Perimeter Insitute f. Theoretical Physics   *MPI für Gravitationsphysik*   *Institut für Physik und Astronomie*
Universität Potsdam

Quantum Gravity   *Dynamics of Quantum Gravity*
31 Caroline St. N.   *Am Mühlenberg 1*   *Karl–Liebknecht Str. 24/25*
Waterloo, ON, N2L 2Y5, Kanada   *D–14476 Potsdam, Deutschland*   *D–14476 Potsdam, Deutschland*

Constructing quantum spacetime: Relation to classical gravity

Publikationsbasierte Dissertation
zur Erlangung des akademischen Grades
„doctor rerum naturalium"
(Dr. rer. nat.)
in der Wissenschaftsdisziplin: Physik

eingereicht an der
Mathematisch–Naturwissenschaftlichen Fakultät der
Universität Potsdam

von
Sebastian Peter Steinhaus

verteidigt am 13. Oktober 2014 vor der Kommission

Prof. Achim Feldmeier	Kommissionsvorsitzende
Dr. Bianca Dittrich	Betreuerin
Prof. Martin Wilkens	Betreuer
Prof. Markus Klein	Kommissionsmitglied
PD Dr. Carsten Henkel	Kommissionsmitglied

Abstract

Despite remarkable progress made in the past century, which has revolutionized our understanding of the universe, there are numerous open questions left in theoretical physics. Particularly important is the fact that the theories describing the fundamental interactions of nature are incompatible. Einstein's theory of general relative describes gravity as a dynamical spacetime, which is curved by matter and whose curvature determines the motion of matter. On the other hand we have quantum field theory, in form of the standard model of particle physics, where particles interact via the remaining interactions – electromagnetic, weak and strong interaction – on a flat, static spacetime without gravity.

A theory of quantum gravity is hoped to cure this incompatibility by heuristically replacing classical spacetime by 'quantum spacetime'. Several approaches exist attempting to define such a theory with differing underlying premises and ideas, where it is not clear which is to be preferred. Yet a minimal requirement is the compatibility with the classical theory, they attempt to generalize.

Interestingly many of these models rely on discrete structures in their definition or postulate discreteness of spacetime to be fundamental. Besides the direct advantages discretisations provide, e.g. permitting numerical simulations, they come with serious caveats requiring thorough investigation: In general discretisations break fundamental diffeomorphism symmetry of gravity and are generically not unique. Both complicates establishing the connection to the classical continuum theory.

The main focus of this thesis lies in the investigation of this relation for spin foam models. This is done on different levels of the discretisation / triangulation, ranging from few simplices up to the continuum limit. In the regime of very few simplices we confirm and deepen the connection of spin foam models to discrete gravity. Moreover, we discuss dynamical, e.g. diffeomorphism invariance in the discrete, to fix the ambiguities of the models. In order to satisfy these conditions, the discrete models have to be improved in a renormalisation procedure, which also allows us to study their continuum dynamics. Applied to simplified spin foam models, we uncover a rich, non–trivial fixed point structure, which we summarize in a phase diagram. Inspired by these methods, we propose a method to consistently construct the continuum theory, which comes with a unique vacuum state.

Abstrakt

Trotz bemerkenswerter Fortschritte im vergangenen Jahrhundert, die unser Verständnis des Universums revolutioniert haben, gibt es noch zahlreiche ungeklärte Fragen in der theoretischen Physik. Besondere Bedeutung kommt der Tatsache zu, dass die Theorien, welche die fundamentalen Wechselwirkungen der Natur beschreiben, inkompatibel sind. Nach Einsteins allgemeiner Relativitätstheorie wird die Gravitation durch eine dynamische Raumzeit dargestellt, die von Materie gekrümmt wird und ihrerseits durch die Krümmung die Bewegung der Materie bestimmt. Dem gegenüber steht die Quantenfeldtheorie, die die verbliebenen Wechselwirkungen – elektromagnetische, schwache und starke Wechselwirkung – im Standardmodell der Teilchenphysik beschreibt, in dem Teilchen auf einer statischen Raumzeit – ohne Gravitation – miteinander interagieren.

Die Hoffnung ist, dass eine Theorie der Quantengravitation diese Inkompatibilität beheben kann, indem, heuristisch, die klassische Raumzeit durch eine ‚Quantenraumzeit' ersetzt wird. Es gibt zahlreiche Ansätze eine solche Theorie zu definieren, die auf unterschiedlichen Prämissen und Ideen beruhen, wobei a priori nicht klar ist, welche zu bevorzugen sind. Eine Minimalanforderung an diese Theorien ist Kompatibilität mit der klassischen Theorie, die sie verallgemeinern sollen.

Interessanterweise basieren zahlreiche Modelle in ihrer Definition auf Diskretisierungen oder postulieren eine fundamentale Diskretheit der Raumzeit. Neben den unmittelbaren Vorteilen, die Diskretisierungen bieten, z.B. das Ermöglichen numerischer Simulationen, gibt es auch gravierende Nachteile, die einer ausführlichen Untersuchung bedürfen: Im Allgemeinen brechen Diskretisierungen die fundamentale Diffeomorphismensymmetrie der Gravitation und sind in der Regel nicht eindeutig definiert. Beides erschwert die Wiederherstellung der Verbindung zur klassischen, kontinuierlichen Theorie.

Das Hauptaugenmerk dieser Doktorarbeit liegt darin diese Verbindung insbesondere für Spin–Schaum–Modelle (spin foam models) zu untersuchen. Dies geschieht auf sehr verschiedenen Ebenen der Diskretisierung / Triangulierung, angefangen bei wenigen Simplizes bis hin zum Kontinuumslimes. Im Regime weniger Simplizes wird die bekannte Verbindung von Spin–Schaum–Modellen zu diskreter Gravitation bestätigt und vertieft. Außerdem diskutieren wir dynamische Prinzipien, z.B. Diffeomorphismeninvarianz im Diskreten, um die Ambiguitäten der Modelle zu fixieren. Um diese Bedingungen zu erfüllen, müssen die diskreten Modelle durch Renormierungsverfahren verbessert werden, wodurch wir auch ihre Kontinuumsdynamik untersuchen können. Angewandt auf vereinfachte Spin–Schaum–Modelle finden wir eine reichhaltige, nicht–triviale Fixpunkt–Struktur, die wir in einem Phasendiagramm zusammenfassen. Inspiriert von diesen Methoden schlagen wir zu guter Letzt eine konsistente Konstruktionsmethode für die Kontinuumstheorie vor, die einen eindeutigen Vakuumszustand definiert.

Acknowledgements

Most of my advances were by mistake.
You uncover what is when you get rid of what isn't.
– R. Buckminster Fuller

Contents

1 Introduction

Many technological advances achieved in the last one hundred years, which have greatly changed and influenced human life, go back to the discovery of two fundamental physical theories: on the one hand, we have quantum theory, i.e. quantum mechanics and quantum field theory, describing nature on small scales, e.g. subatomic particles interacting via the electromagnetic, strong and weak forces encoded in the so–called Standard Model. Quantum theories not only solved long lasting problems, e.g. the ultraviolet catastrophe of electromagnetism, and explained the stability of atoms, they stimulated condensed matter physics, which lead to the development of computers and with it our modern communication society with all of its opportunities and perils. Additionally, it gave rise to classically unknown effects such as entanglement, which opened up completely new fields of research and may spark another revolution of its own, namely quantum computing.

On the other hand, we have general relativity, the classical theory of gravity, the last and comparably weakest of the known fundamental interactions in nature. Thus it is mostly associated to interactions at very large scales to describe the dynamics of celestial bodies. General relativity, together with special relativity, revolutionized our understanding of space and time: In contrast to Newton's theory of gravity, it does not consider an absolute space and time as a given background structure on which gravitational interactions take place. Instead space and time are tied together into a dynamical spacetime, whose curvature, induced by matter, describes then again the universal gravitational interaction between massive objects. In short, the gravitational interactions are encoded into the dynamical geometry of spacetime. Hence, there exists no preferential choice of spacetime or coordinate system, which gives rise to the fundamental symmetry of general relativity, namely diffeomorphism symmetry, also known as general covariance. In brief, the dynamics of gravity are invariant under all smooth bijective maps from the underlying manifold to itself, such that only diffeomorphism invariant quantities are physically relevant. Of course general relativity can claim its personal share in novel physical predictions, to name a few such as the perihelion precession of Mercury and bending of light rays by heavy objects in the sky, known as gravitational lensing. From a technological perspective, it contributed the necessary corrections to Newtonian gravity for the Global Positioning System (GPS) to work flawlessly. An inquiring phenomenon discovered as a particular solution to Einstein's equations are black holes, special regions in spacetime characterized by mass, angular momentum, etc. that causally disconnect their interior from the surrounding spacetime by an event horizon. These objects, whose existence still has to be confirmed directly, e.g. by the direct detection of gravitational waves, are a topic of active research.

Remarkably, both theories are very well tested and still mark the most predictive theories developed in theoretical physics. To mention a very recent result at the LHC, the highly celebrated detection of (probably) the Higgs boson experimentally [1, 2] confirms the last missing piece in the Standard Model of particle physics, whereas, up to now, no indication of supersymmetry, extra dimensions or a fifth force have been observed. On the gravitational side, experiments rather appear to put more and more strict bounds onto alternative theories of gravity or (conjectured) quantum gravity effects, yet new experiments might uncover novel effects challenging general relativity, see [3] for a recent review. Very recent results from cosmological experiments, such as the BICEP2 experiment [4], which detected an imprint of primordial gravitational waves in the cosmic microwave background, appear promising to blaze the trail towards new insights in cosmology, which will hopefully affect quantum gravity.

Indeed, quantum field theory and classical gravity are physically well established theories that describe the phenomena currently experimentally accessible to us very well. However, this neither

implies that no new physical effects will be uncovered at higher energy scales nor does it mean that our understanding of the theories are complete, e.g this can concern the values of the parameters of the theories, their interpretation and origin: the cosmological constant is a prime example. Originally introduced by Einstein in 1917 to model a static universe, it has been measured to be positive, yet very small, and it is a vital parameter in modern models of cosmology [5, 6]. However we are lacking a convincing explanation of its origin and value; an attempt well–known for its obvious failure is the explanation of the cosmological constant as the zero–point energy of quantum fields, cut–off at the Planck scale, which gives a result roughly 120 orders of magnitude too large. This is usually referred to as the 'Cosmological constant problem' [7].

In fact, it is frequently argued that many of the current shortcomings in our understanding of nature is rooted in the fact that we do not have a theory of quantum gravity. Indeed, such a theory is necessary for two reasons: First, general relativity is not a complete theory, since it exhibits singularities, e.g. at the origin of our universe or other cosmological scenarios like black holes, where either curvature or energy density diverges and the theory loses its validity. Generically, this is expected to happen at energies close to the Planck scale. Second, and even more troubling, classical gravity is incompatible with quantum theories: indeed, the two most tested and predictive theories are very well understood on scales, where either one of the two is negligible. On scales of the size of a nucleus, gravity is insignificantly weak in comparison to strong, weak and electromagnetic force, whereas on scales of the solar system (and beyond), the weak and strong force are non–relevant and the electromagnetic interactions are well approximated by the classical theory (or semi–classical approximations). However in cosmological situations like the Big Bang, the cosmological singularity at the beginning of the universe, matter and gravitational interactions (and backreactions) are crucial and require compatible theories.

The incompatibility between general relativity and quantum field theory is caused by opposing initial assumptions and different technical ingredients: In general relativity, spacetime itself, i.e. the metric on a (differential) manifold, is dynamical and determined by the Einstein equations of motion, in which matter is universally coupled to gravity. As a result, it is not reasonable to distinguish one particular spacetime as a special *background*, nor should physics depend on the special choice of spacetime coordinates. This is encoded as diffeomorphism invariance in GR, implemented as a symmetry of the Einstein–Hilbert action, which is deeply intertwined with the dynamics of gravity: e.g. in the canonical formalism, gravity is totally constrained, i.e. the Hamiltonian governing time evolution is a constraint itself and forced to vanish. That means that time evolution, generated by the constraint, itself is a gauge transformation, which is often referred to as the 'problem of time' or 'frozen time formalism' [8–11]. Hence, diffeomorphism symmetry is an essential ingredient of the classical theory of gravity and can serve as a test or guiding principle in the construction of a quantum theory of gravity. Indeed, as we will see the fate of diffeomorphism symmetry plays an important role in the definition of non–perturbative quantum gravity theories.

In contrast to general relativity, quantum field theory is defined on one particular spacetime, which can be seen as the 'stage' on which the dynamics of quantum fields takes place. This background spacetime, frequently chosen to be flat Minkowski space, is fixed and not dynamical, i.e. spacetime is not interacting with the matter content. In other words, (full) gravity is excluded from the dynamics by construction. In many scenarios, like collider experiments on earth, this is a very good approximation, since the involved energies and particle masses are too small to get non–negligible backreaction effects. Gravity can be partially, or rather passively, incorporated by choosing a curved background spacetime, an essential generalization to derive Hawking radiation of black holes[1]. Indeed fixing a background spacetime is essential in providing the technical tools for

---

[1]Since a black hole emits thermal radiation, it will eventually evaporate due to energy conservation. However, this process is far from understood and a very active, and controversially discussed, area of research. In particular the information paradox is investigated: Information that is hidden behind the event horizon of the black hole, e.g. matter that has fallen in, gives rise to an entanglement entropy of the black hole. Under evaporation, this information should be released, however, if only thermal radiation is emitted, how can this thermal radiation

the (perturbative) (Fock–)quantization of fields and computing scattering processes of excitations of the quantum fields.

Hence, the most straightforward idea to define a quantum field theory of gravity and matter is to drop background independence of gravity: Instead of quantizing the full gravitational field, i.e. the metric, one quantizes the (weak) fluctuations around a fixed background, e.g. Minkowski space, as a typical quantum field theory in a perturbative expansion in Feynman diagrams. Classically this approach is known as linearized gravity and describes gravitational waves. The quantum excitations of gravitational waves are particles of spin 2, called gravitons, that interact universally with all other matter fields and, more importantly, with themselves. However this theory, also for pure gravity, is not predictive: As for any quantum field theory, there exist Feynman diagrams that diverge, however these divergences can be absorbed by renormalizing the theory and performing a measurement for each independent parameter of the theory. Yet in perturbative quantum gravity, the divergences cannot be absorbed into a finite number of independent couplings, e.g. the first non–renormalizable term has been identified at the two–loop level [12, 13]. This can either be inferred from the dimensionality of the gravitational coupling constant, which comes with a positive mass dimension. As a result, this form of perturbative quantum gravity is called perturbatively non–renormalizable.

There exist several research fields that explore possible non–perturbative theories of quantum gravity to circumvent or solve this issue. Roughly these can be split into two categories: the first relies on the idea that gravity cannot be consistently quantized just by itself, but should rather be contained in a unified theory with all other interactions. String theory typically falls into this category, which however relies on a background spacetime (or sometimes a background boundary spacetime in the AdS / CFT correspondence). The second one, which we will focus on in this thesis, deals with the non–perturbative quantization of *pure* gravity, characterized by preserving the dynamical nature of spacetime, to which the matter content and interactions are coupled. Tentatively, one might be tempted to call this approach 'constructing quantum spacetime'.

1.1 Non–perturbative quantum gravity

The term 'non–perturbative quantum gravity' joins several different approaches, which can be well distinguished by considering their main underlying ideas. Asymptotic safety [14, 15] assumes that gravity can be formulated as a quantum field theory, since it is expected that the renormalization group flow, i.e. the change of the fundamental coupling constants of the theory under integration of higher momentum–modes, has a non–trivial (non–Gaussian) fixed point in the ultraviolet, which is also called the UV completion of the theory. Or take causal dynamical triangulations [16], a numerical approach simulating quantum spacetime by summing over all possible (equilateral) triangulations weighted by the Regge action [17, 18], a form of discrete gravity, which exhibits a phase (in parameter space) in which the three–volume of spatial slices (on average) resembles a de Sitter spacetime.

One of the best–known approaches is loop quantum gravity [19, 20], a background independent attempt to canonically quantize gravity, in which the spin–network states, i.e. states in the kinematical Hilbert space, live on discrete graphs embedded in a 3D hypersurface. Physical information is contained in the physical states, i.e. all states that are annihilated by the quantum constraint operators. The covariant approach related to loop quantum gravity is known as spin foam models [21, 22], which are defined on a 2–complex and can be understood as discrete versions of the gravitational path integral. E.g. they give the transition amplitudes between two 3–geometries by assigning amplitudes to the connecting discrete 4–geometry, where it has been shown that the amplitudes assigned to (one of the) basic building blocks are proportional to the discrete Regge action in a semi–classical limit [23–29], see also the papers [30, 31] presented in chapters 2 and 3.

---

contain this information? What is the process that reduces the entanglement entropy under evaporation?

A related approach is group field theory (GFT) [32, 33], which defines a field theory on a group, generating pre–geometric complexes via its perturbative expansion in Feynman diagrams. Group field theories are related to spin foam models, since their Feynman diagrams actually resemble spin foam amplitudes.

This little excursion is meant to illustrate the variety of different approaches that can be summarized under the topic 'quantum gravity'. Interestingly, several approaches listed above have common ideas, at least at the conceptual level: As quantum field theories, asymptotic safety and group field theory explicitly examine the renormalization group flow of the theory, namely whether the theory is renormalizable, i.e. there exists a scheme to absorb the divergences of the theory, and how the dynamics of the theory changes at different energy scales. On the other hand, loop quantum gravity[2], spin foam models, causal dynamical triangulations and group field theories rely on discrete structures in their construction, which serve as a truncation of the number of degrees of freedom and allow to non–perturbatively define the dynamics. In some approaches to quantum gravity the discreteness of spacetime is postulated to be fundamental, take for example causal set theory [36].

One goal of this thesis is to define and develop a renormalization group method for discrete approaches, to be more concrete for (analogue) spin foam models, so–called spin nets [37–39], in order to examine the (effective) dynamics of the theory depending on the number of discrete building blocks involved. The hopes are on the one hand that this scheme helps to fix the ambiguities (and pathologies) involved in the definition of the discrete theory, while on the other hand it allows us to explore the different phases of the theory and, furthermore, give a consistent construction method for the associated continuum theory.

This goal is very ambitious, but a crucial point if we consider discretisations, in particular in gravitational theories. Despite their desirable properties, the introduction of discretisations (in both classical and quantum theories) has serious repercussions:

- Discretisations of a continuous action are usually not uniquely defined, that means one can define a plethora of different discrete actions that all converge to the same continuum action in an appropriate continuum limit. This is particularly troubling if one considers (this form of) discreteness to be fundamental.

- Generically, discretisations break the fundamental diffeomorphism symmetry of general relativity [40–43]; in the discrete this symmetry is associated with an invariance under vertex translations [40–46]. As a consequence, former gauge degrees of freedom are 'promoted' to physical degrees of freedom and are a priori indistinguishable from the 'true' physical ones, thus called pseudo–gauge degrees of freedom [41, 42]. This can have serious repercussions e.g. in a path integral formulation, where a naive integration would lead to (additional) divergences once the diffeomorphism symmetry is restored in a continuum limit.

- An issue related to the breaking of diffeomorphism symmetry is the (unphysical) dependence of the theory on the choice of the discretisation / regulator. There exist several proposals to remove this regulator, where it is a priori unclear which one is to be preferred. Should one some over all possible triangulations as in spin foam models and causal dynamical triangulations, or also all topologies as suggested by group field theory? Or should one rather consider a refinement limit, in which the theory is defined on finer and finer triangulations? Under certain conditions in spin foam models, summing over all foams and refining a single foam

---

[2]Even though loop quantum gravity uses graphs to define (kinematical) states, it is a continuum theory: two states defined on two different graphs can be compared by embedding them into a common refinement, i.e. a graph, which is a refinement of both previous graphs. For this to work consistently, the embedding maps have to satisfy cylindrical consistency conditions. In an inductive / projective limit, one can then construct the continuum Hilbert space [20, 34, 35].

may be identical [47]. In a canonical formulation, for broken diffeomorphism symmetry, the constraints of the theory rather occur as pseudo–constraints [41, 42, 48–50].

- Covariant approaches to quantum gravity have the goal to give meaning to the (formal) gravitational path integral

$$\int_{\partial M} \mathcal{D}g \, \exp\{i \, S_{\text{E–H}}[g]\} \quad , \tag{1.1.1}$$

where $\mathcal{D}g$ is the measure on the space of geometries, i.e. the space of metrics modulo diffeomorphisms. In the discrete setting, one not only has to replace the Einstein–Hilbert action $S_{\text{E–H}}[g]$ by a discrete action, but also choose a measure on the set of discrete geometries, which will directly translate into a choice on the measure on the space of geometries. Since diffeomorphism symmetry is generically broken, this raises the question whether the measure factor is anomaly free with respect to diffeomorphisms [51]. Additionally, choices on the measure in spin foam models influence the divergent behaviour of the model [46, 52–55].

- Lorentz invariance is generically broken by the introduction of a discretisation, e.g. in Regge calculus [17], yet its fate in quantum gravity is not clear. It has been frequently argued that quantum gravity effects at the Planck scale may result in a breaking or modification / deformation of Lorentz symmetry, which could be potentially observed as modified dispersion relations of matter propagating on this quantum gravitational background. A possible experimental test could be by observing highly energetic particles, which travelled over long, i.e. cosmological, distances, e.g. emitted in a gamma ray burst [56, 57].

The various issues stated above are very much related to one another and are rooted in the lack of good understanding of the relation between the discrete and the continuous description of gravity, which even arises on the classical level. This particularly affects the fate of diffeomorphism symmetry in the discrete setting. See also [58] for a review on the interplay between discretizations, diffeomorphism symmetry and constraints in various models of quantum gravity and how discretizations can be constructed to circumvent some of the issues.

However, exactly this understanding is crucial in making the case for any of the discrete quantum gravity approaches above. Due to the lack of observational evidence and data indicating quantum gravity effects, the least a quantum gravity theory must achieve is consistency with the classical theory it intends to generalize. This can already be explored on the discrete level, where one would compare the candidate theory to discrete gravity, e.g. Regge calculus [17], yet the full consistency can only be checked for a continuum formulation. Hence the overarching question is, whether quantum gravity models defined in the discrete possess a phase, in which the collective dynamics of many building blocks exhibits a smooth description consistent with general relativity. This consistency certainly should also include (a realization of) diffeomorphism symmetry. In case such a scenario is realized one might be able to predict quantum gravity corrections to general relativity that motivate new experiments and tests, which might eventually verify or falsify the theory.

1.1.1 Introduction to Regge calculus

To get a better understanding of this, let us concretely discuss a discretisation of classical general relativity, namely Regge calculus [17, 59]. Regge calculus is defined on a triangulation of a d–dimensional manifold, where the geometric information is encoded into the distance between the vertices, i.e. the length of the edges of the triangulation. Thus the edge lengths are the dynamical variables of the theory. Note that this formulation is inherently coordinate independent, since only the relative distances between the vertices determine the theory. The Regge action S_R is given as follows:

$$S_R := - \sum_{h \subset \text{bulk}} V_h \left(2\pi - \sum_{\sigma^d \supset h} \theta_h^{(\sigma^d)} \right) - \sum_{h \subset \text{bdry}} V_h \left(\pi - \sum_{\sigma^d \supset h} \theta_h^{(\sigma^d)} \right) \quad , \tag{1.1.2}$$

where σ^d denotes a d–simplex and V_h is the volume of a $(d-2)$–simplex, also called a 'hinge'. The d–dim. (interior) dihedral angle of the d–simplex σ^d located at the hinge h is denoted by $\theta_h^{(\sigma^d)}$ and is determined by the edge lengths of the simplex. The terms in brackets resemble the bulk and boundary deficit angles respectively:

$$\omega_h^{(\text{bulk})} := 2\pi - \sum_{\sigma^d \ni h} \theta_h^{(\sigma^d)} \quad , \tag{1.1.3}$$

$$\omega_h^{(\text{bdry})} := k\pi - \sum_{\sigma^d \ni h} \theta_h^{(\sigma^d)} \quad , \tag{1.1.4}$$

where k depends on the number of pieces one is glueing together at this boundary. If there are only two pieces we have $k = 1$. The deficit angles $\omega_h^{(\text{bulk})}$ define a notion of distributional curvature in Regge calculus: If the dihedral angles located at a hinge shared by several simplices do not sum up to 2π, then the geometry is locally curved.

Since the edge lengths are the dynamical variables of Regge calculus, one obtains an equation of motion for each bulk edge by varying the action with respect to this edge length l_e[3]:

$$\frac{\partial S_R}{\partial l_e} = - \sum_{h \supset e} \frac{\partial V_h}{\partial l_e} \omega_h = 0 \quad . \tag{1.1.5}$$

To provide an intuitive example, in 3D, this formula simplifies notably because the edges are the hinges of the triangulation. Each bulk edge carries one bulk deficit angle, for which the equations of motion state that it has to vanish. Hence 3D Regge calculus is locally flat, which is consistent with the 3D continuous theory: Regge calculus 'perfectly' matches a flat geometry by glueing intrinsically flat simplices in a flat way, i.e. with vanishing deficit angles.

In fact, this example can help us to better understand the issues mentioned above, since it illustrates a particular discretisation with an intact diffeomorphism symmetry in the discrete, i.e. a vertex translation invariance [40–46]. Another example is 3D Regge calculus with a cosmological constant [42,60], where the flat tetrahedra are replaced by constantly curved ones. Similar examples also exist in non–topological theories, for instance in 4D Regge calculus, in case the boundary data allow for a flat solution in the bulk [44,45]. The key point in these examples is that the continuum dynamics are 'perfectly' represented in the discretisation; these approaches are thus called 'perfect discretisations' [61–63]. In more general situations, their construction becomes highly non–trivial: In order to pull back the continuum dynamics onto the discretisation, one first has to solve the continuum dynamics. On the other hand, one can observe that the symmetry is 'less' broken the finer the discretisation is. Thus one can attempt to improve the discretisation [42, 64, 65] by combining, i.e. coarse graining, building blocks of the discretisation into a new (effective) building block, such that the dynamics are endowed onto the discretisation in steps and eventually, in the limit of infinite refinement, diffeomorphism symmetry gets restored.

For interacting systems, such as quantum gravity, the perfect realization of a diffeomorphism symmetry in the discrete is highly non–trivial and may not be possible, however, a suitable coarse graining algorithm should be able to at least *approximately* restore diffeomorphism symmetry. The hope is that given such a good approximation one can draw conclusions on the issues explained above and eventually uncover the relation of the (improved) quantum gravity model and general relativity. Indeed, building this connection between discrete quantum gravity models and general relativity is the main topic of this thesis, which will be mainly discussed for spin foam models. Therefore we will present a brief introduction into spin foams in the next section with particular focus on the current status of these models with respect to the issues discussed above.

---

[3] Note the Schläfli identity: $\sum_{h \subset \sigma^d} V_h \, \delta\theta_h^{(\sigma^d)} = 0$.

1.2 Spin foam models

The modern spin foam models are usually constructed as follows. Consider the Plebanski formulation of gravity [66]:

$$S_{\text{Pleb}} = \int_M B \wedge F(A) + \phi B \wedge B \quad , \qquad (1.2.1)$$

where B is a Lie–algebra valued 2–form and F is the curvature 2–form of the gauge connection (1–form) A. If we just consider the first part of this action, i.e. $B \wedge F(A)$, this gives a topological theory, called BF theory [67]. Topological means that there are no local degrees of freedom and the global ones are completely fixed by the topology of the manifold M^4. In order to get a theory of gravity, constraints have to be imposed that break the (too many) symmetries of this action. These constraints are called simplicity constraints and are imposed via the Lagrange multipliers ϕ; if satisfied one returns to Palatini's first order formulation of gravity.

To construct a spin foam model, one usually starts with topological BF theory, for which it is rather well–known how to discretize and quantize it [67, 70], see also [46, 71, 72] for discussions on the issues in this construction. In many cases the chosen discretization is (dual to) a triangulation, but it can be generalized to arbitrary 2–complexes, i.e. a collection of vertices, edges and faces. Then, in order to break the symmetries of BF theory, one has to impose simplicity constraints in the discrete, quantized theory: the question, which constraints to impose and how is the key difference between the currently proposed spin foam models for 4D gravity, see e.g. the Barrett–Crane model [73], the EPRL–model [74] and the FK–model [75]. We would also like to mention the KKL–model [76], which generalizes the EPRL–model to arbitrary 2–complexes. In general, the dynamical ingredients of spin foam models can be summarized as follows:

Spin foam models defined on 2–complexes assign an amplitude to this complex, if it connects e.g. two (discrete) 3–geometries on its boundaries, then this amplitude can be interpreted as a transition amplitude. The 2–complex itself is coloured with additional data: the faces carry irreducible representations of the symmetry group the spin foam is defined on, e.g. SO(4) in 4D Riemannian gravity or SL(2, $\mathbb{C}$) in Lorentzian 4D gravity, whereas the edges carry projectors onto (a subspace of) the invariant subspace of the tensor product of irreducible representations meeting at this edge. Which subspace the projectors project on depends on the imposition of the simplicity constraints. If no constraints are imposed at all, we have the usual Haar projectors on the edges, which project onto the full invariant subspace. Then this prescription coincides with the strong coupling expansion of lattice gauge theories[5]. Thus spin foam models can be regarded as generalized lattice gauge theories, which is nicely explained in the holonomy representation of spin foam models [69]. The entire amplitude of the complex (or foam) is then computed by summing over all the colourings on the faces[6].

The overlying issue of spin foam models are their complexity, which greatly hinders the exploration of their dynamics. In fact, most of our knowledge and confidence for the validity of spin foam models comes from calculations involving only one simplex, i.e. one of the basic building blocks: A highly celebrated result is the asymptotic expansion of the vertex–amplitude, essentially the amplitude assigned to (the dual of) a simplex [23–29]. By scaling up the areas (of the triangles) of this simplex, which is frequently interpreted as a semi–classical limit, one can identify

---

[4]The Plebanski formulation of gravity is strikingly similar to the action of Yang–Mills theory: $S_{\text{YM}} = \int B \wedge F + g^2 B \wedge (\star B)$ [68]. This action explicitly depends on a background, encoded in the Hodge dual $\star$. As one can see, if $g \to 0$ one obtains BF theory as the weak coupling limit of Yang–Mills theory. We will argue below that one can understand spin foam models as generalized lattice gauge theories [69].

[5]This formulation can be obtained by performing a group Fourier transform of the functions associated to the faces / plaquettes of the lattice.

[6]A prescription more commonly used in the literature is by directly assigning amplitudes to the vertices, edges and faces of the foam. This prescription is equivalent to the one discussed here. The vertex amplitude is directly constructed by a contraction of intertwiners, i.e. the basis elements of the invariant subspace, associated to the edges meeting at the vertex. See the review [77] for a nice explanation.

the dominating phase of the amplitude by a stationary phase approximation. This dominating phase (in the geometric sector) turns out to be the Regge action [17] associated to the simplex. Hence for the simplest possible triangulation, one obtains discrete gravity (in the geometric sector of) spin foam models in this particular limit. Note also that the amplitude is proportional to $\cos(S_R) = \frac{1}{2}(e^{iS_R} + e^{-iS_R})$ instead of just e^{iS_R} as for 'ordinary' path integrals. This is due to the fact that in a spin foam model one has to sum over both orientations of the simplex[7].

Unfortunately, similar results relating spin foams and discrete gravity are rare for larger triangulations / foams, not to mention the continuum theory. In [78], the asymptotic geometry of arbitrary triangulations in the large spin limit of the boundary variables has been examined (without additional assumptions on the bulk triangulation), where one found that the amplitude is suppressed unless the geometry in the bulk satisfies accidental curvature constraints. This indicates that the large spin limit by itself might not be sufficient to explore the semi–classical geometry of spin foams, but also a refinement of the bulk (and the boundary) might be necessary, see e.g. [79]. Additionally even the asymptotics of one vertex amplitude are not completely understood, e.g. the measure factor, which is a possible indicator for the measure on the space of geometries chosen in spin foam models, is unknown.

The work bundled in this thesis can be generally seen as the attempt to extend and deepen our understanding of the connection between spin foams and discrete / continuous general relativity. We explore this relation at very diverse numbers of involved building blocks, with particular focus on dynamical principles either to determine the theory or to improve the theory / discretisation, e.g. via coarse graining. At the lowest level, namely a single simplex / vertex amplitude, we revisit the asymptotic expansion of vertex amplitudes of the Ponzano–Regge model (in 3D) [23,80] and the Barrett–Crane model (in 4D) [73] in chapters 2 / [30] and 3 / [31] with particular focus on deriving the measure factor from a coherent state approach (see [81] for a nice introduction); the result in [31] for the Barrett–Crane model is indeed the first of its kind. Starting from a conjecture derived in [43] relating discrete diffeomorphism invariance to triangulation independence, we investigate whether triangulation independence can be used as a dynamical principle to fix ambiguities in discrete gravity theories, e.g. define the path integral measure unambiguously. Invoking the relation between spin foams and Regge calculus from asymptotic expansions of vertex amplitudes, we study invariance of the (linearized) Regge path integral under local changes of the triangulation, so–called Pachner moves [82,83], in chapters 4 / [59] and 5 / [84]. In 4D such a measure can almost be constructed, but turns out to be non–local, motivating more general coarse graining schemes that also affect the boundary of the discretisation. Such methods were invented in condensed matter theory, e.g. tensor network renormalization [85,86], in order to study effective dynamics of many degrees of freedom by only truncating the least relevant degrees of freedom. We apply these methods to (analogue) spin foam models (defined on quantum groups) in chapter 6 / [87] and uncover a rich fixed point structure with extended phases and phase transitions. Remarkably, the truncation scheme can also be understood as a tool to dynamically relate Hilbert spaces associated to fine or coarse boundaries. In chapter 7 / [88] we argue that such dynamical embedding maps can be interpreted as time evolution maps that allow us to define a consistent continuum theory from the discrete one, if these embedding maps satisfy so–called cylindrical consistency conditions [20,34,35,89].

Before including the manuscripts in the order described above, we would like to give a brief introduction to them and elaborate on their context to the overarching question of this thesis.

---

[7]This can be interpreted as a feature instead of an issue, since one can argue that in a gravitational path integral one has to integrate over all values of lapse and shift in order to impose the constraints of the theory, which can be seen as an evolution 'back and forth in time'.

1.3 Overview of presented manuscripts

1.3.1 Coherent states, 6j symbols and properties of the next to leading order asymptotic expansions

In chapter 2, we present the paper [30], which directly deals with the question of how to compute asymptotic expansions of spin foam models, to be more precise the vertex amplitude / the amplitude associated to a simplex. In this particular paper we revisit the Ponzano–Regge model [23, 80], a theory for 3D (Riemannian) quantum gravity defined on a triangulation.

The Ponzano–Regge model is actually the very first spin foam model. Its partition function Z is defined as follows:

$$Z = \sum_j \prod_{\text{edges}} (-1)^{2j}(2j+1) \prod_{\text{triangles}} (-1)^{j_1+j_2+j_3} \prod_{\text{tetrahedra}} \begin{Bmatrix} j_1 & j_2 & j_3 \\ j_4 & j_5 & j_6 \end{Bmatrix} \quad , \qquad (1.3.1)$$

where j_i denote spins, i.e. irreducible representations of SU(2), which are attached to the edges of the triangulation. This can be understood as assigning a length to the edge. In the partition function then, each edge is weighted with the dimension (of the vector space) of the representation j, whereas each tetrahedron is weighted by the $6j$ symbol made up of the six spins assigned to the six edges of the tetrahedron.

One way to check the relation between spin foam models and classical (discrete) gravity is to extract a semi–classical geometry and action via an asymptotic expansion from the spin foam amplitude. To do so one identifies the dominating phase of the spin foam, which is then usually interpreted as the effective action of this system. One method to achieve this, which proved to be very useful in the examination of modern spin foam models [28, 29], is a coherent state approach. This concept is nicely explained in [81], here we will briefly discuss the idea in 3D:

In a given representation j of SU(2) coherent states [90] are labelled by a vector $\vec{n} \in S^2$, denoted as $|\alpha_j(\vec{n})\rangle$. This state is defined up to a phase by the following equations:

$$\vec{n} \cdot \vec{L}_j \alpha_j(\vec{n}) = i\,j\,\alpha_j(\vec{n}) \quad , \qquad (1.3.2)$$

$$\left\langle \alpha_j(\vec{n}) \left| \left(\vec{L}_j\right)^m \right| \alpha_j(\vec{n}) \right\rangle = i\,j\,(\vec{n})^m \quad . \qquad (1.3.3)$$

$\vec{L}_j$ denotes the generator of rotations, represented in the representation j. The first equation states that $\alpha_j(\vec{n})$ is an eigenstate of the rotation operator pointing in direction $\vec{n}$, whereas the second one gives the expectation value of the m component of $\vec{L}_j$, which basically is the m component of $\vec{n}$ times the spin j. In short, the coherent state is peaked on the vector pointing in the direction $\vec{n}$.

From these coherent states one can construct so–called coherent intertwiners, i.e. basis elements in the invariant subspace of the vector space of the tensor product of irreducible representations, by taking the group averaged tensor product of several coherent states. For a 3–valent intertwiner, basically a Clebsch–Gordan coefficient, this is a tensor product of three coherent states, which can be regarded as a 'quantized triangle'. The vector associated to the coherent state is then interpreted as the edge vector. Remarkably, the amplitude for a Clebsch–Gordan coefficient is dominated by geometries for which $\sum_{i=1}^3 j_i \vec{n}_i = 0$, which is known as the closure constraint. Such a triangle is also referred to as a coherent triangle, since it is peaked on a classical geometry.

From these basic intertwiners, one can construct larger spin networks by contracting these intertwiners according to the combinatorics of the network. One particular example is the $6j$ symbol, the central building block of the Ponzano–Regge model, which is a contraction of four 3–valent intertwiners, i.e. a distinct glueing of four triangles forming a tetrahedron. Using the coherent states defined above, one performs a stationary phase approximation of the group integrations by uniformly scaling up the spins on the edges; the tetrahedron is 'blown up' to a macroscopic size. Remarkably, the stationary point conditions allow for a clear geometric interpretation. First, all

four triangles have to close, i.e. their edge vectors have to sum to zero. Second, one can define normal vectors to the triangles, which have to sum to zero as well, i.e. the tetrahedron constructed from the triangles has to close, too. The angles enclosed by the normal vectors of the triangles are the (exterior) dihedral angles of this tetrahedron. Eventually, one finds that the dominating phase of the $6j$ symbol is given by the Regge action [17] associated to the tetrahedron, a result known for about 45 years [23] and derived in a plethora of ways [91–95].

However, despite the nice geometric interpretation the coherent state approach generically fails to produce the complete asymptotic expansion. While it is straightforward to obtain the dominating phase via a stationary phase approximation, the latter cannot be completed, since the determinant of the Hessian matrix, sometimes called the measure factor[8], cannot be computed. This also troubles the calculations for 4D spin foam models, where the measure factor is generically unknown. Furthermore, even for the $6j$ symbol, where the measure factor is known, the coherent state approach fails and only numerical results are available [96].

To overcome this drawback, we introduce modified coherent states in [30], see also chapter 2, which allow for the same geometric interpretation as the usual ones, yet come with an additional smearing angle ϕ. The major advantage of these coherent states is that the stationary phase approximation can be performed in steps, first with respect to the smearing angles and then with respect to the group elements. The new effective action obtained after the first one turns out to be the first order Regge action [97], which already establishes the connection to discrete gravity and actually is the first derivation of this action from the asymptotics of spin foam models. Given the geometric interpretation of Regge calculus, we complete the asymptotic expansion by deriving several identities from curved Regge calculus [98] and derive properties of higher order corrections [99–102].

The main purpose of this work has been to develop important tools and ideas that might help in also extracting measure factors for 4D spin foam models. Indeed, we succeeded in this endeavour, as we will explain in the next section.

1.3.2 The Barrett-Crane model: asymptotic measure factor

The paper [31] presented in chapter 3 can be seen as a direct continuation of [30] in chapter 2 and deals with the asymptotic expansion of the vertex amplitude of the so–called Barrett–Crane model, i.e. the amplitude assigned to a 4–simplex of the triangulation.

The Barrett–Crane model is the very first, and arguably the simplest, spin foam model for 4D (Riemannian) gravity. In fact, the construction of the modern spin foam models is very similar as it is nicely illustrated in [69]: Starting from discretized and quantized BF theory, they differ in the implementation (and choice) of the simplicity constraints. In case of the Barrett–Crane model, these constraints are imposed 'strongly', such that they are generically satisfied. Indeed, this choice is very constricting, which is reflected in the fact that the 4–valent intertwiner (also called Barrett–Crane intertwiner), dual to a tetrahedron, is unique [73]. Thus, the Barrett–Crane model has no intertwiner degrees of freedom, in contrast to the other 4D spin foam models.

Actually, the Barrett–Crane model is nowadays commonly disregarded as a viable theory of quantum gravity, for a recent discussion see [103]. One of the issues is the presence of non–geometric sectors, for example a BF sector, in the asymptotic expansion, i.e. the semi–classical limit of the model contains contributions that do not allow for a geometric (gravitational) interpretation. In fact this is also a feature shared by the other spin foam models. Additionally, the Barrett–Crane model lacks glueing constraints, that is the tetrahedra along which the simplices are glued together are made up of triangles with the same areas, yet the shapes of these triangles are not matching. Thus, in a semi–classical limit, the Barrett–Crane model rather gives area Regge calculus [104], a theory in which areas, instead of edge lengths, are the dynamical variables. This theory is troubled

---

[8]This term is not to be confused with 'measure' in spin foam literature, which refers to edge and face amplitudes.

by vanishing deficit angles, such that it is locally flat, and, due to the non–matching of the shapes of the faces, the metric, locally defined for each 4–simplex, is discontinuous [105, 106].

Despite the comparable simplicity of the Barrett–Crane model to the other 4D spin foam models, the asymptotic expansion of the vertex amplitude, i.e. the $10j$ symbol, is still incomplete, even when only the geometric contributions are considered. Remarkably, starting from a nice identity of the $10j$ symbol derived in [27], the tools and identities for Regge calculus developed in [30], see also chapter 2, can be almost analogously applied to the Barrett–Crane vertex amplitude. Surprisingly, the result, which is the first of its kind, has a nice geometric interpretation and is almost completely explicit; the only implicit contribution is a Jacobian from a variable transformation from areas to edge lengths. Indeed, this Jacobian can be absorbed by considering a peculiar triangulation. Instead of examining only one 4–simplex, we discuss two 4–simplices glued together along all of their tetrahedra, which is the simplest possible triangulation of a 4–sphere. Then the Jacobian can be absorbed by introducing shape–matching constraints, i.e. constraints that enforce that the areas (triangles) are constructed from edge lengths and thus have matching shapes.

1.3.3 Path integral measure and triangulation independence in discrete gravity

Chapter 4 includes paper [59], in which we address the choice of the path integral measure in (linearized) Regge calculus. Regge calculus [17, 18] is a discretization of classical general relativity defined on a triangulation, see also chapter 1.1.1 for a brief introduction.

Asymptotic expansions in spin foam models indicate, as discussed above, that one obtains Regge gravity in a semi–classical limit. Since the measure factors for spin foam models are hardly known, one can invert the logic and ask, whether one can derive and define a suitable measure factor for quantum Regge calculus, which then presents a 'blueprint' spin foams can be compared to. Indeed, many different measure factors have been proposed for Regge calculus [107–109], yet none has been derived from a dynamical principle.

In chapter 4, see also [59], we propose to use triangulation independence as the determining property for the measure. This is motivated by the work [43], in which perfect discretisations [41, 42, 61, 62], i.e. discretisations with intact discrete diffeomorphism symmetry, have been constructed using a coarse graining scheme. There it has been conjectured that having a discrete diffeomorphism invariant theory is equivalent to the fact that this theory is triangulation / discretisation independent. This conjecture is explained in more detail in the discussion (see chapter 8.2).

Let us emphasize that this is a desirable feature: A theory being both discretisation independent and equipped with a discrete (remnant of) diffeomorphism symmetry fixes many ambiguities in the choices of possible discretisations. Additionally, due to discretisation independence the continuum limit can be performed trivially, which allows to check consistency with the continuum theory, while calculations, such as expectation values of observables, can be performed in the discrete, even on the simplest triangulation possible. Most importantly, the discrete version of diffeomorphism symmetry ensures the realization of diffeomorphism symmetry in the continuum.

Clearly, satisfying these conditions is highly non–trivial. Thus, instead of applying a full fledged coarse graining scheme to (quantum) Regge calculus, we approach the problem from the opposite direction, namely triangulation independence. For a triangulation, this can be tackled on a local level: A triangulation of a manifold can be converted into any other triangulation of the same manifold by a consecutive application of Pachner moves [82, 83], i.e. local changes of the triangulation. A theory is triangulation independent, if it gives the same result for any triangulation of the same manifold, which is equivalent to invariance of the theory under Pachner moves.

On the classical level, it is well–known that the discrete Regge action is fully triangulation invariant in 3D, where gravity is topological, and almost invariant in 4D [59]. Hence we examine, whether one can derive a measure for quantum Regge calculus that renders the path integral triangulation independent, i.e. invariant under Pachner moves. Instead of discussing the full

theory, we instead perturb the Regge action around a flat background solution, i.e. vanishing deficit angles, up to quadratic order and perform the path integral for the perturbations. The resulting path integral measure only depends on the background variables.

To sum up, in chapter 4, see also [59], we use triangulation independence, i.e. invariance under Pachner moves, as a dynamical principle to construct the path integral measure in quantum Regge calculus. In 3D, this construction is successful and consistent with the asymptotics of the Ponzano–Regge model [23]. However in 4D, already the Regge action is not invariant under all Pachner moves and the construction of a triangulation invariant measure (for the remaining moves) is complicated by the appearance of an overall factor in the Hessian matrix, which is the topic of the paper briefly introduced in the next section.

1.3.4 Discretization independence implies non–locality in 4D discrete quantum gravity

The work [84] presented in chapter 5 is the direct continuation of the attempt in [59], see also chapter 4, to construct a triangulation invariant path integral measure in 4D (linearized) Regge calculus. While the calculation is strikingly similar to the 3D case, the Hessian matrix in 4D additionally possesses an overall factor, which resisted a geometric interpretation and has been conjectured in [59] to be non–local. Indeed this factor troubles the construction of a triangulation invariant measure in 4D, such that the purpose of the paper [84] is to derive its geometric meaning and actually prove its non–local nature.

Interestingly, this overall factor turns out to be a criterion determining whether the six vertices involved in the 4D Pachner move lie on the same 3–sphere [110], see also [111]; if this is the case, the factor vanishes. Therefore we carefully analyse the situations, in which this can happen, which includes a careful examination of the relative orientation of simplices in simplicial complexes, see also [112]. Indeed, we identify configurations in which the factor vanishes, yet all involved simplices are non–degenerate. Thus we show that the factor necessarily is non–local and cannot be written as a product of amplitudes associated to (sub)simplices. The result is surprising since one might have hoped for the existence of a topological sector in 4D gravity, which describes flat geometries. Whereas this is the case for the classical theory, it does not exist in the quantum theory.

In fact, non–localities are expected to appear under coarse graining of interacting theories, which generically complicates the calculations and demands the implementation of approximations to keep the scheme feasible, e.g. the truncation scheme invented by Migdal [113] and Kadanoff [114] outright removes the non–local interactions, but is remarkably predicting a phase transition for the 2D Ising model. Yet the error made by such ad hoc truncations is difficult to estimate, such that more efficient truncation schemes are desirable, which are capable of treating the non–local excitations effectively, e.g. by also changing the boundary data in the process. Such coarse graining schemes, e.g. tensor network renormalization [85, 86], originally developed in condensed matter theory, are applied to (analogue) spin foam models defined on quantum groups in the paper [87] in chapter 6, which is briefly introduced in the next section.

1.3.5 Quantum group spin nets: refinement limit and relation to spin foams

Up to this point of the thesis, we have not addressed the elephant in the room: how can we extract the collective dynamics of many building blocks of spin foam models? This questions is very difficult to answer due to the complexity of spin foam models. An idea to make progress is employing numerical simulations, yet quantum Monte Carlo simulations are already out of the game, since they cannot handle complex amplitudes appearing in spin foam models.

Surprisingly the initial setup of spin foam models is not too different from the initial starting point in condensed matter theory: given a discretisation with (locally) interacting degrees of freedom placed e.g. on the vertices of the discretisation, one intends to extract the macroscopic behaviour

from the many–body dynamics, e.g. ground states and the spectrum of the Hamiltonian. Tools to study effective dynamics are summarized under the term real space renormalization techniques [115], in contrast to momentum space renormalization in quantum field theories, of which many can be seen as coarse graining schemes, i.e. mechanisms to combine finer degrees of freedom into new, coarser ones. Generically, this leads to non–localities namely the coarser degrees of freedom start to interact (more) non–locally in comparison to the finer ones. However in the past twenty years many new renormalization schemes have been developed, which are much more suited to effectively deal with non–local interactions, e.g. density matrix renormalization group (DMRG) [116, 117], matrix product states (MPS) and Projected Entangled Pair States (PEPS) [118, 119] and tensor network renormalization [85, 86] in different flavours [120].

The idea of the latter is to encode the dynamics of the system into a tensor network, where each tensor carries the dynamics of the local degrees of freedom. Then the partition function is rewritten as a contraction of this tensor network. Since this is only a rewriting of the initial problem, tensor network renormalization attempts to approximate the partition function of the original system by a contraction of a coarser network by (locally) combining tensors into a new, locally interacting tensor. However under consecutive application of this coarse graining method, the boundary data of the tensor grow exponentially, such that one has to employ truncations. In order to still provide a good approximation to the initial system, it is thus vital to identify the relevant degrees of freedom: this is achieved by employing a singular value decomposition (of a recombination of the tensors), which transforms the fine degrees of freedom into an orthogonal basis, ordered according to their relevance indicated by the associated singular value. On the one hand this particular variable transformation allows to employ good approximations by only keeping the most relevant degrees of freedom, i.e. with the largest singular values, while on the other hand it serves as a direct translation between the degrees of freedom on the fine and the coarser discretisation. If interpreted the other way around, this variable transformation can be seen as an embedding map, computed directly from the dynamical ingredients of the system, embedding the coarse boundary data into the fine data. To be more precise, such an embedding map relates the Hilbert spaces associated to the coarser and finer boundaries. This is a crucial feature which partially motivated the conceptual work [88] in chapter 7, in which we describe how to construct a consistent continuum theory using these embedding maps.

Remarkably, the dynamical ingredients of spin foam models, i.e. the projectors (onto invariant subspaces of the tensor product of irreducible representations) located on the edges, fit very well into the language of tensors. For each face meeting the edge, the tensor carries an index, which runs over all labellings assigned to the pair (edge, face)[9], usually representation labels (magnetic indices). Instead of coarse graining such networks, which is currently work in progress, we consider simplified versions, so–called spin nets, in [87], see also [39].

Spin nets are dimensionally reduced spin foams, so instead of a 2–complex they are defined on a 1–complex, a graph, yet we keep the main dynamical ingredients of spin foams, i.e. the projectors, which are now located on vertices. In fact, one can assign the entire dynamical ingredients to the vertices of the lattice, such that these models are also known as vertex models. Then the corresponding tensor network is straightforward to construct and consists only of one type of tensors. Crucially, the projectors permit an interpretation in terms of simplicity constraints. A second simplification is the replacement of the underlying Lie group e.g. by a finite group, in order to only have finitely many representation labels to sum over in the partition function, which allows for efficient numerical simulations. In [87], see also chapter 6, we instead define spin nets on the quantum groups $SU(2)_k$, which on the one hand also contains a natural cut–off on the representation labels (depending on the level k), yet on the other hand is the *full* 'group'[10] used

---

[9]To write a spin foam as a tensor network, one has to additionally introduce auxiliary tensors on the faces that ensure that the face carries the same irreducible representation [37]. This is also necessary in order to rewrite lattice gauge theories as tensor networks [121].

[10]Despite their name, quantum groups are no groups, but quasi-triangular Hopf algebras [122, 123]. Here we

in spin foam models describing gravity with a non–vanishing cosmological constant. This intuition originates from the Turaev–Viro spin foam model [124] describing 3D quantum gravity with a non–vanishing, positive cosmological constant, which essentially resembles a q–deformed version of the Ponzano–Regge model. In recent years it has also been explored to define loop quantum gravity with a non–vanishing cosmological constant, in particular in (2+1)D to establish the connection to the Turaev–Viro model [125–129], and similarly to extend 4D spin foam models to quantum groups [130–132].

To these quantum group spin nets we apply a symmetry preserving version of tensor network renormalization, see also [39] for this method, to examine their many–body dynamics. We put special focus on the projectors, now located on the vertices: In the modern spin foam model construction, these are not projectors onto the full invariant subspace (of the tensor product of irreducible representations), but only a smaller subspace via the implementation of simplicity constraints. The question is how these projectors change under coarse graining, or to put it differently, how the simplicity constraints change: does the additional structure, added by allowing smaller invariant subspaces, survive under coarse graining or does the system flow back to the standard (analogue) lattice gauge theory phases, namely either the weak coupling, ordered BF phase or the degenerate, strong coupling phase? In a refinement limit, reached once the system has arrived at a fixed point of the coarse graining procedure, we thus examine whether spin nets allow for more structure, e.g. more fixed points than lattice gauge theories or even extended phases (with phase transitions). Indeed we find a rich fixed point structure beyond the standard phases equipped with extended phases in parameter space with phase transitions that show tentative indications to be of second order. This is very encouraging evidence that also spin foam models possess more structure than standard lattice gauge theories and may potentially have a phase with effective dynamics consistent with general relativity.

1.3.6 Time evolution as refining, coarse graining and entangling

As briefly mentioned in the previous section, tensor network renormalization provides a scheme to compute embedding maps from the dynamics of the theory relating fine to coarse boundary data. Such dynamical embedding maps possess a greater potential than merely providing a truncation scheme under coarse graining: If we use them to refine the discretisations, we should eventually arrive at a continuum description from the discrete theory.

To improve our understanding in this direction, we tackle the conceptual issues in defining a continuum theory from a discrete one in [88], see also chapter 7. As the title of the paper suggests, the key idea is to understand time evolution in discrete systems as a map that relates different discretisations, in particular discretisations that are variably coarse (or fine), i.e. discretisations that are capable to capture differing numbers of degrees of freedom. This idea is in fact motivated from local time evolution moves in (canonical) Regge calculus [133–135], which time evolve a triangulated hypersurface to another one, where the latter can capture more, less or the same number of degrees of freedom, possibly organized in a different way. On the classical level, this is captured by phase spaces of differing dimension associated to the hypersurfaces. Remarkably, if the number of degrees of freedom change under local time evolution, this *always* results in the appearance of constraints, even if one does not model gravity or diffeomorphism symmetry is broken. The occurring constraints are called pre– and post–constraints: the pre–constraints are conditions that have to be satisfied in order for time evolution to take place, while the post–constraints are automatically satisfied once time evolution has taken place. Notably for gravity, in the example of a refining time evolution, the post–constraints also contain diffeomorphism and Hamiltonian constraints. In a quantum theory one assigns Hilbert spaces to the triangulated hypersurfaces.

---

understand $SU(2)_k$ as the q-deformation of the universal enveloping algebra of $SU(2)$, denoted as $\mathcal{U}_q(\mathfrak{su}(2))$. $q = \exp\{i\frac{\pi}{k+2}\}$ is a root of unity, k denotes the level of the quantum group.

Then local time evolution acts as an embedding map of the initial into a different Hilbert space. See also [136, 137] for discussions of the quantum case.

The observant reader may immediately object that time evolution generated by local moves may depend on the particular choice and order of the moves, which may render this approach to be unphysical. Indeed, to avoid such pathologies, time–evolution has to be path–independent [138], which translates into consistency conditions called (dynamical) cylindrical consistency for the embedding maps, a concept well–known (on the kinematical level) in loop quantum gravity [20, 34, 35]. The extension of the concept towards dynamical embedding maps has already been explored in [89], a viewpoint we extend upon in chapter 7, see also [88]. The important feature of dynamical cylindrical consistency is that, if realized, states represented on different discretisations can be compared to one another and identified as describing the same *physical* situation, i.e. physics should not depend on which discretisation it is represented on. As a consequence, the state of the system only implicitly depends on the specific discretisation, in fact it can already be represented in the continuum. Furthermore, in gravity the interpretation of embedding maps as time evolution is particularly appealing, since in gravity, as a totally constrained system, time evolution is a gauge transformation. Thus, the physical state of the system does not change under time evolution; indeed if cylindrical consistency is satisfied, time evolving the state means embedding it into a different discretisation, which by definition lies in the same equivalence class. The physical state therefore does not change, it is simply expressed on a different discretisation.

Candidate's contribution to the presented manuscripts

Before including the manuscripts representing the bulk of this thesis, we have to clarify and outline the candidate's contribution to the multi–authored papers:

In the projects concerning the asymptotic expansions of vertex amplitudes in spin foam models [30, 31] the author of this thesis was involved in all major steps, yet his main contribution was for the calculations on the partial approximations of stationary phase, i.e. first with respect to the smearing angles and afterwards for the dihedral angles. To complete the latter the candidate derived several non–trivial identities for first order Regge calculus crucial for the extraction of the asymptotic measure factor in both papers [30, 31]. Also, the calculations in [30] were quite involved: The candidate's knowledge of numerical methods were crucial for finishing the project, even though they are not directly visible in the final version of the paper. The papers were written collaboratively, yet the candidate wrote significant portions of the introduction and discussion in both papers, and is mainly responsible for the organisation of the paper [30].

The papers [59, 84] concerning triangulation independence of the linearized Regge path integral were mainly developed and authored by the author of this thesis, of course with several discussions and consultations with the co–authors.

The project on coarse graining quantum group spin nets [87] was a joint effort by all three authors. Again the candidate was involved in all main steps of the work, including the definition of the model and dealing with the intricacies of quantum groups in the development of the algorithm. Most of the candidate's efforts were invested in coding and optimizing the algorithm, in particular the higher accuracy version, running of the simulations and analyzing the data. The paper was written collaboratively, where the candidate wrote the parts on diagrammatic calculus, the coarse graining algorithm and the results of the simulations.

Finally, the conceptual paper on interpreting embedding maps as time evolution maps [88] was a result of long contemplation on fundamental and conceptual issues in quantum gravity. As a result the paper is mostly conceptual and many points arose in discussions between the candidate and Bianca Dittrich clarifying the direction and interpretation of our research. Concurring the explicit writing, the candidate contributed the sections on topological theories and the geometric interpretation.

2 Coherent states, $6j$ symbols and properties of the next to leading order asymptotic expansions

Wojciech Kamiński[1,2,3] and Sebastian Steinhaus[2,3]

[1] Wydział Fizyki, Uniwersytet Warszawski
Hoża 69, 00-681, Warsaw, Poland

[2]Perimeter Institute for Theoretical Physics
31 Caroline Street North, Waterloo, Ontario, Canada N2L 2Y5

[3]Max Planck Institute for Gravitational Physics
Am Mühlenberg 1, D-14476 Potsdam, Germany

Abstract

We present the first complete derivation of the well-known asymptotic expansion of the $SU(2)$ $6j$ symbol using a coherent state approach, in particular we succeed in computing the determinant of the Hessian matrix. To do so, we smear the coherent states and perform a partial stationary point analysis with respect to the smearing parameters. This allows us to transform the variables from group elements to dihedral angles of a tetrahedron resulting in an effective action, which coincides with the action of first order Regge calculus associated to a tetrahedron. To perform the remaining stationary point analysis, we compute its Hessian matrix and obtain the correct measure factor. Furthermore, we expand the discussion of the asymptotic formula to next to leading order terms, prove some of their properties and derive a recursion relation for the full $6j$ symbol.

2.1 Introduction

Spin foam models [A1–A4] are candidate models for quantum gravity invented as a generalization of Feynman diagrams to higher dimensional objects. Their popularity is rooted in the fact that they were well adapted to descibe 3D Quantum Gravity theories such as the Ponzano-Regge [A5, A6] or the Turaev-Viro model [A7]. To examine whether these models are a quantum theory of 4D General Relativity, in particular whether one obtains Gravity in a semi-classical limit is an active area of topical research. One of the strongest positive implications comes from the asymptotic analysis of single simplices in spin foam models: A first attempt to compute the asymptotic expansion of the amplitude associated to a 4-simplex in the Barrett-Crane model [A8] can be found in [A9, A10]. This was continued for the square of (the Euclidean and Lorentzian) $6j$ and $10j$ symbols in [A11], whereas the most recent asymptotic results for modern spin foam models, i.e. the EPRL-model [A12] or the FK-model [A13], were obtained using a coherent state approach [A14–A19]:

The basic amplitudes of the spin foam model are their vertex amplitudes ($SU(2)$ $6j$ symbols in the 3D Ponzano Regge model). They are defined in a representation theoretic way and can be constructed from coherent states of the underlying Lie group [A20] as a multidimensional integral to which the stationary point approximation is applicable [A21]. This method has proven to be very efficient in determining the dominating phase in the asymptotic formula as well as the geometric interpretation of the contributions to the asymptotic expansion in spin foam models [A14–A19]. In 3D, on the points of stationary phase, $6j$ symbols are geometrically interpreted as tetrahedra, their dominating phase given by the Regge action [A22, A23], a discrete version of General Relativity on a triangulation. Similar results were proven by this method for the 4-simplex [A9, A14–A18] in spin foam models. Until today, this is still one of the most promising evidences that spin foam models are viable Quantum Gravity theories.

Despite this success, the coherent state approach fails to produce the full amplitude. It has not yet been possible to compute the so-called measure factor, a proportionality constant (depending on the representation labels) in the asymptotic expansion, which is given by the determinant of the matrix of second derivatives, i.e. the Hessian matrix, evaluated on the stationary point. This failure even applies to the simplest spin foam model in 3D, the Ponzano-Regge model [A6], whose vertex amplitude is the $SU(2)$ $6j$ symbol. To the authors' best knowledge the Ponzano and Regge formula [A5] has not yet been obtained this way; we can only refer to numerical results in [A19]. This is particularly troubling for the coherent state approach, since the full asymptotic formula for $SU(2)$ $6j$ symbols introduced in [A5] has been proven in many different ways, for example, by geometric quantization [A24], Bohr-Sommerfeld approach [A25], Euler-MacLaurin approximation [A26] or the character integration method [A11].

The source of the problem is the size of the Hessian matrix and the lack of immediate geometric formulas for its determinant. For the $6j$ symbol, for example, this matrix is 9 dimensional and its entries are basis dependent. This is a major drawback of the coherent state approach, in particular, since the full expansion is necessary to discuss and examine the properties of spin foams models of Quantum Gravity. To obtain this measure factor and compare it to other approaches [A27, A28], the complete asymptotic expansion is indispensable. This is an important open issue for 4D spin foam models.

Our approach to overcome this problem can be seen (as we will show in Appendix 2.H) as a combination of the coherent state approach [A14–A19] and the propagator kernel method [A29]. It inherits nice geometric properties from the coherent state analysis with a similar geometric interpretation of the points of stationary phase. Moreover, the Hessian matrix is always described in terms of geometrical quantities and, most importantly, its determinant can be computed for the $6j$ symbol.

In addition to the computation of the asymptotic formula of the $6j$ symbol [A5], our approach allows us to propose a new way to compute higher order corrections to the asymptotic expansion. These corrections have already been discussed in [A30, A31]: it was conjectured that the asymptotic

expansion has an alternating form

$$\{6j\} = A_0 \cos \left(\sum \left(j_i + \frac{1}{2} \right) \theta_i + \frac{\pi}{4} \right) + A_1 \sin \left(\sum \left(j_i + \frac{1}{2} \right) \theta_i + \frac{\pi}{4} \right) + \dots \quad , \qquad (2.1.1)$$

where A_n are consecutive higher order corrections and homogeneous functions in $j + \frac{1}{2}$. Our method allows us to prove this conjecture to any order in the asymptotic expansion.

2.1.1 Coherent states and integration kernels

The coherent state approach is based on the following principle: Invariants (under the action of the group) can be constructed by integration of a tensor product of vectors (living in the tensor product of vector spaces of irreducible representations) over the group, i.e. group averaging. Since the invariant subspace of the tensor product of three representations of $SU(2)$ is one-dimensional, the invariant is uniquely defined up to normalization. However, in order to apply the stationary point analysis the vectors in the construction above cannot be chosen arbitrarily. The choice, from which the method takes its name, is the coherent states class, which consists of eigenvectors of the generators of rotations with highest eigenvalues [A20]. Although these states are very effective in obtaining the dominating phase of the amplitude, the associated Hessian matrix turns out to be very complicated. This problem occurs since the action is not purely imaginary, which is also related to the problem of choice of phase for the coherent states which has not yet been fully understood.

Both latter problems disappear if, instead of eigenstates with maximal eigenvalues, we take null eigenvectors for a generator of rotations L. Since this vector is trivially invariant with respect to rotations generated by L, the phase problem disappears. Similarly the contraction of invariants can be expanded in terms of an action that actually is purely imaginary. There is a trade-off, though: The quantity of stationary points increases and their geometric interpretation becomes more complicated. Moreover, frequently there exist no such eigenvectors for certain representations, (half-integer spins for $SU(2)$) and their tensor product gives thus vanishing invariants.

The solution to these issues comes from the simple observation that null eigenvectors can be obtained by the integration of a coherent state, pointing in direction perpendicular to the axis of L, over the rotations generated by L. Like that the geometric interpretation usually obtained when using coherent states is restored. Furthermore, if we first perform the partial stationary phase approximation with respect to the additional circle variables, we obtain a purely imaginary action. In the special case of the $6j$ symbol, our construction allows us to write the invariant purely in terms of edge lengths and dihedral angles of a tetrahedron, in particular we perform a variable transformation from group elements to dihedral angles of the tetrahedron. The resulting phase of the integral is given be the first order Regge action [A32].

2.1.2 Relation to discrete Gravity

Regge calculus [A22, A23] is a discrete version of General Relativity defined upon a triangulation of the manifold. Influenced by Palatini's formulation, a first order Regge calculus was derived in [A32], in which both edge lengths and dihedral angles are considered as independent variables and their respective equations of motion are first order differential equations. Additional constraints on the angles have to be imposed in order to reobtain their geometric interpretation. These consist of the vanishing of the angle Gram matrix that implies the existence of the flat n-simplex with the given angles. Our derivation of the Ponzano-Regge formula shows astonishing similarity to this procedure. Moreover, from our calculation one can deduce a suitable measure for first order (linearized) Quantum Regge calculus, such that the expected Ponzano-Regge factor $\frac{1}{\sqrt{V}}$ appears, which naturally leads to a triangulation invariant measure [A27].

Another version of 4D Regge calculus was explored in [A33] with areas of triangles and (a class of) dihedral angles as fundamental and independent variables. Several local constraints guarantee that the geometry of a 4-simplex is uniquely determined. These variables were chosen in the pursuit to better understand the relation between discrete gravity and 4D spin foam models. The latter are based on a similar paradigm as the Ponzano-Regge or the Turaev-Viro models [A5, A7] in 3D, yet enhanced by the implementation of the simplicity constraints from the Plebanski formulation of General Relativity [A34]. Area-angle variables as a discretization of Plebanski rather than Einstein-Hilbert formulation were conjectured to be more suitable to describe the semi-classical limit of those models.

Although it is known that the asymptotic limit of the amplitude of a 4-simplex for 4D gravity models is proportional to the cosine of the Regge action [A15–A17], the proportionality factor still remains unknown. We hope that the method presented in this work can help in filling the gap.

2.1.3 Problem of the next to leading order (NLO) and complete asymptotic expansion

The asymptotic expansion for the $SU(2)$ $6j$ symbol, in particular for the next to leading order (NLO), is still a scarcely examined issue, since it is very non-trivial to write the (NLO) contributions in a compact form. Steps forward in this direction can be found in [A30, A31, A35], where the latter gives the complete expansion in the isosceles case of the $6j$ symbol.

The stationary point analysis applied in this work allows for a natural extension in a Feynman diagrammatic approach. From this approach the full expansion can be computed in principle, however in a very lengthy way. We derive a recursion relations of the Ward-Takesaki type, which is surprisingly similar to the one invented in [A36, A37] however in very different context, that, basically can be used in the asymptotic expansion to derive the NLO in a more concise way. Moreover, we can show explicitly that the consecutive terms in the expansion (2.1.1) are of the conjectured 'sin/cos' form.

2.1.4 Organization of the paper

This paper is organized as follows: In section 2.2 we will present our modified coherent states, how to use them to construct invariants and how to contract these invariants to compute spin network amplitudes. The contracted invariants will be used to define an action for the stationary point analysis, which will be examined whether it allows for the same geometric interpretation on its stationary points as other coherent state approaches [A14–A19]. Its symmetries as well as the group generated by the symmetry transformations will be discussed. Section 2.3 deals with the partial stationary point analysis with respect to the introduced circle variables. This will allow us to write the amplitude, after a variable transformation, purely in terms of angle variables, which will be identified as exterior dihedral angles of a polyhedron. In section 2.4 we focus on the example of the $6j$ symbol. After another variable transformation, we obtain the action of first order Regge calculus and perform the remaining stationary point analysis. Eventually we obtain the asymptotic formula from [A5]. In section 2.5 we prove the conjecture from [A30, A31] that the full asymptotic expansion is of alternating form (2.1.1) and derive the recursion relations for the full $6j$ symbol. We conclude with a discussion of the results and an outlook in section 2.6.

We would like to point out that several results of this paper have been obtained by tedious calculations which we did not include in its main part to improve readability. Interested readers are welcome to look them up in the appendices.

2.2 Modified coherent states, spin-network evaluations and symmetries

In this section we are going to present the modified coherent states, how to construct the spin-network evaluation from them and that they allow for the same geometric interpretation in the stationary point analysis as similar coherent state approaches. Furthermore the symmetries of the action will be investigated.

Consider a three-valent spin network, i.e. a graph with three-valent nodes carrying $SU(2)$ intertwiners and edges carrying irreducible representations of $SU(2)$. For each edge of the spin network we introduce a (fiducial) orientation such that each node of the network can be denoted as the 'source' $s(e)$ or the 'target' $t(e)$ of the edge e. Later in this work we intend to give a geometrical meaning to the spin network, in terms of polyhedra, triangles, etc. so we denote the set of nodes by F and the set of edges by E, which will become the set of triangles / faces and set of edges of the triangulation respectively. This dual identification is not always possible but we restrict our attention to the case of planar (spherical) graphs, where such notions are natural.

2.2.1 Intertwiners from modified coherent states

Intertwiners are invariant vectors (with respect to the action of the group) in the tensor product of vector spaces associated to irreducible representations of that group. In the case of 3 irreducible representations of $SU(2)$ the space of invariants is one dimensional and, moreover, there is a unique choice for the invariant for a given cyclic order of representations [A38, A39].

Suppose $\xi \in V_{j_1} \otimes \cdots \otimes V_{j_n}$ is a vector in the tensor product of vector spaces of representations, then

$$\int_{SU(2)} dU \ U\xi \tag{2.2.1}$$

is invariant under the action of $SU(2)$. If ξ is chosen in a clever way, such an invariant is nontrivial. In the case of three representations it must be proportional to the unique invariant defined in [A38, A39]. In the following we present a choice which has the advantage that the method of stationary phase can be directly applied.

For every face f, which is bounded by three edges, we choose a cyclic order of these edges $(j_{fe_1}, j_{fe_2}, j_{fe_3})$, labelled by the carried representations. These choices influence the orientation of the spin network [A38, A39] and are used to define and determine the sign of its amplitude, see also appendix 2.A. We introduce the following intertwiners for every face f:

$$C_f = \int_{SU(2)} dU_f \ U_f \int \prod_j \frac{d\phi_{ji}}{2\pi} f_f \left(\{\phi_{fe}\}_{e \in F} \right) \prod_{e \in F} \left(O_{\phi_{fe}} |^1/_2\rangle \right)^{2j_e} \quad , \tag{2.2.2}$$

where f_f is a function of the three angles ϕ_{fe}, $e \subset f$, $|^1/_2\rangle$ is the basic state of the fundamental representation and O_ϕ is a rotation matrix on $\mathbb{R}^2$:

$$O_\phi = \begin{pmatrix} \cos\phi & \sin\phi \\ -\sin\phi & \cos\phi \end{pmatrix} \quad . \tag{2.2.3}$$

As mentioned above, (2.2.2) is invariant under the action of $SU(2)$.

Before moving on, we would like to outline the key differences between the approach described above and the usual coherent state approach [A15–A17, A19].

- Coherent states of $SU(2)$ are labelled by vectors in $\mathbb{R}^3$. On the stationary point with satisfied reality conditions, one obtains the geometric interpretation that for every face these three vectors form the edge vectors of a triangle. Later on we will prove the same geometric interpretation for the invariant C_f.

- Furthermore we smear the coherent state by a rotation, which is the key ingredient of our approach. In addition to the stationary point analysis with respect to the $\{U_f\}$, we will also perform a stationary point analysis for the smearing angles $\{\phi_{fe}\}$. Clearly, this will result in more stationary points contributing to the final amplitude. To suppress their contributions, we introduce modifiers f_f which will be described in the next section.

Prescription of the modifiers

In order to make (2.2.2) complete, we have to describe the function f_f.

For every face f we choose three vectors v_e ($e \subset f$) on $\mathbb{R}^2$ with norms j_e such that $\sum_{e \subset f} v_e = 0$, i.e. they form a triangle with edge lengths j_e. The vectors are ordered anti-clockwise, their choice is unique up to Euclidean transformations, i.e rotations and translations.

Let us denote the edges (in cyclic order) by $1, 2, 3$. The angles (counted clockwise) between the vectors v_k and v_j are denoted by $2(\psi_{kj} - \pi)$, where $2(\psi_{kj} - \pi)$ is the $SO(3)$ angle taking values in $(0, \pi)$ for $(k, j) \in \{(2, 1), (3, 2), (1, 3)\}$. Due to the ordering, the $SU(2)$ angles ψ_{21}, ψ_{32} and ψ_{13}
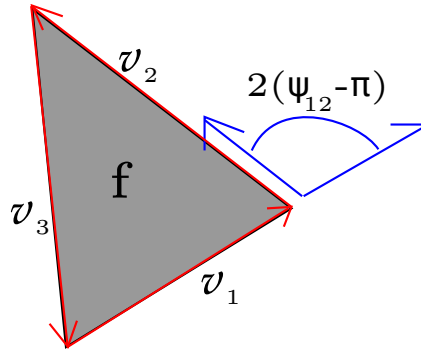
Figure 2.1: The choice of vectors v_i.

are positive and smaller than 2π, in fact, one can also check that ψ_{kj} is in $(\pi, 2\pi)$. This choice contributes an overall sign to the invariant, to be more precise, there are two different choices of cyclic order giving two invariants that may differ by a sign factor. This will be discussed in more detail in appendix 2.A.2. In particular we compare them to the intertwiner introduced in [A38, A39]. The angles ψ_{kj} satisfy the relation

$$\psi_{21} + \psi_{32} + \psi_{13} = 4\pi \ . \tag{2.2.4}$$

We introduce a function $f(x \bmod 2\pi, y \bmod 2\pi)$ such that

- it is equal to 1 in the neighbourhood of $x = \psi_{21}$, $y = \psi_{32}$,

- it is equal to zero in the neighbourhood of points

$$(x, y) = \pm(\psi_{21} + \pi, \psi_{32}), \pm(\psi_{21}, \psi_{32} + \pi), \pm(\psi_{21} + \pi, \psi_{32} + \pi), (-\psi_{21}, -\psi_{32}) \quad . \tag{2.2.5}$$

Hence, we define

$$f_f(\phi_{f1}, \phi_{f2}, \phi_{f3}) = f(\phi_{f2} - \phi_{f1}, \phi_{f3} - \phi_{f2}) \quad . \tag{2.2.6}$$

The spin network evaluation

Given the definition of invariants in (2.2.2) it is straightforward to define the evaluation of a given spin network: The intertwiners are contracted with each other according to the combinatorics of

the network. The resulting amplitude has to be normalized, i.e. divided by the product of norms of our intertwiners, see section 2.3.4. It is, however, not sufficient in order to agree with the canonical definition [A38, A39]. The remaining sign ambiguity will be resolved in Appendix 2.A.

As in the standard coherent state approach the amplitude (contraction of intertwiners) then reads:

$$
(-1)^s \int \prod_{f \in F} dU_f \prod_{e \subset f} \frac{d\phi_{fe}}{2\pi} \prod_f f_f \left(\{\phi_{fe}\}_{e \subset f}\right)
$$
$$
\underbrace{\prod_{e \in E} \epsilon\Big(U_{s(e)} O_{\phi_{s(e)e}}|1/2\rangle \ , \ U_{t(e)} O_{\phi_{t(e)e}}|1/2\rangle\Big)^{2j_e}}_{e^S} \quad , \tag{2.2.7}
$$

where s is the sign factor as prescribed in [A38, A39] (see Appendix 2.A), and $\epsilon(\cdot, \cdot)$ is an invariant bilinear form defined by

$$
\epsilon(|1/2\rangle, |1/2\rangle) = \epsilon(|-1/2\rangle, |-1/2\rangle) = 0, \quad \epsilon(|1/2\rangle, |-1/2\rangle) = -\epsilon(|-1/2\rangle, |1/2\rangle) = 1 \ . \tag{2.2.8}
$$

The choice of the orientation of edges, faces and the sign factor prescription will be described in appendix 2.A.1. To perform the stationary point analysis we rewrite (part of) the integral kernel as an exponential function and define the 'action' S. From (2.2.7) one can deduce that

$$
S = \sum_e S_e \quad , \tag{2.2.9}
$$

where the action S_e (labelled by the edge e) is given by:

$$
S_e = 2j_e \ln \epsilon\left(U_{s(e)} O_{\phi_{s(e)e}}|1/2\rangle \ , \ U_{t(e)} O_{\phi_{t(e)e}}|1/2\rangle\right) \quad . \tag{2.2.10}
$$

2.2.2 The action

In order to examine the geometric meaning of the action on its points of stationary phase, let us introduce the following geometric quantities. For each face $f \in F$ we introduce vectors n_f (as traceless Hermitian matrices, which can be naturally identified with vectors in $\mathbb{R}^3$) defined by:

$$
n_f = U_f H U_f^{-1} \quad , \tag{2.2.11}
$$

where

$$
H = \begin{pmatrix} 0 & i \\ -i & 0 \end{pmatrix} \quad . \tag{2.2.12}
$$

For each pair $\{f, e\}$ with $e \subset f$, we define vectors B_{fe} (also as traceless matrices):

$$
B_{fe} = j_e(2U_f O_{\phi_{fe}}|1/2\rangle\langle 1/2|O_{\phi_{fe}}^{-1} U_f^{-1} - \mathbb{I})
$$
$$
= U_f O_{\phi_{fe}} \left[j_e \begin{pmatrix} 1 & 0 \\ 0 & -1 \end{pmatrix} \right] O_{\phi_{fe}}^{-1} U_f^{-1} \quad . \tag{2.2.13}
$$

Note that the length of B_{fe} is equal to j_e.

We can already deduce that $\Re S \leq 0$. The stationary point analysis contains the conditions $\partial S = 0$ and $\Re S = 0$. These are as follows

- The reality condition is satisfied if and only if

$$
U_{s(e)} O_{\phi_{s(e)e}}|1/2\rangle \perp U_{t(e)} O_{\phi_{t(e)e}}|1/2\rangle \quad , \tag{2.2.14}
$$

where $\perp$ means perpendicular in the $SU(2)$ invariant scalar product. This is equivalent to $B_{s(e)e} = -B_{t(e)e}$.

- Using both the reality condition and the definition of B_{fe} we obtain from the variation of S with respect to U_f:

$$X \frac{\partial S_e}{\partial U_f} = \begin{cases} \operatorname{Tr} X B_{fe} & e \subset f \\ 0 & e \not\subset f \end{cases} , \qquad (2.2.15)$$

where X is a generator of the Lie algebra. Hence the action is stationary with respect to U_f if:

$$\sum_{e \subset f} B_{fe} = 0 \quad . \qquad (2.2.16)$$

- Similarly we obtain for the variation of S with respect to ϕ_{fe} (again using the reality condition):

$$\frac{\partial S_e}{\partial \phi_{fe'}} = \begin{cases} \operatorname{Tr} n_f B_{fe} & e = e' \subset f \\ 0 & \text{otherwise} \end{cases} . \qquad (2.2.17)$$

So the condition from variation with respect to ϕ is

$$\forall_{e \subset f} \; n_f \perp B_{fe} \quad . \qquad (2.2.18)$$
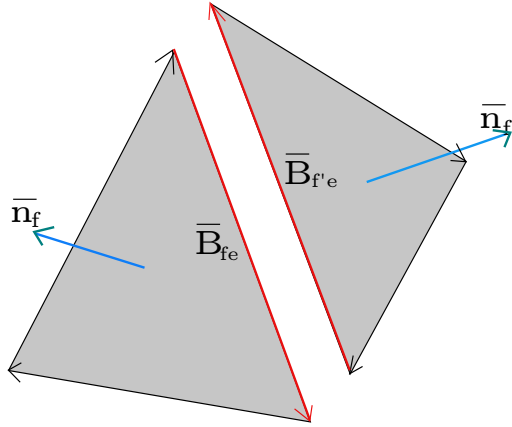
Figure 2.2: Stationary point condition.

Before we discuss the geometric meaning of the just derived conditions, we first have to examine the symmetries of the action to determine the amount of stationary points and their relations.

2.2.3 Symmetry transformations of the action

There exist several variable transformations that only change e^S by a sign such that a stationary point is transformed into another stationary point. Some of the transformations below are continuous so the stationary points form submanifolds of orbits under the action of these symmetries. We will explain the geometric interpretation of these orbits in section 2.2.5, and show that these orbits are isolated for many spin networks, e.g. the $6j$ symbol.

The above mentioned transformations are as follows:

- u-symmetry:
  $\forall u \in SU(2)$,

$$\forall_{f \in F}, \; U_f \to u U_f \qquad (2.2.19)$$

  applied to all U_f simultaneously preserves e^S. This is the only symmetry which has to be applied to all group elements simultaneously showing that one of the $SU(2)$ integrations in (2.2.7) is redundant (gauge).

- o_f-rotation:
  For a chosen face f and ϕ,

$$U_f \to U_f O_\phi, \quad \forall_{e \subset f} \phi_{fe} \to \phi_{fe} - \phi \tag{2.2.20}$$

  preserves e^S, in fact, each e^{S_e} is preserved.

- $-u_f$-symmetry:
  For any chosen face $f \in F$,

$$U_f \to (-1)U_f \tag{2.2.21}$$

  preserves e^S because for every face $\sum_{e \subset f} j_e$ is an integer.

- r_f-reversal transformation:
  For any chosen face f,

$$U_f \to U_f \underbrace{\begin{pmatrix} i & 0 \\ 0 & -i \end{pmatrix}}_{D}, \quad \forall_{e \subset f} \ \phi_{fe} \to -\phi_{fe} \ . \tag{2.2.22}$$

  Because

$$D^{-1} O_\phi D = O_{-\phi}, \quad D|1/2\rangle = i|1/2\rangle \ , \tag{2.2.23}$$

  e^S is multiplied by

$$i^{2 \sum_{e \subset f} j_e} = (-1)^{\sum_{e \subset f} j_e} \ . \tag{2.2.24}$$

  Let us notice that $2j_e \in \mathbb{Z}$ and $\sum_{e \subset f} j_e$ is an integer,

- $-o_{fe}$ transformation:
  For any chosen pair $e \subset f$

$$\phi_{fe} \to \phi_{fe} + \pi \tag{2.2.25}$$

  This multiplies the integrated term by $(-1)^{2j_e}$.

Note that the transformations o_f, $-u_f$ $-o_{fe}$, r_f are restricted to variables associated to one face. They transform the functions f_f as follows:

- o_f shifts all angles ϕ_{fe} on f by an angle ϕ:

$$f'_f(\{\phi_{fe}\}) = f_f(\{\phi_{fe} + \phi\}) = f_f(\{\phi_{fe}\}) \quad , \tag{2.2.26}$$

  since f_f only depends on differences of angles.

- $-o_{fe}$

$$f'_f(\{\phi_{fe'}\}) = f_f(\{\phi_{fe'} + \delta_{ee'}\pi\}) \quad . \tag{2.2.27}$$

- r_f

$$f'_f(\{\phi_{fe}\}) = f_f(\{-\phi_{fe}\}) \quad . \tag{2.2.28}$$

To sum up, the functions f_f are preserved by u-, $-u_f$- and o_f-transformations, since the first two do not affect the angles ϕ and the last one translates all angles by a constant.

In addition to that, let us also define an additional transformation c, which we call parity transformation:

$$\forall f : \quad U_f \to U_f \begin{pmatrix} 0 & 1 \\ -1 & 0 \end{pmatrix} \quad . \tag{2.2.29}$$

It transforms the integral into its complex conjugate due to the fact that

$$\bar{U} = \begin{pmatrix} 0 & 1 \\ -1 & 0 \end{pmatrix}^{-1} U \begin{pmatrix} 0 & 1 \\ -1 & 0 \end{pmatrix} \quad , \tag{2.2.30}$$

and the f_f, the matrix O_ϕ and the vectors $|\pm 1/2\rangle$ are real.

In the next section we will examine which group is generated by the transformations, i.e. the symmetry group of the action.

2.2.4 Groups generated by symmetry transformations

The transformations described in 2.2.3 generate a group $\tilde{G}$ with the following relations:

$$
\begin{aligned}
&u_{(-1)} = \prod_f (-u_f), \\
&\forall_f, \quad r_f^2 = (-u_f), \quad (-u_f)^2 = 1, \quad o_f(2\pi) = 1, \\
&\forall_{e \subset f}, \quad (-o_{fe})^2 = 1, \\
&\forall_f, \quad o_f(\pi) \prod_{e \subset f} (-o_{fe}) = 1 \ .
\end{aligned}
\tag{2.2.31}
$$

and all its elements commute besides u (that form $SU(2)$) and

$$
\forall f, \ r_f o_f(\alpha) r_f^{-1} = o_f(-\alpha) \ .
\tag{2.2.32}
$$

The group generated by all transformations except u is denoted by G.

In $\tilde{G}$ (resp. G), there is a normal subgroup generated by the transformations $u, o_f, -u_f$ (resp. $o_f, -u_f$), which preserves the modifiers f_f. We denote these subgroups by $\tilde{H}$ (and H respectively); their quotient groups are given by

$$
K = \tilde{G}/\tilde{H} = G/H \ \ .
\tag{2.2.33}
$$

This is an Abelian group generated by

$$
\forall_{e \subset f} \quad [r_f], \ [-o_{fe}]
\tag{2.2.34}
$$

with relations

$$
\forall_f \ \prod_{e \subset f} [-o_{fe}] = 1, \ [r_f]^2 = [-o_{fe}]^2 = 1 \ \ ,
\tag{2.2.35}
$$

which show that K is isomorphic to $\mathbb{Z}_2^{3|F|}$.

In the next two sections, we will discuss the geometric interpretation of the points of stationary phase.

2.2.5 Geometric lemma

Our goal in this section is to describe the geometric interpretation of the stationary point orbits introduced in section 2.2.2. In particular, we will show how these points are related to the standard stationary point interpretation in the coherent state method.

Lemma 1. *For every set of vectors B_{fe} of length j_e satisfying*

$$
\begin{aligned}
&\forall_e B_{s(e)e} = -B_{t(e)e} \quad , \\
&\forall_f \sum_{e \subset f} B_{fe} = 0 \quad ,
\end{aligned}
\tag{2.2.36}
$$

there exist ϕ_{fe} and U_f being a point of stationary phase with vectors B_{fe}. Moreover, all these points are related via G transformations.

Proof. For every f we can choose the unit vector n_f perpendicular to all B_{fe} (for all $e \subset f$). Such a normal is only determined up to a sign. Let us choose U_f such that

$$
n_f = U_f H U_f^{-1} \quad .
\tag{2.2.37}
$$

Such a choice always exists, but it is not unique. U_f is only determined up to the transformation

$$U_f \to U_f DO_\phi \tag{2.2.38}$$

since D, defined in (2.2.22), stabilizes H up to a sign:

$$DHD^{-1} = -H \quad . \tag{2.2.39}$$

This is called the D_∞ group.

The vectors $U_f^{-1} B_{fe} U_f$ are orthogonal to H. The operators $U_f^{-1} B_{fe} U_f$ are thus real and we can choose their eigenvectors with positive eigenvalues as

$$\begin{pmatrix} \cos \phi_{fe} \\ \sin \phi_{fe} \end{pmatrix} \quad . \tag{2.2.40}$$

Hence ϕ_{fe} is fixed (up to π).

It is straightforward to check that this construction gives a stationary point, in fact, each stationary point with vectors B_{fe} must be constructed in this way. The ambiguities in the choices above are all related by o_f-, $-u_f$-, $-o_f$- and r_f-transformations, i.e. G-transformations. $\qquad \square$

For every face f on the stationary point $\sum_{e \subset f} B_{fe} = 0$ and given the definition of f_f in section 2.2.1, there is a unique choice (up to o_f transformations) of the stationary point angles ϕ_{fe} such that f_f is nonzero. In the neighbourhood of those stationary point $f_f = 1$, whereas around all remaining ones at least one of the functions f_f is zero:

Lemma 2. *For given vectors B_{fe} satisfying (2.2.36), there exists only one orbit (orbit of the action of the group $\tilde{H}$) of stationary points of the action, such that*

$$\prod f_f(\{\phi_{fe}\}) \neq 0 \quad , \tag{2.2.41}$$

and in the neighbourhood of this orbit

$$\prod f_f(\{\phi_{fe}\}) = 1 \quad . \tag{2.2.42}$$

Note that the normals to the faces change sign under r_f transformations:

$$n_f \to -n_f \quad . \tag{2.2.43}$$

Under the c-transformation, the B_{fe} are inverted, but the normals to the faces are not affected, i.e. they behave as pseudovectors.

$$\begin{aligned} B_{fe} &\to -B_{fe} \quad , \\ n_f &\to n_f \quad . \end{aligned} \tag{2.2.44}$$

In the next section we will specify the definition of the normals n_f.

2.2.6 Normal vectors to the faces

We will now give a precise geometric definition of n_f (normal to the face). To simplify notation we will omit the subscript ϕ in $O_{\phi_{fe}}$. Note that

$$n_f = U_f O_{fe} H O_{fe}^{-1} U_f^{-1} \tag{2.2.45}$$

for any edge $e \subset f$, since O_{fe} and H commute.

Take two consecutive edges $e_1, e_2 \subset f$ and their respective edge vectors B_{fe_i}:

$$B_{fe_1} = U_f O_{fe_1} \left[j_{e_1} \begin{pmatrix} 1 & 0 \\ 0 & -1 \end{pmatrix} \right] O_{fe_1}^{-1} U_f^{-1} \quad , \tag{2.2.46}$$

$$B_{fe_2} = U_f O_{fe_1} (O_{fe_1}^{-1} O_{fe_2}) \left[j_{e_2} \begin{pmatrix} 1 & 0 \\ 0 & -1 \end{pmatrix} \right] (O_{fe_1}^{-1} O_{fe_2})^{-1} O_{fe_1}^{-1} U_f^{-1} \quad . \tag{2.2.47}$$

Rotating all three vectors by $U_f O_{fe_1}$ one obtains (the rotated vectors are denoted by B'_{fe_i}, n'_f):

$$n'_f = H, \quad B'_{fe_1} = j_{e_1} \begin{pmatrix} 1 & 0 \\ 0 & -1 \end{pmatrix}, \quad B_{fe_2} = O_{fe_1}^{-1} O_{fe_2} \left[j_{e_2} \begin{pmatrix} 1 & 0 \\ 0 & -1 \end{pmatrix} \right] (O_{fe_1}^{-1} O_{fe_2})^{-1} \quad . \tag{2.2.48}$$

For a stationary point with non-vanishing modifier f_f, $O_{fe_1}^{-1} O_{fe_2}$ describes the rotation by the $SO(3)$ angle $0 < 2(\psi_{12} - \pi) < \pi$. We thus conclude:

$$n_f \cdot (B_{fe_1} \times B_{fe_2}) = n'_f \cdot (B'_{fe_1} \times B'_{fe_2}) > 0 \quad , \tag{2.2.49}$$

where we regard n_f and B_{fe_i} as vectors using the natural identification of hermitian matrices with $\mathbb{R}^3$ (tracial scalar product). Condition (2.2.49) fixes the sign of n_f and also completes the geometric interpretation of the points of stationary phase.

2.2.7 Interpretation of planar (spherical) spin-networks as polyhedra

In the last section we obtained an interpretation of the stationary points in terms of a set of vectors B_{fe} satisfying closure conditions for every face f

$$\sum_e B_{fe} = 0 \quad . \tag{2.2.50}$$

However, these conditions do not specify a unique reconstruction of the according surface dual to the spin network. In fact, already each triangle allows for two different configurations of B_{fe} vectors. Therefore, we will here describe a method to reconstruct the surface from B_{fe} vectors for the spherical case:

Let us draw the graph on the sphere (on the plane) as described in appendix 2.A.1. From the possible ways of drawing it, which in the case of 2-edge irreducible spin networks is in one-to-one correspondence with the orientation of the spin network, we have to choose one. In the case of 2-edge irreducible graphs the polyhedra obtained from different choices only differ by orientation. In addition to nodes and edges, there is also a natural notion of two-cells. The latter are defined as areas bounded by loops of edges. We are mainly interested in the dual picture that in this case is a triangulation of the sphere. Thus there is a unique identification of the vertices in the dual picture. A cyclic ordering of the edges for each f is inherited from the orientation of the sphere.

In the following, we will construct an immersion (not an embedding) of this triangulation of the sphere into $\mathbb{R}^3$, such that every edge e is given by $B_{t(e)e}$ (with the right orientation).

Let us choose one vertex v_0. Every other vertex v' can be connected to v_0 by a path

$$v_0, e_0, v_1, e_1, \ldots, v' \quad . \tag{2.2.51}$$

Every edge e_i in the sequence belongs to two faces. Exactly one of these faces is such that v_i, v_{i+1} are the consecutive vertices w.r.t the cyclic order of the face. We denote this face by f_i (see figure 2.3). We introduce the vector

$$\tilde{v}' = \sum_i B_{f_i e_i} \quad . \tag{2.2.52}$$

One can prove that this vector does not depend on the chosen path. To see this, let us consider a basic move that consists of replacing v_i, e_i, v_{i+1} by v_i, e, v, e', v_{i+1} where all three vertices belong to the same face f. Using the property

$$\sum_{e \subset f} B_{fe} = 0 \qquad (2.2.53)$$

and the proper orientation, one can show that the vector $\tilde{v}'$ is invariant with respect to this move. In fact any two paths can be transformed into one another by a sequence of these basic moves (or their inverses) due to the fact that the graph is spherical. A different choice of v_0 gives a translated surface. It is straightforward to check that
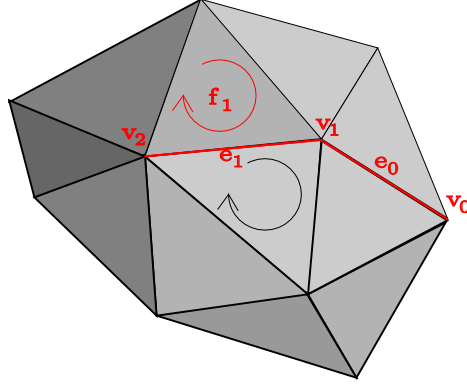
Figure 2.3: Reconstruction of the surface

$$\tilde{v}_b - \tilde{v}_a = B_{fe} \quad , \qquad (2.2.54)$$

where v_a and v_b are vertices joint by the edge e and f is the face such that (v_a, v_b) is the pair of consecutive vertices in the cyclic order of f.

Let us notice that from three vectors B_{fe} satisfying the closure condition one can form a triangle in two ways (see figure 2.4), but only that one depicted on the left appears in the reconstruction discussed here. Moreover the direction of the normal to the face coincides with the orientation
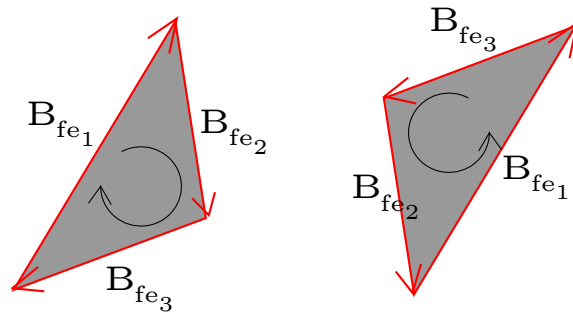
Figure 2.4: Two possible triangles formed by B_{fe} satisfying closure condition.

inherited by the face from the cyclic order of its edges.

For non-planar graphs, in general, we can only reconstruct the universal cover of the surface.

Before we continue with the stationary point analysis for the angles ϕ_{fe} in the next section, let us briefly summarize the results of section 2.2: We have introduced a class of modified coherent states for irreducible representations of $SU(2)$, which contain an additional smearing parameter,

and presented how to construct invariants from them. From the contraction of these invariants (according to the spin network) an effective action has been derived, whose points of stationary phase allow for the same geometrical interpretation as the standard coherent states [A19, A20]. The amount of stationary points is significantly increased by the smearing parameters, yet they are all related by symmetry transformations of the action; a certain set of them can be suppressed by the prescribed modifiers. Eventually, we have depicted a way to reconstruct a triangulation from planar spin networks.

2.3 Variable transformation and final form of the integral

In this section we focus on the stationary point analysis with respect to the angles ϕ_{fe}, which is the key modification in comparison to previously used coherent state approaches, see also section 2.2.1. This analysis allows us to obtain an effective action for S_e associated to the edge e in terms of a phase, which we will identify as the angle between the normals of the faces sharing the edge e. Furthermore we are able to expand the effective action for S_e in orders of $\frac{1}{j}$ and initiate the discussion of next-to-leading order contributions.

2.3.1 Partial integration over ϕ and the new action

Suppose that we have a non-degenerate configuration, i.e.

$$\forall_e n_{s(e)} \cdot n_{t(e)} \neq \pm 1 \quad . \tag{2.3.1}$$

Then the partial stationary point analysis with respect to all ϕ_{fe} can be performed. Its result will be the sum over the contribution from all stationary points with respect to ϕ_{fe} for a given configuration of B_{fe} vectors, but for fixed U_f (so also fixed n_f).

Stationary points for S_e

In this section we will explain the contribution to the integral from the stationary point of the action S_e with respect to $\phi_{s(e)e}, \phi_{t(e)e}$. The $f_{s(e)}, f_{t(e)}$ terms can be ignored, since they are equal to 1 around the stationary point.

We can separately consider terms corresponding to each edge

$$\frac{1}{4\pi^2} \int d\phi_{s(e)e} d\phi_{t(e)e} \, \epsilon \left(U_{s(e)} O_{s(e)e} |1/2\rangle \,, \, U_{t(e)} O_{t(e)e} |1/2\rangle \right)^{2j_e} \quad , \tag{2.3.2}$$

and perform the stationary point analysis that gives the asymptotic result of the integration over $\phi_{s(e)e}, \phi_{t(e)e}$. The stationary point with respect to $\phi_{t(e)e}$ and $\phi_{s(e)e}$ is given by the conditions

$$U_{s(e)} O_{s(e)e} |1/2\rangle \perp U_{t(e)} O_{t(e)e} |1/2\rangle \quad , \tag{2.3.3}$$

which is equivalent to

$$U = O_{s(e)e}^{-1} U_{s(e)}^{-1} U_{t(e)} O_{t(e)e} = (-1)^{\tilde{s}} e^{-i\tilde{\theta} \begin{pmatrix} 1 & 0 \\ 0 & -1 \end{pmatrix}} \begin{pmatrix} 0 & -1 \\ 1 & 0 \end{pmatrix} \quad , \tag{2.3.4}$$

where $\tilde{\theta} \in \left(-\frac{\pi}{2}, \frac{\pi}{2} \right)$ and $\tilde{s} \in \{0, 1\}$ are uniquely determined by this equation. In section 2.3.1 we will show that $2\tilde{\theta}$ can be interpreted as the angle enclosed by the normal vectors $n_{s(e)}$ and $n_{t(e)}$ (w.r.t. the axis $B_{t(e)e}$). Hence, S_e on the stationary point is of the following form:

$$S_e = 2j_e \ln \epsilon(\cdots) = 2j_e \tilde{\theta} + i \, 2j_e \pi \tilde{s} \quad . \tag{2.3.5}$$

As already discussed in section 2.2.5, each stationary point is characterized by the existence of $B_{t(e)e} = -B_{s(e)e}$ orthogonal to both $n_{s(e)}$ and $n_{t(e)}$ (see also stationary point conditions in section 2.2.2). There exist two such configurations that differ by a sign of $B_{s(e)e}$.

For every configuration one has 4 stationary points that can be obtained from one another by $-o_{s(e)}$- and $-o_{t(e)}$-transformations. In case j_e is an integer the contributions from the two stationary points are equal, see also section 2.2.3.

Contributions from B_{fe} configurations with opposite signs are related by complex conjugation.

Geometric interpretation of the angle $\tilde{\theta}$

The missing piece of the description above is the exact value of the angle $\tilde{\theta}$. Here we will provide a geometric interpretation of this angle and its relation to the angle between faces. Let us recall:

$$B_{s(e)e} = j_e U_{s(e)e} O_{s(e)e} \begin{pmatrix} 1 & 0 \\ 0 & -1 \end{pmatrix} O_{s(e)e}^{-1} U_{s(e)}^{-1} \tag{2.3.6}$$

$$n_{s(e)} = U_{s(e)} O_{s(e)e} H O_{s(e)e}^{-1} U_{s(e)}^{-1} \tag{2.3.7}$$

$$n_{t(e)} = U_{t(e)} O_{t(e)e} H O_{t(e)e}^{-1} U_{t(e)}^{-1} = e^{i\tilde{\theta} \frac{B_{t(e)e}}{|B_{t(e)e}|}} n_{s(e)} e^{-i\tilde{\theta} \frac{B_{t(e)e}}{|B_{t(e)e}|}} \tag{2.3.8}$$

The angle $2\tilde{\theta}$ is the angle by which one needs to rotate $n_{s(e)}$ around the axis $B_{t(e)e}$ to obtain $n_{t(e)}$. We will denote this $SO(3)$ angle by

$$\theta = 2\tilde{\theta}, \quad \theta \in (-\pi, \pi) \ . \tag{2.3.9}$$

This remaining ambiguity of the sign factor $\tilde{s}$ will be resolved in appendix 2.A.

2.3.2 Partial integration over ϕ

We introduce new variables

$$\phi_1 = \phi_{s(e)} - \phi_{s(e)}^0, \quad \phi_2 = \phi_{t(e)} - \phi_{t(e)}^0 \ , \tag{2.3.10}$$

where $\phi_{s(e)}^0$ and $\phi_{t(e)}^0$ denote the stationary points. Then using (2.3.4), we can write the action as:

$$\frac{1}{4\pi^2} \int d\phi_1 \, d\phi_2 (-1)^{2j_e \tilde{s}} \left(e^{i\tilde{\theta}} \cos\phi_1 \cos\phi_2 + e^{-i\tilde{\theta}} \sin\phi_1 \sin\phi_2 \right)^{2j} \ , \tag{2.3.11}$$

where we integrate over ϕ_i. By splitting the terms in the bracket in real and imaginary part, we obtain:

$$\cos\tilde{\theta} \underbrace{(\cos\phi_1 \cos\phi_2 + \sin\phi_1 \sin\phi_2)}_{\cos(\phi_1 - \phi_2)} + i \sin\tilde{\theta} \underbrace{(\cos\phi_1 \cos\phi_2 - \sin\phi_1 \sin\phi_2)}_{\cos(\phi_1 + \phi_2)} \ . \tag{2.3.12}$$

We define new variables

$$\alpha := \phi_1 - \phi_2, \quad \beta := \phi_1 + \phi_2 \ , \tag{2.3.13}$$

and the Jacobian for this transformation is given by:

$$\left| \frac{\partial\alpha\partial\beta}{\partial\phi_1\partial\phi_2} \right| = \left| \begin{matrix} 1 & -1 \\ 1 & 1 \end{matrix} \right| = 2 \ . \tag{2.3.14}$$

Hence equation (2.3.11) becomes:

$$\frac{1}{8\pi^2}\int d\alpha d\beta \ (-1)^{2j_e\tilde{s}}\left(\cos\tilde{\theta}\cos\alpha + i\sin\tilde{\theta}\cos\beta\right)^{2j_e} =$$

$$=\frac{1}{8\pi^2}\int d\alpha d\beta \ (-1)^{2j_e\tilde{s}}\exp\left\{\underbrace{2j_e\ln\left(\cos\tilde{\theta}\cos\alpha + i\sin\tilde{\theta}\cos\beta\right)}_{=:S'_e}\right\} \quad , \qquad (2.3.15)$$

where $S_e = S'_e + i\ 2j_e\pi\tilde{s}$.

Expansion around stationary points

Given the definitions from the previous section, we compute the expansion of the following expression:

$$\frac{1}{8\pi^2}\int d\alpha \, d\beta \ (-1)^{2j\tilde{s}}e^{S'_e} \quad . \qquad (2.3.16)$$

The stationary point is given by $\alpha = \beta = 0$, which corresponds to $\phi_i = 0$, i.e. $\phi_{s(e)} = \phi^0_{s(e)}$, $\phi_{t(e)} = \phi^0_{t(e)}$. In this point the action associated to the edge e becomes:

$$S'_e = 2j_e\ln\left(e^{i\tilde{\theta}_e}\right) = i2j_e\tilde{\theta}_e \qquad (2.3.17)$$

In order to compute the first order contribution, one has to consider the matrix of second derivatives (evaluated on the point of stationary phase):

$$\frac{\partial^2 S'_e}{\partial\alpha^2} = -\ 2j_e\frac{\cos\tilde{\theta}\cos\alpha}{\cos\tilde{\theta}\cos\alpha + i\sin\tilde{\theta}\cos\beta} \quad , \qquad (2.3.18)$$

$$\frac{\partial^2 S'_e}{\partial\alpha\partial\beta} = 0 = \frac{\partial^2 S'_e}{\partial\beta\partial\alpha} \quad , \qquad (2.3.19)$$

$$\frac{\partial^2 S'_e}{\partial\beta^2} = -\ 2ij_e\frac{\sin\tilde{\theta}\cos\beta}{\cos\tilde{\theta}\cos\alpha + i\sin\tilde{\theta}\cos\beta} \quad . \qquad (2.3.20)$$

Around the stationary point the action can be expanded (up to second order in the variables α, β):

$$S'_e = i2j_e\tilde{\theta} + \frac{1}{2}\begin{pmatrix} \alpha & \beta \end{pmatrix}\begin{pmatrix} -2j_e\cos\tilde{\theta}e^{-i\tilde{\theta}} & 0 \\ 0 & -2ij_e\sin\tilde{\theta}e^{-i\tilde{\theta}} \end{pmatrix}\begin{pmatrix} \alpha \\ \beta \end{pmatrix} + \cdots \quad . \qquad (2.3.21)$$

In order to correctly perform the stationary phase approximation, it is indispensable to state the right branch of the square root, here for $\tilde{\theta} \in \left(-\frac{\pi}{2}, \frac{\pi}{2}\right)$:

$$\sqrt{\cos\tilde{\theta}e^{-i\tilde{\theta}}} = \sqrt{|\cos\tilde{\theta}|}e^{-i\frac{1}{2}\tilde{\theta}}$$

$$\sqrt{i\sin\tilde{\theta}e^{-i\tilde{\theta}}} = \sqrt{|\sin\tilde{\theta}|}e^{-i\frac{1}{2}\tilde{\theta}}\begin{cases} e^{-i\frac{\pi}{4}} & \tilde{\theta} \in \left(-\frac{\pi}{2}, 0\right) \\ e^{i\frac{\pi}{4}} & \tilde{\theta} \in \left(0, \frac{\pi}{2}\right) \end{cases} \quad . \qquad (2.3.22)$$

Let us notice that

$$\text{sgn}\sin\theta = \text{sgn}\sin\tilde{\theta} \quad \text{for} \quad \tilde{\theta} \in \left(-\frac{\pi}{2}, \frac{\pi}{2}\right) \quad . \qquad (2.3.23)$$

Hence, the leading order contribution from the stationary point is:

$$\frac{1}{8\pi^2}\frac{2\pi(-1)^{2j_e\tilde{s}}}{\sqrt{2j^2\left|\sin 2\tilde{\theta}\right|}}e^{i2\tilde{\theta}\left(j+\frac{1}{2}\right)-i\frac{\pi}{4}\text{sign}(\sin 2\tilde{\theta})}\left(1 + O\left(\frac{1}{j}\right)\right) \quad . \qquad (2.3.24)$$

In the next section we will show an improvement of this result.

The total expansion of the edge integral

Let us introduce a number (see appendix 2.H for a motivation of its origin)

$$C_j = \frac{1}{4^j} \frac{\Gamma(2j+1)}{\Gamma(j+1)^2} \quad . \tag{2.3.25}$$

We can multiply (2.3.24) by $\frac{C_j}{C_j} = 1$ and use the expansion $\frac{1}{C_j} = \sqrt{\pi j}\left(1 + O(\frac{1}{j})\right)$ derived in appendix 2.D.2 to write the result as

$$C_{j_e} \frac{(-1)^{s_e}}{4\sqrt{2\pi j_e \,|\sin\theta|}} e^{i(\theta(j_e+\frac{1}{2}) - \frac{\pi}{4}\text{sign}(\sin\theta))} \left(1 + O\left(\frac{1}{j_e}\right)\right) \quad . \tag{2.3.26}$$

By s_e we denoted the sign factor

$$s_e = \begin{cases} 0 & j_e \text{ integer,} \\ 0 & j_e \text{ half-integer and } \tilde{s} = 0 \\ 1 & j_e \text{ half-integer and } \tilde{s} = 1 \end{cases} \quad . \tag{2.3.27}$$

We will determine the sign s_e in appendix 2.A.

We introduce new 'length' parameters

$$l_e := j_e + \frac{1}{2} \quad , \tag{2.3.28}$$

and using the fact that $\frac{(-1)^{s_e}}{4\sqrt{2\pi l_e|\sin\theta|}} = \frac{(-1)^{s_e}}{4\sqrt{2\pi j_e|\sin\theta|}}\left(1 + O(j^{-1})\right)$ we can express (2.3.26) in terms of l_e. Before we move on, we would like to present a first glimpse at the next-to-leading order contribution: As it will be shown in section 2.5.2 by application of the stationary point analysis (2.3.26) and the recursion relation (2.5.29), the contribution (including next-to-leading order (NLO)) from the integral of e^{S_e} over $\phi_{s(e)e}, \phi_{t(e)e}$ is given by

$$C_{j_e} \frac{(-1)^{s_e}}{4\sqrt{2\pi l_e\,|\sin\theta|}} e^{i(l_e\theta - \frac{\pi}{4}\text{sign}(\sin\theta) - \frac{1}{8l_e}\cot\theta)} \left(1 + O\left(\frac{1}{l_e^2}\right)\right) \quad , \tag{2.3.29}$$

where $\theta \in (-\pi, \pi)$ is the angle by which one has to rotate $n_{s(e)}$ around $B_{t(e)e}$ to obtain $n_{t(e)}$.

2.3.3 New form of the action

In the previous sections we have computed the contribution of one point of stationary phase with respect to the angles ϕ_{fe}. From section 2.3.2 we can also conclude that having one stationary point all others are obtained by application of transformations from $\tilde{G}$ that keep U_f fixed. These are given by compositions of

$$(-u_f)o_f(\pi), \ -o_{fe} \ \forall f \quad . \tag{2.3.30}$$

However, only the orbit generated by the group of $(-u_f)o_f(\pi)$ from a non-trivial stationary point contributes, since all other stationary points are suppressed by the modifiers f_f. Therefore it is sufficient to compute the number of these stationary points. The group generated by $(-u_f)o_f(\pi)$ is equal to $Z_2^{|F|}$ and acts freely on the stationary points; the countability of the orbit is thus $2^{|F|}$.

Around the stationary orbit, the integral is hence of the form:

$$(-1)^s 2^{|F|} \int \prod dU_f \prod_e (-1)^{s_e} C_{j_e} \frac{1}{4\sqrt{2\pi\left(j_e+\frac{1}{2}\right)|\sin\theta_e|}} e^{-i\frac{\pi}{4}\text{sgn}\sin\theta_e}\, e^{i\left(j_e+\frac{1}{2}\right)\theta_e - \frac{1}{8(j_e+\frac{1}{2})}\cot\theta_e} \quad , \tag{2.3.31}$$

where θ_e is the angle between $n_{s(e)}$ and $n_{t(e)}$ with the sign determined by left hand rule with respect to $B_{t(e)e}$. In the neighbourhood of the stationary point this definition is meaningful. The value of the product $\prod_e (-1)^{s_e}$ is discussed in appendix 2.A.2. We use new 'length' parameters introduced in section 2.3.2

$$l_e := j_e + \frac{1}{2} \tag{2.3.32}$$

and perform a change of variables

$$U_f \to n_f \quad , \tag{2.3.33}$$

which is worked out in appendix 2.B.1. The correct integral measure is given by:

$$\mu = \frac{1}{2\pi} \delta(|n|^2 - 1) \, dn_1 \, dn_2 \, dn_3 \quad . \tag{2.3.34}$$

Thus, we can write the integral (integrating out o_f and $-u_f$ gauges) as:

$$\frac{(-1)^s (-1)^{\sum_e s_e} e^{-i\frac{\pi}{4} \sum_e \mathrm{sgn}_e} \prod_e C_{j_e}}{2^{\frac{5}{2}|E|} \pi^{|F| + \frac{1}{2}|E|}}$$

$$\int \prod_{f \in F} \delta(|n_f|^2 - 1) \, d^3 n_f \frac{1}{\sqrt{\prod_e l_e |\sin \theta_e|}} e^{i \sum_e \left(l_e \theta_e + S_1^{l_e}(\theta_e) \right)} \quad . \tag{2.3.35}$$

where from 2.3.2 we know

$$S_1^{l_e}(\theta_e) = -\frac{1}{8 l_e} \cot \theta_e + \dots \quad . \tag{2.3.36}$$

The only present symmetry that has to be discussed is a u-symmetry, which is implemented by $SO(3)$ rotations:

$$n_f \to u n_f u^{-1} \tag{2.3.37}$$

If the configurations of the vectors B_{fe} is rigid, i.e. the only deformations of the configuration of the edges with given lengths are rotations, then the stationary u-orbit is isolated, i.e. there exists a neighbourhood of the orbit that does not intersect any other orbit.

c transformation as parity transformation

Furthermore, we would like to point out that given one orbit of stationary phase, we can always construct a different one via parity transformation of the B_{fe} vectors (see also section 2.2.5 about c transformations). After integrating out gauges these two points are related by

$$\begin{aligned} n'_f &= n_f \quad , \\ B'_{fe} &= -B_{fe} \quad , \end{aligned} \tag{2.3.38}$$

so also the angles are related by $\theta'_e = -\theta_e$ (n_f are preserved as pseudovectors). Finally, we see that the asymptotic contribution from the parity related stationary orbits is just the complex conjugate of the original one, such that the complete expansion is real.

In order to provide the correct expression of the action before performing the remaining stationary point analysis, it is necessary to compute the normalization of the intertwiners, the so-called 'Theta' graph.

2.3.4 Normalization - 'Theta' graph

We need to compute the self-contraction of the invariants C_f using the (in this case) symmetric bilinear form ϵ (as a generalization of the anti-symmetric form ϵ of spin $1/2$ to arbitrary representations). Its special properties allow us to relate the ϵ product $((\cdot, \cdot))$ to the scalar product on $SU(2)$:

$$(C_f, C_f) = \left\langle \overline{C_f}, \begin{pmatrix} 0 & 1 \\ -1 & 0 \end{pmatrix} C_f \right\rangle = \langle C_f, C_f \rangle \quad , \tag{2.3.39}$$

since C_f is real and $SU(2)$ invariant. The integral of the contraction of the intertwiner with itself is given by:

$$
\int_{SU(2)^2 \times S_1^6} dU_1 dU_2 \prod_i \frac{\mathrm{d}\,\phi_{i1}}{2\pi} \prod_i \frac{\mathrm{d}\,\phi_{i2}}{2\pi}
$$
$$
f_1(\{\phi_{i1}\}) f_2(\{\phi_{i2}\}) \prod_i \left(1/2 |, O_{\phi_{i1}}^{-1} U_1^{-1} U_2 O_{\phi_{i2}} | 1/2 \right)^{2j_i} \quad . \tag{2.3.40}
$$

Its stationary point conditions are:

- $B_{i1} = -B_{i2}$.

- $\sum_i B_{i1} = \sum_i B_{i2} = 0$.

As the 'Theta' graph itself is an evaluation of a spin network its effective action have the same transformations on the action as described in 2.2.3.

The u symmetry can be ruled out just by dropping the integration over U_1. Then one is left with the group G generated by the transformations

$$
r_{f1}, \ r_{f2}, \ -u_2, \ o_{f1}, \ o_{f2}, \ -o_{f1,i}, \ -o_{f2,i} \quad . \tag{2.3.41}
$$

On the stationary H orbits, i.e. the normal subgroup of G generated by $\{o_f, -u_f\}$, these transformations act as the group $K = G/H$, which gives $\mathbb{Z}_2^3 \times \mathbb{Z}_2^3$.

This group acts freely on the stationary H orbits and as before the modifiers suppress all but one of the H orbits. If we take $f_1 = f_2 = 1$ and restrict ourselves to the case where $\sum_i j_i$ is even (all j_i integer) then the action is invariant with respect to all transformations, thus every stationary orbit contribute the same $\frac{1}{2^6}$ of the overall result. In the case when $\sum j_e$ is not even, or some j_e are not integer, this choice leads to a vanishing invariant.

The computation of the full expansion of the theta graph in the even case also gives an expansion on the stationary orbit in the presence of f_i. This is briefly discussed in the next section.

Theta graph for integer spins and $\sum j$ even

We will derive the complete expansion for $\sum j$ even. We need to compute

$$
\prod_i C_{j_i} (C_{000}^{j_1 j_2 j_3})^2 \tag{2.3.42}
$$

where C_{j_i} (see also appendix 2.D.2) is the normalization of the $|0\rangle$ vector.

In appendix 2.D.3 we show (following [A40]) that the theta graph $(C_{000}^{j_1 j_2 j_3})^2$ is equal to

$$
\frac{1}{2\pi S} \left(1 + O\left(\frac{1}{l^2} \right) \right) \quad , \tag{2.3.43}
$$

where S is the area of the triangle with edges $j_i + \frac{1}{2}$.

2.3.5 Final formula

Let us state the final formula normalized by the square roots of the 'Theta' diagrams. Those are equal to:

$$
(-1)^{s_f} 2^{-7/2} \sqrt{\frac{\prod_{e \subset f} C_{j_e}}{\pi S_f}} \left(1 + O\left(\frac{1}{l^2} \right) \right) \quad , \tag{2.3.44}
$$

where s_f is a sign factor necessary to be consistent with [A38, A39] that will be derived in 2.A.2.

To summarize the various calculations of this chapter, the contraction of normalized intertwiners has the following asymptotic expansion after the stationary phase approximation for the angles ϕ_{fe} has been performed and the asymptotic expansion from (2.3.44) has been inserted:

$$\frac{(-1)^{s+\sum_f s_f + \sum_e s_e} e^{-i\frac{\pi}{4}\sum_e \operatorname{sgn}_e}}{2^{\frac{5}{2}|E|-\frac{7}{2}|F|}\pi^{\frac{1}{2}|F|+\frac{1}{2}|E|}} \frac{\prod_{f\in F} S_f^{1/2}}{\prod_{e\in E} l_e^{1/2}}$$

$$\int \prod_{f\in F} \delta(|n_f|^2 - 1)\, d^3 n_f \frac{1}{\sqrt{\prod_e |\sin\theta_e|}} e^{i\sum_e \left(l_e\theta_e - \frac{1}{8l_e}\cot\theta_e\right)} \quad . \tag{2.3.45}$$

As it will be shown in appendix 2.A, $s + \sum_f s_f + \sum_e s_e = 0 \mod 2$ and thus the term

$$(-1)^{s+\sum_f s_f + \sum_e s_e} \tag{2.3.46}$$

in the integral can be omitted.

This is the contribution up to next-to-leading order. It is straightforward to generalize it to higher order due to the complete expansion of the edge amplitude (section 2.5.2) and the expansion of 'Theta' diagrams (appendix 2.D.3).

In the next section we will focus our attention on the specific example of the $6j$ symbol. After another variable transformation to the set of exterior dihedral angles of the tetrahedron has been performed, we obtain the action of flat first order Regge Calculus , i.e. Regge Calculus in which both edge lengths and dihedral angles are considered as independent variables. The stationary point conditions (with respect to the dihedral angles) will reduce the action to ordinary Regge calculus, such that the geometry is entirely described by the set of edge lengths, where angles on the stationary point agree with the angles given for a tetrahedron built from the lengths. We will perform the stationary point analysis, in particular compute the determinant of the Hessian matrix, and obtain the correct asymptotic expression for the $SU(2)$ $6j$ symbol [A5].

2.4 Analysis of 6j symbol and first order Regge Calculus

In this section, we will perform the remaining integrations via stationary phase approximation starting from (2.3.45) in the case of the $6j$ symbol. As we are restricting the discussion to a specific spin network, we introduce the following notations:

This spin network consists of 4 faces f, which we will simply count by $i \in \{1, \ldots, 4\}$, and 6 edges e, which we will denote by $ij, i < j$, i.e. the faces sharing it. On the stationary point with respect to $\{\phi_{fe}\}$, we have two configurations of B_{fe}, which we will label accordingly as B_{ij} and similarly θ_{ij} using the convention that θ_{ij} is the angle at the edge l_{ij}.

In [A19] it has been shown that the $6j$ symbol can be interpreted as a tetrahedron on the points of stationary phase (for non-degenerate configurations). In section 2.2.2 we have shown that our approach gives the same interpretation. Hence, we can assume that for one stationary point, the normals to the faces n_i of the tetrahedron are outward pointing and the B_{ij} vectors are oriented such that $\theta_{ij} \in (0, \pi)$. For the second stationary orbit, described by $B'_{ij} = -B_{ij}$, the angles are negative, hence this contributes the complex conjugate.

In order to perform the remaining stationary point analysis, it is necessary to perform another variable transformations from normals of faces n_i to angles between these normals θ_{ij} followed by integrating out gauge degrees of freedom corresponding to u transformations:

$$n_i \to \theta_{ij} \quad . \tag{2.4.1}$$

This transformation is performed in appendix 2.B.2 in great detail, and we obtain the following relation:

$$\prod_i d^3 n_i \delta(|n_i|^2 - 1) \to \prod_{ij} d\theta_{ij} \prod_{ij} |\sin\theta_{ij}|\delta(\det \tilde{G}) \quad , \tag{2.4.2}$$

where $\tilde{G}$ denotes the angle Gram matrix (for exterior dihedral angles) of a tetrahedron with components $G_{ij} = \cos(\theta_{ij})$, with $\theta_{ii} = 0$. Using (2.4.2) and simplifying (2.3.45) for the case of the $6j$ symbol, we obtain in the neighbourhood of the stationary point:

$$\frac{e^{-i\frac{6}{4}\pi} \prod_i S_i^{1/2}}{2\pi^3 \prod_{i<j} l_{ij}^{1/2}} \int \prod_{i<j} \mathrm{d}\,\theta_{ij} \underbrace{\prod_{i<j} |\sin\theta_{ij}| \delta(\det\tilde{G})}_{\text{Jacobian}} \frac{1}{\prod_{i<j}\sqrt{|\sin\theta_{ij}|}} e^{i\sum_{i<j}\left(l_{ij}\theta_{ij} - \frac{1}{8l_{ij}}\cot\theta_{ij}\right)} \quad . \tag{2.4.3}$$

Let us consider one of the stationary points for which $\sin\theta_{ij} > 0$. The second one contributes the complex conjugate of the first because two points (orbits) are related by c (parity) transformations:

$$\frac{i}{4\pi^4} \frac{|l| \prod_i S_i^{1/2}}{\prod_{i<j} l_{ij}^{1/2}} \int \mathrm{d}\,\rho \prod_{i<j} \mathrm{d}\,\theta_{ij} \prod_{i<j}\sqrt{\sin\theta_{ij}} e^{i\left(\sum_{i<j}\left(l_{ij}\theta_{ij} - \frac{1}{8l_{ij}}\cot\theta_{ij}\right) - |l|\rho\det\tilde{G}\right)} \quad , \tag{2.4.4}$$

where $|l|^2 := \sum_{i<j} l_{ij}^2$ and ρ is a Lagrange multiplier.

It is worth to examine the action in (2.4.4) in more detail: This function of edge lengths l_{ij} and angles θ_{ij} is known as the action for 'first order' Regge Calculus [A32]. We will comment on this further in section 2.4.4.

In the next section we will perform a stationary phase approximation for the integrations over the angles θ_{ij}. We will use the improved action $\sum_{i<j} l_{ij}\theta_{ij}$, where we regard higher order corrections as the vertices of a Feynman diagram expansion, and the resulting points of stationary phase will correspond to perturbed stationary points obtained previously from the stationary point analysis w.r.t. the $SU(2)$ group elements U_f in section 2.2.

2.4.1 Stationary point analysis

The stationary point conditions for the action (2.4.4) are:

- Derivative with respect to θ_{ij}:

$$l_{ij} - |l|\rho\frac{\partial\det\tilde{G}}{\partial\theta_{ij}} = 0 \quad . \tag{2.4.5}$$

- Derivative with respect to ρ:

$$-|l|\det\tilde{G} = 0 \quad . \tag{2.4.6}$$

Equations (2.4.5) and (2.4.6) are exactly those equations stating that θ_{ij} are the exterior dihedral angles of a tetrahedron formed by edges of length l_{ij} (see appendix 2.C and [A41]). From the stationary point analysis w.r.t. group elements U_f we know that all normals n_i to the faces are outward directed. The point of stationary phase w.r.t. the angles θ_{ij} is only a small perturbation in comparison to the stationary point w.r.t. group elements. The areas of the respective face are denoted by S_i. For a flat tetrahedron, the following relation holds (see for example [A41, A42]):

$$l_{ij} = \frac{2}{3}\frac{1}{V} S_i S_j \sin\theta_{ij} \ . \tag{2.4.7}$$

On the other hand $\det\tilde{G} = 0$ holds, where a (single) null eigenvector of $\tilde{G}$ is given by the vector of areas of the triangles $(S_1, \ldots, S_4)$ (of the tetrahedron) as $\det\tilde{G} = 0$ imposes the closure of the flat tetrahedron. Thus follows:

$$\frac{\partial\det\tilde{G}}{\partial\theta_{ij}} = -2\frac{\det'\tilde{G}}{\sum_k S_k^2} S_i S_j \sin\theta_{ij} \overset{(2.4.7)}{=} -3\frac{V\det'\tilde{G}}{\sum_k S_k^2} l_{ij} \quad , \tag{2.4.8}$$

where $\det' \tilde{G} = \sum_i \tilde{G}^*_{ii}$ and $\tilde{G}^*_{ii}$ is the (i,i)th minor of $\tilde{G}$. $\det' \tilde{G}$ is computed in appendix 2.C.1:

$$\det'\tilde{G} = \frac{3^4}{2^2} (\sum_i S_i^2) \frac{V^4}{\prod S_i^2} \quad . \tag{2.4.9}$$

Using (2.4.8) and (2.4.9), we solve (2.4.5) for the Lagrange multiplier ρ:

$$\rho = -\frac{2^2 \prod S_i^2}{3^5 V^5 |l|} \quad . \tag{2.4.10}$$

The quadratic order in the expansion around the stationary point, which we also call the kinetic term, i.e. the Hessian matrix of the action, is given by:

$$\mathcal{H} := -i|l| \begin{pmatrix} 0 & \frac{\partial \det \tilde{G}}{\partial \theta_{ij}} \\ \frac{\partial \det \tilde{G}}{\partial \theta_{km}} & \rho \frac{\partial \det \tilde{G}}{\partial \theta_{ij} \partial \theta_{km}} \end{pmatrix} \quad . \tag{2.4.11}$$

To complete the stationary point analysis, we have to compute the determinant of its inverse evaluated on the stationary point.

2.4.2 Propagator and Hessian

Let us introduce a function of lengths l:

$$\lambda = |l|\rho = -\frac{2^2 \prod S_i^2}{3^5 V^5} \quad . \tag{2.4.12}$$

It is of scaling dimension 1 with respect to l.

Propagator

We will prove that the inverse of the kinetic term is equal to

$$\mathcal{H}^{-1} = i \begin{pmatrix} \frac{c}{|l|^2} & \frac{1}{|l|} \frac{\partial \lambda}{\partial l_{ij}} \\ \frac{1}{|l|} \frac{\partial \lambda}{\partial l_{kl}} & \frac{\partial \theta_{ij}}{\partial l_{kl}} \end{pmatrix} \quad , \tag{2.4.13}$$

where c is a constant (defined in Lemma 7 in appendix 2.C). Let us compute

$$i \begin{pmatrix} \frac{c}{|l|^2} & \frac{1}{|l|} \frac{\partial \lambda}{\partial l_{ij}} \\ \frac{1}{|l|} \frac{\partial \lambda}{\partial l_{mn}} & \frac{\partial \theta_{ij}}{\partial l_{mn}} \end{pmatrix} (-i)|l| \begin{pmatrix} 0 & \frac{\partial \det \tilde{G}}{\partial \theta_{kl}} \\ \frac{\partial \det \tilde{G}}{\partial \theta_{mn}} & \rho \frac{\partial \det \tilde{G}}{\partial \theta_{kl} \partial \theta_{mn}} \end{pmatrix} \quad . \tag{2.4.14}$$

This gives

$$|l| \begin{pmatrix} \frac{1}{|l|} \frac{\partial \lambda}{\partial l_{mn}} \frac{\partial \det \tilde{G}}{\partial \theta_{mn}} & \frac{\partial \det \tilde{G}}{\partial \theta_{ij}} \frac{c}{|l|^2} + \frac{1}{|l|} \frac{\partial \lambda}{\partial l_{mn}} \rho \frac{\partial \det \tilde{G}}{\partial \theta_{mn} \partial \theta_{ij}} \\ \frac{\partial \det \tilde{G}}{\partial \theta_{mn}} \frac{\partial \theta_{mn}}{\partial l_{ij}} & \frac{1}{|l|} \frac{\partial \lambda}{\partial l_{ij}} \frac{\partial \det \tilde{G}}{\partial \theta_{kl}} + \frac{\partial \theta_{ij}}{\partial l_{mn}} \rho \frac{\partial^2 \det \tilde{G}}{\partial \theta_{mn} \partial \theta_{kl}} \end{pmatrix} \quad , \tag{2.4.15}$$

using the results of appendix 2.C.2, we see that (2.4.15) is equal to the identity.

Hessian

Similar to the angle Gram matrix discussed in the previous section, $\det \frac{\partial \theta_{ij}}{\partial l_{kl}} = 0$ in the case of a flat tetrahedron. This is due to the fact that given a set of dihedral angles of a flat tetrahedron, the tetrahedron is only defined up to rotations and uniform scaling of its edge lengths. Hence, the null eigenvector of the matrix $\frac{\partial \theta_{ij}}{\partial l_{kl}}$ is given by the edge vector $\vec{l} := (l_{12}, \ldots, l_{34})$. This is equivalent to the Schläfli identity in 3D: $\sum_{ij} l_{ij} d\theta_{ij} = 0$. We rewrite the matrix $\mathcal{H}^{-1}$ in the basis in which its second row is parallel to $\vec{l}$ and the next ones are perpendicular to $\vec{l}$:

$$
i \begin{pmatrix}
\frac{c}{|l|^2} & \frac{1}{|l|}\frac{\partial \lambda}{\partial l} & \cdots & \cdots \\
\frac{1}{|l|}\frac{\partial \lambda}{\partial l} & 0 & 0 & 0 \\
\vdots & 0 & \frac{\partial \theta_{ij}}{\partial l_{kl}} & \vdots \\
\vdots & 0 & \vdots & \vdots
\end{pmatrix} \quad .
\tag{2.4.16}
$$

The determinant of $(-\mathcal{H}^{-1})$ is thus equal to

$$
\det(-\mathcal{H}^{-1}) = -(-i)^7 \Big(\underbrace{\frac{1}{|l|}\frac{\partial \lambda}{\partial l}}_{=\frac{\lambda}{|l|^2}} \Big)^2 {\det}'\frac{\partial \theta_{ij}}{\partial l_{kl}} \quad .
\tag{2.4.17}
$$

Since λ is of scaling dimension 1 (with respect to edge lengths), $l_{ij}\frac{\partial \lambda}{\partial l_{ij}} = \lambda$. More details and the tedious calculation of ${\det}'\frac{\partial \theta_{ij}}{\partial l_{kl}}$ can be found in appendix 2.C:

$$
{\det}'\frac{\partial \theta_{ij}}{\partial l_{kl}} = \frac{3^3}{2^5}\frac{|l|^2}{\prod S_i^2}V^3 \quad .
\tag{2.4.18}
$$

Combining all these results, we obtain:

$$
\det(-\mathcal{H}^{-1}) = -i\frac{1}{|l|^4}\left(-\frac{2^2 \prod S_i^2}{3^5 V^5}\right)^2 \frac{3^3}{2^5}\frac{|l|^2}{\prod S_i^2}V^3 = -i\frac{1}{2\,3^7}\frac{\prod_i S_i^2}{|l|^2 V^7} \quad ,
\tag{2.4.19}
$$

and hence

$$
\sqrt{|\det \mathcal{H}^{-1}|} = \frac{1}{\sqrt{2}\,3^{\frac{7}{2}}}\frac{\prod_i S_i}{|l|V^{\frac{7}{2}}} \quad .
\tag{2.4.20}
$$

Since $\mathcal{H}^{-1}$ is antihermitian, it has only imaginary (and nonzero) eigenvalues. Therefore it is important to count the number of $+i\mathbb{R}$ and $-i\mathbb{R}$ eigenvalues in order to pick the right branch of $\sqrt{\det(-\mathcal{H}^{-1})}$. The number of positive and negative imaginary eigenvalues is constant on the connected components of parameter spaces. For oriented tetrahedra (one of the two components) it can be computed in the equilateral case, i.e. all l_{ij} are equal. This was done in appendix 2.D.4, then $\mathcal{H}^{-1}$ has 4 $i\mathbb{R}$ eigenvalues and 3 $-i\mathbb{R}$. Finally, we conclude:

$$
\frac{1}{\sqrt{\det(-\mathcal{H})}} = e^{-4i\frac{\pi}{4}}e^{3i\frac{\pi}{4}}\sqrt{|\det \mathcal{H}^{-1}|} = \frac{1}{\sqrt{2}\,3^{\frac{7}{2}}}e^{-i\frac{\pi}{4}}\frac{\prod S_i}{|l|V^{\frac{7}{2}}} \quad .
\tag{2.4.21}
$$

The last step is to combine all the previous results to obtain the final formula for the asymptotics of the $6j$ symbol.

2.4.3 Final Result

In this section, we will combine the results of the previous calculations step by step. First we perform the stationary point analysis for (2.4.4):

$$
\frac{i}{4\pi^4}\frac{|l|\prod_i S_i^{1/2}}{\prod_{i<j} l_{ij}^{1/2}}\prod_{i<j}\sqrt{\sin \theta_{ij}}\frac{(2\pi)^{\frac{7}{2}}}{\sqrt{\det(-\mathcal{H})}}e^{i\left(\sum_{ij}\left(l_{ij}\theta_{ij}-\frac{1}{8l_{ij}}\cot\theta_{ij}\right)+\tilde{S}_1\right)}
$$

$$
= i\frac{2^{\frac{3}{2}}}{\pi^{\frac{1}{2}}}\frac{|l|\prod_i S_i^{1/2}\prod_{i<j}\sqrt{\sin\theta_{ij}}}{\sqrt{\det(-\mathcal{H})}\prod_{i<j}l_{ij}^{1/2}}e^{i\left(\sum_{ij}l_{ij}\theta_{ij}+S_1\right)} \quad ,
\tag{2.4.22}
$$

where S_1 is the NLO contribution. As a next step, we substitute $\sin\theta_{ij} = \frac{3}{2}\frac{l_{ij}V}{S_iS_j}$ (for $\sin\theta_{ij} > 0$) and (2.4.21) in (2.4.22):

$$\frac{2^{\frac{3}{2}}}{\pi^{\frac{1}{2}}}\frac{|l|\prod S_i^{1/2}}{\prod l_{ij}^{1/2}}\left(\frac{3}{2}\right)^3\frac{\prod l_{ij}^{1/2}V^3}{\prod S_i^{\frac{3}{2}}}e^{i\frac{\pi}{4}}\frac{\prod S_i}{\sqrt{2}\,3^{\frac{7}{2}}|l|V^{\frac{7}{2}}}e^{i\left(\sum_{ij}l_{ij}\theta_{ij}+S_1\right)}$$
$$=\frac{1}{2}\frac{1}{\sqrt{12\pi\,V}}e^{i\frac{\pi}{4}}e^{i\left(\sum_{ij}l_{ij}\theta_{ij}+S_1\right)} \tag{2.4.23}$$

As previously discussed, the full contribution comes from two stationary points, which are related by parity transformations. Eventually, we obtain:

$$\frac{1}{\sqrt{12\pi V}}\left(\cos\left(\sum_{ij}l_{ij}\theta_{ij}+\frac{\pi}{4}+S_1\right)+O\left(|l|^{-2}\right)\right)\quad, \tag{2.4.24}$$

as in [A5]. In the formula above, we implicitly assumed that S_1 is real. This property will be proven in section 2.5.

2.4.4 First order Regge calculus

A first order formulation of Regge Calculus [A32, A43] is a discretization of General Relativity defined on the triangulation of the manifold in which both edge lengths and dihedral angles are considered as independent variables. Its introduction was motivated by Palatini's formulation of Relativity where equations of motion are first order differential equations. Its action in 3D is given by

$$S_R[l_e] = \sum_e l_e\epsilon_e, \quad \epsilon_e = 2\pi - \sum_{\tau\supset e}\theta_e^{(\tau)} \tag{2.4.25}$$

where l_e denotes the length of the edge e, $\theta_e^{(\tau)}$ denotes the dihedral angle at edge e in the tetrahedron τ. By ϵ_e we denote the deficit angle at edge e. For every tetrahedron an additional constraint is imposed, namely

$$\det\tilde{G} = 0 \tag{2.4.26}$$

that enter the action via a Lagrange multiplier [A32]. $\tilde{G}$ is the angle Gram matrix of the tetrahedron. One can eliminate the θ_e^τ variables by partially solving the equations of motion (given by variations with respect to θ_e^τ), then

$$\theta_e^\tau = \theta_e^\tau(l) \tag{2.4.27}$$

turns out to be the dihedral angle at the edge e for a discrete geometry determined by the edge lengths $\{l_e\}$.

Our derivation of the $6j$ symbol asymptotics follows the same idea. It also suggests a suitable measure in the path integral quantization for (linearized) first order Regge calculus in order to reobtain the factor $\frac{1}{\sqrt{V}}$ from Ponzano-Regge asymptotics. We also hope that our methods might be applied in the 4D case, where a similar action, motivated by the construction of modern spin foam models, was proposed in [A33]. Furthermore, the present results could naturally provide and motivate a triangulation independent measure for first order Regge calculus following the approach in [A27]. Examining first order and area-angle (quantum) Regge calculus in 4D might also give new insights into possible measures for 4D spin foam models.

2.5 Properties of the next to leading order and complete asymptotic expansion

So far, we dealt with the asymptotic expansion of a spherical spin network evaluation in the leading order approximation and managed to work out the example of the $6j$ symbol. However,

our method allows us to derive, in principle, the full asymptotic expansion of the evaluation by the higher order stationary point analysis, e.g. we have already mentioned the next-to-leading order (NLO) corrections to the contribution from edges of the spin network (on the stationary points) in section 2.3.2. Such corrections improve the asymptotic behaviour in particular for small spins. Therefore we will apply our formalism in this section to derive new insights on the NLO corrections (to the $6j$ symbol).

NLO order corrections to the asymptotic formula of the $SU(2)$ $6j$ symbol have been thoroughly discussed in [A30, A31]. In particular, the authors found evidence that the leading contributions in the expansion in $\frac{1}{l}$ are purely real and oscillating as $\cos(S_R + \frac{\pi}{4})$, whereas the next order term (also purely real) behaves like $\sin(S_R + \frac{\pi}{4})$, where S_R denotes the Regge action for the tetrahedron. Furthermore, this behaviour is conjectured to be alternating for consecutive orders.

We will refer to this behaviour introduced in [A30, A31] as "Dupuis-Livine" (DL) property and we will show that it holds for the full expansion of the asymptotics of any evaluation of spin networks, satisfying certain generic conditions, for example the $6j$ symbol in the non-degenerate case. Furthermore we will derive a new recursion relation for the $6j$ symbol which can be applied to obtain a simpler form of the next to leading order correction to the Ponzano-Regge formula.

2.5.1 Properties of the Dupuis-Livine form

In this section we will give a definition to the Dupuis-Livine form and also discuss some of its basic properties.

Consider an asymptotic expansion in the variables $\{j\}$ of the following form

$$\sum_i A_k(\{j\})e^{i\sum j_i\theta_i} \quad , \tag{2.5.1}$$

where A_k is a homogeneous function in all variables j of degree $k + \beta$. It can be rewritten in terms of the variables $\{l\}$ (with $l = j + \frac{1}{2}$):

$$\sum_i \tilde{A}_k(\{l\})e^{i\sum l_i\theta_i} \quad , \tag{2.5.2}$$

where $\tilde{A}_0 = e^{-\frac{i}{2}\sum\theta_i}A_0$.

We will say that it has the Dupuis-Livine (DL) property, if it can be written as

$$\tilde{A}_0(\{l\})e^{i\sum l_i\theta_i}\sum_k B_k \quad , \tag{2.5.3}$$

where $i^k B_k$ is a real and homogeneous function of degree k. Note that if we write this expansion in the form

$$\tilde{A}_0(l)e^{i\sum l_i\theta_i + S} \tag{2.5.4}$$

then S also has DL form (and starts with degree 1). Furthermore, suppose that two asymptotic series f_1 and f_2 have the DL property then also

$$f_1 f_2 \quad , \quad \frac{1}{f_i} \tag{2.5.5}$$

have this property. In particular the last two relations are very useful for our discussion, since they allow us to examine the full expansion of the evaluation of the spin network in steps: first we examine the contributions from the edges, i.e. the partial integrations over the ϕ_{fe}, then the normalization factors until we eventually discuss the full expansion.

2.5.2 Partial integration over ϕ

In this subsection, we will examine whether the contributions from the partial integration over ϕ have the DL property. We will prove it by using a recurrence relation similar to Bonnet's formula for Legendre polynomials. Therefore, it will be necessary to introduce some technical definitions, from which we are able to derive recursion relations.

Weak equivalence

Let $\psi_i = f_i e^S$, where $S = kS_{-1} + \ldots$, $\Re S_{-1} \leq 0$ and f_i grows at most polynomially in k and admits a power series expansion in k.

Definition 1. ψ_1 *is weakly equivalent to* ψ_2 *around the point* x_0,

$$\psi_1 \equiv \psi_2 \quad , \tag{2.5.6}$$

if the expansion in k of the integral of both around x_0 is the same.

If $\psi = f e^S$ then

$$L^* \psi \equiv 0 \tag{2.5.7}$$

where

$$L^* \psi = L \psi + (\text{div } L) \psi \tag{2.5.8}$$

and L is a vector field.

Equivalences and recursion relations

Let us introduce

$$L_\pm = \cos \tilde\theta \sin \alpha \frac{\partial}{\partial \alpha} \pm i \sin \tilde\theta \sin \beta \frac{\partial}{\partial \beta} \quad , \tag{2.5.9}$$

$$A_\pm = \cos \tilde\theta \cos \alpha \pm i \sin \tilde\theta \cos \beta \tag{2.5.10}$$

that we regard as vector fields and functions of the variables α, β. It is straightforward to calculate

$$\text{div } L_\pm = A_\pm \quad , \tag{2.5.11}$$

and

$$L_+ A_+ = L_- A_- = \frac{1}{2} A_+^2 + \frac{1}{2} A_-^2 - \cos 2\tilde\theta \tag{2.5.12}$$

$$L_- A_+ = L_+ A_- = A_+ A_- - 1 \quad .$$

Starting from $L_\pm^* A_+^k \equiv 0$ and using the above identities, we derive the following relation (see appendix 2.D.1 for more details):

$$-\frac{(k+2)^2}{k+1}(A_+)^{k+2} + 2(k+1)\cos 2\tilde\theta \, A_+^k - (k-1)A_+^{k-2} \equiv 0 \quad . \tag{2.5.13}$$

Therefore we introduce the following quantity:

$$\tilde P_l = \frac{1}{C_j} A_+^{2j} \quad , \tag{2.5.14}$$

where $l = j + \frac{1}{2}$ and C_j is given by (2.3.25):

$$C_j = \frac{1}{4^j} \frac{\Gamma(2j+1)}{\Gamma(j+1)^2} \quad . \tag{2.5.15}$$

Furthermore C_j admits a complete expansion in j, see also appendix 2.D.2:

$$C_j = \frac{1}{\sqrt{\pi j}} \left(1 + O\left(\frac{1}{j}\right) \right) \quad . \tag{2.5.16}$$

Moreover, one can show that

$$C_{j+1} = \frac{2j+1}{2j+2} C_j \quad , \quad C_{j-1} = \frac{2j}{2j-1} C_j \quad . \tag{2.5.17}$$

Combining (2.5.14), (2.5.15) and (2.5.17) with (2.5.13) and substituting $k = 2j$ in (2.5.13) we obtain:

$$\begin{aligned}
0 \equiv & 2C_j \left[-\frac{(2j+2)(j+1)}{2j+1} \frac{2j+1}{2j+2} \tilde{P}_{l+1} + (2j+1)\cos 2\tilde{\theta} \tilde{P}_l - \frac{2j-1}{2} \frac{2j}{2j-1} \tilde{P}_{l-1} \right] = \\
= & 2C_j \left[-\left(l+\frac{1}{2}\right) \tilde{P}_{l+1} + 2l\cos 2\tilde{\theta} \tilde{P}_l - \left(l-\frac{1}{2}\right) \tilde{P}_{l-1} \right] \quad .
\end{aligned} \tag{2.5.18}$$

But C_j admits a nonzero asymptotic expansion, thus

$$-\left(l+\frac{1}{2}\right) \tilde{P}_{l+1} + 2l\cos 2\tilde{\theta} \tilde{P}_l - \left(l-\frac{1}{2}\right) \tilde{P}_{l-1} \equiv 0 \tag{2.5.19}$$

around any stationary point. With the definitions given here, (2.3.15), i.e. the amplitude associated to one edge, becomes:

$$\frac{1}{8\pi^2} \int d\alpha d\beta A_+^{2j} = \frac{C_j}{8\pi^2} \int d\alpha d\beta \tilde{P}_l \quad , \tag{2.5.20}$$

which establishes the connection to our previous calculations.

Let us notice that (2.5.19) is exactly Bonnet's recursion formula for Legendre polynomials.

Total expansion and DL property

Over any stationary point we have shown that the integral of $\tilde{P}_l$ can be expanded as

$$(-1)^s \sum_{k\geq 0} \frac{e^{il\theta}}{l^{k+\frac{1}{2}}} A_k(\theta) + O(l^{-\infty}) \quad , \tag{2.5.21}$$

where $\theta = 2\tilde{\theta}$ is now the $SO(3)$ angle and s is a sign factor that comes from the $SU(2)$ angle. Values of the integral for $\tilde{\theta}$ and $\tilde{\theta}+\pi$ differ by the factor $(-1)^s$. This restricts A_k to be of the form described above. Moreover we know from the previous section that

$$-\left(l+\frac{1}{2}\right) \tilde{P}_{l+1} + 2l\cos\theta \tilde{P}_l - \left(l-\frac{1}{2}\right) \tilde{P}_{l-1} \equiv 0 \quad . \tag{2.5.22}$$

Applying the asymptotic form to the recursion relations, we obtain:

Lemma 3. *For every $m \geq 0$*

$$\sum_{k\leq m} (2\beta_{m+1-k}^k + \beta_{m-k}^k) A_k i^{m+1-k} \sin\left(\theta - \frac{\pi}{2}(m-k)\right) = 0 \quad , \tag{2.5.23}$$

where

$$\beta_m^k = \frac{(-k-\frac{1}{2})_m}{m!} \in \mathbb{R} \quad , \tag{2.5.24}$$

and

$$(a)_m = a \cdot (a-1) \cdot \ldots \cdot (a-m+1), \quad (a)_0 = 1 \quad . \tag{2.5.25}$$

We will prove the lemma in appendix 2.D.2.

Consider the case where $k = m$ in (2.5.23). For any $m \geq 0$ one obtains that

$$2\beta_1^m + \beta_0^m = -2\left(m + \frac{1}{2}\right) + 1 = -2m \quad , \tag{2.5.26}$$

such that (2.5.23) can be rewritten in the following way:

$$2m A_m i \sin(\theta) = \sum_{k<m}(2\beta_{m+1-k}^k + \beta_{m-k}^k)A_k i^{m+1-k}\sin\left(\theta - \frac{\pi}{2}(m-k)\right) \quad . \tag{2.5.27}$$

Let us introduce

$$B_m := A_m i^{-m} e^{i\frac{\pi}{4}\text{sign}\sin\theta} \quad . \tag{2.5.28}$$

From the asymptotics of the integrations over $\tilde{P}_l$ follows that $B_0 \in \mathbb{R}$ and (2.5.27) can be rewritten as

$$2m \underbrace{A_m i^{-m} e^{i\frac{\pi}{4}\text{sign}\sin(\theta)}}_{=B_m}\sin(\theta) = \sum_{k<m}\left(2\beta_{m+1-k}^k + \beta_{m-k}^k\right)\underbrace{A_k i^{-k} e^{i\frac{\pi}{4}\text{sign}\sin(\theta)}}_{=B_k}\sin\left(\theta - \frac{\pi}{2}(m-k)\right)$$

$$\Longleftrightarrow 2m B_m \sin(\theta) = \sum_{k<m}\left(2\beta_{m+1-k}^k + \beta_{m-k}^k\right)B_k \sin\left(\theta - \frac{\pi}{2}(m-k)\right) \quad . \tag{2.5.29}$$

This implies that all $B_k \in \mathbb{R}$ and it proves that the asymptotic terms (in the connected component expansion - e^S) are of the form

$$\tilde{A}_k \in i^k\mathbb{R} \text{ for } k > 0 \quad . \tag{2.5.30}$$

This proves that the contributions from the integration over ϕ evaluated on the points of stationary phase are of DL form.

The total expansion of the original integral

We know that the total expansion of the original integral around the stationary point is of the form given in (2.3.26). Using the recurrence relation (2.5.29) we can compute its next-to-leading order:

$$C_j \frac{(-1)^s}{4\sqrt{2\pi l\,|\sin\theta|}}e^{i(l\theta - \frac{\pi}{4}\text{sign}(\sin\theta) - \frac{1}{8l}\cot\theta)}\left(1 + O\left(\frac{1}{l^2}\right)\right) \quad . \tag{2.5.31}$$

As a next step, we will examine whether the normalization factors computed from the self-contraction of intertwiners is of DL form as well.

2.5.3 Different forms of intertwiners and DL property

To examine whether the normalization factors satisfy the DL property, we will construct different forms of invariants. Since the (three-valent) intertwiner is unique, all new constructions are proportional to the original one.

Let U_i be distinct group elements from a sufficiently small neighbourhood of the identity. Let

$$C_{U_i,f} = \int dU \int \prod \frac{d\phi_i}{2\pi}f(\phi_1,\phi_2,\phi_3)$$
$$UU_1 O_{\phi_1}|1/2\rangle^{2j_{e_1}} \otimes UU_2 O_{\phi_2}|1/2\rangle^{2j_{e_2}} \otimes UU_3 O_{\phi_3}|1/2\rangle^{2j_{e_3}} \tag{2.5.32}$$

be the new invariant, where f is such a function that it is constant in the neighbourhood of the angles, which satisfy the stationary phase conditions, i.e. where all

$$B_i = j_{e_i} UU_1 O_{\phi_1}\begin{pmatrix} 1 & 0 \\ 0 & -1 \end{pmatrix}(UU_1 O_{\phi_1})^{-1} \tag{2.5.33}$$

sum to zero. We will choose U_i in such a way (described below) that such points are separated. In such a case we can choose f to be nonzero around only one of them.

Let us now describe U_i. For given three vectors B_i in the plane perpendicular to $H = \begin{pmatrix} 0 & i \\ -i & 0 \end{pmatrix}$ (see also section 2.2 for more details) such that

$$\sum B_i = 0 \quad , \tag{2.5.34}$$

we choose U_i in the neighborhood of identity such that $U_i H U_i^{-1} \perp B_i$. There are many such choices which will be used in the sequel.

Let us take contraction of such a $C_{U_i,f}$ with the intertwiner $C_{f'}$ obtained with the help of modifiers.

$$\left(C_{U_i,f}, C_{f'} \right) \tag{2.5.35}$$

Due to the definition of $C_{U_i,f}$, there is only one $-u$ and o_f orbit of stationary points on which f and f' are nonzero. These are given by the conditions

$$
\begin{aligned}
B_{fe_i} &= -B_i \quad , \\
n_f &\perp B_{fe_i} \quad , \\
\underbrace{U U_i H U_i^{-1} U^{-1}}_{n_{f'}} &\perp B_{fe_i} \quad .
\end{aligned}
\tag{2.5.36}
$$

Hence, on the stationary point U is of the form

$$U = \begin{pmatrix} \cos\alpha & \sin\alpha \\ -\sin\alpha & \cos\alpha \end{pmatrix} \quad . \tag{2.5.37}$$

If we choose U_i in such a way that

$$U_i H U_i^{-1} \cdot H \neq \pm 1 \quad , \tag{2.5.38}$$

i.e. the two normal vectors are not (anti)parallel, then also

$$U U_i H U_i^{-1} U^{-1} \cdot H \neq \pm 1 \quad . \tag{2.5.39}$$

This guarantees that this configuration is non-degenerate, such that the partial integration over ϕ (see section 2.5.2) and the fixing of the o_f and u_f symmetry can be performed. Following the same method as presented in section 2.5.2 we prove that the asymptotic expansion of $\left(C_{U_i,f}, C_{f'} \right)$ has the DL property. Similar considerations apply to

$$\left(C_{U_i^1,f^1}, C_{U_i^2,f^2} \right) \tag{2.5.40}$$

if $U_i^1 H (U_i^1)^{-1} \cdot U_i^2 H (U_i^2)^{-1} \neq \pm 1$.

Finally, using the uniqueness of the intertwiner, we obtain

$$(C_f, C_f) = \pm \frac{\left(C_f, C_{U_i^2,f^2} \right) \left(C_{U_i^1,f^1}, C_f \right)}{\left(C_{U_i^1,f^1}, C_{U_i^2,f^2} \right)} \quad . \tag{2.5.41}$$

As a product of functions whose asymptotic expansion is of DL form, it follows directly that (2.5.41) is of DL form, too.

2.5.4 Leading order expansion and a recursion relation for the $6j$ symbol

In the two previous sections we have shown that both the contributions from partial integrations over ϕ and the normalization factors satisfy the DL property. Hence using properties explained in appendix 2.E we have proven the conjecture from [A30, A31].

In this section we will discuss the next-to-leading order expansion for the $6j$-symbol. Therefore we do a brief recap of the results of section 2.4.

From the stationary point (with outward pointing normals) we have contributions from the Hessian, i.e. the kinetic term, and higher order terms, which are computed using a Feynman diagrammatic approach:

$$\propto \frac{1}{\sqrt{\det(-\mathcal{H})}} e^{i \sum l_{ij} \theta_{ij} + S_1} \quad , \qquad (2.5.42)$$

where S_1 are the evaluations of the connected Feynman diagrams of the expansion in $\{\theta, \rho\}$ evaluated on the stationary point of the action $i \sum l_{ij} \theta_{ij}$, using $-\mathcal{H}^{-1}$ as the propagator of this theory. We are interested only in $|l|^{-1}$ contributions, the respective Feynman rules are briefly discussed in appendix 2.G.

The expansion up to the next to leading order is of the form (see also section 2.4.3):

$$\frac{1}{2} \frac{1}{\sqrt{12\pi V}} e^{i\left(\sum_{ij} \left(l_{ij}\theta_{ij} - \frac{1}{8l_{ij}} \cot \theta_{ij}\right) + \tilde{S}_1\right)} = \frac{1}{2} \frac{1}{\sqrt{12\pi V}} e^{i\left(\sum_{ij} l_{ij}\theta_{ij} + S_1\right)} \qquad (2.5.43)$$

where S_1 is of order $|l|^{-1}$. The full contribution comes from two stationary point that are related via parity transformation, see also section 2.3.3; their contributions are related by complex conjugation. Hence, we obtain up to $|l|^{-1}$:

$$\frac{1}{\sqrt{12\pi V}} \left(\cos \left(\sum_{ij} l_{ij}\theta_{ij} + \frac{\pi}{4} + S_1 \right) + O\left(|l|^{-2}\right) \right) \qquad (2.5.44)$$

The next to leading order expansion is briefly described in appendix 2.G. Although, this method is algorithmically more involved than the method proposed in [A30, A31], the final expression is also more geometric. We will now derive a recursion relation for the full $6j$ symbol using a similar idea as in [A36, A37] that, we hope, can serve to compute the NLO expansion in more concise way.

Recursion relation for $6j$ symbols

In this section we derive a recursion relation for the whole $6j$ symbol. First, let us introduce a multiplication operator

$$N(l) = \sqrt{\prod_i \Theta_i(l)} \qquad (2.5.45)$$

where Θ_i is normalization (of a three-valent intertwiner) computed from the Theta graph. Furthermore we define the operator T_{ij}^v via its action on a function of edge lengths $\{l\}$:

$$T_{ij}^v C(l) = \left(1 + v\frac{1}{2l_{ij}}\right) C(\{l_{km} + v\delta_{(ij)(km)}\}) \quad . \qquad (2.5.46)$$

We assume that $T_{ii}^v = 1$.

As a next step, recall the definition of $\tilde{P}_l$ (2.5.14) and its recursion relation (2.5.19). The latter can be written as follows:

$$\cos \theta \tilde{P}_l \equiv \left(\frac{1}{2} + \frac{1}{4l}\right) \tilde{P}_{l+1} + \left(\frac{1}{2} - \frac{1}{4l}\right) \tilde{P}_{l-1} \quad . \qquad (2.5.47)$$

and we can write the non-normalized $6j$ amplitude as

$$Z''(l) = \int \prod \mathrm{d}\,\theta_{ij} \prod_{(ij)} \sin \theta_{ij} \prod_{(ij)} \tilde{P}_{l_{ij}}(\theta_{ij}) \delta(\det \tilde{G}) \quad . \tag{2.5.48}$$

In order to derive the recursion relation, we insert an additional $\det \tilde{G}$ into (2.5.48):

$$\int \prod \mathrm{d}\,\theta_{ij} \det \tilde{G} \prod_{(ij)} \sin \theta_{ij} \prod_{(ij)} \tilde{P}_{l_{ij}}(\theta_{ij}) \delta(\det \tilde{G}) = 0, \tag{2.5.49}$$

since $\det \tilde{G}$ is constrained to vanish. Similar to [A36, A37], $\det \tilde{G}$ can be expanded as a sum over perturbations:

$$\det \tilde{G} = \sum_{\sigma \in S_4} \mathrm{sgn}\sigma \frac{1}{16} \sum_{\vec{v} \in \{-1,1\}^4} e^{iv_i \theta_{i\sigma_i}} \quad , \tag{2.5.50}$$

with the convention that $\theta_{ij} = \theta_{ji}$ and $\theta_{ii} = 0$. Using (2.5.50), equation (2.5.49) can be rewritten as:

$$\sum_{\sigma \in S_4} \mathrm{sgn}\,\sigma \frac{1}{16} \sum_{\vec{v} \in \{-1,1\}^4} \prod_i T_{i\sigma_i}^{v_i} Z''(l) = 0 \quad . \tag{2.5.51}$$

On the other hand, we know from previous calculations that

$$\{6j\} \equiv N^{-1} Z''(l) + c.c + O(l^{-\infty}) \quad , \tag{2.5.52}$$

such that we can summarize both (2.5.51) and (2.5.52) into the following recursion relation for the $6j$ symbol that has been verified numerically for several $6j$ symbols:

$$\det \left[\frac{T_{ij}^1 + T_{ij}^{-1}}{2} \right] N\{6j\} \equiv 0 \quad , \tag{2.5.53}$$

where T_{ij}^v is defined as in (2.5.46).

Another useful form is the following

$$\sum_{\sigma \in S_4} \mathrm{sgn}\,\sigma \frac{1}{16} \sum_{\vec{v} \in \{-1,1\}^4} \frac{N(l + v_{i\sigma_i})}{N(l)} \left(\prod_i T_{i\sigma_i}^{v_i} \right) \{6j\} \equiv 0 \quad , \tag{2.5.54}$$

since the expansion of $\frac{N(l+v_{i\sigma_i})}{N(l)}$ is straightforward to compute. We have to point out though that the coefficients in this formula are not rational, yet they allow for nice a asymptotic expansion. Thus they should in principle allow for the computation of the higher order expansions of the $6j$ symbol.

2.6 Discussion and outlook

Coherent state approaches are the only available tools so far to successfully compute the asymptotic expansion of spin foam models [A14–A19], which gives us a first, and yet, very incomplete understanding of the relation of spin foam models to gravity. The strength and beauty of this approach is its clear geometrical interpretation and straightforward computation of the dominating phase of the expansion, which is identified as the Regge action of the examined triangulation. Despite these successes, the approach usually fails in the computation of the determinant of the Hessian matrix, which provides the normalization to the path integral and, more importantly, a measure on the space of geometries.

To overcome this drawback, we have introduced modified coherent states, i.e. states labelled by null eigenvectors with respect to a generator of rotations, smeared perpendicular to the axis of rotation. We have shown that these states allow for the same geometrical interpretation as the usual $SU(2)$ coherent states and presented a method to deal with the (due to the smearing) increased number of stationary points. This allowed us to derive the well-known asymptotic expansion of the $SU(2)$ $6j$ symbol [A5] entirely, by computing its amplitude in the stationary phase approximation, first with respect to the smearing parameters and second, after a variable transformation, with respect to the dihedral angles of the tetrahedron. In the process, we have discovered that the resulting amplitude is proportional to the action of the first order formulation of Regge calculus, a result that supports the conjecture given in [A33] that 4D spin foam models can be better described by angle and area variables instead of only edge lengths, the fundamental variables of ordinary Regge calculus. This result could also stimulate new work following the ideas of [A27] to obtain an invariant path integral measure (under Pachner moves [A44, A45]) for first order Regge calculus and to compare it to spin foam models.

In addition to this result, we also extended the calculation to the next to leading order correction for the $6j$ symbol. We have been able to prove the conjecture presented in [A30, A31] that the higher order corrections are alternatingly oscillating with the cosine or the sine of the Regge action, and furthermore we can, in principle, calculate the asymptotic expansion up to arbitrary order. Despite this success, we are not able to present the next-to-leading order in a short and concise way. This is a nuisance of all known derivations of next-to-leading order expansion, see for example [A30, A31]. However, we derived a recursion relation for the $6j$ symbol, very similar in nature to the one in [A36, A37], that can in principle be used to obtain more concise form of the next to leading order term.

The main goal of this work was not the derivation of known results, but to develop and advertise a new coherent state method, which is capable of challenging the determination of the measure in spin foam models [A14–A18]. The computation of the full asymptotic expansion (even only up to leading order) would not only increase the understanding of spin foam models, but could also give a measure on the space of geometries, which could be compared to the proposed measure in [A27]. Given such a measure, one would be able to examine which geometries dominate the spin foam transition amplitudes in the various models, which could also be used to exclude some of them. Our successful and complete derivation of the asymptotic expansion of the $SU(2)$ $6j$ symbol is a good start, however the method still has to prove itself by tackling more complicated models. Therefore, two issues have to be overcome:

The first problem is to extend the presented coherent state approach to groups with non-unique intertwiners. Our calculations are heavily based on the fact that the intertwiner of three irreducible representations of $SU(2)$ is unique, which simplified the construction of our model. The only 4D spin foam model with unique intertwiners is the Barrett-Crane model [A8], which has already been ruled out as a viable quantum gravity theory. Nevertheless, our calculations presented in this work can be applied and can lead to interesting new insights [A46].

The second problem is common to all coherent state approaches to spin foam models so far; all the known calculations are restricted to one simplex of the triangulation. To extract the asymptotic expansion for larger triangulations and to examine possible invariances under (local) changes of the triangulation like Pachner moves is still an open issue. In this work, before computing the asymptotic expansion of the $6j$ symbol, we have kept the discussion as general as possible. It would be interesting to examine, whether the relation to the first order formulation of Regge calculus can also be found in larger triangulations or whether one obtains modifications, which could be understood as quantum gravity effects.

At the end we would like to point out that the application of our method to the case of the non-compact group $SL(2, \mathbb{R})$ is rather straightforward and we leave the determination of the 3D Lorentzian $6j$ symbol for future investigations.

Acknowledgement

2.A Spin network evaluation and sign convention

This appendix is devoted to the sign issue. We will show how one can determine the total sign of our formula using the prescription of [A38, A39].

2.A.1 Penrose prescription for spherical graph

In this section we will describe a canonical way to evaluate spherical (planar) spin networks. Let us draw it on the 2-sphere such that no edges intersect; if the spin network is 2-line irreducible there are two distinct ways to do so, which differ by orientation. The result of the evaluation does not depend on this choice. For every node of the graph (a face in the dual picture) we have a natural
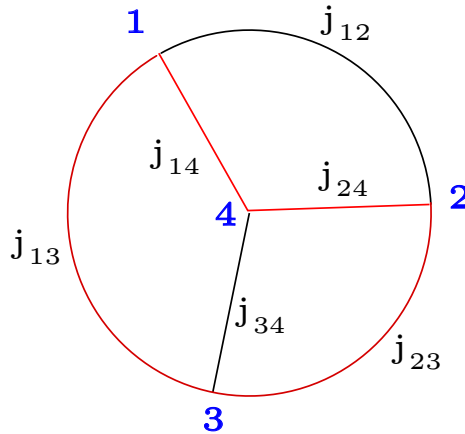
Figure 2.5: Orientation of intertwiners inherited from orientation of the sphere (plane). Half-integer spins colored red.

cyclic order inherited from the orientation of the sphere. In the second step we choose any ordering of nodes (faces). This gives a natural orientation of the edges; they start in nodes lower in the order and end in nodes higher in the order. We draw the graph on the plane as shown on figure 2.5 such that the order of the nodes is preserved and the order of legs in every node is consistent with the cyclic order obtained above.

In the third step we count the number of crossings s of half-integer edges with each other. The spin network is evaluated by contracting invariants, given for every node, by using the ϵ bilinear form oriented according to the edge orientation inherited from the nodes. The ordering of the legs
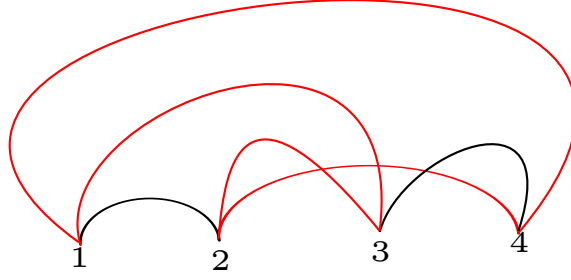
Figure 2.6: Nodes are in the right order and for each intertwiner the legs are in the right cyclic order. The number of crossings for half-integer edges is $s = 2$.

is as in figure 2.6:

$$\prod_e \epsilon^{j_e}_{A_{s(e)e} A_{t(e)e}} \prod_v I_v^{A_{ve_1} A_{ve_2} A_{ve_3}} \quad . \tag{2.A.1}$$

These invariants are described in [A38, A39] (see also section 2.3.4). One can show that the result does not depend on the made choices.

2.A.2 Sign factors and spin structure

In this section we will show how to compute the sign factor for spherical graphs. First of all, let us notice that in the case that all j are integers, the sign disappears completely. We will prove now that this is also the case in general. Explicitly we will prove that (see 2.3.5 for the definitions)

$$s + \sum_f s_f + \sum s_e = 0 \mod 2 . \tag{2.A.2}$$

Sign factor in the intertwiner

In this section we compute the sign s_f. In order to do this, we compare our invariant with the one from [A38, A39] (given for a fixed order of j_1, j_2, j_3). The dual of the latter is given on vectors $\xi_1^{2j_1} \otimes \xi_2^{2j_2} \otimes \xi_3^{2j_3}$ by the formula

$$(-1)^{j_1+j_3-j_2} C \, \epsilon(\xi_1, \xi_2)^{j_1+j_2-j_3} \epsilon(\xi_2, \xi_3)^{j_2+j_3-j_1} \epsilon(\xi_3, \xi_1)^{j_1+j_3-j_2} \tag{2.A.3}$$

with normalization $C > 0$ [A38, A39].

The contraction of (2.A.3) with our invariant is given by:

$$(-1)^{j_1+j_3-j_2} C \int \frac{d\phi_1 \, d\phi_2 \, d\phi_3}{(2\pi)^3} \epsilon(v_{\phi_1}, v_{\phi_2})^{j_1+j_2-j_3} \epsilon(v_{\phi_2}, v_{\phi_3})^{j_2+j_3-j_1} \epsilon(v_{\phi_3}, v_{\phi_1})^{j_1+j_3-j_2} \quad , \tag{2.A.4}$$

where

$$v_\phi = \begin{pmatrix} \cos\phi \\ \sin\phi \end{pmatrix}, \quad \epsilon(v_\phi, v_{\phi'}) = \sin(\phi' - \phi) \quad , \tag{2.A.5}$$

and we skipped the integration over U, since (2.A.3) is invariant. Let us recall our notation:

$$\psi_{ij} = \phi_i - \phi_j \quad . \tag{2.A.6}$$

After a change of variables

$$(\phi_1, \phi_2, \phi_3) \rightarrow (\psi_{21}, \psi_{32}, \phi_1) \tag{2.A.7}$$

and performing one trivial integration over ϕ_1, (2.A.4) is equal to

$$(-1)^{j_1+j_3-j_2}C \int \frac{d\psi_{21}\, d\psi_{32}}{(2\pi)^2}(\sin\psi_{21})^{j_1+j_2-j_3}(\sin\psi_{32})^{j_2+j_3-j_1}(\sin\psi_{13})^{j_1+j_3-j_2} \quad, \qquad (2.A.8)$$

with the constraint $\psi_{21}+\psi_{32}+\psi_{13}=0$.

As the expression is real (since $j_i+j_k-j_l$ is an integer), in the asymptotic limit it is dominated by the stationary point (maxima of the integral) of the action

$$(j_1+j_2-j_3)\ln|\sin\psi_{21}|+(j_2+j_3-j_1)\ln|\sin\psi_{32}|+(j_1+j_3-j_2)\ln|\sin\psi_{13}|+\rho(\psi_{21}+\psi_{32}+\psi_{13}) \quad, \tag{2.A.9}$$

where ρ is a Lagrange multiplier and $\psi_{21},\psi_{32},\psi_{13}$ are treated as independent variables. The stationary point condition reads

$$(j_i+j_k-j_l)\cot\psi_{ij}=\rho\,. \qquad (2.A.10)$$

Now we can use the fact that

$$\cot\psi_{32}\cot\psi_{21}+\cot\psi_{13}\cot\psi_{32}+\cot\psi_{21}\cot\psi_{13}=1 \qquad (2.A.11)$$

to obtain

$$\rho^2=\frac{(j_1+j_2-j_3)(j_2+j_3-j_1)(j_1+j_3-j_2)}{j_1+j_2+j_3} \quad. \qquad (2.A.12)$$

Furthermore, we see that

$$\cot^2\psi_{32}=\frac{(j_1+j_2-j_3)(j_1+j_3-j_2)}{(j_2+j_3-j_1)(j_1+j_2+j_3)}=\frac{j_1^2-(j_2-j_3)^2}{(j_2+j_3)^2-j_1^2} \quad. \qquad (2.A.13)$$

Hence, we compute that

$$\cos 2\psi_{32}=\frac{\cot^2\psi_{32}-1}{\cot^2\psi_{32}+1}=\frac{j_1^2-j_2^2-j_3^2}{2j_2 j_3} \quad, \qquad (2.A.14)$$

$$\sin 2\psi_{32}=\frac{2\cot\psi_{32}}{\cot^2\psi_{32}+1}=\pm\frac{A}{j_2 j_3} \quad, \qquad (2.A.15)$$

where A is the area of the triangle with edge lengths j_1, j_2, j_3. Thus $\pm 2\psi_{32}$ modulo 2π is the angle in this triangle opposite to the edge j_1. Similar relations hold for ψ_{21} and ψ_{13}. Together with the relation $\psi_{21}+\psi_{32}+\psi_{13}=0$, it gives the condition that

$$2\psi_{21},\; 2\psi_{32},\; 2\psi_{13} \bmod 2\pi \qquad (2.A.16)$$

are oriented (i.e. incorporate sign) angles of the triangle on the plane with edges (j_1, j_2, j_3).

In the presence of a function f_f, only one of those stationary points contributes. Since the Jacobian is real, the only contribution to the sign is given by the value of the integral in the stationary point. We know that $\psi_{ij}\in(\pi,2\pi)$ for consecutive pair of edges (ij) (see 2.2.1), thus $\sin\psi_{ij}<0$ and the total sign is

$$(-1)^{j_1+j_3-j_2}\,(-1)^{j_1+j_2-j_3}(-1)^{j_2+j_3-j_1}(-1)^{j_1+j_3-j_2}=(-1)^{2j_2} \qquad (2.A.17)$$

As already discussed above, this is a relative sign of our invariant with respect to the invariant described in [A38, A39].

The sign $\sum s_e$

In the stationary point we can write (see 2.3.1 and 2.3.1 for the derivation)

$$U_{s(e)}^{-1}U_{t(e)} = (-1)^{\tilde{s}_e}O_{s(e)e}e^{-i\tilde{\theta}_{s(e)t(e)}\begin{pmatrix}1 & 0\\0 & -1\end{pmatrix}}\begin{pmatrix}0 & -1\\1 & 0\end{pmatrix}O_{t(e)e}^{-1} \quad, \tag{2.A.18}$$

where we assumed that $\tilde{\theta}_{s(e)t(e)} \in \left(-\frac{\pi}{2}, \frac{\pi}{2}\right)$. It is straightforward to check that

$$U_{t(e)}^{-1}U_{s(e)} = (-1)^{\tilde{s}_e+1}O_{t(e)e}e^{-i\tilde{\theta}_{t(e)s(e)}\begin{pmatrix}1 & 0\\0 & -1\end{pmatrix}}\begin{pmatrix}0 & -1\\1 & 0\end{pmatrix}O_{s(e)e}^{-1} \quad, \tag{2.A.19}$$

where $\tilde{\theta}_{t(e)s(e)} = -\tilde{\theta}_{s(e)t(e)} \in \left(-\frac{\pi}{2}, \frac{\pi}{2}\right)$. Thus in general we have

$$U_f^{-1}U_{f'} = (-1)^{\tilde{s}_e+c_e}O_{fe}e^{-i\tilde{\theta}_{ff'}\begin{pmatrix}1 & 0\\0 & -1\end{pmatrix}}\begin{pmatrix}0 & -1\\1 & 0\end{pmatrix}O_{f'e}^{-1} \quad, \tag{2.A.20}$$

where

$$c_e = \begin{cases} 0 & f = s(e) \text{ and } f' = t(e) \\ 1 & f = t(e) \text{ and } f' = s(e) \end{cases} \quad. \tag{2.A.21}$$

By a cycle we denote an assignment of a number $\{0,1\}$ to every edge such that

$$\forall_f \sum_{e\subset f} c_e = 0 \bmod 2 \; . \tag{2.A.22}$$

The set of cycles is denoted by Z_1. Abusing the notation, we will also say that the cycle is formed by edges with $c_e = 1$. Let us notice that such edges form a disjoint sum of loops that we will denote by c_i.

For every cycle c holds

$$\prod_i \left(\prod_j U_{f_j^i}^{-1}U_{f_{j+1}^i}\right) = 1 \quad, \tag{2.A.23}$$

where $\{f_j^i f_{j+1}^i\}$ are consequtive pair of faces in the cycle c_i (in the correctly chosen order).

Thus, we can write

$$(-1)^{\tilde{s}(c)} = \prod_{e=[ff']\subset c} (-1)^{c_e}O_{fe}e^{-i\tilde{\theta}_{ff'}\begin{pmatrix}1 & 0\\0 & -1\end{pmatrix}}\begin{pmatrix}0 & -1\\1 & 0\end{pmatrix}O_{f'e}^{-1} \quad, \tag{2.A.24}$$

where we used the same order of multiplications as before. The equations (2.A.23) translate into the set of equations satisfied by $\tilde{s}_e$:

$$\forall\, c \in Z_1 \quad \sum_{e\in c} \tilde{s}_e c(e) = \tilde{s}(c) \bmod 2 \quad . \tag{2.A.25}$$

Given a solution for the $\tilde{s}_e$, U_f can be reconstructed up to a U transformation. The solutions $\{\tilde{s}_e\}$ are not completely determined, but the residual symmetry is given by $\text{Ran}\,\partial$ where

$$\partial : C_0 \to C_1, \tag{2.A.26}$$

is a boundary operator because $C_1 = \ker \partial^* \oplus \text{Ran}\,\partial$. Those correspond exactly to $-U_f$ transformations.

We are interested in 2.3.5

$$\sum s_e = \sum_{e\in c} \tilde{s}_e c(e) \quad, \tag{2.A.27}$$

where c is the cycle formed by all edges that are half-integer.

Sign of basic cycles in spherical case

In this section we will compute the sign factor $\tilde{s}(c)$ for cycles consisting of only a single loop. Every other cycle can be uniquely written as a sum (as the $\mathbb{Z}_2$ module) of such disjoint cycles.

Let us take such a cycle. The cycle is described by the sequence of consecutive faces and edges. The value of $(-1)^{\tilde{s}(c)}$ is thus equal to

$$\prod_{\{ff'\}\in c} O_{fe} e^{-i\tilde{\theta}_{ff'}\begin{pmatrix} 1 & 0 \\ 0 & -1 \end{pmatrix}} \begin{pmatrix} 0 & -1 \\ 1 & 0 \end{pmatrix} O_{f'e}^{-1} \quad . \tag{2.A.28}$$

All parameters (i.e ϕ_{fe} and $\tilde{\theta}_{ff'}$) can be continuously deformed, i.e. there exists a map

$$[0,1] \ni t \to \{\phi_{fe}^t, \tilde{\theta}_{ff'}^t\} \tag{2.A.29}$$

such that

$$\forall_{e\subset f}\ \phi_{fe}^0 = \phi_{fe}, \quad \forall_{ff'}\ \tilde{\theta}_{ff'}^0 = \tilde{\theta}_{ff'}, \tag{2.A.30}$$

that satisfies the following conditions:

- the image of (2.A.28) in $SO(3)$ is always the identity,

- at the end all deformed $SU(2)$ angles $\tilde{\theta}_{ff'}^1$ are equal to 0

- for every face f with ordered pair of edges e, e' (neighbours in the cycle), the difference $\phi_{fe}^t - \phi_{fe'}^t \in \left(\frac{\pi}{2}, \frac{3\pi}{2}\right)$ modulo 2π during the whole deformation process. In fact, it is larger than π if order of edges agrees with the orientation of the face and smaller if it does not.

The final stage of the deformation will be denoted by

$$\forall_{e\subset f}\ \tilde{\theta}'_{ff'} = \tilde{\theta}_{ff'}^1, \quad \forall_{ff'}\ \phi'_{fe} = \phi_{fe}^1 \quad . \tag{2.A.31}$$

Up to 2-dimensional homotopies, there are two possible final stages of such deformations. They differ by orientation of the cycle (loop) drawn on the plane. We assume that the faces are ordered in agreement with total orientation.

The cycle before and after the deformation is shown in figure 2.7. The proces is shown on the
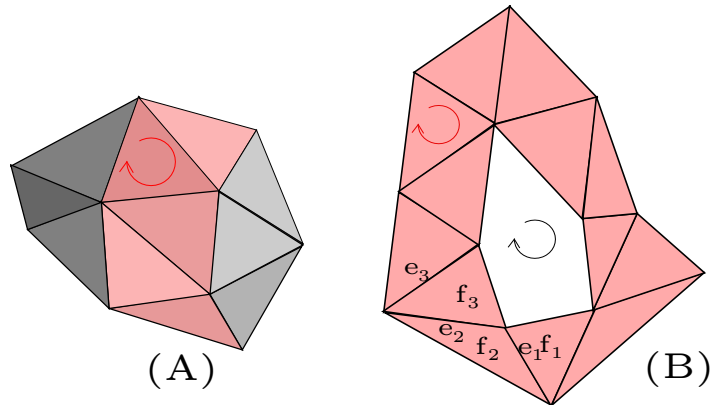
Figure 2.7: (A) Cycle before deformation. (B) Cycle after deformation.

figure 2.8 on example of a single-loop cycle around the vertex. In the end we obtain
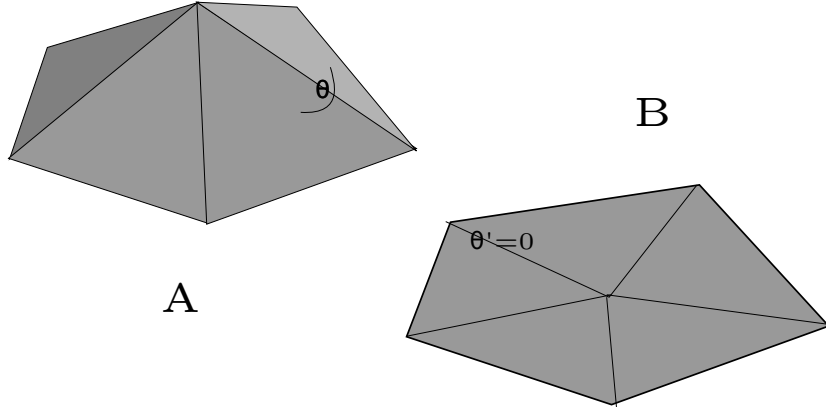
Figure 2.8: Example of the single-loop cycle around a vertex. (A) Cycle before deformation: angle θ between two faces depicted. (B) Cycle after deformation $\theta' = 0$, the faces are parallel.

$$\prod_{\{ff'\}\in c} (-1)^{c_e} O_{fe} e^{-i\tilde{\theta}'_{ff'} \begin{pmatrix} 1 & 0 \\ 0 & -1 \end{pmatrix}} \begin{pmatrix} 0 & -1 \\ 1 & 0 \end{pmatrix} O_{f'e}^{-1} = (-1)^{C_e} \prod_{\{ff'\}} O'_{fe} O'^{-1}_{f'e} \prod_e \begin{pmatrix} 0 & -1 \\ 1 & 0 \end{pmatrix} \quad ,$$

$$(2.A.32)$$

where C_e is the number of edges with $c_e = 1$ because O'_{fe} commutes with $\begin{pmatrix} 0 & -1 \\ 1 & 0 \end{pmatrix}$. The images of O'_{fe} (and related $SO(3)$ angles $\pi(\phi'_{fe})$) satisfy (see figure 2.9)

$$\sum_e \pi(\phi'_{fe}) - \pi(\phi'_{f'e}) = - \sum_{\{ee'\}\subset f} \pi(\phi'_{fe}) - \pi(\phi'_{fe'}) = -(n-2)\pi \quad , \qquad (2.A.33)$$

where n is the number of faces meeting in the cycle c.
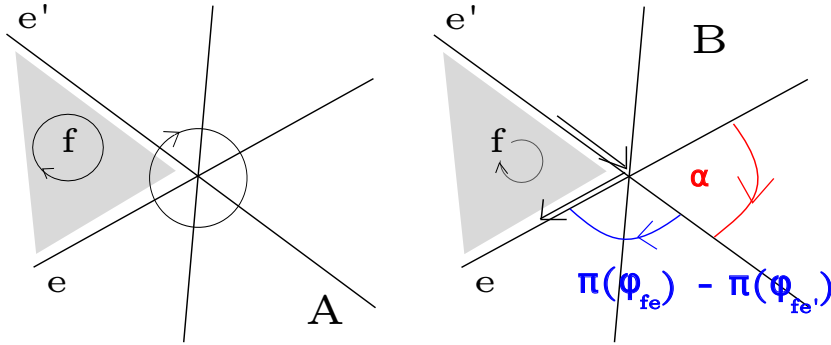
Figure 2.9: (A) example of the cycle with orientations shown, (B) $\pi(\phi'_{fe}) - \pi(\phi'_{fe'})$ and $\alpha = \pi - (\pi(\phi'_{fe}) - \pi(\phi'_{fe'}))$

Using prescription 2.2.1 for $\phi_{fe} - \phi_{fe'}$, the fact that $SU(2)$ is the double cover of $SO(3)$ and

continuity of the deformation we obtain (modulo 2π)

$$\sum_f \phi'_{fe} - \phi'_{fe'} = \sum_f \frac{\pi(\phi'_{fe}) - \pi(\phi'_{fe'})}{2} - \pi = \left(-n + \frac{n}{2} + 1\right)\pi \quad . \tag{2.A.34}$$

Thus

$$\prod_{\{ff'\}} O'_{fe} O'^{-1}_{f'e} \prod_e \begin{pmatrix} 0 & -1 \\ 1 & 0 \end{pmatrix} = \begin{pmatrix} 0 & 1 \\ -1 & 0 \end{pmatrix}^{n-2} \begin{pmatrix} 0 & -1 \\ 1 & 0 \end{pmatrix}^n = -1 \quad . \tag{2.A.35}$$

To sum up, we obtained for a given cycle c

$$\sum_e c(e)\tilde{s}_e = C_e + 1 \bmod 2 \quad . \tag{2.A.36}$$

Since the cycle is oriented in the same way as the faces, C_e is the number of edges oriented according to the cycle.

Other method of computation

Let us consider an arbitrary cycle c. Let us draw it on the graph G as in figure 2.6. We will denote by $s(c)$ the number of crossings in the cycle. For any node (face) f we also denote

$$f(c) = \begin{cases} 0 & \text{if the middle leg edge of } f \text{ does not belong to } c \\ 1 & \text{if the middle leg edge of } f \text{ belongs to } c \end{cases} \tag{2.A.37}$$

In the following, we will present another method of how to compute $\sum_e c_v(e)\tilde{s}_e$ for a basic cycle c. First we will prove:

Lemma 4. *For a single loop cycle c in a spherical network, the quantity*

$$C_e + \sum_f f(c) + s(e) \bmod 2 \tag{2.A.38}$$

does not depend on the choice of a graph G.

Proof. Any two graphs can be transformed into one another by a sequence of basic moves

- One of the Reidemeister moves [A47, A48] for the edge (see figure 2.10 for example). It only changes $s(c)$ by an even number.

(A)   (B)
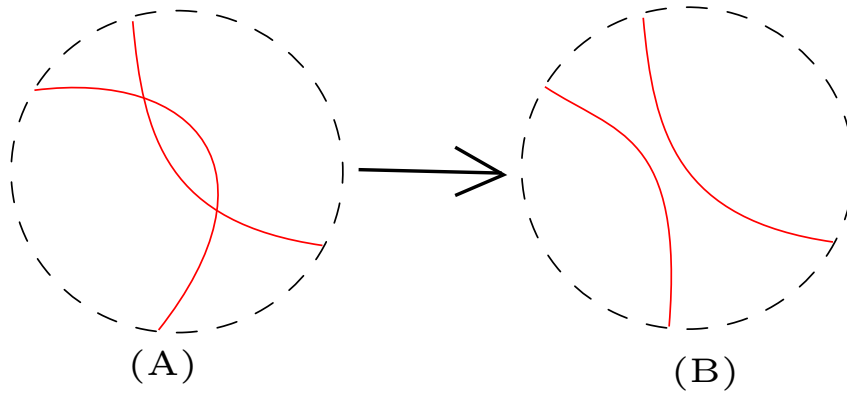
Figure 2.10: Part of the graph changed by the move. Example of a Reidemeister move.

- Transposition of two consecutive nodes belonging to the cycle (see figure 2.11). In the move shown in the figure

$$C'_e = C_e \pm 1, \quad s(c)' = s(c) + 3 \quad , \tag{2.A.39}$$

and all $f(c)$ remain unchanged.
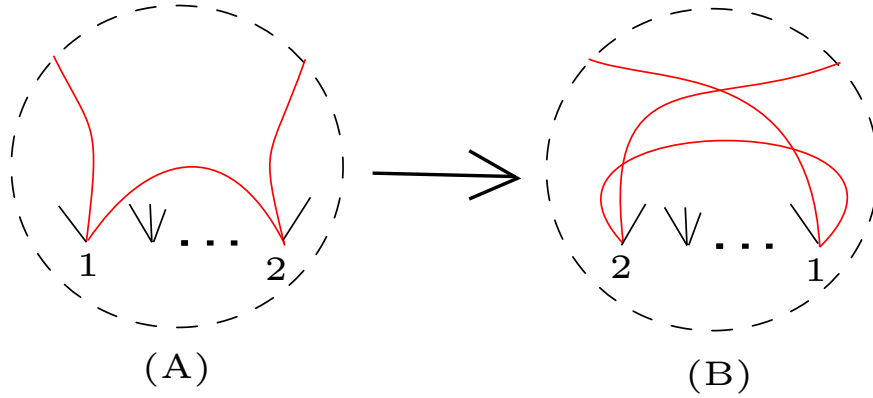
Figure 2.11: Part of the graph changed by the move (edges not belonging to the cycle are not drawn). Two consecutive nodes in the cycle transposed.

- Cyclic permutation of the legs of a node f (figure 2.12). In this case

$$f(c) + s(c) \tag{2.A.40}$$

is preserved.
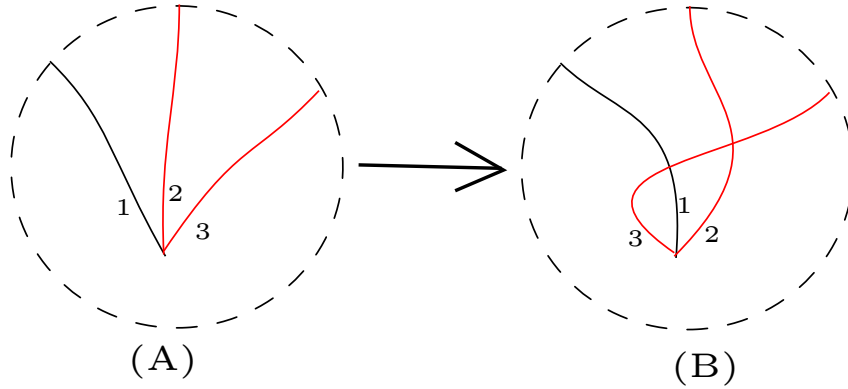
Figure 2.12: Part of the graph changed by the move. Cyclic change of the order of legs.

Thus $C_e + \sum_f f(c) + s(c) \mod 2$ is invariant. $\qquad \square$

We see that $(C_e + 1) + \sum_f f(c) + s(c)$ does not depend on the chosen graph G, hence, we can choose the most convenient one (see figure 2.13). For this particular choice

$$C_e = 1, \quad \forall_{f \subset c} f(c) = 0, \quad s(c) = 0 \quad , \tag{2.A.41}$$

and thus $(C_e + 1) + \sum_f f(c) + s(c) = (1+1) + 0 = 0 \mod 2$ and

$$\sum_e c(e) \tilde{s}_e = C_e + 1 = \sum_f f(c) + s(c) \mod 2 \ . \tag{2.A.42}$$
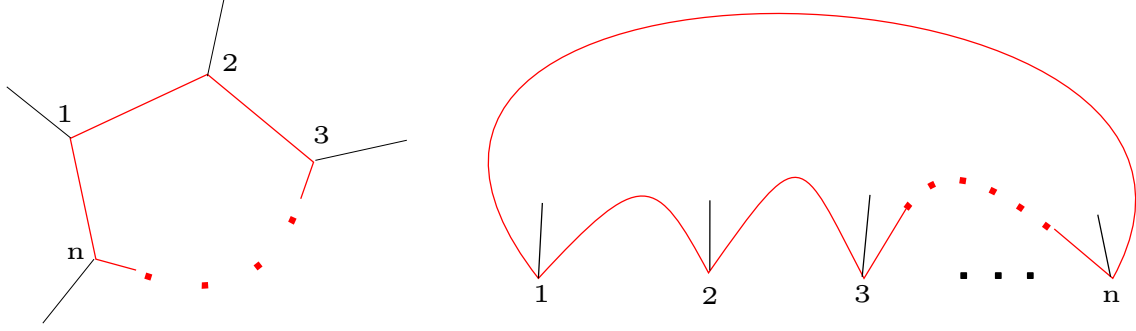
Figure 2.13: Convenient choice for the graph G

Sign of the general cycle in spherical case

Let us state now a few properties of $f(c)$ and $s(c)$ useful in the sequel.

For two cycles c and c' we denote a cycle by $c + c'$ if it satisfies the following property:

$$\forall_e, \ (c + c')(e) = c(e) + c'(e) \bmod 2 \ . \tag{2.A.43}$$

We have for two disjoint cycles c and c'

$$s(c + c') = s(c) + s(c') \bmod 2 \quad , \tag{2.A.44}$$
$$\forall_f \ f(c + c') = f(c) + f(c') \bmod 2 \quad . \tag{2.A.45}$$

We can now write every cycle c in the spherical case as a sum of disjoint single-loop cycles c_α, such that $c = \sum_\alpha c_\alpha$:

$$\sum_e c(e)\tilde{s}_e = \sum_e \left(\sum_\alpha c_\alpha(e) \right) \tilde{s}_e = \sum_\alpha \left(\sum_f f(c_\alpha) + s(c_\alpha) \right) =$$
$$= \sum_f f\left(\sum_\alpha c_\alpha \right) + s\left(\sum_\alpha c_\alpha \right) = \sum_f f(c) + s(c) \bmod 2 \ . \tag{2.A.46}$$

Final sign formula

Let us notice that in the case when c is the cycle of all half-integer spins we have

$$s = s(c), \quad \forall_f s_f = f(c), \quad \sum_e s_e = \sum_e c(e)\tilde{s}_e \ , \tag{2.A.47}$$

since if we denote the spin of the middle leg edge of f by j_{f2} then $f(c) = 2j_{f2} \bmod 2$. Finally

$$s + \sum_f s_f + \sum_e s_e = 2 \left(\sum_f f(c) + s(c) \right) = 0 \bmod 2 \ . \tag{2.A.48}$$

2.B Changes of variables and their Jacobians

Let the Lie group G act transitively on the manifold S and let

$$\chi \colon G \to \mathbb{R} \tag{2.B.1}$$

be a homomorphism. There exists at most one measure μ (up to scaling) on S such that

$$g^* \mu = \chi(g) \mu \quad . \tag{2.B.2}$$

Let

$$H \circlearrowright S_1 \to S_2 \quad , \tag{2.B.3}$$

where S_1 is a principal Lie group bundle with the structure group H and the base space S_2. Any (pseudo-)k-form μ_2 on S_2 can be uniquely represented by a (pseudo-) k-form μ_1 on S_1 that satisfies

$$h^* \mu_1 = \mu_1 \quad \forall h \in H \tag{2.B.4}$$

$$\mu_1 \perp \partial_\xi = 0 \quad \forall \, \partial_\xi \in \mathfrak{h} \quad , \tag{2.B.5}$$

where $\mathfrak{h}$ is the Lie algebra of H and $\perp$ is contraction of the (pseudo-) form with the vector on the first site. Any form μ_1 determines the form μ_2 on S_2. The integration over S_2 is the integration over any section of the projection map $S_1 \to S_2$.

Such a form satisfying conditions (2.B.4) and (2.B.5) can be obtained from the H invariant form μ on S_1 via the formula

$$\mu_2 = \mu \perp \bigwedge_{\xi \text{ basis } \mathfrak{h}} \partial_\xi \quad . \tag{2.B.6}$$

In case of a compact group H it is related to the measure obtained by integration over the fibers, called $\mu_{\int H}$, as follows

$$\mu_2 = (\mu_H \perp \bigwedge \partial_\xi) \mu_{\int H} \quad , \tag{2.B.7}$$

where μ_H is the normalized Haar measure on H.

Let $M \subset S$ be a submanifold described locally by a set of independent equations f_a. For any measure (form) μ on S we can define a measure (form) μ_{f_a} on M by the following integration prescription: Let $g \in C^0(M)$ and $\tilde{g}$ be any continuous extension to S, then

$$\int_M \mu_{f_a} g = \int_M \prod \delta(f_a) \tilde{g} \mu \quad . \tag{2.B.8}$$

Let M be a section of the bundle $H \subset S_1 \to S_2$ described by equations f_a, then we can compare the just described measures on M and S_2 since $M \to S_2$ is a diffeomorphism of M onto S_2:

$$\mu_{f_a} = (\det \partial_{\xi_i} f_a)^{-1} \mu \perp \bigwedge \partial_\xi \quad . \tag{2.B.9}$$

Indeed, we can choose local coordinates such that $S_1 = M \times H$ and the zero section is described by $f_a = 0$. We have

$$\mu = (\mu \perp \bigwedge \partial_\xi) \wedge \bigwedge d\xi \quad . \tag{2.B.10}$$

By extending the function g constantly along fibers from the zero section, we obtain:

$$\int_M g \mu_{f_a} = \int_{S_1} \prod \delta(f_a) \tilde{g} \mu = \int_M \tilde{g} \left(\int_H \prod \delta(f_a) \bigwedge d\xi \right) (\mu \perp \bigwedge \partial_\xi)$$
$$= \int_{S_2} g \, (\det \partial_{\xi_i} f_a)^{-1} (\mu \perp \bigwedge \partial_\xi) \quad . \tag{2.B.11}$$

2.B.1 Change of variables $u_i \to n_i$ (integrating out gauge)

Let us remind from section 2.3.3 that

$$S^2 = SU(2)/S^1 \quad , \tag{2.B.12}$$

given by the right action of S^1 on $SU(2)$. The sphere S^2 can either be represented by unit vectors $|n_i|^2 = 1$ or traceless 2×2 matrices n_i with the condition

$$\frac{1}{2} \operatorname{Tr} n_i n_i = 1 \quad . \tag{2.B.13}$$

Then the quotient map is given by

$$n_i(u) = uHu^{-1} \quad , \tag{2.B.14}$$

where $H = \begin{pmatrix} 0 & i \\ -i & 0 \end{pmatrix}$. The group $SU(2)$ acts on S^2 (as a left action on the quotient) by

$$n_i \to u \, n_i \, u^{-1} \quad . \tag{2.B.15}$$

The Haar measure from $SU(2)$ can be integrated over the fibers giving the invariant measure μ on the sphere with total volume 1.

Another invariant measure is

$$\delta(|n|^2 - 1) \, \mathrm{d} \, n_1 \, \mathrm{d} \, n_2 \, \mathrm{d} \, n_3 \quad . \tag{2.B.16}$$

Since there is only one invariant measure up to scale, both are related by a scaling transformation:

$$\mu = c\delta(|n|^2 - 1) \, \mathrm{d} \, n_1 \, \mathrm{d} \, n_2 \, \mathrm{d} \, n_3 \quad . \tag{2.B.17}$$

The constant is fixed by requiring:

$$1 \overset{!}{=} \int_{S^2} \mu = c \int_0^{2\pi} \mathrm{d} \, \phi \int_0^\pi \sin\theta \, \mathrm{d} \, \theta \int_0^\infty r^2 \delta(r^2 - 1) \, \mathrm{d} \, r = 2\pi c \quad , \tag{2.B.18}$$

thus

$$\mu = \frac{1}{2\pi} \delta(|n|^2 - 1) \, \mathrm{d} \, n_1 \, \mathrm{d} \, n_2 \, \mathrm{d} \, n_3 \quad . \tag{2.B.19}$$

2.B.2 Variables θ in the flat tetrahedron

Let us consider two sets of variables

$$N = (\vec{n}_1, \dots, \vec{n}_{m+1}) \quad , \tag{2.B.20}$$

where $\vec{n}_i$ are m vectors with exactly one dependency, i.e. every subset of m vectors forms a basis. Let

$$M = N^T N, \; m_{ij} = \vec{n}_i \vec{n}_j, \; i \le j \; , \tag{2.B.21}$$

where M is a symmetric positive $(m+1) \times (m+1)$ matrix, which is degenerate with exactly one null eigenvector, whose entries are all non vanishing.

On N there exists a left action of $O(m)$, $\vec{n}_i \to O\vec{n}_i$. The matrix M is $O(m)$ invariant, so the parameters of this action can be regarded as supplementary to M. The vector fields of this action will be denoted by L_{ab}. The map $N \to M$ is an $O(m)$ principal bundle.

In the following, our goal is to compare the pseudo-form

$$\mu_1 = \left| \bigwedge_{i=1\dots m+1, a=1\dots m} \mathrm{d} \, n_i^a \perp \bigwedge_{a<b} L_{ab} \right| \tag{2.B.22}$$

with the form

$$\mu_2 = \left| \delta(\det M) \bigwedge_{i \leq j} \mathrm{d}\, m_{ij} \right| \quad . \tag{2.B.23}$$

Let us notice that both μ_1 and μ_2 are measures on M.

There are additional transformations parametrized by $U \in GL(m+1)$

$$\tilde{N} = NU, \ \tilde{M} = U^T M U , \tag{2.B.24}$$

which commute with the $O(m)$ action on N. The measure μ_1 is χ covariant with respect to this action, where

$$\chi(U) = |\det^m|(U) := |\det(U)|^m \quad \forall U \in GL(m+1) \tag{2.B.25}$$

Furthermore, we have

- μ_2 is invariant for $U \in O(m+1)$,

- for transformations of the form $U = \mathrm{diag}\, \lambda_i$ (diagonal matrix) the measure μ_2 transforms as

$$\left| \underbrace{\frac{1}{\prod_i \lambda_i}}_{\text{from } \det M} \underbrace{\prod_{i \leq j} \lambda_i \lambda_j}_{=\prod_i \lambda_i^{m+1}} \right| \mu_2 \quad , \tag{2.B.26}$$

so it is also χ covariant as rotations and scaling generate the whole group.

Hence the two measures μ_1 and μ_2 differ by a constant c as $GL(m+1)$ acts transitively on M. This constant can be computed for a special value of N:

$$n_i^a = \begin{cases} \delta_i^a, & i \leq m \\ 0, & i = m+1 \end{cases} \quad . \tag{2.B.27}$$

In this choice

$$\mathrm{d}\, m_{ij} = \begin{cases} \mathrm{d}\, n_i^j + \mathrm{d}\, n_j^i, & i, j \leq m \\ \mathrm{d}\, n_{m+1}^i, & j = m+1 \\ 0, & i = j = m+1 \end{cases} \quad . \tag{2.B.28}$$

Moreover

$$\mathrm{d}\, n_i^a \perp L_{cd} = (L_{cd}\vec{n}_i)^a = \delta_{ac}\delta_{id} - \delta_{ad}\delta_{ic} \quad . \tag{2.B.29}$$

The following equalities hold:

$$2^m \left| \bigwedge_{i=1\ldots m+1, a=1..m} \mathrm{d}\, n_i^a \right| = \left| \bigwedge_{1 \leq j \leq i \leq m+1, j \neq m+1} \underbrace{dn_i^j + dn_j^i}_{dm_{ij}} \wedge \bigwedge_{1 \leq j < i \leq m+1} dn_i^j \right| , \tag{2.B.30}$$

but since $\mathrm{d}\, m_{ij} \perp L_{ab} = 0$:

$$2^m \left| \bigwedge_{i=1\ldots m+1, a=1..m} \mathrm{d}\, n_i^a \perp \bigwedge_{a<b} L_{ab} \right| = \left| \bigwedge_{1 \leq j \leq i \leq m+1, j \neq m+1} dm_{ij} \right| = \delta(m_{m+1,m+1}) \left| \bigwedge_{(i,j): \ i \leq j} \mathrm{d}\, m_{ij} \right| \quad . \tag{2.B.31}$$

Moreover in this case

$$M_{ij} = \begin{cases} \delta_{ij}, & i \leq m \\ 0, & i = m+1 \end{cases} \tag{2.B.32}$$

and so $\frac{\partial \det M}{\partial m_{m+1,m+1}} = 1$. Eventually

$$2^m \left| \bigwedge_{i=1\ldots m+1, a=1..m} \mathrm{d}\, n_i^a \perp \bigwedge_{a<b} L_{ab} \right| = \delta(\det M) \left| \bigwedge_{i \leq j} \mathrm{d}\, m_{ij} \right| \quad . \tag{2.B.33}$$

Integration over the $SO(3)$ fiber

In the case $m = 3$ we are interested in integrating over the fiber, however not the whole $O(3)$ but only over one connected component with respect to $SO(3)$. This is due to the u transformation symmetry corresponds to $SO(3)$ not $O(3)$ (see also section 2.2.3).

In this section we continue to compute the correct constant in front of the measure. We will now consider a fibration with the group $SO(m)$ that can still be described locally by a projection $N \mapsto M$. This is, however, enough because we are only interested in local variables.

In general we have [A49]

$$\int_{SO(m)} \left| \bigwedge_{a<b} L_{ab}^* \right| = \prod_{k=2}^{n} \frac{2\pi^{\frac{k}{2}}}{\Gamma\left(\frac{k}{2}\right)} \quad , \tag{2.B.34}$$

so from (2.B.7) our measure integrated over the fibre is equal to

$$\int_{SO(m)} \left| \bigwedge_{i=1...m+1,a=1..m} \mathrm{d}\, n_i^a \right| = \frac{1}{2^m} \prod_{k=2}^{m} \frac{2\pi^{\frac{k}{2}}}{\Gamma\left(\frac{k}{2}\right)} \delta(\det M) \left| \bigwedge_{i\leq j} \mathrm{d}\, m_{ij} \right| \quad . \tag{2.B.35}$$

If we impose the condition $|\vec{n}_i| = 1$, we integrate over a set of unit vectors. This implies for M that we have to skip $\mathrm{d}\, m_{ii}$ in the measure and we define $m_{ij} = \cos\theta_{ij}$. In these new angle variables the measure takes the form

$$\frac{1}{2^m} \prod_{k=2}^{m} \frac{2\pi^{\frac{k}{2}}}{\Gamma\left(\frac{k}{2}\right)} \delta(\det \tilde{G}) \prod_{i<j} |\sin\theta_{ij}| \bigwedge_{i<j} |\mathrm{d}\,\theta_{ij}| \quad , \tag{2.B.36}$$

where $\tilde{G}$ is the Gram matrix with the convention

$$\tilde{G}_{ij} = \cos\theta_{ij}, \quad \theta_{ii} = 0 \quad . \tag{2.B.37}$$

In case $n = 3$ we have

$$\pi^2 \delta(\det \tilde{G}) \prod_{i<j} |\sin\theta_{ij}| \bigwedge_{i<j} \mathrm{d}\,\theta_{ij} \quad . \tag{2.B.38}$$

2.B.3 Variables $\theta/\, l$ in the spherical constantly curved tetrahedron

Let us consider the spaces of matrices

$$\tilde{N} = \{N \in M_n(\mathbb{R}) \colon \det N > 0\} \tag{2.B.39}$$

and

$$\tilde{M} = \{M \in M_n(\mathbb{R}) \colon M > 0\} \quad . \tag{2.B.40}$$

We have a fibration with the group $SO(n)$ (via left action on $\tilde{N}$)

$$\tilde{N} \to \tilde{M}, \quad M = N^T N \quad . \tag{2.B.41}$$

We can compare forms

$$\mu_1 = \left| \bigwedge \mathrm{d}\, n_i^a \perp \bigwedge \partial_\xi \right| \quad ,$$

$$\mu_2 = (\det M)^{-1/2} \left| \bigwedge_{i<j} \mathrm{d}\, m_{ij} \right| \quad . \tag{2.B.42}$$

As in section 2.B.2 there is an action of $SL(n)$ by

$$N \to NU, \quad M \to U^T M U \quad . \tag{2.B.43}$$

We can check that both measures are $\chi = |\text{det}^n|$ covariant. Since $SL(n)$ acts transitively on matrices with positive determinant, we have

$$\mu_1 = c\mu_2 \quad . \tag{2.B.44}$$

Checking for $N = \mathbb{I}$ gives $c = 1$.

Let us notice that $n_i \cdot n_i = m_{ii}$. On the surface $m_{ii} = 1$ we can introduce angle variables $\cos \theta_{ij} = m_{ij}$ and obtain

$$(\det \tilde{G})^{-1/2} \prod \sin \theta_{ij} \bigwedge \mathrm{d}\,\theta_{ij} = \pm \prod \delta(n_i n_i - 1) \bigwedge \mathrm{d}\, n_i^a \quad . \tag{2.B.45}$$

2.B.4 Determinant $\det \frac{\partial \theta}{\partial l}$ for constantly curved simplices

We denote the length Gram matrix by G and the angle Gram matrix by $\tilde{G}$. The dimension is equal to $n - 1$ and we are working in $\mathbb{R}^n$ on the sphere with radius 1.

Our goal is to prove the following formulas for the $n - 1$-dimensional curved simplex. It was first proposed in [A41] and checked using an algebraic manipulator. Now we are presenting the complete derivation.

Lemma 5. *The following formulas hold for a spherical $(n - 1)$-simplex:*

$$\det \frac{\partial \theta_{ij}}{\partial l'_{km}} = (-1)^n \frac{\prod \sin l'_{ij}}{\prod \sin \theta_{ij}} \left(\frac{\det \tilde{G}}{\det G} \right)^{\frac{n+1}{2}} \quad , \tag{2.B.46}$$

and for $n = 4$

$$\det \frac{\partial \theta_{ij}}{\partial l_{km}} = -\det \frac{\partial \theta_{ij}}{\partial l'_{km}} = -\frac{\det \tilde{G}}{\det G} \quad . \tag{2.B.47}$$

Where we used standard convention that the angle θ_{ij} is the angle on the hinge obtained by leaving out indices i and j. The length of the opposite edge, i.e. the edge connecting vertices i and j, is denoted by l'_{ij} and in 3D, l_{ij} is the length of the edge at which the angle sits.

Outline of the proof

We compute how the measure $\bigwedge dl'_{ij}$ transforms under the the change of variables

$$\theta_{ij} \to l'_{ij} \quad . \tag{2.B.48}$$

In fact, introducing variables $m_{ij} = \cos \theta_{ij}$ and $m'_{ij} = \cos l_{ij}$, we have (in the right order)

$$\prod_{i<j} \sin \theta_{ij} \bigwedge_{i\leq j} d\theta_{ij} = \prod_i \delta(m_{ii} - 1) \bigwedge_{i\leq j} \mathrm{d}\, m_{ij} \quad , \tag{2.B.49}$$

$$\prod_{i<j} \sin l'_{ij} \bigwedge_{i\leq j} dl'_{ij} = \prod_i \delta(m'_{ii} - 1) \bigwedge_{i\leq j} \mathrm{d}\, m'_{ij} \quad . \tag{2.B.50}$$

Both measures on the left hand side are on

$$\tilde{M}_1 = \{M \in \tilde{M} : \forall_i m_{ii} = 1\} \quad , \tag{2.B.51}$$

where we introduced the notation $\tilde{M} = GL_+(n)$ for simplicity.

Computation

There is an action of the group of diagonal matrices

$$D = \{d \in GL_+(n) \colon d_{ij} = \lambda_i \delta_{ij}, \quad \lambda_i > 0\} \tag{2.B.52}$$

on $\tilde{M}$ given by

$$M \to d^T M d \quad . \tag{2.B.53}$$

A basis for the Lie algebra $\mathfrak{d}$ of the group D is given by $\partial_{\xi_i} = E_{ii}$ (matrices with only one nonzero entry being the i-th element on the diagonal equal to 1).

We have a fibration

$$\tilde{M} \to \tilde{M}/D \tag{2.B.54}$$

and let $\tilde{M}_1 \subset \tilde{M}$ be a cross section given by the equations

$$\forall_i \ m_{ii} = 1 \ . \tag{2.B.55}$$

Let us introduce maps

$$\begin{aligned}
\psi_1 \colon \tilde{M}_1 \to \tilde{M}/D, \quad & M \mapsto [M] \quad , \\
\psi_2 \colon \tilde{M} \to \tilde{M}, \quad & M \mapsto M^{-1} \quad .
\end{aligned} \tag{2.B.56}$$

Acting with ψ_2 on matrix transformed as in (2.B.53), we have

$$\psi_2(d^T M d) = (d^{-1})^T \psi_2(M)(d^{-1}) \quad , \tag{2.B.57}$$

such that there is a map

$$[\psi_2] \colon \tilde{M}/D \to \tilde{M}/D \quad . \tag{2.B.58}$$

Let us notice that the composition $\psi := \psi_1^{-1}[\psi_2]\psi_1$ transforms $\tilde{M}_1$ into $\tilde{M}_1$.

We define measures

$$\begin{aligned}
\mu_1 &= \prod \delta(m_{ii} - 1) \bigwedge_{i \leq j} \mathrm{d}\, m_{ij} = \bigwedge_{i < j} \mathrm{d}\, m_{ij} \quad , \\
\mu &= (\det M)^{-\frac{n+1}{2}} \bigwedge_{i \leq j} \mathrm{d}\, m_{ij} \quad , \\
\mu_{\tilde{M}/D} &= \mu \perp \bigwedge_i \partial_{\xi_i} \quad ,
\end{aligned} \tag{2.B.59}$$

where ∂_{ξ_i} is the basis of the Lie algebra $\mathfrak{d}$

$$\partial_{\xi_i} m_{kl} = (\delta_{ik} + \delta_{il}) m_{kl} \quad . \tag{2.B.60}$$

Let us notice that according to section 2.B.2 μ is $SL(n)$ invariant (where it acts as D) thus the pullback

$$\psi_2^* \mu = c\mu \quad , \tag{2.B.61}$$

since $SL(n)$ acts transitively on $\tilde{M}$. We can check that $c = 1$ by computing the measures for $M = M^{-1} = \mathbb{I}$.

We have $\psi_2 \partial_{\xi_i} = -\partial_{\xi_i}$ so

$$[\psi_2]^* \mu_{\tilde{M}/D} = (-1)^n \mu_{\tilde{M}/D} \quad . \tag{2.B.62}$$

From basic facts explained in the appendix 2.B we know that (in the right order)

$$\psi_1^* \mu_{\tilde{M}/D} = [\det \partial_{\xi_i}(m_{jj} - 1)] (\det M)^{\frac{n+1}{2}} \mu_1 = 2^n (\det M)^{\frac{n+1}{2}} \mu_1 \quad . \tag{2.B.63}$$

Combining all transformations we obtain

$$\mu_1 = (-1)^n \left(\frac{\det M}{\det \psi(M)} \right)^{\frac{n+1}{2}} \psi^* \mu_1 \quad . \tag{2.B.64}$$

Finally, we obtain

$$\bigwedge d\theta_{ij} = (-1)^n \frac{\prod \sin l'_{ij}}{\prod \sin \theta_{ij}} \left(\frac{\det \tilde{G}}{\det G} \right)^{\frac{n+1}{2}} \bigwedge dl'_{ij} \quad . \tag{2.B.65}$$

So eventually

$$\det \frac{\partial \theta_{ij}}{\partial l'_{km}} = (-1)^n \frac{\prod \sin l_{ij}}{\prod \sin \theta_{ij}} \left(\frac{\det \tilde{G}}{\det G} \right)^{\frac{n+1}{2}} \quad . \tag{2.B.66}$$

Further simplifications for $n = 4$

We can simplify the above formula using equalities from [A42]:

$$\det \tilde{G} = \frac{(\det G)^{n-1}}{\prod G_{ii}^*}, \quad (\sin \theta_{ij})^2 = \frac{\det G \det G_{(ij)}}{G_{ii}^* G_{jj}^*} \quad , \tag{2.B.67}$$

where G_{ii}^* is the ii-element of the minor matrix, $G_{(ij)}$ is the G matrix without ith and jth rows and columns. Eventually we obtain

$$\det \frac{\partial \theta_{ij}}{\partial l'_{km}} = (-1)^n \frac{\prod \sin l'_{ij} \prod (G_{kk}^*)^{\frac{n-1}{2}}}{(\det G)^{\frac{n(n-1)}{4}} \prod \sqrt{\det G_{(ij)}}} \frac{(\det G)^{\frac{(n-1)(n+1)}{2}}}{\prod (G_{kk}^*)^{\frac{n+1}{2}}} \frac{1}{(\det G)^{\frac{n+1}{2}}} \quad . \tag{2.B.68}$$

After simplification it is equal to

$$\det \frac{\partial \theta_{ij}}{\partial l'_{km}} = \underbrace{\left(\prod \frac{\sin l'_{ij}}{\sqrt{\det G_{(ij)}}} \right)}_{=1} \frac{\det \tilde{G}}{\det G} \quad . \tag{2.B.69}$$

Note that this simplification only holds for $n = 4$. Since

$$\det \frac{\partial l_{ij}}{\partial l'_{km}} = -1 \tag{2.B.70}$$

we obtain

$$\det \frac{\partial \theta_{ij}}{\partial l_{km}} = - \det \frac{\partial \theta_{ij}}{\partial l'_{km}} \quad . \tag{2.B.71}$$

2.C Technical computations of determinants

In this section we will prove several technical results.

Let us introduce the notation

$$\det{}' M = \sum_i M_{ii}^* \quad . \tag{2.C.1}$$

It is an invariant of the matrix and, moreover, in the case when the matrix is symmetric and has one null eigenvector, it is the determinant of the matrix restricted to the space perpendicular to that null eigenvector.

Let us also remind some general facts

$$l_{ij}\frac{\partial \theta_{ij}}{\partial l_{kl}} = l_{kl}\frac{\partial \theta_{ij}}{\partial l_{kl}} = 0 \quad , \quad \frac{\partial \theta_{ij}}{\partial l_{kl}} = \frac{\partial \theta_{kl}}{\partial l_{ij}} \quad , \tag{2.C.2}$$

$$l_{ij} = \lambda \frac{\partial \det \tilde{G}}{\partial \theta_{ij}} \quad , \quad \lambda = -\frac{2^2 \prod S_i^2}{3^5 V^5} \quad , \tag{2.C.3}$$

$$\det{'}\tilde{G} = \frac{3^4}{2^2}(\sum_i S_i^2)\frac{V^4}{\prod S_i^2} \quad , \tag{2.C.4}$$

which are proven for completeness in appendix 2.C.1. Our results are (see appendix 2.C.3):

Lemma 6. *For the flat tetrahedron holds*

$$\det{'}\frac{\partial \theta_{ij}}{\partial l_{kl}} = \frac{3^3}{2^5}\frac{|l|^2}{\prod S_i^2}V^3 \quad . \tag{2.C.5}$$

Moreover, in appendix 2.C.2 we prove:

Lemma 7. *Let*

$$\lambda = -\frac{2^2 \prod S_i^2}{3^5 V^5} \quad . \tag{2.C.6}$$

For the flat tetrahedron holds

$$\frac{\partial \lambda}{\partial l_{ij}}\frac{\partial \det \tilde{G}}{\partial \theta_{kl}} + \frac{\partial \theta_{ij}}{\partial l_{mn}}\lambda\frac{\partial^2 \det \tilde{G}}{\partial \theta_{mn}\partial \theta_{kl}} = \delta_{(ij),(kl)} \quad , \tag{2.C.7}$$

$$\exists_c \; \frac{\partial \det \tilde{G}}{\partial \theta_{kl}}c + \lambda\frac{\partial \lambda}{\partial l_{ij}}\frac{\partial^2 \det \tilde{G}}{\partial \theta_{ij}\partial \theta_{kl}} = 0 \quad , \tag{2.C.8}$$

$$\frac{\partial \lambda}{\partial l_{mn}}\frac{\partial \det \tilde{G}}{\partial \theta_{mn}} = 1 \quad . \tag{2.C.9}$$

2.C.1 General knowledge

We know that $\det \tilde{G} = 0$ for a geometric set of θ's. Moreover, the null eigenvector is given by

$$(S_1, S_2, S_3, S_4) \quad , \tag{2.C.10}$$

where S_i denote the areas of the triangles of the tetrahedron. The computation of $\det{'}\tilde{G}$ can be found in appendix 2.C.1. We have

$$\frac{\partial \det \tilde{G}}{\partial \theta_{ij}} = -2\det{'}\tilde{G}\frac{S_i S_j \sin \theta_{ij}}{\sum_k S_k^2} = -\frac{3^5}{2^2}(\sum_k S_k^2)\frac{V^4}{\prod S_k^2}\frac{V l_{ij}}{\sum_k S_k^2} = -\frac{3^5}{2^2}\frac{V^5}{\prod S_k^2}\,l_{ij} = \lambda^{-1}l_{ij} \quad . \tag{2.C.11}$$

In addition to that, we also have

$$0 = \frac{\partial \det \tilde{G}}{\partial l_{kl}} = \frac{\partial \det \tilde{G}}{\partial \theta_{ij}}\frac{\partial \theta_{ij}}{\partial l_{kl}} = \lambda l_{ij}\frac{\partial \theta_{ij}}{\partial l_{kl}} \quad . \tag{2.C.12}$$

We know that θ has scaling dimension 0, thus

$$l_{kl}\frac{\partial \theta_{ij}}{\partial l_{kl}} = 0 \quad . \tag{2.C.13}$$

Expressing $\frac{\partial \theta_{ij}}{\partial l_{kl}}$ in terms of l_{ij}

Here we recall several well-known facts for flat simplices of arbitrary dimension using the notation of l'_{ij} from appendix 2.B.4, see also [A41, A50] for more details. Let M be the following matrix

$$
M = \begin{bmatrix}
0 & 1 & \ldots & 1 \\
1 & l'^2_{11} & \ldots & l'^2_{1n} \\
\vdots & \vdots & \ddots & \vdots \\
1 & l'^2_{n1} & \ldots & l'^2_{nn}
\end{bmatrix} \quad ,
\tag{2.C.14}
$$

where $l'_{11} = \ldots = l'_{nn} = 0$ and $l'_{ij} = l'_{ji}$. Then we have:

$$
V^2 = \frac{(-1)^{n-1}}{2^n (n-1)!^2} \det M \quad , \quad S_i^2 = \frac{(-1)^{n-2}}{2^{n-1}(n-2)!^2} M_{ii}^* \quad ,
\tag{2.C.15}
$$

$$
\cos \theta_{ij} = \frac{M_{ij}^*}{\sqrt{M_{ii}^* M_{jj}^*}} \quad .
\tag{2.C.16}
$$

In three dimension we also have

$$
\sin^2 \theta_{ij} = \left(\frac{3}{2} \right)^2 \frac{V^2 l_{ij}^2}{S_i^2 S_j^2} \quad ,
\tag{2.C.17}
$$

so in the case $\theta_{ij} \in (0, \pi)$ we can write:

$$
\frac{\partial \theta_{ij}}{\partial l_{kl}} = -\frac{1}{\sin \theta_{ij}} \frac{\partial \cos \theta_{ij}}{\partial l_{kl}} = -\frac{2}{3} \frac{S_i S_j}{V l_{ij}} \frac{\partial}{\partial l_{kl}} \frac{M_{ij}^*}{\sqrt{M_{ii}^* M_{jj}^*}} \quad .
\tag{2.C.18}
$$

This, in principle, allows us to compute $\frac{\partial \theta_{ij}}{\partial l_{kl}}$ and all other derivatives in terms of lengths.

Computation of $\det'\tilde{G}$

Let us start with the spherical case, i.e. a tetrahedron with constant non vanishing (positive) curvature – a curved tetrahedron on the unit sphere. In this case we define $\tilde{l}_{ij} := \epsilon l_{ij}$ and $\theta_{ij}^\epsilon := \theta(\epsilon l_{kl})$ and take the limit $\epsilon \to 0$ in order to reobtain the flat case. The angles (θ_{ij}^ϵ) have a limit as the angles of flat tetrahedron (θ_{ij}) with lengths l_{ij}.

First, let us notice that

$$
\det G = \det \begin{pmatrix}
1 & 0 & \cdots \\
1 & G & \cdots \\
\vdots & \cdots & \cdots
\end{pmatrix} = \det \begin{pmatrix}
1 & 0 & \cdots \\
1 & 1 - \frac{1}{2}\epsilon^2 l_{ij}^2 + O(\epsilon^4) & \cdots \\
\vdots & \cdots & \cdots
\end{pmatrix}
\tag{2.C.19}
$$

$$
= \frac{1}{8} \epsilon^6 \underbrace{\det \begin{pmatrix}
0 & 1 & \cdots \\
1 & l_{ij}^2 & \cdots \\
\vdots & \cdots & \cdots
\end{pmatrix}}_{C} + O(\epsilon^8) \quad .
\tag{2.C.20}
$$

We can compute $\det'\tilde{G} = \sum_i \tilde{G}_{ii}^*$ using the following identity from [A42] ($n = 4$, i.e. $D = 3$):

$$
\frac{\tilde{G}_{ii}^*}{G_{ii}^*} = \frac{(\det G)^{n-2}}{\prod G_{ii}^*} \quad ,
\tag{2.C.21}
$$

obtaining

$$\det'\tilde{G} = \sum_i \tilde{G}_{ii}^* = \left(\sum_i G_{ii}^*\right)\frac{(\det G)^{n-2}}{\prod G_{ii}^*} = \frac{3^4}{2^2}\left(\sum_i S_i^2\right)\frac{V^4}{\prod S_i^2} + O(\epsilon^2) \quad . \tag{2.C.22}$$

So in the flat case

$$\det'\tilde{G} = \frac{3^4}{2^2}\left(\sum_i S_i^2\right)\frac{V^4}{\prod S_i^2} \quad . \tag{2.C.23}$$

2.C.2   Collection of results

Let us prove the following useful formulas:

$$\frac{\partial\lambda}{\partial l_{ij}}\frac{\partial\det\tilde{G}}{\partial\theta_{kl}} + \sum_{m<n}\frac{\partial\theta_{ij}}{\partial l_{mn}}\lambda\frac{\partial^2\det\tilde{G}}{\partial\theta_{mn}\partial\theta_{kl}} = \frac{\partial}{\partial l_{ij}}\left(\lambda\frac{\partial\det\tilde{G}}{\partial\theta_{kl}}\right) = \delta_{(ij),(kl)} \quad , \tag{2.C.24}$$

since we know, due to the Schläfli identity, that $\frac{\partial\theta_{ij}}{\partial l_{kl}} = \frac{\partial\theta_{kl}}{\partial l_{ij}}$. This also implies that

$$\sum_{m<n}\frac{\partial\theta_{mn}}{\partial l_{ij}}\lambda\frac{\partial^2\det\tilde{G}}{\partial\theta_{mn}\partial\theta_{kl}} = \delta_{(ij),(kl)} - \frac{\partial\lambda}{\partial l_{ij}}\frac{l_{kl}}{\lambda} \quad . \tag{2.C.25}$$

We will now prove that there exists such a c that

$$\frac{\partial\det\tilde{G}}{\partial\theta_{kl}}c + \lambda\frac{\partial\lambda}{\partial l_{ij}}\frac{\partial^2\det\tilde{G}}{\partial\theta_{ij}\partial\theta_{kl}} = 0 \quad . \tag{2.C.26}$$

Because the range of the matrix $\frac{\partial\theta_{ij}}{\partial l_{kl}}$ is the whole space perpendicular to the vector $\vec{l} = (l_{ij})$ and the vector $\frac{\partial\det\tilde{G}}{\partial\theta_{kl}}$ is proportional to $\vec{l}$, it is enough to compute

$$\left(\frac{\partial\det\tilde{G}}{\partial\theta_{kl}}c + \lambda\frac{\partial\lambda}{\partial l_{ij}}\frac{\partial^2\det\tilde{G}}{\partial\theta_{ij}\partial\theta_{kl}}\right)\frac{\partial\theta_{kl}}{\partial l_{mn}} = \lambda\frac{\partial\lambda}{\partial l_{ij}}\frac{\partial}{\partial l_{mn}}\frac{\partial\det\tilde{G}}{\partial\theta_{ij}} =$$
$$= \lambda\frac{\partial\lambda}{\partial l_{ij}}\frac{\partial}{\partial l_{mn}}\frac{l_{ij}}{\lambda} = \lambda\frac{\partial\lambda}{\partial l_{ij}}\left(\frac{\delta_{(ij)(mn)}}{\lambda} - l_{ij}\frac{\partial\lambda}{\partial l_{mn}}\frac{1}{(\lambda)^2}\right) \quad . \tag{2.C.27}$$

On the other hand we know that, since λ is of scaling dimension 1, $l_{ij}\frac{\partial\lambda}{\partial l_{ij}} = \lambda$, and thus

$$\lambda\frac{\partial\lambda}{\partial l_{ij}}\left(\frac{\delta_{(ij)(mn)}}{\lambda} - l_{ij}\frac{\partial\lambda}{\partial l_{mn}}\frac{1}{(\lambda)^2}\right) = \frac{\partial\lambda}{\partial l_{mn}} - \frac{\partial\lambda}{\partial l_{mn}} = 0 \quad . \tag{2.C.28}$$

Let us also remind that:

$$\frac{\partial\lambda}{\partial l_{mn}}\frac{\partial\det\tilde{G}}{\partial\theta_{mn}} = \frac{\partial\lambda}{\partial l_{mn}}\frac{l_{mn}}{\lambda} = 1 \quad . \tag{2.C.29}$$

2.C.3   Computation of $\det'\frac{\partial\theta_{ij}}{\partial l_{ij}}$

In this section we will prove that

$$\det'\frac{\partial\theta_{ij}}{\partial l_{ij}} = \frac{3^3}{2^5}\frac{|l|^2}{\prod S_i^2}V^3 \quad . \tag{2.C.30}$$

We will start from the formula valid for a spherical tetrahedron (Lemma 5):

$$\det\frac{\partial\theta_{ij}}{\partial\tilde{l}_{ij}} = -\frac{\det\tilde{G}}{\det G} \quad . \tag{2.C.31}$$

As mentioned above we set $\tilde{l}_{ij} = \epsilon l_{ij}$ and $\theta_{ij}^\epsilon = \theta(\epsilon l_{kl})$ and take the limit $\epsilon \to 0$ in the end. In this limit the angles converge to the angles of a flat tetrahedron with lengths l_{ij}.

Let us remind that

$$\det G = \frac{1}{8}\epsilon^6 \det \underbrace{\begin{pmatrix} 0 & 1 & \cdots \\ 1 & l_{ij}^2 & \cdots \\ \vdots & \cdots & \cdots \end{pmatrix}}_{C} + O(\epsilon^8) \quad . \tag{2.C.32}$$

Let us notice that because G (in the spherical case) is a function of $\cos \epsilon l_{ij}$, its expansion around $\epsilon = 0$ is an analytic function in ϵ^2 and not only in ϵ. The same holds for the matrix $\tilde{G}$ since it is

$$\tilde{G}_{ij} = \frac{1}{\sqrt{G_{ii}^*}} G_{ij}^* \frac{1}{\sqrt{G_{jj}^*}} \quad , \tag{2.C.33}$$

where G_{ij}^* is the cofactor matrix of G and $\sqrt{G_{ii}^*}$ is ϵ^3 times an analytic function in ϵ^2.

Hence we know that for the vector $\vec{S} = (S_1, S_2, S_3, S_4)$ (the single null eigenvector in the limit $\epsilon = 0$)

$$\tilde{G}\vec{S} = O(\epsilon^2) \ , \ (\vec{S}, \tilde{G}\vec{S}) = O(\epsilon^2) \ , \tag{2.C.34}$$

then also $\det \tilde{G} = O(\epsilon^2)$ and

$$\det \tilde{G} = \det{}'\tilde{G} \frac{(\vec{S}, \tilde{G}\vec{S})}{|S|^2} + O(\epsilon^4) \ . \tag{2.C.35}$$

Moreover

$$\epsilon \frac{\partial}{\partial \epsilon} \frac{(\vec{S}, \tilde{G}\vec{S})}{|S|^2} = 2\frac{(\vec{S}, \tilde{G}\vec{S})}{|S|^2} + O(\epsilon^3) \ . \tag{2.C.36}$$

We have

$$\epsilon \frac{\partial}{\partial \epsilon} \frac{(\vec{S}, \tilde{G}\vec{S})}{|S|^2} = \sum_{(ij)} l_{ij}\partial_{l_{ij}} \frac{(\vec{S}, \tilde{G}\vec{S})}{|S|^2} = \frac{(\vec{S}, \sum_{(ij)} l_{ij}\partial_{l_{ij}} \tilde{G}\vec{S})}{|S|^2} = \tag{2.C.37}$$

$$= -2\frac{\sum_{(km)(ij)} S_k S_m \sin\theta_{km} l_{ij} \frac{\partial\theta_{km}^\epsilon}{\partial l_{ij}}}{|S|^2} = -3\frac{V}{|S|^2} \sum_{(km)(ij)} l_{km} l_{ij} \frac{\partial\theta_{km}^\epsilon}{\partial l_{ij}} \quad . \tag{2.C.38}$$

Similarly, we know that $\sum_{ij} \frac{\partial\theta_{km}^\epsilon}{\partial l_{ij}} l_{ij} = O(\epsilon^2)$ and $\sum_{ijkm} l_{km} \frac{\partial\theta_{km}^\epsilon}{\partial l_{ij}} l_{ij} = O(\epsilon^2)$, so

$$\det \frac{\partial\theta_{km}}{\partial \tilde{l}_{ij}} = \epsilon^{-6} \det \frac{\partial\theta_{km}^\epsilon}{\partial l_{ij}} = \epsilon^{-6} \det{}' \frac{\partial\theta_{km}^\epsilon}{\partial l_{ij}} \frac{\sum_{(ij)(km)} l_{km} \frac{\partial\theta_{km}^\epsilon}{\partial l_{ij}} l_{ij}}{|l|^2} \quad . \tag{2.C.39}$$

Eventually, we have

$$\epsilon^{-6} \det{}' \frac{\partial\theta_{km}^\epsilon}{\partial l_{ij}} \frac{\sum_{ijkm} l_{km} \frac{\partial\theta_{km}^\epsilon}{\partial l_{ij}} l_{ij}}{|l|^2} = 12\epsilon^{-6} \frac{\det{}'\tilde{G}}{\det C} \frac{V}{|S|^2} \sum_{kmij} l_{km} l_{ij} \frac{\partial\theta_{km}^\epsilon}{\partial l_{ij}} + O(\epsilon^{-3}) \quad . \tag{2.C.40}$$

and so

$$\det{}' \frac{\partial\theta_{km}^\epsilon}{\partial l_{ij}} = \frac{12|l|^2}{|S|^2} \frac{V}{\det C} \det{}'\tilde{G} + O(\epsilon) \quad . \tag{2.C.41}$$

Now we can use the identities from appendix 2.C.1

$$\det{}'\tilde{G} = \frac{3^4}{2^2} \left(\sum_i S_i^2\right) \frac{V^4}{\prod S_i^2}, \quad \det C = 8(3!)^2 V^2 \quad . \tag{2.C.42}$$

Finally, in the limit $\epsilon \to 0$, $(\theta_{ij} = \lim \theta_{ij}^{\epsilon})$:

$$\det' \frac{\partial \theta_{km}}{\partial l_{ij}} = \frac{3^3}{2^5} \frac{|l|^2}{\prod S_i^2} V^3 \quad . \tag{2.C.43}$$

2.D Technical computations

In this appendix we give some explicit computations needed in the main body of the paper.

2.D.1 Weak equivalences

In the following we will use the notation introduced in section 2.5.2. We can compute

$$
\begin{aligned}
0 \equiv L_+ A_+^k &= k(L_+ A_+) A_+^{k-1} + A_+^{k+1} \\
&= \left(\frac{k}{2} + 1 \right) A_+^{k+1} + \frac{k}{2} A_-^2 A_+^{k-1} - k \cos 2\tilde{\theta} \ A_+^{k-1} \quad ,
\end{aligned} \tag{2.D.1}
$$

such that

$$A_-^2 A_+^{k-1} \equiv -\frac{k+2}{k} A_+^{k+1} + 2 \cos 2\tilde{\theta} \ A_+^{k-1} \quad . \tag{2.D.2}$$

Similarly, we can derive an identity by acting on A_+^k with L_-^*:

$$0 \equiv L_-^* A_+^k = (k+1) A_- A_+^k - k A_+^{k-1} \quad , \tag{2.D.3}$$

$$\implies \ A_- A_+^k \equiv \frac{k}{k+1} A_+^{k-1} \quad . \tag{2.D.4}$$

By acting again on (2.D.4) we obtain:

$$L_-^* (A_- A_+^k) = \frac{1}{2} A_+^{k+2} + \left(k + \frac{3}{2} \right) A_-^2 A_+^k - k A_- A_+^{k-1} - \cos 2\tilde{\theta} \ A_+^k \equiv 0 \quad . \tag{2.D.5}$$

Hence using (2.D.2) and (2.D.4) we have

$$
\begin{aligned}
0 &\equiv \frac{1}{2} A_+^{k+2} + \left(k + \frac{3}{2} \right) \left(-\frac{k+3}{k+1} A_+^{k+2} + 2 \cos 2\tilde{\theta} \ A_+^k \right) - k \frac{k+1}{k} A_+^k - \cos 2\theta \ A_+^k \\
&= -\frac{(k+2)^2}{k+1} A_+^{k+2} + 2(k+1) \cos 2\tilde{\theta} \ A_+^k - (k-1) A_+^{k-2} \quad .
\end{aligned} \tag{2.D.6}
$$

2.D.2 Proof of the lemma

In this section we will prove the following lemma:

Lemma 3. *For every $m \geq 0$*

$$\sum_{k \leq m} (2\beta_{m+1-k}^k + \beta_{m-k}^k) A_k i^{m+1-k} \sin \left(\theta - \frac{\pi}{2}(m-k) \right) = 0 \quad , \tag{2.D.7}$$

where

$$\beta_m^k = \frac{(-k - \frac{1}{2})_m}{m!} \in \mathbb{R} \quad , \tag{2.D.8}$$

and

$$(a)_m = a \cdot (a-1) \cdot \ldots \cdot (a - m + 1), \quad (a)_0 = 1 \quad . \tag{2.D.9}$$

To do so, we need:

Lemma 8. *The following equality holds:*

$$\frac{1}{(l \pm 1)^{k+\frac{1}{2}}} = \sum_{m \geq k} \frac{(\pm 1)^{m-k} \beta_{m-k}^k}{l^{m+\frac{1}{2}}} \quad . \tag{2.D.10}$$

Proof.

$$\frac{1}{(l \pm 1)^{k+\frac{1}{2}}} = \sum_{n=0}^{\infty} \binom{-k-\frac{1}{2}}{n} l^{-k-\frac{1}{2}-n} (\pm 1)^n = \sum_{n=0}^{\infty} \frac{(-k-\frac{1}{2})_n}{n!} \frac{1}{l^{k+n+\frac{1}{2}}} (\pm 1)^n$$

$$\stackrel{m:=k+n}{=} \sum_{m \geq k} (\pm 1)^{m-k} \frac{(-k-\frac{1}{2})_{m-k}}{(m-k)!} = \sum_{m \geq k} (\pm 1)^{m-k} \frac{\beta_{m-k}^k}{l^{m+\frac{1}{2}}} \quad . \qquad \square$$

In the following we will use Lemma 8 to prove Lemma 3:

Proof of Lemma 3. In any stationary point we have by Lemma 8

$$\tilde{P}_{l \pm 1} \equiv \sum_{k \geq 0} \frac{e^{i(l \pm 1)\theta}}{(l \pm 1)^{k+\frac{1}{2}}} A_k(\theta) \equiv \sum_{k \geq 0} e^{il\theta} \sum_{m \geq k} \frac{(\pm 1)^{m-k}}{l^{m+\frac{1}{2}}} \beta_{m-k}^k A_k(\theta) e^{\pm i\theta} \quad . \tag{2.D.11}$$

We thus have

$$l(\tilde{P}_{l+1} + \tilde{P}_{l-1} - 2\cos\theta \tilde{P}_l) \equiv \sum_{k \geq 0} \frac{e^{il\theta}}{l^{k-\frac{1}{2}}} A_k \left(\sum_{m \geq k} \frac{\beta_{m-k}^k}{l^{m-k}} (e^{i\theta} + (-1)^{m-k} e^{-i\theta}) - 2\cos\theta \right) \quad . \tag{2.D.12}$$

A simple algebraic manipulation gives

$$e^{i\theta} + (-1)^{m-k} e^{-i\theta} = \begin{cases} 2\cos\theta & \text{if } m = k \\ 2i^{m-k} \cos\left(\theta - \frac{\pi}{2}(m-k)\right) & \text{if } m > k \end{cases} , \tag{2.D.13}$$

such that we obtain:

$$l(\tilde{P}_{l+1} + \tilde{P}_{l-1} - 2\cos\theta P_l) \equiv \sum_{k \geq 0} e^{il\theta} A_k \sum_{m \geq k} \frac{2\beta_{m+1-k}^k}{l^{m+\frac{1}{2}}} i^{m+1-k} \underbrace{\cos\left(\theta - \frac{\pi}{2}(m-k+1)\right)}_{\sin\left(\theta - \frac{\pi}{2}(m-k)\right)} \quad . \tag{2.D.14}$$

We also have

$$\frac{1}{2}(\tilde{P}_{l+1} - \tilde{P}_{l-1}) = \sum_{k \geq 0} e^{il\theta} A_k \sum_{m \geq k} \frac{\beta_{m-k}^k}{l^{m+\frac{1}{2}}} i^{m+1-k} \sin\left(\theta - \frac{\pi}{2}(m-k)\right) \quad . \tag{2.D.15}$$

By combining (2.D.14) and (2.D.15), we obtain for the full recursion relation (2.5.22):

$$\sum_{k \geq 0} e^{il\theta} A_k \left(\sum_{m \geq k} \frac{2\beta_{m+1-k}^k + \beta_{m-k}^k}{l^{m+\frac{1}{2}}} i^{m+1-k} \sin\left(\theta - \frac{\pi}{2}(m-k)\right) \right)$$

$$= \sum_{m \geq 0} \frac{e^{il\theta}}{l^{m+\frac{1}{2}}} \left(\sum_{k \leq m} \left(2\beta_{m+1-k}^k + \beta_{m-k}^k \right) i^{m+1-k} A_k \sin\left(\theta - \frac{\pi}{2}(m-k)\right) \right) = O(l^{-\infty}) \quad . \tag{2.D.16}$$

Thus every single term must be zero. That ends the proof. $\qquad \square$

Expanding C_j

In the following we will expand the normalization factor $C_j = \frac{1}{4^j}\binom{2j}{j}$ up to $O(\frac{1}{j})$. Therefore we use Stirling's series for the logarithm of the factorial:

$$\ln n! = n \ln n - n + \frac{1}{2}\ln(2\pi n) + O\left(\frac{1}{n}\right) \quad . \tag{2.D.17}$$

Hence

$$\ln(C_j) = \ln\left(\frac{1}{\sqrt{\pi j}}\right) + O\left(\frac{1}{j}\right) \quad . \tag{2.D.18}$$

Therefore we obtain:

$$C_j = \frac{1}{\sqrt{\pi j}}e^{O\left(\frac{1}{j}\right)} = \frac{1}{\sqrt{\pi j}}\left(1 + O\left(\frac{1}{j}\right)\right) \quad . \tag{2.D.19}$$

Moreover, since $\ln n!$ admits a complete expansion (neglecting the first terms) in powers of $\frac{1}{n}$, also C_j can be completely expanded in powers of $\frac{1}{j}$. The same is true for an expansion in l.

2.D.3 Theta graph

In this section we explain the result that the theta graph $(C_{000}^{j_1 j_2 j_3})^2$ is equal to

$$\frac{1}{2\pi S}\left(1 + O\left(\frac{1}{l^2}\right)\right) \quad . \tag{2.D.20}$$

From [A40] we have

$$C_{000}^{j_1 j_2 j_3} = (-1)^g \frac{g!}{(g-j_1)!(g-j_2)!(g-j_3)!}\sqrt{\frac{(2g-2j_1)!(2g-2j_2)!(2g-2j_3)!}{(2g+1)!}} \quad , \tag{2.D.21}$$

where $2g = j_1 + j_2 + j_3$. We compute the expansion of $\ln C_{000}^{j_1 j_2 j_3}$ using the Stirling's formula:

$$\ln(n!) = n \ln n - n + \frac{1}{2}\ln n + \frac{1}{2}\ln 2\pi + \frac{1}{12n} + O(n^{-2}) \quad , \tag{2.D.22}$$

obtaining

$$\ln\left((-1)^g C_{000}^{j_1 j_2 j_3}\right) = -\frac{1}{4}\ln\left(\frac{(2\pi)^2}{16}(l_1+l_2+l_3)(-l_1+l_2+l_3)(l_1-l_2+l_3)(l_1+l_2-l_3)\right) \\ + O(l^{-2}) \quad . \tag{2.D.23}$$

This is exactly

$$-\frac{1}{4}\ln 4\pi^2 S^2 + O(l^{-2}) \quad , \tag{2.D.24}$$

where S is the area of the triangle with edge lengths l_i. We conclude that the theta graph $(C_{000}^{j_1 j_2 j_3})^2$ is equal to

$$\frac{1}{2\pi S}\left(1 + O\left(\frac{1}{l^2}\right)\right) \quad . \tag{2.D.25}$$

71

2.D.4 Kinetic term in equilateral case

Let us introduce

$$M_\lambda = \begin{pmatrix}
0 & a & a & a & a & a & a \\
a & b-\lambda & c-\lambda & c-\lambda & c-\lambda & c-\lambda & -\lambda \\
a & c-\lambda & b-\lambda & c-\lambda & c-\lambda & -\lambda & c-\lambda \\
a & c-\lambda & c-\lambda & b-\lambda & -\lambda & c-\lambda & c-\lambda \\
a & c-\lambda & c-\lambda & -\lambda & b-\lambda & c-\lambda & c-\lambda \\
a & c-\lambda & -\lambda & c-\lambda & c-\lambda & b-\lambda & c-\lambda \\
a & -\lambda & c-\lambda & c-\lambda & c-\lambda & c-\lambda & b-\lambda
\end{pmatrix} \quad , \tag{2.D.26}$$

where $a = -\sqrt{2}\frac{64}{81}$, $b = \frac{\sqrt{3}}{4}$ and $c = \frac{1}{2\sqrt{3}}$. In the equilateral case (all l equal to 1) the kinetic term is of the form

$$-iM_0 \quad . \tag{2.D.27}$$

Let us note that

$$\det M_\lambda = \det M_0 \neq 0 \quad , \tag{2.D.28}$$

and all M_λ are symmetric. Thus all of them have the same number of positive and negative eigenvalues. Matrix M_λ for $\lambda = c$ is similar (have the same determinant) by simultaneous permutation of rows and columns to the matrix

$$M' = \begin{pmatrix}
b-c & -c & 0 & 0 & 0 & 0 & a \\
-c & b-c & 0 & 0 & 0 & 0 & a \\
0 & 0 & b-c & -c & 0 & 0 & a \\
0 & 0 & -c & b-c & 0 & 0 & a \\
0 & 0 & 0 & 0 & b-c & -c & a \\
0 & 0 & 0 & 0 & -c & b-c & a \\
a & a & a & a & a & a & 0
\end{pmatrix} \quad . \tag{2.D.29}$$

The matrix M' restricted to its first 6 rows and columns has 3 positive and 3 negative eigenvalues. Applying the min-max principle [A51] to M' and $-M'$ shows that M' has at least three positive and three negative eigenvalues. Together with the fact that determinant is positive it shows that there are 4 positive and 3 negative eigenvalues.

Hence, the matrix of kinetic term has 4 $-i\mathbb{R}_+$ eigenvalues and 3 $i\mathbb{R}_+$ and the same is true for matrix $(-\mathcal{H}^{-1})$.

2.E Dupuis-Livine form and stationary points

In this section we will prove the following lemma:

Lemma 9. *Suppose that the integral is of the form as*

$$\int d\theta \frac{e^{i\eta}}{l^\lambda} e^S \quad , \tag{2.E.1}$$

where $S(\theta_i)$ has an asymptotic expansion around the isolated stationary point of $S_{-1}(\theta)$ of the form

$$S = S_{-1} + S_0 + S_1 + \dots \quad , \tag{2.E.2}$$

and $i^k S_k \in \mathbb{R}$ is a homogeneous function of order $-k$ in l. Then the contribution to the expansion of the integral from this stationary point has the DL property.

Proof. Let us consider the contribution from the isolated stationary point of S_{-1}. They are of the form

$$\frac{1}{\sqrt{\mathcal{H}}}e^{\tilde{S}} \quad , \tag{2.E.3}$$

where $\tilde{S}$ is given by the contraction of all connected Feynman diagrams. They are made up of vertices, given by the derivatives of $S_{\geq 0}$, connected by the propagator H, which is the inverse to (-1) times the matrix of second derivatives of S_{-1}.

$$H = \left(-\partial^2 S_{-1}\right)^{-1}, \quad \mathcal{H} = \det\left(-\partial^2 S_{-1}\right) \ . \tag{2.E.4}$$

Their contribution is computed by contracting the vertices V_k with propagators H. Since vertices are obtained from derivatives of S_m, $m \geq 0$, the homogeneous degree $\deg V_k$ of this vertex is thus m and the matrix elements of $i^{\deg V_k} V_k$ are real. Similarly iH is a real matrix and is of degree 1.

To conclude, the total contraction is thus of degree

$$\sum_k \deg V_k + n \quad , \tag{2.E.5}$$

where n is the number of propagators in the diagram. Moreover, the complete contraction multiplied by

$$i^{\sum_k \deg V_k + n} \tag{2.E.6}$$

is again real as a contraction of real matrices. This proves that expansion is still of DL form. $\quad \square$

2.F Stationary point analysis

In the paper we use an advanced version of the stationary point analysis. This appendix is intended to explain the details of this method.

Lemma 10. *Let $S(x) = i(S_{-1} + S_0) + S_0' + \sum_{i>0} S_i$ be an asymptotic expansion of the action such that*

- *S_i is of homogeneous degree $-i$ in j,*

- *S_0 and S_{-1} are real*

- *$S_{-1} + S_0$ is homogeneous in $l = j + \frac{1}{2}$*

and let x_0 be an isolated stationary point of S_{-1}. Then there is an asymptotic expansion of the contribution to the integral

$$\int dx e^S \tag{2.F.1}$$

from the neighbourhood of x_0 given as follows:

We can write the asymptotic expansion of S in homogeneous terms in l as

$$S = i\tilde{S}_{-1} + S_0' + \sum_{i>0} \tilde{S}_i \quad , \tag{2.F.2}$$

where $\tilde{S}_{-1} = S_{-1} + S_0$. Let x_1 be the stationary point of $\tilde{S}_{-1}$ obtained by perturbation of x_0 (there is exactly one such stationary point if the matrix of second derivatives of S_{-1} is non-degenerate). The asymptotic expansion of the integral is equal to

$$\frac{1}{\sqrt{\det(-H)}}e^{\sum_{i\geq-1} A_i} \tag{2.F.3}$$

where H is the matrix of second derivatives of $\tilde{S}_{-1}$ and $A_{-1} = \tilde{S}_{-1}$ evaluated on x_1. The terms A_i for $i \geq 0$ are homogeneous functions of order $-i$ in l and can be obtained from the Feynman diagram expansion with the propagator $(-H)^{-1}$ and interaction vertices given by derivatives of $\tilde{S}_i$ for $i \geq 0$.

The same fact applies when the isolated point is replaced by the isolated orbit of the symmetry group of the action.

The second fact concerns with integration over only a part of the variables:

Lemma 11. *Let $S(x, y) = iS_{-1}(x, y) + \sum_{i \geq 0} S_i$ has an isolated stationary point (x_0, y_0) with a non-degenerate matrix of second derivatives $\bar{H}$ with the property*

$$H = \begin{pmatrix} H_{xx} & H_{xy} \\ H_{xy} & H_{yy} \end{pmatrix}, \quad H_{yy} \text{ invertible }. \tag{2.F.4}$$

Then there exists a function $y(x)$ such that (in the neighbourhood of stationary point)

$$\nabla_x S_{-1} + \frac{\partial y}{\partial x} \nabla_y S_{-1} = 0 \tag{2.F.5}$$

and the asymptotic expansion of $\int dxdy\ e^S$ is equal to asymptotic expansion of

$$\int dx\ e^{\bar{S}}, \tag{2.F.6}$$

where $\bar{S}$ is obtained by asymptotic expansion of the integral $e^{\bar{S}} = \int dy\ e^S$.

2.G Feynman diagrams

In this subsection we are interested in the next to leading order in the expansion of the $6j$ symbol. We will derive expressions for S_1 in terms of Feynman diagrams. Vertices in this expansion consist of derivatives of

$$-\sum_i \frac{1}{2} \ln \sin \theta_{ij}, \quad \frac{-i}{8l_{ij}} \cot \theta_{ij}, \tag{2.G.1}$$

and higher than second derivatives of $|l|\rho \det \tilde{G}$ with respect to ρ and θ_{ij}. Each propagator contributes a weight $|l|^{-1}$.

We only evaluate closed diagrams, so if the diagram is made up of vertices of valency n_k, i.e. the n_k-th derivative of a function with weight $|l|^{\alpha_k}$, then the scaling behaviour of the whole diagram is as

$$|l|^{\sum_k \left(\alpha_k - \frac{n_k}{2} \right)}. \tag{2.G.2}$$

The only vertices that can contribute up to order $|l|^{-1}$ are thus

Vertex	$-\frac{1}{2} \ln \sin \theta_{ij}$	$-\frac{1}{2} \cot \theta_{ij}$	$-\frac{1}{2} \frac{\partial}{\partial \theta_{ij}} \cot \theta_{ij}$	$-\frac{i}{8l_{ij}} \cot \theta_{ij}$	$i|l|\partial^3 \rho \det \tilde{G}$	$i|l|\partial^4 \rho \det \tilde{G}$
Valency	0	$1_{(ij)}$	$2_{(ij)(ij)}$	0	3	4
Order	$|l|^0$	$|l|^{-1/2}$	$|l|^{-1}$	$|l|^{-1}$	$|l|^{-1/2}$	$|l|^{-1}$

Note that the only diagram that is real (up to the order $|l|^{-1}$) is just the first vertex (being of order 0). Furthermore, this is also the only contribution of order $|l|^0$. All other diagrams are purely imaginary and of order $|l|^{-1}$.

2.H Relation to spin-network kernel formula

We will prove that (for $j \in \mathbb{Z}$)

$$\int_0^\pi \frac{d\phi_1}{\pi} \left(e^{i\theta} \cos\phi_1 \cos\phi_2 + e^{-i\theta} \sin\phi_1 \sin\phi_2 \right)^{2j} = \frac{1}{4^j} \binom{2j}{j} \left(e^{i2\theta} \cos^2\phi_2 + e^{-i2\theta} \sin^2\phi_2 \right)^j \quad . \tag{2.H.1}$$

It is straightforward to check that

$$e^{i2\theta} \cos^2\phi_2 + e^{-i2\theta} \sin^2\phi_2 = \cos 2\theta + i \sin 2\theta \cos 2\phi_2 \quad . \tag{2.H.2}$$

In this way we obtain the formula from [A29].

To prove (2.H.1), we use the following formulas:

$$2 \int_0^{\pi/2} d\phi \ \sin^{2\alpha}\phi \cos^{2\beta}\phi = \frac{\Gamma\left(\alpha + \frac{1}{2}\right) \Gamma\left(\beta + \frac{1}{2}\right)}{\Gamma(\alpha + \beta + 1)} \quad , \tag{2.H.3}$$

$$\Gamma(n+1) = n!, \quad \Gamma\left(n + \frac{1}{2}\right) = \frac{(2n)!}{4^n n!}\sqrt{\pi} \quad . \tag{2.H.4}$$

In the case that $k, l \in \mathbb{N}$, these formulas can be simplified to:

$$\int_0^\pi d\phi \ \sin^{2k}\phi \cos^{2l}\phi = \frac{(2k)!(2l)!\pi}{4^{k+l} k! l! (k+l)!} \quad , \tag{2.H.5}$$

$$\int_0^\pi d\phi \ \sin^{2k+1}\phi \cos^{2l+1}\phi = 0 \quad . \tag{2.H.6}$$

Expanding the left hand side of (2.H.1) and using these formulas we have:

$$\int_0^\pi \frac{d\phi_1}{\pi} \left(e^{i\theta} \cos\phi_1 \cos\phi_2 + e^{-i\theta} \sin\phi_1 \sin\phi_2 \right)^{2j} = \tag{2.H.7}$$

$$\sum_{n=0}^{2j} \binom{2j}{n} e^{i(2j-2n)\theta} \cos^{2j-n}\phi_2 \sin^n\phi_2 \int_0^\pi \frac{d\phi_1}{\pi} \cos^{2j-n}\phi \sin^n\phi \quad . \tag{2.H.8}$$

This is equal to $(k := 2n)$

$$\sum_{k=0}^{j} \binom{2j}{2k} e^{i(j-2k)2\theta} \cos^{2j-2k}\phi_2 \sin^{2k}\phi_2 \frac{1}{\pi} \frac{(2k)!(2j-2k)!\pi}{4^j k! (j-k)! j!} \quad . \tag{2.H.9}$$

The factors in j and k can be rewritten in terms of binomial coefficients

$$\binom{2j}{2k} \frac{(2k)!(2j-2k)!}{4^j k! (j-k)! j!} = \frac{(2j)!}{4^j k! (j-k)! j!} = \frac{1}{4^j} \binom{2j}{j} \binom{j}{k} \quad , \tag{2.H.10}$$

such that we obtain the final result:

$$\frac{1}{4^j} \binom{2j}{j} \sum_{k=0}^{j} \binom{j}{k} \left(e^{i2\theta} \cos^2\phi_2 \right)^{j-k} \left(e^{-i2\theta} \sin^2\phi_2 \right)^k =$$

$$= \underbrace{\frac{1}{4^j} \binom{2j}{j}}_{C_j} \left(e^{i2\theta} \cos^2\phi_2 + e^{-i2\theta} \sin^2\phi_2 \right)^j \quad . \tag{2.H.11}$$

This explains the occurrence of C_j in our formulas, which is absent in integral kernel approach [A29].

References

[A1] A. Perez, "Spin foam models for quantum gravity," *Class.Quant.Grav.* **20** (2003) R43, `arXiv:gr-qc/0301113 [gr-qc]`.

[A2] A. Perez, "The Spin Foam Approach to Quantum Gravity," *Living Rev.Rel.* **16** (2013) 3, `arXiv:1205.2019 [gr-qc]`.

[A3] C. Rovelli, *Quantum Gravity*. Cambridge University Press, 2004.

[A4] J. C. Baez, "Spin foam models," *Class.Quant.Grav.* **15** (1998) 1827–1858, `arXiv:gr-qc/9709052 [gr-qc]`.

[A5] G. Ponzano and T. Regge, *Semiclassical limit of Racah coefficients, in: Spectroscopy and group theoretical methods in physics*. North Holland Publ. Co., Amsterdam, 1968.

[A6] J. W. Barrett and I. Naish-Guzman, "The Ponzano-Regge model," *Class.Quant.Grav.* **26** (2009) 155014, `arXiv:0803.3319 [gr-qc]`.

[A7] V. G. Turaev and O. Y. Viro, "State sum invariants of 3 manifolds and quantum 6j symbols," *Topology* **31** (1992) 865–902.

[A8] J. W. Barrett and L. Crane, "Relativistic spin networks and quantum gravity," *J.Math.Phys.* **39** (1998) 3296–3302, `arXiv:gr-qc/9709028 [gr-qc]`.

[A9] J. W. Barrett and R. M. Williams, "The Asymptotics of an amplitude for the four simplex," *Adv.Theor.Math.Phys.* **3** (1999) 209–215, `arXiv:gr-qc/9809032 [gr-qc]`.

[A10] J. C. Baez, J. D. Christensen, and G. Egan, "Asymptotics of 10j symbols," *Class.Quant.Grav.* **19** (2002) 6489, `arXiv:gr-qc/0208010 [gr-qc]`.

[A11] L. Freidel and D. Louapre, "Asymptotics of 6j and 10j symbols," *Class.Quant.Grav.* **20** (2003) 1267–1294, `arXiv:hep-th/0209134 [hep-th]`.

[A12] J. Engle, E. Livine, R. Pereira, and C. Rovelli, "LQG vertex with finite Immirzi parameter," *Nucl.Phys.* **B799** (2008) 136–149, `arXiv:0711.0146 [gr-qc]`.

[A13] L. Freidel and K. Krasnov, "A New Spin Foam Model for 4d Gravity," *Class.Quant.Grav.* **25** (2008) 125018, `arXiv:0708.1595 [gr-qc]`.

[A14] F. Conrady and L. Freidel, "On the semiclassical limit of 4d spin foam models," *Phys.Rev.* **D78** (2008) 104023, `arXiv:0809.2280 [gr-qc]`.

[A15] J. W. Barrett, W. J. Fairbairn, and F. Hellmann, "Quantum gravity asymptotics from the SU(2) 15j symbol," *Int.J.Mod.Phys.* **A25** (2010) 2897–2916, `arXiv:0912.4907 [gr-qc]`.

[A16] J. W. Barrett, R. Dowdall, W. J. Fairbairn, F. Hellmann, and R. Pereira, "Lorentzian spin foam amplitudes: Graphical calculus and asymptotics," *Class.Quant.Grav.* **27** (2010) 165009, `arXiv:0907.2440 [gr-qc]`.

[A17] J. W. Barrett, R. Dowdall, W. J. Fairbairn, H. Gomes, F. Hellmann, *et al.*, "Asymptotics of 4d spin foam models," *Gen.Rel.Grav.* **43** (2011) 2421–2436, `arXiv:1003.1886 [gr-qc]`.

[A18] J. W. Barrett, R. Dowdall, W. J. Fairbairn, H. Gomes, and F. Hellmann, "Asymptotic analysis of the EPRL four-simplex amplitude," *J.Math.Phys.* **50** (2009) 112504, `arXiv:0902.1170 [gr-qc]`.

[A19] R. Dowdall, H. Gomes, and F. Hellmann, "Asymptotic analysis of the Ponzano-Regge model for handlebodies," *J.Phys.* **A43** (2010) 115203, `arXiv:0909.2027 [gr-qc]`.

[A20] A. Perelomov, *Generalized coherent states and their applications.* Springer, Berlin, 1986.

[A21] L. Hörmander, *The analysis of linear partial differential operators I.* Springer-Verlag, 1990.

[A22] T. Regge, "General relativity without coordinates," *Nuovo Cim.* **19** (1961) 558.

[A23] R. M. Williams, "Recent progress in Regge calculus," *Nucl.Phys.Proc.Suppl.* **57** (1997) 73–81, `arXiv:gr-qc/9702006 [gr-qc]`.

[A24] J. Roberts, "Classical 6j-symbols and the tetrahedron," *Geom. Topol.* **3** (1999) 21–66, `arXiv:math-ph/9812013 [math-ph]`.

[A25] V. Aquilanti, H. M. Haggard, A. Hedeman, N. Jeevanjee, R. G. Littlejohn, *et al.*, "Semiclassical Mechanics of the Wigner 6j-Symbol," *J.Phys.* **A45** (2012) 065209, `arXiv:1009.2811 [math-ph]`.

[A26] R. Gurau, "The Ponzano-Regge asymptotic of the 6j symbol: An Elementary proof," *Annales Henri Poincare* **9** (2008) 1413–1424, `arXiv:0808.3533 [math-ph]`.

[A27] B. Dittrich and S. Steinhaus, "Path integral measure and triangulation independence in discrete gravity," *Phys.Rev.* **D85** (2012) 044032, `arXiv:1110.6866 [gr-qc]`.

[A28] H. W. Hamber and R. M. Williams, "On the measure in simplicial gravity," *Phys.Rev.* **D59** (1999) 064014, `arXiv:hep-th/9708019 [hep-th]`.

[A29] J. M. Garcia-Islas, "(2+1)-dimensional quantum gravity, spin networks and asymptotics," *Class.Quant.Grav.* **21** (2004) 445–464, `arXiv:gr-qc/0307054 [gr-qc]`.

[A30] M. Dupuis and E. R. Livine, "Pushing Further the Asymptotics of the 6j-symbol," *Phys.Rev.* **D80** (2009) 024035, `arXiv:0905.4188 [gr-qc]`.

[A31] M. Dupuis and E. R. Livine, "The 6j-symbol: Recursion, Correlations and Asymptotics," *Class.Quant.Grav.* **27** (2010) 135003, `arXiv:0910.2425 [gr-qc]`.

[A32] J. W. Barrett, "First order Regge calculus," *Class.Quant.Grav.* **11** (1994) 2723–2730, `arXiv:hep-th/9404124 [hep-th]`.

[A33] B. Dittrich and S. Speziale, "Area-angle variables for general relativity," *New J.Phys.* **10** (2008) 083006, `arXiv:0802.0864 [gr-qc]`.

[A34] J. F. Plebański, "On the separation of einsteinian substructures," *J. Math. Phys.* **18** (1977) 2511.

[A35] V. Bonzom, E. R. Livine, M. Smerlak, and S. Speziale, "Towards the graviton from spinfoams: The Complete perturbative expansion of the 3d toy model," *Nucl.Phys.* **B804** (2008) 507–526, `arXiv:0802.3983 [gr-qc]`.

[A36] V. Bonzom, E. R. Livine, and S. Speziale, "Recurrence relations for spin foam vertices," *Class.Quant.Grav.* **27** (2010) 125002, `arXiv:0911.2204 [gr-qc]`.

[A37] V. Bonzom and E. R. Livine, "A New Recursion Relation for the 6j-Symbol," *Annales Henri Poincare* **13** (2012) 1083–1099, `arXiv:1103.3415 [gr-qc]`.

[A38] R. Penrose, *Angular momentum: An approach to combinatorial spacetime in Quantum Theory and Beyond.* Cambridge University Press, Cambridge, 1971.

[A39] L. H. Kauffman and S. Lins, "Temperley-Lieb Recoupling Theory and Invariants of 3-Manifolds," *Annals of Mathematics Studies* **134** (1994) .

[A40] D. A. Varshalovich, A. N. Moskalev, and V. K. Khersonskii, *Quantum Theory of Angular Momemtum.* World Scientific, 1988.

[A41] B. Dittrich, L. Freidel, and S. Speziale, "Linearized dynamics from the 4-simplex Regge action," *Phys.Rev.* **D76** (2007) 104020, `arXiv:0707.4513 [gr-qc]`.

[A42] S. L. Kokkendorff, "Polar duality and the generalized law of sines," *Journal of Geometry* **86** no. 1-2, (2007) 140–149.

[A43] B. Bahr and B. Dittrich, "Regge calculus from a new angle," *New J.Phys.* **12** (2010) 033010, `arXiv:0907.4325 [gr-qc]`.

[A44] U. Pachner, "Konstruktionsmethoden und das kombinatorische Homöomorphieproblem für Triangulationen kompakter semilinearer Mannigfaltigkeiten," *Abh. Math. Sem. Univ. Hamburg* **57** (1986) 69.

[A45] U. Pachner, "P.L. Homeomorphic Manifolds are Equivalent by Elementary Shellings," *Europ. J. Combinatorics* **12** (1991) 129–145.

[A46] W. Kamiski and S. Steinhaus, "The BarrettCrane model: asymptotic measure factor," *Class.Quant.Grav.* **31** (2014) 075014, `arXiv:1310.2957 [gr-qc]`.

[A47] J. W. Alexander and G. B. Briggs, "On types of knotted curves," *Ann. of Math.* **28 (1-4)** (1926/27) 562–586.

[A48] K. Reidemeister, "Elementare Begründung der Knotentheorie," *Abh. Math. Sem. Univ. Hamburg* **5** (1926) 24–32.

[A49] I. Macdonald, "The volume of a compact Lie group," *Inventiones Mathematicae* **56** (1980) 93–95.

[A50] R. Sorkin, "The electromagnetic field on a simplicial net," *J. Math. Phys.* **16** (1975) 2432–2440. [*Erratum-ibid.* **19** (1978) 1800].

[A51] M. Reed and B. Simon, *Methods of Modern Mathematical Physics Vol I.* Academic Press Inc., 1980.

3 The Barrett-Crane model: asymptotic measure factor

Wojciech Kamiński[1,2] and Sebastian Steinhaus[2]

[1]Instytut Fizyki Teoretycznej, Uniwersytet Warszawski
ul. Hoża 69, 00-681, Warszawa, Poland

[2]Perimeter Institute for Theoretical Physics
31 Caroline Street North, Waterloo, Ontario, N2L 2Y5 Canada

Abstract

The original spin foam model construction for 4D gravity by Barrett and Crane suffers from a few troubling issues. In the simple examples of the vertex amplitude they can be summarized as the existence of contributions to the asymptotics from non geometric configurations. Even restricted to geometric contributions the amplitude is not completely worked out. While the phase is known to be the Regge action, the so called measure factor has remained mysterious for a decade. In the toy model case of the $6j$ symbol this measure factor has a nice geometric interpretation of $V^{-1/2}$ leading to speculations that a similar interpretation should be possible also in the 4D case. In this paper we provide the first geometric interpretation of the geometric part of the asymptotic for the spin foam consisting of two glued 4-simplices (decomposition of the 4-sphere) in the Barrett-Crane model in the large internal spin regime.

3.1 Introduction

In spin foam models [B1–B5] the asymptotic expansion of the vertex amplitude in the large spin limit is an important test for their connection to (discrete) gravity. The expansion of the known vertex amplitudes can be written in the form

$$\sum_{\alpha} A_\alpha(\{j_i\}) e^{iS_\alpha(\{j_i\})} \left(1 + O\left(|j|^{-1}\right) \right) \quad , \tag{3.1.1}$$

where $O(|j|^{-1})$ denotes more suppressed terms in the expansion. The sum over indices α indicates that the asymptotic expansion usually contains contributions from different sectors, which differ in their geometric and physical interpretation. According to common terminology we call S_α the phase or the action and A_α the measure factor[1].

The value of the asymptotic expansion lies in its geometric interpretation, for example, in the case of the $6j$ symbol, the expansion consists of two terms (see for example [B6–B9] for derivations). For both the phase is equal to the Regge action (up to a sign) associated to tetrahedra built from the spin labels. This strongly supports the claim that the Ponzano-Regge model [B10, B11], which utilizes SU(2) $6j$ symbols as its basic building block, is a model of 3D quantum gravity. The modern 4D spin foam models, such as the Barrett-Crane- [B12], EPRL- [B13] or FK-model [B14], were invented as generalizations of this case adapted to incorporate the so-called simplicity constraints. Similar results as for the 3D model were obtained for the action of these models [B8, B15–B20], which is a significant support of the relation of these models to Quantum Gravity.

However, the understanding of the asymptotic expansion is far from complete: Besides the troubling fact that non-geometric configurations are contributing, even for geometric contributions the measure factors, which play an important role in asymptotic expansions, pose a challenge. From the simple example of the $6j$ symbol, one expects that they should be given in simple geometric terms. However, known spin foam amplitudes resist attempts to find such formulas. Whereas the phase contribution to the asymptotics is well known, the measure factor has remained mysterious so far. In this paper we are considering the simplest model introduced by Barrett and Crane (BC model) in the case of two glued 4-simplices.

It is known that this model suffers from several issues: One of them is the presence of the topological BF sector common to all spin foams [B8, B16, B17, B21], but in addition it lacks gluing constraints [B14, B22, B23]. The faces along which the simplices are glued have the same area yet their shapes differ in general. The theory obtained in a semiclassical limit, called area Regge calculus [B24], is troubled by metric discontinuities and vanishing deficit angles [B25, B26]. For this reason the model is now commonly disregarded as a viable model for Quantum Gravity, for a recent discussion on this see [B27] and [B28]. This naturally raises the question why we are considering it at all. The simple yet honest answer would be that this is the only model we can cope with, but there is a more profound reason: It is known that the geometric sector of the BC model is supported on the same configurations as the flipped Freidel-Krasnov model ($\overline{\text{FK}}$ model in [B29]). In the latter the γ-flatness property [B29] takes its extreme form as complete SO(4) flatness: The deficit angles on all bulk faces have to vanish like in the BC model. Recently this led to hopes that a semiclassical limit exists, for which this property can assure large scale geometricity, i.e. small curvature on small scales (see [B30] for discussion of a double-scaling limit for the EPRL model in which the representation labels diverge, but curvature goes to zero) [2]. In this context the BC model appears to be a nice 'test and proving ground' [B35]. We hope that this result can provide some insight for more physical models.

---

[1] Here we refer to the asymptotic measure factor of the vertex amplitude. This is not to be confused with the face and edge amplitudes (also called measure factors) of the spin foam model.

[2] To reach this regime one needs, however, more refined tools. For first steps in this direction using coarse-graining techniques see [B31–B34].

In this work we mainly focus on the amplitude of the BC model associated to the geometry of two 4–simplices glued along all of their tetrahedra, forming a triangulation of the 4-dimensional sphere that is given by the product of two vertex amplitudes. The asymptotic behaviour of the latter were analysed in [B15, B16] and finally in [B8]. For simplicity we assume that both face and edge amplitudes are equal to one, even though their importance for the geometric interpretation has been emphasized in [B28]. Our result is only slightly affected by this choice.

As a starting point for our derivation, we will use formula (125) from ref. [B8] for the $10j$ symbol, i.e. the BC amplitude of a single 4-simplex (see [B9] for the derivation of the change of measure, the normalisation factor is equal to $\frac{2^4|O(4)|}{|S_3|^5} = \frac{2}{\pi^6}$):

$$\frac{2}{\pi^6} \int_{[0,\pi]^{10} \cap \{\tilde{G} \geq 0\}} \prod_{i<j} d\theta_{ij} \; \delta(\det \tilde{G}) \prod_{ij} \sin \theta_{ij} \prod_{i<j} \chi_{j_{ij}}(\theta_{ij}) \quad . \tag{3.1.2}$$

Let us briefly explain the notation: Each tetrahedron of the 4–simplex is labelled by an integer $i \in \{1, 2, \ldots, 5\}$. Each face is shared by two tetrahedra and is hence labelled by a pair of indices i, j. Attached to the faces are both the spins j_{ij}, denoting irreducible representations of SU(2), and the exterior dihedral angles θ_{ij}. The function $\chi_j(\theta)$ denotes the SU(2) character function (3.3.1) and $\tilde{G}$ denotes the angle Gram matrix defined in appendix 3.A.1.

Under the necessary assumption that $\forall_i \sum_j j_{ij} \in \mathbb{N}$, the integral (3.1.2) is invariant under the action of the symmetry group $\mathbb{Z}_2^4$, which has the following mutually commuting generators of order 2:

$$g_i \colon \forall_j \; \theta_{ij} \to \pi - \theta_{ij} \; . \tag{3.1.3}$$

with the relation $\prod_i g_i = 1$. Several regions of the domain of integration contribute to the asymptotics:

- Certain values of θ_{ij} on the boundary of the integration domain form the degenerate sector. The contribution from this region may be even dominating in the amplitude, yet it does not correspond to a 4-geometry, but to a so-called vector geometry or the Hodge dual of that [B21].

- θ_{ij} are the angles between the normals in $\mathbb{R}^4$, such that the 4-simplex with tetrahedra perpendicular to the normals (that is determined uniquely up to a scale) has face areas $A_{ij} = 2j_{ij} + 1$. Given only the set of areas $\{A_{ij}\}$, there might be several configurations of angles $\{\theta_{ij}\}$ contributing.

Since we are considering two 4-simplices, we have the same distinction for each of them. However, even if we restrict to non-degenerate configurations, the shapes (of the glued tetrahedra) do not need to match; this is a known problem of the BC model. From now on, we will denote the configurations with matching shapes as geometric and neglect all other, i.e. non-geometric, contributions to the amplitude, even though we are aware of their existence.

We will now proceed to present our result and its derivation in the next sections.

3.2 Main result

Our main result can be formulated as follows. The geometric part of the leading asymptotic expansion of the spin foam built from two glued 4-simplices with faces $A_{ij} = 2j_{ij} + 1$ is given by the formula[3]

$$\frac{3^3}{2^{23}\pi^3} \int_{\mathcal{C}} \prod_{i<j} dl_{ij}^2 \prod_{i<j} \delta(A_{ij}(l)^2 - A_{ij}^2) \; \frac{\prod_i W_i'^2}{V'^7} \cos^2\left(\sum_{i<j} A_{ij}(l)\theta_{ij}(l) - \frac{\pi}{4}\right) \quad , \tag{3.2.1}$$

---

[3] We integrate over all sets of lengths l_{ij} that form a 4-simplex.

where W'_i is the volume of ith tetrahedron, and V' is the volume of the 4-simplex. The integration region $\mathcal{C}$ consists of all geometric lengths (see appendix 3.A.2). The formula is valid for generic configurations A_{ij} such that the map from length variables $\{l_{ij}\} \to \{A_{ij}\}$ is locally invertible for all l_{ij} with given face areas constructed from them[4], and the reconstructed 4-simplices are non degenerate. If the maps $\{l_{ij}\} \to \{A_{ij}\}$ are not locally invertible, this contribution to the total amplitude is less suppressed as the Hessian has an additional null eigenvector. We leave the investigation of these cases for future research.

Although this expression appears to be complicated at first sight, it is possible to perform the integration:

$$\frac{3^3}{2^{23}\pi^3} \sum \det\left(\frac{\partial l_{ij}^2}{\partial A_{ij}^2}\right) \frac{\prod_i W_i'^2}{V'^7} \cos^2\left(\sum_{i<j} A_{ij}(l)\theta_{ij}(l) - \frac{\pi}{4}\right) \quad, \tag{3.2.2}$$

where the summation is with respect to all possible configurations of lengths l_{ij}, from which the given areas can be constructed. Please note that the only non explicit factor is $\det \frac{\partial l_{ij}^2}{\partial A_{ij}^2}$, which corresponds to the change of variables.

The result in the form (3.2.2) can be simply translated into the geometric contribution to the asymptotic expansion for a single 4-simplex amplitude

$$\frac{3^{\frac{3}{2}}}{2^{\frac{23}{2}}\pi^{\frac{3}{2}}} \sum \pm \sqrt{\det\left(\frac{\partial l_{ij}^2}{\partial A_{ij}^2}\right)} \frac{\prod_i W_i'}{V'^{\frac{7}{2}}} \cos\left(\sum_{i<j} A_{ij}(l)\theta_{ij}(l) - \frac{\pi}{4}\right) \quad, \tag{3.2.3}$$

The apparent sign ambiguity needs further research.

3.2.1 Comments

Before we discuss the derivation of this result, we would like to briefly comment on two subjects: first the choice of the examined triangulation and second the omittance of other contributing sectors.

The natural question arising is why we are considering a triangulation of the sphere and not a single 4-simplex. In fact, the latter can be deduced from the second version of our result (3.2.2) (with a sign ambiguity). Then the only non-explicit term is the Jacobian $\det \frac{\partial l_{ij}^2}{\partial A_{ij}^2}$. Surprisingly in the case of the 4-sphere this Jacobian can be absorbed by imposing area data as constraints, such that the asymptotic formula can be simply stated in terms of length variables.

The origin of the phenomenon that the asymptotic formula for the triangulated 4–sphere is simpler than the one for a single 4–simplex is obscure to us. For general spin foam models it is well known that the measure factors, contrary to the phase amplitudes, are inflicted by the spread of the boundary states. Thus one would expect to find nicer results for closed triangulations. Of course, this argument does not apply to the BC model, because its boundary space structure is trivial, i.e. the intertwiner space is 1–dimensional and there is no choice of the spread of the boundary state. Instead, we rather expect the imposition of the area data as constraints to be the root of this property.

The second issue we would like to address is that our result concerns only a part of the contribution to the asymptotic behaviour, yet it has a clear numerical meaning at least in the case of nondegenerate geometries. Precisely, if the asymptotic formula (to leading order) is given by

$$\sum_\alpha A_\alpha(\{j_i\}) e^{iS_\alpha(\{j_i\})} \quad, \tag{3.2.4}$$

---

[4]Please note the subtlety in the notation: A_{ij} denotes the area of the triangle obtained from one 4-simplex by removing the vertices i and j, whereas l_{ij} actually is the edge connecting i and j.

where all phases S_α are different functions of the data, then every term has a separate meaning and is interesting by itself.

In the case of the Barrett-Crane model, the additional contributions omitted in our derivation are known to some extent. They can be treated by the method of coherent states or by the Kirillov character formula [B21]. For the case of a single simplex, their phase turns out to be zero. Thus the additional contributions to our asymptotic formula are indeed of the form (3.2.4) with:

- $S_\alpha = \pm S_{\text{Regge}} \pm S'_{\text{Regge}}$ for non–matching configurations and thus differing Regge actions,

- $S_\alpha = 0$ for matching configurations, but opposite signs or non–geometric configurations and finally

- $S_\alpha = \pm S_{\text{Regge}}$ if one of the simplices is in a non–geometric configuration.

Our result can thus be regarded as a derivation of the measure factors for the terms in the asymptotic formula with phases $\pm 2S_{\text{Regge}}$.

Before we discuss this result further, we will briefly present its derivation in the following two sections.

3.3 Derivation

In this section we sketch our proof, leaving technical details to the next section. In order to simplify notation and to avoid keeping track of numerical factors, we absorb the combinatorial factors into the definition of the volume of simplices, e.g. V is 4! times the volume of a 4-simplex and W_i is 3! times the volume of the ith tetrahedron, A_{ij} denotes the area of the face. Faces are labelled by two vertices, i.e. those which do not belong to the face. From now on, we use the convention that $\vec{l}$, $\vec{A}$, $\vec{W}$ denote vectors consisting of all lengths, areas and tetrahedra respectively. For any vector $\vec{m}$, $|m|$ denotes its Cartesian length. Since the dihedral angles of a 4-simplex sit on the faces of the simplex, i.e. the triangles, they carry the same labels as the faces.

3.3.1 Stationary point conditions

Starting from (3.1.2), we use the character formula (θ is the SU(2) angle)

$$\chi_j(\theta) = \frac{\sin(2j+1)\theta}{\sin\theta} = \frac{e^{i(2j+1)\theta} - e^{-i(2j+1)\theta}}{2i\sin\theta} \tag{3.3.1}$$

to divide the integral into several parts (the sines from (3.1.2) cancel with the sines from the integral)

$$\frac{\pm 1}{2^{10}}\frac{2}{\pi^6} \int_{[0,\pi]^{10}} \prod_{i<j} d\theta_{ij}\; \delta(\det \tilde{G})\; e^{i\sum \pm(2j_{ij}+1)\theta_{ij}} = \pm \frac{|A|}{2^{10}\pi^7} \int_{[0,\pi]^{10}} \prod_{i<j} d\theta_{ij} \int d\rho\, e^{i\left(\sum \pm A_{ij}\theta_{ij} - |A|\rho \det \tilde{G}\right)} \tag{3.3.2}$$

to which stationary point method can be applied – boundary terms contribute non geometric asymptotics as shown in [B8] and will be omitted. The stationary phase conditions are:

- For $\frac{\partial S}{\partial \theta_{ij}} = 0$:

$$\pm A_{ij} = \lambda \frac{\partial \det \tilde{G}}{\partial \theta_{ij}} \quad, \tag{3.3.3}$$

where we introduced notation $\lambda := |A|\rho$.

- For $\frac{\partial S}{\partial \rho} = 0$:

$$\det \tilde{G} = 0 \quad. \tag{3.3.4}$$

The latter condition ensures that θ_{ij} are geometric angles. In fact, the vanishing of the determinant of the angle Gram matrix ensures that the flat 4-simplex with the given angles between normals (associated to tetrahedra) exists. This simplex is determined uniquely up to rotations, parity transformations and scaling. However these normals are not necessarily outward pointing. The before mentioned generators of the $\mathbb{Z}_2^4$ symmetry correspond to the change of normals [5]

$$\tilde{g}_i \colon n_i \to -n_i \quad . \tag{3.3.5}$$

Using this symmetry we can restrict our consideration to the case where all normals are outward pointing. The contribution from the other stationary points are the same and are taken into account by multiplication of the result by 2^4.

Under the restriction that the normals to the tetrahedra should be outward pointing, every 4–simplex determined by the normals (that is unique up to a scale) satisfies:

$$A'_{ij} = \lambda' \frac{\partial \det \tilde{G}}{\partial \theta_{ij}}, \quad \lambda' = -\frac{\prod W_i^2}{4V^7} \quad . \tag{3.3.6}$$

The details of the derivation are similar to [B9] and are also briefly discussed in section 3.4. It turns out [B8] that under such restriction only two of the integrals actually have a point of stationary phase, namely if all signs are either '+' or '−'; then the action in (3.3.2) is the first order Regge action [B36]. Their respective contributions are related by complex conjugation, such that the final result is purely real. Hence, we will consider only the '+' sign case. The calculation for the '−' sign case works analogously. In this case the stationary point conditions (3.3.3) and (3.3.4) are solved by the angles θ_{ij} between outward pointing normals to the 4-simplex with face areas $\{A_{ij}\}$ and the Lagrange multiplier λ'.

3.3.2 The hessian

Most of the calculations following in the remaining sections of this work were derived in great detail for the 3D case [B9] and can be performed almost analogously in the situation under discussion. Even though the calculations are presented in a self-consistent way, we highly recommend that interested readers also study [B9] to better understand the crucial ideas and background information of this approach.

The matrix of second derivatives has the form

$$\mathcal{H} := -i|A| \begin{pmatrix} 0 & \frac{\partial \det \tilde{G}}{\partial \theta_{ij}} \\ \frac{\partial \det \tilde{G}}{\partial \theta_{km}} & \rho \frac{\partial \det \tilde{G}}{\partial \theta_{ij} \partial \theta_{km}} \end{pmatrix} \tag{3.3.7}$$

and its inverse is given by (c is a constant)

$$\mathcal{H}^{-1} = i \begin{pmatrix} \frac{c}{|A|^2} & \frac{1}{|A|} \frac{\partial \lambda}{\partial A_{ij}} \\ \frac{1}{|A|} \frac{\partial \lambda}{\partial A_{kl}} & \frac{\partial \theta_{ij}}{\partial A_{kl}} \end{pmatrix} \quad . \tag{3.3.8}$$

We know that $\frac{\partial \theta_{ij}}{\partial A_{kl}}$ is symmetric and has exactly one null eigenvector $\vec{A}$, since given the dihedral angles, the 4-simplex is determined up to scale: We can scale all edges by ξ (then all areas are scaled by ξ^2) to obtain a 4-simplex with the same dihedral angles. In fact, this is the only remaining freedom, once all θ_{ij} are fixed. We can write the matrix in the basis with $\frac{\vec{A}}{|A|}$ as a basis vector

$$i \begin{pmatrix} \frac{c}{|A|^2} & \frac{1}{|A|} \frac{\partial \lambda}{\partial A} & \cdots & \cdots \\ \frac{1}{|A|} \frac{\partial \lambda}{\partial A} & 0 & 0 & 0 \\ \vdots & 0 & \frac{\partial \theta_{ij}}{\partial A_{kl}} & \vdots \\ \vdots & 0 & \cdots & \ddots \end{pmatrix} \quad , \tag{3.3.9}$$

---

[5] Notice that $\prod \tilde{g}_i$ acts as an element of $O(4)$ and vectors n_i are determined only up to $O(4)$ transformations.

where $\frac{\partial}{\partial A} := \frac{A_{ij}}{|A|}\frac{\partial}{\partial A_{ij}}$[6]. The determinant of $(-\mathcal{H}^{-1})$ is thus equal to

$$\det(-\mathcal{H}^{-1}) = -(-i)^{11}\Big(\underbrace{\frac{1}{|A|}\frac{\partial\lambda}{\partial A}}_{=\frac{\lambda}{|A|^2}}\Big)^2 \det'\frac{\partial\theta_{ij}}{\partial A_{kl}} \quad , \qquad (3.3.10)$$

where $\det'\frac{\partial\theta_{ij}}{\partial A_{kl}}$ is the determinant of the matrix $\frac{\partial\theta_{ij}}{\partial A_{kl}}$ restricted to the subspace orthogonal to the vector $\vec{A}$ (the only null eigenvector of this symmetric matrix)[7]. Now we will expand

$$\frac{\partial\theta_{ij}}{\partial A_{kl}} = \frac{\partial\theta_{ij}}{\partial l_{mn}}\frac{\partial l_{mn}}{\partial A_{kl}} \quad . \qquad (3.3.11)$$

Scaling symmetry (see appendix 3.A.3) ensures that $A_{kl}\frac{\partial l_{ij}}{\partial A_{kl}} = \frac{1}{2}l_{ij}$. A similar argument of scaling shows that $\vec{l}$ is a null eigenvector of $\Big(\frac{\partial\theta_{ij}}{\partial l_{kl}}\Big)$. As before, we write the matrix $\frac{\partial l_{ij}}{\partial A_{kl}}$ in the adapted basis (with the normalized vectors $\frac{\vec{l}}{|l|}$ and $\frac{\vec{A}}{|A|}$)

$$\begin{pmatrix} \frac{|l|}{2|A|} & 0 & \cdots & 0 \\ \hline 0 & & & \\ \vdots & & \frac{\partial l_{ij}}{\partial A_{kl}} & \\ 0 & & & \end{pmatrix} \quad . \qquad (3.3.12)$$

Notice moreover that[8]

$$A_{ij}\frac{\partial\theta_{ij}}{\partial l_{kl}} = l_{kl}\frac{\partial\theta_{ij}}{\partial l_{kl}} = 0 \quad , \qquad (3.3.13)$$

thus working in the bases with vectors $\frac{\vec{l}}{|l|}$ and $\frac{\vec{A}}{|A|}$ we can prove (using (3.3.11)) that

$$\det'\frac{\partial\theta_{ij}}{\partial A_{kl}} = \det'\frac{\partial\theta_{ij}}{\partial l_{kl}}\frac{2|A|}{|l|}\det\frac{\partial l_{ij}}{\partial A_{kl}} \quad . \qquad (3.3.14)$$

Together with the formula

$$\det'\frac{\partial\theta_{ij}}{\partial l_{kl}} = 2^{-10}\frac{|A||l|}{\prod W_i^2}V^7\frac{\prod l_{ij}}{\prod A_{ij}} \quad , \qquad (3.3.15)$$

which is calculated in section 3.4, we get

$$\det(-\mathcal{H}^{-1}) = -i\,2^{-9}\Big(\prod W_i^2\Big)\frac{\prod l_{ij}}{\prod A_{ij}}V^{-7}\frac{1}{|A|^2}\det\frac{\partial l_{ij}}{\partial A_{kl}} \quad . \qquad (3.3.16)$$

The combined contribution from two (conjugated) stationary points for a single 4–simplex is thus

$$\pm\frac{|A|}{2^{\frac{7}{2}}\pi^{\frac{3}{2}}}\sqrt{|\det(-\mathcal{H}^{-1})|}\cos\Big(\sum A_{ij}\theta_{ij} - \frac{\pi}{4}\Big) \quad . \qquad (3.3.17)$$

Inserting the determinant of the Hessian matrix (3.3.16), one obtains the result (3.2.3) with a sign ambiguity and the Jacobian $\frac{\partial l_{ij}}{\partial A_{ij}}$ as the only implicit term.

---

[6]We are using Einstein's summing convention for the index pair (ij) with $i \leq j$.

[7]Consider a symmetric matrix M with exactly one null eigenvector. The determinant of this matrix restricted to the subspace orthogonal to that eigenvector is given by $\det'M := \sum_i M_{ii}^*$, where M_{ii}^* denotes the (i,i)th minor of the matrix M. See [B9] for more details.

[8]The first relation is the well-known Schläfli identity.

Precisely this Jacobian can be 'absorbed' in the case of two 4–simplices, glued together via all of their tetrahedra, i.e. a triangulation of the 4–sphere. However this only works if the shapes of the two 4–simplices match; we call this a geometric configuration. This contribution can be written as a sum over the stationary points for one integral of the square of the amplitude. We obtain

$$\sum \frac{|A|^2 |\det(-\mathcal{H}^{-1})|}{2^7 \pi^3} \cos^2\left(\sum A_{ij}\theta_{ij} - \frac{\pi}{4}\right) \quad , \tag{3.3.18}$$

where the summation is over all angles for which the areas A_{ij} match. We rewrite this summation by an integral over the edge lengths (squared), where we impose the area matching as a constraint:

$$\int \prod dl_{ij}^2 \frac{\prod A_{ij}}{\prod l_{ij}} \det \frac{\partial A_{ij}}{\partial l_{kl}} \prod \delta(A_{ij}(l)^2 - A_{ij}^2) \quad . \tag{3.3.19}$$

Thus the result, after counting also the contributions from stationary points related by the $\mathbb{Z}_2^4$ symmetry, is

$$\frac{1}{2^{12}\pi^3} \int \prod dl_{ij}^2 \prod \delta(A_{ij}(l)^2 - A_{ij}^2) \frac{\prod W_i^2}{V^7} \cos^2\left(\sum A_{ij}\theta_{ij} - \frac{\pi}{4}\right) \quad . \tag{3.3.20}$$

In order to arrive at the result (3.2.1), one just has to extract the combinatorial factors out of V and W_i as described at the beginning of section 3.3. In the following section we will provide all the necessary technical details to fill the gaps on the presented derivation. An even more thorough discussion can be found in [B9].

3.4 Technical details

3.4.1 General facts

Let us also remind some general facts (we assume that $\{A_{ij}\}$ locally constitute a good coordinate system)

$$A_{ij}\frac{\partial \theta_{ij}}{\partial l_{kl}} = l_{kl}\frac{\partial \theta_{ij}}{\partial l_{kl}} = 0 \;,\; A_{ij}\frac{\partial \theta_{ij}}{\partial A_{kl}} = A_{kl}\frac{\partial \theta_{ij}}{\partial A_{kl}} = 0 \;,\; \frac{\partial \theta_{ij}}{\partial A_{kl}} = \frac{\partial \theta_{kl}}{\partial A_{ij}} \;, \tag{3.4.1}$$

$$A_{ij} = \lambda \frac{\partial \det \tilde{G}}{\partial \theta_{ij}} \;,\; \lambda = -\frac{\prod W_i^2}{4V^7} \;,\; 2A_{ij}V = W_i W_j \sin\theta_{ij} \;, \tag{3.4.2}$$

which can be proven analogously as in [B9]. For the flat 4-simplex holds

$$\frac{\partial \lambda}{\partial A_{ij}}\frac{\partial \det \tilde{G}}{\partial \theta_{kl}} + \frac{\partial \theta_{ij}}{\partial A_{mn}}\lambda\frac{\partial^2 \det \tilde{G}}{\partial \theta_{mn}\partial \theta_{kl}} = \delta_{(ij),(kl)} \quad , \tag{3.4.3}$$

$$\exists_c \frac{\partial \det \tilde{G}}{\partial \theta_{kl}}c + \lambda\frac{\partial \lambda}{\partial A_{ij}}\frac{\partial^2 \det \tilde{G}}{\partial \theta_{ij}\partial \theta_{kl}} = 0 \quad , \tag{3.4.4}$$

$$\frac{\partial \lambda}{\partial A_{mn}}\frac{\partial \det \tilde{G}}{\partial \theta_{mn}} = 1 \quad . \tag{3.4.5}$$

Interested reader should consult appendix C in [B9] for more details.

3.4.2 Limits from curved simplex

In the following two subsections we will consider a curved 4-simplex with edge lengths $\epsilon\, l_{ij}$ from which we will derive several quantities for the flat simplex. To do so we will heavily rely on the

duality relations of length and angle Gram matrices in the curved case, which are nicely presented in [B37]. The desired quantities will be obtained in the limit $\epsilon \to 0$. For any dimension d holds

$$\det G^{(d)} = \epsilon^{2d}(V^{(d)})^2 + O(\epsilon^{2d+2}) \quad , \tag{3.4.6}$$

where $G^{(d)}$ is the length Gram matrix and $V^{(d)}$ is $d!$ times the volume of d dimensional simplex [9]. We denote

$$V^{(3)} = W, \quad V^{(4)} = V, \quad V^{(2)} = 2A. \tag{3.4.7}$$

Using the results of [B37] we arrive at the following identity for $\det' \tilde{G}$ (for $d = n - 1 = 4$)

$$\det{}'\tilde{G}^\epsilon = \sum_i \tilde{G}^*_{ii} = \left(\sum_i G^*_{ii}\right) \frac{(\det G)^3}{\prod G^*_{ii}} = \left(\epsilon^6 \sum_i W_i^2\right) \frac{\epsilon^{24} V^6}{\epsilon^{30} \prod W_i^2} + O(\epsilon^2) = |W|^2 \frac{V^6}{\prod W_i^2} + O(\epsilon^2) \quad . \tag{3.4.8}$$

and, moreover, also using [B37], we have

$$\det \tilde{G}^\epsilon = \frac{(\det G)^4}{\prod \det G_i} = -\frac{(\epsilon^8 V^2)^4}{\prod \epsilon^6 W_i^2} + O(\epsilon^4) = \epsilon^2 \frac{V^8}{\prod W_i^2} + O(\epsilon^4) \quad . \tag{3.4.9}$$

We will use the latter identity in the following formula for a curved 4-simplex, which has been stated in [B38] (for derivation see [B9]):

$$\det \frac{\partial \theta^\epsilon_{ij}}{\partial l^\epsilon_{km}} = (-1) \frac{\prod \sin l^\epsilon_{ij}}{\prod \sin \theta^\epsilon_{ij}} \left(\frac{\det \tilde{G}}{\det G}\right)^3 , \tag{3.4.10}$$

where $l^\epsilon_{ij} = \epsilon l_{ij}$. Thus

$$\epsilon^{-10} \det \frac{\partial \theta^\epsilon_{ij}}{\partial l_{km}} = \det \frac{\partial \theta^\epsilon_{ij}}{\partial l^\epsilon_{km}} = -\epsilon^{10} \frac{\prod l_{ij}}{\prod \sin \theta_{ij}} \frac{\epsilon^6 \frac{V^{24}}{\prod W_i^6}}{\epsilon^{24} V^6} + O(\epsilon^{-6}) \tag{3.4.11}$$

and finally substituting $\sin \theta_{ij} = \frac{2 A_{ij} V}{W_i W_j}$

$$\det \frac{\partial \theta^\epsilon_{ij}}{\partial l_{km}} = -\frac{\epsilon^2}{2^{10}} \frac{\prod l_{ij}}{\prod A_{ij}} \frac{V^8}{\prod W_i^2} + O(\epsilon^4) \quad . \tag{3.4.12}$$

3.4.3 Limits of determinant with one null eigenvector

If the matrix M^η has in the limit $\eta \to 0$ one null eigenvector $\vec{m}$ and is holomorphic in η then the following expansion around $\eta = 0$ holds:

$$\det M^\eta = \det{}'M \frac{(\vec{m}, M^\eta \vec{m})}{|m|^2} + O(\eta^2) \quad . \tag{3.4.13}$$

This expansion can be immediately applied to $\det \tilde{G}$, since $\tilde{G}$ (and thus also $\det \tilde{G}$) is holomorphic in ϵ^2 and $\tilde{G}$ has one null eigenvector $\vec{W}$ in the flat case

$$\det \tilde{G}^\epsilon = \det{}'\tilde{G} \frac{(\vec{W}, \tilde{G}^\epsilon \vec{W})}{|W|^2} + O(\epsilon^4) \quad . \tag{3.4.14}$$

Furthermore $\left(\vec{W}, \tilde{G}^\epsilon \vec{W}\right) = O(\epsilon^2)$ and can be expanded as follows:

$$2\left(\vec{W}, \tilde{G}^\epsilon \vec{W}\right) = \epsilon \frac{\partial}{\partial \epsilon}\left(\vec{W}, \tilde{G}^\epsilon \vec{W}\right) + O(\epsilon^3) = \left(\vec{W}, l_{ij} \frac{\partial \tilde{G}^\epsilon}{\partial l_{ij}} \vec{W}\right) + O(\epsilon^3) \quad , \tag{3.4.15}$$

---

[9]Please note that our convention affects only tetrahedra and 4-simplices, but not areas and edge lengths.

and

$$\left(\vec{W}, l_{ij} \frac{\partial \tilde{G}^\epsilon}{\partial l_{ij}} \vec{W} \right) = l_{ij} W_k W_l \sin \theta_{kl}^\epsilon \frac{\partial \theta_{kl}^\epsilon}{\partial l_{ij}} = 2 V l_{ij} A_{kl} \frac{\partial \theta_{kl}^\epsilon}{\partial l_{ij}} + O(\epsilon^3) \quad . \tag{3.4.16}$$

Eventually we can summarize these results in a concise form:

$$l_{ij} A_{kl} \frac{\partial \theta_{kl}^\epsilon}{\partial l_{ij}} = \frac{|W|^2}{V} \frac{\det \tilde{G}^\epsilon}{\det' \tilde{G}} + O(\epsilon^3) = \epsilon^2 V + O(\epsilon^3) \quad . \tag{3.4.17}$$

On the other hand, we can apply the same argument to $\frac{\partial \theta_{ij}^\epsilon}{\partial l_{km}}$, since it also is holomorphic in ϵ^2 and has exactly one null eigenvector in the flat case, namely $\vec{l}$ and respectively $\vec{A}$ (it is not symmetric). Thus

$$\det \frac{\partial \theta_{ij}^\epsilon}{\partial l_{km}} = \det' \frac{\partial \theta_{ij}}{\partial l_{km}} \frac{\left(\vec{A}, \frac{\partial \theta_{ij}^\epsilon}{\partial l_{km}} \vec{l} \right)}{|A||l|} + O(\epsilon^3) \tag{3.4.18}$$

Substituting $\det \frac{\partial \theta_{ij}^\epsilon}{\partial l_{km}}$ and $\left(\vec{A}, \frac{\partial \theta_{ij}^\epsilon}{\partial l_{km}} \vec{l} \right) = l_{ij} A_{kl} \frac{\partial \theta_{kl}^\epsilon}{\partial l_{ij}}$ we obtain

$$\det' \frac{\partial \theta_{ij}}{\partial l_{km}} = 2^{-10} \frac{|A||l|}{\prod W_i^2} V^7 \frac{\prod l_{ij}}{\prod A_{ij}} \quad . \tag{3.4.19}$$

3.5 Conclusions

In this work we have derived a first asymptotic formula for the Barrett-Crane spin foam model, expressed completely in terms of simple geometric quantities, which sheds new light on the possible asymptotic behaviour of more complicated spin foam models. In fact it suggests that edge lengths are the more suitable variables to be used in the asymptotic limit than area variables. Exactly this might be a root of the problem to derive a measure factor in the asymptotic limit of modern spin foam models.

Let us put our derivation in a geometric but heuristic context. Expanding the SU(2) characters in (3.1.2) into exponentials one can obtain the so-called bare action for arbitrary foams. Putting aside the troubling fact that we sum over spins instead of integrating, we can regard the models as a Feynman path integral. The action turns out to be the action of first order (area) Regge calculus, where both areas and 4D dihedral angles are independent variables. One can then argue that the semiclassical expansion of the integral is governed by the expansion of this action around the solutions to the classical equations of motion, which differ from standard Regge calculus [B22, B25, B39, B40]. If we restrict ourselves to geometric solutions for which the shapes of tetrahedra match then there are only flat solutions, but with arbitrary non-matching orientations. Flatness is imposed by the equations of motion originating from the variation over areas. In our asymptotic analysis, however, the areas are fixed and uniformly large. As the suppression of non-flat solutions is related to summing (integrating) over spins (see [B29, B41]), and we do not sum over spins, this part of the equations of motion is absent in our asymptotics. In our case non-flat solutions are not suppressed.

The results of [B41] show that the modern spin foam models correspond to (area, coherent states)-Regge calculus. This is yet another version of Regge calculus, also leading to the flatness problem, yet with matching area shapes [B41]. It is not clear how to extend our result in this setting, nevertheless it suggests new types of factors that might appear in the asymptotic expansion, as the just derived formula can also be stated for a single 4-simplex, although with an additional factor $\sqrt{\det \frac{\partial A_{ij}}{\partial l_{ij}}}$.

It is also worth to speculate about the suggestions from our work for measure factors [B42] in (linearized) Regge calculus due to its close relation to spin foams in the asymptotic limit. One

of the typical constraints for such measures derived in [B43] is triangulation independence, i.e. invariance under Pachner moves. It can be shown (see [B44]) that a product (or fraction) of simple geometric quantities (like volumes, areas or edge lengths) cannot be invariant. However, if the non-local change of variables plays a role in larger simplicial complexes, then the invariance might be restored.

Finally, in the case when the map $\{l_{ij}\} \rightarrow \{A_{ij}\}$ is not locally invertible, the Hessian has an additional null eigenvector and the asymptotic contribution is less suppressed. If a similar phenomenon exists in the Lorentzian EPRL–FK model it would directly influence the result of [B45], which is derived under the assumption of a certain scaling behaviour of the measure factor. Our result suggests, which configurations might show such an anomalous scaling behaviour and are thus crucial for research in this direction.

As we have shown in this work there still exist new insights that can be drawn from the Barrett-Crane model. Let us notice, that the derivation is restricted only to a very specific example and it is not clear how to extend it to more general situation. We hope however that our methods presented here and in [B9] can be expanded to the more advanced spin foam models and might shed some new light on the pressing questions such as the measure factor, the flatness issue or the suitable choice of variables and semi-classical limits.

Acknowledgments

3.A Auxiliary definitions and computations

3.A.1 Definition of the Gram matrix

For the set of numbers $\{\theta_{ij} \in (0, \pi)\}$, the angle Gram matrix $\tilde{G}$ is defined as

$$
\tilde{G} = [\cos\theta_{ij}] = \begin{pmatrix} 1 & \cos\theta_{12} & \cdots & \cos\theta_{15} \\ \cos\theta_{12} & 1 & \cdots & \cos\theta_{25} \\ \vdots & \vdots & \ddots & \vdots \\ \cos\theta_{15} & \cos\theta_{25} & \cdots & 1 \end{pmatrix} \quad , \tag{3.A.1}
$$

with the convention that $\theta_{ii} = 0$. It is well–known that for $\{\theta_{ij}\}$ satisfying $\det\tilde{G} = 0$ ($\tilde{G}$ is semi–positive definite with exactly one null eigenvector) we can associate normals n_i to the tetrahedra forming a 4–simplex, such that $n_i \cdot n_j = \cos\theta_{ij}$ (see for example [B9]). In the case when these normals are all outward (or inward) pointing we will call θ_{ij} an exterior dihedral angle. In such a case the 4–simplex is uniquely determined up to a scale and $\tilde{G}$ has one null eigenvector $(W_1, \cdots, W_5)$. Using this fact we can compute

$$
\frac{\partial \det\tilde{G}}{\partial\theta_{ij}} = -2\det{}'\tilde{G}\frac{W_i W_j \sin\theta_{ij}}{|W|^2} \quad , \tag{3.A.2}
$$

but $2A_{ij}V = W_iW_j\sin\theta_{ij}$ and thus

$$\frac{\partial\det\tilde{G}}{\partial\theta_{ij}} = \underbrace{-\frac{2\det'\tilde{G}}{|W|^2}V}_{\lambda^{-1}}A_{ij} \tag{3.A.3}$$

but we also have (see also [B9])

$$\det'\tilde{G} = \left(\sum_i W_i^2\right)\frac{V^6}{\prod W_i^2} \quad. \tag{3.A.4}$$

Thus we conclude $\lambda = -\frac{\prod W_i^2}{4V^7}$.

3.A.2 Geometric values of l_{ij}

In any dimension d in order for the set of numbers $\{l_{ij}\} \in [0,\infty]^{\frac{(d+1)d}{2}}$ to be a set of lengths of a d-simplex the following Menger condition [B46] must hold: The Cayley- Menger matrix

$$C = \begin{pmatrix} 0 & 1 & 1 & \cdots & 1 \\ 1 & 0 & l_{12}^2 & \cdots & l_{1(d+1)}^2 \\ 1 & l_{12}^2 & 0 & \cdots & l_{2(d+1)}^2 \\ \vdots & \vdots & \vdots & \ddots & \vdots \\ 1 & l_{1(d+1)}^2 & l_{2(d+1)}^2 & \cdots & 0 \end{pmatrix} \tag{3.A.5}$$

must have 1 positive and $d+1$ negative eigenvalues. This is equivalent to the following conditions on the determinants of the upper left corner $n \times n$ submatrices C_n of the matrix C:

$$\forall_{2\leq n\leq d+1}: \ (-1)^n \det C_n < 0 \quad. \tag{3.A.6}$$

We denote the closure of the region of such l_{ij} by $\mathcal{C}$.

3.A.3 Scaling

By applying the field $l_{ij}\frac{\partial}{\partial l_{ij}}$ on any function of $\{l\}$, we can deduce the scaling of the respective function, e.g. the scaling of areas:

$$l_{ij}\frac{\partial}{\partial l_{ij}} = l_{ij}\frac{\partial A_{kl}}{\partial l_{ij}}\frac{\partial}{\partial A_{kl}} \quad, \tag{3.A.7}$$

but since $l_{ij}\frac{\partial A_{kl}}{\partial l_{ij}} = 2A_{kl}$ (areas are two dimensional), it follows:

$$A_{kl}\frac{\partial}{\partial A_{kl}} = \frac{1}{2}l_{ij}\frac{\partial}{\partial l_{ij}} \quad. \tag{3.A.8}$$

References

[B1] A. Perez, "Spin foam models for quantum gravity," *Class.Quant.Grav.* **20** (2003) R43, `arXiv:gr-qc/0301113 [gr-qc]`.

[B2] A. Perez, "The Spin Foam Approach to Quantum Gravity," *Living Rev.Rel.* **16** (2013) 3, `arXiv:1205.2019 [gr-qc]`.

[B3] C. Rovelli, *Quantum Gravity*. Cambridge University Press, 2004.

[B4] J. C. Baez, "Spin foam models," *Class.Quant.Grav.* **15** (1998) 1827–1858, `arXiv:gr-qc/9709052 [gr-qc]`.

[B5] C. Rovelli, "Zakopane lectures on loop gravity," *PoS QGQGS* **2011** (2011) 003, `arXiv:1102.3660 [gr-qc]`.

[B6] J. Roberts, "Classical 6j-symbols and the tetrahedron," *Geom. Topol.* **3** (1999) 21–66, `math-ph/9812013`.

[B7] V. Aquilanti, H. M. Haggard, A. Hedeman, N. Jeevanjee, R. G. Littlejohn, and L. Yu, "Semiclassical Mechanics of the Wigner 6j-symbol," *J. Phys. A* **45** (2012) 065209, `arXiv:1009.2811 [math-ph]`.

[B8] L. Freidel and D. Louapre, "Asymptotics of 6j and 10j symbols," *Class.Quant.Grav.* **20** (2003) 1267–1294, `arXiv:hep-th/0209134 [hep-th]`.

[B9] W. Kamiński and S. Steinhaus, "Coherent states, 6j symbols and properties of the next to leading order expansion," *J. Math. Phys.* **54** (2013) 121703, `arXiv:1307.5432 [math-ph]`.

[B10] G. Ponzano and T. Regge, *Semiclassical limit of Racah coefficients, in: Spectroscopy and group theoretical methods in physics*. North Holland Publ. Co., Amsterdam, 1968.

[B11] J. W. Barrett and I. Naish-Guzman, "The Ponzano-Regge model," *Class. Quant. Grav.* **26** (2009) 155014, `arXiv:0803.3319 [gr-qc]`.

[B12] J. W. Barrett and L. Crane, "Relativistic spin networks and quantum gravity," *J.Math.Phys.* **39** (1998) 3296–3302, `arXiv:gr-qc/9709028 [gr-qc]`.

[B13] J. Engle, E. Livine, R. Pereira, and C. Rovelli, "Lqg vertex with finite Immirzi parameter," *Nucl. Phys. B* **799** (2008) 136, `arXiv:0711.0146 [gr-qc]`.

[B14] L. Freidel and K. Krasnov, "A New Spin Foam Model for 4d Gravity," *Class. Quant. Grav.* **25** (2008) 125018, `arXiv:0708.1595 [gr-qc]`.

[B15] J. W. Barrett and R. M. Williams, "The Asymptotics of an amplitude for the four simplex," *Adv.Theor.Math.Phys.* **3** (1999) 209–215, `arXiv:gr-qc/9809032 [gr-qc]`.

[B16] J. C. Baez, J. D. Christensen, and G. Egan, "Asymptotics of 10j symbols," *Class.Quant.Grav.* **19** (2002) 6489, `arXiv:gr-qc/0208010 [gr-qc]`.

[B17] J. W. Barrett, W. J. Fairbairn, and F. Hellmann, "Quantum gravity asymptotics from the SU(2) 15j symbol," *Int. J. Mod. Phys. A* **25** (2010) 2897, `arXiv:0912.4907 [gr-qc]`.

[B18] J. W. Barrett, R. J. Dowdall, W. J. Fairbairn, F. Hellmann, and R. Pereira, "Lorentzian spin foam amplitudes: Graphical calculus and asymptotics," *Class. Quant. Grav.* **27** (2010) 165009, `arXiv:0907.2440 [gr-qc]`.

[B19] J. W. Barrett, R. J. Dowdall, W. J. Fairbairn, H. Gomes, F. Hellmann, and R. Pereira, "Asymptotics of 4d spin foam models," *Gen. Rel. Grav.* **43** (2011) 2421, `arXiv:1003.1886 [gr-qc]`.

[B20] J. W. Barrett, R. J. Dowdall, W. J. Fairbairn, H. Gomes, and F. Hellmann, "Asymptotic analysis of the EPRL four-simplex amplitude," *J. Math. Phys.* **50** (2009) 112504, `arXiv:0902.1170 [gr-qc]`.

[B21] J. W. Barrett and C. M. Steele, "Asymptotics of relativistic spin networks," *Class.Quant.Grav.* **20** (2003) 1341–1362, `arXiv:gr-qc/0209023 [gr-qc]`.

[B22] J. W. Barrett, M. Rocek, and R. M. Williams, "A Note on area variables in Regge calculus," *Class.Quant.Grav.* **16** (1999) 1373–1376, `arXiv:gr-qc/9710056 [gr-qc]`.

[B23] E. Alesci and C. Rovelli, "The complete LQG propagator: I. Difficulties with the Barrett-Crane vertex," *Phys. Rev. D* **76** (Aug., 2007) 104012, `arXiv:0708.0883 [gr-qc]`.

[B24] C. Rovelli, "The basis of the Ponzano-Regge-Turaev-Viro-Ooguri model is the loop representation basis," *Phys. Rev. D* **48** (1993) 2702–2707, `arXiv:hep-th/9304164 [hep-th]`.

[B25] C. Wainwright and R. M. Williams, "Area Regge calculus and discontinuous metrics," *Class.Quant.Grav.* **21** (2004) 4865–4880, `arXiv:gr-qc/0405031 [gr-qc]`.

[B26] Y. Neiman, "A look at area Regge calculus," `arXiv:1308.1012 [gr-qc]`.

[B27] V. Bonzom and E. R. Livine, "A Lagrangian approach to the Barrett-Crane spin foam model," *Phys. Rev. D* **79** (2009) 064034, `arXiv:0812.3456 [gr-qc]`.

[B28] A. Baratin and D. Oriti, "Quantum simplicial geometry in the group field theory formalism: reconsidering the Barrett-Crane model," *New J. Phys.* **13** (2011) 125011, `arXiv:1108.1178 [gr-qc]`.

[B29] F. Hellmann and W. Kaminski, "Holonomy spin foam models: Asymptotic geometry of the partition function," *JHEP* **1310** (2013) 165, `arXiv:1307.1679 [gr-qc]`.

[B30] M. Han, "Covariant Loop Quantum Gravity, Low Energy Perturbation Theory, and Einstein Gravity with High Curvature UV Corrections," *Phys.Rev.* **D89** (2014) 124001, `arXiv:1308.4063 [gr-qc]`.

[B31] B. Bahr and B. Dittrich, "Improved and Perfect Actions in Discrete Gravity," *Phys. Rev. D* **80** (2009) 124030, `arXiv:0907.4323 [gr-qc]`.

[B32] B. Bahr, B. Dittrich, and S. Steinhaus, "Perfect discretization of reparametrization invariant path integrals," *Phys. Rev. D* **83** (2011) 105026, `arXiv:1101.4775 [gr-qc]`.

[B33] B. Bahr, B. Dittrich, F. Hellmann, and W. Kaminski, "Holonomy Spin Foam Models: Definition and Coarse Graining," *Phys. Rev. D* **87** (2013) 044048, `arXiv:1208.3388 [gr-qc]`.

[B34] B. Dittrich, M. Martn-Benito, and E. Schnetter, "Coarse graining of spin net models: dynamics of intertwiners," *New J. Phys.* **15** (2013) 103004, `arXiv:1306.2987 [gr-qc]`.

[B35] V. Bonzom and B. Dittrich, "Bubble divergences and gauge symmetries in spin foams," *Phys. Rev. D* **88** (2013) 124021, `arXiv:1304.6632 [gr-qc]`.

[B36] J. W. Barrett, "First order Regge calculus," *Class.Quant.Grav.* **11** (1994) 2723–2730, `arXiv:hep-th/9404124 [hep-th]`.

[B37] S. L. Kokkendorff, "Polar duality and the generalized law of sines," *Journal of Geometry* **86** no. 1-2, (2007) 140–149.

[B38] B. Dittrich, L. Freidel, and S. Speziale, "Linearized dynamics from the 4-simplex Regge action," *Phys. Rev. D* **76** (2007) 104020, `arXiv:0707.4513 [gr-qc]`.

[B39] B. Dittrich and S. Speziale, "Area-angle variables for general relativity," *New J. Phys.* **10** (2008) 083006, `arXiv:0802.0864 [gr-qc]`.

[B40] B. Bahr and B. Dittrich, "Regge calculus from a new angle," *New J. Phys.* **12** (2010) 033010, `arXiv:0907.4325 [gr-qc]`.

[B41] V. Bonzom, "Spin foam models for quantum gravity from lattice path integrals," *Phys. Rev. D* **80** (2009) 064028, `arXiv:0905.1501 [gr-qc]`.

[B42] H. W. Hamber and R. M. Williams, "On the measure in simplicial gravity," *Phys.Rev.* **D59** (1999) 064014, `arXiv:hep-th/9708019 [hep-th]`.

[B43] B. Dittrich and S. Steinhaus, "Path integral measure and triangulation independence in discrete gravity," *Phys. Rev. D* **85** (2012) 044032, `arXiv:1110.6866 [gr-qc]`.

[B44] B. Dittrich, W. Kaminski, and S. Steinhaus, "Discretization independence implies non-locality in 4D discrete quantum gravity," *Class.Quant.Grav.* **31** (2014) 245009, `arXiv:1404.5288 [gr-qc]`.

[B45] A. Riello, "Self-Energy of the Lorentzian EPRL-FK Spin Foam Model of Quantum Gravity," *Phys. Rev. D* **88** (2013) 024011, `arXiv:1302.1781 [gr-qc]`.

[B46] K. Menger, "New Foundation of Euclidean Geometry," *American Journal of Mathematics* **53** no. 4, (Oct., 1931) 721–745. `http://www.jstor.org/stable/2371222`.

4 Path integral measure and triangulation independence in discrete gravity

Bianca Dittrich and Sebastian Steinhaus

Max Planck Institute for Gravitational Physics,
Am Mühlenberg 1, D-14476 Potsdam, Germany

Abstract

A path integral measure for gravity should also preserve the fundamental symmetry of general relativity, which is diffeomorphism symmetry. In previous work, we argued that a successful implementation of this symmetry into discrete quantum gravity models would imply discretization independence. We therefore consider the requirement of triangulation independence for the measure in (linearized) Regge calculus, which is a discrete model for quantum gravity, appearing in the semi–classical limit of spin foam models. To this end we develop a technique to evaluate the linearized Regge action associated to Pachner moves in 3D and 4D and show that it has a simple, factorized structure. We succeed in finding a local measure for 3D (linearized) Regge calculus that leads to triangulation independence. This measure factor coincides with the asymptotics of the Ponzano Regge Model, a 3D spin foam model for gravity. We furthermore discuss to which extent one can find a triangulation independent measure for 4D Regge calculus and how such a measure would be related to a quantum model for 4D flat space. To this end, we also determine the dependence of classical Regge calculus on the choice of triangulation in 3D and 4D.

4.1 Introduction

Many approaches to quantum gravity, such as spin foams [C1–C3], group field theories [C4, C5], (causal) dynamical triangulations [C6–C8] and Regge quantum gravity [C9, C10], rely on a path integral approach. A (non–perturbative) path integral has to be regularized to make it well defined. In the process of this regularization, several choices have to be made, that differ in the various approaches. Broadly one can understand these choices as deciding on a measure on the space of all geometries. This includes various aspects, such as to define the space of geometries, for example the space of all triangulations with fixed edge lengths in dynamical triangulations versus the space defined by allowing all possible edge lengths (satisfying generalized triangle inequalities) in a fixed triangulation such as in Regge calculus, or some generalized discrete geometric spaces, as appearing in loop quantum gravity [C11–C13]. A related question is whether to include a sum over triangulations, such as in (causal) dynamical triangulations and group field theories, or even over two–complexes as suggested for spin foam models [C14–C16]. Alternatively the path integral may just include an integration over geometric data associated to a given, fixed, discretization. For discussions on the relation between these approaches, see [C17–C19].

One reason for this many different suggestions, is that the space of all (discrete) geometries and its relation to the corresponding continuum space needs to be better understood [C20, C21]. Many difficulties are rooted in the role of diffeomorphism symmetry, by which the space of metrics has to be quotiened to obtain the space of geometries. Discretizations obscure the role of diffeomorphisms, see [C18,C22] for a discussion. In particular, for a precise notion of diffeomorphism symmetry in the discrete [C18], one can show that this symmetry is broken for 4D Regge gravity [C23,C24]. However, if this symmetry would hold in discrete gravity, one could hope for a unique anomaly–free (with repsect to diffeomorphisms) measure [C25]. As is also argued in [C25, C26], the implementation of this symmetry into discrete gravity (of Regge type, i.e. with geometric data on a fixed triangulation or discretization), would make such a theory triangulation or discretization independent. In this case there would also be no need of summing over triangulations, which is often employed to obtain a triangulation independent theory.

One can expect to find such a discretization independent theory for 3D gravity, which is a topological theory, i.e. there are no local physical (propagating) degrees of freedom. In fact we will succeed to find a triangulation invariant path integral description for 3D (linearized) Regge calculus. 4D gravity features local propagating degrees of freedom and a discretization independent model will require a non–local structure and moreover control over the solutions of the system [C27]. Nevertheless, as argued in [C25] the choice of path integral measure is important for the convergence of the model, also under a renormalization flow, which might be employed to find improved discretizations [C28]. Moreover 4D classical Regge gravity is invariant under a set of certain local changes of the triangulation. One might therefore ask also for invariance of the path integral under this set of local changes.

In this work we will concentrate on finding a measure in a (Euclidean) Regge calculus set up, that is as much triangulation independent, as possible. Before explaining this in more detail we will shortly review different measures suggested so far in the literature [C29]. One method would be to discretize the (formal) continuum path integral

$$I_{cont} = \int \prod_{x,\, \rho \geq \tau} dg_{\rho\tau}(x) \prod_x \left(\sqrt{\det(g_{\mu\nu})} \right)^{\alpha} \exp\left(-S_{EH}\right) \quad . \tag{4.1.1}$$

Here S_{EH} is the (Euclidean) Einstein Hilbert continuum action and $\left(\sqrt{\det(g_{\mu\nu})} \right)^{\alpha}$ is a factor which can be obtained from the DeWitt metric on (geometric) superspace [C30]. More specifically the DeWitt measure [C30] prescribes $\alpha = 0$ in 4D and $\alpha = -1$ in 3D. However also other values of α have been suggested [C29], for instance $\alpha = -(D+1)$ for the Misner measure [C31], where D is the dimension of space time. A priori it is not clear which choice to prefer [C29].

Regge calculus [C9, C10] provides a discretization S_R of the Einstein Hilbert action S_{EH}, defined on a triangulation. The metric data are replaced by edge lengths l_e associated to the edges of the triangulation. As $\sqrt{\det(g_{\mu\nu})}$ gives the local space time volume a natural discretization of this factor is given by the volumes V_Δ of the top–dimensional simplices Δ, i.e. 4–simplices in 4D and tetrahedra in 3D. A straightforward discretization of (4.1.1) is then given by [C29] (modulo numerical constants)

$$I_{discr} = \int \prod_e dl_e^2 \prod_\Delta V_\Delta^\alpha \; \exp\left(-S_R\right) \quad . \tag{4.1.2}$$

Concerning the range of integration it will always be understood that the generalized triangle inequalities are satisfied. These require positive volume for all (sub-) simplices and are therefore equivalent to restricting the integration in the continuum path integral (4.1.1) to positive definite metrics. Apart from this requirement of triangle inequalities (which are technically very difficult to implement) the measure used in (4.1.2) has the advantage of being especially simple, in particular local.[1] The simplicity is also a reason why $\alpha = 0$ in 4D seems to be preferred [C29].

In this paper we will consider a requirement of triangulation independence for the path integral measure. This requirement is also connected [C25] with a discrete notion of diffeomorphism invariance [C26]. Hence asking for triangulation independence amounts to requiring an anomaly free measure with respect to the diffeomorphisms, see also [C32] for a discussion in the spin foam context.

Specifically we ask for invariance of the (linearized) model defined by (4.1.2) under Pachner moves [C33, C34]. These are local changes of the triangulation, that act ergodically, i. e. two topologically equivalent triangulations can always be transformed into each other by a sequence of Pachner moves. Restricting the measure to the local ansatz (4.1.2) we will find that our results suggest to fix the parameter α to $\alpha = -\frac{1}{2}$ both in 3D and in 4D. Interestingly this conforms completely with the semi–classical analysis [C35, C36] of the Ponzano–Regge model [C37] in 3D. This is a triangulation independent (spin foam) model for 3D quantum gravity, based on discrete variables. The case of 4D is much more involved. Firstly, being an interacting theory with propagating degrees of freedom, one cannot expect to obtain a triangulation independent model, with just local interactions, as in the Regge action [C27]. Indeed, we will precisely show in which sense the (linearized) 4D Regge action fails to be triangulation independent. Although the semiclassical analysis of the 4D models [C38–C40] could show that the Regge action appears in a $\hbar \to 0$ limit of the amplitudes, the corresponding measure factor has not been specified yet as a function of the geometric variables. For future work it will be interesting to compare in more detail the spin foam results with Regge gravity. Also a measure ambiguity shows up in choosing so called edge and face amplitudes [C14–C16, C32, C41]. These ambiguities could also be restricted by asking for as much triangulation independence as possible, similar to the method proposed here. Hence it would be very interesting to study the behavior of spin foam amplitudes under Pachner moves [C42].

There are also other suggestions for the Regge measure, which are non–local. As these are far more complicated explicit computations they have mostly been restricted to 2D. The Regge–Lund measure [C29, C43, C44] is obtained by discretizing first the deWitt super metric and then taking the determinant (whereas in (4.1.2) this is performed the other way around). The result is given by

$$I_{RL} = \int \prod_e dl_e^2 \prod_\Delta \sqrt{\det(G_{ee'})} \; \exp\left(-S_R\right) \quad , \tag{4.1.3}$$

---

[1] Another suggestion is to use a measure of the form $\prod_e l_e^{-1} dl_e$, which is scale invariant. (The Regge action without cosmological constant term is invariant -up to an overall factor- under global rescaling of the edge lengths.) However, this measure did not lead to satisfying results in numerical simulations, see [C21] and references therein.

where

$$G_{ee'} = -D! \sum_{\Delta} \frac{1}{V_{\Delta}^{\beta}} \frac{\partial V_{\Delta}}{\partial l_e l_{e'}} \tag{4.1.4}$$

and β is another ambiguous parameter. As the determinant has to be taken of a matrix, which is indexed by all the edges of the triangulation, the result is potentially quite non–local. Further discussion of this measure can be found in [C29, C44].

In 3D, where gravity is a topological theory, we will find that a local measure is sufficient to guarantee triangulation independence of the (linearized) theory. In 4D, as previously mentioned one cannot expect to find complete triangulation independence for the path integral as already the action is not triangulation independent. (More precisely it is the Hamilton–Jacobi function as a functional of the boundary data, that is not invariant under the change of the bulk triangulation.) One can however ask for invariance under a restricted set of Pachner moves, under which the action happens to be invariant. These are the $4-2$ and $5-1$ moves (but not the $3-3$ move). Nevertheless also for these moves we will find that a factor appears that features a certain non-local structure. At this stage it seems however more promising to construct improved measures and actions directly by coarse graining and the method of perfect discretizations [C25, C27, C28].

Ultimately, another criterion that any quantum gravity model has to satisfy, is to display the correct large scale limit. Also here a measure term could be essential. For investigations in 2D Regge see for instance [C45], for discussion of the influence of the measure in the context of dynamical triangulations see [C46, C47]. Another suggestion for constructing a measure for Regge gravity, is to mod out a certain subgroup of the continuum diffeomorphism group [C48]. This results again in a highly non–local measure, where explicit results are mostly restricted to 2D.

In the next section we introduce the Regge action and its expansion up to second order. This requires the calculation of its Hessian matrix, which will be one of the main subjects of this work. Furthermore we discuss the concept of Pachner moves and briefly present the Pachner moves in 3D and 4D. Section 4.3 deals with a general method to compute the Hessian matrix in 3D and presents the application of this method to the Regge actions associated to the Pachner moves. Then we examine invariance of the path integral under Pachner moves and define a suitable measure factor. The results for 3D will be summarized in section 4.4. In section 4.5 we extend our method to compute the Hessian matrix in 4D, examine invariance of the path integral under Pachner moves and discuss a suitable measure. The results in 4D are then summarized in section 4.6. We conclude this work with a discussion of our results in section 4.7.

4.2 Linearized Regge Calculus

The Regge action (which we will denote by S in the following) provides a discretization of the Einstein Hilbert action for gravity. It is defined on a triangulation, the geometry is a piecewise flat one, and the geometric data are encoded in the lengths of the edges in this triangulation. For Regge type actions based on different geometric variables nearer to spin foams, specifically areas and angles, see [C49, C50].

In the following we will consider the Euclidean path integral for the Regge discretization of gravity on a given 3D or 4D triangulation

$$\int_{l_{e|e\subset\partial M}} \prod_{e\subset\text{bulk}} dl_e \,\mu(l_e) \exp\{-S\} \quad . \tag{4.2.1}$$

Here $l_{e|e\subset\partial M}$ denotes the boundary conditions, which we take to be fixed length variables for the edges in the boundary triangulation. $\mu(l_e)$ is a suitable measure factor. In (4.2.1) not all edge lengths combinations are allowed since the edge lengths have to satisfy generalized triangle

inequalities, i.e. all the (2D, 3D and, in case, 4D) volumes have to be positive. The (Euclidean) Regge action in arbitrary dimension D can be written in the following form

$$S := -\sum_{h \subset \text{bulk}} V_h \left(2\pi - \sum_{\sigma^D \supset h} \theta_h^{(\sigma^D)}\right) - \sum_{h \subset \text{bdry}} V_h \left(\pi - \sum_{\sigma^D \supset h} \theta_h^{(\sigma^D)}\right) \quad, \tag{4.2.2}$$

where σ^D denotes D-simplices, i.e. D-dimensional simplices with $D+1$ vertices, h denotes 'hinges', i.e. $D-2$-simplices, V_h is the volume of a hinge and $\theta_h^{(\sigma^D)}$ denotes the internal dihedral angle in the D-simplex σ^D at the hinge h. The terms in brackets in (4.2.2) define the bulk and boundary deficit angles

$$\omega_h^{(\text{bulk})} := 2\pi - \sum_{\sigma^D \ni h} \theta_h^{(\sigma^D)} \quad, \tag{4.2.3}$$

$$\omega_h^{(\text{bdry})} := k\pi - \sum_{\sigma^D \ni h} \theta_h^{(\sigma^D)} \quad, \tag{4.2.4}$$

where k depends on the number of pieces one is glueing together at this boundary. If there are only two pieces we have $k = 1$.

The dihedral angles are complicated functions of the lengths variables, so that the integral in (4.2.1) cannot be computed analytically. Additionally one has to take the generalized triangle inequalities for the range of integration into account.

To circumvent this issue, we consider linearized Regge Calculus in which one chooses a classical background solution (for the edge lengths) $l_e^{(0)}$ satisfying the triangle inequalities and one quantizes, i.e. integrates over, the perturbations λ_e around it.

Therefore consider a small perturbation around a background solution

$$l_e = l_e^{(0)} + \lambda_e \tag{4.2.5}$$

and expand the Regge action up to second order in the perturbation variables λ_e:

$$S = S^{(0)}\Big|_{l_e=l_e^{(0)}} + \frac{\partial S}{\partial l_e}\Big|_{l_e=l_e^{(0)}} \lambda_e + \frac{1}{2}\frac{\partial^2 S}{\partial l_e \partial l_{e'}}\Big|_{l_e=l_e^{(0)}} \lambda_e \lambda_{e'} \quad. \tag{4.2.6}$$

The background edge lengths $l_e^{(0)}$ are defined as the solution to the Regge equations,

$$\frac{\partial S}{\partial l_e} = -\sum_{h \supset e} \frac{\partial V_h}{\partial l_e} \omega_h = 0 \tag{4.2.7}$$

such that the first order term in (4.2.6) vanishes for the bulk edges. More specifically we take the background solution to be (locally) flat, that is $\omega_h^{(\text{bulk})} = 0$. (This is exactly the equation of motion in 3D.) The second order term is defined by the matrix of second derivatives, that is the Hessian.

In three dimension one obtains due to the Schläfli identity[2]

$$\frac{\partial^2 S}{\partial l_e \partial l_{e'}} = -\frac{\partial \omega_e}{\partial l_{e'}} \quad. \tag{4.2.8}$$

In four dimensions we obtain (using again the Schläfli identity):

$$\frac{\partial^2 S}{\partial l_e \partial l_{e'}} = -\sum_h \frac{\partial A_h}{\partial l_{e'}} \frac{\partial \omega_h}{\partial l_e} - \sum_{h \subset \text{bulk}} \frac{\partial^2 A_h}{\partial l_e \partial l_{e'}} \omega_h^{(\text{bulk})} - \sum_{h \subset \text{bdry}} \frac{\partial^2 A_h}{\partial l_e \partial l_{e'}} \omega_h^{(\text{bdry})} \quad. \tag{4.2.9}$$

---

[2]The Schläfli identity $\sum_{h \subset \Delta^{(D)}} V_h \, \delta\theta_h^{(\Delta^{(D)})} = 0$ ensures that terms with second derivatives of the dihedral angles vanish.

The bulk deficit angles $\omega_h^{\text{(bulk)}}$ vanish on a flat (background) solution.

For the evaluation of these Hessian matrices, we will need the first derivatives of the dihedral angles with respect to the length variables. A formula valid for simplices of arbitrary dimension D can be found in [C51]:

$$\frac{\partial \tilde{\theta}_{kl}}{\partial l_{hm}} = \frac{1}{D^2} \frac{l_{hm}}{\sin(\tilde{\theta}_{kl})} \frac{V_h V_m}{V^2} \Big(\cos(\tilde{\theta}_{kh}) \cos(\tilde{\theta}_{ml}) + \cos(\tilde{\theta}_{km}) \cos(\tilde{\theta}_{hl}) +$$
$$+ \cos(\tilde{\theta}_{kl}) \big(\cos(\tilde{\theta}_{kh}) \cos(\tilde{\theta}_{km}) + \cos(\tilde{\theta}_{lh}) \cos(\tilde{\theta}_{lm}) \big) \Big) \quad . \tag{4.2.10}$$

In (4.2.10) $\tilde{\theta}_{kl}$ denotes the dihedral angle (in a D-simplex) between the two $D-1$-simplices formed without the vertices k and l respectively. l_{hm} is the length of the edge between vertices h and m. V_h denotes the volume of the $(D-1)$ simplex formed without vertex h in the D-simplex. V is the volume of the respective D-simplex.

In case the dihedral angle $\tilde{\theta}_{kl}$ and the edge l_{hm} do not share a vertex, which implies that $(kl) = (hm)$, i.e. the hinge is formed without the vertices h and m in the D-simplex, equation (4.2.10) simplifies using the convention $\cos \tilde{\theta}_{ll} = -1$:

$$\frac{\partial \tilde{\theta}_{hm}}{\partial l_{hm}} = \frac{1}{D^2} \frac{l_{hm}}{\sin \tilde{\theta}_{hm}} \frac{V_h V_m}{V^2} \Big(1 - \cos^2 \tilde{\theta}_{hm} \Big)$$
$$= \frac{1}{D^2} \frac{l_{hm} V_h V_m}{V^2} \sin \tilde{\theta}_{hm} = \frac{1}{D(D-1)} \frac{l_{hm} V_{hm}}{V} \quad . \tag{4.2.11}$$

This result (4.2.11) will be crucial for an alternative derivation of the matrix elements of the Hessian (4.2.11) in section 4.3. This alternative derivation applies to configurations defining Pachner moves, which we will discuss in the next section.

4.2.1 Pachner Moves

Pachner moves are local changes of the triangulation which, if applied consecutively, allow to go from any triangulation of a given manifold to any other triangulation of that manifold [C33,C34]. In quantum Regge calculus one usually fixes the triangulation and just integrates over the edge lengths in this given triangulation. Given this definition the question arises of how the result depends on the choice of triangulation. Note that the triangulation is only an auxiliary structure, which is put in in order to regularize the (continuum) path integral. Hence it would be advantageous, if the path integral (with or without given boundary triangulation and condition) would depend minimally on the choice of (bulk) triangulation. In case the path integral does not depend at all on the triangulation, we do not even need to take any refinement limit (here of the bulk triangulation only), as the result will not change under refinement. Such a strong version of discretization independence can actually be expected in 3D, in which gravity is a topological theory, describing the dynamics of only global (topological) variables. Indeed we will find a measure that will render the path integral discretization independent in this sense. (That the linearized action is invariant under refinements has been shown in [C27].) Locally this discretization independence implies that the path integral is form invariant 'under Pachner moves'. More precisely, we will consider here Pachner moves arising by integrating out certain edges in the triangulation, so that the remaining edges still define a triangulation. The form of the (discretized) path integral should then be invariant.

We will consider a similar requirement in 4D. This defines however, a theory with local degrees of freedom, where not even the (linearized) action is invariant under change of triangulation [C27, C52–C54]. This broken invariance can however be isolated into one of the Pachner moves, the $3-3$ move. Hence we can at least ask whether it is possible to define a measure that would render the path integral invariant under the remaining Pachner moves.

A $x - y$ Pachner move changes a complex of x D–simplices into one with y D–simplices without changing the boundary triangulation. Here the parameters x, y are related by $x + y = D + 2$. Since the boundary is not changed, the Pachner moves act locally in the triangulation. This also allows us (for the cases with $x > y$) to consider the initial configuration of x D simplices, to integrate out the bulk edges and to re–interpret the resulting partition function as one for the complex with y simplices. Note also that the $x - y$ and the $y - x$ move are inverse to each other.

In the following sections we will introduce the Pachner moves in 3D and 4D and shortly point out some points pertaining to the dynamics defined by Regge calculus.

4.2.2 Pachner moves in 3D

Here we have two Pachner moves $3 - 2$ and $4 - 1$ (and their inverses). Note that the equation of motion for 3D Regge calculus require flatness, i.e. vanishing deficit angles.

3–2 move

The first Pachner move we will consider is the $3 - 2$ move, see Fig. 4.1. In the initial configuration three tetrahedra (0123), (0124) and (0134) share an edge (01). This is the only bulk edge. Removing (i.e. integrating out) this edge and introducing a triangle (123) we obtain a configuration of two tetrahedra (0234) and (1234) sharing this triangle.

As there is only one bulk edge in the initial configuration, we will also have only one equation of motion. This equation of motion requires the vanishing of the bulk deficit angle ω_{01} and in this way fixes the length l_{01} of the edge (01) as a function of the boundary edge lengths.
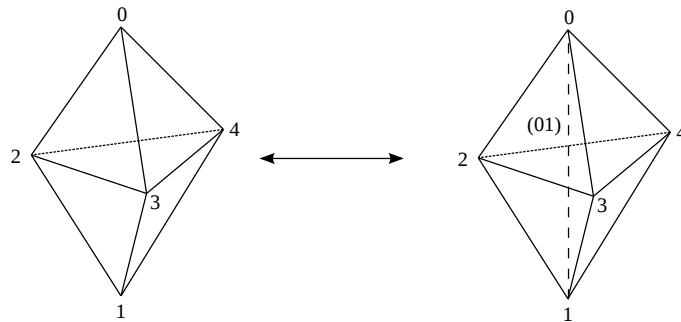
Figure 4.1: $3 - 2$ move. The two tetrahedra can be split into three by connecting the two vertices separated by the shared triangle. The dashed line in the three tetrahedra configuration is the dynamical edge.

4–1 move

The other Pachner move in 3D we are going to discuss is the $4 - 1$ move. Here in the initial configuration four tetrahedra share one vertex. This configuration can be obtained by subdividing a tetrahedron (1234) into four tetrahedra by placing one vertex 0 into the tetrahedron and connecting 0 with the other four vertices. In the $4 - 1$ move this vertex 0 and the adjacent edges are removed, leaving us with one tetrahedron (1234), see also Fig. 4.2.

In the initial configuration with four tetrahedra, there are four bulk edges, and hence four equations of motion. These, again require that the (four) bulk deficit angles have to vanish, i.e. that the complex has to be flat. We know that we can easily construct such solutions by placing a vertex into the (flat) tetrahedron (1234) and determining the lengths of the four bulk edges. There is, of course, a three–dimensional parameter space of where to place the inner vertex exactly, hence the solutions are not uniquely determined. This is the well known gauge freedom in Regge calculus

on flat solutions [C18, C51, C55–C58], a discrete remnant of the diffeomorphism symmetry in the continuum. From this it follows that of the four equations of motions only one is independent and that we have to expect three null modes in the Hessian matrix of the system, signifying three gauge degrees of freedom. Further discussions and extensions to the case with cosmological constant can be found in [C18, C23, C24, C28].
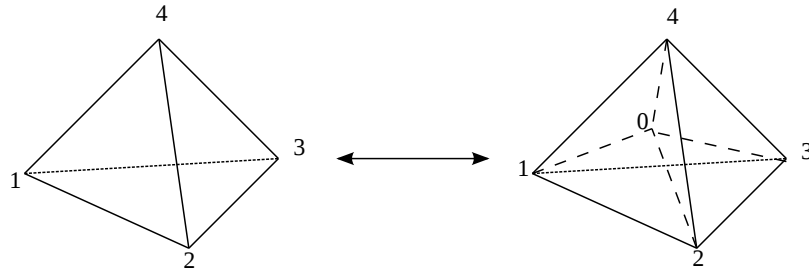
Figure 4.2: $4 - 1$ move. The tetrahedron is split into four by placing one additional vertex inside the tetrahedron and connecting it to the remaining vertices in the boundary giving four internal edges (dashed).

4.2.3 Pachner moves in 4D

4–2 move

This Pachner move is very similar to the $3 - 2$ move in 3D, see Fig. 4.3. The initial configuration is one with four 4–simplices, (01234), (01235), (01245) and (01345), sharing one edge (01). All the other edges are boundary edges. Removing this edge and introducing a tetrahedron (2345), we obtain a configuration with two 4-simplices (02345) and (12345) sharing this tetrahedron.

As there is only one bulk edge we again have only one equation of motion for the initial configuration. A (flat) solution can always be constructed in the following way: The boundary triangulation is the same as for two 4–simplices sharing one tetrahedron. Such a configuration can always (i.e. for all boundary edge lengths satisfying the appropriate inequalities) be embedded into flat 4D space. We can hence straightforwardly determine the distance between the vertices 0 and 1 in the induced metric, which defines the length of the edge (01).

In some exceptional cases there might be also solutions with curvature [C23, C24], however this seems to be rather a discretization artifact. For the perturbative solutions around flat space we are interested in, we can note that the linearized equations of motion have a unique (flat) solution for all (linearized) boundary perturbations.
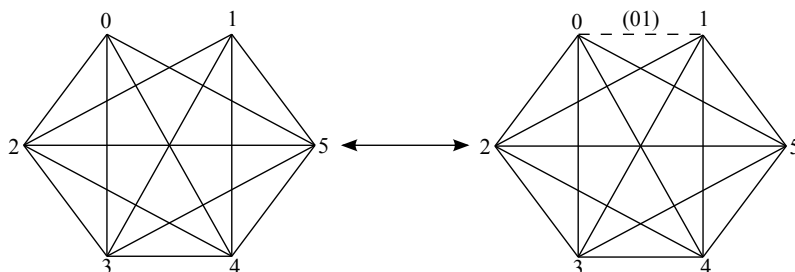
Figure 4.3: $4 - 2$ move. By connecting the vertices (0) and (1) the two 4-simplices are split into four with one bulk edge, here drawn dashed.

5–1 move

The $5 - 1$ is again analogous to the $4 - 1$ move in 3D. In the initial configuration five 4–simplices share one vertex (0) which is adjacent to five bulk edges. Removing this vertex and the adjacent edges we are left with just one simplex (12345), see also Fig. 4.4.

Also here, we can construct for all boundary configurations flat solutions to the equations of motion. These can be found by placing the vertex (0) into the (flat) 4–simplex (12345) and determining the induced lengths of the edges $(0x)$, where $x = 1, \ldots, 5$. For given boundary data there is a four–parameter space of such solutions, according to the four parameters describing the position of the vertex inside the 4–simplex. Hence we can expect four null modes for the Hessian of this configuration.
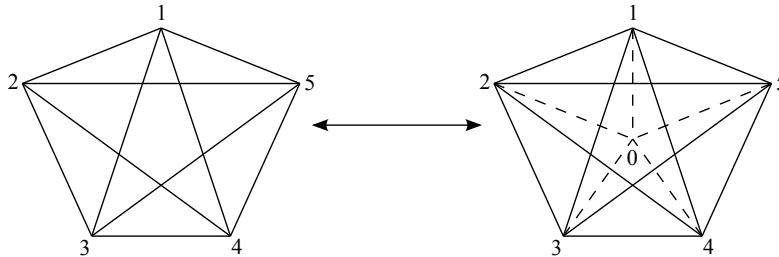
Figure 4.4: $5 - 1$ move. The 4-simplex is split into five 4-simplices by placing one vertex inside the 4-simplex and connecting it to the boundary vertices, hence obtaining five bulk edges (dashed lines).

3–3 move

We are left with the $3 - 3$ move, which is significantly different from all the other Pachner moves discussed so far.

Assume three 4-simplices (01234), (01235) and (01245) sharing one triangle (012). Note that this configuration does not include a triangle (345), as neither of the three 4–simplices contains the three vertices $(3), (4), (5)$.

The $3 - 3$ move rebuilds this configuration into three 4–simplices (01345), (02345) and (12345) which share the triangle (345) and do not include the triangle (012), see also Fig. 4.5.
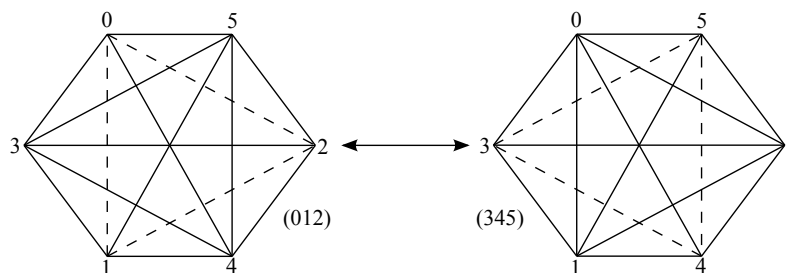
Figure 4.5: $3 - 3$ move. Three 4–simplices sharing the triangle (012) and not containing (345) are rebuilt into three 4–simplices sharing the triangle (345) and not including triangle (012). The shared triangles are drawn dashed in this figure. Note that all edges are boundary edges and are contained in both configurations, so the configurations are determined by the shared triangle.

In contrast to all other Pachner moves discussed so far the $3 - 3$ move does not involve dynamical edges, i.e. all edges are in the boundary and therefore included in both configurations. We therefore do not have an equation of motion. Note however that, again in contrast to the other Pachner

moves, not all boundary configurations define a flat geometry. That is, in both configurations we have only one bulk triangle. The vanishing of the deficit angle for this bulk triangle gives one condition for the length of the boundary edges. In case this condition is violated we do have a curved configuration. In particular, even on a flat background, we can have a curvature excitation, if the boundary perturbations do not satisfy the linearized flatness condition.

In the following section we will specify the Hessian matrix of the Regge action associated to the various configurations appearing in the Pachner moves. We could start with the formula (4.2.10) for the derivatives of the dihedral angles to obtain the derivatives of the deficit angles, so that these can be combined to give the entries in the Hessian. This procedure would however result in very lengthy formulas and not use the flatness of the background solution. We will use an alternative strategy, which will produce a quite enlightening structure for the Hessian, and for which we present some auxiliary formulas in the next section.

4.3 Computation of the Hessian matrix in 3D

In this section we will compute the matrix elements of the Hessian matrix. To do so one has to compute terms of the form $\frac{\partial \omega}{\partial l}$ for which we will present a general strategy, similar to [C59, C60]. We need to extend the ideas in [C59, C60] in order to also obtain the matrix elements of the Hessian indexed by edges in the boundary. First we will derive two auxiliary formulas, which is the subject of the next section.

4.3.1 Auxiliary formulas

For concreteness we will derive the auxiliary formulas for the initial configuration of the $3 - 2$ move (see Fig. 4.1) with the bulk edge (01) as described in the previous section. Assume that this configuration can be embedded into flat (3-dimensional) space, i.e. $\mathbb{R}^3$. This implies that for instance l_{01}, the edge length of the dynamical edge (01), is fixed as a function of all other edge lengths. Hence there is one relation which all edge lenghts have to satisfy, which is $\omega_{01} = 0$, i.e. the deficit angle at the edge (01) vanishes. (Note that this relation can also be derived by requiring that the Cayley-Menger determinant of this configuration, giving the square of the 4D volume, vanishes.) As there is one condition, at least two edge lenghts have to be varied in order to preserve this relation. Therefore consider variations of exactly two edge lenghts, l and l'. Alternatively one can interpret l' as a function of l, where all other edge lengths are (fixed) parameters. We will derive a relation between the edge variations δl and $\delta l'$ or alternatively the partial derivative $\frac{\partial l'}{\partial l}$.

For example, consider $l' = l_{23}$ and $l = l_{34}$. We vary l_{23} and l_{34} such that $\omega_{01} = 0$, i.e. the triangulation is still embeddable in flat space. This implies:

$$0 = \delta\omega_{01} = -\,\delta\theta_{01}^{(0123)} - \delta\theta_{01}^{(0124)} - \delta\theta_{01}^{(0134)}$$
$$= -\,\delta\theta_{01}^{(0123)} - \delta\theta_{01}^{(0134)} \tag{4.3.1}$$

where $\theta_{01}^{(01xy)}$ is the dihedral angle at edge (01) in the tetrahedron $(01xy)$. $\delta\theta_{01}^{(0124)} = 0$ since it neither depends on l_{23} nor on l_{34}, as these edges are not part of the tetrahedron (0124).
Using equation (4.2.11), we obtain:

$$\frac{\partial\theta_{01}^{(0123)}}{\partial l_{23}} = \frac{l_{01}l_{23}}{6V_{\bar{4}}} \quad , \qquad \frac{\partial\theta_{01}^{(0134)}}{\partial l_{34}} = \frac{l_{01}l_{34}}{6V_{\bar{2}}} \tag{4.3.2}$$

where $V_{\bar{i}}$ denotes the volume of the tetrahedron formed by all vertices except i, e.g. $\bar{4} \to (0123)$, such that $V_{\bar{4}} = V_{(0123)}$. Since $\delta\theta_{01}^{(0123)}$ ($\delta\theta_{01}^{(0134)}$) can only depend on l_{23} (l_{34} respectively), we can

use equations (4.3.2) in (4.3.1) and obtain:

$$\frac{\partial l_{23}}{\partial l_{34}} = -\frac{l_{34}}{l_{23}}\frac{V_{\bar{4}}}{V_{\bar{2}}} \quad . \tag{4.3.3}$$

In general one finds (for a five vertex configuration with vanishing Cayley-Menger determinant) [C59, C60]:

$$\left|\frac{\partial l_{ij}}{\partial l_{jk}}\right| = \left|\frac{l_{jk}V_{\bar{k}}}{l_{ij}V_{\bar{i}}}\right| \quad . \tag{4.3.4}$$

The actual sign depends on the geometric configuration under consideration.

In addition to relation (4.3.4) we need an analogous relation between deviations of edges not sharing a vertex. This can be derived from (4.3.4): Consider variations of three edge lengths l_{ij}, l_{jk} and l_{km} such that $\omega_{01} = 0$. That is, l_{ij} can be understood as a function of l_{jk} and l_{km}. Then

$$\delta l_{ij} = \frac{\partial l_{ij}}{\partial l_{jk}}\delta l_{jk} + \frac{\partial l_{ij}}{\partial l_{km}}\delta l_{km} \quad . \tag{4.3.5}$$

Now we restrict the variations further by requiring $\delta l_{ij} = 0$, such that we have to additionally understand l_{jk} as a function of l_{km}, that is $l_{ij} = l_{ij}\Big(l_{jk}(l_{km}), l_{km}\Big)$. Thus one obtains for (4.3.5):

$$0 = \frac{\partial l_{ij}}{\partial l_{jk}}\frac{\partial l_{jk}}{\partial l_{km}}\delta l_{km} + \frac{\partial l_{ij}}{\partial l_{km}}\delta l_{km} \tag{4.3.6}$$

$$\implies \frac{\partial l_{ij}}{\partial l_{km}} = -\frac{l_{ij}}{l_{jk}}\frac{l_{jk}}{l_{km}} \quad . \tag{4.3.7}$$

With (4.3.4) we find (see also [C60]):

$$\left|\frac{\partial l_{ij}}{\partial l_{km}}\right| = \left|\frac{l_{km}V_{\bar{k}}V_{\bar{m}}}{l_{ij}V_{\bar{i}}V_{\bar{j}}}\right| \quad . \tag{4.3.8}$$

To summarize (4.3.4), (4.3.8):

$$\left|\frac{\partial l_{ij}}{\partial l_{jk}}\right| = \left|\frac{l_{jk}V_{\bar{k}}}{l_{ij}V_{\bar{i}}}\right| \quad , \quad \left|\frac{\partial l_{ij}}{\partial l_{km}}\right| = \left|\frac{l_{km}V_{\bar{k}}V_{\bar{m}}}{l_{ij}V_{\bar{i}}V_{\bar{j}}}\right|$$

where in fact (4.3.4) is a special case of (4.3.8).

In the following section we will use relations (4.2.11), (4.3.4) and (4.3.8) to compute terms of the form $\frac{\partial\omega}{\partial l}$.

4.3.2 Computation of $\frac{\partial\omega}{\partial l}$

The Hessian of the Regge action has entries of the form $\frac{\partial\omega}{\partial l}$, which we have to evaluate on configurations where $\omega^{(bulk)} = 0$. As in the previous section we consider the initial configuration of the $3 - 2$ move. We will start with the calculation of $\frac{\partial\omega_{01}}{\partial l_{01}}$, which is the derivative of the bulk deficit angle with respect to the bulk edge length.

The equation of motion for the perturbations λ_{01} around the flat solution $l_{01}^{(0)}$ is given by

$$0 = \sum_b \frac{\partial^2 S}{\partial l_b \partial l_{01}}\lambda_b + \frac{\partial^2 S}{\partial l_{01}\partial l_{01}}\lambda_{01} = -\sum_b \frac{\partial\omega_{01}}{\partial l_b}\lambda_b - \frac{\partial\omega_{01}}{\partial l_{01}}\lambda_{01} \quad . \tag{4.3.9}$$

Here b indicates edges in the boundary triangulation, and the sum is over all such edges.

Now we know that these equation of motion specify λ_{01}, such that the linearized deficit angle at (01) is still flat. That is, if we choose the boundary perturbations, such that for instance only

$\lambda_{23} \sim \delta l_{23}$ is non–vanishing, we know that the ration of $\lambda_{01} \sim \delta l_{01}$ and $\lambda_{23} \sim \delta l_{23}$ has to satisfy (4.3.8). This specifies the ratio of the derivatives $\partial \omega_{01}/\partial l_{01}$ and $\partial \omega_{01}/\partial l_{23}$. For the latter derivative, as l_{23} is only included in one of the three tetrahedra we have via (4.2.11)

$$\frac{\partial \omega_{01}}{\partial l_{23}} = -\frac{\partial \theta_{01}^{(0123)}}{\partial l_{23}} = -\frac{l_{01} l_{23}}{6 V_{\bar{4}}} \quad . \tag{4.3.10}$$

This finally gives

$$\left| \frac{\partial \omega_{01}}{\partial l_{01}} \right| = \left| \frac{l_{01} l_{23}}{6 V_{\bar{4}}} \frac{\delta l_{23}}{\delta l_{01}} \right| \underset{(4.3.8)}{=} \left| \frac{l_{01}^2}{6} \frac{V_{\bar{0}} V_{\bar{1}}}{V_{\bar{2}} V_{\bar{3}} V_{\bar{4}}} \right| \quad . \tag{4.3.11}$$

The actual sign is determined by the geometry and discussed in the next section. Note that we could have also used the lengths l_{24} or l_{34} instead of l_{23}, which would have however all lead to the same result.

Next we consider terms of the form $\frac{\partial \omega_{01}}{\partial l_b}$, i.e. derivatives of the deficit angle at the bulk edge with respect to a boundary edge length. Note that for $b = 23, 24, 34$ the result is already given by (the analogue of) (4.3.10).

To find the derivative with respect to the remaining boundary lengths consider again (4.3.9) with all boundary perturbations vanishing except, say $\lambda_{0i} \sim \delta l_{0i}$. Then, with the same line of arguments as used previously we can conclude

$$\frac{\partial \omega_{01}}{\partial l_{0i}} = -\frac{\partial \omega_{01}}{\partial l_{01}} \frac{\delta l_{01}}{\delta_{0i}} \tag{4.3.12}$$

and hence

$$\left| \frac{\partial \omega_{01}}{\partial l_{0i}} \right| \underset{(4.3.4)}{=} \left| \frac{l_{01} l_{0i}}{6} \frac{V_{\bar{0}}}{V_{\bar{j}} V_{\bar{k}}} \right| \tag{4.3.13}$$

where $i \in \{2, 3, 4\}$ and j, k are such that $i, j, k = 2, 3, 4$. Again, the sign is determined by the geometry under consideration.

Note that due to the symmetry of second derivatives of the Regge action we have

$$\frac{\partial \omega_e}{\partial l_{e'}} = \frac{\partial \omega_{e'}}{\partial l_e} . \tag{4.3.14}$$

Hence we can deduce terms of the form $\frac{\partial \omega_b}{\partial l_{01}}$ from $\frac{\partial \omega_{01}}{\partial l_b}$. Thus only terms of the form $\frac{\partial \omega b}{\partial l_{b'}}$ remain to be computed, i.e. derivatives of exterior angles with respect to boundary edge lengths.

To this end, remember that the initial configuration of the $3 - 2$ Pachner move is flat. During the Pachner move the edge (01) is removed and replaced by a triangle (234), such that neither the intrinsic geometry (i. e. flatness) nor the extrinsic geometry (the embedding into flat space) of the boundary changes. In particular we will have that the extrinsic curvature angles $\omega_b^{(3)}(l_{b'}, l_{01}(l_{b'})) = \omega_b^{(2)}$ coincide in the initial and finial configuration of the Pachner moves, involving three or two tetrahedra respectively. Here we understand l_{01} as a function of the boundary lengths $l_{b'}$ as it is determined by the requirement of flatness.

Now varying just one boundary edge lengths $l_{b'}$, together with $l_{01} = l_{01}(l_{b'})$ as function of this lengths we obtain:

$$\frac{d\omega_b^{(2)}}{dl_{b'}} = \frac{d\omega_b^{(3)}}{dl_{b'}} = \frac{\partial \omega_b^{(3)}}{\partial l_{b'}} + \frac{\partial \omega_b^{(3)}}{\partial l_{01}} \frac{\partial l_{01}}{\partial l_{b'}} \tag{4.3.15}$$

$$\implies \frac{\partial \omega_b^{(3)}}{\partial l_{b'}} = \underbrace{\frac{d\omega_b^{(2)}}{dl_{b'}}}_{\frac{\partial \omega_b^{(2)}}{\partial l_{b'}}} - \underbrace{\frac{\partial \omega_b^{(3)}}{\partial l_{01}}}_{\frac{\partial \omega_{01}}{\partial l_{b'}}} \frac{\partial l_{01}}{\partial l_{b'}} \quad . \tag{4.3.16}$$

This gives finally

$$\frac{\partial \omega_b^{(3)}}{\partial l_{b'}} = \frac{\partial \omega_b^{(2)}}{\partial l_{b'}} + s \, \frac{l_b l_{b'}}{6} \frac{V_{\bar{i}} V_{\bar{j}} V_{\bar{m}} V_{\bar{n}}}{\prod_n V_{\bar{n}}} \tag{4.3.17}$$

for $b = (ij)$ and $b' = (mn)$. Here $s = \pm 1$ denotes a sign, that will be determined in the next section.

Determining the sign of $\frac{\partial l_e}{\partial l_{e'}}$

In the previous section we have seen that in order to compute the full expression for the matrix elements of the Hessian, the actual sign of the derivatives of the form $\frac{\partial l_e}{\partial l_{e'}}$ has to be determined. To be more precise, one only needs to determine the signs of $\frac{\partial l_{01}}{\partial l_b}$, where one has to treat the cases in which l_b shares a vertex with l_{01} and where it does not share a vertex separately.

We start with the case where l_b shares a vertex with l_{01}, e.g. l_{0i} with $i \in \{2, 3, 4\}$. In the derivation of the formula for $\frac{\partial \omega_{01}}{\partial l_{0i}}$, we considered variations of the edge lengths l_{01} and l_{0i}, while keeping all other edge lengths fixed, under the condition that the triangulation is supposed to remain flat. This allowed us to understand l_{01} as a function of l_{0i}, $l_{01} = l_{01}(l_{0i})$. To determine the sign of this dependence, consider Fig. 4.6:
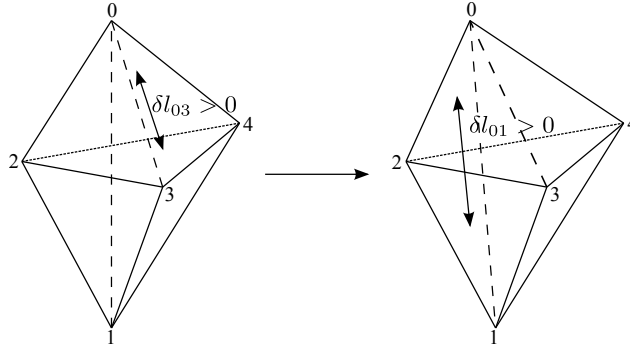
Figure 4.6: As one increases the edge lengths l_{03}, one also has to increase l_{01} in order to keep the triangulation flat, i.e. $\omega_{01} = 0$

Assume that we enlarge l_{0i} slightly, i.e. $\delta l_{0i} > 0$. If we do not change l_{01} as well, the condition $\omega_{01} = 0$ will be violated since all other edge lengths are fixed. However, if one allows l_{01} to vary as well, the vertex (0) will be 'pushed' away from the vertex i, but since the edge lengths l_{0j} and l_{0k} are fixed, l_{01} has to be increased, i.e. $\delta l_{01} > 0$. Hence:

$$\delta l_{0i} > 0 \implies \delta l_{01} > 0 \underset{(4.3.4)}{\implies} \frac{\delta l_{01}}{\delta l_{0i}} = \frac{l_{0i} V_{\bar{i}}}{l_{01} V_{\bar{1}}} \quad . \tag{4.3.18}$$

We follow a similar line of argumentation for terms of the form $\frac{\partial l_{ij}}{\partial l_{01}}$, with $i, j \in \{2, 3, 4\}$. Consider Fig. 4.7:

Assume that we slightly increase l_{ij}, i.e. $\delta l_{ij} > 0$. Since the edge lenghts l_{ik} and l_{jk} are fixed, the vertex k is being 'pulled' towards the edge (ij). Furthermore the edge lengths l_{0i}, l_{0j} and l_{0k} are fixed, such that the vertex (0) is 'dragged' towards the edge (ij). This configuration can only remain flat, if l_{01} is decreased, i.e. $\delta l_{01} < 0$. Hence:

$$\delta l_{ij} > 0 \implies \delta l_{01} < 0 \underset{(4.3.8)}{\implies} \frac{\delta l_{01}}{\delta l_{ij}} = -\frac{l_{ij} V_{\bar{i}} V_{\bar{j}}}{l_{01} V_{\bar{0}} V_{\bar{1}}} \quad . \tag{4.3.19}$$

This is also consistent with (4.3.10).
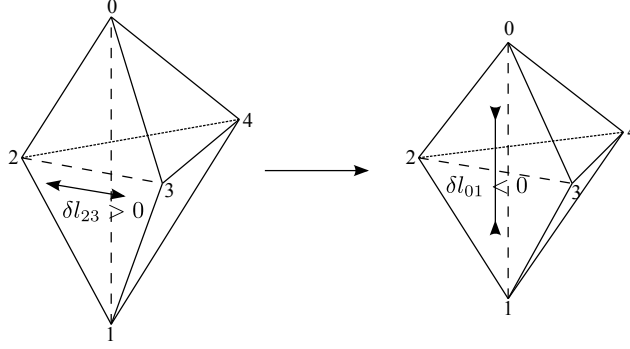
Figure 4.7: As one increases the edge lengths l_{23}, one has to decrease l_{01} in order to keep the triangulation flat, i.e. $\omega_{01} = 0$

4.3.3 Summary for the 3–2 move

Let us summarize the results of the previous paragraphs.

- In case either edge (ij) or the edge (km) is in the bulk, one obtains:

$$H^{(3)}_{(ij),(km)} := \frac{\partial^2 S}{\partial l_{km} \partial l_{ij}} = -\frac{\partial \omega_{ij}}{\partial l_{km}} = (-1)^{s_i+s_j+s_k+s_m} \frac{l_{ij} l_{km}}{6} \frac{V_{\bar{i}} V_{\bar{j}} V_{\bar{k}} V_{\bar{m}}}{\prod_n V_{\bar{n}}} \tag{4.3.20}$$

  where

$$s_i = \begin{cases} 1 & \text{if } i \in \{0,1\} \\ 0 & \text{else} \end{cases} \tag{4.3.21}$$

  and the product in the denominator runs over all vertices in the triangulation.

- In case both the edges (ij) and (km) are in the boundary, one obtains:

$$H^{(3)}_{(ij),(km)} := \frac{\partial^2 S}{\partial l_{km} \partial l_{ij}} = -\frac{\partial \omega^{(3)}_{ij}}{\partial l_{km}} = (-1)^{s_i+s_j+s_k+s_m} \frac{l_{ij} l_{km}}{6} \frac{V_{\bar{i}} V_{\bar{j}} V_{\bar{k}} V_{\bar{m}}}{\prod_n V_{\bar{n}}} - \frac{\omega^{(2)}_{ij}}{\partial l_{km}} \tag{4.3.22}$$

  where $\omega^{(i)}_{km}$ denotes the exterior angle at the (boundary) edge (km) in the i tetrahedra configuration, s_i is defined as above.

Notice the simple form of the Hessian,

$$H^{(3)}_{(ij),(km)} = H^{(2)}_{(ij),(km)} + c\, h_{(ij)}\, h_{(km)} \quad , \tag{4.3.23}$$

in particular that the second summand in (4.3.23) factorizes. (Here $H^{(2)}_{(ij),(km)} = 0$ if either (ij) of (km) equals (01).)

We have now all the prerequisites to discuss the (form-) invariance of the path integral associated to the $3-2$ move.

4.3.4 Invariance of the path integral

For the $3-2$ move we have to consider an expression of the following form:

$$P_{3-2} = \int d\lambda_{01}\, \mu(l)\, \exp\left[-\sum_{(ij),(km)} \frac{1}{2} H^{(3)}_{(ij),(km)} \lambda_{ij} \lambda_{km} \right] \tag{4.3.24}$$

where:

- $\mu(l)$ is a measure factor, which we assume to only depend on the background variables l, such that the configuration is flat.

- $H^{(3)}_{(ij),(km)}$ is the $(ij),(km)$-matrix element of the Hessian in the three tetrahedra configuration, which we computed in the previous section, see (4.3.20), (4.3.22).

- Since λ_{01} is the only dynamical edge (variation) in the configuration under discussion, the sign of $H^{(3)}_{(01),(01)}$ is crucial for the convergence of (4.3.24). In the sign convention introduces in equation (4.2.2) $H^{(3)}_{(01),(01)} > 0$, such that (4.3.24) converges.

We can easily perform the integral in (4.3.24) as it is a (partial) Gaussian integration. For an integral of the form

$$I = \int dq_1 \ldots dq_r \, \exp\left\{-\frac{1}{2} \vec{q}^T M \vec{q}\right\} \tag{4.3.25}$$

where M is a real, symmetric, positive-definite $n \times n$-matrix and $\vec{q} = (q_i)$ denotes a vector with $i = 1, \ldots, r, r+1, \ldots n$. Splitting the matrix M accordingly into submatrices

$$M = \begin{pmatrix} W_0 & V \\ V^T & U_0 \end{pmatrix} \tag{4.3.26}$$

we can write

$$I = \frac{(2\pi)^{\frac{r}{2}}}{\sqrt{\det(W_0)}} \exp\left\{-\frac{1}{2} \vec{u}^T U \vec{u}\right\} \qquad \text{with} \qquad U := U_0 - V^T W_0^{-1} V \quad . \tag{4.3.27}$$

Using this result for the $3 - 2$ move (4.3.24), we identify:

$$W_0 = H^{(3)}_{(01),(01)} = -\frac{\partial \omega_{01}}{\partial l_{01}} \tag{4.3.28}$$

$$(U_0)_{b,b'} = \underbrace{-\frac{\partial \omega_b^{(2)}}{\partial l_{b'}}}_{H^{(2)}_{b,b'}} + \frac{\partial \omega_{01}}{\partial l_b} \frac{\partial l_{01}}{\partial l_{b'}} \tag{4.3.29}$$

$$(V)_{(01),b} = -\frac{\partial \omega_{01}}{\partial l_b} \quad . \tag{4.3.30}$$

Furthermore requiring form invariance of (4.3.24) implies

$$P_{3-2} \propto \exp\left\{-\sum_{(ij)\neq(01),(km)\neq(01)} \frac{1}{2} H^{(2)}_{(ij)(km)} \lambda_{ij} \lambda_{km}\right\} \tag{4.3.31}$$

such that in order to show that (4.3.24) is invariant (on the level of the action), one has to show that $U = H^{(2)}$, which implies

$$-\frac{\partial \omega_{01}}{\partial l_b} \frac{\partial l_{01}}{\partial l_{b'}} = \left[\frac{\partial \omega_{01}}{\partial l_{01}}\right]^{-1} \frac{\partial \omega_{01}}{\partial l_b} \frac{\partial \omega_{01}}{\partial l_{b'}} \quad . \tag{4.3.32}$$

Note that we have already proven that (4.3.32) holds due to the identity (4.3.12). This shows form invariance of the action.

For the invariance of the measure $\mu(l)$ in (4.3.24) we examine the contribution from the Gaussian integral:

$$\frac{\sqrt{2\pi}}{\sqrt{\det(W_0)}} = \frac{\sqrt{2\pi}}{\sqrt{H^{(3)}_{(01),(01)}}} = \frac{\sqrt{2\pi}}{\sqrt{-\frac{\partial \omega_{01}}{\partial l_{01}}}} = \frac{\sqrt{12\pi}}{l_{01}} \sqrt{\frac{V_{\bar{2}} V_{\bar{3}} V_{\bar{4}}}{V_{\bar{0}} V_{\bar{1}}}} \tag{4.3.33}$$

Hence, choosing the measure factor as

$$\mu(l) = \frac{\prod_e \frac{l_e}{\sqrt{12\pi}}}{\prod_\tau \sqrt{V_\tau}} \tag{4.3.34}$$

we obtain a partition function, invariant under $3 - 2$ Pachner moves. Here e denotes the edges and τ the tetrahedra in the triangulation.

4.3.5 4–1 move

For 3D gravity, in addition to the $3 - 2$ move, we have also to consider the $4 - 1$ move. This move amounts to the subdivision of one tetrahedron, denoted by (1234), into four by adding one additional vertex (0), placing it inside the original tetrahedron and connecting it with all of the remaining vertices, see section 4.2.2.

In contrast to the $3 - 2$ move, the edge lengths of the new edges, i.e. the position of the new vertex inside the original tetrahedron, is not uniquely fixed. In fact the action is invariant under translations of the vertex (0) inside the tetrahedron (1234), such that one expects the Hessian matrix to have three null eigenvectors. In order to compute this matrix, terms of the form $\frac{\partial \omega_e}{\partial l_{e'}}$ have to be evaluated just as in the $3 - 2$ move. Following a similar derivation as in the previous section, one arrives at the following terms:

- In case either the edge $e = (ij)$ or edge $e' = (km)$ are in the bulk, one obtains:

$$\frac{\partial^2 S}{\partial l_{km} \partial l_{ij}} = (-1)^{s_i + s_j + s_k + s_m + 1} \frac{l_{ij} l_{km}}{6} \frac{V_{\bar{i}} V_{\bar{j}} V_{\bar{k}} V_{\bar{m}}}{\prod_n V_{\bar{n}}} \tag{4.3.35}$$

  where

$$s_i = \begin{cases} 1 & \text{if } i = 0 \\ 0 & \text{else} \end{cases} . \tag{4.3.36}$$

- In case both edges are in the boundary, one obtains:

$$\frac{\partial^2 S}{\partial l_{km} \partial l_{ij}} = (-1)^{s_i + s_j + s_k + s_m + 1} \frac{l_{ij} l_{km}}{6} \frac{V_{\bar{i}} V_{\bar{j}} V_{\bar{k}} V_{\bar{m}}}{\prod_n V_{\bar{n}}} - \frac{\partial \omega_{ij}^{(1)}}{\partial l_{km}} \tag{4.3.37}$$

  where $\omega^{(1)}$ denotes an exterior dihedral angle in the one tetrahedron configuration.

Again, notice the simple form of the Hessian,

$$H_{(ij),(km)}^{(4)} = H_{(ij),(km)}^{(1)} + c\, h_{(ij)}\, h_{(km)} \quad, \tag{4.3.38}$$

with a factorizing summand. This form of the Hessian makes the appearance of null vectors obvious.

Null eigenvectors

Since the pure bulk part $H_{(0i),(0j)}^{(4)}$ of the Hessian matrix factorizes, we can easily examine the condition for null vectors $\vec{v}$:

$$\sum_j H_{(0i),(0j)} v_j = c h_{0i} \sum_j h_{0j} v_j \overset{!}{=} 0 \tag{4.3.39}$$

Hence, due to the factorizing form of the Hessian, we just have one condition for the null vectors. Therefore the Hessian has three null eigenvectors and of the four bulk degrees of freedom three are gauge.

Furthermore we have to discuss the sign of the Hessian. The only non–vanishing eigenvalue of the submatrix $H_{(0i),(0j)}$ can also easily be determined due to the factorizing form to be $\sum_j H_{(0j),(0j)}$. This gives a negative eigenvalue, hence the Gaussian integral would not be convergent. This is a trace of the conformal mode problem in Euclidean gravity: the kinematic term of the conformal mode comes with the 'wrong' sign, so that the Euclidean action is not bounded from below. We see that the Pachner moves allow a nice isolation of this mode problem into the $4-1$ moves. We will change the global sign for the action of the $4-1$ move, such that the integral (over the one non-gauge mode) converges. This can be understood as selecting a complex contour for the integration for the conformal and the other modes separately, see [C61] for a discussion in the continuum.

Invariance of the path integral

Similar to the $3-2$ move, we have to consider

$$P_{4\to 1} = \int \prod_i d\lambda_{0i}\, \mu(l)\, \exp\left\{ -\sum_{(ij),(km)} \frac{1}{2} H^{(4)}_{(ij),(km)}\, \lambda_{ij}\, \lambda_{km} \right\} \tag{4.3.40}$$

where $\mu(l)$ is again a measure factor, which we assume to depend only on background variables l, which have to make up a flat configuration. (4.3.40) is again a partial Gaussian integral but with three gauge degrees of freedom, for which we will modify the general method of section 4.3.4.

Again the general form for the Gaussian integral is:

$$I = \int dq_1 \ldots dq_r \exp\left\{ -\frac{1}{2} \vec{q}^T M \vec{q} \right\} \quad . \tag{4.3.41}$$

Since there are gauge degrees of freedom one integrates over the matrix M is singular. Assume that there are m gauge degrees of freedom such that we can split $\vec{q}$ in the following way:

$$\vec{q} = (\underbrace{q_1, \ldots, q_{r-m}}_{=:\vec{w}}, \underbrace{q_{r-m+1}, \ldots, q_r}_{=:\vec{g}}, \underbrace{q_{r+1}, \ldots, q_n}_{=:\vec{u}}) \quad . \tag{4.3.42}$$

(Here we assume that the transformation between $q_{r-m+1}, \ldots, q_r$ and the m gauge parameters is not singular.) This implies the following split for the matrix M

$$M = \begin{pmatrix} W_0 & V_g & V \\ V_g^T & G_0 & Z_0 \\ V^T & Z_0^T & U_0 \end{pmatrix} \tag{4.3.43}$$

where W_0 is non-singular. Integrating out the degrees of freedom summarized in $\vec{w}$ one obtains:

$$I = \frac{(2\pi)^{\frac{(r-m)}{2}}}{\sqrt{\det(W_0)}} \exp\left\{ -\frac{1}{2}\left(\vec{g}^T G \vec{g} + \vec{g}^T Z \vec{u} + \vec{u}^T Z^T \vec{g} + \vec{u}^T U \vec{u} \right) \right\} \tag{4.3.44}$$

with

$$G = G_0 - V_g^T W_0^{-1} V_g \quad , \tag{4.3.45}$$

$$Z = Z_0 - V_g^T W_0^{-1} V \quad , \tag{4.3.46}$$

$$U = U_0 - V^T W_0^{-1} V \quad . \tag{4.3.47}$$

Applying this formalism to the problem under discussion, one identifies (here $i, j \neq 0, 1$):

$$(W_0)_{(01),(01)} = H^{(4)}_{(01),(01)} = -\frac{\partial\omega_{01}}{\partial l_{01}} \quad , \qquad\qquad (G_0)_{(0i),(0j)} = \frac{\partial\omega_{01}}{\partial l_{0i}}\frac{\partial l_{01}}{\partial l_{0j}} \quad ,$$

$$(U_0)_{b,b'} = H^{(1)}_{b,b'} + \frac{\partial\omega_{01}}{\partial l_b}\frac{\partial l_{01}}{\partial l_{b'}} \quad , \qquad\qquad (V_g)_{(01),(0i)} = -\frac{\partial\omega_{01}}{\partial l_{0i}} \quad ,$$

$$(V)_{(01),b} = -\frac{\partial\omega_{01}}{\partial l_b} \quad , \qquad\qquad (Z_0)_{(0i),b} = \frac{\partial\omega_{01}}{\partial l_{0i}}\frac{\partial l_{0i}}{\partial l_b} \quad . \tag{4.3.48}$$

We therefore obtain:

$$(G)_{(0i),(0j)} = \frac{\partial \omega_{01}}{\partial l_{0i}} \frac{\partial l_{01}}{\partial l_{0j}} + \left[\frac{\partial \omega_{01}}{\partial l_{01}}\right]^{-1} \frac{\partial \omega_{01}}{\partial l_{0i}} \frac{\partial \omega_{01}}{\partial l_{0j}} \overset{(4.3.12)}{=} 0 \tag{4.3.49}$$

$$(Z)_{(0i),b} = \frac{\partial \omega_{01}}{\partial l_{0i}} \frac{\partial l_{01}}{\partial l_b} + \left[\frac{\partial \omega_{01}}{\partial l_{01}}\right]^{-1} \frac{\partial \omega_{01}}{\partial l_{0i}} \frac{\partial \omega_{01}}{\partial l_b} \overset{(4.3.12)}{=} 0 \tag{4.3.50}$$

$$(U)_{b,b'} = H^{(1)}_{b,b'} + \frac{\partial \omega_{01}}{\partial l_b} \frac{\partial l_{01}}{\partial l_{b'}} + \left[\frac{\partial \omega_{01}}{\partial l_{01}}\right]^{-1} \frac{\partial \omega_{01}}{\partial l_b} \frac{\partial \omega_{01}}{\partial l_{b'}} \overset{(4.3.12)}{=} H^{(1)}_{b,b'} \quad . \tag{4.3.51}$$

This proves form invariance of the action, as the remaining term in the exponential corresponds to the action of the tetrahedron (1234) (after we have rotated back the global sign of the action).

Note that after having only integrated over λ_{01} the other bulk variables λ_{0i}, $i = 2, 3, 4$ do not appear anymore in the exponential.

Let us first consider how the measure factor is modified by the Gaussian integration over λ_{01}. The additional factor is given by

$$\frac{\sqrt{2\pi}}{\sqrt{\det(W_0)}} = \frac{\sqrt{12\pi}}{l_{01}} \sqrt{\frac{V_{\bar{2}} V_{\bar{3}} V_{\bar{4}}}{V_{\bar{0}} V_{\bar{1}}}} \quad . \tag{4.3.52}$$

If we consider $\mu(l)$ in (4.3.40) to be the same measure which gives an invariant amplitude under the $3 - 2$ move, namely

$$\mu(l) = \frac{\prod_e \frac{l_e}{\sqrt{12\pi}}}{\prod_\tau \sqrt{V_\tau}} \tag{4.3.53}$$

where e includes all boundary and bulk edges and τ the four tetrahedra of the initial configuration, we obtain:

$$P_{4-1} = \frac{\prod_b l_b}{\sqrt{12\pi V_{\bar{0}}}} \exp\left\{-\sum_{b,b'} \frac{1}{2} H^{(1)}_{b,b'} \lambda_b \lambda_{b'}\right\} \int \frac{\prod_{i \neq 1} \frac{l_{0i}}{\sqrt{12\pi}} d\lambda_{0i}}{V_{\bar{1}}} \quad . \tag{4.3.54}$$

The remaining integral over the variables $\lambda_{02}, \ldots, \lambda_{04}$ can be identified with an integration over the gauge orbit, which is given by the displacement of the inner vertex (0). As one can show [C60, C62], see also appendix 4.A, the following identity between integration measures holds

$$d^3 x_0^\alpha = \frac{\prod_{i=2,3,4} l_{0i} \, dl_{0i}}{6 V_{\bar{1}}} \quad . \tag{4.3.55}$$

Here $d^3 x_0^\alpha$ is the integration measure of the Euclidean coordinates x_0^α, $\alpha = 1, 2, 3$ of the vertex (0). The displacement of this vertex corresponds exactly to the gauge action of the discrete remnant of the diffeomorphisms [C18, C58, C63]. Hence we will replace the last factor in (4.3.54) by 1. This can be understood as resulting from a gauge fixing procedure, including the appropriate Faddeev-Popov determinant. (The numerical factors are chosen to conform with the integration measure found for the $3 - 2$ move, however it is not possible to fix them uniquely.)

4.4 Summary for 3D gravity

For a general 3D triangulation we define the path integral for linearized Regge calculus by

$$P := \int \frac{\prod_e \frac{l_e}{\sqrt{12\pi}}}{\prod_\tau \sqrt{V_\tau}} \prod_{e \subset \text{bulk}} d\lambda_e \exp\left\{-\frac{1}{2} \sum_{e,e'} H_{e,e'} \lambda_e \lambda_{e'}\right\} \quad . \tag{4.4.1}$$

l_e is the length of the edge e, V_τ is the volume of the tetrahedron τ, λ_e is the edge length perturbation of the edge e and $H_{e,e'}$ is the e-e' matrix element of the Hessian matrix of the Regge action. The

considerations conducted in the previous section show that (4.4.1) is invariant under Pachner moves, in case one follows the gauge fixing and sign rotation procedure for the $4-1$ move discussed above. Hence (4.4.1) does not depend on the choice of bulk triangulation and in this sense it is discretization independent.

Here we assigned the numerical pre–factor $(12\pi)^{-1/2}$ to the edges of the triangulation (as the π factors result from integration over edges). Another possibility would be to associate this pre–factor to the tetrahedra of the triangulation, in which case one needs to appropriately adjust the numerical constant in the gauge fixing prescription for the $4-1$ move.

Amazingly, the path integral measure which we found for linearized Regge calculus, coincides with the semi-classical limit of the Ponzano–Regge model [C35–C37]. This is a triangulation independent[3] spin foam model for 3D quantum gravity. Here the numerical pre–factors (also given by $(12\pi)^{-1/2}$) are associated to the tetrahedra.

It would be interesting to see, whether this correspondence can be extended to 3D Regge calculus with a cosmological constant. This theory can be (classically) formulated in a triangulation independent way, by using curved tetrahedra [C28, C50]. The corresponding quantization is given by the Turaev-Viro model [C64], for which the semi–classical limit has been obtained [C65]. Hence (4.4.1) should give a triangulation independent amplitude for linearized Regge calculus with a (positive) cosmological constant by replacing l_e and V_τ by their respective counterparts on the sphere, i.e. $\sin(l_e)$, where $l_e \in [0, \pi]$, and $\mathcal{V}_\tau$, the determinant of the Gram matrix.

4.5 Computation of the Hessian matrix in 4D

We are now going to discuss the 4D case. We will proceed as for 3D, that is first determine the matrix elements of the Hessian and then consider the path integral for the Pachner moves. It will turn out that the $4-2$ and $5-1$ moves behave very similarly to the $3-2$ and the $4-1$ move, respectively, in 3D. There is however an additional Pachner move in 4D, namely the $3-3$, which is significantly different, and thus responsible for the non–trivial dynamics of 4D Regge gravity.

The Hessian of the Regge action is given by

$$\frac{\partial^2 S}{\partial l_{ij} \partial l_{mn}} = -\sum_{stu} \frac{\partial A_{stu}}{\partial l_{mn}} \frac{\partial \omega_{stu}}{\partial l_{ij}} - \sum_{stu \in \text{bulk}} \frac{\partial^2 A_{stu}}{\partial l_{ij} \partial l_{mn}} \omega_{stu}^{(bulk)} - \sum_{stu \in \text{bdry}} \frac{\partial^2 A_{stu}}{\partial l_{ij} \partial l_{mn}} \omega_{stu}^{(bdry)} \tag{4.5.1}$$

where ω_{stu} is the deficit angle at the (bulk or boundary) triangle (stu). In the following we will not discuss the last two terms in (4.5.1) because we will consider flat background solutions, i.e. $\omega^{(bulk)} = 0$. That is the second term in (4.5.1) vanishes and the third term is unaffected by Pachner moves, since the extrinsic geometry, defined by the embedding into flat space, is not changed. (Furthermore this term is only multiplied by boundary perturbations, which are not integrated over in the path integrals.)

Hence we define a reduced Hessian matrix:

$$H_{(ij),(km)} := -\sum_\Delta \frac{\partial A_\Delta}{\partial l_{ij}} \frac{\partial \omega_\Delta}{\partial l_{km}} \tag{4.5.2}$$

which can be rewritten as the product of the following two matrices:

$$H = - \begin{pmatrix} \frac{\partial A_{\Delta_1}}{\partial l_{01}} & \frac{\partial A_{\Delta_2}}{\partial l_{01}} & \cdots \\ \frac{\partial A_{\Delta_1}}{\partial l_{02}} & \ddots & \\ \vdots & & \end{pmatrix} \begin{pmatrix} \frac{\partial \omega_{\Delta_1}}{\partial l_{01}} & \frac{\partial \omega_{\Delta_1}}{\partial l_{02}} & \cdots \\ \frac{\partial \omega_{\Delta_2}}{\partial l_{01}} & \ddots & \\ \vdots & & \end{pmatrix} \tag{4.5.3}$$

---

[3]also requiring a gauge fixing procedure for the $4-1$ moves

Here the index summation is over all triangles in the triangulation. So as in 3D we have to compute terms of the form $\frac{\partial \omega_\triangle}{\partial l_e}$. To this end we will proceed similarly as in the 3D case, as described in the next sections.

4.5.1 4–2 move

Auxiliary formulas

As in 3D we will need additional formulas to derive all entries of the Hessian matrix in a compact way. We start with the derivatives of the dihedral angles at a given triangle with respect to the length of the opposite edge (4.2.11)

$$\frac{\partial \theta_{ijk}^{(ijkmn)}}{\partial l_{mn}} = \frac{l_{mn} A_{ijk}}{12V}$$

where A_{ijk} denotes the area of the triangle (ijk), l_{mn} is the lengths of the edge (mn) and V is the volume of the 4-simplex $(ijkmn)$.

Now given a flat triangulation with six, i.e. $D+2$, vertices, we will consider edge lengths variations of at least two edges under the condition that the triagulation remains flat, i.e. the deficit angles are vanishing, $\omega = 0$. Then, along the same line of arguments as in 3D, we obtain [C66]:

- In case the varied edges share a vertex:

$$\left| \frac{\partial l_{ij}}{\partial l_{jk}} \right| = \left| \frac{l_{jk}}{l_{ij}} \frac{V_{\bar{k}}}{V_{\bar{i}}} \right| \tag{4.5.4}$$

- In case the varied edges do not share a vertex:

$$\left| \frac{\partial l_{ij}}{\partial l_{km}} \right| = \left| \frac{l_{km}}{l_{ij}} \frac{V_{\bar{k}} V_{\bar{m}}}{V_{\bar{i}} V_{\bar{j}}} \right| \tag{4.5.5}$$

where $V_{\bar{k}}$ denotes the volume of the 4-simplex formed without the vertex k. To determine the sign of the derivatives in (4.5.4,4.5.5) one has to consider the geometric set–up in detail. Note that (4.5.4) and (4.5.5) are the exact 4D analogues of (4.3.4) and (4.3.8) respectively.

Computation of $\frac{\partial \omega}{\partial l}$

Consider the $4-2$ move, that is two 4-simplices (02345) and (12345), which share one common tetrahedron (2345). By connecting vertices (0) and (1), the two 4-simplices are split into four, namely $(01ijk)$. This edge is the only bulk edge in the configuration with 4 simplices. As for the $3-2$ move we can use two facts, to specify the matrix elements of the Hessian. Namely on the one hand, that the equations of motions for the perturbation variable λ_{01} require flatness, on the other hand that lengths perturbations around flat space have to satisfy equations (4.5.4,4.5.5). The equation of motion is given by

$$\sum_{e \neq (01)} H_{(01),e} \lambda_e + H_{(01)(01)} \lambda_{01} = 0 \quad . \tag{4.5.6}$$

But as the perturbative solutions are also flat, the perturbation variables λ_e have to satisfy the relations (4.5.4,4.5.5). Hence considering boundary data, such that only one $\lambda_e \neq 0$ for $e = (km) \neq (01)$ and $\lambda_{01} \neq 0$ we can deduce

$$\left| \frac{H_{(01),(km)}}{H_{(01),(01)}} \right| = \left| \frac{\delta l_{01}}{\delta l_{km}} \right| = \left| \frac{l_{km}}{l_{01}} \frac{V_{\bar{k}} V_{\bar{m}}}{V_{\bar{0}} V_{\bar{1}}} \right| \quad . \tag{4.5.7}$$

To specify the (reduced) Hessian even further, we can use that the linearized deficit angles also have to vanish. That is consider variations of two edge lengths, here $\delta l_{01} = \lambda_{01}$ and $\delta l_{34} = \lambda_{34}$. Using that the linearized deficit angle $\delta\omega_{012}$ has to vanish we obtain

$$0 = \delta\omega_{012} = -\frac{\partial\theta_{012}^{(01234)}}{\partial l_{34}}\delta l_{34} + \frac{\partial\omega_{012}}{\partial l_{01}}\delta l_{01} \tag{4.5.8}$$

$$\overset{(4.2.11)}{=} -\frac{l_{34}A_{012}}{12V_{\bar{5}}}\delta l_{34} + \frac{\partial\omega_{012}}{\partial l_{01}}\delta l_{01} \tag{4.5.9}$$

$$\Longrightarrow \left|\frac{\partial\omega_{012}}{\partial l_{01}}\right| = \left|\frac{l_{01}A_{012}}{12V_{\bar{5}}}\frac{\delta l_{34}}{\delta l_{01}}\right| \overset{(4.5.5)}{=} \left|\frac{l_{01}A_{012}}{12}\frac{V_{\bar{0}}V_{\bar{1}}}{V_{\bar{3}}V_{\bar{4}}V_{\bar{5}}}\right| \quad . \tag{4.5.10}$$

This can be repeated for all bulk deficit angles:

$$\left|\frac{\partial\omega_{01i}}{\partial l_{01}}\right| = \left|\frac{l_{01}A_{01i}}{12}\frac{V_{\bar{0}}^2V_{\bar{1}}^2V_{\bar{i}}}{\prod_n V_{\bar{n}}}\right| \quad . \tag{4.5.11}$$

The sign is again determined by the geometry under consideration.

The rest of the derivations proceeds in the same way as for the $3-2$ move. That is for the derivation of the bulk deficit angle with respect to a boundary edge length l_b we obtain

$$\frac{\partial\omega_{01i}}{\partial l_b} = -\frac{\partial\omega_{01i}}{\partial l_{01}}\frac{\partial l_{01}}{\partial l_b} \quad . \tag{4.5.12}$$

To determine the derivatives of the (boundary) exterior angles one again uses that these angles agree in both configurations of the $4-2$ move. This results in

$$\left|\frac{\partial\omega_{ijk}^{(4)}}{\partial l_{01}}\right| = \left|\frac{l_{01}A_{ijk}}{12}\frac{V_{\bar{0}}V_{\bar{1}}V_{\bar{i}}V_{\bar{j}}V_{\bar{k}}}{\prod_n V_{\bar{n}}}\right| \tag{4.5.13}$$

and furthermore in

$$\frac{\partial\omega_{ijk}^{(4)}}{\partial l_b} = \frac{\partial\omega_{ijk}^{(2)}}{\partial l_b} - \frac{\partial\omega_{ijk}^{(4)}}{\partial l_{01}}\frac{\partial l_{01}}{\partial l_b} \quad . \tag{4.5.14}$$

The missing signs are dependent on the geometry under discussion and determined by similar considerations as in section 4.3.2. To summarize the results for the $4-2$ move:

- In the case that either the triangle or the edge is in the bulk:

$$\frac{\partial\omega_{ijk}^{(4)}}{\partial l_{mn}} = (-1)^{s_i+s_j+s_k+s_m+s_n+1}\frac{l_{mn}A_{ijk}}{12}\frac{V_{\bar{i}}V_{\bar{j}}V_{\bar{k}}V_{\bar{m}}V_{\bar{n}}}{\prod_p V_{\bar{p}}} \tag{4.5.15}$$

 where

$$s_i = \begin{cases} 1 & \text{if } i \in \{0,1\} \\ 0 & \text{else} \end{cases} \quad . \tag{4.5.16}$$

- In the case that both triangle and edge are in the boundary:

$$\frac{\partial\omega_{ijk}^{(4)}}{\partial l_{mn}} = (-1)^{s_i+s_j+s_k+s_m+s_n+1}\frac{l_{mn}A_{ijk}}{12}\frac{V_{\bar{i}}V_{\bar{j}}V_{\bar{k}}V_{\bar{m}}V_{\bar{n}}}{\prod_p V_{\bar{p}}} + \frac{\partial\omega_{ijk}^{(2)}}{\partial l_{mn}} \tag{4.5.17}$$

Note that as in 3D the formulas for $\frac{\partial\omega}{\partial l}$ factorize.

Hessian matrix

In order to complete the calculation for the (reduced) Hessian matrix, the terms $\frac{\partial A_\Delta}{\partial l_{ij}} \frac{\partial \omega_\Delta}{\partial l_{km}}$ have to be summed up, where

$$\frac{\partial A_{ijk}}{\partial l_{ij}} = \frac{l_{ij}}{8 A_{ijk}} \underbrace{(l_{ik}^2 + l_{jk}^2 - l_{ij}^2)}_{=:F_{ij;k}}. \tag{4.5.18}$$

Note that (4.5.18) is only non-vanishing for four triangles in the triangulation for a given edge (ij). This implies (in case either (op) or (mn) are in the bulk):

$$H^{(4)}_{(op),(mn)} = -\sum_{(ijk)} \frac{\partial A_{ijk}}{\partial l_{op}} \frac{\partial \omega_{ijk}}{\partial l_{mn}} = -\sum_{k \neq o,p} \frac{\partial A_{opk}}{\partial l_{op}} \frac{\partial \omega_{opk}}{\partial l_{mn}} \tag{4.5.19}$$

$$= \sum_{k \neq o,p} \frac{1}{8} \frac{l_{op} l_{mn}}{12} (-1)^{s_o + s_p + s_k + s_m + s_n} \frac{V_{\bar{o}} V_{\bar{p}} V_{\bar{m}} V_{\bar{n}}}{\prod_l V_{\bar{l}}} V_{\bar{k}} F_{op;k}$$

$$= \underbrace{(-1)^{s_o + s_p + s_m + s_n} \frac{l_{op} l_{mn}}{96} \frac{V_{\bar{o}} V_{\bar{p}} V_{\bar{m}} V_{\bar{n}}}{\prod_l V_{\bar{l}}}}_{\text{symmetric in } (op) \leftrightarrow (mn)} \underbrace{\sum_{k \neq o,p} (-1)^{s_k} V_{\bar{k}} F_{op;k}}_{=:D_{op}} \tag{4.5.20}$$

where D_{op} is a factor independent of the choice of (mn). In case (op) and (mn) are in the boundary, we obtain:

$$H^{(4)}_{(op),(mn)} = D_{op} (-1)^{s_o + s_p + s_m + s_n} \frac{l_{op} l_{mn}}{96} \frac{V_{\bar{o}} V_{\bar{p}} V_{\bar{m}} V_{\bar{n}}}{\prod_l V_{\bar{l}}} - \underbrace{\sum_{k \neq o,p} \frac{l_{op}}{8 A_{opk}} F_{op;k} \frac{\partial \omega^{(2)}_{opk}}{\partial l_{mn}}}_{=H^{(2)}_{(op),(mn)}}. \tag{4.5.21}$$

$H^{(4)}$ and $H^{(2)}$ are equal to matrices of second derivatives of the Regge action up to symmetric terms. Hence $H^{(4)}$ and $H^{(2)}$ are also symmetric matrices. From this it follows that the factor D_{op} is the same for all choices of op:

$$D := D_{op} = D_{mn} \quad . \tag{4.5.22}$$

Note that the elements $H^4_{(ij),(01)}$ satisfy the relation (4.5.7).

Invariance of the path integral

We have to consider:

$$P_{4-2} = \int d\lambda_{01} \, \mu(l) \, \exp\left\{ -\sum_{(ij),(km)} \frac{1}{2} H^{(4)}_{(ij),(km)} \lambda_{ij} \lambda_{km} \right\} \tag{4.5.23}$$

where the measure factor $\mu(l)$ is supposed to depend only on the background edge lengths l. Note that $H^{(4)}_{(01),(01)} > 0$ such that (4.5.23) converges. (Note that in (4.5.23) we did not include boundary terms which only depend on the boundary perturbations.)

The computation is analogous to section 4.3.4. That is to show (form) invariance of the action, i. e.

$$P_{4-2} \propto \exp\left\{ -\sum_{(ij) \neq (01), (km) \neq (01)} \frac{1}{2} H^{(2)}_{(ij)(km)} \lambda_{ij} \lambda_{km} \right\} \tag{4.5.24}$$

we have to proof that

$$H^{(4)}_{(ij),(mn)} = \left[H^{(4)}_{(01),(01)}\right]^{-1} H^{(4)}_{(ij),(01)} H^{(4)}_{(01),(mn)} + H^{(2)}_{(ij),(mn)}$$

$$\stackrel{(4.5.14)}{\Longleftrightarrow} -\sum_{k \neq i,j} \frac{\partial A_{ijk}}{\partial l_{ij}} \frac{\partial \omega_{ijk}}{\partial l_{01}} \frac{\partial l_{01}}{\partial l_{mn}}$$

$$= \left[\sum_{k \neq 0,1} \frac{\partial A_{01k}}{\partial l_{01}} \frac{\partial \omega_{01}}{\partial l_{01}}\right]^{-1} \left(\sum_{k \neq i,j} \frac{\partial A_{ijk}}{\partial l_{ij}} \frac{\partial \omega_{ijk}}{\partial l_{01}}\right) \left(\sum_{k \neq 0,1} \frac{\partial A_{01k}}{\partial l_{01}} \frac{\partial \omega_{01k}}{\partial l_{mn}}\right) \quad . \tag{4.5.25}$$

(ij) and (mn) denote two boundary edges. Applying (4.5.14) to the last term on the right hand side of (4.5.25) gives:

$$\left(\sum_{k \neq 0,1} \frac{\partial A_{01k}}{\partial l_{01}} \frac{\partial \omega_{01k}}{\partial l_{mn}}\right) \stackrel{(4.5.14)}{=} -\left(\sum_{k \neq 0,1} \frac{\partial A_{01k}}{\partial l_{01}} \frac{\partial \omega_{01k}}{\partial l_{01}}\right) \frac{\partial l_{01}}{\partial l_{mn}} \quad , \tag{4.5.26}$$

which shows that (4.5.25) holds.

For the measure factor we examine the contribution from the Gaussian integral:

$$\frac{\sqrt{2\pi}}{\sqrt{H^{(4)}_{(01),(01)}}} = \frac{\sqrt{2\pi}}{\sqrt{-\sum_{k \neq 0,1} \frac{\partial A_{01k}}{\partial l_{01}} \frac{\partial \omega_{01k}}{\partial l_{01}}}} = \frac{\sqrt{192\pi}}{l_{01}} \sqrt{\frac{V_{\bar{2}} V_{\bar{3}} V_{\bar{4}} V_{\bar{5}}}{V_{\bar{0}} V_{\bar{1}}}} \frac{1}{\sqrt{D}} \tag{4.5.27}$$

Apart from the additional factor $\frac{1}{\sqrt{D}}$, (4.5.27) is of a similar form as (4.3.33) for the $3-2$ move in 3D. Hence the invariant measure factor $\mu(l)$ should be proportional to:

$$\mu(l) = \frac{\prod_e \frac{l_e}{\sqrt{192\pi}}}{\prod_\Delta \sqrt{V_\Delta}} \tag{4.5.28}$$

where e denotes the edges and Δ the 4–simplices in the triangulation. However, with this form, we will still get factors of $\frac{1}{\sqrt{D}}$ by applying $4-2$ Pachner moves. The factor D does not factorize into contributions that could be associated to 4–simplices or other subsimplices. It is rather a sum of terms involving the edge lengths of the entire triangulation associated to the $4-2$ move. We will therefore defer the discussion of this factor D until after we have considered all the Pachner moves in 4D.

4.5.2 5–1 move

Let us now consider the $5-1$ move in 4D. Again, many derivations will be similar to the ones for the $4-1$ move in 3D. The $5-1$ move corresponds to the subdivision of one 4–simplex, denoted by (12345), into five by adding one additional vertex (0), placing it inside the original 4–simplex and connecting it with all of the remaining vertices, see section 4.2.3.

Here, the edge lengths of the new edges, i.e. the position of the new vertex inside the original 4–simplex, are not uniquely fixed. Accordingly there is a 4–parameter set of solutions and we expect to find four null modes in the Hessian.

The derivation of the matrix elements for the Hessian proceeds as for the $4-2$ move. We arrive at the following terms:

- In case either the edge $e = (op)$ or edge $e' = (mn)$ are in the bulk, one obtains:

$$H^{(5)}_{(mn),(op)} = (-1)^{s_o+s_p+s_m+s_n+1} \frac{l_{op} l_{mn}}{96} \frac{V_{\bar{o}} V_{\bar{p}} V_{\bar{m}} V_{\bar{n}}}{\prod_l V_{\bar{l}}} \underbrace{\sum_{k \neq o,p} (-1)^{s_k} F_{op;k} V_{\bar{k}}}_{:=D^{(5)}} \tag{4.5.29}$$

where

$$s_i = \begin{cases} 1 & \text{if } i = 0 \\ 0 & \text{else} \end{cases} \tag{4.5.30}$$

and $F_{op;k}$ is defined as in the previous section. Note, that as for the $4 - 2$ move the factor $D^{(5)}$ does not depend on the choice of indices (op) in (4.5.29).

- In case both edges are in the boundary, one obtains:

$$H_{(mn),(op)}^{(5)} = (-1)^{s_o + s_p + s_m + s_n + 1} \frac{l_{op} l_{mn}}{96} \frac{V_{\bar{o}} V_{\bar{p}} V_{\bar{m}} V_{\bar{n}}}{\prod_l V_{\bar{l}}} D^{(5)} + H_{(op),(mn)}^{(1)} \tag{4.5.31}$$

where $H_{(op),(mn)}^{(1)}$ denotes the (op)-(mn) matrix element of the Hessian of the one 4–simplex configuration.

This gives all matrix elements of the Hessian of the $5 - 1$ move. In the next section we will discuss the pure bulk terms more closely, in particular with respect to null eigenvectors.

Null eigenvectors

In this section we examine the pure bulk terms of the Hessian matrix, i.e. equation (4.5.29) for edges $(0i)$ and $(0j)$ for arbitrary i, j. Then (4.5.29) can be rewritten as:

$$H_{(0i),(0j)}^{(5)} = -\frac{l_{0i} l_{0j}}{96} \frac{V_0^2 V_{\bar{i}} V_{\bar{j}}}{\prod_l V_{\bar{l}}} D^{(5)} = \underbrace{l_{0i} V_{\bar{i}}}_{h_{0i}} \underbrace{l_{0j} V_{\bar{j}}}_{h_{0j}} \underbrace{(-1) D^{(5)} \frac{V_{\bar{0}}}{96 V_{\bar{1}} V_{\bar{2}} V_{\bar{3}} V_{\bar{4}} V_{\bar{5}}}}_{c} \tag{4.5.32}$$

So, as in 3D, the bulk terms in the Hessian $H_{(0i),(0j)}^{(5)}$ factorize:

$$H_{(0i),(0j)}^{(5)} = c \, h_{0i} h_{0j} \quad . \tag{4.5.33}$$

Hence, following the argument in section 4.3.5, we can conclude that $H_{(0i),(0j)}^{(5)}$ features four null vectors. The one non-vanishing eigenvalue is again given by $\sum_j H_{(0j),(0j)}$, which amounts to a negative value. We will proceed as for the $4 - 1$ move and change the global sign for the action associated to the $5 - 1$ move. This can again be interpreted as taking care of the conformal factor problem in Euclidean gravity [C61].

Invariance of the path integral

Similar to the $4 - 2$ move, we have to consider

$$P_{5-1} = \int \prod_i d\lambda_{0i} \, \mu(l) \, \exp\left\{ -\sum_{(ij),(km)} \frac{1}{2} H_{(ij),(km)}^{(4)} \, \lambda_{ij} \, \lambda_{km} \right\} \tag{4.5.34}$$

where $\mu(l)$ is a measure factor, which we assume to depend only on the background variables l, making up a flat configuration. (4.5.34) is again a partial Gaussian integral but with four gauge degrees of freedom. The treatment of this integral will be completely analogous to the $4 - 1$ move. Due to the gauge modes we will first integrate only over λ_{01}.

This integration will result in an exponential that is independent of the other variables λ_{0i}, $i = 2, 3, 4, 5$. To show that we obtain the action associated to the one remaining simplex (12345) we

need to invoke the identities

$$
H^{(5)}_{(ij),(mn)} = \left[H^{(5)}_{(01),(01)} \right]^{-1} H^{(5)}_{(ij),(01)} H^{(5)}_{(01),(mn)} + H^{(1)}_{(ij),(mn)}
$$

$$
\overset{(4.5.14)}{\Longleftrightarrow} - \sum_{k \neq i,j} \frac{\partial A_{ijk}}{\partial l_{ij}} \frac{\partial \omega_{ijk}}{\partial l_{01}} \frac{\partial l_{01}}{\partial l_{mn}}
$$

$$
= \left[\sum_{k \neq 0,1} \frac{\partial A_{01k}}{\partial l_{01}} \frac{\partial \omega_{01k}}{\partial l_{01}} \right]^{-1} \left(\sum_{k \neq i,j} \frac{\partial A_{ijk}}{\partial l_{ij}} \frac{\partial \omega_{ijk}}{\partial l_{01}} \right) \left(\sum_{k \neq 0,1} \frac{\partial A_{01k}}{\partial l_{01}} \frac{\partial \omega_{01k}}{\partial l_{mn}} \right) \tag{4.5.35}
$$

Similar to (4.5.25), we apply (4.5.14) to the last term in (4.5.35), which gives:

$$
\sum_{k \neq 0,1} \frac{\partial A_{01k}}{\partial l_{01}} \frac{\partial \omega_{01k}}{\partial l_{mn}} = - \sum_{k \neq 0,1} \frac{\partial A_{01k}}{\partial l_{01}} \frac{\partial \omega_{01k}}{\partial l_{01}} \frac{\partial l_{01}}{\partial l_{mn}} \quad . \tag{4.5.36}
$$

This proves (4.5.35) and hence form invariance of the linearized action under the $5-1$ move.

The measure factor $\mu(l)$ in (4.5.34) changes by the λ_{01} integration by a factor

$$
\frac{\sqrt{2\pi}}{\sqrt{H_{(01),(01)}}} = \frac{\sqrt{192\pi}}{l_{01}} \sqrt{\frac{V_{\bar{2}} V_{\bar{3}} V_{\bar{4}} V_{\bar{5}}}{V_{\bar{0}} V_{\bar{1}}}} \frac{1}{\sqrt{D^{(5)}}} \tag{4.5.37}
$$

which turns out to be of a similar form as the contribution in the $4-2$ move. If we consider $\mu(l)$ in (4.5.34) to be given by

$$
\mu(l) = \frac{\prod_e \frac{l_e}{\sqrt{192\pi}}}{\prod_\Delta \sqrt{V_\Delta}} \tag{4.5.38}
$$

we obtain for the path integral

$$
P_{5-1} = \frac{\prod_b \frac{l_b}{\sqrt{192\pi}}}{\sqrt{V_{\bar{0}}}} \frac{1}{\sqrt{D^{(5)}}} \exp \left\{ - \sum_{b,b'} \frac{1}{2} H^{(1)}_{b,b'} \lambda_b \lambda_{b'} \right\} \int \frac{\prod_{i \neq 1} \frac{l_{0i}}{\sqrt{192\pi}} d\lambda_{0i}}{V_{\bar{1}}} \tag{4.5.39}
$$

Also here the remaining integral can be identified with an integration over the gauge orbit, which is again given by the displacement of the inner vertex (0). In 4D we have the identity

$$
d^4 x_0^\alpha = \frac{\prod_{i=2,3,4,5} l_{0i} \, dl_{0i}}{24 V_{\bar{1}}} \tag{4.5.40}
$$

where $d^4 x_0^\alpha$ is the integration measure for the Euclidean coordinates x_0^α, $\alpha = 1, 2, 3, 4$ of the vertex (0). Hence we will replace the remaining integral in (4.5.39) by 1.

4.5.3 3–3 move

In addition to the $5-1$ and $4-2$ moves, the set of Pachner moves in 4D includes the $3-3$ move. Here a complex of three 4–simplices is replaced with another complex of 3 4–simplices, such that the boundary triangulation is not changed. This move does not involve any bulk edge, hence, differing from all the other moves considered so far, we do not have an equation of motion associated to this move.

There is another essential difference to the other Pachner moves, namely that the action is not invariant under $3-3$ moves. Evaluating the (full) Regge action for the two configurations of the $3-3$ move, one finds a difference, that grows quadratically with the deficit angle of the (only) bulk triangle [C52]. Hence the action is not invariant in general under 3-3 moves, in fact, such an invariance applies only on flat configurations. This violation of the invariance of the action holds

also for the quadratic action of the linearized theory, as can be expected from the behavior in the full theory and as can be checked explicitly on configurations with non–vanishing (linearized) curvature.

The derivation of the (reduced) Hessian matrix for the $3-3$ move proceeds in a slightly different way, as we now have to take into account that the boundary perturbations might describe curvature. The result will however have the same structure as for the other Pachner moves.

To start the derivation note that in both configurations A (with simplices (01234), (01235), (01245)) and B (with simplices (01345), (02345), (12345) there is only one bulk triangle, namely (012) and (345) respectively in A and B. The vanishing of the linearized deficit angles defines boundary perturbations in flat directions:

$$\sum_{(ij)} \frac{\partial \omega_{012}^A}{\partial l_{ij}} \lambda_{ij} = 0 = \sum_{(ij)} \frac{\partial \omega_{345}^B}{\partial l_{ij}} \lambda_{ij} \quad . \tag{4.5.41}$$

For such flat variations λ_{ij} we can again derive, along the same arguments as in section 4.5.1, the relations (4.5.5)

$$\left| \frac{\lambda_{ij}}{\lambda_{km}} \right| = \left| \frac{l_{km}}{l_{ij}} \frac{V_{\bar{k}} V_{\bar{m}}}{V_{\bar{i}} V_{\bar{j}}} \right| \quad . \tag{4.5.42}$$

Note that equation (4.5.41) also implies that the gradients of the deficit angles in the two configurations are parallel to each other. That is the space of flat boundary perturbations λ_{ij} in both configurations is the same, the linearized curvature will however have different values in the general case, if evaluated on the same set of (non–flat) boundary perturbations λ_{ij}.

Now, starting with the derivatives

$$\frac{\partial \omega_{012}^A}{\partial l_{34}} = -\frac{\partial \theta_{012}^{01234}}{\partial l_{34}} = -\frac{l_{45} A_{123}}{12 V_{\bar{5}}} \quad , \qquad \frac{\partial \omega_{345}^B}{\partial l_{12}} = -\frac{\partial \theta_{345}^{12345}}{\partial l_{12}} = -\frac{l_{12} A_{345}}{12 V_{\bar{0}}} \tag{4.5.43}$$

and using (4.5.41) and (4.5.42), assuming that only two appropriately chosen length perturbations $\lambda_{ij}, \lambda_{mn}$ are not vanishing, we can obtain all other derivatives of the bulk deficit angle in both configurations. The signs can again be determined as in section 4.3.2.

The result is given by

$$\begin{aligned} \frac{\partial \omega_{012}^A}{\partial l_{ij}} &= (-1)^{s_i^A + s_j^A + 1} \frac{l_{ij} A_{012}}{12} \frac{V_{\bar{0}} V_{\bar{1}} V_{\bar{2}} V_{\bar{i}} V_{\bar{j}}}{\prod_p V_{\bar{p}}} \\ \frac{\partial \omega_{345}^B}{\partial l_{ij}} &= (-1)^{s_i^B + s_j^B + 1} \frac{l_{ij} A_{345}}{12} \frac{V_{\bar{3}} V_{\bar{4}} V_{\bar{5}} V_{\bar{i}} V_{\bar{j}}}{\prod_p V_{\bar{p}}} \end{aligned} \tag{4.5.44}$$

Here we defined the sign factors as

$$s_i^A = \begin{cases} 1 & \text{if } i \in \{0, 1, 2\} \\ 0 & \text{else} \end{cases} \quad , \qquad s_i^B = \begin{cases} 1 & \text{if } i \in \{3, 4, 5\} \\ 0 & \text{else} \end{cases} \quad . \tag{4.5.45}$$

With the understanding that $\omega_{345}^A \equiv 0 = \omega_{012}^B$ we can write the relation between the derivatives as

$$\frac{\partial \omega_{opk}^A}{\partial l_{ij}} - \frac{\partial \omega_{opk}^B}{\partial l_{ij}} = \underbrace{(-1)^{s_i^A + s_j^A + s_o^A + s_p^A + s_k^A}}_{=(-1)^{s_i^B + \dots + s_k^B + 1}} \frac{l_{ij} A_{opk}}{12} \frac{V_{\bar{o}} V_{\bar{p}} V_{\bar{k}} V_{\bar{i}} V_{\bar{j}}}{\prod_p V_{\bar{p}}} \tag{4.5.46}$$

where (opk) is either the set (012) or (345). Note that (4.5.46) is consistent with (4.5.45) under change $A \leftrightarrow B$, i.e. change of sign.

We will soon discover that (4.5.46) holds also for the other (boundary) angles. To this end we use that the linearized boundary extrinsic curvature angles coincide in both configurations A and B, if evaluated on flat boundary perturbations. Hence we can conclude that the difference of the gradients of a given boundary angle has to be proportional to the gradient of one of the bulk angles, i. e.

$$\frac{\partial \omega^A_{mnl}}{\partial l_{ij}} - \frac{\partial \omega^B_{mnl}}{\partial l_{ij}} = c^A_{mnl} \frac{\partial \omega^A_{012}}{\partial l_{ij}} \quad . \tag{4.5.47}$$

Again we can start with an especially simple derivative, i.e.

$$\frac{\partial \omega^A_{345}}{\partial l_{12}} = -\frac{l_{12} A_{345}}{12} \frac{V_{\bar 3} V_{\bar 4} V_{\bar 5} V_{\bar 1} V_{\bar 2}}{\prod_p V_{\bar p}} \quad , \qquad \frac{\partial \omega^B_{345}}{\partial l_{12}} = 0 \tag{4.5.48}$$

to get hold of all the other derivatives of this exterior curvature angle. In this way we obtain

$$\frac{\partial \omega^A_{opk}}{\partial l_{ij}} - \frac{\partial \omega^B_{opk}}{\partial l_{ij}} = (-1)^{s^A_i + s^A_j + s^A_o + s^A_p + s^A_k} \frac{l_{ij} A_{opk}}{12} \frac{V_{\bar o} V_{\bar p} V_{\bar k} V_{\bar i} V_{\bar j}}{\prod_p V_{\bar p}} \tag{4.5.49}$$

for all the boundary and bulk angles.

To finally arrive at the (reduced) Hessian, we have to multiply this result (4.5.49) with the area derivatives as in (4.5.19). This allows us to express the difference of the (reduced) Hessians in the A and B configurations as

$$H^A_{(op),(mn)} - H^B_{(op),(mn)} = \underbrace{(-1)^{s^A_o + s^A_p + s^A_m + s^A_n}}_{=(-1)^{s^B_i + \ldots + s^B_p}} \frac{l_{op} l_{mn}}{96} \frac{V_{\bar o} V_{\bar p} V_{\bar m} V_{\bar n}}{\prod_l V_{\bar l}} \underbrace{\sum_{k \neq o,p} \underbrace{(-1)^{s^A_k + 1}}_{=(-1)^{s^B_k}} F_{op;k} V_{\bar k}}_{:= D^A} \tag{4.5.50}$$

Also here D does not depend on the choice of indices o, p in (4.5.50). Note that $D^A = -D^B$. Unless $D^A = D^B = 0$, the (quadratic) action of the linearized theory is different in the A and the B configuration. This equality $D^A = D^B = 0$ does not hold on general (flat) background configurations, but might hold in very symmetric cases.

Furthermore, a measure of the form

$$\mu(l) = \frac{\prod_e \frac{l_e}{\sqrt{192\pi}}}{\sqrt{\prod_l V_{\bar l}}} \tag{4.5.51}$$

is only invariant under the $3 - 3$ move in the case that

$$V_{\bar 0} V_{\bar 1} V_{\bar 2} = V_{\bar 3} V_{\bar 4} V_{\bar 5} \quad . \tag{4.5.52}$$

Again, this equality does not hold for generic cases.

4.6 Summary for 4D gravity

4D classical Regge calculus is invariant under the $4 - 2$ and $5 - 1$ moves, but not under the $3 - 3$ moves. Our calculations provided the evidence for the linearized theory, in particular isolating the invariance breaking term for the $3 - 3$ move.

But this invariance behavior also holds for the full theory: there is always a flat solution to the equation of motions associated to the $4 - 2$ and $5 - 1$ Pachner moves. Hence the contribution from the bulk to the Hamilton-Jacobi function is vanishing. The Hamilton-Jacobi function is therefore just given by the boundary terms, which do not change under the $4 - 2$ and $5 - 1$ moves.

Concerning the quantum theory for linearized Regge Calculus in 4D, we define the path integral for general triangulations as

$$P := \int \frac{\prod_e \frac{l_e}{\sqrt{192\pi}}}{\prod_\Delta \sqrt{V_\Delta}} \prod_{e \subset \text{bulk}} d\lambda_e \, \exp\left\{-\frac{1}{2} H_{e,e'} \lambda_e \lambda_{e'}\right\} \quad . \tag{4.6.1}$$

l_e denotes the length of edge e, V_Δ the volume of 4–simplex Δ, λ_e is the edge length perturbation of edge e and $H_{e,e'}$ is the e-e' matrix element of the Hessian matrix of the Regge action.

In the previous section we have shown that (4.6.1) is invariant – modulo the factor D – under $4-2$ and $5-1$ Pachner moves (using the gauge fixing conventions discussed above), but in general not under the $3-3$ Pachner move. The non-invariance under $3-3$ moves is already present in the classical theory and should be overcome by constructing a perfect discretization [C22–C25, C27, C28].

It might be possible to implement a full invariance of the path integral under either the $4-2$ or the $5-1$ move, that is by including the factor $\sqrt{D}$ into the measure. For the $4-2$ moves one would need to associate a corresponding factor to the edges of the triangulation, for the $5-1$ move rather to the vertices. (Alternatively, one would have to change the gauge fixing procedure for the $5-1$ move, i.e. the factor associated to the gauge orbit, but this seems to be rather unnatural.) Still there are several open questions left to address, as how to generalize the definition of the D factors to more complicated triangulations (the bulk edges in the Pachner moves are always shared by four triangles) and how the D factors associated to boundary edges or vertices will interfere. Furthermore, the factor D is slightly non-local, but its actual form might be due to the linearized theory.

Here it might be helpful to reconsider the topological BF theory, from which gravity can be obtained by implementing (simplicity) constraints. This is the route followed by spin foams. The advantage of this approach is, that a triangulation invariant path integral can be constructed for BF theory. To apply this to Regge calculus one would need a formulation based on the same geometric variables as used in 4D BF theory. Such a formulation is provided by area-angle Regge calculus [C49]. The corresponding action can also be split into a piece describing a topological theory and constraints acting in the same way as the simplicity constraints. Studying this action might help to construct a triangulation independent quantum theory describing flat space dynamics. For other work in this direction, related to BF theory see [C67–C71].

Despite all these subtleties and drawbacks, the simple form of the Hessian matrix for all Pachner moves and its similar form to the 3D case are remarkable. Therefore it will be very interesting to compare our results to spin foam asymptotics and possibly help to fix measure ambiguities (by requiring invariance under Pachner moves) there.

4.7 Discussion

In this work we provided extensive analytical calculations for linearized Regge calculus, very much enlightening the structure of the theory. In particular we obtained the linearized Regge actions associated to all the Pachner moves in 3D and 4D, explicitly showing that the Regge action[4] is invariant under all Pachner moves, with the exception of the $3-3$ move. We isolated the gauge symmetries and the conformal factor problem, which both are potential sources for divergencies. Amazingly the structure of the linearized Regge actions associated to the Pachner moves lead in all cases to a very transparent factorizing structure, similar in 3D and in 4D. These formulae might be also helpful in other contexts, for instance in a canonical formulation of Regge calculus [C53, C54] or in numerical larger scale calculations.

---

[4]This invariance result holds also for the full theory.

Furthermore we proposed a dynamical principle to fix the measure for Regge calculus, namely to consider the behavior of the theory under Pachner moves. Restricting to a local ansatz as in (4.1.2) this fixes the measure uniquely. Indeed the invariance under change of triangulation is related to an implementation of diffeomorphism symmetry [C18, C22, C25, C28]. This condition can therefore be understood as requiring an anomaly–free measure, which can be expected to be unique. A simple reason for this is that for a theory completely invariant under changes of the triangulation, there is also no (bulk) discretization scale. That is the only discretization scale is provided by the boundary data. For compact manifolds without boundary the continuum limit is even trivial, as such a limit would be obtained via a refinement of the triangulation [C26]. In other words a triangulation independent path integral provides already the continuum result.

This is the reason why we cannot expect to obtain a fully triangulation independent local theory in 4D. However one might ask for invariance of the quantum theory under the same set of local triangulation changes under which the local classical theory is invariant. Such a set can be understood as trivial subdivisions of the triangulation, as the associated equations of motions lead to flat space–time. The question therefore is, whether one can define a topological sub–sector of the theory [C11, C12, C69, C70], which would provide a quantum description of flat space dynamics, see also [C71]. Such an invariance of the theory under trivial subdivisions seems also be crucial to realize scenarios as proposed in [C26], i. e. the convergence of the theory to a topological sector, under refinement.

We found a path integral measure for linearized Regge calculus, which provides such an invariance, in 4D modulo a factor, which features a certain non–local structure. In 3D we found an exactly invariant measure, which also coincides with the asymptotics of the (triangulation independent) Ponzano Regge model. This is quite astonishing, as we performed a calculation in the linearized theory. Furthermore the Ponzano Regge model includes in addition also a sum over orientations, which we do not consider here[5]. The question arises, whether this result can be extended to the full non-linear theory and shed light on the problem, whether to include a sum over orientations into a quantum gravity path integral or not [C72, C73].

The factor appearing in 4D, disturbing invariance at least under the $5-1$ and $4-2$ moves, is related to a transformation from area to length variables. It might therefore be helpful, in order to further enlighten this issue, to consider area-angle Regge calculus [C49, C50]. This formulation allows a split into a topological theory, which would be triangulation independent, and constraints. Another possibility to obtain path integral measures is a derivation from the canonical theory, which has recently became available for Regge calculus [C53, C54]. Indeed the path integral measure is important to obtain correlation functions, which are annihilated by the Hamiltonian constraints [C25].

A fully triangulation independent theory can be constructed via the method of perfect discretizations [C23–C25, C27, C28], which is based on a Wilsonian renormalization flow. This has the advantage of providing at the same time informations on the continuum limit of the theory. Here two different strategies can be thought of. One is based on local considerations, namely to study the behavior of a given theory under local refinements, e. g. Pachner moves, see for instance [C42] for related studies in (topological) spin foam models. This can result in recursion relations, whose fixed points provide the continuum limit (and perfect discretization) of the path integral, see [C25] for an example in 1D. Another strategy is to extract the large scale behavior, which might depend on the choice of measure [C21, C74]. First steps towards extracting large scale behavior of (simplified) spin foam models via real space renormalization can be found in [C75, C76].

---

[5]In this work we considered a background triangulation with positive orientation. The results can however be extended to Pachner moves leading to negatively oriented simplices. In this case the Regge action has to be adjusted to take the negative orientation of these simplices into account, the measure does not need to be changed however.

Acknowledgements

4.A Euclidean integration measure

The usual Lebesgue measure of D-dimensional Euclidean space can be rewritten with respect to the edge lengths of a (non-degenerate) D-simplex [C62].

Assume $D + 1$ vertices making up a D-simplex embedded in $\mathbb{R}^D$, their positions given by $\{\vec{x}_i\}_{i=0,\ldots,D}$, such that the D-simplex is not degenerate, i.e. its D-volume is non-vanishing. Next, we define the position of the vertices of the D-simplex with respect to one of its vertices by defining $\vec{l}_i := \vec{x}_i - \vec{x}_0$. Since the D-simplex is non-degenerate, the set of vectors $\{\vec{l}_i\}_{i=1,\ldots,D}$ form a (non-orthonormal) basis of $\mathbb{R}^D$, where the lengths of the vectors $\vec{l}_i$ give the edge lengths l_{0i} of the D-simplex. To write the Lebesgue measure in these coordinates, one has to compute the Jacobian of the linear function which maps the orthonormal basis $\{\vec{e}_i\}$ to $\{\vec{l}_i\}$. To simplify notation, we will denote $\vec{y} := \vec{x}_0$.

$$\prod_{i=1}^{D} l_{0i}\, dl_{0i} = \prod_{i=1}^{D} d\left(\frac{l_{0i}^2}{2}\right) = \prod_{i=1}^{D} d\left(\frac{(\vec{y} - \vec{x}_i)^2}{2}\right) = \prod_{i=1}^{D} dy_i \left|\det\left[\frac{\partial}{\partial y^j} \frac{(\vec{y} - \vec{x}_i)^2}{2}\right]\right| \tag{4.A.1}$$

where the determinant in the last term is the Jacobian of the coordinate transformation. For the matrix elements of the Jacobian one obtains:

$$\frac{\partial}{\partial y^j} \frac{(\vec{y} - \vec{x}_i)^2}{2} = \vec{e}_j \cdot (\vec{y} - \vec{x}_i) \quad . \tag{4.A.2}$$

Given (4.A.2), the Jacobian can be rewritten in terms of the volume of the D-simplex:

$$\left|\det\left(\vec{e}_j \cdot (\vec{y} - \vec{x}_i)\right)\right| = \sqrt{\det\left((\vec{y} - \vec{x}_j) \cdot (\vec{y} - \vec{x}_i)\right)} = D!\, V \quad . \tag{4.A.3}$$

Using (4.A.2,4.A.3) in (4.A.1) gives:

$$\prod_{i=1}^{D} l_{0i}\, dl_{0i} = \prod_{i=1}^{D} dy_i\, D!\, V \tag{4.A.4}$$

$$\implies \prod_{i=1}^{D} dy_i = \frac{\prod_{i=1}^{D} l_{0i}\, dl_{0i}}{D!\, V} \quad . \tag{4.A.5}$$

From (4.A.5) one obtains (4.3.55) in 3D and (4.5.40) in 4D.

4.B Determinant formula for D

In the calculations of the Hessian matrix in 4D, see section 4.5, we have encountered the factors D_{op} (see for instance (4.5.19)) which are slightly non-local. In this section we will present a different way to compute these factors in terms of a determinant of a matrix which will additionally allow us to show that (some) factors D_{op} are equal without using that the Hessian matrix is symmetric.

Consider six vertices embedded in $\mathbb{R}^4$ making up a triangulation which can be modified by one of the Pachner moves discussed in section 4.2.3. We define the position vectors of the vertices with

respect to vertex (0), which we place in the origin of the coordinate system for simplicity. Hence the position vector of vertex (i) is defined by $\vec{x}^i \equiv \vec{x}^i - \vec{x}^0$, its components are denoted by x_a^i with $a = 1, 2, 3, 4$. Given this definition, consider the following determinant:

$$
\det
\begin{bmatrix}
x_1^1 & x_1^2 & \dots & x_1^5 \\
x_2^1 & x_2^2 & \dots & \\
\vdots & & \ddots & \\
x_4^1 & x_4^2 & \dots & x_4^5 \\
(\vec{x}^1)^2 & (\vec{x}^2)^2 & \dots & (\vec{x}^5)^2
\end{bmatrix} .
\tag{4.B.1}
$$

We will show that this determinant is proportional to the factors D_{0i}, for $i = 1, \dots, 5$.

The determinant of a matrix remains unchanged if a scalar multiple of one of its rows / columns is added to one of its rows / columns respectively. Hence we will subtract x_a^i times the ath row from the last for $1 \leq a < 5$. Then one obtains for instance for $i = 1$:

$$
\det
\begin{bmatrix}
x_1^1 & x_1^2 & \dots & x_1^5 \\
x_2^1 & x_2^2 & \dots & \\
\vdots & & \ddots & \\
x_4^1 & x_4^2 & \dots & x_4^5 \\
0 & (\vec{x}^2)^2 - \vec{x}^2 \cdot \vec{x}^1 & \dots & (\vec{x}^5)^2 - \vec{x}^5 \cdot \vec{x}^1
\end{bmatrix} .
\tag{4.B.2}
$$

The terms in the last row can be rewritten as

$$
(\vec{x}^k)^2 - \vec{x}^k \cdot \vec{x}^1 = \frac{1}{2} \underbrace{\left((\vec{x}^k)^2 - (\vec{x}^1)^2 + (\vec{x}^k - \vec{x}^1)^2 \right)}_{= l_{0k}^2 - l_{01}^2 + l_{1k}^2} = \frac{1}{2} F_{01;k} \quad ,
\tag{4.B.3}
$$

where $F_{01;k}$ is the same factor as in (4.5.18). Expanding (4.B.2) with respect to the last row, the subdeterminants of the matrix correspond to (oriented) volumes of 4-simplices (see (4.A.3)). Hence one obtains:

$$
\underbrace{\det[\dots]}_{(4.B.2)} = 4! \sum_{i=2}^{5} (-1)^{i-1} s_i \, F_{01;i} \, V_{\bar{i}} \; \propto \; D_{01}
\tag{4.B.4}
$$

where s_i are appropriate sign factors taking into account the orientation of the volumes. By analogous considerations, one computes the other factors D_{0j}, $j = 2, 3, 4, 5$, from the same determinant, which implies that these factors are all equal (although the symmetry of the Hessian matrix has not been used). The signs s_i depend on the relative orientation of the vectors $\vec{x}_i$ of the respective 4-simplex and hence they depend on the geometry under discussion. We would like to demonstrate that explicitly with the example of the $4 - 2$ move.

Consider the D_{01} for the $4 - 2$ move, see (4.5.19). Four of the five edge vectors $\vec{x}_i$ of the vertices, defined with respect to the vertex (0), form a basis of $\mathbb{R}^4$ since the 4-simplices are not degenerated. In the following we assume that $\vec{x}_2, \dots, \vec{x}_5$ is a positively oriented orthonormal basis. Hence, we can rewrite the determinant (4.B.2) as

$$
\det
\begin{bmatrix}
\sum_{i=2}^{5} v_i \vec{x}_i & \vec{x}_2 & \vec{x}_3 & \vec{x}_4 & \vec{x}_5 \\
0 & F_{01;2} & F_{01;3} & F_{01;4} & F_{01;5}
\end{bmatrix}
\tag{4.B.5}
$$

where the v_i are the coefficients of $\vec{x}_1$ in the basis formed by $\vec{x}_2, \dots, \vec{x}_5$. Note that the configuration of the $4 - 2$ move can be chosen such that $v_i > 0$. If (4.B.5) is expanded with respect to the last row, the submatrices are of the following form:

$$
\det
\begin{bmatrix}
\sum_{i=2}^{5} v_i \vec{x}_i & \vec{x}_j & \vec{x}_k & \vec{x}_l
\end{bmatrix} = \epsilon_{ijkl} \, v_i \quad ,
\tag{4.B.6}
$$

where ϵ_{ijkl} is the Levi-Cevita symbol in 4D. Hence the signs s_i in (4.B.4) are alternating, which, together with the alternating signs $(-1)^{i-1}$ verifies formula (4.B.4).

References

[C1] A. Perez, "Spin foam models for quantum gravity," *Class.Quant.Grav.* **20** (2003) R43, `arXiv:gr-qc/0301113 [gr-qc]`.

[C2] A. Perez, "The spin foam approach to quantum gravity," *Living Rev. Rel.* **16** (2013) 3, `arXiv:1205.2019 [gr-qc]`.

[C3] C. Rovelli, *Quantum Gravity.* Cambridge University Press, Cambridge, 2004.

[C4] D. Oriti, "The Group field theory approach to quantum gravity," `arXiv:gr-qc/0607032 [gr-qc]`. Published in In *Oriti, D. (ed.): Approaches to quantum gravity* 310-331.

[C5] R. Gurau and J. P. Ryan, "Colored Tensor Models - a review," *SIGMA* **8** (2012) 020, `arXiv:1109.4812 [hep-th]`.

[C6] J. Ambjørn and J. Jurkiewicz, "Four-dimensional simplicial quantum gravity," *Phys.Lett.* **B278** (1992) 42–50.

[C7] M. Agishtein and A. A. Migdal, "Critical behavior of dynamically triangulated quantum gravity in four-dimensions," *Nucl.Phys.* **B385** (1992) 395–412, `arXiv:hep-lat/9204004 [hep-lat]`.

[C8] J. Ambjørn, A. Görlich, J. Jurkiewicz, R. Loll, J. Gizbert-Studnicki, *et al.*, "The Semiclassical Limit of Causal Dynamical Triangulations," *Nucl.Phys.* **B849** (2011) 144–165, `arXiv:1102.3929 [hep-th]`.

[C9] T. Regge, "General Relativity Without Coordinates," *Nuovo Cim.* **19** (1961) 558–571.

[C10] R. M. Williams, "Recent progress in Regge calculus," *Nucl.Phys.Proc.Suppl.* **57** (1997) 73–81, `arXiv:gr-qc/9702006 [gr-qc]`.

[C11] B. Dittrich and J. P. Ryan, "Phase space descriptions for simplicial 4d geometries," *Class. Quant. Grav.* **28** (2011) 065006, `arXiv:0807.2806 [gr-qc]`.

[C12] B. Dittrich and J. P. Ryan, "Simplicity in simplicial phase space," *Phys. Rev. D* **82** (2010) 064026, `arXiv:1006.4295 [gr-qc]`.

[C13] L. Freidel and S. Speziale, "Twisted geometries: A geometric parametrisation of SU(2) phase space," *Phys. Rev. D* **82** (2010) 084040, `arXiv:1001.2748 [gr-qc]`.

[C14] W. Kaminski, M. Kisielowski, and J. Lewandowski, "Spin-Foams for All Loop Quantum Gravity," *Class.Quant.Grav.* **27** (2010) 095006, `arXiv:0909.0939 [gr-qc]`.

[C15] B. Bahr, "On knottings in the physical Hilbert space of LQG as given by the EPRL model," *Class.Quant.Grav.* **28** (2011) 045002, `arXiv:1006.0700 [gr-qc]`.

[C16] B. Bahr, F. Hellmann, W. Kaminski, M. Kisielowski, and J. Lewandowski, "Operator Spin Foam Models," *Class.Quant.Grav.* **28** (2011) 105003, `arXiv:1010.4787 [gr-qc]`.

[C17] L. Freidel, "Group field theory: An Overview," *Int.J.Theor.Phys.* **44** (2005) 1769–1783, `arXiv:hep-th/0505016 [hep-th]`.

[C18] B. Dittrich, "Diffeomorphism symmetry in quantum gravity models," *Adv. Sci. Lett.* **2** (2009) 121, `arXiv:0810.3594 [gr-qc]`.

[C19] C. Rovelli and M. Smerlak, "In quantum gravity, summing is refining," *Class. Quant. Grav.* **29** (2012) 055004, `arXiv:1010.5437 [gr-qc]`.

[C20] J. Ambjørn, M. Carfora, and A. Marzuoli, "The Geometry of dynamical triangulations," *Lect.Notes Phys.* **50** (1997) 197, `arXiv:hep-th/9612069 [hep-th]`.

[C21] R. Loll, "Discrete approaches to quantum gravity in four-dimensions," *Living Rev.Rel.* **1** (1998) 13, `arXiv:gr-qc/9805049 [gr-qc]`.

[C22] B. Bahr, R. Gambini, and J. Pullin, "Discretisations, constraints and diffeomorphisms in quantum gravity," *SIGMA* **8** (2012) 002, `arXiv:1111.1879 [gr-qc]`.

[C23] B. Bahr and B. Dittrich, "(Broken) Gauge Symmetries and Constraints in Regge Calculus," *Class.Quant.Grav.* **26** (2009) 225011, `arXiv:0905.1670 [gr-qc]`.

[C24] B. Bahr and B. Dittrich, "Breaking and restoring of diffeomorphism symmetry in discrete gravity," *AIP Conf. Proc.* **1196** (2009) 10–17, `arXiv:0909.5688 [gr-qc]`.

[C25] B. Bahr, B. Dittrich, and S. Steinhaus, "Perfect discretization of reparametrization invariant path integrals," *Phys. Rev. D* **83** (2011) 105026, `arXiv:1101.4775 [gr-qc]`.

[C26] C. Rovelli, "Discretizing parametrized systems: The Magic of Ditt-invariance," `arXiv:1107.2310 [hep-lat]`.

[C27] B. Bahr, B. Dittrich, and S. He, "Coarse graining free theories with gauge symmetries: the linearized case," *New J. Phys.* **13** (2011) 045009, `arXiv:1011.3667 [gr-qc]`.

[C28] B. Bahr and B. Dittrich, "Improved and Perfect Actions in Discrete Gravity," *Phys.Rev.* **D80** (2009) 124030, `arXiv:0907.4323 [gr-qc]`.

[C29] H. W. Hamber and R. M. Williams, "On the measure in simplicial gravity," *Phys.Rev.* **D59** (1999) 064014, `arXiv:hep-th/9708019 [hep-th]`.

[C30] B. S. DeWitt, "Quantum Theory of Gravity. 1. The Canonical Theory," *Phys. Rev.* **160** (1967) 1113–1148.

[C31] C. W. Misner, "Feynman quantization of general relativity," *Rev. Mod. Phys.* **29** (1957) 497–509.

[C32] M. Bojowald and A. Perez, "Spin foam quantization and anomalies," *Gen.Rel.Grav.* **42** (2010) 877–907, `arXiv:gr-qc/0303026 [gr-qc]`.

[C33] U. Pachner, "Konstruktionsmethoden und das kombinatorische Homöomorphieproblem für Triangulationen kompakter semilinearer Mannigfaltigkeiten," *Abh. Math. Sem. Univ. Hamburg* **57** (1986) 69.

[C34] U. Pachner, "P. L. Homeomorphic Manifolds are Equivalent by Elementary Shellings," *Europ. J. Combinatorics* **12** (1991) 129–145.

[C35] J. Roberts, "Classical 6j-symbols and the tetrahedron," *Geom. Topol.* **3** (1999) 21.

[C36] R. J. Dowdall, H. Gomes, and F. Hellmann, "Asymptotic analysis of the Ponzano-Regge model for handlebodies," *J. Phys. A* **43** (2010) 115203, `arXiv:0909.2027 [gr-qc]`.

[C37] G. Ponzano and T. Regge, *Semiclassical limit of Racah coefficients, in: Spectroscopy and group theoretical methods in physics.* North Holland Publ. Co., Amsterdam, 1968.

[C38] J. W. Barrett, R. J. Dowdall, W. J. Fairbairn, H. Gomes, and F. Hellmann, "Asymptotic analysis of the EPRL four-simplex amplitude," *J. Math. Phys.* **50** (2009) 112504, `arXiv:0902.1170 [gr-qc]`.

[C39] J. W. Barrett, R. J. Dowdall, W. J. Fairbairn, H. Gomes, F. Hellmann, and R. Pereira, "Asymptotics of 4d spin foam models," *Gen. Rel. Grav.* **43** (2011) 2421–2436, `arXiv:1003.1886 [gr-qc]`.

[C40] F. Conrady and L. Freidel, "On the semiclassical limit of 4d spin foam models," *Phys.Rev.* **D78** (2008) 104023, `arXiv:0809.2280 [gr-qc]`.

[C41] E. Bianchi, D. Regoli, and C. Rovelli, "Face amplitude of spinfoam quantum gravity," *Class. Quant. Grav.* **27** (2010) 185009, `arXiv:1005.0764 [gr-qc]`.

[C42] V. Bonzom, E. R. Livine, and S. Speziale, "Recurrence relations for spin foam vertices," *Class. Quant. Grav.* **27** (2010) 125002, `arXiv:0911.2204 [gr-qc]`.

[C43] F. Lund and T. Regge *unpublished* (1974) .

[C44] H. W. Hamber and R. M. Williams, "Gauge invariance in simplicial gravity," *Nucl.Phys.* **B487** (1997) 345–408, `arXiv:hep-th/9607153 [hep-th]`.

[C45] J. Ambjørn, J. L. Nielsen, J. Rolf, and G. K. Savvidy, "Spikes in quantum Regge calculus," *Class.Quant.Grav.* **14** (1997) 3225–3241, `arXiv:gr-qc/9704079 [gr-qc]`.

[C46] J. Laiho and D. Coumbe, "Evidence for Asymptotic Safety from Lattice Quantum Gravity," *Phys. Rev. Lett.* **107** (2011) 161301, `arXiv:1104.5505 [hep-lat]`.

[C47] D. Benedetti and R. Gurau, "Phase Transition in Dually Weighted Colored Tensor Models," *Nucl. Phys.* **B855** (2012) 420–437, `arXiv:1108.5389 [hep-th]`.

[C48] P. Menotti and P. P. Peirano, "Diffeomorphism invariant measure for finite dimensional geometries," *Nucl.Phys.* **B488** (1997) 719–734, `arXiv:hep-th/9607071 [hep-th]`.

[C49] B. Dittrich and S. Speziale, "Area-angle variables for general relativity," *New J.Phys.* **10** (2008) 083006, `arXiv:0802.0864 [gr-qc]`.

[C50] B. Bahr and B. Dittrich, "Regge calculus from a new angle," *New J. Phys.* **12** (2010) 033010, `arXiv:0907.4325 [gr-qc]`.

[C51] B. Dittrich, L. Freidel, and S. Speziale, "Linearized dynamics from the 4-simplex Regge action," *Phys. Rev. D* **76** (2007) 104020, `arXiv:0707.4513 [gr-qc]`.

[C52] B. Bahr.

[C53] B. Dittrich and P. A. Höhn, "From covariant to canonical formulations of discrete gravity," *Class. Quant. Grav.* **27** (2010) 155001, `arXiv:0912.1817 [gr-qc]`.

[C54] B. Dittrich and P. A. Höhn, "Canonical simplicial gravity," *Class. Quant. Grav.* **29** (2012) 115009, `arXiv:1108.1974 [gr-qc]`.

[C55] M. Rocek and R. M. Williams, "Quantum Regge Calculus," *Phys. Lett. B* **104** (1981) 31.

[C56] M. Rocek and R. M. Williams, "The Quantization of Regge Calculus," *Z. Phys. C* **21** (1984) 371.

References

[C57] P. A. Morse, "Approximate diffeomorphism invariance in near flat simplicial geometries," *Class. Quant. Grav.* **9** (1992) 2489.

[C58] L. Freidel and D. Louapre, "Diffeomorphisms and spin foam models," *Nucl.Phys.* **B662** (2003) 279–298, `arXiv:gr-qc/0212001 [gr-qc]`.

[C59] I. Korepanov, "Multidimensional analogues of the geometric s <–> t duality," *Theor.Math.Phys.* **124** (2000) 999–1005, `arXiv:solv-int/9911008 [solv-int]`.

[C60] I. G. Korepanov, "Invariants of PL manifolds from metrized simplicial complexes: Three-dimensional case," *J.Nonlin.Math.Phys.* **8** (2001) 196–210, `arXiv:math/0009225 [math-gt]`.

[C61] G. W. Gibbons, S. W. Hawking, and M. J. Perry, "Path Integrals and the Indefiniteness of the Gravitational Action," *Nucl. Phys.* **B138** (1978) 141.

[C62] A. Baratin and L. Freidel, "Hidden Quantum Gravity in 3-D Feynman diagrams," *Class.Quant.Grav.* **24** (2007) 1993–2026, `arXiv:gr-qc/0604016 [gr-qc]`.

[C63] H. W. Hamber and R. M. Williams, "Simplicial quantum gravity in three-dimensions: Analytical and numerical results," *Phys.Rev.* **D47** (1993) 510–532.

[C64] V. G. Turaev and O. Y. Viro, "State sum invariants of 3 manifolds and quantum 6j symbols," *Topology* **31** (1992) 865–902.

[C65] Y. U. Taylor and C. T. Woodward, "Spherical Tetrahedra and Invariants of 3-manifolds," `arXiv:math/0406228 [math]`.

[C66] I. G. Korepanov, "Euclidean 4-simplices and invariants of four-dimensional manifolds. I. Moves 3 —> 3," *Theor.Math.Phys.* **131** (2002) 765–774, `arXiv:math/0211165 [math-gt]`.

[C67] V. Bonzom, "From lattice BF gauge theory to area-angle Regge calculus," *Class. Quant. Grav.* **26** (2009) 155020, `arXiv:0903.0267 [gr-qc]`.

[C68] V. Bonzom, "Spin foam models for quantum gravity from lattice path integrals," *Phys. Rev. D* **80** (2009) 064028, `arXiv:0905.1501 [gr-qc]`.

[C69] V. Bonzom, "Spin foam models and the Wheeler-DeWitt equation for the quantum 4-simplex," *Phys. Rev. D* **84** (2011) 024009, `arXiv:1101.1615 [gr-qc]`.

[C70] V. Bonzom and A. Laddha, "Lessons from toy-models for the dynamics of loop quantum gravity," *SIGMA* **8** (2012) 009, `arXiv:1110.2157 [gr-qc]`.

[C71] A. Baratin and L. Freidel, "Hidden Quantum Gravity in 4-D Feynman diagrams: Emergence of spin foams," *Class.Quant.Grav.* **24** (2007) 2027–2060, `arXiv:hep-th/0611042 [hep-th]`.

[C72] D. Oriti, "The Feynman propagator for quantum gravity: Spin foams, proper time, orientation, causality and timeless-ordering," *Braz.J.Phys.* **35** (2005) 481–488, `arXiv:gr-qc/0412035 [gr-qc]`.

[C73] C. Rovelli *private communication* .

[C74] H. W. Hamber, "Phases of simplicial quantum gravity in four-dimensions: Estimates for the critical exponents," *Nucl.Phys.* **B400** (1993) 347–389.

[C75] B. Bahr, B. Dittrich, and J. P. Ryan, "Spin foam models with finite groups," *J. Grav.* **2013** (2013) 549824, `arXiv:1103.6264 [gr-qc]`.

[C76] B. Dittrich, F. C. Eckert, and M. Martín-Benito, "Coarse graining methods for spin net and spin foam models," *New J. Phys.* **14** (2012) 035008, `arXiv:1109.4927 [gr-qc]`.

5 Discretization independence implies non–locality in 4D discrete quantum gravity

Bianca Dittrich, Wojciech Kamiński and Sebastian Steinhaus

Perimeter Institute for Theoretical Physics,
31 Caroline Street North, Waterloo, Ontario, Canada N2L 2Y5

Abstract

The 4D Regge action is invariant under 5–1 and 4–2 Pachner moves, which define a subset of (local) changes of the triangulation. Given this fact one might hope to find a local path integral measure that makes the quantum theory invariant under these moves and hence makes the theory partially triangulation invariant. We show that such a local invariant path integral measure does not exist for the 4D linearized Regge theory.

To this end we uncover an interesting geometric interpretation for the Hessian of the 4D Regge action. This geometric interpretation will allow us to prove that the determinant of the Hessian of the 4D Regge action does not factorize over 4–simplices or subsimplices. It furthermore allows to determine configurations where this Hessian vanishes, which only appears to be the case in degenerate backgrounds or if one allows for different orientations of the simplices.

We suggest a non–local measure factor that absorbs the non–local part of the determinant of the Hessian under 5–1 moves as well as a local measure factor that is preserved for very special configurations.

5.1 Introduction

Many quantum gravity approaches rely on a path integral construction as their foundation, for example spin foam models [D1, D2], group and tensorial field theory [D3, D4], (causal) dynamical triangulations [D5] or quantum Regge calculus [D6–D9]. These approaches have the same goal, namely to provide a way to compute (and give meaning to) the gravitational path integral, i.e. the sum over all histories between two 3–dimensional boundary geometries, where each history is a 4–geometry describing a possible transition weighted by the (exponential of the) Einstein–Hilbert action. An essential part in this path integral is the measure over the space of geometries, i.e. the space of all metrics modulo diffeomorphisms.

To propose a well–defined path integral, one generically has to introduce a regulator to truncate the degrees of freedom of the theory. In gravitational theories mentioned above this is achieved by discretizing the theory, e.g. on a triangulation. However, the introduction of discretizations comes with a caveat: In general, a discretization of the classical theory cannot be chosen uniquely, if the only requirement is that this discretization leads to the correct continuum action. Whereas some agreement has been reached on the Regge action as a preferred discrete action [D10], at least for the theory without cosmological constant, the debate on the measure in Regge calculus [D11–D14] and spin foams [D15, D16] is not settled.

Even more troubling in the context of gravity, discretizations generically break diffeomorphism symmetry [D17–D19], which is deeply intertwined with the dynamics of general relativity. Furthermore, this might induce an unphysical dependency of this theory on the choice of the discretization. Different approaches to quantum gravity differ in how they deal with these problems, e.g. in Regge calculus one considers only one triangulation with varying edge lengths, whereas in causal dynamical triangulations one keeps equilateral simplices and sums over all triangulations. Group field theories additionally sum over all topologies. Which of these schemes leads to a sensible theory of quantum gravity cannot be determined a priori.

These intricacies are deeply rooted in the fact that diffeomorphism symmetry is broken by the discretisation and that the relation between discrete and continuous gravity is still hardly understood. This particularly affects the choice of measure in quantum gravity theories, which is crucially important for the dynamics in the continuum limit, since it also resembles a choice of the measure on the space of geometries.

For spin foam models, arguments that link diffeomorphism symmetry, choice of (anomaly free) measure and divergence structure due to having non–compact gauge orbits from the diffeomorphism group have been made in [D15, D20]. This led also to the suggestion to choose a measure which has a certain (weak) notion of discretization independence, e.g. such that the amplitudes become independent under 'trivial' edge and face subdivisions [D16, D21–D23]. As mentioned the choice of measure heavily influences the divergence structure of the models [D23–D25]. Thus one can adjust the measure to obtain the divergence structure that fits the divergences one expects from diffeomorphism symmetry. This of course does not fully guarantee diffeomorphism symmetry or triangulation independence, as divergences might also arise due to other reasons.

In Regge calculus, several measures have been proposed: in [D11] Hamber and Williams propose a discretization of the formal continuum path integral, with a local discretization of the (DeWitt) measure [D11, D12], conflicting with the proposal by Menotti and Peirano [D13], who mod out a subgroup of the continuum diffeomorphisms resulting in a highly non–local measure. A different discretization, also leading to a non–local measure due to discretizing first the DeWitt super metric [D26] and then forming the determinant, was proposed in [D14].

In this work we will pick up the suggestion in [D27], to choose a measure that, at least for the linearized (Regge) theory, leads to as much discretization invariance as possible. These considerations require to actually integrate out degrees of freedom and thus take the dynamics into account.

The requirement of discretisation independence seems to be at odds with interacting theories, which possess local / propagating degrees of freedom. This apparent contradiction can be resolved

by allowing a non–local action or non–local amplitudes for the quantum theory – which in fact are unavoidable if one coarse grains the theory. Non–local amplitudes are however difficult to deal with. We therefore ask in this paper the question, whether in the quantum theory we can retain as much symmetry as in the classical theory, with a choice of local measure. The classical 4D Regge action is known to be invariant under $5-1$ moves and $4-2$ moves, but not under $3-3$ moves [D27]. Here the non–invariance under the $3-3$ moves – in fact the only move involving bulk curvature for the solution – allows the local Regge action to nevertheless lead to a theory with propagating degrees of freedom. We therefore ask whether it is possible to have a local measure for linearized Regge calculus that leads to invariance under $5-1$ and / or $4-2$ moves. Such a measure would therefore reproduce the symmetry properties of the Regge action. We will however show that such a local path integral measure does not exist.

Our requirement of (maximal) discretisation independence is motivated by the 'perfect action / discretisation' approach [D28, D29] that targets to construct a discretisation, which 'perfectly' encodes the continuum dynamics and has a discrete remnant of the continuum diffeomorphism symmetry. Examples of such 'perfect discretisations' are 3D Regge calculus with and without a cosmological constant [D30] and also 4D Regge calculus, if the boundary data impose a flat solution in the bulk. In these examples, the basic building blocks mimic the continuum dynamics, e.g. one takes constantly curved tetrahedra for 3D gravity with a cosmological constant. Such perfect discretisations can be constructed as the fixed point of a coarse graining scheme, see for instance [D30–D32].

Once such a discretisation is constructed, the predictions of the theory become independent of the fineness of the discretisation. On the one hand one can compute observables for the coarsest discretisation, while on the other hand one can straightforwardly define the continuum limit and return to a description with local degrees of freedom. Indeed, the examples that have been considered so far lead to the conjecture that diffeomorphism symmetry is equivalent to discretisation independence. For quantum mechanical systems (with time discretization), it has been proven in [D32] that diffeomorphism symmetry implies discretization invariance. Recently, the relationship between diffeomorphism symmetry and discretization independence has been strengthened in the principle of dynamical cylindrical consistency [D33] for time–evolving discrete systems [D34], see also [D35–D38].

This conjecture has been the main motivation of [D27]: the question has been, whether requiring triangulation independence, i.e. invariance under Pachner moves [D39, D40], can be used as a dynamical determination of the path integral measure in (linearized) Regge calculus. One would expect that this requirement would also single out a unique measure. In 3D this lead to a simple measure factor invariant under all Pachner moves, which is consistent with the asymptotics of the Ponzano–Regge (spin foam) model [D41–D46]. The 4D case, that is the expressions for the determinants of the Hessians of the action evaluated on the solution, turned out to be astonishingly similar to the 3D one, yet these expressions were modified by an overall factor, which appears to be non–factorising with respect to the (sub)simplices of the triangulation and resisted so far a geometric interpretation. More importantly, it has been conjectured in [D27] to be non–local and, thus, effectively hindering a construction of a local path integral invariant under a subset of Pachner moves in 4D [D27].

This factor will be the main focus of this paper, in which we will derive a geometric interpretation, namely as a criterion determining whether $d + 2$ vertices (in d dimensions) lie on a $(d - 1)$– sphere [D47] (see also [D48]). This interpretation allows us to prove that this intricate factor is non–factorising, i.e. it cannot be expressed as a simple product of amplitudes associated to the (sub)simplices of the triangulation. (We will refer to this property as 'non–local'.)

This paper is organized as follows: In section 5.2 we review the setup and main results of [D27]. Section 5.3 deals with the derivation of the new interpretation of the non–factorising factor, namely as a criterion determining whether six vertices lie on a 3–sphere, uncovering the factor's non–local

nature. To examine the general cases, we have to generalize the study of [D27] to more general orientations in section 5.4. We discuss different choices for the measure (see also appendix 5.B). The paper is concluded by a discussion of the result in section 5.5. In appendix 5.A we discuss some particular cases of the non–local factor.

5.2 Linearized Regge calculus and previous results

In the work [D27] it has been examined whether one can define a triangulation invariant path integral measure for (linearized) length Regge calculus. Let us briefly recap the setup: Consider the Euclidean path integral for the Regge discretization of gravity given on a 3D or a 4D triangulation:

$$\int_{l_e|e \subset \partial M} \prod_e dl_e \, \mu(l_e) e^{-S_R[l_e]} \quad , \tag{5.2.1}$$

where $l_e|e \subset \partial M$ denotes the fixed edge lengths on the boundary of the triangulated manifold M. $S_R[l_e]$ is called the Regge action and is given by the following expression in d dimensions:

$$S_R[l_e] := - \sum_{h \subset \text{bulk}} V_h \, \omega_h^{(\text{bulk})} - \sum_{h \subset \text{bdry}} V_h \, \omega_h^{(\text{bdry})} \quad , \tag{5.2.2}$$

where V_h is the volume of the $(d-2)$–simplex h, also called 'hinge', and $\omega_h^{(\text{bulk})}$ and $\omega_h^{(\text{bdry})}$ denote the deficit angle or the exterior boundary angle respectively, located at the hinge h in the d–dimensional simplex σ^d. The deficit angles at a hinge are defined as a sum of the dihedral angles of the d–simplices sharing the hinge modulo 2π and relative orientation of the simplices. The definition for matching orientations of the simplices, also considered in [D27], is:

$$\omega_h^{(\text{bulk})} := 2\pi - \sum_{\sigma^d \supset h} \theta_h^{(d)} \quad , \tag{5.2.3}$$

$$\omega_h^{(\text{bdry})} := k\pi - \sum_{\sigma^d \supset h} \theta_h^{(d)} \quad , \tag{5.2.4}$$

where $\theta_h^{(d)}$ is the d-dimensional dihedral angle at the hinge h in the d–simplex σ^d. k depends on the number of pieces glued together at this boundary. In case only two pieces are put together $k = 1$.

This action (5.2.2) has been linearized, i.e. expanded (up to quadratic order) around a flat background solution, denoted by edge lengths $l_e^{(0)}$, that is a solution of the equations of motion $\frac{\partial S_R}{\partial l_e} = 0$ with vanishing deficit angles $\omega_h^{(\text{bulk})}$ [1]:

$$l_e = l_e^{(0)} + \lambda_e \quad . \tag{5.2.5}$$

The integration is then performed over the perturbations λ_e, such that the Hessian matrix of the Regge action, i.e. $\frac{\partial^2 S_R}{\partial l_e \partial l_{e'}}$, becomes the (inverse) 'propagator' of the theory. The motivating question of [D27] has been whether it is possible to define a measure factor $\mu(l_e^{(0)})$, as a function of the background edge lengths, that allows for a triangulation invariant Regge path integral. To examine triangulation independence, it is enough to only consider local changes of the triangulation, so–called Pachner moves [D39, D40]: a consecutive application of these transfers a triangulation of a manifold into any other possible triangulation of the same manifold.

In [D27] exact formulas for the Hessian matrix in 3D and 4D have been derived in great detail from which one concludes a very specific form of measure factors. In the following, we will restrict ourselves to just recalling the main results:

---

[1] In 3D, the solution to the Regge equations of motion (for positive orientation) always implies vanishing deficit angles, however in 4D this is only possible if the boundary data admit a flat solution.

The Hessian matrices one has to compute are of the following form. In 3D we have

$$\frac{\partial^2 S_R}{\partial l_e \partial l_{e'}} = -\frac{\partial \omega_e}{\partial l_{e'}} \quad , \tag{5.2.6}$$

where the dihedral angles are associated to the edges. In 4D the situation is more complicated

$$\frac{\partial^2 S_R}{\partial l_e \partial l_{e'}} = -\sum_h \frac{\partial A_h}{\partial l_e} \frac{\partial \omega_h}{\partial l_{e'}} - \sum_h \frac{\partial^2 A_h}{\partial l_e \partial l_{e'}} \omega_h - \sum_h \frac{\partial^2 A_h}{\partial l_e \partial l_{e'}} \omega_h^{(\text{bdry})} \quad , \tag{5.2.7}$$

yet only the first term survives, since we are considering a flat background solution ($\omega_h = 0$) and only local changes of the triangulation, which leave the boundary unchanged. Thus for both cases of 3D and 4D Regge calculus, the main task is to compute the first derivatives of the deficit angles.

Although these first derivatives of the deficit angles can be computed explicitly [D49], it is much more effective to use techniques of [D50, D51], see also [D52]. This utilizes the flat background (for the linearized Regge action) and hence the fact that the simplicial complex is embeddable into $\mathbb{R}^d$. One then considers small deviations in the edge lengths so that the complex remains embeddable, i.e. the deficit angles ω_h are unchanged, $\delta\omega_h \equiv 0$. This requirement automatically translates into a requirement on the variations of the dihedral angles $\delta\theta_h$, which are part of the respective deficit angle. Then one computes the derivatives of the dihedral angles [D49] under the assumption that only two edge lengths are varied at the same time [D50, D51]; starting from the simplest case, one derives all other derivatives of the deficit angles by considering the relative change of edge lengths under infinitesimal deviations. Eventually, one finds in 3D:

$$\frac{\partial^2 S_R}{\partial l_{ij} \partial l_{km}} = -\frac{\partial \omega_{ij}}{\partial l_{km}} = (-1)^{s_i + s_j + s_k + s_m} \frac{l_{ij} l_{km}}{6} \frac{V_{\bar{i}} V_{\bar{j}} V_{\bar{k}} V_{\bar{m}}}{\prod_n V_{\bar{n}}} + \text{bdry terms} \quad , \tag{5.2.8}$$

where l_{ij} is the edge lengths between the vertices i and j, ω_{ij} is the deficit angle at the edge (ij) and $V_{\bar{i}}$ is the volume of the tetrahedron obtained by removing the vertex i [2]. The signs s_i depend on the orientation and the considered Pachner move. We provide a different derivation of them in section 5.3. In this work we will neglect the boundary terms, since they are not relevant for the main argument of this paper, yet they are essential to show that the classical Regge action is invariant under Pachner moves [D27].

Indeed, the idea to construct a triangulation invariant measure factor, relies crucially on the invariance of the classical Regge action under Pachner moves. In 3D this is the case for all Pachner moves, such that we were able to derive an invariant measure factor, which is factorising, and hence local, with a straightforward geometrical interpretation:

$$\mu(\{l\}) = \frac{\prod_e \frac{1}{\sqrt{12\pi}} l_e}{\prod_\tau \sqrt{V_\tau}} \quad . \tag{5.2.9}$$

To each edge e of the triangulation one associates the edge length l_e and a numerical factor of $(12\pi)^{-\frac{1}{2}}$, to each tetrahedron τ one associates the inverse (square root) of its volume V_τ. This measure factor is consistent, even up to the numerical factor[3], with the asymptotic expansion of the SU(2) $6j$ symbol [D41–D46], the amplitude associated to a tetrahedron in the Ponzano Regge model, which is triangulation invariant (and topological) as well.

In 4D Regge calculus the situation is more complicated, as one might expect: First the Regge action itself is in general not invariant under the 3–3 Pachner move [D27]. It is a peculiar move, since both possible configurations only differ by the triangle shared by all three 4–simplices of this

---

[2] This assignment is unique in subsets of the triangulation, which are subject to a Pachner move. These subsets consist of $d + 2$ vertices in d dimensions; by removing one vertex, $d + 1$ vertices remain, which span a d–simplex.

[3] The association of the factor $(\sqrt{12\pi})^{-1}$ is not unambiguous. It can either be assigned to edges or tetrahedra.

configuration, no dynamical edge is involved. Hence the configurations are solely determined by the boundary data, which might be chosen such that the deficit angle on the bulk triangle does not vanish, i.e. the configuration is not flat. However as soon as this is the case, the Regge action is not invariant under this Pachner move any more. Thus the Regge action is not a suitable starting point to define an invariant measure under all 4D Pachner moves.

Nevertheless the 4D Regge action is invariant under the 5–1 and 4–2 Pachner moves (and their inverses), so it has been examined whether one can define a measure factor that is at least invariant under these two local changes of the triangulation. Surprisingly, the (considered part of the) Hessian matrix is very similar to the 3D case:

$$\frac{\partial^2 S_R}{\partial l_{op} \partial l_{mn}} = -\sum_{k \neq o,p} \frac{\partial A_{opk}}{\partial l_{op}} \frac{\partial \omega_{opk}}{\partial l_{mn}} = D_{op} \, (-1)^{s_o+s_p+s_m+s_n} \frac{l_{op} l_{mn}}{96} \frac{V_{\bar{o}} V_{\bar{p}} V_{\bar{m}} V_{\bar{n}}}{\prod_l V_{\bar{l}}} + \text{bdry terms} \quad ,$$

(5.2.10)

where the factor D_{op} is the only difference to the 3D case, besides the fact that the $V_{\bar{i}}$ now denote volumes of 4–simplices. Note that for the 5–1 move in 4D (and similarly the 4–1 move in 3D), the Hessian matrix possesses four null eigenvectors, which correspond to a vertex translation invariance of the subdividing vertex. The divergent part of the integral is then identified as an integral over a 4D volume and is gauge fixed to 1. We also provide a brief derivation of (5.2.10) in section 5.4 for more general orientations.

The emphasis of this paper lies on this factor D_{op}, which is given by the following expression:

$$D_{op} := \sum_{k \neq o,p} (-1)^{s_k} \left(l_{ok}^2 + l_{pk}^2 - l_{op}^2 \right) V_{\bar{k}} \quad .$$

(5.2.11)

Since the Hessian matrix is symmetric, one concludes that D_{op} actually does not depend on the vertices o and p, such that it turns into an overall factor of the Hessian matrix. Thus we will only refer to it as D in the following.

Ignoring D for the time being, one can construct an 'almost' triangulation invariant measure, very similar to the 3D case:

$$\mu(\{l\}) = \frac{\prod_e \frac{1}{\sqrt{192\pi}} l_e}{\prod_\Delta \sqrt{V_\Delta}} \quad ,$$

(5.2.12)

where V_Δ now denotes the volume of the 4–simplex Δ. The numerical factors are again assigned to the edges[4].

Despite the concise expression (5.2.11) of D, it both impedes the construction of a triangulation invariant measure and resists a nice geometric interpretation, since it is not obvious, whether it can be written as a product of amplitudes associated to (sub)simplices. Hence it has been conjectured in [D27] that D is non–local and cannot be written in a factorising way. The purpose of this paper is to provide a geometric interpretation for the factor D, namely it is a criterion that determines whether the 6 vertices, that make up the simplicial complex (in 4D) to which the Pachner move is applied, lie on a 3–sphere. We will use this to prove that the factor D generically cannot be accommodated by a local measure factor, in particular not by simple product (or quotient) of volumes of (sub)simplices.

5.3 A geometric interpretation for D

In this section we will derive a geometric interpretation for the factor D mentioned above. Actually, the definition (5.2.11) of D is valid in any dimension $d \geq 3$, such that we will derive its geometric interpretation for arbitrary dimensions[5].

---

[4]As in 3D, the assignment of numerical factors is not unambiguous.

[5]Note that it is not clear whether D will also arise in higher dimensions in the framework of linearized Regge calculus. We can only confirm this for $d = 4$ [D27].

In the following we will discuss a simplicial complex in d dimensions, to which a Pachner move will be applied. Consider $d + 2$ vertices embedded in $\mathbb{R}^d$, such that they form non–degenerate d–simplices. The geometry can be completely characterized by the set of the edge lengths $\{l_{ij}\}$, describing the Euclidean distances between the vertices. Given a set of vertices and the edge lengths between them, one can define the associated Cayley–Menger matrix C [D47,D50,D51,D53]. In the case we consider here, this is a $(d + 3) \times (d + 3)$–dim. matrix given by:

$$
C := \begin{pmatrix}
0 & 1 & 1 & 1 & \cdots & 1 \\
1 & 0 & l_{01}^2 & l_{02}^2 & \cdots & l_{0(d+1)}^2 \\
1 & l_{01}^2 & 0 & l_{12}^2 & \cdots & l_{1(d+1)}^2 \\
\vdots & \vdots & \vdots & \vdots & \ddots & \vdots \\
1 & l_{0(d+1)}^2 & l_{1(d+1)}^2 & l_{2(d+1)}^2 & \cdots & 0
\end{pmatrix} \quad .
\tag{5.3.1}
$$

In general, the determinant of the Cayley–Menger matrix, $\det C$, associated to a d–simplex is proportional to the square of its d–volume. However, in the example at hand, the $d + 2$ vertices are embedded in $\mathbb{R}^d$, such that they form a degenerate $(d + 1)$–simplex, hence $\det C = 0$. Since we have required that the d–simplices are non–degenerate, C has exactly one null eigenvector, corresponding to changes of the edge lengths, such that the $d + 2$ vertices remain (embeddable) in $\mathbb{R}^d$. To describe this null eigenvector, let us introduce some notation.

By C_j^i we denote the submatrix of C obtained by deleting its i'th column and its j'th row with $i, j \in \{0, 1, 2, \ldots, d+2\}$. The determinant of the submatrix, i.e. the (i, j)th minor of C, is denoted by $\left| C_j^i \right| := \det C_j^i$. To simplify notation we simply call the diagonal minors $|C_i|$. In fact, since $\det C = 0$, all off-diagonal minors can be expressed in terms of the diagonal ones [D54]:

$$
\left| C_j^i \right| = \sqrt{|C_i|} \sqrt{|C_j|} \quad .
\tag{5.3.2}
$$

Before we construct the null eigenvector of C, it is instructive to examine the minors C_0 and C_i for $i > 0$ in more detail and discuss their geometric interpretation.

The matrix C_0, obtained by deleting the '0'th column and row of C is particularly important in this paper. It is given by:

$$
C_0 = \begin{pmatrix}
0 & (l_{01})^2 & \cdots & (l_{0(d+1)})^2 \\
(l_{01})^2 & 0 & \cdots & (l_{1(d+1)})^2 \\
\vdots & \vdots & \cdots & \vdots \\
(l_{0(d+1)})^2 & (l_{1(d+1)})^2 & \cdots & 0
\end{pmatrix} \quad .
\tag{5.3.3}
$$

It has been shown in [D47] (see also [D48]) that $|C_0|$ has a very specific geometric meaning. In case $|C_0| = 0$ the $d + 2$ vertices lie on a $(d-1)$–dimensional sphere, see fig. 5.1 for an example in $d = 2$. In a sense, this is a non–local statement, since it can only be deduced if the positions of all $d + 2$ vertices are known; it cannot be inferred from just $d + 1$ vertices. From the construction of the null eigenvector, we will show that $D \sim \sqrt{|C_0|}$. Hence we argue that D is non–local in section 5.3.1.

The second interesting minor we want to discuss is $|C_i|$ for $i \in \{1, 2, \ldots, d+1\}$. If one takes a look at the definition of C in (5.3.1) again, then one realizes that by removing the i'th row and column, one removes all edge lengths with the index $i - 1$. The remaining matrix is again a Cayley-Menger matrix, yet for a d–simplex. Hence

$$
|C_i| = (-1)^{d+1} 2^d (d!)^2 \left(V_{\overline{i-1}} \right)^2 \quad .
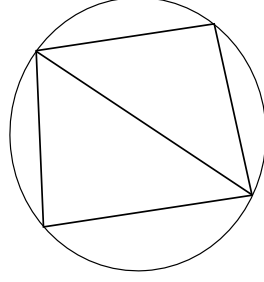\tag{5.3.4}
$$

Figure 5.1: The situation in 2D: Four vertices on a 1–sphere.

The single null eigenvector of C is given by[6]

$$\vec{v}_c := \left((-1)^s \sqrt{|C_0|}, (-1)^{s_0} \sqrt{|C_1|}, \ldots, (-1)^{s_{d+1}} \sqrt{|C_{d+2}|}\right) \tag{5.3.5}$$

$$= \left((-1)^s \sqrt{|C_0|}, (-1)^{s_0} 2^{d/2} d! \, V_{\bar{0}}, \ldots, (-1)^{s_{d+1}} 2^{d/2} d! \, V_{\overline{d+1}}\right) \quad . \tag{5.3.6}$$

The signs s and s_i are determined only up to an overall sign ambiguity. We will show below that we can choose s_i to be the same signs that appear also in (5.2.10) and (5.2.11). The action of the matrix C on $\vec{v}_c$ gives the following relations:

$$\sum_{i=0}^{d+1} (-1)^{s_i} V_{\bar{i}} = 0 \quad , \tag{5.3.7}$$

$$\forall_{j\geq 0} \qquad (-1)^s \sqrt{|C_0|} + \sum_{i=0}^{d+1} (-1)^{s_i} 2^{d/2} d! \, l_{ij}^2 V_{\bar{i}} = 0 \quad . \tag{5.3.8}$$

The first condition fixes the relative signs s_i and is straightforward to interpret if one recalls the change of the triangulation under the Pachner move. Take a $1 - (d+1)$ move for example, where the new vertex 0 is added inside to the $d+1$ vertices forming the d–simplex. The relation shows that the volume before and after the Pachner move is the same:

$$V_{\bar{0}} = \sum_{i=1}^{d+1} V_{\bar{i}} \quad , \tag{5.3.9}$$

which fixes the signs $s_0 = 1$ and $s_i = 0 \, \forall \, i \geq 1$, consistent with the results of [D27]. Similar relations also hold for the other Pachner moves. For different (relative) orientations (see section 5.4), one or more signs get flipped such that such a clear separation between volumes 'before' and 'after' the Pachner move is not possible any more. In fact, since we mainly discuss the 5–1 move in this paper, we fix $s_0 = 1$, i.e. the orientation of the coarse simplex, because it is determined by the boundary data and is thus not affected by moving the vertex 0. This singles out the coarse simplex as a particular reference frame with respect to which the relative orientation of the other simplices is defined.

At this point we can also determine the sign s using equation (5.3.8) for $j = 0$

$$(-1)^s \sqrt{|C_0|} = -2^{d/2} d! \sum_{i=1}^{d+1} (-1)^{s_i} l_{i0}^2 V_{\bar{i}} = -2^{d/2} d! \sum_{i=1}^{d+1} l_{i0}^2 V_{\bar{i}} < 0 \quad . \tag{5.3.10}$$

Thus we conclude $s = 1$.

---

[6]The null eigenvector can be deduced from the expansion of $\det C$ with respect to different rows.

The relations (5.3.7) can be used to derive a relation between the non–local factor D and the criterion $|C_0|$ determining whether $(d+2)$ vertices lie on a $(d-1)$–sphere. Recall that for arbitrary $i \neq j$, D was defined as:

$$D_{ij} = \sum_{k \neq i,j} (-1)^{s_k} (l_{ik}^2 + l_{jk}^2 - l_{ij}^2) V_{\bar{k}} \quad . \tag{5.3.11}$$

Let us expand D_{ij} as follows:

$$D_{ij} = \underbrace{\sum_k (-1)^{s_k} (l_{ik}^2 + l_{jk}^2) V_{\bar{k}}}_{\overset{(5.3.7)}{=} -2(-1)^s 2^{-d/2} (d!)^{-1} \sqrt{|C_0|}} \underbrace{- \left((-1)^{s_j} l_{ij} V_{\bar{j}} + (-1)^{s_i} l_{ij} V_{\bar{i}} \right) - \sum_{k \neq i,j} (-1)^{s_k} l_{ij}^2 V_{\bar{k}}}_{= -l_{ij}^2 \sum_k (-1)^{s_k} V_{\bar{k}} \overset{(5.3.7)}{=} 0}$$

$$= -2^{1-d/2} (d!)^{-1} (-1)^s \sqrt{|C_0|} \quad . \tag{5.3.12}$$

This proves the relation between the non–local measure D and the criterion $|C_0|$.

This automatically gives a new interpretation to the non–factorising factor $D \sim \sqrt{|C_0|}$ appearing in the 4D Pachner moves. If it vanishes[7] all six vertices of the 4–simplices involved in the Pachner move lie on a 3–sphere. To determine whether this is the case or not, one has to know the positions of all six vertices with respect to each other, it cannot be inferred from a subset. Thus it is already implied that the factor D has to be non–local, since its geometric meaning can only be deduced if the relative positions of all six vertices are known. We will use this fact in section 5.3.1 to show that D does not factorise.

This geometric interpretation is even more pronounced if we express the factor D in affine coordinates. To this end we specialize to the $(d+1) - 1$ move, in which we integrate out d edge lengths, that start from a subdividing vertex 0, which lies inside the final simplex.

An efficient way to describe the coordinate of the subdividing vertex 0 with respect to the final simplex $\bar{0}$ is by using affine coordinates. The idea is to write the position vector $\vec{x}_0$ of the new vertex as a weighted sum of the position vectors $\vec{x}_i, i \neq 0$, with weights α_i. The condition $\sum_{i \neq 0} \alpha_i = 1$ ensures that this prescription is well–defined. If one additionally requires that $\alpha_i \geq 0$, $\forall i \neq 0$, then the new vertex is inside the final simplex. As soon as one of the α_i is negative, the vertex 0 is located outside.

Hence, the position vector $\vec{x}_0$ is given by

$$\vec{x}_0 = \sum_{i \neq 0} \alpha_i \vec{x}_i \quad , \tag{5.3.13}$$

thus

$$\vec{x}_k - \vec{x}_0 = \left(\sum_{i \neq 0} \alpha_i \right) \vec{x}_k - \sum_{i \neq 0} \alpha_i \vec{x}_i = \sum_{i \neq 0} \alpha_i (\vec{x}_k - \vec{x}_i) \quad . \tag{5.3.14}$$

The (square of the) new edge lengths is given by $l_{0k}^2 = (\vec{x}_k - \vec{x}_0)^2$:

$$l_{0k}^2 = \sum_{i \neq 0, j \neq 0} \alpha_i \alpha_j (\vec{x}_k - \vec{x}_i) \cdot (\vec{x}_k - \vec{x}_j)$$

$$= \frac{1}{2} \sum_{i \neq 0, j \neq 0} \alpha_i \alpha_j \left((\vec{x}_k - \vec{x}_i)^2 + (\vec{x}_k - \vec{x}_j)^2 - ((\vec{x}_k - \vec{x}_i) - (\vec{x}_k - \vec{x}_j))^2 \right)$$

$$= \frac{1}{2} \sum_{i \neq 0, j \neq 0} \alpha_i \alpha_j (l_{ik}^2 + l_{jk}^2 - l_{ij}^2) = \sum_{i \neq 0} \alpha_i l_{ik}^2 \underbrace{\left(\sum_{j \neq 0} \alpha_j \right)}_{=1} - \underbrace{\sum_{0 < i < j} \alpha_i \alpha_j l_{ij}^2}_{=:b^2} = \sum_{i \neq 0} \alpha_i l_{ik}^2 - b^2 \quad . \tag{5.3.15}$$

---

[7]The result is that the quadratic part of the action vanishes and the integral diverges.

Recalling the determinant expression of D^2, i.e. (5.3.12) and (5.3.3), l_{0k}^2 are the entries of the first row and column of the matrix C_0. Without changing the determinant we subtract α_i times the $(i+1)$'th row from the first one for all $i \neq 0$ and obtain:

$$D^2 = \left(\frac{1}{48}\right)^2 \det \begin{pmatrix} -b^2 & & -b^2 & -b^2 & \cdots & -b^2 \\ \sum_{i\neq 0}\alpha_i l_{i1}^2 - b^2 & 0 & l_{12}^2 & \cdots & l_{15}^2 \\ \sum_{i\neq 0}\alpha_i l_{i2}^2 - b^2 & l_{12}^2 & 0 & \cdots & l_{25}^2 \\ \vdots & \vdots & \vdots & \ddots & \vdots \\ \sum_{i\neq 0}\alpha_i l_{i5}^2 - b^2 & l_{15}^2 & l_{25}^2 & \cdots & 0 \end{pmatrix} \quad , \tag{5.3.16}$$

where it is straightforward to derive that $\sum_{j\neq 0}\alpha_j \left(\sum_{i\neq 0}\alpha_i l_{ij}^2 - b^2\right) = b^2$. Again, we repeat the procedure for the columns by subtracting α_i times the $(i+1)$'th column from the first one for all $i \neq 0$. Then the result can be written as

$$D^2 = \left(\frac{1}{48}\right)^2 \det \begin{pmatrix} 0 & -b^2 & -b^2 & \cdots & -b^2 \\ -b^2 & 0 & l_{12}^2 & \cdots & l_{15}^2 \\ -b^2 & l_{12}^2 & 0 & \cdots & l_{25}^2 \\ \vdots & \vdots & \vdots & \ddots & \vdots \\ -b^2 & l_{15}^2 & l_{25}^2 & \cdots & 0 \end{pmatrix} = 4b^4 V_{\bar{0}}^2 = 4\left(\sum_{0<i<j}\alpha_i\alpha_j l_{ij}^2\right)^2 V_{\bar{0}}^2 \quad . \tag{5.3.17}$$

Indeed, (5.3.17) is a remarkable identity for D (in the 5–1 move[8]): The non–locality of D here is encoded in the choice of reference frame, namely the final simplex. In particular from the perspective of the five simplex configuration, this is not obvious. Moreover, the dependence on the position of the new vertex only enters into the factor b^2 through the weights α_i.

Let us describe the geometric meaning of $b^2 = \sum_{0<i<j}\alpha_i\alpha_j l_{ij}^2$. Let $\vec{x}$ denote the position vector of the circumcenter of the 4–simplex $\bar{0}$, i.e. the circumcenter of the 3–sphere circumscribing the 4–simplex. Then the distance between this point and the vertex 0 is given by:

$$(\vec{x}_0 - \vec{x})^2 = \sum_{i\neq 0, j\neq 0} \alpha_i\alpha_j(\vec{x}_i - \vec{x})(\vec{x}_j - \vec{x}) = \frac{1}{2}\sum_{i\neq 0, j\neq 0}\alpha_i\alpha_j\left((\vec{x}_i - \vec{x})^2 + (\vec{x}_i - \vec{x})^2 - (\vec{x}_i - \vec{x}_j)^2\right) \quad , \tag{5.3.18}$$

yet, by definition of $\vec{x}$, $(\vec{x}_i - \vec{x})^2 = r^2 \; \forall i \neq 0$. Thus

$$(\vec{x}_0 - \vec{x})^2 = r^2 - \sum_{0<i<j}\alpha_i\alpha_j l_{ij}^2 \tag{5.3.19}$$

and finally

$$b^2 = r^2 - (\vec{x}_0 - \vec{x})^2 \quad . \tag{5.3.20}$$

From this fact and (5.3.17) we can simply deduce several properties of D: First of all, since $V_{\bar{0}} \neq 0$ (by assumption), we conclude that $D = 0$ exactly if $b^2 = 0$. From identity (5.3.20) it is clear that this happens only if the vertex 0 lies on the circumscribing sphere of the 4–simplex $\bar{0}$, namely $(\vec{x} - \vec{x}_0)^2 = r^2$. On the other hand, we can directly consider the definition of b^2:

$$b^2 = \sum_{0<i<j}\alpha_i\alpha_j l_{ij}^2 \quad . \tag{5.3.21}$$

It is straightforward to recognize that if we restrict the vertex 0 to stay inside the 4–simplex, i.e. $\alpha_i \geq 0 \; \forall i$, then $b^2 = 0$ is only possible if all α_i except one vanish.

---

[8] As discussed in section 5.4, it is also possible to describe D in a similar way for the 4–2 move. However, there one has to choose one of the two 4–simplices (in the 2 simplex configuration) as a reference frame to describe the fixed position of the additional vertex. Clearly, this is not unambiguous.

This is exactly the case when the vertex 0 is moved on top one of the vertices of the final (coarser) simplex. See fig. 5.2 for the 2D case. In 4D four of the initial five simplices become degenerate and from the limits

$$\lim_{(0)\to(1)} l_{01} = 0 \quad , \lim_{(0)\to(1)} l_{0k} = l_{1k}, \ \forall k \neq 0, 1 \quad , \tag{5.3.22}$$

$$\lim_{(0)\to(1)} V_{\bar{1}} = V_{\bar{0}} \quad , \lim_{(0)\to(1)} V_{\bar{k}} = 0, \ \forall k \neq 0, 1 \quad , \tag{5.3.23}$$

for the volumes and the length variables it is clear that $\lim_{(0)\to(1)} D = 0$. This limit, in which one vertex is moved on top of another plays a crucial role in the relation between diffeomorphism symmetry and triangulation independence [D32]: in the discrete diffeomorphism symmetry is realized as an invariance with respect to moving vertices. Indeed finding a triangulation invariant measure for the $5 - 1$ move would also imply invariance of the path integral under changing the position of the subdividing vertex 0. The classical action (or rather Hamilton–Jacobi functional, i.e. the action evaluated on the solution) already has this symmetry.

An extreme case is given by moving vertices to on top of other vertices, which effectively coarse grains the triangulation. One would expect a singular behaviour in this case, as the lengths variables one integrates over become redundant (we are in the linearized theory, and moving the vertex actually affects the background variables).

Apart from these degenerate cases it can happen that D vanishes, if we move the subdividing vertex outside the coarser simplex. In this case some some $\alpha_i < 0$. Indeed, the conditions $b^2 = 0$ and $\sum_i \alpha_i = 1$ fix three of the five α_i, parametrising a 3–sphere, thus explaining the previous geometric interpretation. Yet these cases involve a change of orientation, which will be reflected in the definition of the deficit angle and hence the action. One might be concerned that the formulas derived in [D27] are no longer valid, but we will show in section 5.4 that the same arguments work also in this case.
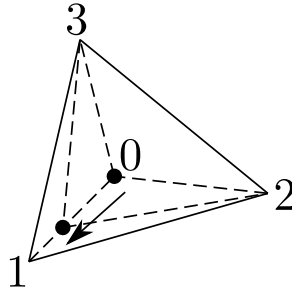

Figure 5.2: The degenerate limit in 2D, in which the inner vertex 0 is moved on top of one of the vertices, here 1, of the original triangle. Clearly, once the limit is reached the areas of the triangles (012) and (013) vanish.

5.3.1 Non–locality of the measure

The geometric interpretation of the factor D reveals its non–local structure, that it does not factorize over (sub)simplices of the triangulation. Assuming that it would factorize, i.e. D is of the form

$$D = \prod_\sigma A_\sigma(l) \quad , \tag{5.3.24}$$

where the product is over the 4–simplices and all the other lower dimensional simplices in the complex under consideration. Note that factors in (5.3.24) are allowed to be constant. A factor $A_\sigma(l)$ depends only on the length variables of the edges contained in this simplex (which completely

specify the geometry of this simplex). The zeros of D would be given by the union of the zeros of all its subfactors. However each subfactor can only depend on the lengths of the edges connecting these five vertices of the simplicial complex in question (which has six vertices), whereas the vanishing of D is equivalent to a condition involving all six vertices.

Assume that D, and hence at least one of the factors in (5.3.24) is vanishing. Thus the six vertices of the simplicial complex in question lie on one 3–sphere. Choose one of the vanishing factors, say $A_{\sigma'}$. As σ' does not include all vertices, we can change the position of one of the vertices not in σ' so that the six vertices do not lie on a 3–sphere any more. In this case D still vanishes due to the factorizing nature assumed in (5.3.24), which contradicts that D is only vanishing if the six vertices are on the 3–sphere. Thus D cannot be of the factorizing form (5.3.24).

5.4 Orientation

In this section we will discuss the changes of orientation that occur once the additional vertex is moved outside the coarser 4–simplex. As we will explain below, this will only result in the change of certain signs; the entire derivation performed in [D27] works analogously.

Before we move the vertex outside, let us first consider how the null eigenvector $\vec{v}_c$ of C (see eq. (5.3.5)) is affected, when we move the vertex toward the boundary of the coarser simplex along a straight line. As we will see, one or more entries of $\vec{v}_c$ will vanish once the boundary is reached; which ones and how many depends on the dimension of the subsimplex the internal vertex is placed upon. The vanishing entries will change sign once the boundary is crossed (through this subsimplex), which corresponds to a change of orientation of the d–simplices, which share the before mentioned subsimplex.

To illustrate this point, let us revisit the simple 2D example. Consider again the triangle (123) spanned by three vertices, which is subdivided in a 1–3 move by the vertex 0 placed in its center. If one intends to move the vertex 0 outside the triangle (123), one has two options: either one crosses through an edge or a vertex, i.e. a 1–dim. or a 0–dim. subsimplex. If one moves 0 closer to the edge (12) as illustrated in fig. 5.3, the volume of the triangle (012), $V_{\bar{3}} \to 0$. Once the vertex is moved across the boundary, the component $\sim V_{\bar{3}}$ in $\vec{v}_c$ changes its sign, here s_3.
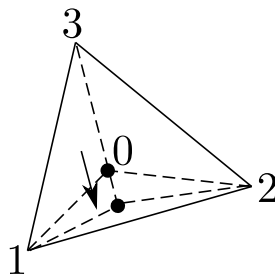

Figure 5.3: Approaching the boundary of the triangle (123) with vertex 0 via the edge (12). If the vertex 0 reaches the edge, the area of the triangle (012), i.e. $V_{\bar{3}}$, vanishes.

The other situation, when the vertex 0 is moved on top of one of the other vertices has been already discussed in section 5.3 and illustrated in figure 5.2: The vertex 0 is moved towards the vertex 1, such that, once they are on top of each other, the areas of the triangles (012) and (013) vanish, i.e. $V_{\bar{2}} = V_{\bar{3}} = 0$. Additionally, since all four vertices lie on the same 1–sphere, $C_0 = 0$. Hence, three signs in $\vec{v}_c$ change, namely s, s_2 and s_3.

It is straightforward to generalize these ideas to arbitrary dimensions d: The relative signs s, s_i depend on the position of the subdividing vertex 0 with respect to $(d-1)$–dim. hypersurfaces: In the case of the sign s, it is the $(d-1)$–sphere circumscribing the initial d–simplex. For the sign

s_i, it is the hypersurface orthogonal to the normal vector associated to one $(d-1)$–simplex formed without the vertex i. We illustrate this in 2D in fig. 5.4.
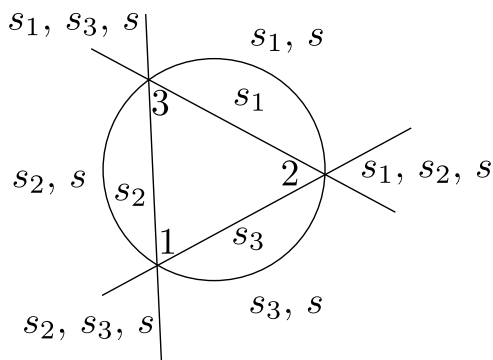

Figure 5.4: The triangle (123) and the 1–dim. hypersurfaces determining the change of sign. A region with s_i inside denotes that the sign s_i is changed, if the vertex is moved 0 is moved from inside the triangle into this labelled region.

To be more concrete, let us examine all possible situations in 4D: Consider the initial 4–simplex (12345) formed by five vertices. The vertex 0 can 'leave' the initial 4–simplex either through a tetrahedron, a triangle, an edge or a vertex. We have summarized the respective changes of signs in the following table:

Approached / crossed subsimplex:	Vanishing entries of $\vec{v}_c$	Changes of signs
Tetrahedron (1234)	$V_{\bar{5}} = 0$	s_5
Triangle (123)	$V_{\bar{4}} = V_{\bar{5}} = 0$	s_4, s_5
Edge (12)	$V_{\bar{3}} = V_{\bar{4}} = V_{\bar{5}} = 0$	s_3, s_4, s_5
Vertex 1	$C_0 = V_{\bar{2}} = \cdots = V_{\bar{5}} = 0$	s and $s_2, \cdots s_5$

Let us now focus on the change of deficit angles in the action that occurs when we cross the boundary of the initial simplex. To explain our point and provide an intuitive example, let us consider the two different orientations drawn in fig. 5.5 for the 1–3 Pachner move in 2D. On the left, we show the well–known configuration, in which the original triangle gets subdivided by an additional vertex 0 into the three triangles (012), (013) and (023). There are three triangles meeting at this new vertex and in order to form a flat triangulation, the dihedral angles located at vertex 0, called $\theta_0^{(0ij)}$ for $i, j \in \{1, 2, 3\}$ with $i \neq j$, have to sum up to 2π. On the right, the same new triangles are created by adding the vertex 0, but this new vertex is now located outside the triangle, which corresponds to a change of orientation. Let us discuss this further.

To be more precise, moving the vertex 0 outside the triangle (123) through the edge (12) changes the relative orientation of the triangle (012) with respect to the triangles (013) and (023). This results into one sign swap in the definition of the deficit angle at the vertex 0 (modulo 2π):

$$\omega_0 = \theta_0^{(013)} + \theta_0^{(023)} - \theta_0^{(012)} = \sum_t \epsilon_t \theta_0^t \quad . \tag{5.4.1}$$

The last part of equation (5.4.1) denotes the formal sum over all triangles t meeting at the vertex 0, where each triangle now carries a colouring $\epsilon_t \in \{\pm 1\}$ denoting its relative orientation, see also [D52]. This simplicial complex is embeddable into $\mathbb{R}^2$, if the deficit angle ω_0 at vertex 0 vanishes modulo 2π[9]. This condition can be automatically translated into the fact that the dihedral angles

---

[9]Due to the peculiar relative orientation of simplices one can argue [D55] that the curvature does not vanish at this vertex.
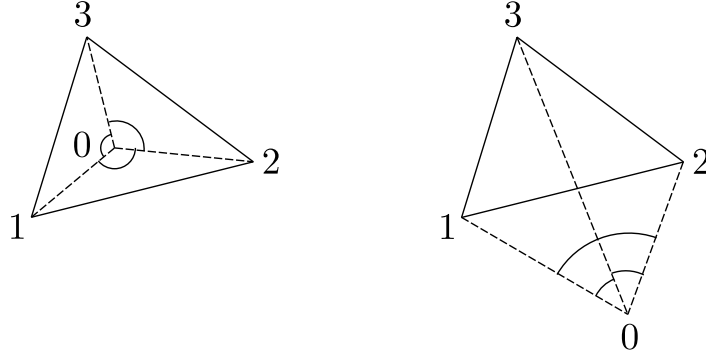
Figure 5.5: We consider here the 1–3 Pachner, in which the triangle (123), formed by the vertices 1, 2 and 3, is subdivided into three triangles (012), (013) and (023) by adding a new vertex 0 and connecting it to all old vertices. On the left the 'usual' configuration after the 1–3 Pachner move with the vertex 0 inside the triangle is depicted, on the right the vertex 0 is outside the triangle, which results here in the opposite orientation of the triangle (012).

(at vertex 0) in the triangles (013) and (023) have to sum up to the one in the triangle (012), which can be nicely seen in fig. 5.5.

Let us return to the 4D case. As the argument above shows, the change of relative signs in the definition of the deficit angle coincides with the change of relative signs of the 4–simplices, i.e. the signs s_k. From that we deduce

$$\epsilon_{\bar{k}} = (-1)^{s_k} \quad . \tag{5.4.2}$$

Finally the general definition of the deficit angle (modulo 2π) located at the triangle (ijk) is:

$$\omega_{ijk} = \sum_l (-1)^{s_l} \theta_{ijk}^{\bar{l}} \bmod 2\pi \quad . \tag{5.4.3}$$

Naturally the questions arises, how this affects the derivation of the Hessian matrix of the Regge action. As it turns out, it hardly does. Let us prove it now:

The starting point of the derivation remains the same, namely we consider a simplicial complex made up of $d+2$ points embedded in $\mathbb{R}^d$ with non–degenerate d–simplices. Hence the Cayley–Menger determinant $\det C$ is vanishing and the Cayley–Menger matrix C has exactly one null eigenvector. The embeddebility into $\mathbb{R}^d$ and also the vanishing of the Cayley–Menger determinant is due to the vanishing of the deficit angles ω_h (modulo 2π), such that we require that the deficit angles do not change under deviations of the edge lengths, i.e. $\delta\omega_h \equiv 0$.

To put it differently, the condition $\det C = 0$, where C only has one null eigenvector, ensures that the given lengths form geometric d–dim. flat configurations. Thus, independent of the details of the definition of the deficit angles, we have:

$$\delta\omega_h \neq 0 \implies \delta \det C \neq 0 . \tag{5.4.4}$$

As a consequence, the variations of the deficit angles ω_h and $\det C$ are related. This shows that under the condition $\det C = 0$, we conclude for the 4D deficit angles ω_{ijk}:

$$\delta\omega_{ijk} = B_{ijk} \, \delta \det C, \quad \frac{\partial \omega_{ijk}}{\partial l_{mn}} = B_{ijk} \frac{\partial \det C}{\partial l_{mn}} \quad , \tag{5.4.5}$$

where B_{ijk} denote some implicit functions. It turns out that the bulk part of the Hessian satisfies (5.2.7)

$$\frac{\partial^2 S_R}{\partial l_{op} \partial l_{mn}} = -\sum_h \frac{\partial A_h}{\partial l_{op}} \frac{\partial \omega_h}{\partial l_{mn}} + \text{bdry terms} = E_{op} \frac{\partial \det C}{\partial l_{mn}} + \text{bdry terms} \quad , \tag{5.4.6}$$

where E_{op} again are some implicit functions. Since the Hessian matrix is symmetric, we can determine it up to an overall factor F:

$$\delta^2 S_R = F \, \delta \det C \otimes \delta \det C + \text{bdry terms} \quad . \tag{5.4.7}$$

Since we only consider variations on the surface defined by $\det C = 0$, $\delta \det C$ is straightforward to determine:

$$\frac{\partial \det C}{\partial l_{mn}} = \text{Tr}|_{\det C = 0}\left(\text{adj}(C)\frac{\partial C}{\partial l_{mn}}\right) = \left(\vec{v}_c \Big| \frac{\partial C}{\partial l_{mn}} \vec{v}_c\right) = 2^{-2}(4!)^{-2} \, l_{mn}(-1)^{s_m} V_{\bar{m}}(-1)^{s_n} V_{\bar{n}} \quad . \tag{5.4.8}$$

Finally,

$$\delta^2 S_R = F \, \frac{(-1)^{s_i + s_j + s_m + s_n}}{48^2} \, l_{ij} l_{mn} \, V_{\bar{i}} V_{\bar{j}} V_{\bar{m}} V_{\bar{n}} \, \delta l_{ij} \otimes \delta l_{mn} + \text{ bdry terms} \quad . \tag{5.4.9}$$

In order to identify F, let us repeat the reasoning from [D27]. Let us denote by $\{ijkmno\}$ a permutation of the vertices $\{012345\}$. It is straightforward to compute $\frac{\partial \omega_{ijk}}{\partial l_{mn}}$, since it only depends on the dihedral angle in the 4–simplex $(ijkmn)$. Using a formula from [D49] for $\frac{\partial \omega_{ijk}}{\partial l_{mn}}$, we get:

$$\frac{\partial \omega_{ijk}}{\partial l_{mn}} = (-1)^{s_o} \frac{l_{mn} A_{ijk}}{12 V_{\bar{o}}}$$

$$\Rightarrow \delta \omega_{ijk} = (-1)^{\sum_l s_l} \frac{(-1)^{s_i} V_{\bar{i}} (-1)^{s_j} V_{\bar{j}} (-1)^{s_k} V_{\bar{k}} \, A_{ijk}}{12 \prod_l V_{\bar{l}}} \underbrace{(-1)^{s_m} V_{\bar{m}} (-1)^{s_n} V_{\bar{n}} \, l_{mn} \, \delta l_{mn}}_{48^2 \delta \det C} \quad . \tag{5.4.10}$$

Thus in any case we have (for edge lengths not on the boundary)

$$\frac{\partial^2 S_R}{\partial l_{mn} \partial l_{ij}} = -\sum \frac{\partial A_{ijk}}{\partial l_{ij}} \frac{\partial \omega_{ijk}}{\partial l_{mn}}$$

$$= -\frac{\left(\sum_k (l_{ik}^2 + l_{jk}^2 - l_{ij}^2)(-1)^{s_k} V_{\bar{k}}\right)}{96 \prod_l V_{\bar{l}}} \underbrace{(-1)^{s_i} V_{\bar{i}}(-1)^{s_j} V_{\bar{j}} l_{ij}}_{48^2 \frac{\partial \det C}{\partial l_{ij}}} \underbrace{(-1)^{s_m} V_{\bar{m}}(-1)^{s_n} V_{\bar{n}} l_{mn}}_{48^2 \frac{\partial \det C}{\partial l_{mn}}} \quad , \tag{5.4.11}$$

where we used the fact that

$$\frac{\partial A_{ijk}}{\partial l_{ij}} = \frac{l_{ij}}{8 \, A_{ijk}}(l_{ik}^2 + l_{jk}^2 - l_{ij}^2) \quad . \tag{5.4.12}$$

We can thus identify $F = -24\frac{D}{\prod_l V_{\bar{l}}}$.

In this section, we have thoroughly discussed the changes of orientation that occur, if one moves the subdividing vertex outside the coarser 4–simplex. This vertex can be moved outside in different ways, which can be summarized by stating through which subsimplex it has 'left' the coarser 4–simplex. Then all 4–simplices sharing this subsimplex change their relative orientation, which directly translates into a change of sign in the definition of the deficit angles for all dihedral angles stemming from these 4–simplices. Yet these intricacies of the deficit angles do not interfere with the derivations of [D27] as long as the configuration is embeddable in $\mathbb{R}^4$, which is equivalent to stating that the Cayley–Menger determinant $\det C = 0$ or the deficit angles $\omega_h = 0$ modulo 2π.

We have the same factor D appearing in the Hessian of the action, which is vanishing if the subdividing vertex is moved onto the 3–sphere defined by the five vertices of the coarser 4–simplex.

In this case the fluctuation matrix $\delta^2 S_R$ becomes singular[10]. Interestingly there is a recent conjecture, that not including the sum over orientations (and thus avoiding this situation), would avoid divergences in spin foams [D55]. The findings here support this conjecture in a further way: not only may the sum over orientations lead to non–compact (potential) gauge orbits. Additionally there is a submanifold of configurations, on which the fluctuation matrix becomes singular, which only appears if the subdividing vertex is moved outside the coarser simplex (and if one adds up the actions for the different simplices with their correct orientations).

5.4.1 A D factor absorbing measure for the 5–1 move

Given the concise version of D in affine coordinates, see (5.3.17), one may ask whether one can construct a measure factor that absorbs the D factor under the 5–1 move. That is one needs to know which five simplices are coarse grained to one simplex $\sigma_{\bar{0}}$ as the factor D refers to this simplex $\sigma_{\bar{0}}$. The measure one has to choose is then

$$\mu(\{l\})_{5-1} = 2b\sqrt{V_{\bar{0}}}\frac{\prod_e \frac{1}{\sqrt{192\pi}}\, l_e}{\prod_i \sqrt{V_{\bar{i}}}} \quad , \text{ with } b^2 = \sum_{0<i<j} \alpha_i \alpha_j l_{ij}^2 \quad , \tag{5.4.13}$$

where the α_i can be expressed in terms of the lengths l_{i0} and the lengths of the simplex $\sigma_{\bar{0}}$. Again, 'non–locality' arises because it is impossible to rewrite this expression into factors that would only refer to the initial five 4–simplices (or other subsimplices). Instead we have one factor referring to a complex of five simplices.

Here the modifications to the measure due to the non–local factor are specifically made to absorb these contributions, which still requires to identify (and specify) the complexes to which a 5–1 move can (and will) be applied. Thus subdividing one 4–simplex arbitrary many times by 1–5 moves and integrating out again by 1–5 moves with the measure above we will finally end up with an amplitude for the one final simplex, which of course will be 'local', i.e. only refer to the geometry of this simplex.

One can nevertheless ask whether there exists a local measure invariant under a 5–1 move, restricted to special configurations. An example of such a restriction is to consider only barycentric subdivisions. The ansatz of a local measure (factorizing over (sub)simplices) leads to a functional equation that has to be solved, yet whether a solution exists is an open question. In appendix 5.B, we present a measure

$$\mu(\{l\}) = \frac{\prod_e \frac{2^{\frac{1}{10}}5^{\frac{1}{8}}}{\sqrt{192\pi}}\, l_e^{6/5}}{\prod_\Delta V_\Delta^{3/8}} \tag{5.4.14}$$

that is preserved under a single barycentric 5–1 move, if the coarse simplex is equilateral. This local factor should be taken with a grain of salt: Although it gives invariance for a subdivided equilateral simplex, it will not be invariant under repeated subdivisions, as equilateral simplices do not stay equilateral under subdivisions.

5.5 Discussion

In this note we have revisited the work in [D27], in which it has been examined whether one can construct a triangulation invariant path integral measure for (linearized) Regge calculus. While this is possible for the 3–dimensional topological theory, the 4–dimensional case is complicated by the appearance of an overall non–trivial factor D, see (5.2.11), which cannot be factorized over

---

[10] In case of the 5–1 move the Hessian matrix is singular, since it possesses four null eigenvectors corresponding to the vertex translation symmetry of the subdividing vertex. If additionally the factor D vanishes, the whole Hessian matrix vanishes.

(sub)simplices of the triangulation. As we have shown in this paper, this factor has a peculiar geometric interpretation, which is the key ingredient to uncover its non–factorising and, therefore, non–local nature.

This result was derived for the linearized theory. It however also excludes a local measure both invariant under $5-1$ moves and gauge invariant in the sense described in the following for the full theory. The classical equation of motions for this move, which determine the solutions to be flat, display diffeomorphism symmetry as the position of the subdividing vertex can be anywhere (if it is outside the coarser simplex one needs to take the change of (relative) orientation into account). One thus needs to gauge fix (as in the linearized theory). If we assume that a local gauge invariant measure exists that leads to invariance under $5-1$ moves we could use this to define a local measure for the linearized theory, which however does not exist.

We suggested a non–local measure that would absorb the non–local D factor under $5-1$ moves. Alternatively one can devise measure factors that are local and lead to an approximate invariance near very symmetric configurations. Such measure factors could be taken as a hint for choosing the measure for spin foams, see for instance [D56] for a first geometric interpretation of the measure factor for a 4D model.

We additionally found that allowing for a sum over orientations (in our case having simplices of different orientations as background), can lead to more singular Hessians[11] for the linearized Regge action. This resonates with the conjecture in [D55], that not summing over orientations might avoid divergences in spin foams, see however the discussion in [D34], pointing out the significance of summing over orientations for refining boundary states in gravity.

One could have hoped to find a measure that makes the path integral for the linearized theory invariant under $5-1$ moves (and also $4-2$ moves) and is local [D57]. After all this kind of invariance holds for the Regge action and it was the initial motivation for the work [D27]. This work indeed turned out to reproduce successfully the measure factor found in the Ponzano–Regge asymptotics [D41–D46], the (topological) spin foam model for 3D gravity. We see that a theory with propagating degrees of freedom can have quite different properties in this respect even for a sector that leads to only flat solutions as is the case for the $5-1$ and $4-2$ move. Such a flat sector was also discussed in [D58, D59] from a canonical viewpoint where the flatness indeed allows for anomaly free discretizations of the constraint algebra for a special class of boundaries. That is the Hamiltonian and diffeomorphism constraints can be defined, are local and are first class, which so far is not possible to achieve for the general 4D (discrete) case. The results in the work at hand question the possibility to find an anomaly free quantization for this flat (in a sense topological, as the boundaries do not allow for propagating degrees of freedom) sector with only local constraints.

We now have to expect that it is not possible to find a local invariant measure (i.e. a one–loop effective action), even if one just wants to achieve invariance under $5-1$ moves. In fact the concept of 'invariance' under local moves involving non–local amplitudes is rather hard to define: the amplitude for the initial complex in the 5–1 move is non–local, as it can be non–factorizing over the 5 simplices, however the final amplitude only refers to the final, coarser simplex. We therefore suggested a measure that would absorb the non–local part, which results from the Hessian of the action (where 'non–local part' is not without ambiguities). The difficulties of formulating invariance conditions for non–local amplitudes arise also because one is keeping simplices as fundamental building blocks and the principle that these simplices are 'glued' together by integrating over boundary variables. This can be taken as a hint that an alternative formulation, as presented in [D34], is worthwhile: This formulation replaces simplices by building blocks with arbitrarily complicated boundaries and focuses on the amplitudes associated to these boundaries. The requirement of triangulation invariance (which has become empty as it refers to the bulk, whereas in this formulation everything is defined via boundary geometries) is replaced by the condition of cylindrical consistency for the amplitudes associated to these boundaries [D33]. Such a formulation

---

[11]In fact, the Hessian vanishes entirely if $D = 0$.

is much better suited for situations where non–local amplitudes arise and moreover does not refer to bulk triangulations at all.

On the level of the (classical) action, this non–locality has already to be expected if one wants to achieve full triangulation invariance [D60], i.e. under all Pachner moves, as is the case with other perfect actions [D28, D29].

Our arguments relied on the Regge action, using length variables. An interesting question is whether these findings would change if one would use other variables, e.g. involving angles and / or areas [D61–D63]. A first order formulation with length and (4D dihedral) angles as in [D61] would also lead to a non–local measure, as the angles can be integrated out in each simplex locally, and a local measure in first order variables would lead to a local measure in length variables. Area–Regge calculus itself has non–local constraints [D64, D65], thus one would even expect a non–local measure (for the associated Lagrange multipliers) for this reason. In contrast, area–angle Regge calculus [D62, D63] has local constraints, which become non–local (reducing to the area constraints) after integrating out the angles. Here the question of non–locality might depend on whether to impose the gluing (or shape matching) constraints, which are part of the constraints reducing are–angle Regge calculus to length Regge calculus [D62, D63]. The status of these constraints in spin foams (or loop quantum gravity) is debated, see [D66, D67] for a discussion. Let us also mention [D68], which finds a local measure for a 4D model with a Regge like (first order) action. This model is however topological, and hence it is not surprising that one can find a local measure factor in this case. It also shows that the issue of imposing gluing constraints, that are essential in regaining standard Regge calculus with propagating degrees of freedom, might be crucial.

The encountered non–localities are characteristic of interacting theories and unavoidable, but might be more effectively handled if other degrees of freedom are used. One possibility are dynamically determined recombinations of the initial degrees of freedom to obtain new effective degrees of freedom, which can be non–local in terms of the initial triangulation, but may interact only locally among each other. This can also be interpreted as combining the initial basic building blocks into new effective ones, which may require transformations that are more general than Pachner moves. These transformations can be for example be given by dynamical embedding maps [D33, D34], which relate the Hilbert spaces of finer and coarser boundary data. In fact the idea is to use these embedding maps to define the physical (continuum) Hilbert space via an inductive limit and requiring cylindrical consistency. Interestingly, these ideas naturally translate to ideas and real–space renormalization schemes in condensed matter physics, such as tensor network renormalization [D69, D70], which recently have been applied to analogue spin foam models [D71, D72].

Acknowledgments

5.A Special cases of D

5.A.1 Placing the subdividing vertex far outside

In special situations it is possible to derive simpler expressions for the factor D. Assume for example that the inner vertex 0 in the 5–1 move is moved very far outside the original simplex as sketched

in fig. 5.6. These configurations, called 'spikes', are important in determining the divergence behaviour of spin foam models [D23–D25] and hence it is interesting to look for a simpler form of the factor D in this limit. If sufficiently far out, we can approximate the new edge lengths $l_{0i} \approx l$. Inserting this into (5.3.12), we get:

$$D^2 \approx \left(\frac{1}{48}\right)^2 l^4 \det \begin{pmatrix} 0 & 1 & \cdots & 1 \\ 1 & 0 & \cdots & (l_{1(d+1)})^2 \\ \vdots & \vdots & \cdots & \vdots \\ 1 & (l_{1(d+1)})^2 & \cdots & 0 \end{pmatrix} = 4l^4 V_0^2 \quad . \tag{5.A.1}$$
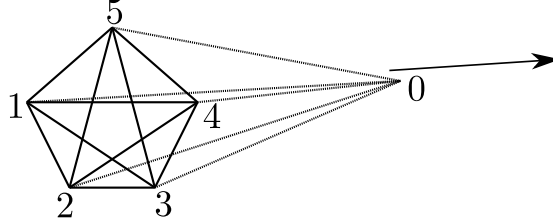
Figure 5.6: A schematic picture of the limit, in which the vertex 0 is moved far away from the initial 4–simplex.

5.A.2 Circumcentric subdivision

The same argument works out exactly in a circumcentric subdivision of the initial 4–simplex. In this subdivision, the subdividing vertex has the same distance to all vertices of the initial 4–simplex, i.e. it is placed in the center of circumscribing sphere of the initial simplex. Depending on the shape of the initial simplex, this can mean that the new vertex is inside or outside the simplex, yet by definition, it cannot be on the circumscribing sphere. In the following we denote the radius of the sphere as r, thus $l_{0i} = r$:

$$D^2 = \left(\frac{1}{48}\right)^2 \det \begin{pmatrix} 0 & r^2 & r^2 & \cdots & r^2 \\ r^2 & 0 & l_{12}^2 & \cdots & l_{15}^2 \\ r^2 & l_{12}^2 & 0 & \cdots & l_{25}^2 \\ \vdots & \vdots & \vdots & \ddots & \vdots \\ r^2 & l_{15}^2 & \cdots & \cdots & 0 \end{pmatrix} = 4r^4 V_0^2 \tag{5.A.2}$$

In both these cases the non–locality of D is rather hidden in the simplicity of the considered geometry.

5.B Measure for barycentric subdivision

Here, we will consider a barycentric subdivision, which in affine coordinates is given by choosing all α_i to be equal. In 4D, $\alpha_i = \frac{1}{5}$ and many equations given above are simplified:

$$b^2 = \frac{1}{25} \sum_{0<i<j} l_{ij}^2 \quad , \quad l_{0k}^2 = \frac{1}{25} \left(4 \sum_{i \neq k} l_{ik}^2 - \sum_{m,n \neq k} l_{mn}^2 \right) \quad . \tag{5.B.1}$$

In case one considers an equilateral initial 4–simplex, i.e. all edge lengths $l_{ij} = l$, $\forall i, j \neq 0$, the factor D simplifies even further. In fact, for this 4–simplex, the circumcentric subdivision coincides

with the barycentric subdivision, $b^2 = r^2$. Then the subdividing edges also have the same length l', with $(l')^2 := b^2 = \frac{2}{5}l^2$ and each of the five 4–simplices $\bar{i}$, $i \neq 0$, has the same volume V', namely $V' := V_{\bar{i}} = \frac{1}{5}V_{\bar{0}} \; \forall i \neq 0$. We consider again D_{01}:

$$D_{01} = \sum_{k=2}^{5} \underbrace{(-1)^{s_k}}_{=1}(l_{0k}^2 + l_{1k}^2 - l_{01}^2)V_{\bar{k}} = \frac{4}{5}l^2 V_{\bar{0}} = 10\,(l')^2\,V' \quad . \tag{5.B.2}$$

Thus we can construct a local measure, which is (approximately) invariant for integrating out subdivided (approximately) equilateral simplices.

Consider the following measure[12]

$$\mu(\{l\}) = \frac{\prod_e \frac{2^{\frac{1}{10}}5^{\frac{1}{8}}}{\sqrt{192\pi}}\,l_e^{6/5}}{\prod_\Delta V_\Delta^{3/8}} \tag{5.B.3}$$

for the initial complex of five simplices in the (equilateral, barycentric) $5 - 1$ move. From this $5 - 1$ move integration we obtain the following factors from the (square root of the inverse of the determinant of the) Hessian and the gauge fixing procedure described in [D27], by which the initial measure factor is multiplied:

$$F_{5-1} = (192\pi)^{\frac{5}{2}}\,\frac{1}{\sqrt{D}}\sqrt{\frac{V_{\bar{1}}\cdots V_{\bar{5}}}{V_{\bar{0}}}}\,\frac{1}{l_{01}\cdots l_{05}} \quad . \tag{5.B.4}$$

For the equilateral barycentric $5 - 1$ move we thus obtain

$$\mu_{\text{initial}}F_{5-1} = \frac{2^{\frac{3}{2}}5^{\frac{15}{8}}}{(192\pi)^{\frac{15}{2}}}\,(192\pi)^{\frac{5}{2}}\,\frac{1}{5^{\frac{5}{8}}}\,\frac{1}{2^{\frac{1}{2}}}\,\frac{l^{\frac{6}{5}\cdot 10}}{V_{\bar{0}}^{\frac{3}{8}}} = \mu_{\text{final}} \tag{5.B.5}$$

and hence invariance for this highly symmetric configuration. Note that this procedure is not without ambiguities, apart from the question of how to distribute numerical coefficients, we could have also exchanged length variables for volumina and vice versa using the relation $V_{\bar{0}} = \sqrt{5}\,(2^3 \cdot 3)^{-1}l^4$ for the equilateral 4–simplex.

5.C Radius of circumscribing sphere

The radius r of the $(d - 1)$–sphere S circumscribing the d–simplex Δ can be computed from the Cayley–Menger matrix C of Δ [D47] (see also [D48]):

$$r(S) = -\frac{1}{2}\frac{|C_0(\Delta)|}{\det C(\Delta)} \quad , \tag{5.C.1}$$

where the numerator $|C_0(\Delta)|$ is the determinant of the '$(0,0)$' minor of $C(\Delta)$, see also (5.3.3), and the denominator is simply the Caley–Menger determinant of Δ. See section 5.4 for the notation.

---

[12] Here we choose to assign numerical factors to the edges as in [D27]. Other choices are possible as well.

References

[D1] A. Perez, "The Spin Foam Approach to Quantum Gravity," *Living Rev.Rel.* **16** (2013) 3, `arXiv:1205.2019 [gr-qc]`.

[D2] C. Rovelli, "Zakopane lectures on loop gravity," *PoS* **QGQGS2011** (2011) 003, `arXiv:1102.3660 [gr-qc]`.

[D3] D. Oriti, "The Group field theory approach to quantum gravity," `arXiv:gr-qc/0607032 [gr-qc]`. Published in In *Oriti, D. (ed.): Approaches to quantum gravity* 310-331.

[D4] R. Gurau and J. P. Ryan, "Colored Tensor Models - a review," *SIGMA* **8** (2012) 020, `arXiv:1109.4812 [hep-th]`.

[D5] J. Ambjørn, A. Goerlich, J. Jurkiewicz, and R. Loll, "Quantum Gravity via Causal Dynamical Triangulations," `arXiv:1302.2173 [hep-th]`.

[D6] T. Regge, "General Relativity without coordinates," *Nuovo Cim.* **19** (1961) 558–571.

[D7] R. M. Williams, "Recent progress in Regge calculus," *Nucl.Phys.Proc.Suppl.* **57** (1997) 73–81, `arXiv:gr-qc/9702006 [gr-qc]`.

[D8] M. Rocek and R. M. Williams, "Quantum Regge calculus," *Phys.Lett.* **B104** (1981) 31.

[D9] M. Rocek and R. Williams, "The Quantization of Regge Calculus," *Z.Phys.* **C21** (1984) 371.

[D10] J. Cheeger, W. Muller, and R. Schrader, "On the Curvature of Piecewise Flat Spaces," *Commun.Math.Phys.* **92** (1984) 405.

[D11] H. W. Hamber and R. M. Williams, "On the measure in simplicial gravity," *Phys.Rev.* **D59** (1999) 064014, `arXiv:hep-th/9708019 [hep-th]`.

[D12] H. W. Hamber and R. M. Williams, "Gauge invariance in simplicial gravity," *Nucl.Phys.* **B487** (1997) 345–408, `arXiv:hep-th/9607153 [hep-th]`.

[D13] P. Menotti and P. P. Peirano, "Diffeomorphism invariant measure for finite dimensional geometries," *Nucl.Phys.* **B488** (1997) 719–734, `arXiv:hep-th/9607071 [hep-th]`.

[D14] F. Lund and T. Regge 1974. Princeton preprint , unpublished.

[D15] M. Bojowald and A. Perez, "Spin foam quantization and anomalies," *Gen.Rel.Grav.* **42** (2010) 877–907, `arXiv:gr-qc/0303026 [gr-qc]`.

[D16] W. Kaminski, M. Kisielowski, and J. Lewandowski, "Spin-Foams for All Loop Quantum Gravity," *Class.Quant.Grav.* **27** (2010) 095006, `arXiv:0909.0939 [gr-qc]`.

[D17] B. Dittrich, "Diffeomorphism symmetry in quantum gravity models," *Advanced Science Letters* **11** (2008) 2–151, `arXiv:0810.3594 [gr-qc]`.

[D18] B. Bahr and B. Dittrich, "(Broken) Gauge Symmetries and Constraints in Regge Calculus," *Class.Quant.Grav.* **26** (2009) 225011, `arXiv:0905.1670 [gr-qc]`.

[D19] B. Bahr and B. Dittrich, "Breaking and restoring of diffeomorphism symmetry in discrete gravity," *AIP Conf. Proc.* **1196** (2009) 10–17, `arXiv:0909.5688 [gr-qc]`.

[D20] L. Freidel and D. Louapre, "Diffeomorphisms and spin foam models," *Nucl.Phys.* **B662** (2003) 279–298, `arXiv:gr-qc/0212001 [gr-qc]`.

[D21] B. Bahr, "On knottings in the physical Hilbert space of LQG as given by the EPRL model," *Class.Quant.Grav.* **28** (2011) 045002, `arXiv:1006.0700 [gr-qc]`.

[D22] B. Bahr, F. Hellmann, W. Kaminski, M. Kisielowski, and J. Lewandowski, "Operator Spin Foam Models," *Class.Quant.Grav.* **28** (2011) 105003, `arXiv:1010.4787 [gr-qc]`.

[D23] V. Bonzom and B. Dittrich, "Bubble divergences and gauge symmetries in spin foams," *Phys.Rev.* **D88** (2013) 124021, `arXiv:1304.6632 [gr-qc]`.

[D24] C. Perini, C. Rovelli, and S. Speziale, "Self-energy and vertex radiative corrections in LQG," *Phys.Lett.* **B682** (2009) 78–84, `arXiv:0810.1714 [gr-qc]`.

[D25] A. Riello, "Self-energy of the Lorentzian Engle-Pereira-Rovelli-Livine and Freidel-Krasnov model of quantum gravity," *Phys.Rev.* **D88** no. 2, (2013) 024011, `arXiv:1302.1781 [gr-qc]`.

[D26] B. S. DeWitt, "Quantum Theory of Gravity. 1. The Canonical Theory," *Phys.Rev.* **160** (1967) 1113–1148.

[D27] B. Dittrich and S. Steinhaus, "Path integral measure and triangulation independence in discrete gravity," *Phys.Rev.* **D85** (2012) 044032, `arXiv:1110.6866 [gr-qc]`.

[D28] P. Hasenfratz and F. Niedermayer, "Perfect lattice action for asymptotically free theories," *Nucl.Phys.* **B414** (1994) 785–814, `arXiv:hep-lat/9308004 [hep-lat]`.

[D29] P. Hasenfratz, "Prospects for perfect actions," *Nucl.Phys.Proc.Suppl.* **63** (1998) 53–58, `arXiv:hep-lat/9709110 [hep-lat]`.

[D30] B. Bahr and B. Dittrich, "Improved and Perfect Actions in Discrete Gravity," *Phys.Rev.* **D80** (2009) 124030, `arXiv:0907.4323 [gr-qc]`.

[D31] J. Marsden and M. West., "Discrete mechanics and variational integrators," *Acta Numerica* **10** (2001) 357.

[D32] B. Bahr, B. Dittrich, and S. Steinhaus, "Perfect discretization of reparametrization invariant path integrals," *Phys.Rev.* **D83** (2011) 105026, `arXiv:1101.4775 [gr-qc]`.

[D33] B. Dittrich, "From the discrete to the continuous: Towards a cylindrically consistent dynamics," *New J.Phys.* **14** (2012) 123004, `arXiv:1205.6127 [gr-qc]`.

[D34] B. Dittrich and S. Steinhaus, "Time evolution as refining, coarse graining and entangling," *New J. Phys.* **16** (2014) 123041, `arXiv:1311.7565 [gr-qc]`.

[D35] B. Dittrich and P. A. Hohn, "Canonical simplicial gravity," *Class.Quant.Grav.* **29** (2012) 115009, `arXiv:1108.1974 [gr-qc]`.

[D36] B. Dittrich and P. A. Hoehn, "Constraint analysis for variational discrete systems," *J. Math. Phys.* **54** (2013) 093505, `arXiv:1303.4294 [math-ph]`.

[D37] P. A. Höhn, "Quantization of systems with temporally varying discretization I: Evolving Hilbert spaces," *J.Math.Phys.* **55** (2014) 083508, `arXiv:1401.6062 [gr-qc]`.

[D38] P. A. Höhn, "Quantization of systems with temporally varying discretization II: Local evolution moves," *J.Math.Phys.* **55** (2014) 103507, `arXiv:1401.7731 [gr-qc]`.

[D39] U. Pachner, "Konstruktionsmethoden und das kombinatorische Homöomorphieproblem für Triangulationen kompakter semilinearer Mannigfaltigkeiten," *Abh. Math. Sem. Univ. Hamburg* **57** (1986) 69.

[D40] U. Pachner, "P. L. Homeomorphic Manifolds are Equivalent by Elementary Shellings," *Europ. J. Combinatorics* **12** (1991) 129–145.

[D41] G. Ponzano and T. Regge, *Semiclassical limit of Racah coefficients, in: Spectroscopy and group theoretical methods in physics.* North Holland Publ. Co., Amsterdam, 1968.

[D42] J. W. Barrett and I. Naish-Guzman, "The Ponzano-Regge model," *Class.Quant.Grav.* **26** (2009) 155014, `arXiv:0803.3319 [gr-qc]`.

[D43] R. Gurau, "The Ponzano-Regge asymptotic of the 6j symbol: An Elementary proof," *Annales Henri Poincare* **9** (2008) 1413–1424, `arXiv:0808.3533 [math-ph]`.

[D44] M. Dupuis and E. R. Livine, "Pushing Further the Asymptotics of the 6j-symbol," *Phys.Rev.* **D80** (2009) 024035, `arXiv:0905.4188 [gr-qc]`.

[D45] M. Dupuis and E. R. Livine, "The 6j-symbol: Recursion, Correlations and Asymptotics," *Class.Quant.Grav.* **27** (2010) 135003, `arXiv:0910.2425 [gr-qc]`.

[D46] W. Kamiński and S. Steinhaus, "Coherent states, 6j symbols and properties of the next to leading order asymptotic expansions," *J.Math.Phys.* **54** (2013) 121703, `arXiv:1307.5432 [math-ph]`.

[D47] M. Berger, *Geometry I.* Springer, Berlin, 1994.

[D48] C. D'Andrea and M. Sombra, "The Cayley-Menger determinant is irreducible for $n \geq 3$," *Sib. Math. J.* **46** (2005) 71–76, `arXiv:math/0406359`.

[D49] B. Dittrich, L. Freidel, and S. Speziale, "Linearized dynamics from the 4-simplex Regge action," *Phys.Rev.* **D76** (2007) 104020, `arXiv:0707.4513 [gr-qc]`.

[D50] I. G. Korepanov, "Invariants of PL manifolds from metrized simplicial complexes: Three-dimensional case," *J.Nonlin.Math.Phys.* **8** (2001) 196–210, `arXiv:math/0009225 [math-gt]`.

[D51] I. Korepanov, "Multidimensional analogues of the geometric s <–> t duality," *Theor.Math.Phys.* **124** (2000) 999–1005.

[D52] A. Baratin and L. Freidel, "Hidden Quantum Gravity in 3-D Feynman diagrams," *Class.Quant.Grav.* **24** (2007) 1993–2026, `arXiv:gr-qc/0604016 [gr-qc]`.

[D53] R. Sorkin, "The Electromagnetic field on a simplicial net," *J.Math.Phys.* **16** (1975) 2432–2440.

[D54] S. L. Kokkendorff, "Polar duality and the generalized law of sines," *Journal of Geometry* **86** no. 1-2, (2007) 140–149.

[D55] M. Christodoulou, M. Langvik, A. Riello, C. Roken, and C. Rovelli, "Divergences and Orientation in Spinfoams," *Class. Quant. Grav.* **30** (2013) 055009, `arXiv:1207.5156 [gr-qc]`.

[D56] W. Kamiski and S. Steinhaus, "The BarrettCrane model: asymptotic measure factor," *Class.Quant.Grav.* **31** (2014) 075014, `arXiv:1310.2957 [gr-qc]`.

[D57] L. Freidel private communication.

[D58] B. Dittrich and J. P. Ryan, "Phase space descriptions for simplicial 4d geometries," *Class.Quant.Grav.* **28** (2011) 065006, `arXiv:0807.2806 [gr-qc]`.

[D59] V. Bonzom and B. Dittrich, "Diracs discrete hypersurface deformation algebras," *Class.Quant.Grav.* **30** (2013) 205013, `arXiv:1304.5983 [gr-qc]`.

[D60] B. Bahr, B. Dittrich, and S. He, "Coarse graining free theories with gauge symmetries: the linearized case," *New J.Phys.* **13** (2011) 045009, `arXiv:1011.3667 [gr-qc]`.

[D61] J. W. Barrett, "First order Regge calculus," *Class.Quant.Grav.* **11** (1994) 2723–2730, `arXiv:hep-th/9404124 [hep-th]`.

[D62] B. Dittrich and S. Speziale, "Area-angle variables for general relativity," *New J.Phys.* **10** (2008) 083006, `arXiv:0802.0864 [gr-qc]`.

[D63] B. Bahr and B. Dittrich, "Regge calculus from a new angle," *New J.Phys.* **12** (2010) 033010, `arXiv:0907.4325 [gr-qc]`.

[D64] J. W. Barrett, M. Rocek, and R. M. Williams, "A Note on area variables in Regge calculus," *Class.Quant.Grav.* **16** (1999) 1373–1376, `arXiv:gr-qc/9710056 [gr-qc]`.

[D65] J. Makela and R. M. Williams, "Constraints on area variables in Regge calculus," *Class.Quant.Grav.* **18** (2001) L43, `arXiv:gr-qc/0011006 [gr-qc]`.

[D66] B. Dittrich and J. P. Ryan, "Simplicity in simplicial phase space," *Phys.Rev.* **D82** (2010) 064026, `arXiv:1006.4295 [gr-qc]`.

[D67] B. Dittrich and J. P. Ryan, "On the role of the Barbero-Immirzi parameter in discrete quantum gravity," *Class.Quant.Grav.* **30** (2013) 095015, `arXiv:1209.4892 [gr-qc]`.

[D68] A. Baratin and L. Freidel, "Hidden Quantum Gravity in 4-D Feynman diagrams: Emergence of spin foams," *Class.Quant.Grav.* **24** (2007) 2027–2060, `arXiv:hep-th/0611042 [hep-th]`.

[D69] M. Levin and C. P. Nave, "Tensor renormalization group approach to 2d classical lattice models," *Phys. Rev. Lett.* **99** (2007) 120601, `cond-mat/0611687`.

[D70] Z.-C. Gu and X.-G. Wen, "Tensor-Entanglement-Filtering Renormalization Approach and Symmetry Protected Topological Order," *Phys.Rev.* **B80** (2009) 155131, `arXiv:0903.1069 [cond-mat.str-el]`.

[D71] B. Dittrich, M. Martn-Benito, and E. Schnetter, "Coarse graining of spin net models: dynamics of intertwiners," *New J.Phys.* **15** (2013) 103004, `arXiv:1306.2987 [gr-qc]`.

[D72] B. Dittrich, M. Martin-Benito, and S. Steinhaus, "Quantum group spin nets: refinement limit and relation to spin foams," *Phys.Rev.* **D90** (2014) 024058, `arXiv:1312.0905 [gr-qc]`.

6 Quantum group spin nets: refinement limit and relation to spin foams

Bianca Dittrich, Mercedes Martín-Benito and Sebastian Steinhaus

Perimeter Institute for Theoretical Physics,
31 Caroline Street North, Waterloo, Ontario, Canada N2L 2Y5

Abstract

So far spin foam models are hardly understood beyond a few of their basic building blocks. To make progress on this question, we define analogue spin foam models, so called spin nets, for quantum groups $SU(2)_k$ and examine their effective continuum dynamics via tensor network renormalization. In the refinement limit of this coarse graining procedure, we find a vast non-trivial fixed point structure beyond the degenerate and the BF phase. In comparison to previous work, we use fixed point intertwiners, inspired by Reisenberger's construction principle [E1] and the recent work [E2], as the initial parametrization. In this new parametrization fine tuning is not required in order to flow to these new fixed points. Encouragingly, each fixed point has an associated extended phase, which allows for the study of phase transitions in the future. Finally we also present an interpretation of spin nets in terms of melonic spin foams. The coarse graining flow of spin nets can thus be interpreted as describing the effective coupling between two spin foam vertices or space time atoms.

6.1 Introduction

The aim of spin foam quantization is to provide a non–pertubative and background–independent quantization of gravity via an auxiliary discretization. A key outstanding question for these models is to show that they reproduce familiar low energy physics, in particular a phase describing a smooth manifold, in a limit in which the scale of the discretization is much smaller than other relevant length scales in the system [E3].

In this work we will provide first conjectures on the possible large scale behaviour of spin foams. These are based on the investigation of the coarse graining or renormalization flow of spin net models, which, as we will show in this work, can be interpreted as a coarse graining flow of (melonic) spin foams and as describing the effective coupling between two spin foam vertices.

To lay out the context of this work, explicit investigations of the coarse graining and renormalization flow of spin foam models [E3–E8], have been hindered by the overwhelming complexity of the models, apart from an incomplete understanding of possible infinities [E9–E13] and a number of conceptual questions [E14–E16], for instance the meaning of scale in coarse graining background independent systems. Regarding these questions a conceptual understanding was reached in [E17, E18], that allows to interpret the coarse graining flow as the construction of the continuum limit of the theory via the concept of dynamical cylindrical consistency and embedding or refinement maps. To tackle the concrete implementation of this coarse graining flow, after establishing the importance of coarse graining for the recovery of diffeomorphism symmetries in discrete systems and therefore the recovery of a correct continuum dynamics [E19–E24], a program was started in [E25–E27], which considers the corresponding question in simplified systems, that keep however key dynamical principles, in particular the imposition of so–called simplicity constraints [E3–E8], of spin foams.

The simplifications considered can be summarized into three types: (a) the replacement of the structure group $SU(2) \times SU(2)$ of the full gravitational models by a finite group [E25, E28, E29], (b) a dimensional reduction of spin foams to so–called spin nets [E25–E27], and (c) the consideration of a regular lattice [E26, E27, E30].

In this work we lift the simplification (a), regarding (b) we show that spin net coarse graining can be interpreted as a coarse graining of (melonic) spin foams and confirm again [E19–E24, E30] that (c) does lead to triangulation invariant models, at least for the non–critical fixed points. This latter fact is deeply related to the restoration of a notion of diffeomorphism symmetry [E19–E24] at the fixed points. In fact the recovery of a sensible continuum limit and the regaining of diffeomorphism symmetry might even be only possible if certain regularity conditions on the coarse graining process are satisfied [E18, E31].

For these reasons we will be able to present for the first time[1] the coarse graining flow in a non–trivial spin foam system and investigate the fixed points it leads to. This allows us to draw first conclusions about the possible phases that might describe the continuum limit of spin foams.

To be more precise, we introduce here spin net models with structure group $SU(2)_k$, the quantum deformation (at the root of unity) of the group $SU(2)$. This makes a numerical investigation of the models possible, as in the quantum group only finitely many representations appear. On the technical level this requires the introduction of the Haar projector for the quantum group which we construct in this work. Models based on the quantum deformation of the rotation group describe gravitational systems with a cosmological constant [E35–E42]. For the 4D systems one would need $SU(2)_k \times SU(2)_k$, however also an effective description in terms of $SU(2)_k$ alone might be possible [E43]. Thus we lift the simplification, considered in [E26, E27, E44], of the structure group almost completely. Moreover considering the behaviour of the models for growing level k allows to

---

[1] An exception is [E28, E29, E32] which considered a sequence of $4-1$ and $5-1$ Pachner moves for spin foam models based on finite groups. However, as mentioned, the question arises whether such a flow, based on coarse graining moves [E18] only, allows to make definite conclusions about the continuum limit. In contrast the tensor network algorithm [E33, E34] considered here includes, in a sense, refining, coarse graining, and entangling moves [E18].

make conjectures on the limit $k \to \infty$, which gives back the classical group $SU(2)$.

As in previous work [E26, E27, E44] we will employ tensor network techniques [E33, E34] to derive a coarse graining flow equation, which is then investigated numerically. This flow equation describes the change of intertwiner degrees of freedom under coarse graining, as exemplified for the first time in [E44]. As is outlined in [E17, E18] these tensor network techniques are particularly suited for the construction of the continuum limit for spin nets and spin foams. In [E26, E27] a tensor network representation of spin foams appeared which might allow to derive similar coarse graining flow equations directly for spin foams. Also [E18] points out, that the geometric building blocks of spin foams, the simplices, allow to be interpreted as coarse graining, refining or entangling moves, in dependence of how these are glued together. Such moves are the basic ingredients of tensor network renormalization. This might lead to an even more geometric way to derive such coarse graining flow equations.

Another innovation that we present in this work is a change in the parametrization for the (phase) space of spin net and spin foam models. This new parametrization takes the lesson from [E44] seriously, that the relevant degrees of freedom are given by intertwiners. We thus introduce a new parametrization, based on Reisenberger's construction principle [E1], that leads us to employ so–called *fixed point intertwiners* [E2, E45], which encode the simplicity constraints. Reisenberger's principle ensures that the models so obtained are physically reasonable, i.e. that the simplicity constraints they encode appear to be the same in (physically equivalent) different recoupling schemes.

We will find that this new parametrization is highly advantageous: in contrast to the parametrization introduced in [E28, E29] and employed in [E44], models flow generically to non–trivial fixed points (in particular different from the degenerate fixed point, in which only the spin representation $j = 0$ appears). We conjecture that this behaviour is due to the projector property that is satisfied for models based on fixed point intertwiners. Modern spin foams are rather based on a parametrization like that employed in [E28, E29], and the reconstruction of the projector property is rather complicated [E46]. The findings here therefore suggest to reconsider Reisenberger's construction principle, in particular since it allows the construction of vertices of arbitrary valence [E1], as was also later realized for the EPRL model [E5–E8] in [E47, E48]. Similar to the arguments on the uniqueness of the Barrett–Crane model [E49] in [E1], it is even possible to find a parametrization of all physically sensible models, by finding all fixed point intertwiners for a given structure group [E2, E45].

The outline of the paper is the following: The next section 6.2 introduces the basic ingredients of spin foam and spin net models that we need for the work here. It will also explain the parametrization for the models based on Reisenberger's construction principle, for which we need the fixed point intertwiners. In section 6.3 we introduce the essential notions and tools related with the quantum group $SU(2)_k$ that will be needed to define spin net models based on this group. Using these tools we introduce the general structure of our models in section 6.4. In section 6.5 we adapt to the quantum group case the symmetry preserving coarse graining algorithm introduced in [E44]. This will lead to a flow equation describing the behaviour of intertwiner degrees of freedom under coarse graining. We will give a (3D) geometrical interpretation of the flow equation which might lead to a more intuitive understanding of the coarse graining flow. Section 6.6 contains the explicit definition of the weights for the initial models. We then investigate the behaviour under coarse graining of these models and analyze and describe the results obtained. We comment on the interpretation of spin net coarse graining in the context of spin foam coarse graining in section 6.7. We discuss our main findings in Section 6.8. Finally appendix 6.A includes technical (diagrammatic) calculations that might help the understanding of some equations in the main text, in particular those appearing in sections 6.3 and 6.5.

6.2 Reisenberger's principle and intertwiner models

Spin foam models are generalization of lattice gauge theories and as such are defined on 2–complexes, i.e. generalizations of graphs, in which in addition to vertices and edges, also faces are specified. There is an important difference though: whereas for lattice gauge theories the main dynamical ingredient are weights on the faces, these weights are not as essential for the dynamics of spin foams (they are crucial for the divergence properties of the model [E9–E13], but are not supposed to include i.e. a coupling constant). Rather for the dynamics of spin foams the choice of an intertwiner for the edges is crucial – equivalent to choosing a certain implementation of the so called simplicity constraints.

To be more specific, consider lattice gauge theory based on a gauge (or structure) group G, which we assume to be either a compact semi–simple Lie group or a finite group.[2] The variables are given as group elements associated to oriented edges of a graph. The dynamics is encoded into face weights ω_f, which are class functions on the group. These face weights are evaluated on the face holonomies h_f, i.e. the (oriented) product of group elements g_e associated to the edges e around a face $h_f = \prod_{e \subset f} g_e$. Let us assume that all edges agree in their orientation with the orientation induced from the face.

The partition function is then given as

$$Z = \int \prod_e \mathbf{d}g_e \prod_f \omega_f(h_f) \quad . \tag{6.2.1}$$

Here $\mathbf{d}g$ denotes the (normalized) Haar measure on G. We can change to a dual description by applying a group Fourier transform. Due to the invariance of the face weight under group conjugation we can expand the face weights as a linear combination of characters

$$\omega_f(h) = \sum_\rho \tilde{\omega}_f(\rho) \chi_\rho(h) \quad , \tag{6.2.2}$$

where $\chi_\rho = \rho_m{}^m$ and $\rho(\cdot)_m{}^n$ denotes a matrix element of a irreducible unitary representation ρ (irreps) of the group G. In (6.2.2) we sum over a complete set of (equivalence classes) of irreps.

Expanding h_f into the product of group elements and using the representation property $\rho(g_1 g_2) = \rho(g_1) \cdot \rho(g_2)$ one finds that the partition function is now given as

$$Z = \sum_{\rho_f} \prod_f \tilde{\omega}_f(\rho_f) \prod_e (\mathcal{P}^e_{Haar})^{n_{f_1} n_{f_2} \cdots n_{f_{N_e}}}_{m_{f_1} m_{f_2} \cdots m_{f_{N_e}}} \quad . \tag{6.2.3}$$

Here $\mathcal{P}^e_{Haar}$ is the so–called Haar projector, which absorbs the integrations over the group elements g in (6.2.1). For an edge whose N_e adjacent faces agree in orientation with the one of the edge the Haar projector is given as

$$(\mathcal{P}^e_{Haar})^{n_{f_1} n_{f_2} \cdots n_{f_{N_e}}}_{m_{f_1} m_{f_2} \cdots m_{f_{N_e}}} = \int \mathbf{d}g \prod_{f \supset e} \rho_f(g_e)_{m_f}{}^{n_f} \quad . \tag{6.2.4}$$

The group integration or averaging enforces gauge invariance. Indeed the Haar projector is an intertwining map between the group invariant (singlet) subspace of the tensor product of representations

$$\mathcal{P}_{Haar} : \mathrm{Inv}(V_{\rho_1} \cdots V_{\rho_{N_e}}) \to \mathrm{Inv}(V_{\rho_1} \cdots V_{\rho_{N_e}}) \tag{6.2.5}$$

or, if seen as a map on $V_{\rho_1} \cdots V_{\rho_{N_e}}$ it acts as a projector onto $\mathrm{Inv}(V_{\rho_1} \cdots V_{\rho_{N_e}})$.

---

[2]For a basic introduction into spin foams as statistical systems see [E25].

Choosing any orthonormal basis[3] $\{|\iota_d\rangle\}_d$ in $\mathrm{Inv}(V_{\rho_1}\cdots V_{\rho_{N_e}})$ we can write the Haar intertwiner as

$$\mathcal{P}_{Haar} = \sum_d |\iota_d\rangle \langle \iota_d| \quad , \tag{6.2.6}$$

which makes the projection property $\mathcal{P} \cdot \mathcal{P} = \mathcal{P}$ of $\mathcal{P}_{Haar}$ obvious.

As mentioned the important dynamical ingredient in spin foams are intertwiners, whereas the face weights are rather chosen due to kinematical considerations, for instance as delta functions on the group in the group representation. For non–trivial spin foam models, that is models which cannot be rewritten into standard lattice gauge theories, one replaces $\mathcal{P}_{Haar}$ by a smaller projector $\mathcal{P}$, selecting a smaller subspace of $\mathrm{Inv}(V_{\rho_1}\cdots V_{\rho_{N_e}})$.

With an appropriate choice of orthonormal basis of intertwiners we can write

$$\mathcal{P}^{(N)} = \sum_{d \in \mathcal{S}_N} |\iota_d\rangle \langle \iota_d| \quad , \tag{6.2.7}$$

where $\mathcal{S}_N$ denotes a subset of intertwiner labels specified by the choice of simplicity constraints. Again the form (6.2.7) makes the projector property $\mathcal{P} \cdot \mathcal{P} = \mathcal{P}$ explicit. In the context of spin foams this projector property ensures a notion of (weak) independence of the underlying two–complex, namely invariance under edge subdivisions [E28, E29, E46, E50–E52].

On the other hand the form (6.2.7) makes it non–obvious how to relate the sets $\mathcal{S}_N$ for different valencies N (i.e. number of faces sharing the edge e) of the edges. To solve this problem, Reisenberger proposed the following principle in [E1]:

Reisenberger's construction: We consider multiplicity free representation categories, where in the reduction of the tensor product of any two irreps each irrep can only appear once. In this case, by choosing a recoupling scheme, intertwiners can be labelled by sets of representation labels: an intertwiner for valency N is characterized by the N representation labels plus $(N-3)$ further representation labels. Note that the choice of recoupling scheme can be encoded in a three–valent graph with N outer edges, and that the representation labels are attached to the edges of this graph. We will denote with $\mathcal{S}_1$ the set of allowed representations implied by the simplicity constraints.

In Reisenberger's construction this set $\mathcal{S}_1$ then determines all the other sets $\mathcal{S}_N$ via the following principle: For every possible choice of recoupling scheme, i.e. three–valent graph, only representations in $\mathcal{S}_1$ should appear.

Reisenberger applies this to the Barret-Crane model [E49] and shows that choosing $\mathcal{S}_1$ accordingly the intertwiners $\mathcal{P}^{(N)}$ are uniquely determined. It actually turns out that if we take the intertwiner as a model for a partition function, as introduced in [E2] (with boundary data given by the n representation and summing over all the intertwiner labels) the Barrett-Crane model leads even to a triangulation invariant model.[4]

In [E2] so–called intertwiner models were introduced, which are 2D statistical models determining an intertwining map between representation spaces associated to the boundary components of the 2D bulk. The models are defined on three–valent graphs. Dualizing these graphs we obtain a triangulation (under certain regularity assumptions). It turns out that intertwiner models whose partition function are invariant under the change of (2D) triangulation, are also – at least in the planar case – a realization of Reisenberger's conditions. In particular each triangulation invariant model is characterized by a set $\mathcal{S}_1$ of representations that are allowed to appear as intertwiner labels and as boundary data.

---

[3]Often the elements of $\mathrm{Inv}(V_{\rho_1}\cdots V_{\rho_{N_e}})$ themselves are referred to as intertwiners.

[4]Indeed it can be seen as a re–interpretaion of an analogue BF spin net model [E25–E27], which is also topological. Related, the Barrett-Crane intertwiner is given as a square of the BF intertwiner [E25].

Let us explain this statement in more detail, restricting to four–valent intertwiners, i.e. $N = 4$. Fixing the 4 outer representations $\rho_1, \ldots, \rho_4$, a choice of intertwiner basis, labeled by ρ_5, can then be represented graphically by the following three graphs Γ:

$$A = \underset{\rho_3 \quad \rho_4}{\overset{\rho_2 \quad \rho_1}{\times}}_{\rho_5} \quad ; \quad B = \underset{\rho_3 \quad \rho_4}{\overset{\rho_2 \quad \rho_1}{\times}}_{\rho_5} \quad ; \quad C = \underset{\rho_3 \quad \rho_4}{\overset{\rho_2 \quad \rho_1}{\times}}_{\rho_5} \quad . \tag{6.2.8}$$

A specific intertwiner is then specified by the basis coefficients $a_\Gamma(\rho_1, \ldots, \rho_4; \rho_5)$. Here one has to make one choice of basis $\Gamma = A, B$ or C. Once the intertwiner coefficients are fixed in one basis, say A, it can of course be re–expressed in the two other bases B and C. Reisenberger's principle demands that a_A has to vanish if any of the arguments $\rho_1, \ldots, \rho_4$ is not in $\mathcal{S}_1$ or if ρ_5 is not in $\mathcal{S}_1$. Additionally the coefficients a_A have to be chosen so that also a_B and a_C vanish as soon as ρ_5 is not in $\mathcal{S}_1$.

The triangulation invariant intertwiners constructed in [E2, E45] are characterized by a certain set $\mathcal{S}_1$ of allowed representations. Additionally the basis coefficients are invariant under changes which keep the graph planar, i.e. we even have $a_A = a_B$. As for a graph with crossing (note that for a quantum group one has to specify whether this is a over or under–crossing), only a certain subset of the fixed point intertwiners satisfies $a_A = a_B = a_C$. However, using the braiding operation for quantum groups, see for instance [E2], one can find for the change of basis from C to B

$$\sum_{\rho_5} a_C(\rho_1, \rho_2, \rho_3, \rho_4; \rho_5) \underset{\rho_3 \quad \rho_4}{\overset{\rho_2 \quad \rho_1}{\times}}_{\rho_5} = \sum_{\rho_5} a_C(\rho_1, \rho_2, \rho_3, \rho_4; \rho_5) \underset{\rho_3 \quad \rho_4}{\overset{\rho_2 \quad \rho_1}{\diamondsuit}}_{\rho_5}$$

$$= \sum_{\rho_5} a_C(\rho_1, \rho_2, \rho_3, \rho_4; \rho_5) \underset{\rho_3 \quad \rho_4}{\overset{\rho_2 \quad \rho_1}{\times}}_{\rho_5} \; b(\rho_3, \rho_4, \rho_5) \quad , \tag{6.2.9}$$

where in the first step we used the triangulation invariance, i.e. invariance under a planar change of graph, and in the second step we resolved the braiding, described by non–vanishing coefficients $b(\rho_3, \rho_4, \rho_5)$. For a certain set of triangulation invariant models these coefficients b can be replaced by 1 in the sum over ρ_5. For most models (for instance the family described in section 6.6.1) this is however not the case. Nevertheless Reisenberger's principle still holds: if a_C vanishes for a certain representation ρ_5 this will also hold for the A basis coefficient, given by $a_C \times b$. Thus Reisenberger's principle is satisfied at least for four–valent intertwiners, relevant for simplicial lattices in 4D. For 3D spin foams (also on non–simplicial lattices) one could even restrict to planar graph changes only, as the intertwiners are attached to edges and so the expansion might be argued to take place in a plane orthogonal to this edge.

There exists a rich structure of these triangulation invariant models [E2, E45]. These models define in particular fixed points for the renormalization flow in the space of intertwiner models. This suggest to indeed use these particular fixed point models for defining intertwiners for spin foams. We will call such an intertwiner coming from a fixed point model a *fixed point intertwiner*. Such a fixed point intertwiner, characterized by a set $\mathcal{S}_1$ of irreps, leads to a family of intertwiners $|\iota_{\mathcal{S}_1}^N\rangle$, labelled by the valency N of the edge, so that we can define a projector just as

$$\mathcal{P}_{\mathcal{S}_1}^{(N)} = |\iota_{\mathcal{S}_1}^N\rangle \langle \iota_{\mathcal{S}_1}^N| \quad . \tag{6.2.10}$$

Assuming normalization the projector property is obviously satisfied.

Note that a spin foam model defined via such a fixed point intertwiner does in general *not* define a fixed point of the renormalization flow in the space of spin foam models. The same holds for spin nets, that we will define as lower dimensional analogues of spin foams further below.

Alternatively we can also consider linear combinations of different fixed point intertwiners

$$\mathcal{P}^{(N)}_{\alpha^N_i} = \sum_i \alpha^N_i |\iota^N_{\mathcal{S}^i_1}\rangle \langle \iota^N_{\mathcal{S}^i_1}| \quad . \tag{6.2.11}$$

These also satisfy Reisenberger's principle (at least for $N = 4$) , as now only representations in $\cup_i \mathcal{S}^i_1$ appear in any possible recoupling scheme. However as the $|\iota^N_{\mathcal{S}^i_1}\rangle$ are not necessarily orthogonal to each other[5], the projector property will be only satisfied for specific choices of the coefficients α^N_i. Nevertheless it is interesting to consider (6.2.11) for general coefficients, as it allows to obtain phase diagrams and in this way to determine phase transitions. The latter might allow to define a continuum limit theory with propagating degrees of freedom.

The main result of this paper is the following: Using these fixed point intertwiners to define (2D) spin net models, these spin nets flow in general to 'non–trivial' triangulation invariant models without the necessity of fine tuning.

Here we mean with 'trivial' fixed points, those in which no simplicity constraints occur, and which can be expressed as standard lattice gauge theories. E.g. for the so–called degenerate fixed point only the representation $j = 0$ is excited (appearing as high temperature fixed point in the statistical physics interpretation). Another example are fixed points which can be understood as analogues of BF theories. In these cases the models can all be described by the Haar projector and a choice of edge weights (the analogues of spin foam face weights for the spin nets).

Furthermore we have to explain the notion of fine tuning, as this depends highly on the parametrization that one chooses for the initial models, which are then subjected to the coarse graining flow. To compare the parametrization (6.2.11) introduced here and another parametrization used in [E44] let us explain the latter. It is based on so–called E–functions, introduced in [E28, E29]. These E–functions encode the simplicity constraints. This parametrization covers all the standard models for spin foams [E3, E5–E8, E49]. In this case the Haar projector is replaced by operators of the form

$$\mathcal{P}^{(N)} = \mathcal{P}_{Haar} \cdot E^{\rho_1} \otimes \cdots \otimes E^{\rho_N} \cdot \mathcal{P}_{Haar} \tag{6.2.12}$$

where E^{ρ_I} denotes a (non–intertwining) map: $V_{\rho_I} \to V_{\rho_I}$ on a representation space associated to one of the faces adjacent to the edge in question. This gives another possibility to define consistently spin foam models for vertices or edges with arbitrary valency [E47, E48]. However, for instance for the EPRL model [E5–E8] the projector property needs to be implemented by an additional construction [E46], in which the factorizing structure of the operators (6.2.12) over the representation spaces V_{ρ_I} is a priori changed.

Indeed the form (6.2.12) can be expanded in an intertwiner basis again

$$\mathcal{P}^{(n)} = \sum_{d,d'} |\iota_d\rangle\langle \iota_d| \mathcal{P}_{Haar} \cdot E^{\rho_1} \otimes \cdots \otimes E^{\rho_n} \cdot \mathcal{P}_{Haar} |\iota_{d'}\rangle\langle \iota_{d'}| \tag{6.2.13}$$

where now in general non–diagonal terms proportional to $|\iota_d\rangle\langle \iota_{d'}|$ appear. The question whether this is a projector turns then into the question whether a diagonaliztion leads to eigenvalues 0 and 1 only.

[E44] used the E–function parametrization for models based on the structure group S_3. (The fusion categories of the permutation group S_3 and $SO(3)_{k=4}$ are actually gauge equivalent as fusion categories[6], hence we can compare the coarse graining results of [E44] with the examples considered

---

[5]Of course the intertwiners can in principle be orthogonalized with the Gram Schmidt procedure.

[6]We thank Oliver Buerschaper for pointing this out.

here.) A phase space diagram based on this parametrization leads to the following picture: Basically all models given by this parametrization flow either to the high temperature phase or to a 'trivial' S_3 or $\mathbb{Z}_2$ ordered phase, analogous to either BF theory on S_3 or BF theory on the subgroup $\mathbb{Z}_2$ for spin foams. Only by fine tuning to a phase transition, in the case of [E44] between high temperature and S_3 ordered phase, one might flow to a non–trivial fixed point. It was this instance of a non–trivial fixed point, which motivated the investigations in [E2], which revealed the possibility of a very rich structure of non–trivial fixed points in spin net models. However a posteriori it was rather a case of good fortune to have seen this fixed point at all, as it appeared (a) only for a tiny subset of initial models in the parametrization used, and (b) only for a certain truncation, as higher truncations turned on couplings that would lead to a flow away from this fixed point.

The picture that we will find for the parametrization (6.2.11) introduced in this work will be very different. Rather models flow generically to non–trivial fixed points. Thus with the parametrization of the phase diagram here, the fixed points define a phase, i.e. an extended region in our phase diagram[7]. We will work with quantum groups $SO(3)_k$ which makes a systematic investigation for different choices of k possible (bounded by the available computer power of course). This allows us to conjecture that the essential picture will not change in the limit $k \to \infty$ and therefore holds for general (quantum) groups.

These results give new weight to the point suggested in [E46, E50–E52], which is to build models and select measure factors such that invariance under certain subdivisions of edges and faces is guaranteed. For edge subdivisions this leads to the projector property for the 'edge operators' $\mathcal{P}$. The investigations here show that models which implement this property (or are in a certain sense near such models) flow rather to non–trivial fixed points. Whereas for models of the form (6.2.12) the implementation of the projector property is rather involved [E46] and as [E44] shows for the structure group S_3, most of these models flow to trivial fixed points.

Finally let us explain spin net models. Very simply whereas for spin foams the $\mathcal{P}^{(N)}$ are based on edges, for spin nets the $\mathcal{P}^{(N)}$ are based on vertices and define the vertex weights. The edges are labelled by the representation labels ρ, as well as two magnetic indices, labelling a basis in V_ρ and V_{ρ^*} (the dual representation space) respectively. Thus every edge carries a Hilbert space

$$\mathcal{H}_e = \oplus_\rho V_\rho \otimes V_{\rho^*} \quad , \tag{6.2.14}$$

where the sum is over all irreducible representations. The contraction of indices of vertex weights $\mathcal{P}^{(N)}$ and the sum over representation labels j corresponds then to integrating out all degrees of freedom associated to the edges.

Thus the partition function for a spin net is defined as

$$Z = \sum_{\rho_e, m_e, n_e} \prod_v \mathcal{P}_v^{(N_v)}(\{\rho_e\}_{e \supset v}, \{m_e\}_{e \supset v}, \{n_e\}_{e \supset v}) \tag{6.2.15}$$

where we made the index structure of the intertwiners explicit.

Spin nets can be imagined as dimensional reductions to spin foams, in the sense that one considers a cut orthogonal to a spin foam edge, which now will appear as vertex. Objects which are based on faces in spin foams, are based on edges in spin nets. Spin nets were introduced in [E26, E27] to allow numerical coarse graining investigations for 2D models, which is naturally much simpler than considering 4D models. In addition, for (standard) lattice gauge theory, a certain duality exist

---

[7]A parametrization independent definition of a stable phase would require stability with respect to all possible perturbations of the fixed point (or all possible perturbations respecting a given symmetry [E53–E55]), that is loosely said an extended region in the infinite dimensional phase space encoding all possible models. For practical reasons we will use the parametrization dependent definition of 'phases' here and investigate stability properties of the phases in future work.

between 2D 'Ising type' models and 4D lattice gauge theory models. In many examples statistical properties are similar between a given 4D lattice gauge model and the corresponding Ising type analogue 2D model. Spin net models have been defined based on the same principle, therefore we can hope that some of the findings on the phase structure of spin nets hold also for the 4D spin foam models.

In section 6.7 we will show that the partition function for a spin net can be understood as the partition function for a melonic spin foam with only two vertices and a large number of edges and faces (with two edges). This will allow us to interpret the renormalization flow of spin nets as a renormalization flow of spin foams.

6.3 Quantum group SU(2)$_k$

6.3.1 Basic ingredients

Before defining our quantum group spin net models, based on the quantum deformation of the rotation group, we need some basic tools that we summarize in this section. We follow [E56] in notation and conventions, where the interested reader can find a thorough introduction to SU(2)$_k$, see also [E57].

Following [E56] we understand the quantum group SU(2)$_k$ as the q-deformation $\mathcal{U}_q(su(2))$ of the universal enveloping algebra $U(su(2))$ of the Lie algebra $su(2)$. The algebra $\mathcal{U}_q(su(2))$ is generated by three operators $J_\pm, J_z$ with commutation relations

$$
\begin{aligned}
[J_z, J_\pm] &= \pm J_\pm \\
[J_+, J_-] &= \frac{q^{J_z} - q^{-J_z}}{q^{1/2} - q^{-1/2}} \quad .
\end{aligned}
\tag{6.3.1}
$$

As for the classical case, the finite dimensional representations of SU(2)$_k$ are labelled by half integers j and can be defined on $(2j + 1)$ dimensional representation spaces V_j. The so–called quantum dimensions are given by

$$
d_j = [2j + 1] \quad , \tag{6.3.2}
$$

where

$$
[n] = \frac{q^{\frac{n}{2}} - q^{-\frac{n}{2}}}{q^{\frac{1}{2}} - q^{-\frac{1}{2}}} \tag{6.3.3}
$$

are the so–called quantum numbers. Here q can be a root of unity or $q \in \mathbb{R}/\{0\}$. For q a root of unity, $q = \exp(\frac{2\pi}{(k+2)}i)$, the quantum numbers are periodic

$$
[n] = \frac{\sin(\frac{2\pi i n}{2k+4})}{\sin(\frac{2\pi i}{2k+4})} \quad , \tag{6.3.4}
$$

having zeros at $n = 0$ and $n = k + 2$. Thus $j = \frac{k}{2}$ with $d_{k/2} = 1$ is the 'last' representation with a strictly positive quantum dimension. Representations $j = 0, \frac{1}{2}, \ldots, \frac{k}{2}$ are called admissible, representations $j > \frac{k}{2}$ are of so–called quantum trace zero. The number $k \in \mathbb{N}$ is referred to as level.

Assuming two representations V_{j_1}, V_{j_2} the tensor product is defined via the co–product Δ. The action of the SU(2)$_k$ algebra on $V_{j_1} \otimes V_{j_2}$ is defined as

$$
\begin{aligned}
\Delta(J_\pm) &= q^{-J_z/2} \otimes J_\pm + J_\pm \otimes q^{J_z/2} \\
\Delta(J_z) &= \mathbb{I} \otimes J_z + J_z \otimes \mathbb{I} \quad .
\end{aligned}
\tag{6.3.5}
$$

As in the classical case we can reduce the tensor product $V_{j_1} \otimes V_{j_2}$ into a direct sum of irreducible representations and a part consisting of trace zero representations (which will be modded out). Assuming orthogonal bases $|j, m\rangle$ in the representation spaces, we can describe this by Clebsch-Gordan coefficients

$$|j, m\rangle = \sum_{m_1, m_2} {}_q C^{j_1 j_2 j}_{m_1 m_2 m} |j_1 m_1\rangle \otimes |j_2, m_2\rangle \quad . \tag{6.3.6}$$

When coupling three admissible representations j_I, j_K and j_L in this way, the coupling coefficients are only non–vanishing if the following conditions hold:

$$\begin{aligned}
j_I + j_K &\geq j_L \quad \text{for all permutations } \{J, K, L\} \text{ of } \{1, 2, 3\} \quad , \\
j_1 + j_2 + j_3 &= 0 \mod 1 \quad , \\
j_1 + j_2 + j_3 &\leq k \quad .
\end{aligned} \tag{6.3.7}$$

Note the last condition in (6.3.7), that is special to the quantum deformed case at root of unity. This condition signifies that $V_{j_1} \otimes V_{j_2}$ can include trace zero parts. These trace zero parts can be modded out [E57]. Some equations (for instance the one defining the $[6j]$ symbol) will however hold only modulo such trace zero parts [E57].

In particular we have the completeness relation

$$\sum_{m_3, \, j_3 \text{ admiss.}} {}_q C^{j_1 j_2 j_3}_{m_1 m_2 m_3} \, {}_q C^{j_1 j_2 j_3}_{m'_1 m'_2 m_3} = \Pi^{j_1 j_2}_{m_1 m_2, m'_1 m'_2} \tag{6.3.8}$$

where $\Pi^{j_1 j_2}_{m_1 m_2, m'_1 m'_2}$ projects out the trace zero part in $V_{j_1} \otimes V_{j_2}$. The orthogonality relation for the Clebsch-Gordan coefficients is given as

$$\sum_{m_1, m_2} {}_q C^{j_1 j_2 j}_{m_1 m_2 m} \, {}_q C^{j_1 j_2 j'}_{m_1 m_2 m'} = \delta_{jj'} \delta_{mm'} \theta_{j_1 j_2 j} \tag{6.3.9}$$

where $\theta_{j_1 j_2 j} = 1$ if the coupling conditions (6.3.7) are satisfied and vanishing otherwise.

When defining our spin net models we will restrict to integer j, that is to $\mathrm{SO}(3)_k$ representations.

6.3.2 Diagrammatic Calculus

The quantum group introduces certain subtleties into the definition, for instance the notion of dual needs to be specified. To this end we will use diagrammatic calculus, which is just a convenient form of representing combinations of Clebsch-Gordan coefficients. This can indeed be seen as an embellished form of tensor network calculus. The quantum group requires to specify a special direction, which we will take as the vertical direction. All graphs can then be interpreted as representing maps from a tensor product of representation spaces of $\mathrm{SU}(2)_k$, represented by lines coming in from below, to a tensor product of representation spaces, drawn as lines going out on top. Each of these lines carries a representation label j and a magnetic index m. One basic example of such a map are the Clebsch-Gordan coefficients, denoted by ${}_q \mathcal{C}^{j_1 \, j_2 \, j_3}_{m_1 \, m_2 \, m_3}$[8]. They are interpreted as a map $V_{j_1} \otimes V_{j_2} \to V_{j_3}$, symbolizing how the spins j_1 and j_2 (with their respective magnetic indices) couple to j_3. We represent them graphically as follows:

$$\begin{array}{c} j_3 \\ \diagdown\!\!\!\diagup \\ j_1 \quad j_2 \end{array} := {}_q \mathcal{C}^{j_1 \, j_2 \, j_3}_{m_1 \, m_2 \, m_3} \quad . \tag{6.3.10}$$

---

[8]This is not the standard Clebsch-Gordan coefficient defined in [E56], but it is modified by the quantum dimension:
$${}_q \mathcal{C}^{j_1 \, j_2 \, j_3}_{m_1 \, m_2 \, m_3} = {}_q C^{j_1 \, j_2 \, j_3}_{m_1 \, m_2 \, m_3} \left(\sqrt{d_{j_3}} \right)^{-1} .$$

A particular version of this Clebsch-Gordan coefficient will be important later on: If we choose $j_1 = j_2 = j$ and take $j_3 = 0$, we define the 'cap' as a map: $V_j \otimes V_j \to \mathbb{C}$, namely

$$
\overset{j}{\underset{m \quad m'}{\cap}} := {}_q\mathcal{C}^{j\,j\,0}_{m\,m'\,0}\sqrt{d_j} = (-1)^{j-m}q^{\frac{m}{2}}\delta_{m,-m'} \quad . \tag{6.3.11}
$$

From this 'cap' we can similarly define a 'cup' by requiring that they give the identity if we concatenate them:

$$
\overset{m''}{\underset{m}{\cap}}\overset{m''}{\underset{m}{\cup}} = \overset{m''}{\underset{m}{\big|}} = \delta^{m''}_m \quad , \tag{6.3.12}
$$

which gives:

$$
\overset{m \quad m'}{\underset{j}{\cup}} = (-1)^{j+m}q^{\frac{m}{2}}\delta_{m,-m'} \quad . \tag{6.3.13}
$$

Using these 'cups' and 'caps', we can construct the Clebsch-Gordan coefficients for the quantum group with inverse (here: complex conjugate) deformation parameter $\bar{q}$ by 'bending up' one of the lower legs of the Clebsch-Gordan in (6.3.10).

$$
{}_{\bar{q}}\mathcal{C}^{j_1\,j_2\,j_3}_{m_1\,m_2\,m_3} = \quad\overset{j_2 \quad j_1}{\underset{j_3}{\vee}} \quad = \quad \overset{j_2 \qquad j_1}{\underset{j_3}{\wedge}} \quad = \quad \overset{j_2 \qquad j_1}{\underset{j_3}{\cup}} \quad . \tag{6.3.14}
$$

This map can hence be interpreted as mapping $V_{j_3} \to V_{j_1} \otimes V_{j_2}$, thus it is dual to (6.3.10). With a 'cap' we can 'pull down' one of the legs again and arrive back at (6.3.10):

$$
\overset{j_5}{\underset{j_3 \quad j_4}{\vee}} \quad = \quad \overset{j_5}{\underset{j_3 \quad j_4}{\wedge}} \quad = \quad \overset{j_5}{\underset{j_3 \quad j_4}{\cap}} \quad . \tag{6.3.15}
$$

Concatenating these two maps, we obtain a map $V_{j_3} \to V_{j_3}$ proportional to the identity.

$$
\overset{j_3}{\underset{j_3}{j_1\diamondsuit j_2}} \quad = \quad \overset{j_3}{\underset{j_3}{j_1\,\,\,j_2}} \quad = \quad (-1)^{j_1+j_2-j_3}d^{-1}_{j_3}\delta_{m_3\,m'_3} \quad . \tag{6.3.16}
$$

Now we have all the necessary graphical ingredients to express the $SU(2)_k$ $6j$ symbol graphically: As for $SU(2)$, the $6j$ symbol is a particular contraction of four Clebsch-Gordan coefficients, which gives a purely real number. Graphically this is expressed in a closed diagram as follows:

$$
\overset{j_4}{\underset{j_3\,\,j_6\,\,j_2\,\,j_1}{}}j_5 \quad = \quad \overset{j_3}{\underset{j_1\,\,j_6\,\,j_4\,\,j_2}{}}j_5 \quad = \quad \begin{Bmatrix} j_1 & j_2 & j_5 \\ j_4 & j_3 & j_6 \end{Bmatrix} = \frac{(-1)^{j_1+j_2+j_3+j_4}}{\sqrt{d_{j_5}d_{j_6}}}\begin{bmatrix} j_1 & j_2 & j_5 \\ j_4 & j_3 & j_6 \end{bmatrix} \quad . \tag{6.3.17}
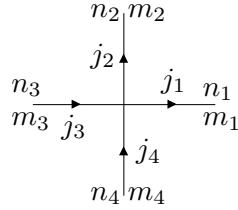$$

Figure 6.1: Vertex in the square lattice. Edges are ordered anticlockwise and have fixed orientation: edges 1 and 2 are outgoing, and edges 3 and 4 are incoming.

6.4 Structure of quantum group spin net models

A spin net model can be understood as a vertex model or as a tensor network model. In both cases weights are associated to the vertices of a graph – in the case of the tensor network model the weights, which depend on variables attached to edges, are given as tensors where the variables are now indices of these tensors. The partition function is expressed as a sum over the variables attached to the edges. For the tensor network this amounts to contracting tensors with each other according to the connectivity of the underlying graph.

We will consider a regular 4–valent graph here. As proposed in [E19–E24, E26, E27], and the results in [E2, E30, E44] show, coarse graining on a regular lattice might be sufficient to regain fully triangulation invariant models.[9]

We will introduce here spin net models with quantum group symmetry, i.e. the vertex weights will be invariant under a certain quantum group symmetry. These are much easier to deal with in the spin representation, where the (oriented) edges carry labels j, m, n which corresponds to the association of a Hilbert space

$$\mathcal{H}_e = \oplus_j V_j \otimes V_{j^*} \tag{6.4.1}$$

to a given edge e.

Here

- j denotes an irrep of the quantum group $\mathrm{SO}(3)_k$ and m, n are labelling elements of a basis in the representation space $V_j \otimes V_{j^*}$.
- For a representation in $\mathrm{SO}(3)_k$ we have $j \in \mathbb{N}$. Additionally, we will restrict to admissible representations, namely $j \leq k/2$ for k even and $j \leq (k-1)/2$ for k odd.
- j^* denotes the dual representation to j, which for $\mathrm{SO}(3)_k$ is unitarily equivalent to j.
- An orientation of the edges is needed as the action of the symmetry on a vertex depends on whether edges are ingoing or outgoing. We will choose an orientation and labelling of edges as in figure 6.1.

As said before, the quantum group requires to specify a special direction, which we have taken as vertical direction. For the horizontal direction we will assume an infinitely extended lattice. Alternatively one can consider periodic boundary conditions, however this requires braiding, see

---

[9]Coarse graining on a regular square lattice in a very regular way might lead to so–called CDL fixed points of the renormalization flow, that are non–isolated [E34,E58]. As pointed out in [E2] these do not define fully triangulation invariant models– however each of the non–isolated families of fixed points defines one triangulation invariant model. As is noted in [E34, E59], changing the renormalization procedure, to include a so–called entanglement filtering, would reduce these families automatically to the triangulation invariant fixed point. This could be obtained by including apart from refining and coarse graining moves also entangling moves into the renormalization algorithm [E18, E60].

[E2,E61,E62]. It turns out that due to the specification of the vertical direction as special, we have to amend the gluing rule for the horizontal direction. This will be explained further below in section 6.5. Modulo this subtlety the tensor network contraction can be understood as concatenation of (intertwiner) maps.

As mentioned, to implement the (quantum) group symmetry, the vertex weights have to be intertwining maps with respect to the representations involved. Such intertwining maps can be obtained by projecting an arbitrary tensor with the appropriate index structure from the 'left' and the 'right' with the Haar projector, which in the case of groups is given by (6.2.4). This can be expanded into Clebsch-Gordan coefficients, see [E44]. As then no group elements appear, this form is also the appropriate one for quantum groups. Indeed we will be defining a Haar projector with the help of diagrammatic calculus. This will in particular help to resolve subtleties regarding the definition of the dual representation j^* for the quantum group. The technical difficulties are due to the fact that the dual of a dual is actually not given by the identity, but by a phase factor. A clean definition of 'dual' is therefore crucial for a consistent definition of the models.

6.4.1 Haar projector

The four–valent Haar projector naturally splits into two three–valent Haar projectors, which are connected by a sum over a representation j_5. This index actually gives the intertwiner label d in (6.2.6), which for the four–valent projector under consideration reads

$$\mathcal{P}_{(\{m\},\{m'\})}(j_1, j_2, j_3, j_4) = \sum_{j_5} \iota_{\{m\}}^{j_5}(j_1, j_2, j_3, j_4)\iota_{\{m'\}}^{*j_5}(j_1, j_2, j_3, j_4) \quad . \tag{6.4.2}$$

The following contraction of Clebsch-Gordan coefficients, associated to the recoupling scheme $j_1 \otimes j_2 \ni j_5 \in j_3 \otimes j_4$, gives the intertwiner $\iota_{\{m\}}^{j_5}(j_1, j_2, j_3, j_4)$ up to normalization:

$$\vcenter{\hbox{}} = \sum_{m_5} {}_{\bar{q}}\mathcal{C}_{m_1\,m_2\,m_5}^{j_1\,j_2\,j_5}\; {}_q\mathcal{C}_{m_3\,m_4\,m_5}^{j_3\,j_4\,j_5} \quad . \tag{6.4.3}$$

Now, with the help of the previously defined 'cups' and 'caps', we can define its dual:

$$\vcenter{\hbox{}} = \vcenter{\hbox{}} = (-1)^{2j_5} \sum_{m_5} q^{m_5}\; {}_{\bar{q}}\mathcal{C}_{m_1\,m_2\,m_5}^{j_1\,j_2\,j_5}\; {}_q\mathcal{C}_{m_3\,m_4\,m_5}^{j_3\,j_4\,j_5} \quad , \tag{6.4.4}$$

which is equal to $\iota_{\{m'\}}^{*j_5}(j_1, j_2, j_3, j_4)$, again up to normalization. Substituting in Eq. (6.4.2) and demanding that $\mathcal{P}$ is a projector, namely $\mathcal{P}^2 = \mathcal{P}$, we fix the normalization. The result is (see the proof in Appendix 6.A.1)[10]

$$\mathcal{P}_{(\{m\},\{m'\})}(j_1, j_2, j_3, j_4) = \sum_{j_5} (-1)^{j_1+j_2+j_3+j_4} d_{j_5} \vcenter{\hbox{}} \otimes \vcenter{\hbox{}} \quad . \tag{6.4.5}$$

---

[10]To alleviate the notation we have omitted the magnetic indices attached to the diagrams. Here the left diagram carries $\{m\}$ indices and the right diagram carries $\{m'\}$ indices.

Note that for the Haar projector (6.4.5) we have the same intertwiner label j_5 appearing for the left and right (dualized) copy. This will actually change for the spin net models introduced in (6.4.12). There basis elements $j_5 \neq j_5'$ appear in the recoupling scheme.

The definition of this Haar projector corresponds to a particular recoupling scheme: $j_1 \otimes j_2 \ni j_5 \in j_3 \otimes j_4$, associated to a vertical splitting of the 4–valent vertex in two three–valent ones. Similarly we can define the Haar projector for the recoupling scheme: $j_2 \otimes j_3 \ni j_6 \in j_4 \otimes j_1$, which leads to a horizontal splitting of the 4–valent vertex. Instead of repeating the same procedure, we can derive it from the previous Haar projector. First we define:

$$\tag{6.4.6}$$

These two different splittings (or recoupling schemes) are not independent. It is straightforward to realize that (see proof in Appendix 6.A.2)

$$= \sum_{j_5} \sqrt{\frac{d_{j_5}}{d_{j_6}}} \begin{bmatrix} j_1 & j_2 & j_5 \\ j_3 & j_4 & j_6 \end{bmatrix} \qquad . \tag{6.4.7}$$

Similarly one can derive an analogue relation to arrive back at the previous splitting.

$$= \sum_{j_6} \sqrt{\frac{d_{j_6}}{d_{j_5}}} \begin{bmatrix} j_1 & j_2 & j_5 \\ j_3 & j_4 & j_6 \end{bmatrix} \qquad , \tag{6.4.8}$$

because of the orthogonality relation of the $[6j]$ symbol:

$$\sum_{j_5} \begin{bmatrix} j_1 & j_2 & j_5 \\ j_3 & j_4 & j_6 \end{bmatrix} \begin{bmatrix} j_1 & j_2 & j_5 \\ j_3 & j_4 & j_6' \end{bmatrix} = \delta_{j_6,j_6'} \cdot (\text{admissibility cond.}) \qquad . \tag{6.4.9}$$

Now by dualizing (6.4.6), one can analogously define a Haar projector for the horizontal splitting:

$$\mathcal{P}_{(\{m\},\{m'\})}(j_1,j_2,j_3,j_4) = \sum_{j_6} (-1)^{j_1+j_2+j_3+j_4} d_{j_6} \qquad \otimes \qquad . \tag{6.4.10}$$

6.4.2 Vertex weights

Attached to each vertex, we consider weights $t(\{j\}, \{m\}, \{n\})$. The partition function for the model is then (basically) defined by summing over all indices attached to the edges. As mentioned previously, there is a subtlety of how to contract the horizontal edges – here one has to include a certain phase. This will be explained in detail in section 6.5.

With the Haar projector $\mathcal{P}$ at hand it is straightforward to characterize the vertex weights, by the condition

$$t(\{j\}, \{m\}, \{n\}) = \sum_{\{m'\},\{n'\}} \mathcal{P}_{(\{m\},\{m'\})}(\{j\}) \, t(\{j\}, \{m'\}, \{n'\}) \, \mathcal{P}_{(\{n'\},\{n\})}(\{j\}) \qquad , \tag{6.4.11}$$

namely $t(\{j\}, \{m\}, \{n\})$ is invariant under the action of $\mathcal{P}$ from the left and from the right. This gauge invariance is the quantum group symmetry we referred to at the beginning of this section. It implies that if $j_1 \otimes j_2 \otimes j_3 \otimes j_4$ does not couple to the identity, then the tensor $t(\{j\}, \{m\}, \{n\})$ vanishes. To exploit this quantum group symmetry and avoid redundancies in the representation (6.4.11), we will reexpress the vertex weights in the intertwiner basis. As we will see this is advantageous for the coarse graining algorithm.

Indeed, by using the intertwiner basis, we can write [11]

$$
t(\{j\}, \{m\}, \{n\}) = \sum_{j_5, j_5'} \hat{t}_1^{(j_5, j_5')}(j_1, j_2; j_3, j_4)\, d_{j_5} d_{j_5'} \quad \otimes \quad \tag{6.4.12}
$$

$$
= \sum_{j_6, j_6'} \hat{t}_2^{(j_6, j_6')}(j_1, j_4; j_2, j_3)\, d_{j_6} d_{j_6'} \quad \otimes \quad . \tag{6.4.13}
$$

These equations are actually two different changes of basis according with the two recoupling schemes. Let us look e.g. at the first equation: On the right hand side the only relevant information is the tensor $\hat{t}_1^{(j_5, j_5')}(j_1, j_2; j_3, j_4)$, which describes how the representations j_1 and j_2 couple to (the pair) (j_5, j_5') and how j_3 and j_4 also couple to that pair [12]. Note that $\hat{t}_1$ does not depend on the magnetic indices, but only on the representation labels and their recoupling into the representations (j_5, j_5'); hence $\hat{t}_1$ provides the vertex weight expressed in the intertwiner basis. In the same way, $\hat{t}_2$ is the vertex weight expressed in the intertwiner basis associated with the other recoupling scheme, in which the pairs j_1 and j_4, and j_2 and j_3, both couple to the pair (j_6, j_6') .

Using the relations (6.4.7) it is straightforward to get the relation between the tensors in the two recoupling schemes:

$$
\hat{t}_2^{(j_6, j_6')}(j_1, j_4; j_2, j_3) = \sum_{j_5, j_5'} \hat{t}_1^{(j_5, j_5')}(j_1, j_2; j_3, j_4) \sqrt{\frac{[2j_5 + 1][2j_5' + 1]}{[2j_6 + 1][2j_6' + 1]}} \begin{bmatrix} j_1 & j_2 & j_5 \\ j_3 & j_4 & j_6 \end{bmatrix} \begin{bmatrix} j_1 & j_2 & j_5' \\ j_3 & j_4 & j_6' \end{bmatrix} .
$$
$$
\tag{6.4.14}
$$

Via the inverse transformation any choice of tensor $\hat{t}$ leads to a vertex weight t satisfying (6.4.11). Additionally one might want to demand certain symmetries, for instance under a reflection of the underlying four–valent vertex, etc.. This translates into certain conditions on the form of $\hat{t}_1$. In section 6.6 we will explicitly define the models that we will analyze, and we will discus the extra symmetries that they enjoy.

6.5 The coarse graining algorithm

As we have motivated in the previous section, the previously introduced quantum group spin net models can be cast into a tensor network form, to which one can apply tensor network renormalization [E33, E34] as a coarse graining procedure. In the following we will describe this algorithm.

---

[11] Recall that, for the sake of clarity in the notation, we have omitted the magnetic indices in the diagrams. In Eqs. (6.4.12)-(6.4.13), the diagrams on the left carry $\{m\}$ indices, while the diagrams on the right carry $\{n\}$ indices.

[12] Recall that every edge carries two representations, j and j^*. Here we explicitly allow them to couple to different representations $j_5' \neq j_5^*$.
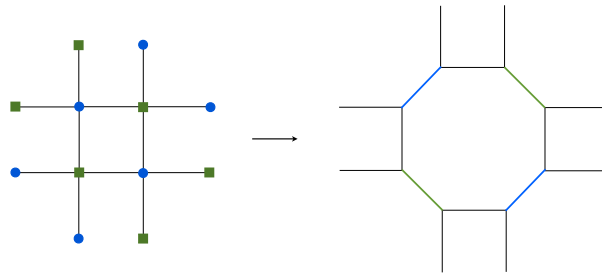
Figure 6.2: Rewriting of the four–valent tensor network as a three–valent tensor network.
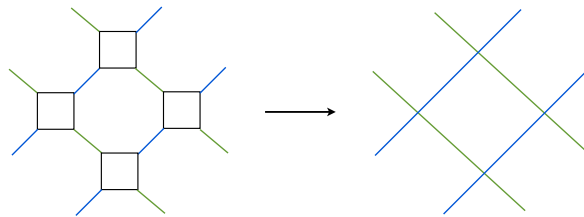

Figure 6.3: The contraction of the three–valent tensor network yields a coarser (rotated) square
lattice.

We consider our quantum group spin net models defined on the square lattice. To each four-valent
vertex of the lattice we attach the tensors

$$t(\{j\}, \{m\}, \{n\}) = \begin{matrix} m_2\, n_2 & m_1\, n_1 \\ j_2 & j_1 \\ j_3 & j_4 \\ m_3\, n_3 & m_4\, n_4 \end{matrix} \qquad . \tag{6.5.1}$$

To complete the definition of our models, we require an additional ingredient in the horizontal
edges: to every horizontal edge, with labels $\{j_a, m_a, n_a\}$, we attach the 'swirl'

$$(-1)^{2j_a} q^{-n_a} \delta_{n_a, n'_a} = \begin{matrix} n_a \\ n'_a \end{matrix} \bigg) j_a \qquad . \tag{6.5.2}$$

This extra factor will be justified when explaining the contraction scheme. We will see that,
thanks to it, under coarse graining the contributions coming from the $\{n\}$ indices (which undergo
a dualization) will behave in the same way as those coming from the indices $\{m\}$. As a result, the
contraction carried out to coarse grain will lead to a flow equation with a very nice compact form,
which will be given in terms of the recoupling symbols of the group.

The partition function for the model then reads

$$Z = \sum_{a,\dots} \dots t(\{j\}, \{m\}, \{n\})_{abcd} \, (-1)^{2j_a} q^{-n_a} \, t(\{j\}, \{m\}, \{n\})_{b'c'ad'} \dots \quad , \tag{6.5.3}$$

namely it is given by the contraction, according with the connectivity of the lattice, of all the
tensors and the extra factors in the horizontal edges.

In order to coarse grain this tensor network we consider the algorithm employed in [E34], which
is the adaptation to the square lattice of the original algorithm introduced in [E33] for a hexagonal

lattice. The idea is simple: we first rewrite the four–valent tensor network into a three–valent tensor network as depicted in Figure 6.2. In this way we can contract the three-valent tensors into new effective four–valent tensors forming a coarser rotated lattice, as in Figure 6.3.

The splitting carried out in Figure 6.2 is achieved by regarding the four–valent tensors as matrices and employing a singular value decomposition. We adapt this singular value decomposition to the recoupling schemes that we discussed in previous section, obtaining an algorithm that preserves the group symmetry properties of our tensors. This symmetry preserving algorithm was already introduced in [E44], where we discussed its advantages. Let us describe how it works for the current quantum group spin net models.

6.5.1 Symmetry preserving algorithm

As explained in the previous section (see Eqs (6.4.12)-(6.4.13)), given the tensor $t(\{j\}, \{m\}, \{n\})$ we can perform a change of basis to the recoupling basis, defining either $\hat{t}_1^{(j_5, j_5')}(j_1, j_2; j_3, j_4)$, associated to the recoupling scheme $j_1 \otimes j_2 \ni \{j_5, j_5'\} \in j_3 \otimes j_4$, or $\hat{t}_2^{(j_6, j_6')}(j_1, j_2; j_3, j_4)$, associated to the recoupling scheme $j_2 \otimes j_3 \ni \{j_6, j_6'\} \in j_4 \otimes j_1$. In the recoupling basis the tensor is then block-diagonal, where blocks are labelled by pairs of representations (j, j') associated to the recoupling scheme. We can regard these blocks as matrices and perform a singular value decomposition, that we truncate to certain cut-off μ:

$$\hat{t}_1^{(j_5, j_5')}(j_1, j_2; j_3, j_4) \equiv (M_1)^{(j_5, j_5')}_{A=\{j_1, j_2\}, B=\{j_3, j_4\}} \simeq \sum_{i=1}^{\mu(j_5, j_5')} (U_1)^{(j_5, j_5')}_{A=\{j_1, j_2\}, i} (\lambda_1)^{(j_5, j_5')}_{ii} (V_1)^{(j_5, j_5')}_{i, B=\{j_3, j_4\}} \quad , \tag{6.5.4}$$

$$\hat{t}_2^{(j_6, j_6')}(j_1, j_2; j_3, j_4) \equiv (M_2)^{(j_6, j_6')}_{A=\{j_2, j_3\}, B=\{j_4, j_1\}} \simeq \sum_{i=1}^{\mu(j_6, j_6')} (U_2)^{(j_6, j_6')}_{A=\{j_2, j_3\}, i} (\lambda_2)^{(j_6, j_6')}_{ii} (V_2)^{(j_6, j_6')}_{i, B=\{j_4, j_1\}} \quad . \tag{6.5.5}$$

Without the cut–off the dimension of the effective index i, the so–called *bond* dimension, would grow exponentially when iterating the coarse graining procedure. Thanks to this cut–off we render the coarse graining procedure a feasible task. Note that we have control on the error made by imposing this truncation: The larger the cut–off the better the approximation.

The above singular value decompositions allow us to split the four–valent tensors $t(\{j\}, \{m\}, \{n\})$ in two three–valent tensors. We can carry out two different splittings, according with the two different recoupling schemes. For vertices located in odd positions (blue circles in Fig. 6.2) we write

$$t(\{j\}, \{m\}, \{n\}) = \sum_{j_5, j_5'} \sum_{m_5, n_5} \sum_{i=1}^{\mu(j_5, j_5')} (S_1)^{j_5, j_5'}_{m_5, n_5}(\{I\}_{\{1,2\}}, i)(S_2)^{j_5, j_5'}_{m_5, n_5}(\{I\}_{\{3,4\}}, i) \quad , \tag{6.5.6}$$

while for vertices located in even positions (green squares in Fig. 6.2) we have

$$t(\{j\}, \{m\}, \{n\}) = \sum_{j_6, j_6'} \sum_{m_6, n_6} \sum_{i=1}^{\mu(j_6, j_6')} (S_3)^{j_6, j_6'}_{m_6, n_6}(\{I\}_{\{2,3\}}, i)(S_4)^{j_6, j_6'}_{m_6, n_6}(\{I\}_{\{4,1\}}, i) \quad . \tag{6.5.7}$$

Here we have have simplified the notation by introducing $\{I\}_{\{a,b\}} = \{j_a, m_a, n_a, j_b, m_b, n_b\}$. In the
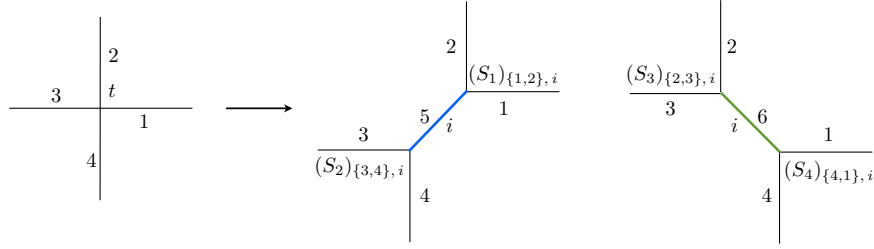
Figure 6.4: Splitting of the tensor $t(\{j\}, \{m\}, \{n\})$ according with the two different recoupling schemes, as expressed in equations (6.5.6)-(6.5.7).

above splittings, which are sketched in Figure 6.4, we have defined the following objects

$$(S_1)^{j_5,j_5'}_{m_5,n_5}(\{I\}_{\{1,2\}}, i) = \sqrt{d_{j_5} d_{j_5'}} (\lambda_1)^{(j_5,j_5')}_{ii} (U_1)^{(j_5,j_5')}_{\{j_1,j_2\},i} \quad \otimes \quad , \qquad (6.5.8)$$

$$(S_2)^{j_5,j_5'}_{m_5,n_5}(\{I\}_{\{3,4\}}, i) = \sqrt{d_{j_5} d_{j_5'}} (\lambda_1)^{(j_5,j_5')}_{ii} (V_1)^{(j_5,j_5')}_{i,\{j_3,j_4\}} \quad \otimes \quad , \qquad (6.5.9)$$

$$(S_3)^{j_6,j_6'}_{m_6,n_6}(\{I\}_{\{2,3\}}, i) = \sqrt{d_{j_6} d_{j_6'}} (\lambda_2)^{(j_6,j_6')}_{ii} (U_2)^{(j_6,j_6')}_{\{j_2,j_3\},i} \quad \otimes \quad , \qquad (6.5.10)$$

$$(S_4)^{j_6,j_6'}_{m_6,n_6}(\{I\}_{\{4,1\}}, i) = \sqrt{d_{j_6} d_{j_6'}} (\lambda_2)^{(j_6,j_6')}_{ii} (V_2)^{(j_6,j_6')}_{i,\{j_4,j_1\}} \quad \otimes \quad . \qquad (6.5.11)$$

In the next section we will use these expressions when computing the contraction that yields the new effective tensor. For that purpose it is convenient to use the following identities, which can be easily proven with the help of the identity $_q\mathcal{C}^{j_1\,j_2\,j_3}_{m_1\,m_2\,m_3} = (-1)^{j_1+j_2-j_3} {}_{\bar{q}}\mathcal{C}^{j_1\quad j_2\quad j_3}_{-m_1\,-m_2\,-m_3}$:

$$\qquad = \qquad ; \qquad \qquad = \qquad , \qquad (6.5.12)$$

$$\qquad = \qquad ; \qquad \qquad = \qquad . \qquad (6.5.13)$$

In view of expression (6.5.13), we can already clarify why we need the extra factor (6.5.2) associated with the horizontal edges, here labeled by 1 and 3, namely the factors $(-1)^{2j_1}q^{-n_1}$ $(-1)^{2j_3}q^{-n_3}$: Their role is to remove the swirl (double arc) that is attached in the equalties (6.5.13) to the edges with labels j_1 and j_3.

6.5.2 Derivation of the flow equation

With the splitting of the four–valent tensors into three-valent ones, it is now straightforward to get the new effective four–valent tensor by contraction, as depicted in Figure 6.5. We note that
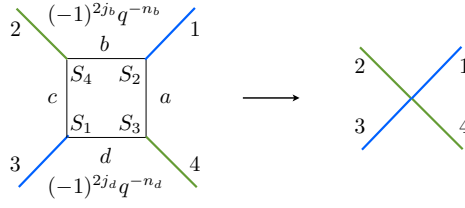
Figure 6.5: The new tensor $t(\{j\},\{m\},\{j'\},\{n\},\{i\})_{1,2,3,4}$ is the result of contracting $(S_1)_{m_3,n_3}^{j_3,j_3'}(\{I\}_{\{d,c\}},i_3)$, $(S_2)_{m_1,n_1}^{j_1,j_1'}(\{I\}_{\{b,a\}},i_1)$, $(S_3)_{m_4,n_4}^{j_4,j_4'}(\{I\}_{\{a,d\}},i_4)$, and $(S_4)_{m_2,n_2}^{j_2,j_2'}(\{I\}_{\{b,c\}},i_2)$, together with the factors $(-1)^{2j_b}q^{-n_b}$ $(-1)^{2j_d}q^{-n_d}$ associated to horizontal edges.

the effective edges now carry labels $I' = \{j,m,j',n,i\}$, with i running from 1 to $\mu(j,j')$, so that the Hilbert space associated to every edge gets a more general structure than that of the original Hilbert space (6.4.1), namely

$$\mathcal{H}_e = \oplus_{j,j'}\mu(j,j')V_j \otimes V_{j'}. \tag{6.5.14}$$

In consequence, the effective tensor also gets more general than (6.5.1), as its structure is of the form

$$t(\{j\},\{m\},\{j'\},\{n\},\{i\}) = \begin{matrix} I_2' & & I_1' \\ & \times & \\ I_3' & & I_4' \end{matrix} \quad ; \quad I_a' = \{j_a,m_a,j_a',n_a,i_a\} \quad . \tag{6.5.15}$$

Thus we have in particular now the possibility $j \neq j'$ also for the 'outer' edges. In addition multiplicity labels i (whose range can depend on the representation labels (j,j')) can appear.

This new tensor possesses the quantum group symmetry of the original vertex weight, namely it is invariant under the left action of $\mathcal{P}_{(\{m\},\{m'\})}(\{j\})$ and under the right action of $\mathcal{P}_{(\{n'\},\{n\})}(\{j'\})$. Our symmetry preserving algorithm gives us directly the tensor in the recoupling basis. Let us compute the new block $\hat{t}_1^{(j_5,j_5')}(J_1,J_2;J_3,J_4)$, with $J_a = \{j_a,j_a',i_a\}$, :

$$\hat{t}_1^{(j_5,j_5')}(J_1,J_2;J_3,J_4) = \sum_{a,b,c,d}\sum_{\{m\}}\sum_{\{n\}}(-1)^{j_1+j_2,+j_3,+j_4}(-1)^{j_1'+j_2',+j_3',+j_4'} \begin{matrix} j_2\,j_1 \\ \\ j_3\,j_4 \end{matrix} j_5 \quad \otimes \quad \begin{matrix} j_2' & j_1' \\ & j_5' \\ j_3' & j_4' \end{matrix}$$

$$\times (-1)^{2j_b}q^{-n_b}(S_2)_{m_1,n_1}^{j_1,j_1'}(\{I\}_{\{b,a\}},i_1)(S_4)_{m_2,n_2}^{j_2,j_2'}(\{I\}_{\{b,c\}},i_2)$$

$$\times (-1)^{2j_d}q^{-n_d}(S_1)_{m_3,n_3}^{j_3,j_3'}(\{I\}_{\{d,c\}},i_3)(S_3)_{m_4,n_4}^{j_4,j_4'}(\{I\}_{\{a,d\}},i_4) \quad . \tag{6.5.16}$$

Substituting in this equation the expressions (6.5.8)-(6.5.11), we can contract the involved Clebsch-Gordan coefficients. It is straightforward to check that the contraction of those coefficients carrying indices $\{j,m\}$ (left part of the diagrams) gives the following $9j$-symbol:

$$\begin{matrix} j_2 & & j_1 \\ & j_b & \\ j_c & & j_a \\ & & \\ j_3 & j_d & j_4 \end{matrix} j_5 = \frac{(-1)^{j_c+j_a+j_5}(-1)^{j_1+j_2+j_3+j_4}}{d_{j_5}\sqrt{d_{j_b}d_{j_d}}} \begin{bmatrix} j_c & j_a & j_5 \\ j_1 & j_2 & j_b \end{bmatrix} \begin{bmatrix} j_c & j_a & j_5 \\ j_4 & j_3 & j_d \end{bmatrix} \quad . \tag{6.5.17}$$

This equality is shown in Appendix 6.A.3.

As for the right side of the diagrams, which come from a dualization and that are formed by Clebsch-Gordan coefficients that carry indices $\{j', n\}$, they also contract to the 9j-symbol, which is obvious once we consider the identities (6.5.12)-(6.5.13), and we remove the swirls with the extra factors $(-1)^{2j_b}q^{-n_b}\,(-1)^{2j_d}q^{-n_d}$. As we anticipated before, without the introduction of these extra factors for the horizontal edges, we would not get the 9j-symbol when contracting the Clebsch-Gordan coefficients that come from the dual contributions.

In conclusion, the new effective tensor in the recoupling scheme 1 reads

$$
\hat{t}_1^{(j_5,j_5')}(J_1, J_2; J_3, J_4) = \sum_{a,b,c,d} \sum_{\{m\}} \sum_{\{n\}} \frac{(-1)^{j_c+j_a+j_5}(-1)^{j_c'+j_a'+j_5'}}{d_{j_5} d_{j_5'} \sqrt{d_{j_b} d_{j_b'} d_{j_d} d_{j_d'}}} \sqrt{d_{j_1} d_{j_1'} d_{j_2} d_{j_2'} d_{j_3} d_{j_3'} d_{j_4} d_{j_4'}}
$$
$$
\times \sqrt{(\lambda_1)_{i_1 i_1}^{(j_1,j_1')} (\lambda_2)_{i_2 i_2}^{(j_2,j_2')} (\lambda_1)_{i_3 i_3}^{(j_3,j_3')} (\lambda_2)_{i_4 i_4}^{(j_4,j_4')}}
$$
$$
\times (V_1)_{i_1,\{j_b,j_b',j_a,j_a'\}}^{(j_1,j_1')} (V_2)_{i_2,\{j_b,j_b',j_c,j_c'\}}^{(j_2,j_2')} (U_1)_{\{j_d,j_d',j_c,j_c'\},i_3}^{(j_3,j_3')} (U_2)_{\{j_a,j_a',j_d,j_d'\},i_4}^{(j_4,j_4')}
$$
$$
\times \begin{bmatrix} j_c & j_a & j_5 \\ j_1 & j_2 & j_b \end{bmatrix} \begin{bmatrix} j_c & j_a & j_5 \\ j_4 & j_3 & j_d \end{bmatrix} \begin{bmatrix} j_c' & j_a' & j_5' \\ j_1' & j_2' & j_b' \end{bmatrix} \begin{bmatrix} j_c' & j_a' & j_5' \\ j_4' & j_3' & j_d' \end{bmatrix} \quad , \quad (6.5.18)
$$

where $j_i = j_i'$ with $i \in \{a, b, c, d\}$ for the first iteration, while they are a priori independent for subsequent iterations. The blocks $\hat{t}_2^{(j_6,j_6')}(J_1, J_4; J_2, J_3)$ for the second splitting can in general be obtained from $\hat{t}_1^{(j_5,j_5')}(J_1, J_2; J_3, J_4)$ by convoluting it with 6j-symbols, as in equation (6.4.14). Nevertheless, as we will further comment in section 6.6, the models that we will consider have the symmetry $\hat{t}_2^{(j_6,j_6')}(J_1, J_4; J_2, J_3) = \hat{t}_1^{(j_6,j_6')}(J_1, J_4; J_2, J_3)$, which is preserved under coarse graining, hence this step of computing $\hat{t}_2$ is actually not necessary.

The above equation (6.5.18) can be regarded as the *coarse graining flow equation* for $\hat{t}_1$, in the sense that the factors $\{\lambda, U, V\}$ are determined by the tensor in the previous step of the iteration procedure. By choosing initial data, we can analyze the behaviour of the vertex weights under this coarse-graining flow. In the next section we carry out this analysis for a particular set of models, determining the fixed points and phases of this flow, as well as phase transitions.

Note that this flow equation is still quite challenging numerically. The coarse grained tensor $\hat{t}$ will have in general χ^5 components where even in the simplest (useful) approximation $\chi = (j_{max} + 1)^2$, with $j_{max} = k/2$ for k even and $j_{max} = (k - 1)/2$ for k odd. To save and compute more efficiently with these tensors we developed the method of super indices. These super indices summarize combinations of indices, and keep only those that actually lead to non–vanishing entries due to the coupling rule. This leads already to a huge saving for the $[6j]$ symbol – instead of $(j_{max} + 1)^6$ entries one only saves the components non–vanishing due to coupling rules.

6.5.3 Geometric interpretation of the flow equation

Here we wish to point out that the flow equation (6.5.18) for the 2D spin nets has an interesting 3D geometric interpretation. A similar 3D interpretation of the 2D models has also been noticed in [E2]. The 3D geometrical interpretation is due to the $[6j]$ symbols appearing in (6.5.18). The 3D spin foam models without and with (positive) cosmological constant are given by the Ponzano–Regge [E63] and the Turaev–Viro model [E64] respectively. These models are topological, that is triangulation invariant, and built by associating $[6j]$ symbols to the tetrahedra. Similarly we can associate tetrahedra to the $[6j]$ symbols appearing in (6.5.18). The edges of the tetrahedra are labelled by the spins appearing in the $[6j]$ symbol, so that the coupling conditions of the $[6j]$ symbol reflect the triangle inequalities for the tetrahedron. The summation over common j and j' is then interpreted as gluing of edges.

This gluing of tetrahedra appears in stages:

- For the left and right copy separately (i.e. for unprimed and primed spins) we have the gluing of two tetrahedra to a double pyramid. Here the gluing is along the triangle with edges labelled by j_a, j_c and j_5 (and similarly for the primed indices).

- The triangles of the double pyramid, i.e. for the left copy, are given by $T_1 = \{(j_1, j_2, j_5), (j_3, j_4, j_5)\}$ as well as $T_2 = \{(j_1, j_a, j_b), (j_2, j_b, j_c), (j_3, j_c, j_d), (j_4, j_a, j_d)\}$, as shown in Figure 6.6. One will notice that T_1 corresponds to the indices of the new effective tensor, whereas the triangles in T_2 are glued with the appropriate U and V's from the singular value decomposition. This singular value decomposition results in three–valent tensors, dual to triangles, and we can indeed interpret this as gluing triangle amplitudes onto the pyramides. Note, that for some families of intertwiner fixed point models described in the next section 6.6 these amplitudes themselves are given by $[6j]$ symbols. Hence we can interpret this case as gluing further tetrahedra onto the pyramids.

  The gluing of the triangle amplitudes is also the place where a coupling between the left and right copy, i.e. primed and unprimed spins occur. We can interpret this as a gluing of the two double pyramids via the triangle amplitudes, that depend on both primed and unprimed indices. However, in the case of factorizing models, described in section 6.6, all quantities factorize with respect to primed and unprimed spins, and so does the coarse graining flow.
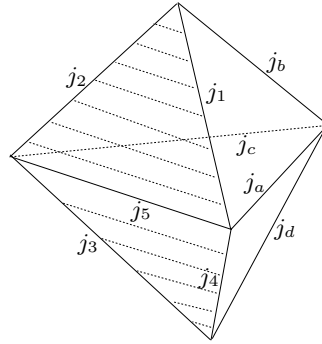
Figure 6.6: Double pyramid with triangles $T_1 = \{(j_1, j_2, j_5), (j_3, j_4, j_5)\}$, those filled with doted lines, and triangles $T_2 = \{(j_1, j_a, j_b), (j_2, j_b, j_c), (j_3, j_c, j_d), (j_4, j_a, j_d)\}$.

This geometric interpretation, in particular in the case that the 'triangle amplitudes' themselves correspond to geometric objects, might help to obtain an intuition about the coarse graining flow. For instance, if only $[6j]$ symbols (with appropriate face and edge factors and signs) are involved, the complex will describe a Turaev–Viro model. This is invariant under changes of the triangulation, which will explain some of the occurring fixed points.

This geometric interpretation might also help to approximate the coarse graining flow equation by a simpler equation. For instance it seems possible to consider instead of the flow equation related to the double pyramid a flow equation related to just one tetrahedron. This applies if $\hat{t}_1 = \hat{t}_2$ in the sense explained below equation (6.6.3), which is preserved under coarse graining. Preliminary numerical investigations have shown that this leads indeed to the same phase diagram as the more complicated flow equation. We will investigate this possibility further as it will allow us to consider more easily the replacement of the structure group $SU(2)_k$ with i.e. $SU(2)_k \times SU(2)_k$, as appear for the 4D gravitational models.

6.6 Fixed point intertwiners as initial data and coarse graining results

The space of possible tensors $\hat{t}_1$, and therefore spin net models is huge. One therefore needs to add further selection principles to arrive at a suitable phase space. For instance [E28, E29, E44] introduces and uses the so–called E–function parametrization, which for the spin foams encompasses all current models. It also allows an interpretation as imposing simplicity constraints, which are encoded in the choice of the E–function. However there are several problems with this parametrization. First of all, it turns out that for a quantum group, models based on E–functions have not the expected[13] symmetries, for instance under changing the recoupling scheme, via a 2–2 move. Furthermore, the models mostly flow to trivial phases and a fine tuning is necessary to arrive at a non–trivial fixed point, i.e. for which simplicity constraints are realized.

Here we will introduce another parametrization, which can be understood as an application of Reisenberger's construction outlined in section 6.2. This parametrization is based on fixed points (i.e. triangulation invariant instances) of so–called intertwiner models, that have been introduced and constructed in [E2, E45].

We will use specific families of these fixed points for intertwiner models here, for a specification of all possible fixed points, see [E2, E45]. In this section we will describe them briefly and explain that they do not define fixed points of the here considered spin net models, but, moreover, flow to non trivial fixed points, i.e. fixed points beyond the degenerate or analogue BF phase. Hence they define new phases and by linear combination we can additionally study phase diagrams.

6.6.1 Description of the fixed point intertwiners

The *fixed point intertwiners* can be written as a modification of the Clebsch-Gordan coefficients[14], which we diagrammatically denote as 'fat' vertices introduced in [E2]:

$$
\begin{matrix} j_3 \\ {\LARGE \bullet} \\ j_1 \quad j_2 \end{matrix} := a(j_1, j_2, j_3) \; {}_q\mathcal{C}^{j_1 \, j_2 \, j_3}_{m_1 \, m_2 \, m_3} \quad , \qquad \begin{matrix} j_2 \quad j_1 \\ {\LARGE \bullet} \\ j_3 \end{matrix} = a'(j_1, j_2, j_3) \; {}_{\bar{q}}\mathcal{C}^{j_1 \, j_2 \, j_3}_{m_1 \, m_2 \, m_3} \quad . \tag{6.6.1}
$$

At first sight such a modification appears to be an arbitrary choice and indeed without further requirements it allows for a parametrization with a plethora of parameters. Nevertheless, as it has been shown in [E2], one can uniquely fix these factors by (a) requiring invariance under planar (i.e. $2 - 2$, $3 - 1$ and $1 - 3$) Pachner moves, i.e. triangulation independence with respect to the dual triangulation, and (b) specifying the allowed representations, i.e. the set of labels j which do not lead to vanishing weights $a(j, \cdot, \cdot)$ and $a'(j, \cdot, \cdot)$. These special factors define the before mentioned *fixed point intertwiners*, of which we will present a few in the following subsections.

Note that this class of tensors leads in general to complex weights. Fortunately this is not a problem at all for the tensor network algorithm that we will be using. To our knowledge it gives a first example where the tensor network algorithm is applied to a statistical system with complex weights.

---

[13]Such symmetries are realized in the S_3 group case [E44].

[14]This modification only depends on the triple of representation labels, not on the magnetic indices m. The vertices define therefore still $SU(2)_k$ intertwining maps.

Thus the models that we will analyze have initial tensors of the form

$$t(\{j\}, \{m\}, \{n\}) = \sum_{j_5, j_5'} \frac{1}{d_{j_5} d_{j_5'}} \quad \otimes \quad$$

$$= \sum_{j_6, j_6'} \frac{1}{d_{j_6} d_{j_6'}} \quad \otimes \quad . \tag{6.6.2}$$

We note that

$$\hat{t}_1^{(j_5, j_5')}(j_1, j_2; j_3, j_4) = \frac{a'(j_1, j_2, j_5) a(j_3, j_4, j_5) a(j_2, j_1, j_5') a'(j_4, j_3, j_5')}{(d_{j_5} d_{j_5'})^2} \quad , \tag{6.6.3}$$

$$\hat{t}_2^{(j_6, j_6')}(j_2, j_3; j_1, j_4) = \frac{a'(j_1, j_6, j_4) a(j_3, j_6, j_2) a(j_4, j_6', j_1) a'(j_2, j_6', j_3)}{(d_{j_6} d_{j_6'})^2} \quad . \tag{6.6.4}$$

As indicated already, due to the fixed point property of the intertwiners, the amplitudes for initial tensor (and as it happens also for the coarse grained tensors) are the same in the two recoupling bases, namely the tensors verify the symmetry property $\hat{t}_1^{(j_5, j_5')}(j_1, j_2; j_3, j_4) = \hat{t}_2^{(j_5, j_5')}(j_1, j_2; j_3, j_4)$. This is indeed a very physical requirement, imposing that the weights are the same if expanded in the two possible (planar) recoupling schemes. A asymmetry would specify a special direction, which we avoid by choosing the fixed point intertwiners as initial data. This equality of the tensor components in the two recoupling schemes will be preserved under the coarse graining flow.

Further symmetries that our tensors verify are

$$\begin{aligned}
\hat{t}_1^{(j_5, j_5')}(j_1, j_2; j_3, j_4) &= \hat{t}_1^{(j_5, j_5')}(j_3, j_4; j_1, j_2) = \hat{t}_1^{(j_5, j_5')}(j_2, j_1; j_4, j_3) \quad , \\
\hat{t}_1^{(j_5, j_5')}(j_1, j_2; j_3, j_4) &= \hat{t}_1^{(j_5', j_5)}(j_1, j_2; j_3, j_4) \quad ,
\end{aligned} \tag{6.6.5}$$

which represent discrete rotation and reflection symmetries.

Note that in (6.6.2) the spin labels at the outer edges are the same in the left and right copy, whereas the intertwiner labels j_5, j_5' or j_6, j_6' can a priori differ. (They do not for models analogous to standard gauge theories, which are based on the Haar intertwiner.) This might actually change under the renormalization flow: we allow generalized tensors carrying two spin labels j, j' per edge. As we will see, in the extreme case we will obtain factorizing models as fixed points of the renormalization flow. In this case the sum over j and j' can be performed independently and the partition function is equal to a square of an intertwiner model partition function. In cases in which that happens, we do regain the square of the model associated to the intertwiner we started with.

To characterize the fixed points we will give the non–vanishing intertwiner channels. I.e. an intertwiner channel (j, j') means that there are non–vanishing tensor components with $j_5 = j$ and $j_5' = j'$. Due to the symmetry under changing the recoupling scheme this holds also for $j_6 = j$ and $j_6' = j'$. We will speak of an 'excited' representation, if this representation is allowed by the simplicity constraints encoded in the model, that is if $j \in \mathcal{S}_1$ in the sense of section 6.2. I.e. the representation does not lead to a vanishing weight for the initial model.

Only $j = 0$ and j_{max} excited

A straightforward but exceptional example, which can be defined for even k, is to require that only representations $j = 0$ and $j_{max} = \frac{k}{2}$ are excited. There are only two non–vanishing a-factors (and

permutations) appearing, namely:

$$a(0,0,0) = a'(0,0,0) = 1 \quad , \quad a(j_{max}, j_{max}, 0) = a'(j_{max}, j_{max}, 0) = 1 \quad . \tag{6.6.6}$$

This is because j_{max} is of quantum dimension one and additionally has to satisfy the coupling rule $j_{max} \otimes j_{max} \equiv 0$. Also note that the factors a are invariant under permutations of their arguments.

If we plug in these fixed point intertwiners as initial data of our spin net models, we do not observe a flow; these initial data already define a fixed point. It only has two excited intertwiner channels, namely $(0,0)$ and (j_{max}, j_{max}). In fact one can easily see that the model is equivalent to the Ising model at zero temperature, but in a 'spin representation', equivalent to a (analogue) BF spin net model on $\mathbb{Z}_2$ [E25–E27]. That is j_{max} corresponds to the non–trivial representation of $\mathbb{Z}_2$ and there has always to meet an even number of such non–trivial representations at every vertex.

Only $j = 0$ and $j = j_1 < j_{max}$ excited

We study here two examples of models based on fixed point intertwiners that have only two representations excited, the trivial representation and a $j = j_1$ different from j_{max}. The two examples are the following:

- $k = 6, j_1 = 2$

  The fixed point intertwiner is defined by the amplitudes

  $$a(0,0,0) = a'(0,0,0) = 1 , \quad a(2,2,2) = a'(2,2,2) = \sqrt{d_2(d_2 - 1)}, \quad a(2,2,0) = a'(2,2,0) = \sqrt{d_2}, \tag{6.6.7}$$

  and permutations of them, with a being invariant under permutations of its arguments.

- $k = 10, j_1 = 3$

  The fixed point intertwiner is defined by the amplitudes

  $$a(0,0,0) = a'(0,0,0) = 1 , \quad a(3,3,3) = a'(3,3,3) = i\sqrt{d_3(d_3 - 1)}, \quad a(3,3,0) = a'(3,3,0) = \sqrt{d_3}, \tag{6.6.8}$$

  and permutations of them, with a being invariant under permutations of its arguments.

Taking these amplitudes as initial data for our spin net models, the resulting model flows to a fixed point with only contributing intertwiner channels $(0,0)$, $(0,j_1)$, $(j_1,0)$ and (j_1,j_1). This fixed point is factorizing: the partition function is the product of two partition functions, where each factor corresponds to the partition function of the intertwiner model we started with.

Only even representations excited

For a quantum group with k multiple of 4, one can construct fixed point intertwiners by only allowing representation with even j excited [E45]. This fixed point intertwiners are characterized by the following amplitudes:

$$a(j_1, j_2, j_3) = a'(j_1, j_2, j_3) = \sqrt{(-)^{J-j_1}} \sqrt{(-)^{J-j_2}} \sqrt{(-)^{J-j_3}} (-)^{2J-j_1-j_2} \times$$

$$\times \sqrt{\frac{[2j_1 + 1][2j_2 + 1]}{[J+1]}} \begin{bmatrix} j_1 & j_2 & j_3 \\ \frac{k}{4} & \frac{k}{4} & \frac{k}{4} \end{bmatrix} \quad , \tag{6.6.9}$$

if j_1, j_2 and j_3 are all even, otherwise the amplitude vanishes.

Starting with these intertwiners, we analyzed cases $k = 8$ and $k = 12$.

For $k = 8$ we obtain the following fixed point under coarse graining: only intertwiner channels $(0,0)$, $(0,4)$, $(4,0)$, $(4,4)$, and $(2,2)$ are excited. This fixed point is not factorizing, as the channels

$(0,0)$ and $(2,2)$ appear, but not for instance the channel $(0,2)$. This constitutes an example of a so-called 'mixed' fixed point. I.e. non–diagonal entries appear but the fixed point is not of factorizing type. These type of fixed points will play a crucial role in the interpretation of the fixed points as phases for spin foams.

In contrast, for $k = 12$ we do find the expected factorizing fixed point with all the intertwiner channels labeled by two even representations excited.

Maximal spin J

At last we introduce a whole family of fixed point intertwiners for each level k. A member of this family is labelled by an integer spin $J \leq k/2$. For a given J all representations $j \leq J$ are excited, where J is independent (apart from the bound) of the maximal spin $\frac{k}{2}$ of the quantum group. In fact these fixed points generalize to the classical group $SU(2)$ and provide a cut–off in spins there. (The coarse graining flow could still lead to arbitrary large spins.) Here the simplicity constraints can be interpreted as forbidding spins larger than J.

The a factors are given by:

$$a_{CDL}^J(j_1, j_2, j_3) = a'^J_{CDL}(j_1, j_2, j_3) = \sqrt{(-)^{J-j_1}}\sqrt{(-)^{J-j_2}}\sqrt{(-)^{J-j_3}}(-)^{2J-j_1-j_2} \times$$

$$\times \sqrt{\frac{[2j_1+1][2j_2+1]}{[J+1]}} \begin{bmatrix} j_1 & j_2 & j_3 \\ \frac{J}{2} & \frac{J}{2} & \frac{J}{2} \end{bmatrix} \quad , \qquad (6.6.10)$$

Note that when $J = k/2$, and j_1, j_2 and j_3 are all even, the amplitudes coincide with those of case 6.6.1, but now also odd representations are allowed.

To understand why the a_{CDL}^J define fixed points intertwiner models it is instructive to interpret them diagrammatically [E2]. Ignoring normalization (edge) factors, one three–valent intertiner is given as
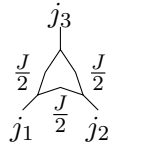
$$(6.6.11)$$

If one glues several of these vertices together, one can sum over the intermediate spins and replace the single line by a double line (see identity (6.A.8)). This explains our notation a_{CDL}^J denoting these tensors as 'corner double line', see also figure 6.7; for such tensor networks it is straightforward to see that they are fixed points of the coarse graining algorithm for intertwiner models [E2].

The initial tensor for the spin net model can then be represented as (again modulo edge normalization factors)
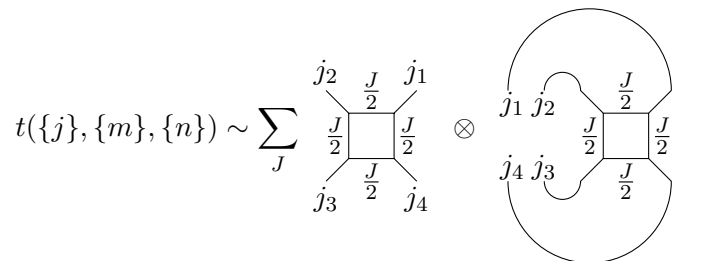
$$(6.6.12)$$

The symmetry of the graphical representation under rotations of $\frac{\pi}{2}$ explains the invariance of the tensor under change of recoupling basis from (j_5, j_5') to (j_6, j_6').

At this point the thoughtful reader may wonder, why we choose 'fixed points' as the initial data of a statistical system, which we intend to coarse grain. In order to guard against confusion we strongly stress that the previously defined a_{CDL}^J do *not* define fixed points of the here considered
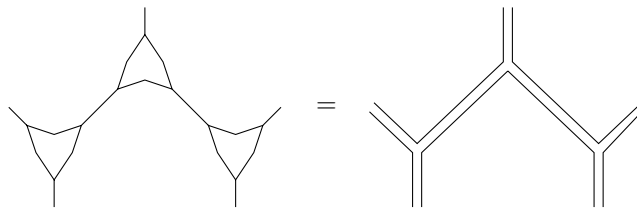
Figure 6.7: Diagrammatic explanation of the 'CDL' structure. With identity (6.A.8) one can replace the intermediate edges by double lines (we ignore normalization factors associated to the edges), which turn the tensor network into a ribbon graph. This ribbon graph structure gives a fixed point under renormalization flow, as the strands going around inner faces form closed loops, which just give constant factors and hence drop out. The remaining graph gives a rescaled version of the original graph.

J	k even	k odd
$J = 0$	degenerate	degenerate
$J = 1$	factorizing $J = 1$	factorizing $J = 1$
$J = 2$	factorizing $J = 2$	factorizing $J = 2$
$\vdots$	$\vdots$	$\vdots$
$J = \frac{k}{2} - 2$ even / $J = \frac{k-1}{2} - 1$ odd	factorizing $J = \frac{k}{2} - 2$	factorizing $J = \frac{k-1}{2} - 1$
$J = \frac{k}{2} - 1$ even / $J = \frac{k-1}{2}$ odd	analogue BF	analogue BF
$J = \frac{k}{2}$	"mixed"	−

Table 6.1: Table of the fixed points obtained from the initial intertwiners labelled by the maximal spin J. For odd k there is no model for $J = \frac{k}{2}$ since the initial model is only defined for even J.

spin net models. To explain why, consider the definition of the initial tensor given in Eq. (6.6.2). Even though it is written in this product form, the intertwiners for one copy and its dual do not decouple: During the contraction of the outer edges in the coarse graining algorithm (6.5.18), the summations over the primed and unprimed representation labels cannot be taken individually. Thus already the first coarse graining step will result in a different model from the initial one and the system 'flows' away from the initial condition.

There are however fixed points of the full spin net models, for which both copies indeed decouple and are thus denoted as 'factorizing'. As we will explain below, most of the initial a^J_{CDL} models actually flow to their 'corresponding' factorizing fixed point, meaning that the fixed point shares the same maximal spin J with the initial models. We have seen such a behaviour already for the $k = 12$ example in section 6.6.1.

After the introduction and justification of the initial data let us focus on the results: Remarkably every single initial fixed point intertwiner model flows to a different fixed point and furthermore the flow in different quantum groups follows a clear pattern, which we summarize in table 6.1[15]. Let us briefly describe the different types of fixed points:

As we have commented in the introduction (see also [E44]) the intertwiner channels are the relevant degrees of freedom in spin net models, such that it is sufficient to know the excited intertwiner channels (and the associated singular values) to identify the phase / fixed point. Thus we will not

---

[15]The pattern is confirmed for quantum groups $SU(2)_k$ with $k = \{4, 5, \ldots, 10\}$. For $k = 4$, the initial model for $J = 1$ flows to the factorizing fixed point, not the analogue BF one.

state the final fixed point tensor but focus on the description of the excited intertwiner channels. Since for all discovered fixed points the excited intertwiner channels are just excited once, they can be characterized by a matrix of singular values, where rows and columns are labelled by the representation label of the 'left' and the 'right' copy: A non–vanishing entry $m_{jj'}$ of this matrix indicates a contributing intertwiner channel (j, j'). For the fixed points the non–vanishing singular values are all equal to one, which is intwined with the triangulation independence of the corresponding three–valent models, obtained from splitting the four–valent vertices into three–valent ones [E18]. The following fixed points appear as a result of the coarse graining flow:

- *Degenerate:*
  On the degenerate fixed point, which coincides with the initial model with $J = 0$, only the trivial representation $j = 0$ is allowed.

- *Analogue BF:*
  In the topological (analogue) BF theory all 'diagonal' intertwiner channels allowed by the quantum group are excited, i.e. channels with $j' = j$. The matrix of singular values is just the identity matrix.

- *Factorizing with spin J:*
  In the factorizing model all intertwiner channels $(j, j'), j, j' \leq J$ are excited with the same singular value. In particular $j' \neq j$ is allowed. As a matrix of singular values, this model has a quadratic upper left block matrix of size $J \times J$ with all entries 1. The other entries vanish.

- *Mixed:*
  For k even and the fixed point intertwiners with maximal spin $J = \frac{k}{2}$, i.e. the maximal spin of the quantum group, the system flows to a peculiar fixed point. It is described by exciting all intertwiner channels (j, j') for which the sum $j + j'$ is even. E.g. for $k = 4$ one finds the following matrix of singular values:

$$\begin{pmatrix} 1 & 0 & 1 \\ 0 & 1 & 0 \\ 1 & 0 & 1 \end{pmatrix} \quad . \tag{6.6.13}$$

  Note that the difference in the even/odd behaviour originates from the fixed point intertwiner weights $a(j_1, j_2, j_5) = a'(j_1, j_2, j_5)$, that vanish if the sum $j_1 + j_2 + j_5$ is odd, see [E2]. This initial condition, which involves the left copy and the right copy of the model separately, results under the coarse graining flow in a non–trivial coupling condition between the left and right copy, namely that $j_1 + j_1'$ has to be even and $j_2 + j_2'$ has to be even.

  This is a fixed points of mixed type as also occurring for the $k = 8$ example in section 6.6.1. Here the 'left and right copy' of the model do not decouple completely as is the case for the factorizing fixed points.

The results are remarkable in two ways: Alone the mere existence of the additional fixed points (with respect to the degenerate and the analogue BF phase) is positive evidence that spin net models possess interesting phases. More importantly we have specified initial data in form of the fixed point intertwiners for which these models actually flow to these fixed points, thus we can state that these phases exist indeed.

At this point we would like to add a comment on the accuracy applied in our simulations. For most of our simulations we used a particular approximation: For each intertwiner channel we picked its largest singular value, namely $\mu(j, j') = 1$ for all j and j'. This truncation is suggested by the investigations in [E44] which put forward the intertwiner degrees of freedom as relevant degrees of freedom. We will name this truncation 'one–singular–value per intertwiner channel algorithm'. Note that for $k = 12$, for which $j_{max} = 6$ this already results in a necessary bond dimension

of $\chi = 49 = (6+1)^2$ (not even taken into account the large number of magnetic indices, that have been absorbed into the recoupling symbols appearing in the flow equation (6.5.18)). Thus such a truncation might be unavoidable if considering more complicated structure groups, i.e. $SU(2)_k \times SU(2)_k$.

By comparison, the full algorithm takes all singular values in all intertwiner channels and picks the largest χ ones, where χ is the fixed bond-dimension. Thus it may happen that some intertwiner channels obtain multiplicity three, whereas others do not appear at all.

In what we have presented so far, the results of both algorithms[16] are consistent, which indicates that already the 'one–singular–value per intertwiner channel' algorithm is a very well suited approximation to study the intertwiner dynamics. (Additionally it avoids the appearance of so–called non–isolated CDL fixed points [E34], which slow down the algorithm very much and are argued to not contain essential information [E59].) This confirms the 'one–singular–value per intertwiner channel' truncation, and the conjecture that the intertwiner degrees of freedom are the relevant ones, i.e. determine the large scale behaviour of the system.

As a next step it is worthwhile to study phase diagrams for these models and phase transitions between these new phases. To do so one can linearly combine the fixed point intertwiners to give new initial data and vary their respective coefficients to tune the system towards a phase transition.

6.6.2 Superposition of intertwiners

As already pointed out in (6.2.11) in section 6.2, one can additionally consider a linear combination of fixed point intertwiners as initial data. Here we will consider linear combinations of models based on the CDL fixed point intertwiners, defined in section 6.6.1, whose amplitudes are characterized by a maximal representation $J \leq j_{max}$ excited:

$$t(\{j\}, \{m\}, \{n\}) = \sum_J \alpha_J \left(\sum_{j_5, j_5'} \begin{array}{c} j_2 \quad j_1 \\ J \\ j_5 \\ J \\ j_3 \quad j_4 \end{array} \otimes \begin{array}{c} J \\ j_2\, j_1 \\ j_5' \\ j_3\, j_4 \\ J \end{array} \right) \quad , \tag{6.6.14}$$

where we have used the notation

$$\begin{array}{c} j_3 \\ J \\ j_1 \quad j_2 \end{array} := a_{CDL}^J(j_1, j_2, j_3) \, {}_q\mathcal{C}_{m_1\, m_2\, m_3}^{j_1\, j_2\, j_3} \quad , \qquad \begin{array}{c} j_2 \quad j_1 \\ J \\ j_3 \end{array} = a_{CDL}'^J(j_1, j_2, j_3) \, {}_{\bar{q}}\mathcal{C}_{m_1\, m_2\, m_3}^{j_1\, j_2\, j_3} \quad . \tag{6.6.15}$$

Also these initial tensors satisfy Reisenberger's principle, at least with respect to the 2–2 move recoupling $(j_5, j_5') \to (j_6, j_6')$. As already mentioned before, these intertwiners are not necessarily orthonormal, hence they only satisfy the projector property for particular choices of the parameters α_J. Nevertheless to plot the phase diagram we will choose the parameter α_J rather freely, we only require that $\sum_J \alpha_J = 1$.

To obtain the phase diagrams we used the 'one-singular-value per intertwiner channel' algorithm, described above. Although it is very well suited for our models, as we argued above, it is not as accurate as the full algorithm with equal or larger bond dimension. This means, e.g. that possible phase transition lines might change in position and shape if we would employ the more accurate version, however, it will not change the qualitative behaviour of the phase diagram, i.e. the phases will also exist in the full algorithm.

---

[16]We can confirm this up to bond dimension $\chi = 22$.

Phase diagram for $k = 5$

For $k = 5$, we have three fixed point intertwiners that we can linearly combine: $J = 0$, which is identical to the degenerate fixed point, $J = 1$, which flows to the factorizing model with maximal spin $J = 1$ and $J = 2$, which flows to the analogue BF fixed point. This gives us two parameters, α_0 and α_1, to tune, α_2 is fixed by the requirement that $\sum_J \alpha_J = 1$. The phase diagram is shown in figure 6.8.
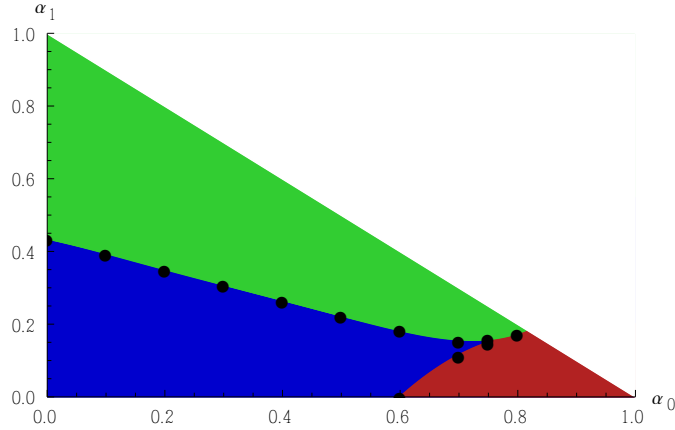

Figure 6.8: The phase diagram for $k = 5$. The red area (in the right corner of the diagram) shows the set of parameters for which the model flows to the degenerate fixed point, which is also located in the bottom right corner. For parameteres in the green area (upper corner), the system flows to the factorizing model with maximal spin $J = 1$ and the blue area (bottom left corner) covers the models that flow to the analogue BF fixed point. Note that neither the factorizing nor the BF fixed point itself can be described by the chosen parametrization.

From the phase diagram we can readily see that we find an extended phase for each fixed point associated to an (initial) fixed point intertwiner. This is an important difference to the results in [E44], where also a factorizing fixed point has been found, however no choice of initial parameters has led to a flow (for high accuracy) to this fixed point and thus it has no associated phase. The second important observation is the relative size of the phases: The two dominating phases are the factorizing and the analogue BF one whereas the degenerate one is the smallest[17]. This is an indication that the chosen fixed point intertwiners define initial models 'far away' from the degenerate fixed point. Since the degenerate phase is not of our major interest, we will thus neglect it in the next phase diagram.

Phase diagram for $k = 8$

For the quantum group with $k = 8$, we discuss the linear combintation of four fixed point intertwiners, each labelled with a maximal (even) spin $1 \leq J \leq 4$, where we neglect $J = 0$ as argued above. Together with the requirement that $\sum_J \alpha_J = 1$, we have three free parameters. In figure 6.9 we show the full parameter space, with a raster of coloured points indicating the fixed point they flow to. In figure 6.10 we show the interesting slice, where $\alpha_3 = 0$.

As in the previous diagram, we find extended phases for all fixed points, here the two factorizing fixed points for $J = 1$ and $J = 2$, a phase for analogue BF theory and one for the 'mixed' fixed point. Again, the two dominating phases are analogue BF theory and the factorizing fixed point

---

[17]As mentioned above the shape of the phases is likely to change for higher accuracy.
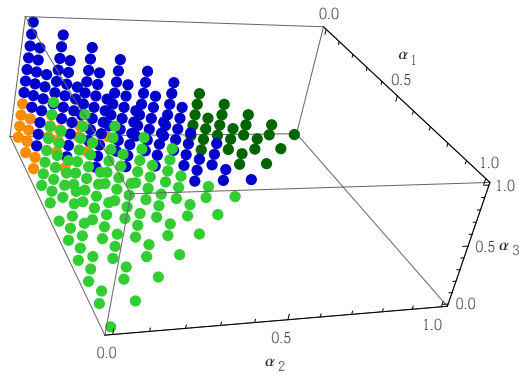
Figure 6.9: Phase diagram for $k = 8$ with $\alpha_0 = 0$. The coloured dots indicate to which fixed point the respective initial models flow to: The green dots show the factorizing models, lighter green for $J = 1$ (area that starts at the vertex $(\alpha_1, \alpha_2, \alpha_3) = (1, 0, 0)$), darker for $J = 2$ (area that starts at the vertex $(0,1,0)$). Analogue BF theory is blue (area that starts at the vertex $(0,0,1)$). The so-called 'mixed' fixed point is orange (area that starts at the vertex $(0,0,0)$).
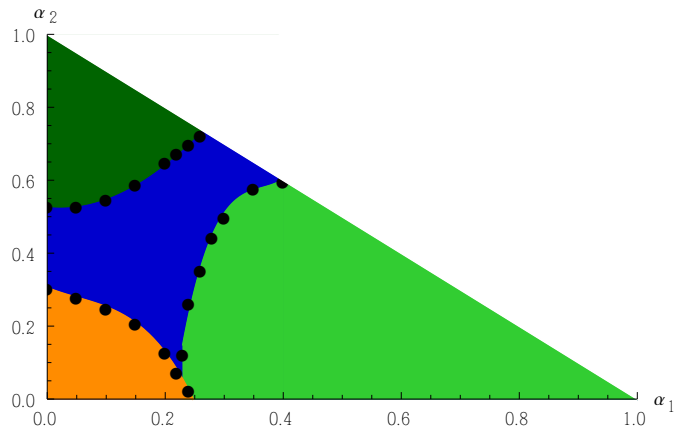
Figure 6.10: Slice of the phase diagram for $k = 8$ with $\alpha_0 = \alpha_3 = 0$. The colouring is the same as in the previous diagram, namely the right corner corresponds to models flowing to the factorizing fixed point with $J = 1$, the upper left corner corresponds to models that flow to the factorizing fixed point with $J = 2$, the models at the bottom left corner flow to the 'mixed' fixed point, and the phase in between these three phases corresponds to analogue BF.

with $J = 1$. Of particular interest is the special slice that we picked in figure 6.10 because of the following two observations: First this slice shows clearly that the analogue BF fixed point is very attractive, since in this slice its associated fixed point intertwiner is not excited, $\alpha_3 = 0$. Even if we stay on the line given by $\alpha_1 + \alpha_2 = 1$, i.e. the diagonal boundary in figure 6.10, the system flows to BF for an intermediate region between the two phases and spoils a direct phase transition between the two factorizing phases. Second we want to emphasize the 'mixed' fixed point in the bottom left corner because it is a highly non-trivial fixed point and might allow for a direct phase transition to one of the factorizing models[18].

---

[18]It might happen that the system flows to analogue BF theory for an intermediate region if the accuracy of the algorithm is increased.

Figure 6.11: To each vertical face of the considered row of cubes, we attach $\mathcal{P}^e$ to the vertical edges and δ's to the horizontal edges. These δ's contract the vertical projectors $\mathcal{P}^e$.

6.7 Spin foam interpretation of spin nets and fixed points

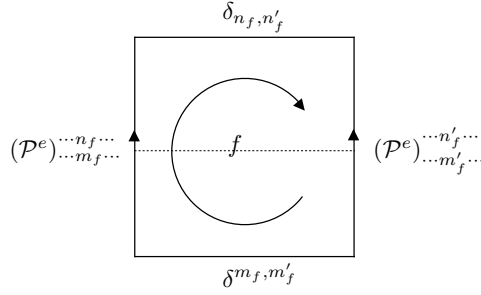As explained shortly in section 6.2 spin nets can be understood as dimensional reductions of spin foams. Here we will make this picture more concrete, which will enable us to provide an interpretation of the coarse graining flow and the fixed points in terms of spin foams.

Let us consider a 3D spin foam defined on a cubical regular lattice. We will actually just need to consider 'one slice of cubes'. In (6.2.3) we gave the partition function of a general spin foam as

$$Z = \sum_{j_f} \prod_f \tilde{\omega}_f(j_f) \prod_e (\mathcal{P}^e)^{n_{f_1} n_{f_2} n_{f_3} n_{f_4}}_{m_{f_1} m_{f_2} m_{f_3} m_{f_4}} \qquad (6.7.1)$$

where we already specialized to the case of four–valent edges. To obtain a spin net model we choose the edge intertwiners anisotropically. That is for the vertical edges we take the original $\mathcal{P}^e$ of the spin foam model. However for the horizontal edges we replace the intertwining operators with $(\mathcal{P}_{hor})^{n_1 n_2}_{m_1 m_2} = \delta_{n_1,n_2} \delta^{m_1,m_2}$. Here we consider just a two–valent intertwining operator – this can be understood as imposing $j = 0$ on all horizontal faces. Thus the magnetic indices for these horizontal faces can be omitted. Furthermore $\mathcal{P}_{hor}$ is chosen such that the contributions from different horizontal rows of cubes factorize. Then, as anticipated before, we just need to consider one row of cubes.

The contraction of indices among the vertical edge operators $\mathcal{P}^e$ proceeds as indicated in Figure 6.11. That is given a face f the δ's from the horizontal edges contract the n and m indices of this face from the two vertical edge operators $\mathcal{P}^e$. Hence we can replace the face by an edge with indices j, m, n connecting now vertices, which represent the former edges.

Thus the spin net model is given by

$$Z_{net} = \sum_{j_e} \prod_e \tilde{\omega}_e(j_e) \prod_v (\mathcal{P}^v)^{n_{e_1} n_{e_2} n_{e_3} n_{e_4}}_{m_{e_1} m_{e_2} m_{e_3} m_{e_4}} \quad , \qquad (6.7.2)$$

where the edge weights $\tilde{\omega}_e$ can be absorbed into the vertex weights $(\mathcal{P}^v)$.

In this sense we can understand a spin net as a spin foam with just two vertices and a very large number of faces, all of which have only two edges. All edges and faces share the same two vertices, which leads to a (super) melon in the sense of [E65, E66], see Figure 6.12. The fact that there are only two vertices explains why the local gauge symmetry of spin foams is converted into a global symmetry for the spin net. This is given by a left and right action of the group (on the m and on the n indices) corresponding to the two vertices.

Such melons play a crucial role in the investigation of coloured tensor models [E65, E66]. Note however that the renormalization flow considered here is quite different from the one usually considered (which rather integrates out complete melons). In this work a (super) melon with many edges
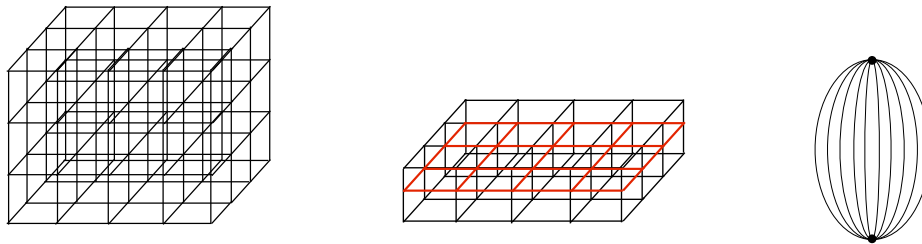
Figure 6.12: Given a spinfoam model defined in the cubic lattice, for the corresponding spin net model we just need to consider one row of cubes. The spin net model is then defined on the 1-dimensional reduction of the row of cubes, namely the square lattice, here distinguished by thick red lines. We can understand this reduction as making all the horizontal edges of the spinfoam belonging to the same slice to collapse in a single vertex. For the slice of cubes we then get two vertices linked by all the vertical edges, like the super melon spinfoam of the right.

is coarse grained into another melon with fewer (effective) edges. For the spin net this corresponds to blocking a number of vertices into effective vertices.

We can therefore interpret spin net coarse graining as a highly anisotropic way of coarse graining (anisotropic) spin foams. (In this case the analogue BF phase is indeed the BF phase for spin foams.) It focusses on the change of coupling between two spin foam vertices with the coarse graining flow. Following this interpretation, we see that the models that flow to factorizing fixed points lead in the spin foam interpretation to a factorization of vertex amplitudes. That is the contribution of the two vertices decouples into two parts associated to the upper and lower vertex of the super melon. That is gluing two spin foam vertices with many edges and blocking these into effective edges, we actually end up with two decoupled vertices, that is the melon is cut into two halves.

The decoupling of vertices is certainly a possible scenario of spin foams, of course not a very attractive one. It will be interesting to see whether this also occurs for Barrett–Crane like models with $SU(2)_k \times SU(2)_k$ structure group. For these models concerns have been voiced, that neighbouring tetrahedra are not sufficiently glued with each other, see the discussion in [E5–E8, E67–E71].

Of course we cannot be certain whether the corresponding spin foam models will really flow to the corresponding factorizing fixed points, as we are considering a very anisotropic situation. Here an investigation at least into 3D spin foams seems to be in reach employing a coarse graining algorithm proposed in [E26, E27], which has been already tested for Abelian models [E72]. Alternatively it may be possible to devise a coarse graining scheme in which the coarse graining in equatorial direction of the melons, and integrating out entire melons, alternate.

From the spin foam point of view the 'mixed fixed points' seems to be particular interesting and encouraging, as here the vertices do not decouple. It has to be investigated whether these (spin net) fixed points give also triangulation invariant spin foam models.

Such mixed fixed points seem to result from a subtle interplay between the two different sources of the spin foam models: On the one hand spin foams can be understood as generalized lattice gauge theories. However, as noticed in [E44], the phases of standard lattice gauge theory seem to be dominating. The BF phase can be understood as leading to a maximal gluing between the 'two spin foam vertices' in the spin net model. Simplicity constraints indeed weaken this gluing (alone by restricting the sum over intertwiner degrees of freedom) and allow to flow out of the standard lattice gauge theory phases. However if this effect is too strong the two spin foam vertices (in the spin net model) decouple. In this sense the mixed fixed point represents a balance between these two effects.

We think that it will be very worthwhile to push and test such an interpretation, as it could reveal the effect that the imposition of simplicity constraints has on the large scale limit of spin foams and in this way possibly resolve the question whether these have to imposed more strongly or not, see for instance [E5–E8, E67–E71].

6.8 Discussion

In this work we have taken several important steps towards a full understanding of the continuum limit of spin foam models. We in particular introduced and defined models based on the structure group $SU(2)_k$ that can encode the dynamics of the full gravitational models, but are still feasible to investigate numerically. Note that apart from certain technical subtleties (e.g. the definition of the duals) for the quantum group coarse graining, that we resolved, this nevertheless requires very efficient numerical algorithms[19]. For this the symmetry protected tensor network algorithm developed here and in [E44] is absolutely crucial.

We considered mainly spin nets, as dimensional reductions of spin foams, in this work. However, we point out that the spin net coarse graining flow is equivalent to a coarse graining flow of spin foam melons into spin foam melons. It particular focusses on the coupling of (two) spin foam vertices with each other – which is of course crucial to understand the macroscopic behaviour of spin foams. Indeed it allows us to describe the properties of the fixed points found via coarse graining in terms of this coupling. Note that this question cannot even be considered if one performs coarse graining only by $5 - 1$ Pachner moves [E28, E29, E32].

The coarse graining of the spin net models is encoded in a flow equation (6.5.18), which describes the behaviour of the intertwiner degrees of freedom. We believe that spin foam coarse graining (including non–melonic spin foams of course) will lead to quite similar coarse graining equations. Thus one might speculate whether the phases we find are already the ones one will encounter for spin foam models.

The coarse graining flow equation describes that the effective intertwiner degrees of freedom are obtained from the old intertwiner degrees of freedom basically by two operations: the first is a contraction of the tensors encoding the intertwiners, the second is a convolution with recoupling symbols. This convolution leads to a non–trivial flow of intertwiner degrees of freedom, i.e. intertwiner channels which are not excited initially, can become excited by the coarse graining flow. This is again not the case, if considering coarse graining via $5 - 1$ Pachner moves only [E32].

Here again two effects seem to compete with each other: without simplicity constraints, i.e. models described by the Haar intertwiner where we have a restriction to $j_5 = j_5'$, the recoupling symbols appearing in the flow equation, contract with each other (approximately) to a Kronecker Delta. In this case one can indeed approximate the flow by a Migdal Kadanoff recursion [E73–E75], see also [E26, E27], where recoupling symbols do not appear. The flow is (approximately) restricted to the phase space where the spins of left and right copy agree, i.e. $j_5 = j_5'$ throughout the coarse graining. In the case of BF fixed points it leads to a gluing/coupling of the (two) spin foam vertices. This however only allows to reach the degenerate fixed point or a BF theory, either of the full structure group or of a normal subgroup (in the case that one actually deals with a proper group).

Simplicity constraints, which lead to components with $j_5 \neq j_5'$ in the tensor $\hat{t}_1$, do change this picture in an essential way: now the convolution with the recoupling symbols appearing in the flow equation (6.5.18) becomes crucial and leads to a large set of additional fixed points. Indeed an

---

[19]Even the one–singular value algorithm leads to a bond dimension of e.g. $\chi = 49$ for $k = 12$. The tensors we are employing have five such indices, which run from 1 to 49. Thus already for saving these tensors one needs to employ an efficient scheme, not speaking off contracting indices of several such tensors. A technique we developed for this work are 'super indices' which allow to save and deal only with entries not–vanishing as given by the coupling rules. This leads already to a huge reduction of components from $(49)^5$ to $(2359)^2$.

open issue is the understanding of all possible fixed points, which might be possible with techniques developed in [E2, E45] which allows already the understanding of all factorizing fixed points.

As we have seen for a number of examples the flow can now lead to factorizing fixed points, where the copy labelled by j indices and the copy labelled by j' indices decouple. In terms of (melonic) spin foams this means a decoupling of the two spin foam vertices involved. For reasons discussed below it would be interesting to see whether such a decoupling appears in the Barrett Crane model [E49] with a quantum group [E76].

However we have also examples which flow to so–called mixed fixed points, in which both a coupling between the two spin foam vertices persists and nevertheless simplicity constraints persists. It will therefore be very interesting to investigate these fixed points further and in particular study whether these can be lifted to fixed points for (non–melonic) spin foam models. Furthermore a full classification of these fixed points, along the lines of [E2, E45], would reveal further possible phases for spin nets and spin foams.

Both cases constitute non–trivial possible phases for spin nets and for spin foams (at least the factorizing models lead to phases for spin foams as all vertices decouple). As discussed in section 6.7 a decoupling of spin foam vertices might indeed be related to concerns that tetrahedra are not properly glued to each other, e.g. in the Barrett Crane model [E5–E8, E67–E71]. It would therefore help and potentially resolve the discussions on the correct way to impose simplicity constraints, to study coarse graining for other geometric configurations. Starting from a coarse graining of melons, it might be possible to alternate the coarse graining considered here – in equatorial direction of the melon – with a coarse graining in vertical direction. This might already lead to a less anisotropic coarse graining, which takes also the blocking of spin foam vertices (and not only edges as happens for the melonic flow considered here) into account.

Apart from the identification of possible phases for spin foams we can draw another important lesson from the work here, in particular compared to [E44]. This is related to the introduction of a new parametrization of the space of models, based on Reisenberger's construction principle and fixed point intertwiners [E2, E45]. We have argued that this parametrization makes it much easier to satisfy the projector property, which guarantees invariance under edge subdivisions in spin foams.

Indeed the picture that this parametrization gives is quite different from the one based on E–functions in [E44], in which the projector property is quite complicated to implement [E46]. The parametrization in [E44] requires a fine tuning between the degenerate and BF phase, to flow to a non–trivial (actually factorizing) model. This is not the case for the fixed point intertwiner based parametrization, which leads to a rich spectrum of non–trivial fixed points, of both factorizing and non–factorizing type. We conjecture that this is due to the projector property, which itself can be interpreted as a very weak imposition of diffeomorphism symmetry [E50–E52]. The fine tuning in [E44] can thus be understood as satisfying this weak requirement of diffeomorphism invariance, as already argued in [E44]. The results here therefore stresses the importance of this concept [E19–E24, E77].

Interestingly the phase diagrams, obtained by considering linear combinations of fixed point intertwiners, support this conclusion even more. Non–trivial fixed points appear in particular around the fixed point intertwiners itself. In the intermediate regions the models flow typically to the BF fixed point. Although there seem to occur phase transition between non–trivial phases, e.g. in figure 6.10, this might disappear if a higher accuracy is employed: It might happen, that all non–trivial phases are separated by models flowing to the BF fixed point. We leave the falsification or verification of this picture for future work.

Apart from the open questions mentioned so far there are numerous other directions for further work, some of which we outline here:

- Given the results we have found here, i.e. that fixed point intertwiner models flow to interesting fixed points, it would be of high interest to classify such fixed points for intertwiner

models, for $SU(2)_k \times SU(2)_k$, as is performed in [E2, E45] for $SU(2)_k$. The Barrett–Crane model constitutes one such fixed point, the question is, whether a Barbero–Immirzi parameter, as appearing in the EPRL, FK and BO models[20] [E5–E8] can be accommodated by such a fixed point.

- Further approximations and therefore simplifications of the flow equation (6.5.18) will be useful to allow the treatment of $SU(2)_k \times SU(2)_k$ and similar structure groups.

- Coarse graining involving non–melonic spin foams should be developed along the lines of spin net coarse graining. As is discussed in [E18] the tensor network algorithm might be adaptable to the case of spin foams in a more straightforward way then envisaged in [E26, E27], which presented a tensor network formulation of spin foams.

- It would be interesting to investigate in further detail the phase transitions. Indeed one would expect that an interacting theory, such as 4D gravity, can only occur there. Here the first question is, whether the models along the phase transition carry 'only' conformal symmetry, or lead to a fully (cylindrically) consistent continuum limit as outlined in [E17, E18]. As is argued in [E18] such a cylindrically consistent continuum limit is deeply entangled with the restoration of diffeomorphism symmetry, which is typically broken by the discretization itself [E19–E24]. From a more tensor network renormalization point of view [E34, E75] discusses the investigation of fixed point tensors at critical fixed points and the extraction of critical exponents.

In summary, we hope to have convinced the reader, that the tensor network coarse graining methods [E33, E34] and the many refinements thereof developed here and in [E26, E27, E44], together with the conceptual understanding of how to construct the continuum limit in [E17, E18], put the understanding of the possible phases of spin foam models within the very near future.

Acknowledgements

6.A Additional diagrammatic calculations

6.A.1 Normalization of Haar projector

The Haar projector $\mathcal{P}$ reads

$$\mathcal{P}_{(\{m\},\{m'\})}(j_1, j_2, j_3, j_4) := \sum_{j_5} c(j_5) \quad \text{[diagram]} \quad \otimes \quad \text{[diagram]} \quad , \qquad (6.A.1)$$

---

[20]i.e. Engle-Pereira-Rovelli-Livine, Freidel-Krasnov and Baratin-Oriti models.

where $c(j_5)$ is the normalization constant that we want to determine. For $\mathcal{P}$ to be a projector, it has to satisfy the relation $\mathcal{P}^2 = \mathcal{P}$, namely

$$\mathcal{P} \cdot \mathcal{P} = \sum_{j_5, j_5'} c(j_5)\, c(j_5') \quad \underset{(-1)^{j_1+j_2+j_3+j_4}\left(d_{j_5}\right)^{-1}\delta_{j_5 j_5'}}{\underbrace{\qquad\qquad\qquad\qquad}} \otimes \quad \overset{!}{=} \mathcal{P} \quad . \qquad (6.A.2)$$

We therefore deduce that

$$c(j_5) = (-1)^{j_1+j_2+j_3+j_4} d_{j_5} \quad , \qquad (6.A.3)$$

as we wanted to proof.

6.A.2 Relation between the two different recoupling schemes

We are looking for the relation

$$\quad = \sum_{j_5} c(j_5, j_6) \quad . \qquad (6.A.4)$$

In order to find the coefficient $c(j_5, j_6)$ we contract the above expression with the diagram (6.4.4):

$$\quad = \sum_{j_5} c(j_5, j_6) \quad \qquad (6.A.5)$$

The evaluation of both sides of this equation gives

$$(-1)^{j_1+j_2+j_3+j_4} \left(d_{j_5} d_{j_6}\right)^{-\frac{1}{2}} \begin{bmatrix} j_1 & j_2 & j_5' \\ j_3 & j_4 & j_6 \end{bmatrix} = (-1)^{j_1+j_2+j_3+j_4} \sum_{j_5} c(j_5, j_6) \left(d_{j_5}\right)^{-1} \delta_{j_5, j_5'} \quad , \qquad (6.A.6)$$

from which we deduce

$$\quad = \sum_{j_5} \sqrt{\frac{d_{j_5}}{d_{j_6}}} \begin{bmatrix} j_1 & j_2 & j_5' \\ j_3 & j_4 & j_6 \end{bmatrix} \quad . \qquad (6.A.7)$$

6.A.3 Splitting of the $9j$-symbol into two $6j$-symbols

Let us prove the equality (6.5.17). By using the identities

$$j_2 \quad \left| \quad \right|_{j_4} = \quad (-1)^{j_2+j_4-j_9} d_{j_9} \quad , \qquad = \quad \frac{(-1)^{2j_9}}{d_{j_9}} \quad , \qquad (6.A.8)$$

we can manipulate the $9j$-symbol in the following fashion,

$$
\ldots = (-1)^{j_2+j_4-j_9} d_{j_9} \ldots \Bigg| j_9 = (-1)^{j_2+j_4-j_9} \ldots \quad . \quad (6.A.9)
$$

The diagrams of the right are the $6j$-symbols defined in Eq. (6.3.17), and then we get

$$
\ldots = (-1)^{j_2+j_4+j_9} \left\{ \begin{matrix} j_2 & j_4 & j_9 \\ j_5 & j_6 & j_1 \end{matrix} \right\} \left\{ \begin{matrix} j_2 & j_4 & j_9 \\ j_8 & j_7 & j_3 \end{matrix} \right\}
$$

$$
= \frac{(-1)^{j_2+j_4+j_9}(-1)^{j_5+j_6+j_7+j_8}}{d_{j_9}\sqrt{d_{j_1}d_{j_3}}} \begin{bmatrix} j_2 & j_4 & j_9 \\ j_5 & j_6 & j_1 \end{bmatrix} \begin{bmatrix} j_2 & j_4 & j_9 \\ j_8 & j_7 & j_3 \end{bmatrix} \quad , \quad (6.A.10)
$$

as we wanted to proof.

References

[E1] M. P. Reisenberger, "On relativistic spin network vertices," *J.Math.Phys.* **40** (1999) 2046–2054, `arXiv:gr-qc/9809067 [gr-qc]`.

[E2] B. Dittrich and W. Kaminski, "Topological lattice field theories from intertwiner dynamics," `arXiv:1311.1798 [gr-qc]`.

[E3] A. Perez, "The Spin Foam Approach to Quantum Gravity," *Living Rev.Rel.* **16** (2013) 3, `arXiv:1205.2019 [gr-qc]`.

[E4] C. Rovelli, *Quantum gravity.* Cambridge University Press, Cambridge, 2004.

[E5] J. Engle, E. Livine, R. Pereira, and C. Rovelli, "LQG vertex with finite Immirzi parameter," *Nucl. Phys. B* **799** (2008) 136–149, `arXiv:0711.0146 [gr-qc]`.

[E6] E. R. Livine and S. Speziale, "A New spinfoam vertex for quantum gravity," *Phys. Rev. D* **76** (2007) 084028, `arXiv:0705.0674 [gr-qc]`.

[E7] L. Freidel and K. Krasnov, "A New Spin Foam Model for 4d Gravity," *Class. Quant. Grav.* **25** (2008) 125018, `arXiv:0708.1595 [gr-qc]`.

[E8] A. Baratin and D. Oriti, "Quantum simplicial geometry in the group field theory formalism: reconsidering the Barrett-Crane model," *New J. Phys.* **13** (2011) 125011, `arXiv:1108.1178 [gr-qc]`.

[E9] L. Freidel and D. Louapre, "Diffeomorphisms and spin foam models," *Nucl.Phys.* **B662** (2003) 279–298, `arXiv:gr-qc/0212001 [gr-qc]`.

[E10] C. Perini, C. Rovelli, and S. Speziale, "Self-energy and vertex radiative corrections in LQG," *Phys.Lett.* **B682** (2009) 78–84, `arXiv:0810.1714 [gr-qc]`.

[E11] V. Bonzom and M. Smerlak, "Bubble divergences from cellular cohomology," *Lett.Math.Phys.* **93** (2010) 295–305, `arXiv:1004.5196 [gr-qc]`.

[E12] A. Riello, "Self-energy of the Lorentzian Engle-Pereira-Rovelli-Livine and Freidel-Krasnov model of quantum gravity," *Phys.Rev.* **D88** no. 2, (2013) 024011, `arXiv:1302.1781 [gr-qc]`.

[E13] V. Bonzom and B. Dittrich, "Bubble divergences and gauge symmetries in spin foams," *Phys.Rev.* **D88** (2013) 124021, `arXiv:1304.6632 [gr-qc]`.

[E14] F. Markopoulou, "An Algebraic approach to coarse graining," `arXiv:hep-th/0006199 [hep-th]`.

[E15] R. Oeckl, "Renormalization of discrete models without background," *Nucl.Phys.* **B657** (2003) 107–138, `arXiv:gr-qc/0212047 [gr-qc]`.

[E16] J. A. Zapata, "Loop quantization from a lattice gauge theory perspective," *Class.Quant.Grav.* **21** (2004) L115–L122, `arXiv:gr-qc/0401109 [gr-qc]`.

[E17] B. Dittrich, "From the discrete to the continuous: Towards a cylindrically consistent dynamics," *New J. Phys.* **14** (2012) 123004, `arXiv:1205.6127 [gr-qc]`.

[E18] B. Dittrich and S. Steinhaus, "Time evolution as refining, coarse graining and entangling," *New J. Phys.* **16** (2014) 123041, `arXiv:1311.7565 [gr-qc]`.

[E19] B. Dittrich, "Diffeomorphism symmetry in quantum gravity models," *Adv. Sci. Lett.* **2** (2009) 151, `arXiv:0810.3594 [gr-qc]`.

[E20] B. Bahr and B. Dittrich, "(Broken) Gauge Symmetries and Constraints in Regge Calculus," *Class. Quant. Grav.* **26** (2009) 225011, `arXiv:0905.1670 [gr-qc]`.

[E21] B. Bahr and B. Dittrich, "Improved and Perfect Actions in Discrete Gravity," *Phys. Rev. D* **80** (2009) 124030, `arXiv:0907.4323 [gr-qc]`.

[E22] B. Bahr and B. Dittrich, "Breaking and restoring of diffeomorphism symmetry in discrete gravity," *AIP Conf. Proc.* **1196** (2009) 10–17, `arXiv:0909.5688 [gr-qc]`.

[E23] B. Bahr, B. Dittrich, and S. Steinhaus, "Perfect discretization of reparametrization invariant path integrals," *Phys. Rev. D* **83** (2011) 105026, `arXiv:1101.4775 [gr-qc]`.

[E24] B. Dittrich, "How to construct diffeomorphism symmetry on the lattice," *PoS* **QGQGS2011** (2011) 012, `arXiv:1201.3840 [gr-qc]`.

[E25] B. Bahr, B. Dittrich, and J. P. Ryan, "Spin foam models with finite groups," *J. Grav.* **2013** (2013) 549824, `arXiv:1103.6264 [gr-qc]`.

[E26] B. Dittrich, F. C. Eckert, and M. Martin-Benito, "Coarse graining methods for spin net and spin foam models," *New J. Phys.* **14** (2012) 035008, `arXiv:1109.4927 [gr-qc]`.

[E27] B. Dittrich and F. C. Eckert, "Towards computational insights into the large-scale structure of spin foams," *J. Phys. Conf. Ser.* **360** (2012) 012004, `arXiv:1111.0967 [gr-qc]`.

[E28] B. Bahr, B. Dittrich, F. Hellmann, and W. Kaminski, "Holonomy Spin Foam Models: Definition and Coarse Graining," *Phys. Rev. D* **87** (2013) Phys.Rev. D87 (2013) 044048, `arXiv:1208.3388 [gr-qc]`.

[E29] B. Dittrich, F. Hellmann, and W. Kaminski, "Holonomy Spin Foam Models: Boundary Hilbert spaces and Time Evolution Operators," *Class. Quant. Grav.* **30** (2013) 085005, `arXiv:1209.4539 [gr-qc]`.

[E30] B. Bahr, B. Dittrich, and S. He, "Coarse graining free theories with gauge symmetries: the linearized case," *New J. Phys.* **13** (2011) 045009, `arXiv:1011.3667 [gr-qc]`.

[E31] P. A. Morse, "Approximate diffeomorphism invariance in near-flat simplicial geometries," *Class. Quant. Grav.* **9** (1992) 2489.

[E32] B. Bahr and B. Dittrich unpublished, 2012.

[E33] M. Levin and C. P. Nave, "Tensor renormalization group approach to 2d classical lattice models," *Phys. Rev. Lett.* **99** (2007) 120601, `arXiv:cond-mat/0611687 [cond-mat]`.

[E34] Z.-C. Gu and X.-G. Wen, "Tensor-Entanglement-Filtering Renormalization Approach and Symmetry Protected Topological Order," *Phys. Rev. B* **80** (2009) 155131, `arXiv:0903.1069 [cond-mat.str-el]`.

[E35] L. Smolin, "Linking topological quantum field theory and nonperturbative quantum gravity," *J.Math.Phys.* **36** (1995) 6417–6455, `arXiv:gr-qc/9505028 [gr-qc]`.

[E36] S. Major and L. Smolin, "Quantum deformation of quantum gravity," *Nucl.Phys.* **B473** (1996) 267–290, `arXiv:gr-qc/9512020 [gr-qc]`.

[E37] R. Borissov, S. Major, and L. Smolin, "The Geometry of quantum spin networks," *Class.Quant.Grav.* **13** (1996) 3183–3196, `arXiv:gr-qc/9512043 [gr-qc]`.

[E38] K. Noui and P. Roche, "Cosmological deformation of Lorentzian spin foam models," *Class.Quant.Grav.* **20** (2003) 3175–3214, `arXiv:gr-qc/0211109 [gr-qc]`.

[E39] W. J. Fairbairn and C. Meusburger, "Quantum deformation of two four-dimensional spin foam models," *J.Math.Phys.* **53** (2012) 022501, `arXiv:1012.4784 [gr-qc]`.

[E40] M. Han, "4-dimensional Spin-foam Model with Quantum Lorentz Group," *J.Math.Phys.* **52** (2011) 072501, `arXiv:1012.4216 [gr-qc]`.

[E41] M. Dupuis and F. Girelli, "Quantum hyperbolic geometry in loop quantum gravity with cosmological constant," *Phys.Rev.* **D87** no. 12, (2013) 121502, `arXiv:1307.5461 [gr-qc]`.

[E42] M. Dupuis and F. Girelli, "Observables in Loop Quantum Gravity with a cosmological constant," *Phys.Rev.* **D90** (2014) 104037, `arXiv:1311.6841 [gr-qc]`.

[E43] J. Hnybida private communication.

[E44] B. Dittrich, M. Martín-Benito, and E. Schnetter, "Coarse graining of spin net models: dynamics of intertwiners," *New J. Phys.* **15** (2013) 103004, `arXiv:1306.2987 [gr-qc]`.

[E45] B. Dittrich and W. Kaminski, "Ground states in fusion categories,". in preparation.

[E46] W. Kaminski, M. Kisielowski, and J. Lewandowski, "The EPRL intertwiners and corrected partition function," *Class.Quant.Grav.* **27** (2010) 165020, `arXiv:0912.0540 [gr-qc]`.

[E47] W. Kaminski, M. Kisielowski, and J. Lewandowski, "Spin-Foams for All Loop Quantum Gravity," *Class.Quant.Grav.* **27** (2010) 095006, `arXiv:0909.0939 [gr-qc]`.

[E48] B. Bahr, F. Hellmann, W. Kaminski, M. Kisielowski, and J. Lewandowski, "Operator Spin Foam Models," *Class.Quant.Grav.* **28** (2011) 105003, `arXiv:1010.4787 [gr-qc]`.

[E49] J. W. Barrett and L. Crane, "Relativistic spin networks and quantum gravity," *J. Math. Phys.* **39** (1998) 3296–3302, `gr-qc/9709028`.

[E50] M. Bojowald and A. Perez, "Spin foam quantization and anomalies," *Gen.Rel.Grav.* **42** (2010) 877–907, `arXiv:gr-qc/0303026 [gr-qc]`.

[E51] B. Bahr, "On knottings in the physical Hilbert space of LQG as given by the EPRL model," *Class.Quant.Grav.* **28** (2011) 045002, `arXiv:1006.0700 [gr-qc]`.

[E52] B. Dittrich and S. Steinhaus, "Path integral measure and triangulation independence in discrete gravity," *Phys.Rev.* **D85** (2012) 044032, `arXiv:1110.6866 [gr-qc]`.

[E53] X. Chen, Z.-C. Gu, and X.-G. Wen, "Classification of Gapped Symmetric Phases in 1D Spin Systems," *Phys. Rev. B* **83** (2011) 035107, `arXiv:1008.3745 [cond-mat.str-el]`.

[E54] N. Schuch, I. Cirac, and D. Perez-Garcia, "PEPS as ground states: degeneracy and topology," *Annals of Physics* **325** (2010) 2153, `arXiv:1001.3807 [quant-ph]`.

[E55] N. Schuch, D. Perez-Garcia, and I. Cirac, "Classifying quantum phases using matrix product states and PEPS," *Phys. Rev. B* **84** (2011) 165139, `arXiv:1010.3732 [cond-mat.str-el]`.

[E56] L. C. Biedenharn and M. A. Lohe, *Quantum Group Symmetries and q-Tensor Algebras.* World Scientific, Singapore, 1995.

[E57] J. S. Carter, D. E. Flath, and M. Saito, *The Classical and Quantum 6j–symbols.* Princeton University Press, Princeton, 1995.

[E58] M. Levin. `https://www.ipam.ucla.edu/publications/tqc2007/tqc20076595.ppt`, 2007.

[E59] A. J. Ferris, "The area law and real-space renormalization," *Phys. Rev. B* **87** (2013) 125139, `arXiv:1301.2608 [cond-mat.str-el]`.

[E60] G. Vidal, "Entanglement Renormalization," *Phys. Rev. Lett.* **99** (2007) 220405, `arXiv:cond-mat/0512165 [cond-mat]`.

[E61] R. N. C. Pfeifer, P. Corboz, O. Buerschaper, M. Aguado, M. Troyer, and G. Vidal, "Simulation of anyons with tensor network algorithms," *Phys. Rev. B* **82** (2010) 115126, `arXiv:1006.3532 [cond-mat.str-el]`.

[E62] S. Singh and G. Vidal, "Tensor network states and algorithms in the presence of a global SU(2) symmetry," *Phys.Rev.* **B86** (2012) 195114, `arXiv:1208.3919 [cond-mat.str-el]`.

[E63] G. Ponzano and T. Regge, *Semiclassical limit of Racah coefficients, in: Spectroscopy and group theoretical methods in physics.* North Holland Publ. Co., Amsterdam, 1968.

[E64] V. Turaev and O. Viro, "State sum invariants of 3 manifolds and quantum 6j symbols," *Topology* **31** (1992) 865–902.

[E65] V. Bonzom, R. Gurau, A. Riello, and V. Rivasseau, "Critical behavior of colored tensor models in the large N limit," *Nucl. Phys. B* **853** (2011) 174–195, `arXiv:1105.3122 [hep-th]`.

[E66] A. Baratin, S. Carrozza, D. Oriti, J. Ryan, and M. Smerlak, "Melonic phase transition in group field theory," *Lett.Math.Phys.* **104** (2014) 1003–1017, `arXiv:1307.5026 [hep-th]`.

[E67] B. Dittrich and J. P. Ryan, "Phase space descriptions for simplicial 4d geometries," *Class. Quant. Grav.* **28** (2011) 065006, `arXiv:0807.2806 [gr-qc]`.

[E68] B. Dittrich and J. P. Ryan, "Simplicity in simplicial phase space," *Phys.Rev.* **D82** (2010) 064026, `arXiv:1006.4295 [gr-qc]`.

[E69] B. Dittrich and J. P. Ryan, "On the role of the Barbero-Immirzi parameter in discrete quantum gravity," *Class.Quant.Grav.* **30** (2013) 095015, `arXiv:1209.4892 [gr-qc]`.

[E70] S. Alexandrov, M. Geiller, and K. Noui, "Spin Foams and Canonical Quantization," *SIGMA* **8** (2012) 055, `arXiv:1112.1961 [gr-qc]`.

[E71] M. Geiller and K. Noui, "Testing the imposition of the Spin Foam Simplicity Constraints," *Class.Quant.Grav.* **29** (2012) 135008, `arXiv:1112.1965 [gr-qc]`.

[E72] B. Dittrich and S. Steinhaus. w.i.p.

[E73] A. A. Migdal, "Recursion Equations in Gauge Theories," *Sov.Phys.JETP* **42** (1975) 413.

[E74] L. Kadanoff, "Notes on Migdal's Recursion Formulas," *Annals Phys.* **100** (1976) 359–394.

[E75] E. Efrati, Z. Wang, A. Kolan, and L. P. Kadanoff, "Real Space Renormalization in Statistical Mechanics," *Rev. Mod. Phys.* **86** (2014) 647, `arXiv:1301.6323 [cond-mat.stat-mech]`.

[E76] I. Khavkine and J. D. Christensen, "q-Deformed spin foam models of quantum gravity," *Class.Quant.Grav.* **24** (2007) 3271–3290, `arXiv:0704.0278 [gr-qc]`.

[E77] C. Rovelli, "Discretizing parametrized systems: The M agic of Ditt-invariance," `arXiv:1107.2310 [hep-lat]`.

7 Time evolution as refining, coarse graining and entangling

Bianca Dittrich and Sebastian Steinhaus

Perimeter Institute for Theoretical Physics,
31 Caroline Street North, Waterloo, Ontario, Canada N2L 2Y5

Abstract

We argue that refining, coarse graining and entangling operators can be obtained from time evolution operators. This applies in particular to geometric theories, such as spin foams. We point out that this provides a construction principle for the physical vacuum in quantum gravity theories and more generally allows to construct a (cylindrically) consistent continuum limit of the theory.

7.1 Introduction

Renormalization and coarse graining have become powerful tools to connect microscopic and macroscopic regimes of a given theory. In particular many approaches to quantum gravity postulate or aim to derive macroscopic space time as arising from the collective dynamics of basic building blocks [F1–F5]. To validate such a picture one has to show that the many body dynamics of such systems gives indeed a smooth space time if sufficiently coarse grained.

To this end coarse graining techniques [F6] need to be employed. The question of how to coarse grain or block fine degrees of freedom into coarser ones is essential for determining good truncations for the coarse graining schemes. Coarse graining maps are dual to refining maps, in fact tensor network renormalization schemes [F7, F8] put the emphasis rather on refining maps, that then also determine the properties of the truncation in these schemes [F9].

In this document we point out that time evolution maps, which appear in simplicial discretizations [F10, F11], can also be interpreted as refining and coarse graining maps. As we will argue here this applies in particular to gravitational dynamics, e.g. spin foams [F12–F20].

One reason why the appearance of time evolution as coarse graining or refining maps applies in particular to gravitational or other diffeomorphism invariant systems is the following: As argued in [F21–F27] diffeomorphism symmetry in discrete systems translates to a symmetry, which can be interpreted as moving vertices in the discrete space time described by the dynamical variables of the theory. These vertex translations can also be understood as time evolution. Now, vertices can be even moved on top of each other, which gives a coarse graining of the underlying state. Alternatively vertices can split into two and in this way give a refinement. Indeed this argument was used in [F27] to show that diffeomorphism symmetry implies discretization independence.

More generally diffeomorphism invariant systems are totally constrained, i.e. the Hamiltonian is given by a combination of constraints. In the case of a totally constrained system the time evolution operator should be a projection operator [F28–F30], projecting onto so–called physical states. Thus physical states should not evolve.[1]

For discrete time evolutions that change the number of degrees of freedom, this leads to the puzzle of how to identify states from Hilbert spaces of 'different size'.[2] We will argue that such states describe indeed the same physical state, however expressed on two different discretizations. The equivalence relation is provided by the refining time evolution operator. We will explain how this notion can be formalized into the construction of an inductive limit Hilbert space. Such an inductive limit construction is also used for the (kinematical) Hilbert space of loop quantum gravity [F35–F37].

The inductive limit Hilbert spaces, which are defined via an equivalence relation between states from Hilbert spaces based on different discretizations, require however (so called cylindrical) consistency conditions: physical observables should not depend on which representative they have been determined on. Indeed we will connect these consistency conditions with a notion of path independence for (refining) time evolution. This relates then to the requirement of diffeomorphism invariance.

Discrete (non–topological) theories typically break the diffeomorphism symmetry [F25, F26]. The hope however is that diffeomorphism symmetry can be recovered in the continuum limit. We will explain how to formulate the continuum limit of the dynamics of a given quantum gravity theory

---

[1] Introducing relational observables, a notion of relational time evolution can be reconstructed [F31–F34]. In this paper we mean with time evolution always evolution with respect to (unphysical) coordinate time, which just acts as gauge transformation and hence acts as an identity on physical states.

[2] This assumes finite dimensional Hilbert spaces. Even for infinite dimensional Hilbert spaces we can make 'size' more precise: In a discrete dynamics, Hilbert spaces carrying the degrees of freedom, are associated to sites, edges or other geometrical objects. The Hilbert space describing the states at a given time is then (typically) given as a tensor product of these basic Hilbert spaces. 'Size' then refers to the complexity of the underlying discretization, that is the number of sites, edges etc.

and how such a continuum limit can be constructed by an iterative coarse graining procedure akin to tensor network renormalization schemes.

Topological theories can be often discretized without breaking diffeomorphism symmetry. In this case refining time evolution maps indeed satisfy the consistency conditions. We point out that this provides a construction principle for inductive limit Hilbert spaces, that can for instance be applied to find new quantum representations for loop quantum gravity [F38].

The idea that time evolution can be interpreted as coarse graining, refining or entangling occurs in many approaches. Tensor network coarse graining algorithms can be easily seen as time evolution in radial direction (in an Euclidean space time), which itself leads to holographic renormalization [F39]. Entanglement renormalization [F40], which is also based on tensor network techniques, can be interpreted in a space time picture, again involving holographic renormalization, see for instance [F41–F43]. Here the tensor network and the entanglement it encodes are interpreted as a (background) AdS space time. Although such geometrical interpretations appear very naturally, the interpretation of the underlying geometry as a background geometry might not apply straightforwardly to gravity. The reason is that the dynamical variables include the geometric degrees of freedom. Hence the geometry is encoded in the boundary state itself, and has to be extracted from it.

A main point of this paper is to bring together coarse graining tools developed in condensed matter with methods developed in loop quantum gravity and to point out the many peculiarities that arise if one considers totally constrained systems such as general relativity. This leads to our proposal of how to construct the continuum limit of a given quantum gravity theory, together with a notion of a physical vacuum state. Furthermore we point out a general construction principle for inductive limit Hilbert spaces based on time evolution maps of topological theories.

7.1.1 Overview

In this paper we will employ a generalized meaning of time evolution, which will be explained in sections 7.2 and 7.3.2. The first generalization applies in particular to discretized field theories, where we allow for a time evolution, which changes the number of variables, that is phase space or Hilbert space dimension, from one time step to the next. The second issue we will discuss, is the meaning of time evolution in a totally constrained system, such as general relativity.

Usually one considers a discretization that does not change in time, and thus the number of degrees of freedom stays also constant. However, for theories involving a curved background, or gravity as a dynamical theory, one often uses an irregular lattice, where the discretization and the number of variables do change in time.

In section 7.2 we will discuss time evolution in simplicial discretizations, where in general the number of degrees of freedom change. Such simplicial discretizations are in particular used for (the quantization of) gravity, for instance in Regge calculus [F44] or spin foams [F15].

The quantization of the Hamiltonian constraint in loop quantum gravity [F45–F47] also involves a change of the underlying discretization (in the form of a graph). The interpretation of this graph changing Hamiltonian is an open issue. In this work we will suggest an interpretation for a graph or discretization changing time evolution. On the other hand this interpretation will help to actually design reasonable discrete dynamics involving a change of phase or Hilbert space.

In sections 7.2 and 7.3 we will also explain how to formulate such a dynamics with varying number of degrees of freedom in the classical and quantum realm respectively and propose that such a dynamics can be interpreted to refine or coarse grain a given state. This is underlined with a number of examples in section 7.2.

This interpretation is strengthened if we consider totally constrained systems, such as general relativity or topological field theories. In a totally constrained system the Hamiltonian is given as a combination of constraints C_i, that generate gauge transformations. Thus time evolution is

equivalent to a gauge transformation, realizing the fact that in such systems the choice of time coordinate is arbitrary.

The classical evolution of such systems does not change the states, as these are defined as gauge equivalence classes. The quantum evolution in the form of a path integral

$$\int_{X_{ini}, X_{fin}} \mathcal{D}X \, \exp\left(\frac{i}{\hbar} S(X)\right) \tag{7.1.1}$$

is supposed to act as a projector onto physical states $\psi_{phys}(X)$ annihilated by the quantized constraints $\hat{C}_i \psi_{phys} = 0$ [F28, F29]. Thus evolution with respect to (coordinate) time is 'frozen'.

Consider a discretization of a totally constrained system and allow for the number of degrees of freedom to change during time evolution. Here we will understand time evolution in the sense of (7.1.1), that is we consider a discretized path integral. How should we interpret this time evolution, which is supposed to be 'frozen', in the case that the number of variables involved (including physical and gauge degrees of freedom) does change?

We will propose in section 7.3 that in this case time evolution is equivalent to a refining or coarse graining of a state. (In case the initial state is not physical, unphysical degrees of freedom might be also projected out.) We will connect the case of refining time evolution to the construction of a continuum Hilbert space via an inductive limit, explained in section 7.3.1, as is used in loop quantum gravity [F35, F36]. Such a construction provides a precise sense in which states from Hilbert spaces of 'different size' can be equivalent. Note that this inductive limit construction for the continuum Hilbert space has so far been used only for the kinematical Hilbert space in loop quantum gravity. We propose here a construction which involves the dynamics. Thus the dynamics defines which states are equivalent, as one would expect for the physical Hilbert space, i.e. the space of states, satisfying the constraints.

Considering a time evolution where the number of degrees of freedom change, we can go to the extreme, and start from an 'empty' discretization, supporting no variables at all. This will be discussed in section 7.3.2. A state resulting from such a refining time evolution with such initial conditions defines the (Hartle–Hawking) no–boundary state. The different stages of evolution just represent this state on different discretizations, which is consistent with the construction of a Hilbert space via an inductive limit. We will propose that refining a given state via time evolution, means to put the additional degrees of freedom into a state, that resembles this Hartle–Hawking state in some localized form. It is thus natural to see the Hartle–Hawking state as the vacuum state of the system. (Note that in constrained systems the definition of vacuum via minimal energy is usually not available - all states satisfy the Hamiltonian constraints and have therefore zero energy, at least in systems without a boundary.)

Often discretizations provide the only method to make sense of the formal continuum path integral. However for (non–topological) systems the continuum diffeomorphism symmetry is typically broken by the discretization [F25, F26]. But without a realization of diffeomorphism invariance in the path integral (7.1.1), it cannot act as a projector onto the physical states. To deal with this issue one attempts to restore diffeomorphism invariance via refining the building blocks and finding effective amplitudes for the coarser building blocks by integrating out the finer degrees of freedom [F48, F49]. This we usually refer to as coarse graining flow (although the initial step is a refining). We will explain how this defines a continuum limit of (7.1.1), which can be expressed as a cylindrically consistent amplitude map on an inductive limit Hilbert space in section 7.4. For such an inductive limit Hilbert space one needs to again define refinement maps, which we propose to be given by (effective) time evolution maps. This holds in particular if one wants to express the physical Hilbert space as an inductive limit.

Thus what has been said above about equivalence of time evolution and refining and coarse graining will hold in general only in some approximate sense. In fact, one can now attempt to construct discretizations for which this holds to a good approximation. This will also provide the

means to define the continuum limit via a coarse graining flow. In this continuum limit one then expects this equivalence to hold exactly.

Section 7.5 will explain that tensor network renormalization schemes provide a means to construct cylindrically consistent amplitude maps and an inductive limit physical Hilbert space. On the other hand the insight that time evolution maps provide refining maps might help to develop new tensor network renormalization schemes.

The breaking of diffeomorphism symmetry by discretizations can often be avoided in topological theories, such as three–dimensional gravity. Here the relation between time evolution and refining or coarse graining can be made exact. We will therefore illustrate our claims with examples from topological field theories in section 7.6. In particular the (refining) time evolution maps can be taken as refinement maps for the construction of an inductive limit Hilbert space. Note that the applicability of this idea is not exclusive to topological field theories: one can also use the time evolution maps of topological field theories to define inductive limit Hilbert spaces for other theories. Based on this idea a new representation for loop quantum gravity has been recently defined in [F38], based on the time evolution maps for BF–theory. We will explain in section 7.6.4 that this construction can be generalized to other (discretized) topological field theories. It provides a method to find Hilbert space representations for non–topological theories based on vacua provided by the topological theories.

Section 7.7 will comment more on the peculiarities in gravitational theories, where the geometric scale is part of the dynamical variables. It will provide a geometric interpretation of the refining time evolution maps and make clear that these should indeed be rather seen as refining than time evolution. Furthermore the properties of these maps are related to the appearance of (bubble) divergences in spin foams [F23, F50–F52].

7.2 Time evolving phase spaces

Here we are going to explain, how to understand discrete time evolution in systems where the phase space dimension (or the 'size' of the Hilbert space) can change from one time step to the next. We will consider theories which assume a notion of equal time states, which indeed is the case is many discrete theories, such as Regge calculus [F44] or loop quantum gravity restricted to discrete graphs [F53–F55].

First let us illustrate that the need for such a time evolution scheme appears naturally in simplicial discretizations, i.e triangulations. Assume a triangulated hypersurface. The configuration space of the theory is given by an association of variables to certain type(s) of simplices or combinations of simplices. For instance in (length) Regge calculus [F44] one associates lengths to the edges of the triangulations, other formulations work also with areas [F56] or areas and angles [F57, F58] and references therein. Scalar fields can be associated to vertices, discrete n–forms to n–simplices or their n–duals, etc. [F59].

Time evolution in a d–dimensional theory is given by gluing d–simplices to the triangulated $(d-1)$–dimensional theory. This discrete time evolution appears as a change of triangulation – indeed a Pachner move [F60, F61] – in the triangulated hypersurface, see also [F62]. One can understand Pachner moves as the most elementary change of a triangulation, Pachner moves divide time evolution into basic steps.

'Gluing' a d–simplex to the hypersurface, means identifying the variables on the (sub)–simplices that are now shared between this d–simplex and the hypersurface as well as solving for (integrating over) the variables that are now in the bulk, i.e. not associated to the hypersurface any more.

The d–simplices can be glued to the hypersurface in different ways. Depending on how many faces ($(d-1)$–subsimplices) of a d–simplex are identified with $(d-1)$ subsimplices of the triangulated hypersurface, the number of variables associated to the hypersurface might either increase, decrease or stay constant. Accordingly we will interpret these Pachner moves as refining, coarse graining, or

1–3 move in 3D picture   1–3 move in 2D picture

Figure 7.1: A $1-3$ move in the 2D hypersurface can be obtained by gluing a tetrahedron with one of its triangles to the hypersurface.

of 'mixed type'.[3] These 'mixed type' Pachner moves can be seen as entangling moves, appearing in the entanglement renormalization approach [F40, F63], see the discussion in section 7.6.

For example in $(1+1)$ dimensions, gluing triangles to a triangulated line can be done in two ways, which are named $1-2$ and $2-1$ Pachner move. For the $1-2$ Pachner move we glue a triangle with its base to an edge of the 1D line. This edge is mapped to two edges under time evolution – which alternatively can be interpreted as refining the state. Indeed we will later see that this is exactly the case in topological theories. In the $2-1$ move we glue a triangle with two edges to two neighbouring edges of the 1D line.

In 3D one can reproduce the coarse graining $3-1$ and refining $1-3$ Pachner moves by gluing a tetrahedron with three triangles and one triangle respectively, to the triangulated hypersurface, see figure 7.1.

However if one wants to produce a very refined state and uses only $1-3$ Pachner moves one will end up with a very peculiar geometry, known as stacked sphere. Even in 4D, where gravity is non–topological and interacting, such stacked sphere geometries are not dynamical (do not allow for curvature) and span the flat sector of the theory as defined in [F53]. Thus, to arrive at more interesting spatial geometries one needs to include other Pachner moves. For $(2+1)$ dimensions these are the $2-2$ moves which can also be obtained by gluing a tetrahedron with two triangles to the hypersurface, see figure 7.2. Such $2-2$ moves can be used as entangling moves to produce the long range entanglement in topological phases [F63]. For $(3+1)$ dimensions one can generate analogously $4-1$ and $1-4$ as well as $3-2$ and $2-3$ Pachner moves by gluing a 4–simplex to the 3D triangulated hypersurface.

These moves can be described via canonical evolution equations, despite the change in phase space dimension [F10, F11, F64]. Generalizing work of [F65–F70] such discrete time evolution maps can be understood as canonical transformations generated by an action. This action is associated to the d–simplices and can be understood as Hamilton's principal function depending on the boundary data of this simplex.[4] Hamilton's principal function is a generating function for the momenta, that

---

[3]Such moves of 'mixed type' can be avoided, if one considers so called Alexander moves instead of Pachner moves. These Alexander moves can be understood as combinations of Pachner moves, thus they will both refine the hypersurface and entangle certain degrees of freedom of this hypersurface.

[4]The advantage of such a formulation is that it reflects how simplicial path integrals are defined. There, i.e. in spin foams, one associates an amplitude to a d–simplex, which in the semi–classical limit does indeed give the Regge action for the simplex [F71–F74]. The path integral (say with boundary) is then defined by summing the product of all simplex amplitudes over all bulk variables. Thus changing the boundary state by gluing a simplex to the
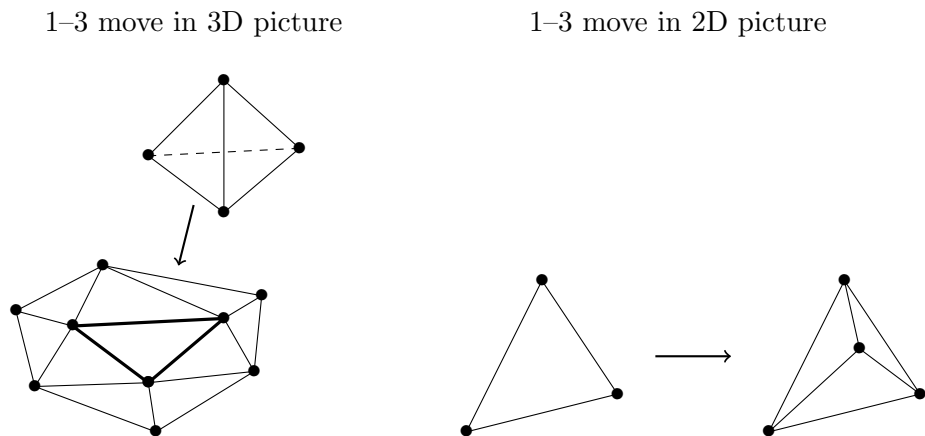
2–2 move in 3D picture   2–2 move in 2D picture
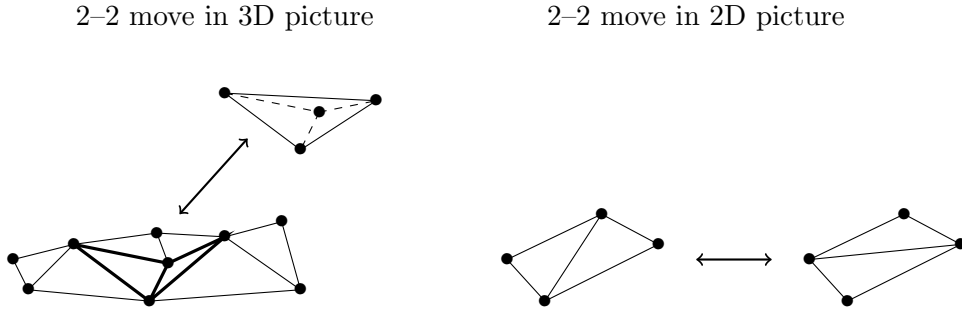
Figure 7.2: A $2-2$ move in the 2D hypersurface can be obtained by gluing a tetrahedron with two of its triangles to the hypersurface.

is we use the action associated to a simplex S_s to define old momenta p and new momenta p'. Schematically we have

$$p = \frac{\partial S(q,q')}{\partial q} \quad , \qquad p' = -\frac{\partial S(q,q')}{\partial q} \quad , \tag{7.2.1}$$

where we denote old and new configuration data by q and q' respectively.[5]

How can the equations (7.2.1) describe a canonical, i.e. symplectic, transformation, if the number of old and new variables differ? The answer is that pre– and/or post– constraints appear on the initial or final phase space respectively. One has to reduce the phase spaces with respect to these constraints and finds a symplectic transformation on these reduced phase spaces.

The constraints have to appear for a simple reason from the equations (7.2.1). There one would have to solve the first set of equations for the new configurations in terms of the old configurations and old momenta. However, if we have $N_{old} > N_{new}$ variables, the first set of equations will give N_{old} relations for N_{new} unknowns. Thus, if the equations are independent, they will give the solutions $q'(q,p)$ but also $(N_{old}-N_{new})$ pre–constraints $C_i(q,p), i = 1, \ldots, (N_{old}-N_{new})$, that is constraints on the initial phase space. Similarly we obtain post–constraints, if $N_{new} > N_{old}$. (Constraints can also appear independently of this mechanism, that is $N_{new} = N_{old}$ does not guarantee that constraints will not appear.) As the pre– or post–constraints are defined via a generating function, they are first class. Thus the evolution equations (7.2.1) leave a number of configurations undetermined ('pre–and post gauge degrees of freedom), corresponding to the number of constraints that appear. The status of these gauge degrees of freedom might change under further evolution: constraints appearing in the future might lead to a gauge fixing. The pre–constraints have to be satisfied for an evolution move to take place. The post–constraints are automatically satisfied, after an evolution move has taken place.

We should point out that the pre– and post–constraints include constraints which might arise due to gauge symmetries, including Hamiltonian and diffeomorphism constraints. For instance the $4-1$ Pachner move in 4D leads to Hamiltonian and diffeomorphism constraints [F10, F53]. In this case the post–constraints exactly coincide with the Hamiltonian and diffeomorphism constraints, no new truly physical degree of freedom is added by such a refinement move. There are however also the $2-3$ moves that add degrees of freedom and therefore lead to constraints, which do however not

---

boundary (i.e. multiplying the state with the simplex amplitude and summing over the variables which are now bulk variables), we automatically obtain the amplitude for the evolved state. Hence one would expect that the semi–classical limit reproduces the equation of motion as obtained from the canonical transformation generated by the action associated to this simplex.

[5]Some configuration variables are neither old or new, as these are represented in the hypersurface before and after the move. Such variables count as (non–dynamical) parameters in this move. Here we will only need this schematic discussion, for explicit discussion of all Pachner moves see [F10].

coincide with the Hamiltonian and diffeomorphism constraints. As noted further evolution might fix the gauge degrees of freedom implied by the Hamiltonian and diffeomorphism constraints. This is due to the breaking of diffeomorphism symmetry in discretization of 4D gravity [F25, F26]

Post– and pre– constraints also appear for theories without any a priori gauge symmetries, such as a scalar field theory. We propose here that such constraints can be interpreted as describing the state of finer degrees of freedom. We will motivate this proposal with examples.

7.2.1   Example: evolution of a scalar field on an extending triangulation

As a first example we consider a massless scalar field on a 2D (Euclidean) equilateral triangulation. The action associated to one triangle is given as

$$S_\Delta \;\; = \;\; \frac{1}{4} \sum_{e \subset \Delta} (\phi_{s(e)} - \phi_{t(e)})^2 \quad , \tag{7.2.2}$$

where $s(e), t(e)$ denote the source and target vertex of an oriented edge respectively. We now consider a time evolution between two spatial periodically identified 1D triangulations, i.e. circles subdivided into edges. We assume that the earlier equal time hypersurface has N edges and the later one N' edges and we connect these two hypersurfaces by "one slice of triangles", see figure 7.3. The triangulation can be described by an adjacency matrix $A_{vv'}$, where $A_{vv'} = 1$ if the vertex v at the earlier time is connected to the vertex v' at the later time, and $A_{vv'} = 0$ if this is not the case. The canonical time evolution map can be easily computed in this case. In particular the momenta $\pi'_{v'}$ at the later time step are given by

$$\pi'_{v'} \;\; = \;\; \frac{\partial S}{\partial \phi_v} = \left(\sum_v A_{vv'} (\phi'_{v'} - \phi_v) \right) + \phi'_{v'} - \tfrac{1}{2}\phi'_{v'+1} - \tfrac{1}{2}\phi'_{v'-1} \quad , \tag{7.2.3}$$

where S is the action associated to the interpolating triangulation obtained by summing the action contributions (7.2.2) of the triangles. If $A_{vv'}$ has right null vectors $R_r^{v'}$, i.e. such that $A_{vv'} R_r^{v'} = 0$, we obtain constraints by contracting (7.2.3) with these null vectors. These constraints are of the form

$$C_r \;\; = \;\; \sum_{v'} R_r^{v'} \pi'_{v'} \; + \; f_r(\phi') \tag{7.2.4}$$

with some specific functions f_r of the fields $\phi'_{v'}$ at the later time step. Coming from a generating function the constraints are Abelian. They generate gauge transformations in the sense that the evolution step leaves indeed certain combinations of field values unspecified. Assuming an orthogonal basis of the null vectors, these combinations are given as $\lambda_r = \sum_{v'} R_r^{v'} \psi'_{v'}$. For a refining evolution step we have a larger number N' of vertices at the later time than the number of vertices N at the earlier time, $N' > N$. In this case there are at least $N' - N$ right null vectors R_r, with $r = 1, \dots, N' - N$. We want to argue that these gauge degrees of freedom correspond to the finer degrees of the field.

Consider specifically a regular refinement as in figure 7.3, with $N' = 2N$. The corresponding adjacency matrix is given by

$$A_{vv'} \;\; = \;\; \delta_{2v-1,v'} + \delta_{2v,v'} + \delta_{2v+1,v'} \quad . \tag{7.2.5}$$

The matrix can be 'diagonalized' by a Fourier transform. Let us formally introduce the notation

$$|k\rangle = \sum_{v=1}^{N} e^{-2\pi i \frac{kv}{N}} |v\rangle \qquad , \qquad |v\rangle = \frac{1}{N} \sum_{k=0}^{N-1} e^{2\pi i \frac{kv}{N}} |k\rangle$$

$$|k'\rangle = \sum_{v'=1}^{2N} e^{-2\pi i \frac{k'v'}{2N}} |v'\rangle \qquad , \qquad |v'\rangle = \frac{1}{2N} \sum_{k'=0}^{2N-1} e^{2\pi i \frac{k'v'}{2N}} |k'\rangle \quad , \tag{7.2.6}$$
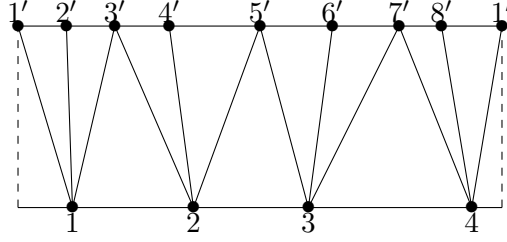
Figure 7.3: The scalar field on a circle and its time evolution. The circle is drawn as an interval with periodic boundary conditions indicated by the dashed lines.

so that we can write

$$\langle k|A|k'\rangle, = \sum_{vv'}\langle k|v\rangle A_{vv'}\langle v'|k'\rangle \;\; = \;\; \left(1 + e^{\pi i\frac{k'}{N}} + e^{-\pi i\frac{k'}{N}}\right)\delta^{(N)}(k,k')$$

$$= \;\; \left(1 + 2\cos\left(\frac{k\pi}{N}\right)\right)\delta(k,k') + \left(1 - 2\cos\left(\frac{k\pi}{N}\right)\right)\delta(k+N,k') \;\; (7.2.7)$$

We thus have N right null vectors $R_k^{k'}$ (here k labels the null vectors) given by

$$\sum_{k'} R_k^{k'}|k'\rangle \;\; := \;\; \left(1 - 2\cos\left(\frac{k\pi}{N}\right)\right)|k\rangle \; - \; \left(1 + 2\cos\left(\frac{k\pi}{N}\right)\right)|k+N\rangle \;\; . \quad\quad (7.2.8)$$

In general the coefficient in front of the higher momentum $|k + N\rangle$ is non–vanishing (it only vanishes for $k = 2N/3$). Thus we can say that (almost) all momenta $\pi'_{k'}$ associated to finer degrees of freedom, i.e. with momenta $k' > N$ are determined by the constraints (7.2.4). The same holds if we add a potential V to the scalar field, and discretize this in a local manner, i.e. as a term $\sum_{v\in\Delta} Ar(\Delta, v)\, V(\phi_v)$ added to the action (7.2.2) with $Ar(\Delta, v)$ denoting some association of an area to the vertex–triangle pair.

The post–constraints signify in particular that no new information is added, the physical phase space cannot be enlarged during evolution.[6] In fact, we can interpret this in the following way: given a state with a certain coarse graining, i.e. discretization scale, we can apply refining time evolution steps. This will lead to a state with the same coarse graining scale, however represented on a finer discretization.

It is preferable that the finer degrees of freedom that are added during refining time evolution are in a vacuum state. In the case of a scalar field we have a notion of energy, thus the statement is that the refining time evolution should not increase the energy as defined by some energy functional on the two different discretizations. See also the discussion in [F75], which considers this issue however in a covariant quantization scheme. Whether this is actually the case will depend on the quality of the discretization.

This is particularly true because the degrees of freedom that are added are typically defined on scales near the discretization scale. Typical discretizations will rather give unreliable results on this scale. A way out is to design discretizations, so that the added degrees of freedom are in fact in a vacuum state.

---

[6]For a complete discussion on how these constraints propagate and a classification of the constraints, see [F11].

7.2.2 Refinement as adding degrees of freedom in the vacuum state

In the last section 7.2.1 we have used the Fourier transform to identify finer degrees of freedom (higher modes) and coarser degrees of freedom (lower modes). In fact in a free theory the Fourier modes decouple and allow us to assign an energy per mode.

We can thus make the argument that refining time evolution should add degrees of freedom in a vacuum state and design a discretization for which this is the case. This will in general result in a non–local (in space) discretization – as can be already suspected if one uses the Fourier transform.

The general idea is to match for a set of Fourier modes up to a cut–off K exactly the dynamics of the continuum, see also the related arguments in [F76, F77].

The construction is as follows: We consider the canonical data of a continuum scalar field on a 1D circle, representing the spatial hypersurface. We only consider fields that include Fourier modes $\tilde{\phi}(k_1)$ up to a cut-off $K \in \mathbb{N}$ on the spatial momentum component $|k_1| \leq K$, so that the fields are superpositions of $N = 2K + 1$ modes. Such fields can therefore be parametrized one–to–one (in the general case) by the set of N values of the field at pre–specified positions along the circle.

We thus have a mapping $\mathcal{M}_K$ from the phase space describing continuum field configurations with a cut–off K to a phase space describing a discretized scalar field on $N = 2K + 1$ vertices.

We have now to decide on an embedding map $\mathcal{C}_{K,K'}$ from the phase space with cut–off K to a phase space with $K' \geq K$. Once such a map is chosen we can construct the corresponding map $\mathcal{D}_{K,K'} = \mathcal{M}_{K'} \circ \mathcal{C}_{K,K'} \circ (\mathcal{M}_K)^{-1}$ for the phase spaces describing the discretized fields.

As an example, one can choose $\mathcal{C}_{K,K'}$ such that in a mode expansion the coefficients of the additional modes are vanishing. This minimizes the energy of the additional modes for a free theory. For interacting theories one can choose more generally $\mathcal{E}_{K,K'}$ such that the energy of the refined configurations (in the space of fields with a mode cut-off K') is minimized, keeping the coarser modes fixed.

Note also that one can attempt to define an embedding $\mathcal{C}_{K,K'}$ such that it includes some proper time evolution step $\mathcal{T}$. However a time evolution will entangle the modes up to the cut-off K, with (possibly) all continuum degrees of freedom, that is the image of $\mathcal{T}$ applied to a phase space given by modes with cut–off K will in general include modes $K' \to \infty$. We therefore face a problem in pulling back the evolved continuum configuration to a discrete one, as the evolved continuum configuration might be infinitely refined with respect to the embedding maps chosen.

Thus one must find an (embedding) map of discrete configurations into continuous ones, where this is not the case. In this sense the choice of the (generalized) maps $\mathcal{M}_K$ should be informed by the dynamics. We believe however that such examples are rare, see section 7.2.3 for one of these cases. Alternatively, one chooses a truncation of the image of $\mathcal{T}$ back to the phase space describing modes with a cut–off K'. This introduces an approximation to the continuum dynamics. However for sufficiently refined configurations, one would of course expect, that these errors do not affect sufficiently coarse grained observables.

In general the discrete embedding maps $\mathcal{D}_{K,K'}$ will be highly non–local, but this will be necessary to obtain a good approximation also for modes near the discretization scale. This construction will be very involved for an interacting theory, as it basically requires the solution of the dynamics.

However it can serve as a guide line of what to expect from 'good' discretizations, that also involve a possible change of degrees of freedom. Thus even if one has a discretization that does not exactly mirror this behaviour (i.e. is not 'perfect') one can hope that via coarse graining one reaches an effective theory, that actually does so. This is the philosophy behind perfect discretization, which can be constructed as fixed points of renormalization flows [F49, F78–F80] or by pulling back continuum physics to the lattice ('blocking from the continuum') [F81]. A more abstract approach is to select as observables spectra of geometric operators [F82].

The construction described in this section allows a more explicit choice of the (post)–constraints, than in the discussion in section 7.2, where the post–constraints are determined by the chosen discretization of the action. Here the post–constraints are determined by the choice of vacuum

state, given by the minimization of an energy functional. Note that the constraints are second class. For instance for a free theory these are given by the vanishing of all higher modes in the fields and momenta. Thus in comparison with the discussion in section 7.2 one has gauge fixed the first class post–constraints appearing there with additional constraints.

This is what one would however expect also from the quantization of a (free) scalar field: the vacuum functional in a given mode is given as a Gaussian of the field variable. Such a Gaussian can also be found by minimizing the 'master constraint' $M(k_1) = \omega^2(k)\tilde{\phi}^2(k_1) + \tilde{\pi}(k_1)$, given as sum of (weighted) squares of the individual constraints [F83–F85]. For gravity the situation is less clear what kind of vacuum to expect. On the one hand (continuum) gravity constitutes a first class constrained system, so all physical states have to satisfy these constraints. Thus, physical states are squeezed states in the conjugated degrees of freedom describing the gauge choice and the constraints. In 4D we of course have additional physical degrees of freedom, however the characterization of a vacuum state (without a background and boundary) is an open issue. We will discuss in section 7.3.2 the Hartle Hawking no–boundary proposal [F86] for a vacuum state, that can be naturally implemented with a refining time evolution.

7.2.3 Massless scalar field in a 2D Lorentzian space time

Here we will discuss an example of a perfect discretization with local embedding maps, namely the discretization of a massless scalar field in 2D Minkowskian space time. Note that this is the only such example of a non–topological theory that we are aware of, and that the locality of the embedding maps might actually change in the quantum theory. We will consider equal time hypersurfaces given by piecewise null lines, akin to characteristic evolution schemes [F87].

We will identify a given discrete configuration of field values with a continuous configuration by assuming the continuum field to be piecewise linear. Such a piecewise linear field can be parametrized by a discrete set of scalar field values at points where the derivative of continuum field is not continuous.

One motivation for this example is to provide an interpretation for graph changing Hamiltonians appearing in loop quantum gravity [F45–F47, F88, F89] or for the parametrized scalar field [F90–F92]. This example will illustrate that indeed refining evolution splits into an embedding map and a proper evolution.

The example is furthermore interesting as it introduces the concept of piecewise null hypersurfaces, that on 'larger scales' can be either put together to a spatial hypersurface, or alternatively to a null hypersurface. Thus problems involving a null boundary can be easily treated, with a natural specification of 'boundary conditions' at the null hypersurface (or null line). For a discussion of issues related to holography involving such discretizations, see [F93], which very much inspired the development of this example. Null surface formulations also attracted recent interest in (loop) gravity [F94–F97].

To be concrete we consider a 2D cylinder space time endowed with the Minkowski metric. We consider piecewise null 'hyperlines' that close around the cylinder. Thus we will have null edges connected via kinks.

For every such kink we have to introduce a vertex ν. We allow furthermore vertices ν on the null edges themselves. We will associate scalar field values ϕ_ν to these vertices ν.

As we will show in the following, such a configuration of scalar fields ϕ_ν specifies a piecewise linear solution to the continuum dynamics.

Let us start with the set of continuum solutions to $\Box\phi = 0$, which are given by

$$\phi(u, v) = f(u) + g(v) \tag{7.2.9}$$

where $(u = t + x, v = t - x)$ are light cone coordinates[7]. We will consider functions of the form (7.2.9) with f and g piecewise linear (continuous) functions. Thus $\phi(u, v)$ will be smooth (even

---

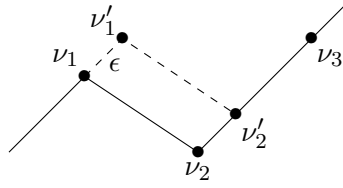[7] Choosing $x \in [0, 2\pi)$ we have $\frac{1}{2}(u - v) \in [0, 2\pi)$.

Figure 7.4: The time evolution proceeds by moving the null edge (ν_1, ν_2) to (ν'_1, ν'_2).

linear) everywhere except at a set of null lines $u = c_I$ or $v = c'_J$, where $\{c_I, c'_J\}$ are a set of constants. Such a solution induces a scalar field configuration on any piecewise null line in the following way:

As outlined above, we have a vertex at every kink of the piecewise null line. Additionally we introduce vertices for every null line $u = c_I$ or $v = c'_J$ that cuts our 'equal time hypersurface' transversally. The values of the scalar field at these vertices are now just given by the values of the solution (7.2.9) at the position of the vertices.

This gives a configuration of scalar field values on a piecewise null hyperline. From this configuration we can re–construct the solution. We basically do the inverse of the above procedure: For every kink we draw two null lines $u = c_I$ and $v = c'_J$ emanating from this kink. Furthermore we draw from every vertex on a null edge a transversal null line. These null lines give the possible non–smooth behaviour of the solution. We can reconstruct the solution everywhere by linear extrapolation.

A concrete way of constructing such a solution is given by a time evolution of the scalar field configuration on a piecewise null line, by pushing the null line forward in time.

Note that the scalar field values on a given piecewise null line are sufficient to reconstruct the full space time solution. There are no additional momenta needed. Intuitively this can be imagined the following way: drawing a null zigzag line we obtain a set of initial fields at two consecutive time steps. Thus the fields themselves provide the momenta.

To describe the time evolution consider a piecewise null line with a vertex ν_1 at a kink. We wish to evolve this vertex by an amount ϵ in say the direction of u, see figure 7.4. (Note that there is no absolute length attached to ϵ as it is an affine parameter. The time evolution itself can only be characterized by the area of the rectangular diamond that will be glued to the hypersurface.) Let us assume (for simplicity) that the next vertex ν_2 to the right of ν_1 is also a kink. If we want to move the vertex ν_1 and keep the hypersurface null we have to also move the vertex ν_2 to a new vertex ν'_2. Thus we move an entire null edge of the hyperline.

Note however that although we move the vertex ν_1 to a new vertex ν'_1 we actually have to keep the vertex ν_1 as a vertex in our hypersurface. This is due to the possible non–smooth behaviour in the field that might still occur at ν_1. Thus the new hypersurface will have one additional vertex. In this way time evolution is necessarily[8] refining.

Thus we have to determine the values of the scalar field at the new vertices ν'_1 and ν'_2. We construct the field $\phi(\nu'_2)$ by linearly interpolating between $\phi(\nu_2)$ and the field $\phi(\nu_3)$ at the next vertex ν_3 to the right of ν_2:

$$\phi(\nu'_2) = \phi(\nu_2) + \frac{\phi(\nu_3) - \phi(\nu_2)}{u(\nu_3) - u(\nu_2)}(u(\nu'_2) - u(\nu_2)) \quad . \tag{7.2.10}$$

(One might consider this step to be somewhat non–local.) Having constructed the field $\phi(\nu'_2)$ we now know three fields at the vertices of the diamond formed by $\nu_1, \nu'_1, \nu_2, \nu'_2$. The field at the tip

---

[8]One can also time evolve by gluing diamonds that fit into the zigzag null line. This would keep the number of vertices constant, but would also pre–define the size of the time evolution step.
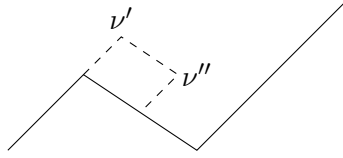
Figure 7.5: Time evolution can also proceed by gluing small diamonds to the hypersurface, which will however produce past directed null edges. Note that in this case $\phi(\nu'')$ will be constrained and determined by the fields at the other vertices on the 'equal time' hypersurface.

ν'_1 of this diamond is imposed by the form of the solution (7.2.9) to be

$$\phi(\nu'_1) = \phi(\nu_1) + \phi(\nu'_2) - \phi(\nu_2) \quad . \tag{7.2.11}$$

This description can be easily generalized to other situations. In the end time evolution proceeds by gluing rectangular diamonds to the null hypersurface. Allowing the side length of these diamonds to vary, we do not pick out a Lorentz frame, thus we have a Lorentz independent cut–off.

Here we have a situation very similar to loop quantum gravity [F45–F47], or parametrized and polymerized scalar field theory [F90–F92], with a 'graph changing' Hamiltonian. One can choose ϵ (or the area of the diamond if one generalizes the framework to allow also 'past directed' null edges, see figure 7.5) arbitrarily small – there remains a discontinuous action of the time evolution, which is to produce new vertices.

The time evolution map can be also split into two parts: one is a pure refining part, introducing the vertex ν'_2 and the associated field value (7.2.10). The second part is the 'proper' time evolution step, in which a diamond with vertices $\nu_1, \nu'_1, \nu_2, \nu'_2$ is glued to the hypersurface. This part keeps the number of vertices constant, as the new vertex ν'_1 is compensated by the loss of the old vertex ν_2.

The scheme we have described is a perfect discretization, that exactly mirrors the continuum solutions. We can also embed any discrete configuration into a refined configuration, where the new field values are given by linear interpolation as in (7.2.10). This allows to identify discrete and continuum configurations, which can be formalized into an inductive limit construction, which we will explain in section 7.3.1 for the quantum theory. See [F98, F99] for an alternative proposal to identify discrete and continuous phase space configurations, based on gauge fixing infinitely many degrees of freedom of the continuum theory.

7.2.4 Refinement moves in simplicial gravity: adding gauge and vacuum degrees of freedom

The examples discussed here involved scalar field theories, for which a notion of energy and hence vacuum is available. In section 7.2.1 we proposed to use directly an energy functional to characterize the state of the additional degrees of freedom. For the massless scalar field on null lines we determine the values of additional 'finer' fields by demanding piecewise linearity of the field.

In case of gravitational theories the notion of energy is less clear, in particular if one considers compact spatial slices.[9] Time evolution itself is rather understood as a gauge transformation and energy is constrained to vanish (on space times with compact spatial slices). Indeed as mentioned in section 7.2, part of the degrees of freedom added in a refining time evolution will be gauge (or

---

[9] However one can attempt to proceed similar to the examples in the previous sections: For instance for simplicial (Regge) gravity one can construct, similar to the massless field, a refining based on piecewise flat geometry, at least on the classical level. Another possibility is to use some quasi-local notion of energy and to minimize this energy for the region that is being refined, in analogy to the procedure described in section 7.2.1.

pseudo gauge if diffeomorphism symmetry is broken [F25, F26, F66–F69]). But in general refining time evolution also adds physical (non–gauge) degrees of freedom. Thus refining time evolution leads to states that are supposed to be gauge equivalent, but seem to be based on different number of degrees of freedom.

To resolve this puzzle, we need to understand states resulting from a refining time evolution as equivalent – they represent the same state on different discretizations. We will discuss quantum theory in section 7.3.1 in which this notion can be indeed made precise. For this interpretation it is important that the refined degrees of freedom are indeed in a state, that can be interpreted as vacuum. For instance in loop quantum gravity one uses the so–called Ashtekar–Lewandowski vacuum [F35, F36], in which spatial geometry is sharply peaked to be totally degenerate. An alternative vacuum state has been recently introduced [F38], in which the vacuum is rather peaked on flat connections. In both cases these vacua are used to define a notion of refining, in the second case this refining origins indeed from a time evolution of BF theory, a topological theory that describes flat connections.

However both these choices are rather kinematical vacua, at least in 4D gravity ([F38] gives actually the physical vacuum for 3D gravity). The interpretation as vacua is not tied to an energy functional, but rather to the fact that these states are the simplest possible ones from different viewpoints. The Ashtekar–Lewandowski vacuum can be understood as the state giving a constant value to all connection fields, whereas the BF vacuum [F38] gives a constant value to the conjugated variables, the flux fields describing spatial geometry.

Thus, although these vacua are not physical, they show an important property of vacua (in homogeneous systems), namely to be homogeneous. We expect a physical vacuum to be given by a state satisfying the constraints and carrying a notion of homogeneity. Again the peculiarities of general relativity make this description of homogeneity non–trivial. Physical observables have to be invariant under space–time diffeomorphisms. To nevertheless allow for local observables one can use relation observables [F31–F34] , that often use a reference system built from matter (fields). Such a reference system requires, however, an inhomogeneity in these matter fields, which are used as rods and clocks. An alternative are reference systems built out of gravitational degrees of freedom, such as in [F100, F101]. There physical observables are constructed that describe perturbations away from homogeneity, thus a vacuum state can be described via a prescription for the expectation values and fluctuations of these observables.

A different characterization of vacuum uses the notion of path integral as a projector on physical states. Assuming one can construct such a (consistent) projector we can define the image of any of the kinematical vacua under this projector as a physical vacuum. The kinematical vacua are homogeneous states – therefore one would expect the physical vacuum obtained by projection (assuming it can be constructed) also to be homogeneous. A priori it is not clear whether e.g. the Ashtekar–Lewandowski vacuum [F35, F36] and the vacuum, based on BF theory [F38] would lead to the same physical vacuum. As we will describe later, if we construct the projector on physical states via a refining time evolution operator (i.e. a path integral) such vacua can be also understood to realize the Hartle–Hawking no–boundary proposal for a vacuum [F86].

7.3 Refining in quantum theory

Here we will discuss some aspects of refining time evolution in quantum theory. See also [F102, F103], which introduces a framework for time evolving Hilbert spaces, in which the number of degrees of freedom can increase and decrease. In this work we will base our discussion more on inductive limit Hilbert spaces and rather see refining time evolution as a means to define embedding maps needed for the construction of these inductive limit Hilbert spaces. We will explain this construction shortly in section 7.3.1.

So far, this framework has been used on the kinematical level in loop quantum gravity. The main

proposal of this work is that one should actually use the dynamics, that is time evolution, to define the embedding maps needed for this framework. With this proposal one adopts a no–boundary Hartle Hawking state as vacuum state, thus the vacuum (and a notion of equivalence between states of different refinement degree) is determined by the dynamics of the theory. This will be lined out in section 7.3.2.

7.3.1 Inductive limit construction of a continuum Hilbert space

The inductive limit construction allows to define a continuum Hilbert space from a family of Hilbert spaces associated to discretizations (for instance graphs as in the Ashtekar Lewandowski representation [F35, F36] or triangulations as in the BF vacuum introduced in [F38]). The discretizations need to be organized into a directed partially ordered set, denoted by $(\{b\}, \prec)$. The ordering provides a notion of coarser and finer discretizations, that is $b \prec b'$ denotes that b' is a refinement of b. In a directed partially ordered set one can always find a common refinement b'' for two discretizations b and b'.

We associate to each such discretization b a Hilbert space of states $\mathcal{H}_b$. For any two Hilbert spaces $\mathcal{H}_b$ and $\mathcal{H}_{b'}$ with $b \prec b'$, we need to define an embedding map

$$\iota_{bb'} : \mathcal{H}_b \to \mathcal{H}_{b'} \quad . \tag{7.3.1}$$

These embedding maps have to satisfy consistency conditions: For any $b \prec b' \prec b''$ we demand

$$\iota_{b'b''} \circ \iota_{bb'} \;\; = \;\; \iota_{bb''} \quad . \tag{7.3.2}$$

As we will see, these conditions encode, under the identification of the embedding maps with time evolution maps, a path independence requirement of the time evolution maps.

Given such a system, we can define the continuum limit of the theory, as an inductive limit. This limit is defined as the space of equivalence classes $\mathcal{H} := \cup_b \mathcal{H}_b / \sim$. The equivalence relation is defined as follows: two states ψ_b and $\psi'_{b'}$ are equivalent, if there exist a b'' with $b \prec b''$ and $b' \prec b''$, i.e. a discretization b'' refining both b and b', such that $\iota_{bb''}(\psi_b) = \iota_{b'b''}(\psi'_b)$.

In words, two states on different discretizations b, b' are equivalent, if they can be refined to the same state. This notion of inductive limit allows to embed any 'discrete state' ψ_b into the continuum Hilbert space $\mathcal{H}$ via an embedding ι_b.

As mentioned this construction is used in loop quantum gravity on the kinematical level, that is the choice of embedding maps is not tied to a dynamics. Indeed, in a theory with a proper time evolution one would need to separate the refining time evolution steps into a 'purely refining' part and a 'proper evolution' part, as in the example in section 7.2.3. Otherwise one would identify time evolved states as equivalent.

However, in gravitational theories, time evolution is a gauge transformation. In the quantum theory, the time evolution operator (7.1.1) is supposed to act as a projector onto physical states and thus as an identity on physical states. Hence one can indeed attempt to use refining time evolution, to define the embedding maps $\iota_{bb'}$ between different discretizations. As we will discuss, the difficulty is that refining time evolution maps based on 'naive' discretizations, will not satisfy the consistency conditions (7.3.2). Here coarse graining provides a means to reach theories in which the consistency conditions are actually satisfied.

7.3.2 Refining time evolution and no–boundary vacuum

Let us return to the time evolution operator (kernel) defined from the path integral (7.1.1)

$$K(X_{ini}, X_{fin}) \;\; = \;\; \int_{X_{ini}, X_{fin} \text{fixed}} \mathcal{D}X \, \exp\left(\frac{i}{\hbar} S(X)\right) \quad . \tag{7.3.3}$$

Here we denote by X_{ini} and X_{fin} initial and final configuration data. In, for instance simplicial, discretizations of the path integral (7.3.3) the wave functions $\psi_i(X_i)$ and $\psi_f(X_{fin})$ might be from two Hilbert spaces $\mathcal{H}_{b_i}$ and $\mathcal{H}_{b_f}$ associated to two different discretizations b_i and b_f.

Even if we consider a system with proper time evolution the path integral (7.3.3) will project onto states satisfying the pre– and post constraints discussed in section 7.2. The reason is similar to the mechanism turning path integrals for gauge theories into projectors [F28, F29], we will sketch an argument here, valid for linearized theories [F104]: Consider for instance the case of post–constraints $C_i(X, P)$, where P are the momentum variables conjugated to X.

We discussed in section 7.2 that these post–constraints are first class and lead to post–gauge degrees of freedom, that is part of the configuration data X at final time remain undetermined. On the other hand there will be also post–Dirac observables, i.e. functions on phase space that Poisson commute with the post–constraints $C(X, P)$. The structure of the constraints allows to make a canonical variable transformation such that the configuration variables separate into post gauge X^G and post–Dirac X^D degrees of freedom. The constraints then involve only variables conjugated to the post–gauge variables X^G and the variables X^G themselves.

By integrating over all bulk variables in (7.3.3) we can define an effective action that only depends on initial and final configuration variables:

$$K(X_{ini}, X_{fin}) \;=\; \exp\left(\frac{i}{\hbar}S_{eff}(X_{ini}, X_{fin})\right) \tag{7.3.4}$$

We can use the canonical variable transformation for the final configuration data X_{fin}. The fact that the classical action leads to post–constraints means that the effective action decouples gauge and Dirac degrees of freedom

$$S_{eff} \;=\; S^D(X_{ini}, X_{fin}^D) + S^G(X_{fin}^G) \quad . \tag{7.3.5}$$

This makes the appearance of constraints $C(X_{fin}^G, P_{fin}^G)$ obvious

$$P_{fin}^G \;=\; -\frac{\partial S_{eff}}{\partial X_{fin}^G} \;=\; -\frac{\partial S^G(X_{fin}^G)}{\partial X_{fin}^G} \quad . \tag{7.3.6}$$

The time evolution kernel (7.3.4) is therefore of the form

$$K(X_{ini}, X_{fin}) \;=\; \exp\left(\frac{i}{\hbar}S^G(X_{fin}^G)\right) \times \exp\left(\frac{i}{\hbar}S^D(X_{ini}, X_{fin}^D)\right) \quad . \tag{7.3.7}$$

All states resulting from a time evolution

$$\psi_f(X_{fin}) \;=\; \int \mathbf{d}X_{ini} \exp\left(\frac{i}{\hbar}S^G(X_{fin}^G)\right) \times \exp\left(\frac{i}{\hbar}S^D(X_{ini}, X_{fin}^D)\right) \psi_i(X_{ini}) \tag{7.3.8}$$

have a prescribed factor $\exp\left(\frac{i}{\hbar}S^G(X_{fin}^G)\right)$ determining the dependence of the wave function in the gauge variables. Adopting a Schroedinger quantization scheme, with the momenta quantized as derivative operators $\hat{P} = \partial/\partial X$ and configurations as multiplication operators, the states (7.3.8) satisfy the quantized constraints

$$\hat{C} \;=\; -i\hbar\frac{\partial}{\partial X_{fin}^G} + \frac{\partial S^G(X_{fin}^G)}{\partial X_{fin}^G} \quad . \tag{7.3.9}$$

In summary the choice of discrete action for a refining time evolution leads to constraints that determine the behaviour of the resulting wave functions in the 'finer' degrees of freedom, which here are characterized as post-gauge degrees of freedom.

As mentioned this mechanism holds also for theories which a priori do not show any gauge symmetries and thus we deal with a proper time evolution operator. General relativity is a totally constraint system. Formal arguments show that the path integral (7.3.3) is equivalent to a projector onto the Hamiltonian and diffeomorphism constraints C_I of the theory [F28, F29]

$$\int \mathcal{D}N^I \exp\left(\frac{i}{\hbar}N^I\hat{C}_I\right) \quad . \tag{7.3.10}$$

Here N^I denote Lagrange multiplier, known as lapse and shift. The integration over these multipliers induces a averaging over the action of the Hamiltonian and diffeomorphism constraints. For a discussion of the many subtleties involving this proposal see for instance [F30, F37, F83–F85].) The averaging would therefore project onto states that satisfy the constraints.

In our discrete context, allowing for the possibility of discretizations changing in time, one expects that the Hamiltonian and diffeomorphism constraints will be part of the post– or pre– constraints. As mentioned this issue is however involved, as discretizations typically break diffeomorphism symmetry, which leads to the constraints. For the moment we will ignore this issue and comment later how to deal with it.

Thus we can hope[10] that a simplicial discretization of a path integral describing refining time evolution will lead to states which (a) satisfy the Hamiltonian and diffeomorphism constraints and (b) in which the finer (Dirac) degrees of freedom are also put into a specific state, characterized by the remaining post– constraints.

With a simplicial path integral, we can in particular consider the extreme case of a refining time evolution; that is, we can start with zero-dimensional configuration space and evolve to a large triangulated spherical hypersurface [F10]. That is the first evolution step evolves from a vertex to the boundary of a d–dimensional simplex, where d denotes the space time dimension. The wave function will be just given as the (path integral) amplitude associated to this simplex. The following evolution steps can be understood as gluing further simplices to the one we started with, by multiplying the wave function with the corresponding simplex amplitudes and integrating over all variables that become bulk.

In this case we will have at every step as many post constraints as (configuration) variables, i.e. the reduced phase space is zero–dimensional. Indeed all momenta P_b are generated by Hamilton's principal function S_H, i.e. the action evaluated on a solution prescribed by the boundary configurations X:

$$P = \frac{\partial S_H}{\partial X}(X) \quad . \tag{7.3.11}$$

We thus have constraints $C = P - \frac{\partial S_H}{\partial X}$. These are Abelian, as the momenta are coming from a generating function. The phase space is foliated by gauge orbits, generated by the constraints, i.e. all configurations X are post–gauge degrees of freedom.

In the quantum theory this corresponds to a unique physical wave function[11], given by a (Hartle Hawking) no–boundary vacuum [F86]. In the semi–classical approximation we have

$$\psi_{HH}(X) \sim \exp\left(\frac{i}{\hbar}S_H\right) \quad . \tag{7.3.12}$$

Here one would indeed expect the appearance of the standard vacuum, at least in the limit of infinitely large regions [F105]. Gravitational theories play a special role here, as the size of the

---

[10]In fact, a naive discretization will break diffeomorphism symmetry and thus the statement regarding (a) can hold only in some approximate sense.

[11]In fact, this wave function will in general depend on the underlying discretization, which can be interpreted as a choice of order for refining time evolution maps. Thus proper 'uniqueness' requires a notion of path independence, as will be explained in section 7.3.3

region is encoded in the state itself, thus the wave function gives rather a probability distribution for the geometrical volume of the hypersurface. 'Radial' evolution, as described here should not change physical states as it is just another form of time evolution. Thus we can hope that a vacuum is reached for degrees of freedom describing scales (much) larger than the discretization scale of the boundary.

We note that a framework, which permits time evolution with phase spaces or Hilbert spaces that change in time, allows to define a notion of vacuum. For instance starting with a very coarse state and refining this state in an homogeneous manner should result into a state describing homogeneous geometries. This allows for applications for cosmology based on lattice treatments, for instance [F106–F108].

An interesting question for future research will be to investigate which simplicial quantum gravity models will lead to an acceptable (Hartle Hawking) vacuum and to investigate the properties of this vacuum.

Apart from defining a no–boundary wave function, the refining time evolution can of course also be used to refine states – and thus to provide the embedding maps needed for the construction of inductive limit Hilbert spaces, as discussed in section 7.3.1. Such (dynamical) embedding maps are therefore selected by taking the dynamics of the theory into account, which is particularly advised for coarse graining [F9]. Here one has however to address the issue that discretized path integrals will in general break diffeomorphism symmetry and, related to this fact, be triangulation dependent. This will be subject of the next sections.

7.3.3 Path independence of evolution and consistent embedding maps

We argued that a discrete evolution starting from a zero–dimensional phase space or a one dimensional Hilbert space produces a vacuum state. However this vacuum state will in general depend on the order of the time evolution steps, which for a simplicial discretization determines the triangulation of the bulk that is bounded by the triangulated hypersurface on which the vacuum is defined.

Similarly, if we aim to use the refining time evolution defined by the path integral as embedding maps, the consistency conditions (7.3.2) will in general not be satisfied. These consistency conditions can now be interpreted as demanding independence of the evolved state from the chosen evolution path. It can be understood as a discrete version of implementing the Dirac algebra of (Hamiltonian and spatial diffeomorphism) constraints. As pointed out in [F109, F110] the Dirac algebra implies path independence, with respect to evolving through arbitrary choices of spatial hypersurfaces. This constitutes a further[12] relation between diffeomorphism symmetry, that yields the constraints, and triangulation independence [F27].

So far we discussed only consistency for the embedding maps, which is needed to make the projective limit Hilbert space well defined. Observables on this Hilbert space need also to satisfy conditions known as cylindrically consistency: Observables $\mathcal{O}_b$ defined on the family of Hilbert spaces $\mathcal{H}_b$ need to commute with the embedding maps $\iota_{bb'}$:

$$\iota_{bb'}(\mathcal{O}_b \, \psi_b) \,=\, \mathcal{O}_{b'} \, \iota_{bb'}(\psi_b) \tag{7.3.13}$$

for all states $\psi_b \in \mathcal{H}_b$ and all pairs $b \prec b'$. This ensures that the observables are well defined on the continuum Hilbert space, i.e. do not depend on the representative ψ_b chosen. In the case that $\iota_{bb'}$ is given by a refining time evolution consistent observables have therefore to be 'refining

---

[12] In cases where diffeomorphism symmetry is realized, for instance in 3D discrete gravity, 4D gravity restricted to the 'flat' sector [F53], or 4D linearized gravity [F64], one can also introduce a continuum time evolution generated by Hamiltonian constraints [F24–F26, F111, F112] and define a (first class) Dirac algebra of these constraints [F113]. This continuum time evolution reproduces the discrete time evolution [F10, F24], if one integrates the infinitesimal evolution to one with a finite time.

Dirac observables'. The algebra of refining Dirac observables characterizes the resulting continuum Hilbert space, as it provides a representation of this algebra.

Topological theories can often be discretized such that partition functions and physical observables are triangulation independent. This also includes 3D gravity, which is topological. Due to the triangulation invariance the refining time evolution maps defined via the discretized path integral do satisfy the consistency conditions (7.3.2). We will illustrate this situation in section 7.6. As we will comment there, the set of 'refining Dirac observables' is much bigger than the set of (standard) Dirac observables given by the topological theory. This allows to use refining time evolution maps stemming from topological theories to define (kinematical) Hilbert spaces for other theories. They can also be used to construct a new Hilbert space for loop quantum gravity, based on the time evolution map of BF–theory [F38].

We believe that the application of refining time evolution maps is however not restricted to topological theories, despite the challenges posed by the triangulation dependence of the path integral. The strategy to attack this issue is to improve a given discretization by coarse graining. The fixed point of the coarse graining flow is hoped to show enhanced symmetry properties, in particular diffeomorphism symmetry which is tied to triangulation dependence [F27, F114].

Such a coarse graining flow leads however to non–local couplings[13], which are difficult to control. One would then also expect the embedding maps, if defined via refining time evolution, to be highly non–local. In section 7.4 we will discuss a coarse graining framework which avoids this issue, and moreover is based on the concepts introduced so far.

Let us comment on the appearance of discretization changing time evolution in loop quantum gravity. There graph changing (actually graph refining) Hamiltonian constraints have been defined by Thiemann [F45–F47]. These constraints are anomaly free, in the sense that the commutator of two Hamiltonians vanishes if evaluated on the Hilbert space of diffeomorphism invariant states, see [F45–F47, F88, F89, F116, F117] for discussions.

What is missing is a concrete geometric interpretation of the action of these constraints and a concrete connection to the path integral. (The notion of graph changing Hamiltonians inspired the development of spin foams, as time evolved spin networks [F118].) This discussion here suggest a possible interpretation for the graph changing Hamiltonians, the exponentiation of which should lead to a (refining) time evolution. Thus one could attempt to extract a notion of vacuum from the Hamiltonian constraints.

7.3.4 Pre–constraints and coarse graining

We suggested to use the refining time evolution to define embedding maps for the inductive Hilbert space construction. Refining time evolution leads to post–constraints, which we argued characterize the (vacuum) state, into which the finer degrees of freedom are put. Here we want to comment shortly on the role of pre–constraints.

These appear for coarse graining time evolution steps, that is the number of variables decreases. Classically these constraints demand that a state needs to satisfy certain conditions, so that the time evolution move can be applied. By time inversion symmetry we can understand this condition in the following way: the state has to be equivalent to a refining of a coarser state. Although the state is represented on a fine triangulation it does only include degrees of freedom in non–vacuum states on a coarser scale.

Although for classical evolution one has to satisfy these constraints, quantum mechanical evolution is always possible. This also holds for standard gauge systems: a priori a quantum state does not need to satisfy any constraints to serve as a boundary condition in a path integral. Rather the path integral itself will project out non–physical degrees of freedom [F28, F29]. Thus, one can indeed expect that in a quantum evolution, the degrees of freedom which are too fine to be evolved

---

[13]Triangulation invariant theories with local couplings are always topological theories, see for instance [F11, F115].

classically (as identified by the constraints) will be projected to the vacuum. In this sense the quantum mechanical evolution is automatically providing a coarse graining. Note that this will be a non–unitary evolution as it includes a projective part. A unitary description can only be obtained if one restricts to the subspace of the Hilbert space describing only sufficiently coarse degrees of freedom, i.e. the physical Hilbert space with respect to the pre–constraints, see also [F102, F103].

Thus time evolution cannot be inverted: Concatenating coarse graining and refining we isolate the projective part, that can be understood as projecting fine degrees of freedom to the vacuum state, that is the state obtained will automatically satisfy the initial pre–constraints. This provides an interesting asymmetry in time evolution that might serve as an arrow of time. See [F119] for another proposal on the origin of the arrow of time, in which also the notion of complexity of the state is crucial.

7.4 How to define a continuum theory of quantum gravity

The investigation of time evolution with changing phase space or Hilbert space dimension is motivated by the simplicial discretization of gravity [F10, F11, F64]. However, such discretizations break diffeomorphism symmetry for the 4D theory [F24]. This appears both at the classical level [F25, F26], and even in more severe form on the quantum level. For instance, the classical 4D Regge action, is invariant under 5-1 moves, but not under 3-3 moves. The latter fact can be related to a breaking of diffeomorphism symmetry on the classical level. Moreover on the quantum level one can show that no local path integral measure factor exists that makes the theory invariant under 5?1 moves [F120, F121], implying even a breaking of the residual classical symmetry.

This implies in particular that the consistency conditions formulated in (7.3.2) are violated. A way out is to improve the discretization by coarse graining, see [F27, F49] for examples. At fixed points of the coarse graining flow one might arrive at perfect discretizations [F78, F79], for which consistency conditions of the form (7.3.2) are satisfied. These fixed points represent the continuum limit of the theory one started with, however expressed on a discretization.

There are different ways to proceed with the coarse graining. One is to keep basic building blocks but to allow highly non–local couplings, which are naturally induced by the coarse graining [F80, F81]. As was pointed out in [F9], there is an alternative inspired by tensor network renormalization (which we will explain in section 7.5) and the generalized boundary proposal [F122].

This alternative construction of a consistent theory would not put basic building blocks (with simplest possible boundary discretizations) with their amplitudes in the centre but instead amplitude maps for space time regions, with arbitrarily complicated discretization of the boundary. These amplitude maps are built from the basic amplitudes, and agree basically with the (dual of the) Hartle Hawking no boundary wave function. The amplitude maps are defined on Hilbert spaces $\mathcal{H}_b$ associated to the discretized boundaries b of a space time region: $\mathcal{A}_b : \mathcal{H}_b \to \mathbb{C}$ as

$$
\begin{aligned}
\mathcal{A}_b(\psi_b) &:= \int \mathcal{D}X \mathcal{D}X_b \exp\left(\frac{i}{\hbar} S(X, X_b)\right) \psi_b(X_b) \\
&= \langle \psi_\emptyset | (\mathbf{K}_{\emptyset b})^\dagger | \psi_b \rangle =: \langle \psi_\emptyset | \psi_b \rangle_{phys}
\end{aligned}
\tag{7.4.1}
$$

where we denote the bulk configuration variables with X and the boundary variables with X_b. Thus the amplitude map applied to the wave function ψ_b is given by the inner product between this wave function ψ_b and the no–boundary wave function. This no–boundary wave function is here expressed as time evolution operator $\mathbf{K}_{\emptyset b}$ applied to the one–dimensional wave function $\psi_\emptyset$ associated to the empty discretization. The second line in (7.4.1) defines the physical inner product, between the projections onto physical states of the two (kinematical) states $\psi_\emptyset$ and ψ_b.

As usual the path integral in (7.4.1) is a discretized one. Thus the first task is to arrive at amplitude functionals $\mathcal{A}_b$ for fixed boundaries b that are independent of the bulk triangulation.

One way to reach such amplitudes is by coarse graining, as will be explained in the next section 7.5.

For a very coarse boundary b we can triangulate the bulk with very few simplices. For instance the boundary of a simplex can be triangulated with just this simplex and thus the amplitude functional $\mathcal{A}_b$, discretized in this way, would be just given by the pairing of the simplex amplitude with the boundary wave function. However there are infinitely many ways to subdivide this simplex (keeping the boundary), and thus one would have to find a method to determine the actual $\mathcal{A}_b$. Indeed we will specify a further criterion for these amplitudes, which will actually help to construct the coarse graining flow of these amplitudes.

It is important to note that bulk triangulation independence of the amplitude maps $\mathcal{A}_b$ is *not* sufficient for the construction of the continuum limit. (Indeed one could just declare some rule for selecting a particular bulk triangulation for each boundary.) We rather need to demand a condition that connects the amplitude maps $\mathcal{A}_b$ for different boundaries b.

Thus we need first to choose embedding maps $\iota_{bb'}$ that connect the different boundary Hilbert spaces, as explained in section 7.3.1. As we explained, there might be different sets of embedding maps, leading to different continuum Hilbert spaces. We will see that some choices are preferred over others. With a given choice of embedding map we require that the amplitude maps are cylindrically consistent functionals, that is

$$\mathcal{A}_{b'}(\iota_{bb'}(\psi_b)) \quad = \quad \mathcal{A}_b(\psi_b) \quad . \tag{7.4.2}$$

In words, if we take a coarse state and evaluate the corresponding amplitude map $\mathcal{A}_b$ on it, we should get the same result as first embedding the state into the 'finer' Hilbert space $\mathcal{H}_b$ and then evaluating with the 'finer' amplitude map $\mathcal{A}_{b'}$. Thus, the result should not depend on which boundary we choose to represent the equivalence class of states $[\psi_b]$ under the equivalence relations of the inductive limit. This allows to actually define the amplitude map as a functional on the inductive (i.e. continuum) limit Hilbert space $\mathcal{H}$ defined in section 7.3.1. Such a requirement was proposed in [F123] with regard to the (kinematical) embedding maps of the Ashtekar Lewandowski Hilbert space. We will argue here that the construction of cylindrically consistent amplitudes is facilitated by the adoption of dynamical embedding maps, as provided by refining time evolution.

The amplitude map $\mathcal{A}_{[b]}$ is technically not any more labelled by a discretization as such, but by equivalence classes of discretizations. Here two discretizations are equivalent if they can be refined to the same discretization. Thus, the information that is left over could just carry topological information (for gravitational theories where metric variables are dynamical) of the boundary.

In our case we assumed spherical topology, thus a cylindrical consistent family of amplitude maps defines a continuum amplitude $\mathcal{A}$. This amplitude $\mathcal{A}$ replaces the basic amplitude for, say the boundary of a simplex, one starts with in the regularization of the path integral. We can recover a 'perfect' amplitude, by evaluating $\mathcal{A}$ on states that are equivalent to states defined on a simplex boundary under the chosen embedding map.

The cylindrically consistency requirement for the amplitude maps is a very strong requirement – it basically encodes the solution of the theory. We can hope to build such amplitude maps iteratively, for more and more refined boundaries, as will be the subject of the next section. To this end it is important to choose embedding maps that are adapted to the dynamics of the system [F9]. In particular we suggested that refining time evolution should give good embedding maps. A priori these will typically fail to satisfy the consistency requirement (7.3.2). However the improved amplitude maps $\mathcal{A}_b$ also allow to define an improved discretization of the path integral and thus to define a (refining) time evolution, that will satisfy the consistency requirement to a better approximations[14]. In an iterative process one therefore improves both the amplitude maps and the

---

[14] The consistency equations can be tested if one considers the equations on matrix elements $\langle \psi_{b''} | \iota_{bb''}(\psi_b) \rangle \overset{!}{=} \langle \psi_{b''} | \iota_{b'b''} \circ \iota_{bb'}(\psi_b) \rangle$. Under an iterative improvement the equations will be satisfied for a larger and larger class of states involving finer and finer boundaries.

embeddings, if these are defined by refining time evolution.

The reason why such embeddings are particularly apt to define cylindrically consistent amplitudes is in the definition of the amplitudes in (7.4.1). If $\iota_{bb'} = \mathbb{K}_{bb'}$ we will have

$$\mathcal{A}_{b'}(\iota_{bb'}\psi_b) \quad = \quad \langle\psi_\emptyset|(\mathbf{K}_{\emptyset b'})^\dagger|\mathbf{K}_{bb'}\psi_b\rangle \sim \langle\psi_\emptyset|(\mathbf{K}_{\emptyset b})^\dagger|\psi_b\rangle \quad = \quad \mathcal{A}_b(\psi_b) \quad . \tag{7.4.3}$$

Here we wrote $\sim$ in the second equation as $(\mathbf{K}_{\emptyset b'})^\dagger \circ \mathbf{K}_{bb'} \sim (\mathbf{K}_{\emptyset b})^\dagger$ holds only approximately in the discretization. However we see that embedding maps defined via refining time evolution simplify the task of constructing cylindrically consistent amplitudes. Indeed the consistency condition for these embedding maps are tied to the cylindrical consistency of the amplitudes.

We want to remark that we do *not* require a consistent gluing between the cylindrically consistent amplitude maps as long as this gluing is performed on a discrete boundary b. (That is the gluing involves integration only over the variables X_b.) One could for instance require that the amplitude for a region with a more complicated boundary $\mathcal{A}_{b_3}$ arises as the gluing between two amplitudes with less refined boundaries $\mathcal{A}_{b_1}$ and $\mathcal{A}_{b_2}$, similar to the way one would glue simplices together. We expect that such a relation might indeed hold, however only if one preforms a continuum limit for the piece of boundary that is glued over.

Let us emphasize that the amplitude maps $\mathcal{A}_{[b]}$ are the end point of a construction to reach the continuum limit of the theory. Of course one hopes that the 'initial' theory defined via basic building blocks and local couplings, provide the basis for the construction of such a theory. This implies that this 'initial' theory can nevertheless be used to extract sufficiently coarse grained observables from sufficiently refined discretizations.

As mentioned we aim at constructing both, cylindrically consistent amplitudes and consistent embedding maps given by refining time evolution. In the next section 7.5 we will explain that tensor network coarse graining tools provide methods to construct these.

7.5 Tensor network coarse graining: time evolution in radial direction

Tensor network renormalization group methods [F7,F8,F124–F127] can be understood to implement an iterative method to construct cylindrically consistent amplitudes. Coming back to equation (7.4.3)

$$\mathcal{A}_{b'}(\iota_{bb'}\psi_b) \quad = \quad \langle\psi_\emptyset|(\mathbf{K}_{\emptyset b'})^\dagger|\mathbf{K}_{bb'}\psi_b\rangle \sim \langle\psi_\emptyset|(\mathbf{K}_{\emptyset b})^\dagger|\psi_b\rangle \quad = \quad \mathcal{A}_b(\psi_b) \quad . \tag{7.5.1}$$

we can understand the second term to consist of two parts: the first is the computation of $\langle\psi_\emptyset|(\mathbf{K}_{\emptyset b'})^\dagger$, that is the basically the amplitude functional $\mathcal{A}_{b'}$ for a more refined boundary. One would build such an amplitude functional from gluing amplitudes $\mathcal{A}_b$ for less refined boundaries b.

However we want to define an iterative process that improves the amplitude maps $\mathcal{A}_b$, which are functionals on $\mathcal{H}_b$. We thus have to find a way to pull back the amplitudes $\mathcal{A}_{b'}$ to $\mathcal{H}_b$, which is done by using the embedding map $\iota_{bb'} = \mathbf{K}_{bb'}$. Thus one defines the improved amplitudes $\mathcal{A}_b^{imp}$ as

$$\mathcal{A}_b^{imp}(\psi_b) \quad = \quad \langle\psi_\emptyset|(\mathbf{K}_{\emptyset b'})^\dagger|\mathbf{K}_{bb'}\psi_b\rangle \quad . \tag{7.5.2}$$

Here both $(\mathbf{K}_{\emptyset b'})^\dagger$ and $\mathbf{K}_{bb'}$ are built from using the initial $\mathcal{A}_b$ as basic amplitudes.

The process is repeated for the improved amplitudes $\mathcal{A}_b^{imp}$ until the procedure converges to a fixed point $\mathcal{A}_b^{fix}$. This fixed point amplitude can be used to proceed to a more refined pair of boundaries (b', b'') with $b \prec b''$ to find the next fixed point amplitude $\mathcal{A}_{b'}^{fix}$ and so on.

There are many tensor network renormalization algorithms [F7, F8, F124–F127], which differ in their geometric setup and the details of how to define $(\mathbf{K}_{\emptyset b'})^\dagger$ and the embedding $\iota_{bb'}$. We will shortly explain a method that can be interpreted as radial evolution, as this also matches nicely with amplitudes being defined via the no–boundary wave function, as in (7.4.1).
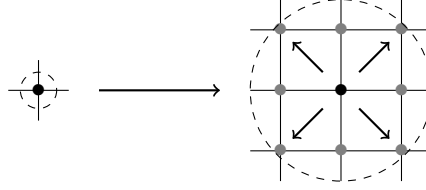
Figure 7.6: Illustration of radial time evolution in tensor networks: By adding eight additional tensors (in gray) we perform one time evolution step. The boundary data grows exponentially from χ^4 to χ^{48}.

The name tensor networks refers to the fact that the amplitudes of a space time region are encoded in tensor of a given rank n, associated to an n–valent vertex, which we can imagine to sit inside this space time region. The indices of this tensor encode the boundary data of the space time region, hence contracting tensors of two neighbouring regions corresponds to gluing the associated amplitudes. The rank n and the bond dimension χ (equal to the number of values the index can take) determines the amount of boundary data and hence the fineness of the boundary in question. Note that one can redefine higher rank tensors to tensors of lower rank by summarizing for instance two indices (i, j) with χ_i, χ_j into effective indices $I = (i, j)$ with bond dimension $\chi_I = \chi_i \cdot \chi_j$.

This interpretation matches nicely with spin nets [F128] and spin foams describing gravitational dynamics. The former can be naturally understood as tensor networks [F2, F3, F129, F130]. A tensor network description of spin foams can be found in [F2, F3].

7.5.1 Radial evolution

As we will see tensor network algorithms are related to transfer matrix methods in which the (Wick rotated) time evolution operator is diagonalized. For the latter, Wick rotation is essential, as the the eigenvalues of the transfer operator need to be ordered in size; in this way we can distinguish relevant from irrelevant degrees of freedom. However one can understand tensor networks to replace the time evolution operator with a radial evolution operator. Even if the (standard) time evolution operator might be unitary, and hence all eigenvalues with absolute value equal to one, the radial evolution operator will include a projective part, that – as we have argued will project out finer degrees of freedom. This can then be used for the construction of an embedding map.

An evolution in radial direction is also expected to project onto the vacuum state [F7, F105], see also the discussion in section 7.3.2 which involves the non–Wick rotated amplitudes.[15]

Consider a radial evolution as in figure 7.6. Here the amplitude / tensor for a larger region is built from the amplitude/ tensor of a basic building block, represented by a (dual) vertex. One would now like to treat the amplitude for the new region as an effective tensor and repeat the procedure. However one has to face the problem, that the number of boundary data, grows exponentially during this procedure, making it impossible to implement in practise.

We thus have to find a method to project back the amplitudes to a boundary with less data, i.e. to coarser boundaries. The radial time evolution can be split into steps with time evolution operators

$$T(R_1, R_2) = \exp(-\int_{R_1}^{R_2} H_r \mathbf{d}r) \quad . \tag{7.5.3}$$

This is a refining time evolution in the sense that the Hilbert space $\mathcal{H}_2$ at R_2 will have more

---

[15]For a (Wick rotated) time evolution operator $\exp(-\int_0^R H_r \mathbf{d}r)$ acts as a projector on the ground states of the Hamiltonian H for R going to infinity. Here H_r denotes the Hamiltonian for radial evolution at the radius r. For large radius, we will have small dr/r, and hence H_r approaches the Hamiltonian H for the time evolution of constant volume hypersurfaces.
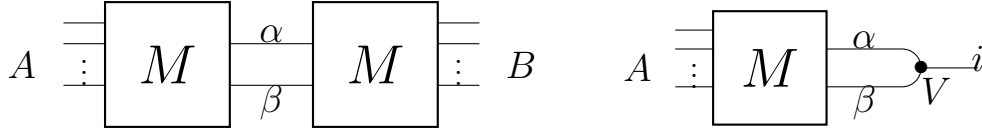
Figure 7.7: Left: Two regions in a tensor network, encoded in the matrices M, are sharing two edges with labels $\{\alpha, \beta\}$, which have a total range of χ^2. Right: From the singular value decomposition we can define the map V depicted as a three–valent vertex, where we restrict the label i of the singular values to be $\leq \chi$.

kinematical degrees of freedom than the Hilbert space $\mathcal{H}_1$ at R_1. Thus $T(R_1, R_2)$ will have a projective part (even if we would not have Wick rotated), which can be identified by a singular value decomposition. This would give a maximal number of $\dim(\mathcal{H}_1)$ singular values. Hence $T(R_1, R_2)$ will have a non–trivial co–image in $\mathcal{H}_2$, which can be projected out. A new amplitude can therefore be defined on a $\dim(\mathcal{H}_1)$ subspace, which can be identified as the subspace carrying coarse boundary data.

Such a scheme might be indeed worthwhile to investigate further (for statistical systems), in order to obtain an intuition about the truncations. One would however expect that the reorganization of the degrees of freedom via the singular value decomposition will be highly non–local, as we have seen for the example in section 7.2.1. The time evolution considered there exactly corresponds to $T(R_1, R_2)$. This non–locality makes it however difficult to turn this into an iterative procedure. The new amplitudes will be expressed with respect to data spread over the entire boundary, which makes a local gluing of these amplitudes difficult.

7.5.2 Truncations via singular value decomposition

In practice one therefore employs schemes which involve more local truncations. The basic idea is as follows. Imagine two space time regions or effective vertices connected with each other by two edges, representing the summation over a certain set of variables, see figure 7.7. We would like to replace these edges carrying an index pair $\{\alpha, \beta\}$ of size χ^2 with an effective edge carrying only a number χ of indices. We choose an optimal truncation for the summation over the index pair $\{\alpha, \beta\}$, which is given by the singular value decomposition of $M_{A\alpha\beta}$:

$$M_{A\alpha\beta} = \sum_{i=1}^{\chi^2} U_{Ai}\lambda_i V_{i\,\alpha\beta} \tag{7.5.4}$$

where $\lambda_1 \geq \lambda_2 \geq \ldots \geq \lambda_{\chi^2} \geq 0$ are positive, and U, V are unitary matrices. The truncation consists then in dropping the smaller set of singular values λ_i with $i > \chi$. Pictorially $V_{i\alpha\beta}$ restricted to $i \leq \chi$ defines a three–valent vertex and we can use these three–valent vertices as in figure 7.7 to arrive at a coarse grained region with less boundary data.

7.5.3 Embedding maps and truncations

We can understand the tensors V as coarse graining maps. Alternatively, if read in the other direction, these maps provide the embeddings $\iota_{bb'}$ from a coarser to a finer discretization. This interpretation comes from seeing the partition function (with boundary) as a functional (or amplitude map) $\mathcal{A}_b$ on a 'boundary' Hilbert space $\mathcal{H}_b$. Gluing several space time regions together we obtain a partition functional $\mathcal{A}'_{b'}$ which a priori acts on a Hilbert space $\mathcal{H}_{b'}$ with finer boundary, see figure 7.8. We can however pull back this functional with the embedding map defined via the

tensors V and in this way obtain an effective amplitude map $\mathcal{A}'_b$:

$$\mathcal{A}'_b(\psi_b) \quad := \quad \mathcal{A}'_{b'}(\iota_{bb'}(\psi_b)) \quad . \tag{7.5.5}$$

This gives a renormalization flow for the amplitude maps, and a fixed point is reached if $\mathcal{A}'_b = \mathcal{A}_b$.
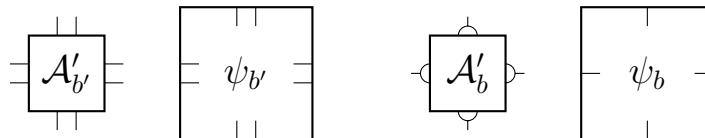

Figure 7.8: To obtain an effective amplitude map $\mathcal{A}'_b$ on the coarser boundary b one can pull back the amplitude $\mathcal{A}'_{b'}$ from the finer boundary b' via the previously defined embedding maps.

We see that it is essential to construct three–valent vertices (with its associated tensors), which we can see as special cases of coarse graining or refining maps. These three–valent vertices should be adapted to the four–valent ones giving the 'regular' dynamics. They can be understood to give a coarse graining or refining version of the regular evolution defined by the four–valent vertices. Note that this adaptation has to happen after each of the coarse graining steps, as the four–valent tensors flow under coarse graining.

The singular value decomposition (or generalizations as in [F125–F127]) provides one method to construct such three–valent tensors. Interestingly, geometric theories such as, spin foams [F14] or spin nets [F2, F3, F128] provide already descriptions for vertices of arbitrary valence [F131–F133]. Thus one can imagine a lattice of say four–valent and three–valent vertices, which automatically implements the coarse graining procedure. However, if one believes that these vertices provide good truncations, in the sense of approximating the summation over an index pair well by a summation over just one index, one needs to adapt the three–valent vertices to the dynamics encoded in the four–valent vertices. That is the embedding maps have to flow together with the effective amplitude maps. Such a relation is provided by the singular value decomposition in (7.5.4). Alternatively, spin foam construction tools [F130–F133] provide methods of how to build vertices of arbitrary valency out of a given vertex. This construction has also to be performed at every step of the coarse graining. It will be interesting to see, whether such a method gives a good truncation. The advantage of such a method is that it might be far easier to implement for spin foams, than the singular value decomposition, and might lead to a closed flow equation.

7.5.4 Embedding maps for the fixed points

Ultimately one would expect that the relation between vertices of different valencies is just given by gluing, i.e. a four–valent vertex is given as a gluing of two three–valent vertices. Indeed this relation can be obtained from the singular value decomposition (7.5.4) in case that (a) all non–vanishing singular values are equal to one and (b) if one is working in a truncation, the number of non–vanishing singular values needs to be smaller than χ. These conditions are satisfied at the stable fixed points of the renormalization flow (describing the phases of a given system), see for instance [F129].

Condition (a) is expected to arise in theories with diffeomorphism symmetry – where time evolution is a projector. (Again the problem is that diffeomorphism symmetry is broken under discretization, so the projector property does not hold exactly and might be rather expected to emerge after sufficient coarse graining. For a computation of the transfer matrix in spin foam theories and a discussion whether these are projectors, see [F128, F134, F135].)

Condition (b), in case that one is working with a cut–off, basically imposes a topological theory for fixed points that are triangulation invariant[16]. For instance fixed points identified in [F2, F3, F129, F130] via a tensor network coarse graining describe triangulation invariant and therefore topological models and χ gives the maximal number of propagating degrees of freedom. Indeed we will see in section 7.6 that all the proposals outlined here are explicitly realized. For an interacting theory, such as 4D gravity, one would expect to need an infinite bond dimension χ, as indeed arises around phase transitions. With a fixed χ one can however approach the phase transition up to a certain precision, and, as the method is designed to keep the variables describing coarse excitations, one can hope to obtain reliable predictions for sufficiently coarse observables. In light of the previous discussion this means to obtain amplitude functionals, which satisfy the cylindrical consistency conditions sufficiently well for coarse boundaries.

7.6 Topological theories

The previously introduced and discussed concepts of time evolution via coarse graining / refining and the concept of cylindrically consistent amplitudes are perfectly realized in topological field theories. In the following we would like to emphasize a few key points. In the first part of this section, we will mainly refer to topological lattice field theories in 2D, for instance [F136]. For theories with a geometric interpretation, see for instance [F115, F130].

Consider a 2D lattice topological field theory with partition functions defined on three–valent graphs. As for a three–valent tensor network we have weights or tensors associated to the vertices and variables and hence Hilbert spaces associated to the edges. The partition function is then defined by summing the variables associated to bulk edges. In case of a boundary, we keep the corresponding variables fixed, thus obtaining a partition function depending on these boundary values. Alternatively we can understand the partition function as an operator (between two boundary Hilbert spaces) or a function (on one boundary Hilbert space).

In this vain a three–valent graph

$$\text{(7.6.1)}$$

represents the simplest graph and the associated partition function, interpolating between a two–site boundary Hilbert space on the lower boundary and a one–site boundary Hilbert space on the upper boundary. In this case we can understand this partition function as a (coarse graining) time evolution map, not involving any bulk summation. The same holds for the time inverted vertex.

Topological lattice theories are triangulation invariant (referring to the triangulation dual to the graph). Thus the partition function does only depend on the topology of the manifold and not on the choice of the triangulation. (We will later show that this also holds in a certain sense for the boundary triangulation, due to the cylindrical consistency of the partition function.) Pictorially this corresponds to the following equalities

$$\text{= } c \quad , \quad \text{= } c \quad , \quad \text{=} \qquad . \qquad \text{(7.6.2)}$$

Here we assume always a summation over the variables or indices associated to the bulk edges. The equations have to hold for all possible choices of the boundary variables. In this section we will assume that the constant c is actually finite and hence can be adjusted to $c = 1$ by a rescaling of the amplitudes.

---

[16]Rank three tensors can be found from a (singular value) decomposition of the rank four ones. These tensors are associated to three–valent vertices dual to triangles, we can therefore consider models on irregular triangulations. The fixed point condition for coarse graining on a regular lattice are then weaker than requiring triangulation invariance.

Given the $2-2$ move invariance, we can replace the $3-1$ move by the so-called bubble move

$$\diamondsuit = c \; \Big|_{j} \quad .$$

$$(7.6.3)$$

The equivalence of bubble and $3-1$ move (given the $2-2$ move holds) follows from the following calculation

$$\triangle = \diamondsuit = c \; \curlyvee \quad . \qquad (7.6.4)$$

7.6.1 Time evolution as coarse graining and refining

Using this pictorial representation we can symbolize a local time evolution operator or transfer matrix acting on a two site boundary Hilbert space as follows:

$$T \; = \; \curlyvee \; = \; \sum_i \lambda_i \left| \iota^{(i)} \right\rangle \left\langle \iota^{(i)} \right| \quad . \qquad (7.6.5)$$

Time is flowing upward. From the bubble move we see that the time evolution operator is actually a projector:

$$T^2 \; = \; \diamondsuit \; = \; \sum_{i,j} \lambda_i \lambda_j \underbrace{\left\langle \iota^{(i)} \big| \iota^{(j)} \right\rangle}_{=\delta_{i,j}} \left| \iota^{(i)} \right\rangle \left\langle \iota^{(j)} \right| \; = \; \sum_i \lambda_i^2 \left| \iota^{(i)} \right\rangle \left\langle \iota^{(i)} \right| \; = \; \curlyvee \; = \; T \quad . \quad (7.6.6)$$

Hence the eigenvalues are $\lambda_i = 1 \vee \lambda_i = 0$. The construction of dynamical embedding maps via a singular value decomposition is trivial and it is straightforward to split the projector into two maps, one that can be interpreted as a coarse graining, the other in terms of a refining:

$$C \; := \; \curlywedge \quad , \quad R \; := \; \curlyvee \quad . \qquad (7.6.7)$$

Each of these maps can be interpreted as maps between Hilbert spaces of different dimension. Concatenating the two gives either the time evolution operator back or is just the identity: This tells us both that the refined state does not carry additional information and that no (physical) information is lost under coarse graining. We will extend this to arbitrarily large triangulations below.

The time evolution operator acts locally, such that it is possible to only locally evolve a state in time, e.g.:

$$\curlyvee \big|\big| \quad . \qquad (7.6.8)$$

However in which order one time evolves pairs of lattice sites is an arbitrary choice, one which should not influence the results of the theory such as the partition function. Therefore we impose the following consistency condition, which is satisfied in topological field theories and allows us to define the transfer matrix for three discretization sites uniquely:

$$\qquad = \qquad = \qquad . \qquad (7.6.9)$$

This construction can be generalised to arbitrarily many discretization sites. In all cases we can replace the time evolution map with a graph of the form on the right hand side of equation (7.6.9). Thus the maximal rank of this time evolution map (which is a projector) is given by the bond dimension of the kink in the middle, i.e. the bond dimension of one edge. This gives also the maximal number of physical degrees of freedom.

7.6.2 Consistent embedding maps and inductive limit

Furthermore if one cuts this diagram into two pieces at the kink, one obtains both more general coarse graining and refining maps. Hence the consistency conditions naturally translate to both the coarse graining and refining maps, as we demonstrate for the refinement map R:

$$
\text{(7.6.10)}
$$

Thus these refinement maps satisfy the path independence conditions as outlined in section 7.3.3, and therefore allow the construction of an inductive limit of Hilbert spaces as described in section 7.3.1. This gives the continuum limit of this theory. Furthermore, understanding the partition function $\mathcal{A}_b$ (with boundary b) as a functional on the boundary Hilbert space

$$
\mathcal{A}_b : \mathcal{H}_b \to \mathbb{C} \quad , \tag{7.6.11}
$$

we also obtain that the partition function is a cylindrically consistent operator [F115]:

$$
\mathcal{A}_{b'}(\iota_{bb'}(\psi_b)) \quad = \quad \mathcal{A}_b(\psi_b) \tag{7.6.12}
$$

(which coincides with the fixed point condition (7.5.5)). Here $\iota_{bb'}$ is built from the refinement maps R, in the way described above. Given a boundary b we choose a triangulation (or dual three–valent graph) interpolating this boundary. As long as we choose a fixed topology for this interpolating triangulation, the partition function will not depend on this choice and hence is a well defined functional on the boundary Hilbert space. Additionally we can refine the boundary via a refinement move. An interpolating triangulation can be obtained by just including a coarse graining move at the appropriate dual edge. This will give a 'bubble' that can be removed due to the bubble move invariance, and we arrive at the previous partition function acting on the unrefined Hilbert space.

Hence the partition function (actually a family of functionals labelled by the boundaries b) is cylindrically consistent with respect to the embeddings provided by the refining time evolution. That automatically allows to define from the (so far) discrete partition functions a continuum limit on the projective limit Hilbert space. This is to our knowledge a new insight, as topological theories are often only discussed with regard to the invariance of the bulk triangulation.

The refinement maps can also be used to construct the Hartle Hawking vacuum states mentioned in section 7.2. To this end one has either to dualize one edge (graphically a bent or cup). Alternatively in examples where the edges are labelled by $(SU(2))$ spins, we start with a refining map for which we fix on the incoming edge $j = 0$, which gives the Hilbert space $\mathbb{C}$ associated to this edge. The (two–site) Hilbert space can then be refined further in an arbitrary way, giving the Hartle Hawking vacuum state on boundaries with different numbers of sites.

Doing this in a linear way, i.e. as for the graph on the right in equation (7.6.10) gives matrix product states (MPS) [F137,F138]. MPS provide ansätze for ground state wave functions of Hamiltonians. The projectors T defined above correspond to exponentiated Hamiltonians and the type of MPS defined in (7.6.10) is the ground state to the following Hamiltonian:

$$
H = \sum_{I=1}^{N-1} \left(\mathbb{I} - \underset{I}{\bigvee\!\!\!\bigwedge} \right) \quad , \tag{7.6.13}
$$

where I denotes the index pair the projector is acting on for a total of N outgoing legs. Thus Hartle Hawking vacuum states appear here as the ground states of the Hamiltonians (7.6.13), justifying again the notion of these states as vacuum states.

7.6.3 3D topological theories and entangling moves

Similar statements hold for higher dimensional theories, for instance BF theories. There are however interesting differences pertaining to the role of Pachner moves in discrete topological theories based on triangulations, such as the Turaev–Viro models [F139]. The physical states of these models can be described as string net states [F140].

For a canonical time evolution in (2+1)D we will have $3 - 1$, $1 - 3$ and $2 - 2$ moves as time evolution moves as described in section 7.2. These allow to build an arbitrary complex triangulated hypersurface from a simple one. In this way one can build up an analogous MPS representation of a string net state on arbitrary complex 2D triangulations or on the corresponding dual graphs. The $3 - 1$ and $1 - 3$ moves serve as (purely) coarse graining or refining moves, whereas the $2 - 2$ moves (dis–)entangle the degrees of freedom. The latter play an important role in entanglement renormalization [F40, F63].

Interestingly MPS states in one (spatial) dimensions do not lead to long range entanglement [F141, F142], whereas the example just described gives a phase with long range entanglement in two (spatial) dimensions [F63]. This might be due to the necessity of the $2 - 2$ move to obtain triangulations not equivalent to a stacked sphere (which would not support long range entanglement). In the case of the stacked sphere the consecutive $1 - 3$ moves can be represented by a tree graph. In (1+1)D all triangulations of a circle can be obtained as 'stacked spheres', which are dual to trees.

In $(3 + 1)$D we have similarly $1 - 4$ and $4 - 1$ moves as refining and coarse graining moves respectively. As mentioned before the $4 - 1$ move does not add physical degrees of freedom, as all additional degrees of freedom are associated to Hamiltonian and diffeomorphism constraints [F10, F25, F26]. Additionally we have $2 - 3$ and $3 - 2$ moves, which can be interpreted as entangling moves, similarly to the $2 - 2$ move in $(2 + 1)$D.

7.6.4 Constructing inductive limit Hilbert spaces for non–topological theories

We discussed that the embedding maps provided by the refining time evolution of topological theories satisfy the consistency conditions (7.3.2). Thus one can use these embeddings to construct an inductive limit Hilbert space as outlined in section 7.3.1.

Note that this Hilbert space will support a much bigger class of observables than just the Dirac, i.e. topological observables of the topological theory. The set of observables supported by this Hilbert space is determined by the cylindrical consistency conditions (7.3.13) for observables. The cylindrical consistent observables then describe excitations from the vacuum state, which is given by the no–boundary wave function of the topological theory. Thus the excitations in particular violate the constraints (implementing the equations of motion) of the topological theory.

This is a general proposal for the construction of inductive Hilbert spaces. It will be interesting to explore more in detail the relation between the set of cylindrical observables which characterize the inductive Hilbert space and the topological theory which provides the embedding maps.

This strategy to construct an inductive limit Hilbert space has been realized recently [F38] for the topological BF theory, which describes the moduli space of flat connections. In this case the excitations are parametrized by curvature observables. The set of cylindrically consistent observables is given by a holonomy–flux algebra underlying the formulation of loop quantum gravity and (lattice) gauge theories. This method therefore resulted in an alternative representation and a new vacuum for loop quantum gravity.

7.7 Geometric interpretation of the refining maps

Here we wish to point out that geometric theories are very special with regards to coarse graining and refining.[17] This is due to the fact that the geometry itself is included into the set of dynamical variables. The (say semi–classical) state on the boundary of a region determines a geometry for the bulk, defined as solution of the Einstein equations for the given boundary data the state is peaked on. (This of course assumes that one has a sensible theory of quantum gravity, which would result in a semi–classical state for the Hartle Hawking state.) Thus setting (geometric) scale and number of coarse graining steps as equal is, at least a priori, senseless in such theories. Rather, a renormalization scale is given by the coarseness or fineness of the boundary data, that is, the scale on which geometric properties, such as curvature, vary.

Even if one peaks the boundary state on a given geometry with a fixed (hypersurface) volume one cannot expect to find that the partition functions peaks on some regular bulk geometry such that the bulk volumes are bounded by the hypersurface volume.

The reason is that one expects diffeomorphism symmetry to emerge in the form of vertex translation invariance. This symmetry even allows to move the vertices such that orientations of building blocks are inverted. This corresponds to 'spikes' in the geometry, see for instance [F51, F144]. These spikes give rise to divergences [F23, F50–F52], related to the non–compactness of the diffeomorphism gauge orbits. As we will argue below this mechanism allows the appearance of arbitrarily large spins even in a region bounded by a small boundary geometry. This might make even a theory describing flat geometry, such as 3D BF, appear as highly fluctuating. However (almost) all these fluctuations are gauge fluctuations [F50], due to the diffeomorphism gauge symmetry. We will illustrate this with a 2D example below.

The relation between the sum of orientations and divergences has been pointed out in [F144] which also argues that allowing only one orientation could cure the problem of divergences. However, we will show here, that from the perspective of time evolution as a refining and coarse graining map, the appearance of two orientations is very natural. (It is also natural as the gravitational constraints are quadratic in the momenta describing time symmetric evolution. The two solutions of the quadratic equation correspond to the two orientations.)

7.7.1 2D example

Let us illustrate this with the intertwiner models introduced in [F115]. These host families of topological theories, which have all the properties discussed in section 7.6. Moreover the theories allow for a natural geometric interpretation, as they are defined on three–valent graphs. The edges carry a spin j ($SU(2)$ representation) and a magnetic quantum number. The spin can be interpreted as a length variable – indeed at the three–valent vertices triangle inequalities have to be satisfied arising from $SU(2)$ recoupling theory.

Consider one upward pointing line as in the examples before: This line can be interpreted as a line in a $(2D)$ space with a length given by the spin j. Using our previously defined refining maps R, we can map it to a different state, which is now labelled by two spins j' and j'':

$$\vdash\!\!\!\frac{}{j}\!\!\!\dashv \qquad \rightarrow \qquad \sum_j \;\overset{j' \wedge j''}{\underset{j}{\longmapsto}} \tag{7.7.1}$$

$$\mid \qquad \rightarrow \qquad \curlyvee \quad , \tag{7.7.2}$$

---

[17]See also the discussion in [F143], which argues that in reparametrization invariant theories all couplings are dimensionless.

where the spins j' and j'' have to satisfy triangle inequalities. However this picture is indistinguishable from adding a triangle with opposite orientation and hence 'removing' it:

$$\vdash\!\!\underset{j}{\rule{2em}{0pt}}\!\!\dashv \quad \rightarrow \quad \underset{j' \quad j''}{\diagdown\!\!\diagup} \quad . \tag{7.7.3}$$

Thus for a quantum theory this means that both possible orientations have to be taken into account in a superposition:

$$\vdash\!\!-\!\!+\!\!-\!\!\dashv \ \sim \ \triangle \ \oplus \ \triangledown \quad . \tag{7.7.4}$$

   This picture conforms with refining the edge and adding a vacuum degree of freedom (this degree of freedom is not physical, as we are considering a topological theory here): This vacuum degree of freedom allows fluctuations of the edge geometry around a flat subdivision – in the sense that the refined edge can bend upwards or downwards. Any asymmetry would appear as proper time evolution, which we do not expect for a topological or gravitational theory. In this case time evolution is generated by constraints and hence gauge – and as explained before realized as a projector in the quantum theory.

   Note that the fluctuation can be arbitrarily large, as argued below. In this case this can be linked to diffeomorphism symmetry realized by a vertex translation symmetry. The middle vertex can be translated an arbitrary large distance forward or backward (or sideways) in 'time'. Moreover, as this is a gauge symmetry, all such configurations have to be gauge equivalent, i.e. come with the same amplitude (and a diffeomorphism invariant measure[18]).

7.7.2 Spin foams

A similar picture applies to spin foams, where gluing a simplex to a boundary can be done with two orientations. From the semi–classical expressions for the simplex amplitude we again obtain a geometric picture: i.e. with a $1-4$ move (from gluing a 4–simplex to one boundary tetrahedron) we replace a boundary tetrahedron with a complex of four tetrahedra, that now allows the inner geometry of the original tetrahedra to fluctuate around a flat subdivision. Note that also in this case one did actually not add a physical degree of freedom, at least not if one deals with Regge geometries [F10,F53,F64]. The reason is that the new kinematical degrees of freedom (the four new edge lengths) are accompanied by four (Hamiltonian and diffeomorphism) constraints, associated to the new vertex. These allow to move the additional vertex arbitrarily forward or backward in time, explaining the appearance of the two orientations. As before the diffeomorphism or vertex translation symmetry also means that configurations with arbitrarily large length of the four inner edges have equal amplitude to those describing a 'flat' subdivision, thus one would expect divergences to appear for every inner vertex, for a discussion in spin foams see [F23, F50–F52, F145]. Thus one should be very careful with treating the spin j variable, which encode the length or area variables in 3D or 4D respectively, as an order parameter. (Indeed one should consider diffeomorphism invariant observables as order parameters, which are however hard to come by [F31–F34].)

   We can provide here an interpretation of the divergences as coming from (extremely) squeezed states: As mentioned we add only degrees of freedom in the vacuum state (including gauge degrees of freedom), in the case of $4-1$ moves these have to satisfy the Hamiltonian and diffeomorphism constraints. Thus, fluctuations in the 'constraint' directions are completely suppressed, whereas fluctuations in the conjugated (i.e. gauge) directions become infinitely large, represented as a non–compact gauge orbit of configurations with equal weight.

---

[18]This actually allows to determine the path integral measure, see [F120].

7.8 Discussion

We pointed out that gravitational theories in a simplicial description, provide with their time evolution maps automatically refining, coarse graining and entangling maps. More generally we interpret the degrees of freedom added during refining time evolution moves as degrees of freedom in the vacuum state (or gauge degrees of freedom). This suggests the construction of a global vacuum state as a state evolved from a one–dimensional Hilbert space $\mathbb{C}$, see also [F10, F102, F103], which gives a simplicial realization of the no–boundary proposal [F86]. Indeed via the notion of dynamical cylindrical consistency [F9], we can identify the vacuum states as representing the equivalence class which includes the unique state in the 'no–boundary' Hilbert space $\mathbb{C}$ on different discretizations.

We argued that the time evolution maps provide embedding maps for the construction of the continuum limit via projective techniques. In section 7.4 we outlined how to define and arrive at a consistent continuum dynamics for quantum gravity. This is based on the dynamical embedding maps and proposes to construct the amplitude maps as cylindrically consistent maps based on these embeddings. This allows to define the amplitude maps as objects of the continuum theory on the continuum Hilbert space.

Such (dynamical) embedding maps have however to satisfy stringent path independence conditions, which we related to the path independence under different choices of interpolating hypersurfaces [F109, F110] and an anomaly free representation of the Dirac algebra of constraints [F45–F47, F113]. These conditions are indeed hard to satisfy exactly for interacting theories but should be valid in some approximate sense if considering sufficiently coarse grained observables.

We explained that tensor network renormalization algorithms provide a method to construct dynamical embedding maps that do satisfy the consistency conditions to a better approximation and the related (approximately) cylindrically consistent amplitudes. An important ingredient in these algorithms are truncations. Good truncations are basically good reorganizations of the degrees of freedom into coarser ones and finer ones. We argued that such a splitting can be found by employing radial, that is refining, evolution.

In topological theories the refining time evolution maps typically satisfy the path independence conditions. This allows the construction of projective limit Hilbert spaces using refining time evolution as embedding maps. This will realize the physical state of the topological theory (satisfying the constraints of the topological theory) as a vacuum in this projective limit Hilbert space. This vacuum coincides with the no–boundary wave functions. Excitations can be produced by cylindrically consistent observables. An example of this construction has been recently provided in [F38].

For non–topological theories, such as 4D gravity, we suggest that an exact satisfaction of the path independence conditions for the embedding maps would rather involve non–local dynamics, as is indicated by the discussion in section 7.2.3. The construction of the continuum limit in section 7.4 allows for such non–local embeddings. The necessity of a non–local dynamics has been recently argued for in [F121], which points out that linearized 4D quantum Regge calculus requires a non–local path integral measure in order to show invariance under $5 - 1$ moves.

From a statistical physics point of view one would expect that a second order phase transition is needed for the continuum limit, leading to long range (in terms of number of lattice cites) correlations and a conformal theory at the boundary. Indeed in the context of tensor network algorithms and radial evolution the appearance of a conformal theory at the fixed point leads to an interpretation in terms of AdS geometries and holographic renormalization, for instance [F41–F43]. For the case of non–perturbative gravity such an interpretation might not apply straightforwardly. Here one would expect that the boundary variables or the quantum state defined on the boundary encodes the geometry of the boundary and – via the equations of motion – of the bulk.

There are still many puzzling features to explore in the context of discretization changing time evolution. This in particular applies to interacting theories, such as 4D gravity. As we outlined here such discretization changing evolution might however provide a definition of the physical vacuum and more generally allow the construction of the continuum limit of the theory. This makes the

explorations of these issues very worthwhile.

Acknowledgements

References

[F1] R. Loll, "Discrete approaches to quantum gravity in four-dimensions," *Living Rev. Rel.* **1** (1998) 13, `arXiv:gr-qc/9805049 [gr-qc]`.

[F2] B. Dittrich, F. C. Eckert, and M. Martin-Benito, "Coarse graining methods for spin net and spin foam models," *New J. Phys.* **14** (2012) 035008, `arXiv:1109.4927 [gr-qc]`.

[F3] B. Dittrich and F. C. Eckert, "Towards computational insights into the large-scale structure of spin foams," *J. Phys. Conf. Ser.* **360** (2012) 012004, `arXiv:1111.0967 [gr-qc]`.

[F4] A. Baratin, S. Carrozza, D. Oriti, J. Ryan, and M. Smerlak, "Melonic phase transition in group field theory," *Lett.Math.Phys.* **104** (2014) 1003–1017, `arXiv:1307.5026 [hep-th]`.

[F5] E. R. Livine, "Deformation Operators of Spin Networks and Coarse-Graining," *Class. Quant. Grav.* **31** (2014) 075004, `arXiv:1310.3362 [gr-qc]`.

[F6] K. G. Wilson and J. B. Kogut, "The renormalization group and the epsilon expansion," *Phys. Rept.* **12** (1974) 75–200.

[F7] M. Levin and C. P. Nave, "Tensor renormalization group approach to 2d classical lattice models," *Phys. Rev. Lett.* **99** (2007) 120601, `arXiv:cond-mat/0611687 [gr-qc]`.

[F8] Z.-C. Gu and X.-G. Wen, "Tensor-Entanglement-Filtering Renormalization Approach and Symmetry Protected Topological Order," *Phys. Rev. B* **80** (2009) 155131, `arXiv:0903.1069 [cond-mat.str-el]`.

[F9] B. Dittrich, "From the discrete to the continuous: Towards a cylindrically consistent dynamics," *New J. Phys.* **14** (2012) 123004, `arXiv:1205.6127 [gr-qc]`.

[F10] B. Dittrich and P. A. Höhn, "Canonical simplicial gravity," *Class. Quant. Grav.* **29** (2012) 115009, `arXiv:1108.1974 [gr-qc]`.

[F11] B. Dittrich and P. A. Höhn, "Constraint analysis for variational discrete systems," *J. Math. Phys.* **54** (2013) 093505, `arXiv:1303.4294 [math-ph]`.

[F12] G. Ponzano and T. Regge, *Semiclassical limit of Racah coefficients, in: Spectroscopy and group theoretical methods in physics.* North Holland Publ. Co., Amsterdam, 1968.

[F13] J. W. Barrett and I. Naish-Guzman, "The Ponzano-Regge model," *Class. Quant. Grav.* **26** (2009) 155014, `arXiv:0803.3319 [gr-qc]`.

[F14] A. Perez, "The Spin Foam Approach to Quantum Gravity," *Living Rev. Rel.* **16** (2013) 3, `arXiv:1205.2019 [gr-qc]`.

[F15] C. Rovelli, *Quantum gravity.* Cambridge University Press, Cambridge, 2004.

[F16] J. W. Barrett and L. Crane, "Relativistic spin networks and quantum gravity," *J. Math. Phys.* **39** (1998) 3296–3302, `arXiv:gr-qc/9709028 [gr-qc]`.

[F17] J. Engle, E. Livine, R. Pereira, and C. Rovelli, "LQG vertex with finite Immirzi parameter," *Nucl. Phys. B* **799** (2008) 136–149, `arXiv:0711.0146 [gr-qc]`.

[F18] E. R. Livine and S. Speziale, "A New spinfoam vertex for quantum gravity," *Phys. Rev. D* **76** (2007) 084028, `arXiv:0705.0674 [gr-qc]`.

[F19] L. Freidel and K. Krasnov, "A New Spin Foam Model for 4d Gravity," *Class. Quant. Grav.* **25** (2008) 125018, `arXiv:0708.1595 [gr-qc]`.

[F20] A. Baratin and D. Oriti, "Quantum simplicial geometry in the group field theory formalism: reconsidering the Barrett-Crane model," *New J. Phys.* **13** (2011) 125011, `arXiv:1108.1178 [gr-qc]`.

[F21] M. Rocek and R. M. Williams, "Quantum Regge Calculus," *Phys. Lett. B* **104** (1981) 31.

[F22] M. Rocek and R. M. Williams, "The Quantization of Regge Calculus," *Z. Phys. C* **21** (1984) 371.

[F23] L. Freidel and D. Louapre, "Diffeomorphisms and spin foam models," *Nucl. Phys. B* **662** (2003) 279–298, `arXiv:gr-qc/0212001 [gr-qc]`.

[F24] B. Dittrich, "Diffeomorphism symmetry in quantum gravity models," *Adv. Sci. Lett.* **2** (2009) 151, `arXiv:0810.3594 [gr-qc]`.

[F25] B. Bahr and B. Dittrich, "(Broken) Gauge Symmetries and Constraints in Regge Calculus," *Class. Quant. Grav.* **26** (2009) 225011, `arXiv:0905.1670 [gr-qc]`.

[F26] B. Bahr and B. Dittrich, "Breaking and restoring of diffeomorphism symmetry in discrete gravity," *AIP Conf. Proc.* **1196** (2009) 10–17, `arXiv:0909.5688 [gr-qc]`.

[F27] B. Bahr, B. Dittrich, and S. Steinhaus, "Perfect discretization of reparametrization invariant path integrals," *Phys. Rev. D* **83** (2011) 105026, `arXiv:1101.4775 [gr-qc]`.

[F28] J. J. Halliwell and J. B. Hartle, "Wave functions constructed from an invariant sum over histories satisfy constraints," *Phys. Rev. D* **43** (1991) 1170–1194.

[F29] C. Rovelli, "The projector on physical states in loop quantum gravity," *Phys. Rev. D* **59** (1999) 104015, `arXiv:gr-qc/9806121 [gr-qc]`.

[F30] K. Noui and A. Perez, "Three-dimensional loop quantum gravity: Physical scalar product and spin foam models," *Class. Quant. Grav.* **22** (2005) 1739–1762, `arXiv:gr-qc/0402110 [gr-qc]`.

[F31] C. Rovelli, "Partial observables," *Phys. Rev. D* **65** (2002) 124013, `arXiv:gr-qc/0110035 [gr-qc]`.

[F32] B. Dittrich, "Partial and complete observables for Hamiltonian constrained systems," *Gen. Rel. Grav.* **39** (2007) 1891–1927, `arXiv:gr-qc/0411013 [gr-qc]`.

[F33] B. Dittrich, "Partial and complete observables for canonical general relativity," *Class. Quant. Grav.* **23** (2006) 6155–6184, `arXiv:gr-qc/0507106 [gr-qc]`.

[F34] A. Dapor, W. Kamiński, J. Lewandowski, and J. wieewski, "Relational Evolution of Observables for Hamiltonian-Constrained Systems," *Phys. Rev. D* **88** (2013) 084007, `arXiv:1305.0394 [gr-qc]`.

[F35] A. Ashtekar and C. J. Isham, "Representations of the holonomy algebras of gravity and nonAbelian gauge theories," *Class. Quant. Grav.* **9** (1992) 1433–1468, `arXiv:hep-th/9202053 [hep-th]`.

[F36] A. Ashtekar and J. Lewandowski, "Projective techniques and functional integration for gauge theories," *J. Math. Phys.* **36** (1995) 2170–2191, `gr-qc/9411046`.

[F37] T. Thiemann, *Modern Canonical Quantum General Relativity.* Cambridge University Press, Cambridge, 2008.

[F38] B. Dittrich and M. Geiller, "A new vacuum for Loop Quantum Gravity," `arXiv:1401.6441 [gr-qc]`.

[F39] K. Skenderis, "Lecture notes on holographic renormalization," *Class. Quant. Grav.* **19** (2002) 5849–5876, `arXiv:hep-th/0209067 [hep-th]`.

[F40] G. Vidal, "Entanglement Renormalization," *Phys. Rev. Lett.* **99** (2007) 220405, `arXiv:cond-mat/0512165 [cond-mat]`.

[F41] B. Swingle, "Constructing holographic spacetimes using entanglement renormalization," `arXiv:1209.3304 [hep-th]`.

[F42] G. Evenbly and G. Vidal, "Tensor network states and geometry," *J. Stat. Phys.* **145** (2011) 891–918, `arXiv:1106.1082 [quant-ph]`.

[F43] M. Nozaki, S. Ryu, and T. Takayanagi, "Holographic Geometry of Entanglement Renormalization in Quantum Field Theories," *JHEP* **1210** (2012) 193, `arXiv:1208.3469 [hep-th]`.

[F44] T. Regge, "General Relativity Without Coordinates," *Nuovo Cim.* **19** (1961) 558–571.

[F45] T. Thiemann, "Anomaly - free formulation of nonperturbative, four-dimensional Lorentzian quantum gravity," *Phys. Lett. B* **380** (1996) 257–264, `arXiv:gr-qc/9606088 [gr-qc]`.

[F46] T. Thiemann, "Quantum spin dynamics (QSD)," *Class.Quant.Grav.* **15** (1998) 839–873, `arXiv:gr-qc/9606089 [gr-qc]`.

[F47] T. Thiemann, "QSD 3: Quantum constraint algebra and physical scalar product in quantum general relativity," *Class.Quant.Grav.* **15** (1998) 1207–1247, `arXiv:gr-qc/9705017 [gr-qc]`.

[F48] M. Lehto, H. B. Nielsen, and M. Ninomiya, "Diffeomorphism Symmetry in Simplicial Quantum Gravity," *Nucl.Phys.* **B272** (1986) 228.

[F49] B. Bahr and B. Dittrich, "Improved and Perfect Actions in Discrete Gravity," *Phys. Rev. D* **80** (2009) 124030, `arXiv:0907.4323 [gr-qc]`.

[F50] V. Bonzom and M. Smerlak, "Bubble divergences from cellular cohomology," *Lett.Math.Phys.* **93** (2010) 295–305, `arXiv:1004.5196 [gr-qc]`.

[F51] A. Riello, "Self-energy of the Lorentzian Engle-Pereira-Rovelli-Livine and Freidel-Krasnov model of quantum gravity," *Phys.Rev.* **D88** no. 2, (2013) 024011, `arXiv:1302.1781 [gr-qc]`.

[F52] V. Bonzom and B. Dittrich, "Bubble divergences and gauge symmetries in spin foams," *Phys.Rev.* **D88** (2013) 124021, `arXiv:1304.6632 [gr-qc]`.

[F53] B. Dittrich and J. P. Ryan, "Phase space descriptions for simplicial 4d geometries," *Class. Quant. Grav.* **28** (2011) 065006, `arXiv:0807.2806 [gr-qc]`.

References

[F54] M. Dupuis, J. P. Ryan, and S. Speziale, "Discrete gravity models and Loop Quantum Gravity: a short review," *SIGMA* **8** (2012) 052, `arXiv:1204.5394 [gr-qc]`.

[F55] C. Rovelli and S. Speziale, "On the geometry of loop quantum gravity on a graph," *Phys. Rev. D* **82** (2010) 044018, `arXiv:1005.2927 [gr-qc]`.

[F56] Y. Neiman, "A look at area Regge calculus," `arXiv:1308.1012 [gr-qc]`.

[F57] B. Dittrich and S. Speziale, "Area-angle variables for general relativity," *New J. Phys.* **10** (2008) 083006, `arXiv:0802.0864 [gr-qc]`.

[F58] B. Bahr and B. Dittrich, "Regge calculus from a new angle," *New J. Phys.* **12** (2010) 033010, `arXiv:0907.4325 [gr-qc]`.

[F59] R. Sorkin, "The Electromagnetic field on a simplicial net," *J. Math. Phys.* **16** (1975) 2432–2440.

[F60] U. Pachner, "Konstruktionsmethoden und das kombinatorische Homöomorphieproblem für Triangulationen kompakter semilinearer Mannigfaltigkeiten," *Abh. Math. Sem. Univ. Hamburg* **57** (1986) 69.

[F61] U. Pachner, "P. L. Homeomorphic Manifolds are Equivalent by Elementary Shellings," *Europ. J. Combinatorics* **12** (1991) 129–145.

[F62] G. Carbone, M. Carfora, and A. Marzuoli, "Hierarchies of invariant spin models," *Nucl. Phys. B* **619** (2001) 654–688, `arXiv:gr-qc/0008011 [gr-qc]`.

[F63] R. Koenig, B. W. Reichardt, and G. Vidal, "Exact entanglement renormalization for string-net models," *Phys. Rev. B* **79** (2009) 195123, `arXiv:0806.4583 [cond-mat.str-el]`.

[F64] B. Dittrich and P. A. Höhn, "From covariant to canonical formulations of discrete gravity," *Class. Quant. Grav.* **27** (2010) 155001, `arXiv:0912.1817 [gr-qc]`.

[F65] J. Marsden and M. West, "Discrete mechanics and variational integrators," *Acta Numerica* **10** (2001) 357.

[F66] R. Gambini and J. Pullin, "Consistent discretizations as a road to quantum gravity," *In *Oriti, D. (ed.): Approaches to quantum gravity* 378-392* (2005) , `arXiv:gr-qc/0512065 [gr-qc]`.

[F67] M. Campiglia, C. Di Bartolo, R. Gambini, and J. Pullin, "Uniform discretizations: A Quantization procedure for totally constrained systems including gravity," *J.Phys.Conf.Ser.* **67** (2007) 012020, `arXiv:gr-qc/0606121 [gr-qc]`.

[F68] M. Campiglia, C. Di Bartolo, R. Gambini, and J. Pullin, "Uniform discretizations: A New approach for the quantization of totally constrained systems," *Phys.Rev.* **D74** (2006) 124012, `arXiv:gr-qc/0610023 [gr-qc]`.

[F69] V. Husain and O. Winkler, "Discrete Hamiltonian evolution and quantum gravity," *Class.Quant.Grav.* **21** (2004) 941–950, `arXiv:gr-qc/0308011 [gr-qc]`.

[F70] B. Bahr, R. Gambini, and J. Pullin, "Discretisations, constraints and diffeomorphisms in quantum gravity," *SIGMA* **8** (2012) 002, `arXiv:1111.1879 [gr-qc]`.

[F71] J. W. Barrett and T. J. Foxon, "Semiclassical limits of simplicial quantum gravity," *Class. Quant. Grav.* **11** (1994) 543–556, `arXiv:gr-qc/9310016 [gr-qc]`.

[F72] J. W. Barrett, R. J. Dowdall, W. J. Fairbairn, H. Gomes, and F. Hellmann, "Asymptotic analysis of the EPRL four-simplex amplitude," *J. Math. Phys.* **50** (2009) 112504, `arXiv:0902.1170 [gr-qc]`.

[F73] F. Conrady and L. Freidel, "On the semiclassical limit of 4d spin foam models," *Phys. Rev. D* **78** (2008) 104023, `arXiv:0809.2280 [gr-qc]`.

[F74] W. Kamiński and S. Steinhaus, "The BarrettCrane model: asymptotic measure factor," *Class. Quant. Grav.* **31** (2014) 075014, `arXiv:1310.2957 [gr-qc]`.

[F75] B. Z. Foster and T. Jacobson, "Quantum field theory on a growing lattice," *JHEP* **0408** (2004) 024, `arXiv:hep-th/0407019 [hep-th]`.

[F76] A. Kempf, A. Chatwin-Davies, and R. T. W. Martin, "A fully covariant information-theoretic ultraviolet cutoff for scalar fields in expanding FRW spacetimes," *J. Math. Phys.* **54** (2013) 022301, `arXiv:1210.0750 [gr-qc]`.

[F77] B. Dittrich and K. Tate, "Exact discretizations." 2012.

[F78] P. Hasenfratz and F. Niedermayer, "Perfect lattice action for asymptotically free theories," *Nucl. Phys. B* **414** (1994) 785–814, `arXiv:hep-lat/9308004 [hep-lat]`.

[F79] P. Hasenfratz, "Prospects for perfect actions," *Nucl. Phys. Proc. Suppl.* **63** (1998) 53–58, `arXiv:hep-lat/9709110 [hep-lat]`. In *Edinburgh 1997, Lattice field theory* 53-58.

[F80] B. Bahr, B. Dittrich, and S. He, "Coarse graining free theories with gauge symmetries: the linearized case," *New J. Phys.* **13** (2011) 045009, `arXiv:1011.3667 [gr-qc]`.

[F81] W. Bietenholz, "Perfect scalars on the lattice," *Int. J. Mod. Phys. A* **15** (2000) 3341–3368, `arXiv:hep-lat/9911015 [hep-lat]`.

[F82] A. Kempf, "Spacetime could be simultaneously continuous and discrete in the same way that information can," *New J. Phys.* **12** (2010) 115001, `arXiv:1010.4354 [gr-qc]`.

[F83] T. Thiemann, "The phoenix project: Master constraint program for loop quantum gravity," *Class. Quant. Grav.* **23** (2006) 2211–2248, `arXiv:gr-qc/0305080 [gr-qc]`.

[F84] B. Dittrich and T. Thiemann, "Testing the master constraint programme for loop quantum gravity. I. General framework," *Class. Quant. Grav.* **23** (2006) 1025–1066, `arXiv:gr-qc/0411138 [gr-qc]`.

[F85] B. Dittrich and T. Thiemann, "Testing the master constraint programme for loop quantum gravity. II. Finite dimensional systems," *Class. Quant. Grav.* **23** (2006) 1067–1088, `arXiv:gr-qc/0411139 [gr-qc]`.

[F86] J. B. Hartle and S. W. Hawking, "Wave Function of the Universe," *Phys. Rev. D* **28** (1983) 2960–2975.

[F87] N. T. Bishop, R. Gomez, L. Lehner, and J. Winicour, "Cauchy characteristic extraction in numerical relativity," *Phys.Rev.* **D54** (1996) 6153–6165.

[F88] A. Henderson, A. Laddha, and C. Tomlin, "Constraint algebra in LQG reloaded : Toy model of a $u(1)^3$ Gauge Theory I," *Phys. Rev. D* **88** (2013) 044028, `arXiv:1204.0211 [gr-qc]`.

[F89] C. Tomlin and M. Varadarajan, "Towards an Anomaly-Free Quantum Dynamics for a Weak Coupling Limit of Euclidean Gravity," *Phys. Rev. D* **87** (2013) 044039, `arXiv:1210.6869 [gr-qc]`.

[F90] M. Varadarajan, "Dirac quantization of parametrized field theory," *Phys. Rev. D* **75** (2007) 044018, `arXiv:gr-qc/0607068 [gr-qc]`.

[F91] A. Laddha and M. Varadarajan, "Polymer Parametrised Field Theory," *Phys. Rev. D* **78** (2008) 044008, `arXiv:0805.0208 [gr-qc]`.

[F92] A. Laddha and M. Varadarajan, "The Hamiltonian constraint in Polymer Parametrized Field Theory," *Phys. Rev. D* **83** (2011) 025019, `arXiv:1011.2463 [gr-qc]`.

[F93] Y. Neiman, "On-shell actions with lightlike boundary data," `arXiv:1212.2922 [hep-th]`.

[F94] M. P. Reisenberger, "The Symplectic 2-form and Poisson bracket of null canonical gravity," `arXiv:gr-qc/0703134 [gr-qc]`.

[F95] M. P. Reisenberger, "The Poisson bracket on free null initial data for gravity," *Phys. Rev. Lett.* **101** (2008) 211101, `arXiv:0712.2541 [gr-qc]`.

[F96] Y. Neiman, "Polyhedra in spacetime from null vectors," *Class. Quant. Grav.* **31** (2014) 015011, `arXiv:1308.1982 [gr-qc]`.

[F97] S. Speziale and M. Zhang, "Null twisted geometries," *Phys.Rev.* **D89** (2014) 084070, `arXiv:1311.3279 [gr-qc]`.

[F98] L. Freidel, M. Geiller, and J. Ziprick, "Continuous formulation of the Loop Quantum Gravity phase space," *Class. Quant. Grav.* **30** (2013) 085013, `arXiv:1110.4833 [gr-qc]`.

[F99] L. Freidel and J. Ziprick, "Spinning geometry = Twisted geometry," *Class.Quant.Grav.* **31** (2014) 045007, `arXiv:1308.0040 [gr-qc]`.

[F100] B. Dittrich and J. Tambornino, "A Perturbative approach to Dirac observables and their space-time algebra," *Class.Quant.Grav.* **24** (2007) 757–784, `arXiv:gr-qc/0610060 [gr-qc]`.

[F101] B. Dittrich and J. Tambornino, "Gauge invariant perturbations around symmetry reduced sectors of general relativity: Applications to cosmology," *Class.Quant.Grav.* **24** (2007) 4543–4586, `arXiv:gr-qc/0702093 [gr-qc]`.

[F102] P. A. Höhn, "Quantization of systems with temporally varying discretization I: Evolving Hilbert spaces," *J.Math.Phys.* **55** (2014) 083508, `arXiv:1401.6062 [gr-qc]`.

[F103] P. A. Höhn, "Quantization of systems with temporally varying discretization II: Local evolution moves," *J.Math.Phys.* **55** (2014) 103507, `arXiv:1401.7731 [gr-qc]`.

[F104] B. Dittrich, P. A. Höhn, and T. Jacobson. to appear.

[F105] F. Conrady, L. Doplicher, R. Oeckl, C. Rovelli, and M. Testa, "Minkowski vacuum in background independent quantum gravity," *Phys.Rev.* **D69** (2004) 064019, `arXiv:gr-qc/0307118 [gr-qc]`.

[F106] M. Bojowald, A. L. Chinchilli, C. C. Dantas, M. Jaffe, and D. Simpson, "Non-linear (loop) quantum cosmology," *Phys. Rev. D* **86** (2012) 124027, `arXiv:1210.8138 [gr-qc]`.

[F107] M. Bojowald, "Mathematical structure of loop quantum cosmology: Homogeneous models," *SIGMA* **9** (2013) 082, `arXiv:1206.6088 [gr-qc]`.

[F108] W. Nelson and M. Sakellariadou, "Lattice Refining Loop Quantum Cosmology from an Isotropic Embedding of Anisotropic Cosmology," *Class. Quant. Grav.* **27** (2010) 145014, `arXiv:0906.0292 [gr-qc]`.

[F109] K. Kuchar, "Geometry of Hyperspace. 1.," *J.Math.Phys.* **17** (1976) 777–791.

[F110] C. Isham, "Canonical quantum gravity and the problem of time," `arXiv:gr-qc/9210011 [gr-qc]`. Published in In *Salamanca 1992, Proceedings, Integrable systems, quantum groups, and quantum field theories* 157-287, and London Imp. Coll. - ICTP-91-92-25 (92/08,rec.Nov.) 124 p.

[F111] R. Sorkin, "Time Evolution Problem in Regge Calculus," *Phys.Rev.* **D12** (1975) 385–396.

[F112] J. W. Barrett, M. Galassi, W. A. Miller, R. D. Sorkin, P. A. Tuckey, *et al.*, "A Paralellizable implicit evolution scheme for Regge calculus," *Int.J.Theor.Phys.* **36** (1997) 815–840, `arXiv:gr-qc/9411008 [gr-qc]`.

[F113] V. Bonzom and B. Dittrich, "Diracs discrete hypersurface deformation algebras," *Class.Quant.Grav.* **30** (2013) 205013, `arXiv:1304.5983 [gr-qc]`.

[F114] B. Dittrich, "How to construct diffeomorphism symmetry on the lattice," *PoS* **QGQGS2011** (2011) 012, `arXiv:1201.3840 [gr-qc]`.

[F115] B. Dittrich and W. Kaminski, "Topological lattice field theories from intertwiner dynamics," `arXiv:1311.1798 [gr-qc]`.

[F116] J. Lewandowski and D. Marolf, "Loop constraints: A Habitat and their algebra," *Int.J.Mod.Phys.* **D7** (1998) 299–330, `arXiv:gr-qc/9710016 [gr-qc]`.

[F117] R. Gambini, J. Lewandowski, D. Marolf, and J. Pullin, "On the consistency of the constraint algebra in spin network quantum gravity," *Int.J.Mod.Phys.* **D7** (1998) 97–109, `arXiv:gr-qc/9710018 [gr-qc]`.

[F118] M. P. Reisenberger and C. Rovelli, "'Sum over surfaces' form of loop quantum gravity," *Phys.Rev.* **D56** (1997) 3490–3508, `arXiv:gr-qc/9612035 [gr-qc]`.

[F119] J. Barbour, T. Koslowski, and F. Mercati, "A Gravitational Origin of the Arrows of Time," `arXiv:1310.5167 [gr-qc]`.

[F120] M. Bojowald and A. Perez, "Spin foam quantization and anomalies," *Gen.Rel.Grav.* **42** (2010) 877–907, `arXiv:gr-qc/0303026 [gr-qc]`.

[F121] B. Dittrich, W. Kaminski, and S. Steinhaus, "Discretization independence implies non-locality in 4D discrete quantum gravity," *Class.Quant.Grav.* **31** (2014) 245009, `arXiv:1404.5288 [gr-qc]`.

[F122] R. Oeckl, "A 'General boundary' formulation for quantum mechanics and quantum gravity," *Phys.Lett.* **B575** (2003) 318–324, `arXiv:hep-th/0306025 [hep-th]`.

[F123] B. Bahr, "Operator Spin Foams: holonomy formulation and coarse graining," *J.Phys.Conf.Ser.* **360** (2012) 012042, `arXiv:1112.3567 [gr-qc]`.

[F124] T. Nishino and K. Okunishi, "Corner Transfer Matrix Renormalization Group Method," *J. Phys. Soc. Jpn.* **65** (1996) 891, `arXiv:cond-mat/9507087 [cond-mat]`.

[F125] Z. Xie, H. Jiang, Q. Chen, Z. Weng, and T. Xiang, "Second Renormalization of Tensor-Network States," *Phys.Rev.Lett.* **103** (2009) 160601, `arXiv:0809.0182 [cond-mat.str-el]`.

[F126] Z. Y. Xie, J. Chen, M. P. Qin, J. W. Zhu, L. P. Yang, and T. Xiang, "Coarse-graining renormalization by higher-order singular value decomposition," *Phys. Rev. B* **86** (2012) 045139, `arXiv:1201.1144 [cond-mat.stat-mech]`.

[F127] L. Wang, Y.-J. Kao, and A. W. Sandvik, "Plaquette renormalization scheme for tensor network states," *Phys. Rev. E* **83** (2011) 056703.

[F128] B. Bahr, B. Dittrich, and J. P. Ryan, "Spin foam models with finite groups," *J. Grav.* **2013** (2013) 549824, `arXiv:1103.6264 [gr-qc]`.

[F129] B. Dittrich, M. Martín-Benito, and E. Schnetter, "Coarse graining of spin net models: dynamics of intertwiners," *New J. Phys.* **15** (2013) 103004, `arXiv:1306.2987 [gr-qc]`.

[F130] B. Dittrich, M. Martin-Benito, and S. Steinhaus, "Quantum group spin nets: refinement limit and relation to spin foams," *Phys.Rev.* **D90** (2014) 024058, `arXiv:1312.0905 [gr-qc]`.

[F131] M. P. Reisenberger, "On relativistic spin network vertices," *J.Math.Phys.* **40** (1999) 2046–2054, `arXiv:gr-qc/9809067 [gr-qc]`.

[F132] W. Kaminski, M. Kisielowski, and J. Lewandowski, "Spin-Foams for All Loop Quantum Gravity," *Class.Quant.Grav.* **27** (2010) 095006, `arXiv:0909.0939 [gr-qc]`.

[F133] B. Bahr, F. Hellmann, W. Kaminski, M. Kisielowski, and J. Lewandowski, "Operator Spin Foam Models," *Class.Quant.Grav.* **28** (2011) 105003, `arXiv:1010.4787 [gr-qc]`.

[F134] B. Bahr, B. Dittrich, F. Hellmann, and W. Kaminski, "Holonomy Spin Foam Models: Definition and Coarse Graining," *Phys. Rev. D* **87** (2013) Phys.Rev. D87 (2013) 044048, `arXiv:1208.3388 [gr-qc]`.

[F135] B. Dittrich, F. Hellmann, and W. Kaminski, "Holonomy Spin Foam Models: Boundary Hilbert spaces and Time Evolution Operators," *Class. Quant. Grav.* **30** (2013) 085005, `arXiv:1209.4539 [gr-qc]`.

[F136] M. Fukuma, S. Hosono, and H. Kawai, "Lattice topological field theory in two-dimensions," *Commun.Math.Phys.* **161** (1994) 157–176, `arXiv:hep-th/9212154 [hep-th]`.

[F137] M. Fannes, B. Nachtergaele, and R. Werner, "FINITELY CORRELATED STATES ON QUANTUM SPIN CHAINS," *Commun.Math.Phys.* **144** (1992) 443–490.

[F138] F. Verstraete, J. I. Cirac, and V. Murg, "Matrix Product States, Projected Entangled Pair States, and variational renormalization group methods for quantum spin systems," *Adv. Phys.* **57** (2008) 143, `arXiv:cond-mat/9503107 [cond-mat]`.

[F139] V. Turaev and O. Viro, "State sum invariants of 3 manifolds and quantum 6j symbols," *Topology* **31** (1992) 865–902.

[F140] M. A. Levin and X.-G. Wen, "String net condensation: A Physical mechanism for topological phases," *Phys.Rev.* **B71** (2005) 045110, `arXiv:cond-mat/0404617 [cond-mat]`.

[F141] N. Schuch, I. Cirac, and D. Perez-Garcia, "PEPS as ground states: degeneracy and topology," *Annals of Physics* **325** (2010) 2153, `arXiv:1001.3807 [quant-ph]`.

[F142] N. Schuch, D. Perez-Garcia, and I. Cirac, "Classifying quantum phases using matrix product states and PEPS," *Phys. Rev. B* **84** (2011) 165139, `arXiv:1010.3732 [cond-mat.str-el]`.

[F143] C. Rovelli, "Discretizing parametrized systems: the magic of Ditt-invariance," `arXiv:1107.2310 [hep-lat]`.

[F144] M. Christodoulou, M. Langvik, A. Riello, C. Roken, and C. Rovelli, "Divergences and Orientation in Spinfoams," *Class. Quant. Grav.* **30** (2013) 055009, `arXiv:1207.5156 [gr-qc]`.

[F145] C. Perini, C. Rovelli, and S. Speziale, "Self-energy and vertex radiative corrections in LQG," *Phys.Lett.* **B682** (2009) 78–84, `arXiv:0810.1714 [gr-qc]`.

8 Discussion

The overarching question of this thesis concerns the intricate relation between discrete models of quantum gravity and the classical continuum theory of general relativity, which we explore at very different levels of the discretisations. Some presented results only deal with one building block, while in others we develop and apply tools to study the collective behaviour of literally infinitely many building blocks and discuss how to consistently construct a continuum theory from the discrete one. At first sight, these results appear to be partially disconnected or isolated. Therefore, the purpose of this discussion is not only to discuss their significance with respect to the overarching questions and how they fit into the already existing knowledge in quantum gravity, but to link them together to form a consistent line of argument. As a guiding principle we will order the discussion of the results by the number of involved fundamental building blocks, starting only from a few moving towards the limit of infinite refinement. Furthermore this ordering is (partially) chronological with respect to insights derived in quantum gravity, such that we can regard the results at few building blocks as a guidance how to explore the dynamics of many building blocks.

8.1 Microscopic building blocks: asymptotic expansion and the measure factor

In this spirit one may ask what one can learn about discrete quantum gravity models, when one considers only one fundamental building block, e.g. one simplex. In spin foam models [21, 22] this corresponds to a single vertex amplitude, the amplitude dual to the simplex, for which one is interested in its relation to other discrete (classical) models of gravity like Regge calculus [17, 18]. A very popular tool to extract geometric information from the vertex amplitude is by considering asymptotic expansions by uniformly scaling up the geometric data, frequently SU(2) spins, to macroscopic sizes and identifying the dominant contribution in terms of an effective action. The scaling of the spins can also be understood as the limit $\hbar \to 0$, such that asymptotic limits are frequently called semi–classical.

The prototype of this idea is the Ponzano–Regge model [23,80], a spin foam model of 3D quantum gravity, which has the SU(2) $6j$ symbol as its vertex amplitude. The famous formula by Ponzano and Regge [23], which has been derived since then by a plethora of other methods [27, 91–96, 99, 100], shows that the $6j$ symbol is proportional to the (cosine of the) discrete Regge gravity action associated to a tetrahedron constructed from SU(2) spins.

Similar results [24–27] also exist for the modern 4D spin foam models [73–75], of which many are obtained via a coherent state approach [28, 29]. The vertex amplitudes are usually constructed via a specific contraction of invariants (under the action of the group) in the tensor product of vector spaces of irreducible representations of the group [77]. In case of the $6j$ symbol, this accounts for a particular contraction of four Clebsch–Gordan coefficients. One way to construct these invariants is by group averaging a tensor product of states (living in the vector space associated to the irreducible representation); for specific choices, namely the eponymous coherent states [90], this leads to non–trivial invariants. Furthermore, the coherent states are peaked on classical geometric notions, e.g. for SU(2) they are labelled by a vector $\vec{n} \in S^2$.

In the asymptotic expansion of the vertex amplitude one scales up the representation labels associated to the simplex and evaluates the amplitude on the points of stationary phase of the group integrations. Due to the geometric data carried by the coherent states, the stationary point

conditions allow for a clear geometric interpretation, e.g. in 3D, the three vectors labelling a 3–valent invariant, which is unique in SU(2) up to normalisation, form a (coherent) triangle [81] if the vectors sum to zero, i.e. $\sum_i j_i \vec{n}_i = 0$. This is also known as the closure constraint of the triangle. Then these vectors are interpreted as the edge vectors of the triangle. This geometric interpretation makes it straight–forward to identify the dominating phase as the Regge action associated to the simplex, yet again as for the $6j$ symbol, the amplitude oscillates with the cosine of the Regge action.

Despite these successes and positive indications underlining the relation of spin foam models to discrete gravity, it is generically not possible to derive the entire leading order contribution of the asymptotic expansion using the coherent state approach. This missing part, sometimes referred to as the 'measure', which one obtains from the determinant of the Hessian matrix, should not be underrated: Essentially it gives us a very first glance at the measure on the space of geometries chosen in spin foam models. Furthermore, it is the most directly accessible, yet naive, quantum correction. The inability to compute these measure factors, besides numerical results [26, 96], even for the well–known SU(2) $6j$ symbol, is rather troubling for the coherent state approach, but can be overcome by introducing modified coherent states.

8.1.1 Modified coherent states and the relation to first order Regge calculus

To solve the issue illustrated above for the SU(2) $6j$ symbol, we introduce new 'smeared' coherent states in [30], see also chapter 2. We would like to emphasize that the purpose of this work is not to invent yet another method to derive the Ponzano–Regge formula [23], which is known for over 40 years, but to test the idea of new coherent states in the context of a well–examined example.

These new coherent states can be understood as follows: Normally, the familiar SU(2) coherent states are eigenstates of highest weight of a generator of rotations. Thus, this state is labelled by a vector $\vec{n} \in S^2$, which labels the axis of rotation. Generically these states are only defined up to a phase, an issue which is not entirely understood in spin foam asymptotics and usually circumvented by choosing a canonical choice of phase [139]. For our smeared coherent states, we circumvent this issue by picking a coherent state orthogonal to the considered generator of rotations and smearing it over the circle of vectors on S^2 orthogonal to the respective generator, expressed as an integration over the smearing angle ϕ. In short, we construct a null eigenvector, with respect to the considered generator of rotations, defined for all representations of SU(2).

The immediate advantage, which eventually allows us to compute the complete expansion (up to leading order) of the $6j$ symbol, is that we can split the stationary phase approximation into two steps, one with respect to the group elements and one with respect to the (artificially) added smearing angles. However, this modification comes with a caveat: due to the smearing, one generically obtains many more points of stationary phase, whose geometric interpretation is less clear and have to be suppressed. Thus, it is a priori not clear whether the new coherent states actually allow for the same geometric interpretation as the familiar ones.

To clarify these two points, we first introduce modifiers for each 3–valent invariant that suppress additional stationary points. Furthermore we carefully examine the stationary phase conditions, the symmetry properties of their solutions and their geometric interpretation, which fortunately coincides with the standard coherent state construction, see e.g. [96]. This property is actually deeply rooted in the fact that the invariant subspace of the tensor product of three SU(2) representations is one–dimensional. Indeed, this agreement with the familiar coherent state approach allows us to perform the stationary phase analysis by parts, that is first with respect to the smearing angles and afterwards with respect to the group elements. This computation can actually be performed for arbitrary planar 3–valent graphs. Interestingly, after a variable transformation from group elements to (exterior) dihedral angles, the resulting effective action for the $6j$ symbol turns out to be the first order Regge action [97] associated to one tetrahedron[1]. This already establishes

---

[1]In first order Regge calculus, both edge lengths $\{l\}$ and dihedral angles $\{\theta\}$ are independent variables. In order

the connection to discrete gravity, which is essential to perform the remaining stationary phase approximation with respect to the angles: The geometric interpretation inherited from Regge calculus allows us to explicitly calculate the determinant of the Hessian matrix by employing several identities of the angle Gram matrix adopted from constantly–curved simplices [98] and rederive the well–known Ponzano–Regge formula [23].

Additionally, our formalism allows to study higher order corrections (in principle). In particular we prove a conjecture in [99,100] on the oscillatory behaviour of higher order corrections that states that sequent orders in the asymptotic expansion alternate between oscillating like a cosine and a sine, e.g. the leading order, i.e. the Ponzano–Regge formula, oscillates like a cosine, while the next–to–leading order oscillates like a sine. Moreover, we derive a recursion relation for the full $6j$ symbol similar to [101,102].

For future applications of the methods developed here, the hope is that one can apply the modified coherent state idea e.g. to the $SL(2,\mathbb{R})$ $6j$ symbol, which corresponds to a Lorentzian version of the Ponzano–Regge model, see also [27,140]. In comparison to the $SU(2)$ case, one certainly faces the complication of a more intricate representation theory and non–trivial invariant subspaces of the tensor product of three irreducible representations. Fortunately, the tools developed for first order Regge calculus [97] can be readily applied to the 4D spin foam model introduced by Barrett and Crane [73], such that we can derive the measure factor for the vertex amplitude of a modern spin foam model for the first time.

8.1.2 Measure factor for a 4D spin foam model

Falling into the same category, the paper [31] in chapter 3 can be seen as a direct follow up of [30]: moving away from 3D, we consider the simplest, yet non–trivial, 4D spin foam model, the Barrett–Crane model [73]. Starting from a nice identity of its vertex amplitude, the $10j$ symbol, in [27] we restrict our attention to strictly geometric contributions to the amplitude. By 'geometric' we refer to two facts: first, the asymptotic expansions of most 4D spin foam models not only contain geometric sectors, but also non–geometric ones, like a BF sector. See [141] for a discussion in the EPRL–model [74]. Second, in the Barrett–Crane model, the tetrahedra along which two 4–simplices are glued together have the same areas (of triangles) yet their shapes generically do not match. Because of such issues this model is nowadays disclaimed to be a viable theory for quantum gravity. For a recent discussion on these issues and a more positive view, see [103].

If we restrict the identity of the $10j$ symbol from [27] to the geometric sector, it exhibits a nice interpretation as first order (area) Regge calculus [104–106], a theory in which areas and 4D dihedral angles are independent variables[2]. Its equations of motion with respect to the areas (of triangles) impose local flatness, i.e. the deficit angles are required to vanish, while the non–matching of tetrahedra gives rise to metric discontinuities [105,106].

In the asymptotic expansion of the $10j$ symbol however, the areas of triangles are uniformly large and fixed, and one computes the stationary phase approximation of the integration over dihedral angles: On the points of stationary phase one obtains the action of standard area Regge calculus, while the determinant of the Hessian can be straightforwardly computed by applying the methods developed in [30], inspired from curved Regge calculus [98]. Remarkably, the so–found measure factor has a nice geometric interpretation as it mostly consists of products of volumes of (sub)simplices of the 4–simplex. The only non–explicit factor appearing is a Jacobian describing the change of variables from areas to edge lengths. If we consider a peculiar triangulation, namely

---

to arrive back at ordinary length Regge calculus, in which the dihedral angles are given as functions of the edge length, the constraint $\det \tilde{G}(\{\theta\}) = 0$ is imposed via a Lagrange multiplier. $\tilde{G}_{ij} = \cos(\theta_{ij})$ is called the angle Gram matrix. For exterior dihedral angles, as discussed in [30], one uses the convention $\tilde{G}_{ii} = 1$.

[2]This theory clearly differs from ordinary length Regge calculus [17,18,97] in 4D, in which the areas of triangles is given by the edge lengths, and should also not be confused with other formulations like area–angle Regge calculus [60,142]

two 4–simplices glued along all of their tetrahedra, giving the simplest triangulation of a 4–sphere as a product of two identical vertex amplitudes, we can absorb the implicit Jacobian into so–called glueing constraints, i.e. conditions that enforce the triangles of the shared tetrahedra to match in shape, not just in areas.

8.1.3 What is the interpretation of the asymptotic expansion?

With the results derived in [30, 31], we reconfirm that the (geometric part of the) asymptotic expansion oscillates like the cosine of the Regge action and also give a first glance at the measure on the space of geometries. However, these encouraging results have to be taken with a grain of salt: even if ignoring the contributions from non–geometric sectors, the physical interpretation of the asymptotics is doubtful. A quantized simplex, blown up to a macroscopic size, asymptotically behaves like a classical simplex, i.e. a basic building block of a triangulation endowed with a discrete gravity action. Indeed, this is only the very first step in establishing the connection between spin foam models and discrete gravity, a relation that has to be generalized to larger triangulations. Unfortunately, due to the complexity of spin foam models, calculations for larger triangulations have proven to be difficult, even Pachner moves, i.e. local changes of the triangulation, have not yet been computed in the full models.

In recent years doubts on the viability of the large spin limit for larger triangulations have been raised in [78]. If one scales up the boundary spins without additional assumptions on the spins in the bulk, one obtains accidental curvature constraints in the bulk forcing the deficit angles to vanish excluding a large class of Regge geometries[3]. Similar constraints have also been found in [143]. Therefore it has been argued that the large spin limit by itself is not semi–classical and should be performed together with a limit, in which the number of building blocks goes to infinity, see e.g. [79]. Later on we will also argue in favour of a refinement limit, yet we do not consider spins to be suitable order parameters, since they do not represent a diffeomorphism invariant quantity, see also chapter 7 (or [88]). Instead we will also consider refinement (and coarse graining) of the boundary itself, relating the states on different boundaries by embedding maps. By imposing cylindrical consistency conditions we propose a construction scheme for the continuum theory from the discrete model.

Another, at first site troubling fact is the oscillation behaviour of spin foams. Instead of oscillating like $e^{i\,S_R}$, which one would understand as a usual behaviour of a path integral, the vertex amplitude asymptotically oscillates (to leading order) like $\frac{1}{2}(e^{i\,S_R} + e^{-i\,S_R}) = \cos(S_R)$. This can be understood as a sum over orientations: In the asymptotic expansion, two conjugated stationary points are contributing that correspond to two different orientations of the simplex. There exist several attempts to suppress this sum over orientations by introducing a notion of causality in spin foam models [144, 145] and it has been argued in [146] that the sum over orientations is a cause of divergences in spin foam models. On the other hand there are important reasons why one should sum over orientations: in gravity, the dynamics (and time evolution) is generated by constraints, such that time evolution itself is a gauge transformation. A path integral should therefore act as a projector onto physical states, i.e. states satisfying the constraints. To realize this property, it is heuristically necessary to integrate over positive and negative values of lapse and shift, which one can understand as evolving forwards and backwards in time or, on the discrete level, as summing over orientations. Of course, these statements are controversial and heuristic, and ignore several subtleties involved in this [20, 147–150].

Still one can also see the asymptotic expansions of spin foam models as a starting point to a different consideration. Assuming the connection between spin foam models and Regge calculus also generalizes to larger triangulations, namely also larger spin foams oscillate as the Regge action

---

[3]Such a feature cannot be observed for asymptotic expansion of a single simplex, since there all spins are on the boundary.

of the underlying triangulation does, one can ask what one can learn about spin foam models from the perspective of Regge calculus. This can indeed be insightful, e.g. it might be used to fix ambiguities in the definition of spin foam models. For example, the edge and face amplitudes in spin foam models, in the literature often referred to as the spin foam measure, are not uniquely defined and are frequently determined by kinematical considerations, e.g. invariance under subdivision of an edge or a face [76, 151, 152], which one can understand as a weak notion of diffeomorphism symmetry. These choices influence the degree of divergence of the model [52–55]. Instead we would like to advocate dynamical principles to fix the ambiguities of the models, where the most desirable, and yet most difficult to achieve, is (discrete) diffeomorphism invariance.

8.2 Lectures from triangulation independence: Regge calculus

As explored in previous work, diffeomorphism invariance is generically broken by discretisations [41–43], hence also in most spin foam models[4], but one can try to resurrect it by consecutively improving the discretisation by a renormalization / coarse graining procedure. The heuristic idea is the following [43]: By infinitely refining and improving the discretisation, one reaches a fixed point, where the system is, by definition of the fixed point, triangulation independent, at which diffeomorphism symmetry is restored. On the other hand, starting with a system that is diffeomorphism invariant in the discrete, i.e. invariant under vertex translations, one can, e.g. move a vertex on top of another one; this induces triangulation independence as well. This relationship can be understood as follows: the consecutive coarse graining and thus improving of the discretisation can be interpreted as 'pulling back' the continuum dynamics onto the discretisation. Once achieved, the dynamics, in its entirety, is represented on the discretisation and with it the entwined symmetry. Thus it is irrelevant how fine or coarse the discretisation is, since it already captures the full dynamical information.

Such discretisations are called 'perfect discretisations' [61, 62]: a demonstrative example is 3D (classical) gravity, whose equations of motion tell us that spacetime is locally flat. 3D Regge calculus captures this perfectly, since it is built up out of intrinsically flat tetrahedra, which are glued together in a flat way, i.e. the deficit angles vanish. Furthermore, the associated discrete Regge action is invariant under vertex translations. However, this symmetry is broken if one considers 3D gravity with a non–vanishing cosmological constant [41, 42], which describes constantly curved spacetime. Then Regge calculus with flat tetrahedra does not capture the continuum dynamics and the deficit angles (on the edges) no longer vanish. However, if one refines the triangulation, one realizes that the deficit angles decrease and the approximation is improved. In the infinite refinement limit, the symmetry gets restored. Alternatively, one can also iteratively improve the tetrahedra to capture the dynamics, which eventually leads to constantly curved building blocks described by the action for (constantly) curved Regge calculus [60]. Again the deficit angles vanish and the action is invariant under vertex translations. Certainly, the construction of such a perfect discretisation for non–topological theories is much more difficult. We will comment on this later on.

The previously mentioned conjecture relating diffeomorphism symmetry and triangulation independence in [43], which also appears in a slightly different form in [88], allows us to interpret triangulation independence as a dynamical principle. Since the modern spin foam models are deliberately constructed not to be triangulation independent[5], we instead examine triangulation independence in (linearized) Regge calculus in chapter 4, see also [59], to determine whether it can be used to fix the ambiguities in the definition of the path integral, in particular the path integral

---

[4]The role of diffeomorphisms in spin foam models has been discussed in [46], where their action has been identified as vertex translations. This concept is realized in the 3D topological models, such as the Ponzano–Regge [23, 80] or the Turaev–Viro model [124].

[5]This is partially rooted in the prejudice that any triangulation invariant theory must be topological.

measure. Indeed, in this context, by requiring triangulation independence one might hope for an anomaly–free path integral measure with respect to diffeomorphisms, see also [51] for a discussion in spin foam models. In contrast to the various other proposals for measures in Regge calculus, see e.g. [107–109], this is the first one to be based on a dynamical principle and, due to the relation to spin foam models, may serve as a blueprint for possible measures in spin foam models.

In this context we study triangulation independence in chapter 4, see also [59], on the local level of Pachner moves [82, 83]: Pachner moves are local changes of the triangulation, whose consecutive application can transfer a triangulation of a manifold into any other triangulation of the same manifold. Therefore it is sufficient to consider just the simplicial complex subject to the Pachner move. By linearisation we mean that the Regge action is expanded (up to quadratic order) around a flat background solution, here vanishing deficit angles. The perturbations around the background are then considered to be the new dynamical variables, whereas we regard the path integral measure to be a function of the background edge lengths. In fact, the flat background structure allows us to explicitly compute the Hessian matrix, i.e. the new 'propagator' of the theory, which can be straightforwardly written in an almost factorising form of geometric quantities, like volumes of simplices. The calculations themselves use and extend identities and results from [153] and [154–156], see also [112, 157]. Furthermore, in case of the 4–1 and 5–1 move in 3D and 4D respectively, we identify the null eigenvectors associated to the vertex translation symmetry of the vertex inside the (coarse) simplex.

Unsurprisingly, full triangulation independence is only achieved in 3D, where the theory is topological and the action itself is fully invariant under all Pachner moves. As a result, the path integral measure is (almost) uniquely determined in a local ansatz, which factorises with respect to the (sub)simplices of the triangulation. Remarkably, this result is compatible with the Ponzano–Regge asymptotics [23], even for the assignment of the numerical constants. No doubt, this is to a large degree due to the topological nature of 3D gravity, but it shows that triangulation independence is indeed a useful requirement to fix the ambiguities of a theory.

Naturally in 4D, full triangulation independence cannot be achieved due to several reasons. The first one, derived in [59, 158], is the fact that the Regge action is not invariant under all Pachner moves, to be more precise the 3–3 Pachner move. The calculations in [59] are performed around a flat background solution, which can be guaranteed for most Pachner move, since there is at least one dynamical edge, which can be chosen such that the deficit angles vanish and the solution is flat. In the 3–3 move however, all edges are in the boundary and thus the deficit angle located at the single bulk triangle is completely determined by this boundary data. Unless these allow for a flat geometry in the bulk, even the linearized Regge action is not invariant under this Pachner move[6]. Indeed, in such a situation the intrinsically flat simplices cannot capture the curvature, which as a consequence leads to a broken diffeomorphism symmetry in larger triangulations. Again, only if the boundary data allow for flat solutions in the bulk, the Regge action possesses a vertex translation invariance [44, 45]. In particular since we intend to study quantum gravity in regions with possibly large curvature, the Regge action – and presumably also spin foams – on a coarse triangulation is not a good approximation in these regions and has to be improved [41, 42].

Nevertheless, it is still instructive to discuss invariance under the two remaining Pachner moves, namely the 5–1 and 4–2 Pachner move. In both cases one can define flat background solutions and we show explicitly that the (linearized) Regge action actually is invariant under both these moves. Surprisingly, the Hessian matrix is strikingly similar to the 3D case, namely highly factorising with respect to (sub)simplices, such that one can define a measure factor analogous to the 3D case that is 'almost' invariant. However, despite these nice properties, full triangulation invariance of the path integral cannot be achieved due to the appearance of an overall factor in the Hessian matrix that at first glance appears to be non–factorising.

---

[6]The two configurations in the 3–3 move differ in the triangle that is shared by all three 4–simplices. The Regge action is only invariant under this move, if the deficit angle at the single bulk triangle vanishes in both configurations.

8.2.1 Triangulation independence implies non–locality

This overall factor is the main focus of the paper [84] presented in chapter 5, in which we derive its geometric interpretation: This factor vanishes if the six vertices involved in the 4D Pachner move lie on a 3–sphere [110], see also [111]. For the 3–3 and the 4–2 Pachner moves, this can only happen if the boundary data is chosen in such a way that all vertices can lie on the same 3–sphere. Yet in case of the 5–1 move, for which the classical action is invariant under translations of the inner vertex, see e.g. [59], such situations can always be constructed by moving the inner vertex onto the circumscribing sphere of the coarse simplex. This can either mean moving the vertex on top of another one, resulting in degenerate simplices, or moving it outside the coarse simplex, which corresponds to a change of relative orientation of one or more simplices [112]. Indeed, if this occurs the entire Hessian matrix vanishes and the integral diverges, which concurs with the thesis in [146] that the change of orientation, by moving the inner vertex outside the coarse simplex, is the cause of divergences in spin foam models. On the other hand we argue below that in spin foams, similar to the asymptotic expansion discussed above, one in fact has to sum over orientations in order to impose Hamiltonian and diffeomorphism constraints.

More importantly, in case the vertex is outside the coarse simplex and at the same time on its circumscribing sphere, the overall factor vanishes, but none of the involved 4–simplices is degenerate, i.e. their volume is non–zero. From this fact we show that this overall factor is non–factorising, i.e. it cannot be written as a product of amplitudes associated to (sub)simplices, and it is necessarily non–local (with respect to the simplices of the triangulation), since its properties can only be inferred if the relative positions of all six vertices are known. Therefore, triangulation independence in 4D Regge calculus implies non–locality. Furthermore, it shows that the factorising measure derived for the Barrett–Crane model in chapter 3, see also [31], is not invariant under Pachner moves, yet the (non–local) change of variables from areas to edge lengths might change this statement for larger simplicial complexes.

In fact, the appearance of non–local couplings is not surprising: since 4D (discrete) gravity is a theory with propagating degrees of freedom and both the 4–2 and the 5–1 Pachner move are coarse graining moves, in the sense that they decimate degrees of freedom, one expects non–localities to occur. Take for example the 2D Ising model [159]: the initial theory defined on a 2D lattice just describes nearest neighbour interactions between the spins located on the lattice sites, encoded in the Hamiltonian of the system. One way to coarse grain this is by a decimation procedure: every second Ising spin is summed over and absorbed into a new effective Hamiltonian. However, already after the first step, this new Hamiltonian describes not only nearest neighbour interactions with respect to the new lattice, but also next–to–nearest neighbour and multiple spin interactions; the theory has left the initial space of models, now containing non–local interactions.

Coarse graining techniques as the one sketched above are called real space renormalization techniques [115], in contrast to momentum space renormalization. Frequently, unless one is dealing with a topological theory, these approaches are troubled with the appearance of non–local interactions enlarging the theory space, which can be naively tamed by introducing ad hoc approximations and restrictions on the allowed couplings. However, it is often not clear how good these approximations are and the non–localities effectively reduced the amount of available real space renormalization methods. One of the most prominent, yet brutal in the approximation, is the Migdal–Kadanoff scheme [113,114] that outright removes non–local interactions, yet is still able to predict the phase transition for the Ising model qualitatively.

At first sight, this seems to diminish the possibilities of improving Regge calculus or even spin foam models in this manner. This is partially due to a particular perspective of these models and the coarse graining scheme: the initial setup of the models is building an amplitude out of basic building blocks that interact locally. In spin foam models these are the vertex, edge and face amplitudes as functions of representation labels, in Regge calculus it is the additive Regge action as a functional of edge lengths. Now the coarse graining schemes, e.g. Pachner moves, intend to

locally manipulate the discretisation, yet at the same time keep the basic building blocks, and the degrees of freedom describing them, as the fundamental ingredients. In particular Pachner moves, as local transformations, keep the boundary data unchanged. However, these data, while suitable to describe physics on the smaller scale, may be very inefficient to capture the dynamics at coarser scales, apparent in the appearance of non–local couplings for interacting theories.

Therefore the question arises whether one can choose more appropriate degrees of freedom to avoid non–local interactions. One suggestion in Regge calculus would be to use area–angle variables [60, 142], since they are more closely related to the construction methods of spin foam models, yet it is not clear whether one can avoid non–localities in this framework. However in practice, it appears to be impossible to circumvent non–localities entirely, such that it is imperative to employ approximations. Indeed, it would be desirable to have a coarse graining scheme capable of controlling both the degree of non–locality and the quality of the approximation. To do so it is indispensable to isolate the relevant degrees of freedom from the less relevant ones, which in most cases will be recombinations of the finer degrees of freedom into coarser, collective ones. Thus we argue that a coarse graining scheme should necessarily affect the boundary data as well.

8.3 A change of perspective: Tensor network renormalization

A possible solution to these issues lies in a change of perspective: instead of keeping the initial basic building blocks fixed and changing the discretisation only locally, one can employ more non–local changes, which modify the building blocks and also affect the boundary data. Essentially, the idea is to replace several locally interacting building blocks by an effective building block, which again interacts locally with the surrounding building blocks. In general, one can construct such a new building block by integrating out / summing over internal degrees of freedom, such that the new object depends on more boundary data than the initial one did. In a way, one 'stores' the non–localities inside the new object by paying the prize of an increasing amount of boundary data.

This increase of the boundary data causes two complementary issues. The first one affects numerical realizations of such a coarse graining scheme. Consecutively performing this procedure gives an exponential growth of the boundary data, which requires the introduction of a truncation. The second one, even more severe, is the question of interpretation of the new building blocks and their comparability to the previous ones. In general, the larger boundary of the new building block is endowed with a 'larger' Hilbert space[7], such that it is not straightforward to compare the two amplitudes and interpret them, i.e. the essential task of any renormalization group approach.

In this particular example of coarse graining, one would like to kill two birds with one stone by suitably 'reducing' the boundary data of the new building block, thus restoring the relation to the previous building block (and the interpretation) and at the same time truncating the boundary data to enable efficient numerical algorithms. To put it differently, one has to define *embedding maps* between Hilbert spaces of different size / complexity, which redefine the fine data in terms of the coarser ones and also provide an approximation. A priori these embedding maps can be chosen arbitrarily, but their choice determines the quality of the approximation and also the interpretation of the new model. The last two conditions are complementary and essentially require the embedding maps to be compatible with the *dynamics* of the system, i.e. the dynamics should determine the embedding maps. Therefore, the embedding maps should combine the fine degrees of freedom into coarse ones in such a way that the symmetries of the system are preserved to allow for an intuitive interpretation. Among these collective degrees of freedom, it has to identify and retain the most relevant ones, such that a good approximation can be achieved.

Interestingly, although working in a very different context, condensed matter theory faces similar issues in the quest to describe many body quantum physics. Even though starting from a simple lattice system equipped with a Hamiltonian describing local interactions, the systems are generically

---

[7]For an infinite dimensional Hilbert space, 'size' refers to the complexity of the discretisation.

not solvable, yet one would like to extract the collective dynamics of many degrees of freedom via a real space renormalization method. Indeed, there exist several new methods tackling these issues, which can be summarized as providing ansätze for groundstates of the Hamiltonians, see e.g. matrix product states (MPS) [118, 119]. In this context, we are particularly interested in tensor network renormalization [85, 86], since it is a proper realization of the ideas illustrated above.

A tensor network can be understood as a reformulation of the lattice system: The local degrees of freedom on the lattice are locally encoded into a tensor $T_{abcd...}$, where the rank of the tensor encodes the valency of the vertices of the lattice. The partition function Z of the system is then computed by contracting all tensors

$$Z = \sum_{a,b,c,d,...} T_{abcd} T_{b'c'ad'} \cdots \tag{8.3.1}$$

according to the combinatorics of the network, here for 4–valent tensors. Thus, the tensors T encode the dynamics of the system. Yet the task to compute the partition function Z is still as difficult as in the original setup, such that one would like to introduce a coarse graining scheme that can approximate Z by a contraction of a coarser tensor network made up out of effective tensors T', which possess a maximum index range χ[8]. To do so, tensor network algorithms aim to iteratively combine a certain amount of tensors into a new tensor, which naively suffers from an exponentially growing index range. Furthermore, since the tensor contains the dynamical information of the system, the new tensor should also be comparable to the previous one in order to observe the change of dynamics at different scales.

In fact there exist many different implementations of tensor network renormalization differing in the way how they construct the embedding maps, relating fine to coarse boundary data, from the tensors, yet all of these algorithms employ singular value decompositions, in short SVD. To do so one rewrites a collection of tensors as a (possibly asymmetric) matrix by an appropriate grouping of tensor indices, to which the SVD can be applied. Then, the SVD can be understood as redefining the variables and ordering them according to their relevance, which can be readily read off from the size of the associated singular value. This allows us to employ a truncation scheme, e.g. by keeping only the χ most relevant degrees of freedom, i.e. the χ largest singular values. The new effective tensor T', labelled by the new degrees of freedom, is the starting point for the next coarse graining step.

Thus the idea is to use this particular approach as a coarse graining scheme for spin foam models. Interestingly, spin foams fit quite naturally into the language of tensor networks as it has been described in [37]: the projectors onto invariant subspaces associated to the edges, can be directly written as a tensor of the same rank as the valency of the edge, i.e. the number of faces sharing the edge. Similarly, one can also absorb the face amplitudes into the tensor. A complication exists however for spin foams, as well as for lattice gauge theories [37, 121]: one has to ensure that each face carries the same representation label and thus, also all tensors on the edges sharing this face must carry the same label in their respective index. Therefore one has to introduce auxiliary tensors on the faces that fix the labels of the adjacent dynamical tensors to be identical.

Yet, even though spin foam models exhibit a nice translation into tensor networks, one faces two obstacles if one intends to apply tensor network renormalization to them:

- Most tensor network renormalization algorithms are defined for spin systems defined on a 1–complex, e.g. a 2D lattice. By spin system we mean a system with a global symmetry, like the Ising model (without external magnetic field), instead of a local gauge symmetry, like $\mathbb{Z}_2$ lattice gauge theory. On the lattice, these systems can be modelled as a vertex model, e.g. with the tensors of the network associated to the vertices. Here no auxiliary tensor are required on the faces, such that the whole network only consists of one type of tensors. Thus,

---

[8]This χ is frequently called the bond dimension.

in order to apply these methods to spin foams, one has to generalize the algorithms to higher dimensional complexes and modify them to deal with the more complicated networks.

- The second, equally troubling issue lies in the underlying symmetry group of spin foam models. Whether one examines Riemannian or Lorentzian gravity, one picks either SO(4) or SL(2, $\mathbb{C}$) as the underlying symmetry groups. These groups generically come with infinitely many representation labels, which would result into tensors with equally ranging indices. At first sight, this appears to doom feasible numerical simulations.

Indeed, each of this issues is very difficult to tackle in full generality: the first one requires the development of a new coarse graining scheme within the tensor network formalism (currently work in progress), while the implementation of the full symmetry group leads to infinities in the partition function. A solution to circumvent this issue is unknown to the author of this thesis.

Thus, instead of tackling these issues head on, it is better to come up with suitable approximations that make currently available methods applicable, while still learning something new about spin foams in the process, e.g. whether tensor network renormalization is (or can be) a useful tool to study the collective dynamics of spin foams. This idea lead to the development of analogue spin foam models, called spin nets [37–39], which can be directly understood as a dimensional reduction of spin foams: the model is defined on a 1–complex, i.e. a graph, e.g. a 2D (regular) lattice, where the dynamical ingredients of spin foams, face weights and projectors (on the edges), are associated to lower dimensional objects, i.e. weights on the edges and projectors on the vertices. Such systems can be readily translated into tensor networks and tensor network renormalization is applicable in principle. Yet due to the infinite number of representation labels one has to sum over for the Lie groups of interest, the index range of the tensors is infinite as well, which poses a serious challenge for numerical simulations. This can be circumvented by replacing the Lie group by a finite group [37–39], which naturally come with only finitely many representation labels. See also [160] for a definition of spin nets and foams for finite groups. Another option are quantum groups like SU(2)$_k$ [87], see also chapter 6, which are equipped with a cut–off on the representation labels depending on the level k [122, 123].

The dimensional reduction might appear ad hoc and is mainly motivated by the restrictions of the coarse graining method, which would be dishonest to neglect. Therefore, we would like to motivate further, why we think even these simplified models can teach us something about the many–body behaviour of spin foams. Actually, it is known that 2D lattice gauge theories are equivalent to 1D spin systems, and also 4D lattice gauge theories have several properties in common with 2D spin systems [161], e.g. one noticed similarities between the 2D Ising model and the 4D $\mathbb{Z}_2$ gauge theory. Similarly, we would like to interpret the results for spin nets as indications for spin foams. Furthermore, as we also show in [87] (see also chapter 6), spin nets can be interpreted as highly anisotropic spin foams, taking the form of a 'melon', similar to [54]: Such a spin foam consists of two vertices connected by many 4–valent edges, which are basically dual to tetrahedra. Then coarse graining of spin nets can be interpreted as defining new effective tetrahedra, which might actually also appear in simplicial 4D spin foam models. Certainly, this does not imply that the same fixed points emerging from spin net simulations also occur in spin foam models, yet this is supportive nonetheless.

Before discussing the results of this approach, we would like to emphasize, what we are looking for and why: As thoroughly discussed above, the intent is to extract effective dynamics of many building blocks from spin net models via tensor network renormalization. Therefore we start the simulation with an initial tensor that encodes the full dynamics of the model. Under coarse graining, we approximate the partition function of a regular, square 2D tensor network by coarse graining the tensors into new effective ones as prescribed above. The tensors will generically change under this procedure until they eventually reach a fixed point, i.e. the tensors remain unchanged under further coarse graining steps. This final tensor resembles the refinement limit of the specific initial

model and encodes its continuum dynamics. Interestingly, these different continuum dynamics can be distinguished by their excited singular values.

8.3.1 Coarse graining spin nets: finite groups

In order to demonstrate the progress in coarse graining spin net models over the past three years, let us briefly summarize previous results. The very first work [37, 38] is based on Abelian finite groups $\mathbb{Z}_n$, and asks the question, in the spirit of related work [41–43], whether broken symmetries get restored under coarse graining. In this context, not (discrete) diffeomorphism symmetry (or reparametrization invariance) is of interest, but rather the global BF symmetry of the system, which is also called the ordered phase. This phase is parametrized by assigning exactly a constant weight to all representation labels; in the dual picture for the Ising model, this corresponds to the state in which all spins are equal. Since this state already defines a fixed point of the renormalization scheme, one has to break this symmetry, e.g. by introducing a cut–off on the representation labels, and study the flow of these 'Abelian cut–off' models under coarse graining. Indeed, [37] already gives a glance at the power of tensor network renormalization, by providing the first phase diagrams for spin foam related models. Depending on the initially chosen cut–off on the representation labels, the models mainly flow to the (analogue) BF phase or to the degenerate phase, in which only the trivial representation is excited. The latter phase is also called disordered or high–temperature phase.

The next logical step is to extend this approach towards non–Abelian finite groups, the simplest of which is S_3, the permutation group of three elements, in [39]. In fact, this work is remarkable in several ways: it is the first study of the effective dynamics of an (analogue) spin foam model that possesses similar features to modern spin foam models [73–75], namely a notion of simplicity constraints [66], which are implemented by special functions analogous to the holonomy formulation of spin foams in [69]. In fact, these simplicity constraints get encoded into the projectors associated to the vertices, which, in comparison to lattice gauge theories, project onto a smaller invariant subspace (of the tensor product of irreducible representations meeting at the vertex). Naturally, the question arises, whether the simplicity constraints persist under coarse graining or whether the model flows back to the standard lattice gauge theory phases, such as the BF or the degenerate phase[9]. In order to answer this question, the coarse graining mechanism has to be adapted in such a way that it preserves the symmetries of the model, in this particular case the group symmetry encoded in the tensors. Therefore a symmetry protecting algorithm has been invented in [39] that works as follows: before performing the SVD, the system is rewritten into the so–called 'recoupling basis', a transformation in the representation theory of the group that brings the tensor into a block diagonal form[10], where each block is then labelled by a pair of representations (ρ, ρ'). Then the SVD is performed for each of the blocks (ρ, ρ'), which is not only computationally more efficient, but also preserves the interpretation of the variables: The representation labels of the blocks, called *intertwiner channels*, are the new labels of the effective tensor.

The work [39] uncovered several remarkable results. First of all, one can determine the phase of the system from the excited intertwiner channels and, moreover, determine directly whether the system is in a standard lattice gauge theory phase. If it is not, one will observe excitations in channels (ρ, ρ'), where $\rho' \neq \rho^*$. This is not only a generalization of the initial model, which started with (ρ, ρ^*), but sheds a new light on the interpretation of spin foams: for spin foams the excited intertwiner channels are the relevant degrees of freedom, specifying the model and the

---

[9] In lattice gauge theory, BF theory is also known as the weak coupling limit, whereas the degenerate phase is also known as the strong coupling limit. In condensed matter, one would refer to these phases, in analogy to the Ising model, as the low temperature or ordered phase or the high temperature, disordered phase respectively.

[10] In fact, [37] already possessed a similar scheme in its algorithm, by preserving the Gauß constraints (at each vertex) under coarse graining. Similarly this protected the interpretation of the labels in the edges in terms of representation labels, yet for a much simpler system.

dynamics. Additionally, as soon as channels with $\rho' \neq \rho^*$ are excited, one can interpret this as an implementation of simplicity constraints.

Despite these interesting insights, the results [39] are mixed: On the one hand one has been able to find one non–trivial fixed point, i.e. with channels (ρ, ρ') and $\rho' \neq \rho^*$ excited, yet in order to flow to it required a high level of fine–tuning and rather low accuracy of the numerical algorithm. As soon as a higher accuracy of the algorithm has been used, i.e. more degrees of freedom were stored in each coarse graining step, the system either flowed to the BF phase, the degenerate phase or BF theory on a normal subgroup, i.e. (analogue) phases known from lattice gauge theories. Thus, even though additional structure in form of the new fixed point has been found, the phase diagram only showed extended phases for the standard lattice gauge theory phases.

8.3.2 Quantum group spin nets

Keeping the results of [39] in mind, the paper [87] presented in chapter 6 extends them in a seminal way. The first, non–trivial change is the definition of spin net models on the quantum group $\mathrm{SU}(2)_k$ [122, 123], which raises these models to a higher level of plausibility: instead of considering finite groups, which are difficult to relate to gravity, quantum groups are expected to model gravity with a non–vanishing cosmological constant. The heuristic argument is that the level k of the quantum group determining the cut–off on the representation labels, here the maximal allowed spin, is anti–proportional to the size of the cosmological constant. Indeed, the very first spin foam model defined on quantum groups is the Turaev–Viro model [124], which describes 3D gravity with a cosmological constant[11]. In recent years, also the modern 4D spin foam models have been defined on quantum groups [130–132] and the possibility to link (2+1)D loop quantum gravity to the Turaev–Viro model has been explored as well [125–129]. Indeed, $\mathrm{SU}(2)_k$ combines the advantages of providing a natural cut–off onto the representation labels with a much more realistic applicability to physics. Furthermore, in contrast to finite groups, quantum groups for different levels k almost have the same representation theory, which makes the study of 'larger' quantum groups straightforward (neglecting the increase of computational cost).

Of course, quantum groups, which are quasi–triangular Hopf–algebras [122], are much more complicated objects than groups. These complications force us to use a different initial parametrization in comparison to [39]. There, simplicity constraint enforcing functions have been used to parametrize the initial tensor, which in the quantum group models however lead to a violation of the quantum group symmetries. Instead we choose initial data lifted from so–called 'intertwiner models' defined in [162], which can be understood as simpler versions of spin nets, since their edges carry only one irreducible representation and thus a simpler Hilbert space. Remarkably, by requiring triangulation independence and certain restrictions on the allowed representations, one can construct a plethora of 'fixed–point intertwiners' of these models, i.e. topological theories, which we use as a new parametrization for our quantum group spin nets[12]. In order to lift these intertwiners to the full spin nets, we revisit Reisenberger's principle [163], a concept prescribing how to uniquely construct higher valent intertwiners from three–valent ones. Additionally, in order to define the dual representation we invent a graphical calculus, which considerably simplifies the calculations and allows us to adapt the symmetry preserving algorithm, and thus the notion of intertwiner channels, invented in [39] to quantum groups. Indeed, as it turns out, this new parametrization, which also permits us to study linear combinations of initial intertwiners, reveals a very rich structure:

The first remarkable difference with respect to [39] is that for each different choice of initial intertwiner (without superposing it with other intertwiners), the system flows (under coarse graining) to a different fixed point, in fact one discovers a whole family of non–trivial fixed points, which

---

[11]In fact, it is closely related to the Ponzano–Regge model, with the difference that the vertex amplitude is the q–deformed $6j$ symbol instead of the standard $\mathrm{SU}(2)$ $6j$ symbol. In discrete, classical gravity this corresponds to replacing flat tetrahedra by constantly curved ones [42, 60].

[12]Ironically, the work [162] has been motivated by the single non–trivial fixed point in [39].

form an interesting pattern for different levels k of the quantum group. More importantly, this behaviour is stable for high accuracy of the simulations, i.e. high number of stored degrees of freedom, and requires no fine–tuning[13]. In fact, most of the fixed points are non–trivial, i.e. they have excited intertwiner channels (j, j'), where $j' \neq j^*$. Even more interesting, if one considers linear combinations of the initial intertwiners, one finds extended phases (in the parameter space) for all fixed points with phase transitions. So, what is the meaning of the fixed points?

As it turns out, all of the fixed points, also the non–trivial ones, describe topological and thus fully triangulation invariant[14] theories. This can actually be deduced from the fact that they can be described by finitely many, locally interacting degrees of freedom, which are all equipped with a singular value equal to one. Of the non–trivial fixed points, most fall into the category of factorising fixed points; the two representations (j, j') assigned to each edge completely decouple. In the 'melonic spin foam' interpretation of spin nets discussed above, this actually implies a complete decoupling of the two spin foam vertices, a rather pessimistic scenario, should these fixed points also occur for the full theory. On the other hand, one finds (analogue) BF theory, which could be understood as maximally 'glueing' the two vertices together. Thus one is tempted to conclude that the factorizing case occurs because the simplicity constraints are too strongly imposed, leading to a complete decoupling of the basic building blocks, whereas introducing them too weakly, the system inevitably returns to analogue BF theory. Interestingly, there exist an intermediate fixed point, called 'mixed', which is not factorising, but also not BF. To better understand this interplay is an interesting prospect for future research.

The observing reader will certainly object that these fixed points describe topological theories and wonder how one might get propagating degrees of freedom back. A preliminary way to 'escape' topological theories is by tuning the system towards a phase transition, where one makes the following observations: The very first peculiarity that attracts attention is that the simulations take considerably longer, the closer the system is tuned towards the phase transition. If one plots for example the singular values against the number of iterations, see e.g. in [164], one notices indications of scale invariance: For many iterations the singular values remain almost constant before eventually converging towards their final value. Actually, the closer the system is tuned towards the transition the longer it takes the system to 'decide' where to flow to. This behaviour can also be spotted at the phase transition of the Ising model (in a tensor network formulation), which is known to be of second order. Another observation worth discussing is the overall list of singular values, concerning the viability of the truncation: in many situations, the singular values drop off reasonably quick, such that one can truncate at a singular value, which is not only much smaller than the largest one, but also considerably smaller than the next larger one. Close to the phase transition however, the choice where to cut off is much more intricate, since the singular values drop off much more slowly, such that one may truncate degrees of freedom that, while being much smaller than the largest one, are of similar size as the smallest considered one. In short, in these cases it would be best not to truncate any degrees of freedom, which indicates that the phase transition probably is of second order and the continuum theory 'on' the phase transition possesses propagating degrees of freedom.

In short, [87] provides a lot of positive implications for spin foams, in particular the vast amount of additional fixed points with extended phases, where the phase transitions appear to provide a possible door towards a theory with propagating degrees of freedom and implemented simplicity constraints. Yet, so far we have only glimpsed at the role of the embedding maps described above, which mainly appear in this context as providing a truncation. In the next section, we will stress the importance of embedding maps, relating coarser to finer boundary data, for the consistent

---

[13]Of course, the term fine–tuning has to be taken with a grain of salt, since it is highly dependent on the employed parametrization. Nevertheless, it is insightful, since it indicates that the parametrization in terms of intertwiners is more suitable for spin foams.

[14]In order to check this statement, the 4–valent tensors have to be split into 3–valent ones, which is part of the particular coarse graining procedure [86].

construction of a continuum theory from the discrete one.

8.4 Embedding maps as time evolution

In this discussion so far, one might get the impression that the main purpose of the dynamical embedding maps, e.g. obtained from tensor network renormalization, is to provide a convenient and good approximation of the dynamics, from which one can obtain an effective macroscopic description of the microscopically defined system. Indeed, as we argue in [88] presented in chapter 7, this viewpoint is too narrow and can be dramatically generalized.

To do so, let us consider a spin foam giving the transition between two boundary states, each represented on a discretisation. On the one hand, this spin foam can be interpreted as one particular time evolution of the initial state to the final state. On the other hand, the two boundary discretisations can be different, e.g. the final state can be finer or coarser than the initial one, such that the spin foam provides an embedding of the initial Hilbert space into the final one. Furthermore, since spin foams implement a dynamics, this embedding is indeed dynamical. Therefore, we argue that dynamical embedding maps can be interpreted as time evolution maps.

To make this idea more clear and concrete, let us elaborate on its origin: the main inspiration comes from work on the canonical formulation of classical Regge calculus [133, 134], or more general, the definition of a canonical formalism for phase spaces of different dimension at different time steps [135]. See also [136, 137] for an extension of the formalism to quantum systems. Imagine a triangulated hypersurface, for concreteness in two dimensions. This hypersurface can be locally evolved in time by glueing a tetrahedron onto it, which results in a new hypersurface at the next time step. From the perspective of the 2D hypersurface, this resembles a 2D Pachner move, depending of how the tetrahedron is glued to the initial hypersurface, either a 2–2 or a 1–3 move. The inverse moves can be understood by removing a tetrahedron (glueing a tetrahedron with opposite orientation). Remarkably, even for non–gravitational systems, this formalism always results in the appearance of constraints, namely so–called pre– and post–constraints. Pre–constraints are basically conditions that have to be fulfilled for time evolution to take place, whereas post–constraints are automatically fulfilled once time evolution has taken place. For a concrete example, consider a refining move, e.g. a 1–3 move in Regge calculus: The final phase space contains three more edges, i.e. three more degrees of freedom. To accommodate them, one has to artificially enlarge the initial phase space to describe this evolution move. As a consequence one obtains three post–constraints, essentially restricting the fictitiously added degrees of freedom. Furthermore, in the gravitational context, these post–constraints implement both diffeomorphism and Hamiltonian constraints [134, 165], where the associated gauge symmetry is interpreted as vertex translations. To put it differently, at first sight the new hypersurface has three more degrees of freedom, which however turn out to only be gauge degrees of freedom[15].

For a quantum system, we argue that something similar happens if one time evolves from a coarser to a finer state. The newly added degrees of freedom are either gauge degrees of freedom or added in a vacuum state. Therefore, similar to the classical case, the refined state does not contain more information than the initial one, but represents the same information on a finer discretisation, possibly arranged in a different way. However, the issue of uniqueness forces itself into the discussion. Given one initial state on a particular discretisation, there exist many different ways to (locally) time evolve this state towards the same final discretisation, where it is a priori not clear that these different embeddings give the same final state. Therefore, one has to discuss consistency

---

[15]From this insight, one can already deduce that refining a hypersurface by purely refining Pachner moves, i.e. 1–$(d + 1)$ moves in $(d + 1)$ dimensions is insufficient. Such a refining procedure leads to geometries known as stacked spheres, which are not dynamical and do not allow curvature. These stacked spheres appear e.g. in the weak coupling phase of simplicial gravity in dynamical triangulations [166] or in the melonic phase in coloured tensor models [167]. On the other hand, one can interpret them to resemble degenerate geometries with a lower Hausdorff dimension [168].

conditions for the embedding maps, which naturally translate into consistency conditions for time evolution.

8.4.1 Cylindrical consistency and the physical vacuum

It is straightforward to outline the immediate conflict between an ambiguous (local) time evolution and time reversibility: assume a particular time evolution of an initial state to a final one. Then one can time evolve the final state back in a different way, which results in the same initial discretisation, yet a different initial state. To avoid this troubling property, one has to require path independence under time evolution: no matter how one chooses to locally time evolve a state to a particular final discretisation, the final state represented on this discretisation is always the same.

Invoking the interpretation of time evolution as embedding maps, this leads to the following consistency conditions the embedding maps have to satisfy: Consider three boundaries b, b' and b'' satisfying the relation $b \prec b' \prec b''$, i.e. b' is a refinement of b and b'' is a refinement of both b and b'. Then the embedding map $\iota_{bb''}$ should not depend on the intermediate boundary b', for any choice of b'. In other words, first evolving from b to b' and then from b' to b'' should give the same embedding map as directly evolving from b to b'', i.e. $\iota_{bb''} = \iota_{b'b''} \circ \iota_{bb'}$. Indeed, this is an essential feature, because it allows the unambiguous comparison of two states, for concreteness ψ_b and $\phi_{b'}$, which are represented on different boundaries b and b'. If these two boundaries have a common refinement, e.g. b'' with $b \prec b''$ and $b' \prec b''$, then both states can be embedded into the Hilbert space $\mathcal{H}_{b''}$ and compared. If $\iota_{bb''}(\psi_b) = \iota_{b'b''}(\phi_{b'})$, then one identifies $\psi_b \sim \phi_{b'}$ and defines an equivalence class for these states. The continuum Hilbert space can then be defined via an inductive limit, i.e. as the disjoint union of all boundary Hilbert spaces $\mathcal{H}_b$ modulo the equivalence relation $\sim$, in short $\mathcal{H} = \bigcup_b \mathcal{H}_b / \sim$. In fact, by embedding the states into the continuum (via the inductive limit), one can represent a state on a given discretisation in the continuum Hilbert space, such that the (equivalence classes of) states only implicitly depend on the discretisation they are represented on.

These consistency conditions are called cylindrical consistency conditions, a concept also used in loop quantum gravity in order to relate states, more precisely spin network states, a convenient basis of the Hilbert space of loop quantum gravity [20], defined on different graphs. A spin network defined on a graph γ can be embedded into a graph γ', if γ is a subset of γ', denoted as $\gamma \prec \gamma'$, by setting the SU(2) spins on all edges added to γ to obtain γ' equal to the trivial representation, $j = 0$. No restrictions on the valency of the vertices of the graph are imposed. Following our previous line of argumentation, the new degrees of freedom available in the larger graph, are added in the vacuum state, here the Ashtekar–Lewandowski vacuum [34, 35], which represents degenerate geometries. Imposing several conditions, e.g. a certain representation of the holonomy–flux algebra of loop quantum gravity and (spatial) diffeomorphism invariance of the vacuum, the F/LOST theorem [169, 170] proves that this representation of loop quantum gravity is unique.

However, there is a key difference between our proposal in chapter 7 [88] and the loop quantum gravity construction: the latter is based on the kinematical states and thus employs kinematical embedding maps to relate these states across different boundaries, while we intend to use dynamical embedding maps to compute 'transition amplitudes' between (kinematical) states, where dynamical means that the embedding maps are supposed to impose the constraints of the theory. Let us elaborate on this further.

Formulating general relativity in a canonical formalism reveals it to be totally constrained: Due to diffeomorphism symmetry of the Einstein–Hilbert action, the solutions of the equations of motion, given initial conditions, are not unique, but one can always obtain a new solution by applying a diffeomorphism. In the canonical formulation this leads to the appearance of constraints, essentially restrictions on the phase space, since one cannot solve the first time derivatives of the configuration variables in terms of their canonical momenta. These constraints are the generators of infinitesimal gauge transformations and form an algebra, in gravity this is known as Dirac's hy-

persurface deformation algebra [171]. For totally constrained systems like gravity, the Hamiltonian itself is a linear combination of constraints and is thus forced to vanish. This implies that time evolution itself is a gauge transformation.

There exist several different methods to canonically quantize constrained systems in principle, where we will here focus on the quantization method by Dirac [171], see also [172] for a nice explanation, which is also employed in loop quantum gravity. Essentially the idea is to quantize the unconstrained system, i.e. the system before constraints are imposed. The associated Hilbert space is called kinematical and the challenge is to define constraint operators on this space, that realize a quantum version of the Poisson algebra of constraints [173]. A physical state is then defined to be annihilated by all constraint operators. In this context, time evolution governed by the exponential of the constraints implies that the physical state should not change, since a physical state, by definition, is annihilated by all generators of gauge transformations, i.e. the constraints. Thus, heuristically, time evolution in quantum gravity should act as a projector onto the physical Hilbert space, leaving physical states unchanged.

This brief, sketchy recollection of the canonical quantization procedure of systems with constraints reveals the crucial difference between the kinematical embedding maps of loop quantum gravity and the dynamical embedding maps we propose in [88]. The kinematical embedding maps relate the kinematical spin network states, defined on a graph, to spin network states defined on a different graph. In the inductive / projective limit [34,35], these embedding maps allow for the construction of the continuum kinematical Hilbert space with a unique kinematical vacuum [169,170], but contain no information on the dynamics. Following our arguments from the previous paragraph, a dynamical embedding map on the other hand, responsible to generate time evolution of the discrete system, must act as a projector onto the physical Hilbert space and therefore impose the (Hamiltonian and diffeomorphism) constraints of the theory. Remarkably, this heuristic picture is in nice agreement with time evolution in canonical quantum gravity: If the (dynamical) embedding maps satisfy cylindrical consistency conditions and one identifies physical states on different boundary discretisations, then the time evolved physical state remains in the same equivalence class as the original one. In fact both physical states describe the same physical situation, such that the physical state of the system is not changed under time evolution, but merely represented on a different discretisation.

Similar to the kinematical construction, the dynamical embedding maps give rise to a notion of a physical vacuum; the unique Hartle–Hawking vacuum [174] of the theory. Consider an 'evolution from nothing', namely starting from an 'empty' universe encoded in the one–dimensional Hilbert space $\mathcal{H}_0 = \mathbb{C}$. Time evolving this state by adding simplices, i.e. embedding it into the larger Hilbert spaces associated to the larger boundary, represents this vacuum on finer and finer discretisations up to the continuum. Yet by definition, the state remains in the same equivalence class as the unique initial one, thus uniquely representing the physical vacuum of the theory, which can be represented on any discretisation and the continuum.

Indeed, this construction principle introduced in [88] has been successfully used to construct a new representation of $(2+1)$–dimensional loop quantum gravity [175] based on the physical vacuum (in $(2 + 1)$D): Instead of considering arbitrary graphs and embeddings of those into finer graphs, one restricts the boundaries to be dual to triangulations, which restricts the vertices of the graph to be 3–valent. These dual triangulations are then refined by Pachner moves instead of (in principle) arbitrary refinements. Then the uniqueness theorem of the loop quantum gravity [169,170] vacuum is circumvented by constructing a different holonomy–flux algebra, which is cylindrically consistent with respect to the new refinement procedure. In a way, this new vacuum can be seen as the dual version of the Ashtekar–Lewandowski vacuum [34,35], since it is peaked on flat closed holonomies, thus also called the BF vacuum. Indeed, this is the physical vacuum of the 3D gravity, since it describes locally flat geometries. Note that this BF vacuum is not the first attempt to construct a vacuum for loop quantum gravity, which is not peaked on completely degenerate geometries, see

also [176] for a review on alternate representations of loop quantum gravity with non–vanishing vacuum expectation values of geometric operators, which are more suited as vacuum states for effective theories.

Nevertheless, a serious word of caution is due: the dynamical cylindrical consistency conditions, and equivalently the path independence of time evolution, are highly non–trivial requirements to satisfy. Indeed, it is very unlikely to readily write down a (family of) embedding maps that can (perfectly) impose Hamiltonian and diffeomorphism constraints, since, very similar to the construction of perfect discretizations [41–43], it requires to solve the dynamics. In fact, as we also describe in [88], the examples in which it is realized all resemble topological theories including the new vacuum for $(2+1)$D loop quantum gravity [175] or the (non–trivial) fixed points obtained from coarse graining quantum group spin nets [87], see chapter 6.

However, we would like to argue that achieving cylindrical consistency might not be necessary in any situation, e.g. consider a kinematical spin network state as the initial state. This state can be time evolved by glueing spin foam amplitudes, dual to simplices, to it, which should at least approximately impose diffeomorphism and Hamiltonian constraints, similar to the description in the classical case [133, 134]. If one stops after a finite number of time evolution steps, this may already suffice to compute good approximations to expectation values of sufficiently coarse grained observables, that is observables sensitive to geometric degrees of freedom on the scale of the discretisation. On the other hand, once sufficiently fine grained, the spin foam should behave as a proper projector onto the physical Hilbert space[16], i.e. in the refinement limit. To put it differently, the spin foam amplitudes have to be improved in order to act as proper projectors onto the physical Hilbert space thus closing the circle back to perfect discretisations [42, 43] and also tensor network renormalization [39, 85–87]. See also [177] for a definition of the transfer matrix from spin foams as a sum over all 2–complexes.

8.4.2 Constructing quantum space time

After these very conceptual considerations, we would like to emphasize more, how one can tackle the construction of a consistent continuum theory of gravity in practise, e.g. via the previously described tensor network renormalization. Therefore, it is instructive to explain in more detail, how these coarse graining methods fit into the scheme of cylindrical consistency and how this affects their interpretation. To be more concrete, we will focus on the tensor network formulation, which also includes spin foams.

Consider a single tensor for now, which we interpret to be dual to a 'chunk' of spacetime. Analogous to our ideas expressed above, the boundary of this chunk carries boundary data, more precisely a state in the Hilbert space associated to that boundary. The legs of the dual tensor pierce the boundary of this chunk and are thus labelled by this data, actually expressing the dependency of the tensor on this data. To put it differently, the tensor is a map from the Hilbert space associated to its boundary into the complex numbers, thus assigning an amplitude to this 'piece of quantum spacetime'. This interpretation is fundamentally inspired by the general boundary formulation [178], a formalism invented to describe quantum mechanics, quantum field theory and quantum gravity in general regions of spacetime by assigning Hilbert spaces to the boundaries of these regions and amplitude maps to the regions itself. Given this interpretation, one might be tempted to tentatively call the tensor, or alternatively the underlying spin foam, an 'atom of spacetime'[17].

---

[16]Another remark on unitarity: The time evolution depicted here is not unitary, since under time evolution, kinematical degrees of freedom get projected out and cannot be recovered by time evolving backwards. Instead, one would time evolve back to the physical state 'hidden' in the kinematical initial state.

[17]The notion of 'atom' must be taken with a pinch of salt: Since we are discussing background independent approaches to quantum gravity, there exists no background scale to compare this atom to. Hence, it is also fuzzy to talk about 'larger' and 'smaller' regions; only relational statements are well–defined.

Of course, a tensor network does not only consist of one tensor, but of a collection of many connected ones, forming a 'large' region of spacetime built up by many 'small' building blocks. This network then gives a fine grained amplitude map by summing over the bulk degrees of freedom and keeping the fine grained boundary data, where so far no approximation has been employed. While this finer amplitude map contains the entire dynamical information, it is also defined on a larger Hilbert space than the previous one. In order to relate this new amplitude map back to the original one and thus define a renormalization group flow for the tensor / the amplitude map, the boundary cannot be left unaffected: one has to define an embedding map, embedding (or rather blocking) the highly fine grained state back into a Hilbert space assigned to a coarser boundary[18]. Thus, we can compare the amplitude maps, i.e. the dynamics, before and after the coarse graining, which one could interpret as different (relative) 'scales'. Tensor network renormalization fits nicely into these ideas, since it provides a clear method to compute the embedding maps: the singular value decomposition applied to the tensor(s), i.e. the ingredients carrying the dynamics of the system, rearranges the degrees of freedom into an orthogonal basis, ordered in their significance by the size of their associated singular value. Therefore, the embedding maps here are essentially convenient variable redefinitions together with a cut–off, the bond dimension, truncating the less important degrees of freedom.

Therefore, we would like to stress again the crucial difference between the embedding maps obtained via tensor network renormalization (TNR) and e.g. the kinematical embedding maps in loop quantum gravity. In TNR the embedding maps themselves are computed from the amplitude maps, i.e. the tensors. Since these amplitude maps define the dynamics of the system, this implies that the so obtained embedding maps are constructed consistent with the dynamics, here explicitly explaining how the effective degrees of freedom on a 'larger' scale arise from the degrees of freedom on a 'smaller' scale. As a consequence, the non–triviality of the cylindrical consistency conditions for dynamical embedding maps becomes apparent in chapter 7 [88]: on the one hand, one has to determine the embedding maps consistent with the dynamics, i.e. the amplitude maps, relating the (partially ordered) boundary Hilbert spaces up to the continuum. Yet on the other hand, one requires the amplitude maps to be cylindrically consistent, i.e. it should not matter whether one evaluates a state on the coarse boundary with the coarse amplitude map or whether one embeds the coarse state into a finer boundary (Hilbert space) and then evaluates it with the finer amplitude map. The vital (and very difficult) feature here is that *both* embedding and amplitude maps have to be mutually consistent with one another.

As already emphasized above, these consistency conditions are very difficult to realize, unless one has solved the dynamics of the continuum theory already and can 'pull it back' onto the discretisation. Indeed, this is a challenge very similar to perfect discretisations [41–43], which aim at constructing a discretisation without breaking diffeomorphism symmetry. In both cases, the idea is to start with a theory, here a particular choice of amplitude maps given by a spin foam model, that is generically not cylindrically consistent, but can be iteratively improved via coarse graining techniques. Concretely, one constructs improved amplitude maps by combining finer ones and dynamically embedding / blocking them back into the previous boundary Hilbert space. Hence, one may wonder whether one can find positive indications that cylindrical consistency can be achieved, e.g. via TNR in the results of [87]. Similar to other coarse graining approaches, e.g. in [43], we observe that the renormalization group flow converges and ceases in a fixed point, where fixed point means that the tensors, the amplitude maps, are not changed under the coarse graining procedure. Indeed, since in TNR the embedding maps are directly computed from the amplitude maps, on the fixed points both the amplitude and the embedding maps do not change under further

---

[18]It may turn out that the previous / initial Hilbert space is just a subspace of the 'full' Hilbert space assigned to that boundary. This actually occurs e.g. in the quantum group spin nets [87]: The initial model has the restriction that only channels (j, j^*) are excited, while under coarse graining (depending on the initial data) also channels (j, j') with $j' \neq j^*$ get (and stay) excited. Just restricting to channels (j, j^*) under coarse graining would be too limited. In principle, one can also permit more general initial data with channels (j, j') excited.

coarse graining transformations, thus they perfectly satisfy the cylindrical consistency conditions. Then, if we interpret the embedding maps again as time evolution maps, they also realize the path independence condition and act as projectors onto the 'fixed point theory'.

Actually, these features are not surprising, since the found (non–trivial) fixed points in [87] all resemble topological field theories. This fact of the fixed points can be read off from the singular value decomposition: In the specific tensor network algorithm used in [87], the singular value decomposition is employed to split the 4–valent tensors into two 3–valent ones; the SVD itself can then be understood as a variable redefinition performed in a symmetry preserving way, retaining an interpretation of the new variables as $SU(2)_k$ representations. On the fixed points of the coarse graining procedure, one realizes that the system actually possesses only a finite number of degrees of freedom, recognizable in the finite number of non–vanishing singular values, which are additionally equal to one. Therefore, these embedding maps clearly satisfy the projector conditions. Combining these properties with the local interactions of the tensors implies that these fixed points describe topological theories. In fact, cylindrical consistency conditions can always be satisfied for topological theories as also discussed in chapter 7, [88]. As already mentioned this is used in the construction of the BF vacuum in (2+1)D loop quantum gravity in [175].

8.4.3 How to (possibly) get propagating degrees of freedom

Despite these encouraging examples and the rich fixed point structure found in [87], we are well aware of the fact that gravity in 4D is not topological and one requires a way to arrive at a theory with propagating degrees of freedom under coarse graining. The frequently uttered route away from these topological theories is to tune the system towards a second order phase transition: at such a transition, one expects that infinitely many degrees of freedom become relevant (or can be reorganized in a non–local way). In a standard lattice approach (with a background lattice constant) one would understand this as a diverging correlation length[19].

The observation that infinitely many degrees of freedom are relevant at the phase transition is in clear conflict with the truncation necessary in tensor network renormalization. To illustrate this issue and why this method necessarily has to break down at the phase transition, let us discuss the situation in quantum group spin nets. Note that these examinations are preliminary and were presented in [164], yet a much more careful analysis of the phase transitions of the systems studied in [87] is required.

Despite the preliminary status of the analysis, one can make two clear observations: The first observation is that the system requires significantly more iterations for the coarse graining procedure to converge to the fixed point the closer it is fine–tuned towards the phase transition. This behaviour becomes visible if one plots a singular value over the number of iterations that can distinguish the two phases meeting at the transition: The closer the system is tuned towards the transition the longer the singular value remains (almost) constant, forming a 'plateau', before either flowing to one or zero depending on to which topological theory the system flows to (see also [164] for a plot). The reason why this has to happen can be drawn from the list of non–vanishing singular values, i.e. the number of relevant degrees of freedom, whose size quickly exceeds the computationally feasible bond dimension, where additionally the singular values slowly decrease in size. This immediately poses an issue to the truncation scheme, which can only provide a reasonable approximation if only irrelevant degrees of freedom are dropped. To determine whether a degree of freedom is irrelevant, the most important criterion is the size of its associated singular value compared to the most important degrees of freedom, e.g. if a singular value is several orders of magnitude smaller than the largest one. Additionally, it is advisable not to neglect the relative sizes of the smallest singular value kept and the largest truncated one. If these are very close together, one

---

[19]The correlation function in a spin system between two spins separated by the distance r usually falls off exponentially with $-\frac{r}{\xi}$, where ξ is the correlation length. At a second order phase transition $\xi \to \infty$, which implies that all spins of the system become correlated.

would actually truncate a degree of freedom of similar significance as the kept one. Indeed, if both these conditions are satisfied during the whole coarse graining process, the result is consistent under increasing the accuracy of the simulations, i.e. the bond dimension of the simulation. Yet close to the phase transition, neither of these conditions can be fulfilled, in fact, no truncation can be employed without significantly altering the dynamics of the system. Hence, the necessarily employed truncation enforces a finite a number of degrees of freedom and together with local embedding maps, the system eventually flows towards a topological theory. As a side remark one can make similar observations if applying the TNR to the Ising model, which indicates that the phase transitions for the quantum group spin net models might be of second order.

In condensed matter physics one is aware of this issue: Methods similar to TNR, e.g. the originally invented density matrix renormalization [116, 117] method or matrix product states [118, 119], were invented to (efficiently) obtain ground states for many–body quantum systems. As it turns out TNR is a well–suited approach to identify these states for 'gapped' systems, i.e. systems with an energy gap between the ground and the first excited state. However close to a second order phase transition, this gap disappears and the tensor network description would require an infinite bond dimension to capture the vastly spread correlation of the microscopic degrees of freedom. This behaviour is referred to as long range entanglement, which requires different methods to efficiently describe these states. One example is called multi–scale entanglement renormalization ansatz (MERA) [179] and is surprisingly analogical to the described 'evolution from nothing' in [88]: One degree of freedom, e.g. a qubit, is embedded via an isometry into a Hilbert space of two qubits. Then one acts with a unitary transformation, called (dis)entangler, on this two–site state, effectively entangling the two degrees of freedom. Afterwards the procedure is iteratively applied until the desired N–site state is generated, which is fully characterized by the chosen isometries and disentanglers. These maps are then specified in a variational scheme such that the expectation value of the Hamiltonian (of the system under discussion) with respect to the just constructed state is minimized. Furthermore, the locally applied entangling maps allow for an long–range entangled many–particle state[20].

Therefore, methods that allow for long–range entanglement may provide a way to escape the topological fixed points encountered in [87]. In fact the importance of entangling maps has been emphasized in [88][21] as well. While tensor network renormalization does entangle the finer degrees of freedom, this only happens in a local way: In order to consecutively apply the algorithm one has to restrict the network to be regular (in terms of combinatorial information) and choose the embedding maps such that the coarse lattice has the same regular combinatorics as the fine one. Then the numerical feasibility of the algorithms dictates the introduction of a cut–off on the degrees of freedom, which in many situations is a reasonable approximation of the dynamics (and the partition function), but inevitably breaks down at a second order phase transition. Hence, non–local embedding maps, e.g. similar to MERA or the radial time–evolution sketched in chapter 7, [88], may constitute the necessary improvement to study the dynamics on the phase transition.

In fact, the idea of radial time evolution in tensor networks is also related to entanglement renormalization [180], which also relies on tensor network techniques and attempts to interpret the network and the encoded entanglement as a background anti de Sitter (AdS) spacetime [181–183], related to holographic renormalization [184]. Even though this idea may appear to be fitting for gravitational theories, it may not be suitable for a dynamical theory of gravity, where one rather expects that the dynamical variables of the tensor network encode the geometric degrees of freedom, which encode a geometry in the boundary state. If one can extract this geometric information from this state, one should be able to fully reconstruct the geometry in the bulk.

---

[20] In condensed matter, this construction scheme is usually seen from the opposite point of view: one starts with an N–site state, where the N sites are entangled on different scales. The (dis)entanglers then remove short–range entanglement between two sites, which is considered not to be universal.

[21] There we particularly discuss the case of trivial refining maps, e.g. 1–4 moves in 4D Regge calculus. In that case one can show that no new physical degrees of freedom are added but gauge degrees of freedom. Thus only refining by these Pachner moves lead to configurations known as 'stacked spheres', which are flat and non–dynamical.

9 Summary and conclusion

In this thesis we have explored the relation between discrete approaches of quantum gravity and classical, continuous general relativity in very different situations and with very different tools, ranging from only a few basic building blocks up to literally infinitely many. While the introduced discretisation constitutes a useful tool to define and examine the dynamics of the quantum theory, it is in general not unique and obscures the relation to the classical continuum theory, e.g. by breaking diffeomorphism symmetry of general relativity [41,42], which is deeply entwined with the dynamics of the theory. We attempt to clarify this relation by employing dynamical principles, e.g. coarse graining procedures improving the discrete theory. As we have argued in the discussion above, one can regard the results at the level of only a few simplices as guiding principles how to explore the collective dynamics of many building blocks in spin foam models. Let us summarize this line of argumentation again:

At the lowest level, namely a single simplex (or vertex amplitude), we have confirmed and extended the results of previous asymptotic expansions in spin foam models [23,25,27–29,99,100] in chapters 2 and 3, see also [30] and [31]: The geometric part of the amplitude oscillates as the cosine of the discrete Regge gravity action [17,18] associated to the simplex, constructed from representation labels of the foam. We modified the frequently used coherent state approach [29,81, 90] to also derive the complete expansion (up to leading order), in particular the missing measure factor, and derived the very first result of such a factor for the 4D Barrett–Crane spin foam model [73]. In fact, this connection between spin foams and Regge calculus at the level of one simplex is a positive direct indication that spin foam models are viable candidate quantum gravity theories.

However, extensions of these results to larger triangulations are rare, see e.g. [78], even simple local changes of the underlying triangulation, so–called Pachner moves [82,83], have not been computed for 4D spin foam models (yet). Also the status of (broken) diffeomorphism symmetry in spin foam models has not been sufficiently analysed, in particular with respect to the ambiguities involved in the definition of these models. Therefore, the conjecture found in [43], stating that discrete diffeomorphism symmetry is equivalent to discretisation independence, together with the connection of spin foams and Regge calculus has motivated us to investigate triangulation independence of the (linearized) Regge path integral in chapters 4 and 5, see also [59,84], with particular focus on the construction of a suitable path integral measure, which one might hope to be anomaly free with respect to diffeomorphisms [51]. Furthermore, the hope is to use such a measure factor as a 'blueprint' for spin foams.

In topological 3D gravity, where the classical Regge action is triangulation independent, an almost unique path integral measure can be constructed, which is furthermore consistent with the asymptotics of the Ponzano–Regge model [23,80]. In 4D, the situation is more complicated and also more interesting: First of all, we show that even the linearized Regge action is not invariant under all Pachner moves, such that full triangulation independence cannot be achieved. Secondly, even though the calculations and Hessian matrix are strikingly similar to the 3D case, independence under the remaining subset of moves cannot be achieved either. This is due to the appearance of non–localities in the action, which do not factorise as a product of amplitudes associated to (sub)simplices.

These results have several important implications: First and foremost, the (linearized) Regge action itself must necessarily be improved in order to realize a diffeomorphism symmetry in the discrete for any choice of boundary data. It has been known that the discrete diffeomorphism

symmetry is only preserved if the boundary data allow for flat solutions in the bulk [44, 45], yet it surprisingly also applies to the linearized scenario. If one then attempts to improve the Regge action by a coarse graining scheme, e.g. via Pachner moves, one obtains non–local interactions already after one step, which complicates the consecutive application of the procedure. This indeed raises the question whether one can invent / apply different real space renormalization techniques [115] to spin foams that are better suited to handle non–local interactions, e.g. by using different degrees of freedom, e.g. area–angle variables [60, 142], or allowing changes on the boundary in contrast to Pachner moves, which leave the boundary unchanged.

Suitable tools can be found in condensed matter theory, in particular tensor network renormalization [85, 86], which can be understood as a tool combining a collection of basic building blocks into a new effective building block; the appearance of non–localities is 'absorbed' into the building block itself, but is instead accompanied by an exponential growth of the boundary data under consecutive application of this method. To solve this issue in tensor network renormalization one identifies the relevant degrees of freedom of the systems (by a singular value decomposition), which allows to truncate less relevant ones and to run efficient numerical simulations. In fact, this identification of relevant degrees of freedom can be understood as a variable redefinition, dynamically relating boundary data on the fine discretisation to effective boundary data on the coarser discretisation, thus serving as an embedding map. Therefore, this tool is capable of studying the effective dynamics of the system and approximately compute the partition function and expectation values.

To test the feasibility of this approach with respect to spin foam models, we have studied it on analogue spin foam models, so–called spin nets [37–39], which can be understood as dimensionally reduced spin foams, defined on the quantum group $SU(2)_k$ [122,123] in chapter 6, see also [87]. Note that these simplified models still capture the important dynamical ingredients of spin foam models, which in principle allows for more structure (by the imposition of simplicity constraints [66]) than in the related lattice gauge theories. Remarkably, we have uncovered a very rich, non–trivial fixed point structure in the spin net models, which form a regular pattern at different levels k of the quantum group, and are characterized by their excited intertwiner channels, see also [39]. Yet in contrast to [39], each of these fixed points exhibits an extended phase (in parameter space) due to the new parametrization of the initial data introduced in [87], which has been inspired by so–called intertwiner models [162]. Furthermore, the theories on the fixed points show an interesting interplay between imposing the constraints too strongly or too weakly. Yet the fixed points themselves resemble topological theories, an accompaniment of the coarse graining scheme: By enforcing a finite number of local interactions between the building blocks, the system naturally flows to a topological theory. Fortunately, close to the phase transition, one realizes that more and more degrees of freedom become relevant and the truncation scheme inevitably breaks down. Therefore we tentatively interpret this behaviour as indications that these phase transitions are of second order [164], which should lead to a theory with propagating degrees of freedom on the transition.

Besides these very encouraging results for the spin foam approach, the idea of the embedding maps relating coarser and finer boundaries can be extended further (see chapter 7 and [88]): If these dynamical embedding maps satisfy so–called cylindrical consistency conditions, which are well–known in loop quantum gravity [20], one can unambiguously relate any pair of boundaries to one another. Then these tools allow us to compare states defined on different boundary Hilbert spaces by embedding them into a common refinement, e.g. the continuum, and identify them if they are identical (on this common refinement). In an inductive limit, one can thus consistently define the continuum Hilbert space of this theory. For gravitational, i.e. totally constrained, theories, this is particularly appealing, since one can then understand these embedding maps as time evolution, which do not change the physical state of the system. In this context, the physical state is merely represented on a different discretisation. Naturally, these are highly non–trivial conditions, which are very difficult to satisfy. One example, in which this is realized are topological theories, e.g. the

previously discussed fixed points of spin net models [87].

Therefore we propose how to use these embedding maps to construct a continuum theory of quantum gravity in principle and approximately, e.g. by a coarse graining scheme like tensor network renormalization. One positive example implementing this idea has already been developed in form of the physical vacuum in (2+1)D loop quantum gravity, called the BF vacuum [175]. Of course, 3D gravity is a topological theory, but nevertheless it proves the potential of this idea. Similarly we expect this to provide the unique Hartle–Hawking vacuum [174] of the theory by starting with an 'evolution from nothing'. Such a construction may require more non–local embedding maps that allow for long range entanglement, which might be the necessary change to escape topological theories. Again, similar tools have also been developed in condensed matter theory in the form of the 'multi–scale entanglement renormalization ansatz' (MERA) [179] that might prove useful in future research.

To conclude this thesis, we would like to emphasize that we have made substantial progress towards defining a continuum / refinement limit of spin foam models and with it towards answering the question whether spin foam models are compatible with general relativity: we have developed new tools that help us to get a better understanding of the basic spin foam amplitudes in terms of discrete gravity, here we get a first glimpse at the chosen measure on the space of geometries. We demonstrate that in 4D discrete gravity, triangulation independence inevitably implies non–local interactions and that the Regge action and spin foam models necessarily have to be improved in order to be diffeomorphism invariant in the discrete. To effectively deal with these non–local interactions, we explore coarse graining methods developed in condensed matter theory and successfully apply them to (analogue) spin foam models, revealing a rich, interesting phase structure that indicates that spin foam models might possess intriguing continuum phases, possibly equipped with dynamics consistent with general relativity. Eventually, we extend the idea of embedding maps, which represent the key ingredients of the coarse graining procedure, to a general consistent construction scheme of the physical continuum theory from spin foam models; a 'user guide' how to construct quantum spacetime.

Beyond doubt, there is still a long road ahead before we can confidently state that spin foam models provide a dynamics consistent with general relativity. In this thesis we provide a suggestion how this question can be investigated with positive evidence underlining the usability of the proposed tools. Following this line of thought it is necessary to extend the coarse graining methods to the full spin foam models and identify their phases. This includes computing expectation values of observables, correlation functions etc. necessary to characterize the systems. We also feel obliged to mention that the systems under discussion in the entirety of this thesis describe pure gravity and in order to check consistency with general relativity also includes coupling matter to the quantum gravity theory.

As a closing remark, let us emphasize again the importance of checking the consistency with the classical theory: Due to the lack of experimental data and therefore a lack of guidance concerning what a theory of quantum gravity must capture, e.g. what are the physical degrees of freedom to quantize, several different approaches to quantum gravity have been developed, each of them with their own premises, advantages and disadvantages. A priori the question which of these research programs is to be favoured cannot be answered and relies heavily on personal opinion. Therefore it is indispensable to make an effort to derive predictions, check consistency with the classical theory, in short, establish a connection to physical reality, such that the theory can be verified or falsified. To accomplish such a task is profoundly ambitious, yet progress might be in reach if one broadens one's horizon and adopts ideas developed in different fields. To be more concrete, we have been able to investigate spin foam models in a novel way, uncovering new insights by using condensed matter techniques; future developments may prove to be mutually beneficial. Therefore, one should not be afraid to reach out for new methods and testable predictions, since even if the outcome is negative, the knowledge that an approach does not work and why is a substantial contribution to

science that should not be underestimated.

Bibliography

[1] **ATLAS** Collaboration, G. Aad *et al.*, "Observation of a new particle in the search for the Standard Model Higgs boson with the ATLAS detector at the LHC," *Phys.Lett.* **B716** (2012) 1–29, `arXiv:1207.7214 [hep-ex]`.

[2] **CMS** Collaboration, S. Chatrchyan *et al.*, "Observation of a new boson at a mass of 125 GeV with the CMS experiment at the LHC," *Phys.Lett.* **B716** (2012) 30–61, `arXiv:1207.7235 [hep-ex]`.

[3] S. G. Turyshev, "Experimental Tests of General Relativity," *Ann.Rev.Nucl.Part.Sci.* **58** (2008) 207–248, `arXiv:0806.1731 [gr-qc]`.

[4] **BICEP2** Collaboration, P. Ade *et al.*, "Detection of B-Mode Polarization at Degree Angular Scales by BICEP2," *Phys.Rev.Lett.* **112** (2014) 241101, `arXiv:1403.3985 [astro-ph.CO]`.

[5] O. Lahav and A. R. Liddle, "The cosmological parameters 2005," `arXiv:astro-ph/0601168 [astro-ph]`.

[6] **Planck** Collaboration, P. Ade *et al.*, "Planck 2013 results. XVI. Cosmological parameters," *Astron.Astrophys.* (2014) , `arXiv:1303.5076 [astro-ph.CO]`.

[7] S. Weinberg, "The Cosmological Constant Problem," *Rev.Mod.Phys.* **61** (1989) 1–23.

[8] K. Kuchar, "Time and interpretations of quantum gravity," *Int.J.Mod.Phys.Proc.Suppl.* **D20** (2011) 3–86. In *Winnipeg 1991, Proceedings, General relativity and relativistic astrophysics* 211-314.

[9] C. Isham, "Canonical quantum gravity and the problem of time," `arXiv:gr-qc/9210011 [gr-qc]`. In *Salamanca 1992, Proceedings, Integrable systems, quantum groups, and quantum field theories* 157-287, and London Imp. Coll. - ICTP-91-92-25 (92/08,rec.Nov.) 124 p.

[10] E. Anderson, "The Problem of Time in Quantum Gravity," `arXiv:1009.2157 [gr-qc]`.

[11] E. Anderson, "Problem of Time in Quantum Gravity," *Annalen Phys.* **524** (2012) 757–786, `arXiv:1206.2403 [gr-qc]`.

[12] M. H. Goroff and A. Sagnotti, "Quantum Gravity At Two Loops," *Phys.Lett.* **B160** (1985) 81.

[13] M. H. Goroff and A. Sagnotti, "The Ultraviolet Behavior of Einstein Gravity," *Nucl.Phys.* **B266** (1986) 709.

[14] M. Niedermaier and M. Reuter, "The Asymptotic Safety Scenario in Quantum Gravity," *Living Rev.Rel.* **9** (2006) 5–173.

[15] R. Percacci, "Asymptotic Safety," `arXiv:0709.3851 [hep-th]`. Published in In *Oriti, D. (ed.): Approaches to quantum gravity* 111-128.

[16] J. Ambjørn, A. Goerlich, J. Jurkiewicz, and R. Loll, "CDT and the Search for a Theory of Quantum Gravity," `arXiv:1305.6680 [gr-qc]`.

[17] T. Regge, "General relativity without coordinates," *Nuovo Cim.* **19** (1961) 558.

[18] R. M. Williams, "Recent progress in Regge calculus," *Nucl.Phys.Proc.Suppl.* **57** (1997) 73–81, `arXiv:gr-qc/9702006 [gr-qc]`.

[19] C. Rovelli, *Quantum gravity.* Cambridge University Press, Cambridge, 2004.

[20] T. Thiemann, *Modern Canonical Quantum General Relativity.* Cambridge University Press, Cambridge, 2008.

[21] A. Perez, "The Spin Foam Approach to Quantum Gravity," *Living Rev.Rel.* **16** (2013) 3, `arXiv:1205.2019 [gr-qc]`.

[22] C. Rovelli, "Zakopane lectures on loop gravity," *PoS* **QGQGS2011** (2011) 003, `arXiv:1102.3660 [gr-qc]`.

[23] G. Ponzano and T. Regge, *Semiclassical limit of Racah coefficients, in: Spectroscopy and group theoretical methods in physics.* North Holland Publ. Co., Amsterdam, 1968.

[24] J. W. Barrett and T. J. Foxon, "Semiclassical limits of simplicial quantum gravity," *Class. Quant. Grav.* **11** (1994) 543–556, `arXiv:gr-qc/9310016 [gr-qc]`.

[25] J. W. Barrett and R. M. Williams, "The Asymptotics of an amplitude for the four simplex," *Adv.Theor.Math.Phys.* **3** (1999) 209–215, `arXiv:gr-qc/9809032 [gr-qc]`.

[26] J. C. Baez, J. D. Christensen, and G. Egan, "Asymptotics of 10j symbols," *Class.Quant.Grav.* **19** (2002) 6489, `arXiv:gr-qc/0208010 [gr-qc]`.

[27] L. Freidel and D. Louapre, "Asymptotics of 6j and 10j symbols," *Class.Quant.Grav.* **20** (2003) 1267–1294, `arXiv:hep-th/0209134 [hep-th]`.

[28] F. Conrady and L. Freidel, "On the semiclassical limit of 4d spin foam models," *Phys.Rev.* **D78** (2008) 104023, `arXiv:0809.2280 [gr-qc]`.

[29] J. W. Barrett, R. J. Dowdall, W. J. Fairbairn, H. Gomes, F. Hellmann, and R. Pereira, "Asymptotics of 4d spin foam models," *Gen. Rel. Grav.* **43** (2011) 2421, `arXiv:1003.1886 [gr-qc]`.

[30] W. Kamiński and S. Steinhaus, "Coherent states, 6j symbols and properties of the next to leading order asymptotic expansions," *J. Math. Phys.* **54** (2013) 121703, `arXiv:1307.5432 [math-ph]`.

[31] W. Kamiski and S. Steinhaus, "The BarrettCrane model: asymptotic measure factor," *Class.Quant.Grav.* **31** (2014) 075014, `arXiv:1310.2957 [gr-qc]`.

[32] L. Freidel, "Group field theory: An Overview," *Int.J.Theor.Phys.* **44** (2005) 1769–1783, `arXiv:hep-th/0505016 [hep-th]`.

[33] D. Oriti, "The Group field theory approach to quantum gravity," `arXiv:gr-qc/0607032 [gr-qc]`. Published in In *Oriti, D. (ed.): Approaches to quantum gravity* 310-331.

[34] A. Ashtekar and C. Isham, "Representations of the holonomy algebras of gravity and nonAbelian gauge theories," *Class.Quant.Grav.* **9** (1992) 1433–1468, `arXiv:hep-th/9202053 [hep-th]`.

[35] A. Ashtekar and J. Lewandowski, "Projective techniques and functional integration for gauge theories," *J.Math.Phys.* **36** (1995) 2170–2191, `arXiv:gr-qc/9411046 [gr-qc]`.

[36] F. Dowker, "Introduction to causal sets and their phenomenology," *Gen.Rel.Grav.* **45** no. 9, (2013) 1651–1667.

[37] B. Dittrich, F. C. Eckert, and M. Martín-Benito, "Coarse graining methods for spin net and spin foam models," *New J. Phys.* **14** (2012) 035008, `arXiv:1109.4927 [gr-qc]`.

[38] B. Dittrich and F. C. Eckert, "Towards computational insights into the large-scale structure of spin foams," *J.Phys.Conf.Ser.* **360** (2012) 012004, `arXiv:1111.0967 [gr-qc]`.

[39] B. Dittrich, M. Martín-Benito, and E. Schnetter, "Coarse graining of spin net models: dynamics of intertwiners," *New J. Phys.* **15** (2013) 103004, `arXiv:1306.2987 [gr-qc]`.

[40] B. Dittrich, "Diffeomorphism symmetry in quantum gravity models," *Adv. Sci. Lett.* **2** (2009) 151, `arXiv:0810.3594 [gr-qc]`.

[41] B. Bahr and B. Dittrich, "(Broken) Gauge Symmetries and Constraints in Regge Calculus," *Class. Quant. Grav.* **26** (2009) 225011, `arXiv:0905.1670 [gr-qc]`.

[42] B. Bahr and B. Dittrich, "Improved and Perfect Actions in Discrete Gravity," *Phys. Rev. D* **80** (2009) 124030, `arXiv:0907.4323 [gr-qc]`.

[43] B. Bahr, B. Dittrich, and S. Steinhaus, "Perfect discretization of reparametrization invariant path integrals," *Phys. Rev. D* **83** (2011) 105026, `arXiv:1101.4775 [gr-qc]`.

[44] M. Rocek and R. M. Williams, "Quantum Regge Calculus," *Phys.Lett.* **B104** (1981) 31.

[45] M. Rocek and R. Williams, "The Quantization of Regge Calculus," *Z.Phys.* **C21** (1984) 371.

[46] L. Freidel and D. Louapre, "Diffeomorphisms and spin foam models," *Nucl.Phys.* **B662** (2003) 279–298, `arXiv:gr-qc/0212001 [gr-qc]`.

[47] C. Rovelli and M. Smerlak, "In quantum gravity, summing is refining," *Class.Quant.Grav.* **29** (2012) 055004, `arXiv:1010.5437 [gr-qc]`.

[48] R. Gambini and J. Pullin, "Consistent discretizations as a road to quantum gravity," `arXiv:gr-qc/0512065 [gr-qc]`. Published in In *Oriti, D. (ed.): Approaches to quantum gravity* 378-392.

[49] M. Campiglia, C. Di Bartolo, R. Gambini, and J. Pullin, "Uniform discretizations: A Quantization procedure for totally constrained systems including gravity," *J.Phys.Conf.Ser.* **67** (2007) 012020, `arXiv:gr-qc/0606121 [gr-qc]`.

[50] M. Campiglia, C. Di Bartolo, R. Gambini, and J. Pullin, "Uniform discretizations: A New approach for the quantization of totally constrained systems," *Phys.Rev.* **D74** (2006) 124012, `arXiv:gr-qc/0610023 [gr-qc]`.

[51] M. Bojowald and A. Perez, "Spin foam quantization and anomalies," *Gen.Rel.Grav.* **42** (2010) 877–907, `arXiv:gr-qc/0303026 [gr-qc]`.

[52] C. Perini, C. Rovelli, and S. Speziale, "Self-energy and vertex radiative corrections in LQG," *Phys.Lett.* **B682** (2009) 78–84, `arXiv:0810.1714 [gr-qc]`.

[53] V. Bonzom and M. Smerlak, "Bubble divergences from cellular cohomology," *Lett.Math.Phys.* **93** (2010) 295–305, `arXiv:1004.5196 [gr-qc]`.

[54] A. Riello, "Self-energy of the Lorentzian Engle-Pereira-Rovelli-Livine and Freidel-Krasnov model of quantum gravity," *Phys.Rev.* **D88** no. 2, (2013) 024011, `arXiv:1302.1781 [gr-qc]`.

[55] V. Bonzom and B. Dittrich, "Bubble divergences and gauge symmetries in spin foams," *Phys.Rev.* **D88** (2013) 124021, `arXiv:1304.6632 [gr-qc]`.

[56] G. Amelino-Camelia, J. R. Ellis, N. Mavromatos, D. V. Nanopoulos, and S. Sarkar, "Tests of quantum gravity from observations of gamma-ray bursts," *Nature* **393** (1998) 763–765, `arXiv:astro-ph/9712103 [astro-ph]`.

[57] G. Amelino-Camelia and L. Smolin, "Prospects for constraining quantum gravity dispersion with near term observations," *Phys.Rev.* **D80** (2009) 084017, `arXiv:0906.3731 [astro-ph.HE]`.

[58] B. Bahr, R. Gambini, and J. Pullin, "Discretisations, constraints and diffeomorphisms in quantum gravity," *SIGMA* **8** (2012) 002, `arXiv:1111.1879 [gr-qc]`.

[59] B. Dittrich and S. Steinhaus, "Path integral measure and triangulation independence in discrete gravity," *Phys. Rev. D* **85** (2012) 044032, `arXiv:1110.6866 [gr-qc]`.

[60] B. Bahr and B. Dittrich, "Regge calculus from a new angle," *New J. Phys.* **12** (2010) 033010, `arXiv:0907.4325 [gr-qc]`.

[61] P. Hasenfratz and F. Niedermayer, "Perfect lattice action for asymptotically free theories," *Nucl. Phys. B* **414** (1994) 785–814, `arXiv:hep-lat/9308004 [hep-lat]`.

[62] P. Hasenfratz, "Prospects for perfect actions," *Nucl. Phys. Proc. Suppl.* **63** (1998) 53–58, `arXiv:hep-lat/9709110 [hep-lat]`. In *Edinburgh 1997, Lattice field theory* 53-58.

[63] J. Marsden and M. West, "Discrete mechanics and variational integrators," *Acta Numerica* **10** (2001) 357.

[64] W. Bietenholz, "Perfect scalars on the lattice," *Int.J.Mod.Phys.* **A15** (2000) 3341–3368, `arXiv:hep-lat/9911015 [hep-lat]`.

[65] B. Bahr, B. Dittrich, and S. He, "Coarse graining free theories with gauge symmetries: the linearized case," *New J. Phys.* **13** (2011) 045009, `arXiv:1011.3667 [gr-qc]`.

[66] J. F. Plebanski, "On the separation of Einsteinian substructures," *J.Math.Phys.* **18** (1977) 2511–2520.

[67] J. C. Baez, "An Introduction to spin foam models of quantum gravity and BF theory," *Lect.Notes Phys.* **543** (2000) 25–94, `arXiv:gr-qc/9905087 [gr-qc]`.

[68] M. Martellini and M. Zeni, "The BF formalism for Yang-Mills theory and the 't Hooft algebra," `arXiv:hep-th/9610090 [hep-th]`.

[69] B. Bahr, B. Dittrich, F. Hellmann, and W. Kaminski, "Holonomy Spin Foam Models: Definition and Coarse Graining," *Phys.Rev.* **D87** (2013) 044048, `arXiv:1208.3388 [gr-qc]`.

[70] L. Freidel and K. Krasnov, "Spin foam models and the classical action principle," *Adv.Theor.Math.Phys.* **2** (1999) 1183–1247, `arXiv:hep-th/9807092 [hep-th]`.

[71] L. Freidel and D. Louapre, "Ponzano-Regge model revisited I: Gauge fixing, observables and interacting spinning particles," *Class.Quant.Grav.* **21** (2004) 5685–5726, `arXiv:hep-th/0401076 [hep-th]`.

[72] V. Bonzom and M. Smerlak, "Gauge symmetries in spinfoam gravity: the case for 'cellular quantization'," *Phys.Rev.Lett.* **108** (2012) 241303, `arXiv:1201.4996 [gr-qc]`.

[73] J. W. Barrett and L. Crane, "Relativistic spin networks and quantum gravity," *J.Math.Phys.* **39** (1998) 3296–3302, `arXiv:gr-qc/9709028 [gr-qc]`.

[74] J. Engle, E. Livine, R. Pereira, and C. Rovelli, "LQG vertex with finite Immirzi parameter," *Nucl.Phys.* **B799** (2008) 136–149, `arXiv:0711.0146 [gr-qc]`.

[75] L. Freidel and K. Krasnov, "A New Spin Foam Model for 4d Gravity," *Class.Quant.Grav.* **25** (2008) 125018, `arXiv:0708.1595 [gr-qc]`.

[76] W. Kaminski, M. Kisielowski, and J. Lewandowski, "Spin-Foams for All Loop Quantum Gravity," *Class.Quant.Grav.* **27** (2010) 095006, `arXiv:0909.0939 [gr-qc]`.

[77] E. Bianchi and F. Hellmann, "The Construction of Spin Foam Vertex Amplitudes," *SIGMA* **9** (2013) 008, `arXiv:1207.4596 [gr-qc]`.

[78] F. Hellmann and W. Kaminski, "Holonomy spin foam models: Asymptotic geometry of the partition function," *JHEP* **1310** (2013) 165, `arXiv:1307.1679 [gr-qc]`.

[79] M. Han, "Covariant Loop Quantum Gravity, Low Energy Perturbation Theory, and Einstein Gravity with High Curvature UV Corrections," *Phys.Rev.* **D89** (2014) 124001, `arXiv:1308.4063 [gr-qc]`.

[80] J. W. Barrett and I. Naish-Guzman, "The Ponzano-Regge model," *Class.Quant.Grav.* **26** (2009) 155014, `arXiv:0803.3319 [gr-qc]`.

[81] F. Hellmann, *State Sums and Geometry*. PhD thesis, University of Nottingham, 2011. `arXiv:1102.1688 [gr-qc]`.

[82] U. Pachner, "Konstruktionsmethoden und das kombinatorische Homöomorphieproblem für Triangulationen kompakter semilinearer Mannigfaltigkeiten," *Abh. Math. Sem. Univ. Hamburg* **57** (1986) 69.

[83] U. Pachner, "P. L. Homeomorphic Manifolds are Equivalent by Elementary Shellings," *Europ. J. Combinatorics* **12** (1991) 129–145.

[84] B. Dittrich, W. Kaminski, and S. Steinhaus, "Discretization independence implies non-locality in 4D discrete quantum gravity," *Class.Quant.Grav.* **31** (2014) 245009, `arXiv:1404.5288 [gr-qc]`.

[85] M. Levin and C. P. Nave, "Tensor renormalization group approach to 2d classical lattice models," *Phys. Rev. Lett.* **99** (2007) 120601, `arXiv:cond-mat/0611687 [cond-mat]`.

[86] Z.-C. Gu and X.-G. Wen, "Tensor-Entanglement-Filtering Renormalization Approach and Symmetry Protected Topological Order," *Phys. Rev. B* **80** (2009) 155131, `arXiv:0903.1069 [cond-mat.str-el]`.

[87] B. Dittrich, M. Martin-Benito, and S. Steinhaus, "Quantum group spin nets: refinement limit and relation to spin foams," *Phys.Rev.* **D90** (2014) 024058, `arXiv:1312.0905 [gr-qc]`.

[88] B. Dittrich and S. Steinhaus, "Time evolution as refining, coarse graining and entangling," *New J. Phys.* **16** (2014) 123041, `arXiv:1311.7565 [gr-qc]`.

[89] B. Dittrich, "From the discrete to the continuous: Towards a cylindrically consistent dynamics," *New J.Phys.* **14** (2012) 123004, `arXiv:1205.6127 [gr-qc]`.

[90] A. Perelomov, *Generalized coherent states and their applications.* Springer, Berlin, 1986.

[91] J. Roberts, "Classical 6j-symbols and the tetrahedron," *Geom. Topol.* **3** (1999) 21–66, `arXiv:math-ph/9812013 [math-ph]`.

[92] V. Aquilanti, H. M. Haggard, A. Hedeman, N. Jeevanjee, R. G. Littlejohn, *et al.*, "Semiclassical Mechanics of the Wigner 6j-Symbol," *J.Phys.* **A45** (2012) 065209, `arXiv:1009.2811 [math-ph]`.

[93] J. M. Garcia-Islas, "(2+1)-dimensional quantum gravity, spin networks and asymptotics," *Class.Quant.Grav.* **21** (2004) 445–464, `arXiv:gr-qc/0307054 [gr-qc]`.

[94] R. Gurau, "The Ponzano-Regge asymptotic of the 6j symbol: An Elementary proof," *Annales Henri Poincare* **9** (2008) 1413–1424, `arXiv:0808.3533 [math-ph]`.

[95] D. Oriti and M. Raasakka, "Asymptotic Analysis of the Ponzano-Regge Model with Non-Commutative Metric Boundary Data," *SIGMA* **10** (2014) 067, `arXiv:1401.5819 [gr-qc]`.

[96] R. Dowdall, H. Gomes, and F. Hellmann, "Asymptotic analysis of the Ponzano-Regge model for handlebodies," *J.Phys.* **A43** (2010) 115203, `arXiv:0909.2027 [gr-qc]`.

[97] J. W. Barrett, "First order Regge calculus," *Class.Quant.Grav.* **11** (1994) 2723–2730, `arXiv:hep-th/9404124 [hep-th]`.

[98] S. L. Kokkendorff, "Polar duality and the generalized law of sines," *Journal of Geometry* **86** no. 1-2, (2007) 140–149.

[99] M. Dupuis and E. R. Livine, "Pushing Further the Asymptotics of the 6j-symbol," *Phys.Rev.* **D80** (2009) 024035, `arXiv:0905.4188 [gr-qc]`.

[100] M. Dupuis and E. R. Livine, "The 6j-symbol: Recursion, Correlations and Asymptotics," *Class.Quant.Grav.* **27** (2010) 135003, `arXiv:0910.2425 [gr-qc]`.

[101] V. Bonzom, E. R. Livine, and S. Speziale, "Recurrence relations for spin foam vertices," *Class.Quant.Grav.* **27** (2010) 125002, `arXiv:0911.2204 [gr-qc]`.

[102] V. Bonzom and E. R. Livine, "A New Recursion Relation for the 6j-Symbol," *Annales Henri Poincare* **13** (2012) 1083–1099, `arXiv:1103.3415 [gr-qc]`.

[103] A. Baratin and D. Oriti, "Quantum simplicial geometry in the group field theory formalism: reconsidering the Barrett-Crane model," *New J.Phys.* **13** (2011) 125011, `arXiv:1108.1178 [gr-qc]`.

[104] C. Rovelli, "The Basis of the Ponzano-Regge-Turaev-Viro-Ooguri quantum gravity model in the loop representation basis," *Phys.Rev.* **D48** (1993) 2702–2707, `arXiv:hep-th/9304164 [hep-th]`.

[105] J. W. Barrett, M. Rocek, and R. M. Williams, "A Note on area variables in Regge calculus," *Class.Quant.Grav.* **16** (1999) 1373–1376, `arXiv:gr-qc/9710056 [gr-qc]`.

[106] Y. Neiman, "A look at area Regge calculus," `arXiv:1308.1012 [gr-qc]`.

[107] H. W. Hamber and R. M. Williams, "On the measure in simplicial gravity," *Phys.Rev.* **D59** (1999) 064014, `arXiv:hep-th/9708019 [hep-th]`.

[108] F. Lund and T. Regge 1974. Princeton preprint , unpublished.

[109] H. W. Hamber and R. M. Williams, "Gauge invariance in simplicial gravity," *Nucl.Phys.* **B487** (1997) 345–408, `arXiv:hep-th/9607153 [hep-th]`.

[110] M. Berger, *Geometry I*. Springer, Berlin, 1994.

[111] C. D'Andrea and M. Sombra, "The Cayley-Menger determinant is irreducible for $n \geq 3$," *Sib. Math. J.* **46** (2005) 71–76, `arXiv:math/0406359 [math]`.

[112] A. Baratin and L. Freidel, "Hidden Quantum Gravity in 3-D Feynman diagrams," *Class.Quant.Grav.* **24** (2007) 1993–2026, `arXiv:gr-qc/0604016 [gr-qc]`.

[113] A. A. Migdal, "Recursion Equations in Gauge Theories," *Sov.Phys.JETP* **42** (1975) 413.

[114] L. Kadanoff, "Notes on Migdal's Recursion Formulas," *Annals Phys.* **100** (1976) 359–394.

[115] E. Efrati, Z. Wang, A. Kolan, and L. P. Kadanoff, "Real-space renormalization in statistical mechanics," *Rev. Mod. Phys.* **86** (May, 2014) 647–667, `arXiv:1301.6323 [cond-mat.stat-mech]`.

[116] S. R. White, "Density matrix formulation for quantum renormalization groups," *Phys. Rev. Lett.* **69** (Nov, 1992) 2863–2866.

[117] K. Hallberg, "New Trends in Density Matrix Renormalization," *Adv. Phys.* **55** (2006) 477–526, `arXiv:cond-mat/0609039 [cond-mat.str-el]`.

[118] F. Verstraete, J. Cirac, and V. Murg, "Matrix Product States, Projected Entangled Pair States, and variational renormalization group methods for quantum spin systems," *Adv. Phys.* **57** (2008) 143, `arXiv:0907.2796 [quant-ph]`.

[119] R. Orus, "A Practical Introduction to Tensor Networks: Matrix Product States and Projected Entangled Pair States," *Annals Phys.* **349** (2014) 117–158, `arXiv:1306.2164 [cond-mat.str-el]`.

[120] R. Orús, "Exploring corner transfer matrices and corner tensors for the classical simulation of quantum lattice systems," *Phys. Rev. B* **85** (2012) 205117, `arXiv:1112.4101 [cond-mat.str-el]`.

[121] Y. Liu, Y. Meurice, M. Qin, J. Unmuth-Yockey, T. Xiang, *et al.*, "Exact blocking formulas for spin and gauge models," *Phys.Rev.* **D88** (2013) 056005, `arXiv:1307.6543 [hep-lat]`.

[122] L. C. Biedenharn and M. A. Lohe, *Quantum Group Symmetries and q-Tensor Algebras*. World Scientific, Singapore, 1995.

[123] J. S. Carter, D. E. Flath, and M. Saito, *The Classical and Quantum 6j–symbols*. Princeton University Press, Princeton, 1995.

[124] V. G. Turaev and O. Y. Viro, "State sum invariants of 3 manifolds and quantum 6j symbols," *Topology* **31** (1992) 865–902.

[125] M. Dupuis and F. Girelli, "Quantum hyperbolic geometry in loop quantum gravity with cosmological constant," *Phys.Rev.* **D87** no. 12, (2013) 121502, `arXiv:1307.5461 [gr-qc]`.

[126] M. Dupuis and F. Girelli, "Observables in Loop Quantum Gravity with a cosmological constant," *Phys.Rev.* **D90** (2014) 104037, `arXiv:1311.6841 [gr-qc]`.

[127] V. Bonzom, M. Dupuis, F. Girelli, and E. R. Livine, "Deformed phase space for 3d loop gravity and hyperbolic discrete geometries," `arXiv:1402.2323 [gr-qc]`.

[128] V. Bonzom, M. Dupuis, and F. Girelli, "Towards the Turaev-Viro amplitudes from a Hamiltonian constraint," *Phys.Rev.* **D90** (2014) 104038, `arXiv:1403.7121 [gr-qc]`.

[129] D. Pranzetti, "Turaev-Viro amplitudes from 2+1 Loop Quantum Gravity," *Phys.Rev.* **D89** (2014) 084058, `arXiv:1402.2384 [gr-qc]`.

[130] I. Khavkine and J. D. Christensen, "q-deformed spin foam models of quantum gravity," *Class. Quant. Grav.* **24** (2007) 3271–3290, `arXiv:0704.0278 [gr-qc]`.

[131] W. J. Fairbairn and C. Meusburger, "Quantum deformation of two four-dimensional spin foam models," *J. Math. Phys.* **53** (2012) 022501, `arXiv:1012.4784 [gr-qc]`.

[132] M. Han, "4-dimensional Spin-foam Model with Quantum Lorentz Group," *J. Math. Phys.* **52** (2011) 072501, `arXiv:1012.4216 [gr-qc]`.

[133] B. Dittrich and P. A. Höhn, "From covariant to canonical formulations of discrete gravity," *Class.Quant.Grav.* **27** (2010) 155001, `arXiv:0912.1817 [gr-qc]`.

[134] B. Dittrich and P. A. Höhn, "Canonical simplicial gravity," *Class.Quant.Grav.* **29** (2012) 115009, `arXiv:1108.1974 [gr-qc]`.

[135] B. Dittrich and P. A. Höhn, "Constraint analysis for variational discrete systems," *J. Math. Phys.* **54** (2013) 093505, `arXiv:1303.4294 [math-ph]`.

[136] P. A. Hoehn, "Quantization of systems with temporally varying discretization I: Evolving Hilbert spaces," *J.Math.Phys.* **55** (2014) 083508, `arXiv:1401.6062 [gr-qc]`.

[137] P. A. Höhn, "Quantization of systems with temporally varying discretization II: Local evolution moves," *J.Math.Phys.* **55** (2014) 103507, `arXiv:1401.7731 [gr-qc]`.

[138] K. Kuchar, "Geometry of Hyperspace. 1.," *J.Math.Phys.* **17** (1976) 777–791.

[139] J. W. Barrett, R. Dowdall, W. J. Fairbairn, H. Gomes, and F. Hellmann, "Asymptotic analysis of the EPRL four-simplex amplitude," *J.Math.Phys.* **50** (2009) 112504, `arXiv:0902.1170 [gr-qc]`.

[140] L. Freidel, "A Ponzano-Regge model of Lorentzian 3-dimensional gravity," *Nucl.Phys.Proc.Suppl.* **88** (2000) 237–240, `arXiv:gr-qc/0102098 [gr-qc]`.

[141] J. Engle, "The Plebanski sectors of the EPRL vertex," *Class.Quant.Grav.* **28** (2011) 225003, `arXiv:1107.0709 [gr-qc]`.

[142] B. Dittrich and S. Speziale, "Area-angle variables for general relativity," *New J.Phys.* **10** (2008) 083006, `arXiv:0802.0864 [gr-qc]`.

[143] V. Bonzom, "Spin foam models for quantum gravity from lattice path integrals," *Phys.Rev.* **D80** (2009) 064028, `arXiv:0905.1501 [gr-qc]`.

[144] D. Oriti, "The Feynman propagator for spin foam quantum gravity," *Phys.Rev.Lett.* **94** (2005) 111301, `arXiv:gr-qc/0410134 [gr-qc]`.

[145] E. R. Livine and D. Oriti, "About Lorentz invariance in a discrete quantum setting," *JHEP* **0406** (2004) 050, `arXiv:gr-qc/0405085 [gr-qc]`.

[146] M. Christodoulou, M. Langvik, A. Riello, C. Roken, and C. Rovelli, "Divergences and Orientation in Spinfoams," *Class. Quant. Grav.* **30** (2013) 055009, `arXiv:1207.5156 [gr-qc]`.

[147] K. Noui and A. Perez, "Three-dimensional loop quantum gravity: Physical scalar product and spin foam models," *Class.Quant.Grav.* **22** (2005) 1739–1762, `arXiv:gr-qc/0402110 [gr-qc]`.

[148] T. Thiemann, "The Phoenix project: Master constraint program for loop quantum gravity," *Class.Quant.Grav.* **23** (2006) 2211–2248, `arXiv:gr-qc/0305080 [gr-qc]`.

[149] B. Dittrich and T. Thiemann, "Testing the master constraint programme for loop quantum gravity. I. General framework," *Class.Quant.Grav.* **23** (2006) 1025–1066, `arXiv:gr-qc/0411138 [gr-qc]`.

[150] B. Dittrich and T. Thiemann, "Testing the master constraint programme for loop quantum gravity. II. Finite dimensional systems," *Class.Quant.Grav.* **23** (2006) 1067–1088, `arXiv:gr-qc/0411139 [gr-qc]`.

[151] B. Bahr, "On knottings in the physical Hilbert space of LQG as given by the EPRL model," *Class.Quant.Grav.* **28** (2011) 045002, `arXiv:1006.0700 [gr-qc]`.

[152] B. Bahr, F. Hellmann, W. Kaminski, M. Kisielowski, and J. Lewandowski, "Operator Spin Foam Models," *Class.Quant.Grav.* **28** (2011) 105003, `arXiv:1010.4787 [gr-qc]`.

[153] B. Dittrich, L. Freidel, and S. Speziale, "Linearized dynamics from the 4-simplex Regge action," *Phys.Rev.* **D76** (2007) 104020, `arXiv:0707.4513 [gr-qc]`.

[154] I. G. Korepanov, "Invariants of PL manifolds from metrized simplicial complexes: Three-dimensional case," *J.Nonlin.Math.Phys.* **8** (2001) 196–210, `arXiv:math/0009225 [math-gt]`.

[155] I. Korepanov, "Multidimensional analogues of the geometric s <–> t duality," *Theor.Math.Phys.* **124** (2000) 999–1005.

[156] I. G. Korepanov, "Euclidean 4-simplices and invariants of four-dimensional manifolds. I. Moves 3 —> 3," *Theor.Math.Phys.* **131** (2002) 765–774, `arXiv:math/0211165 [math-gt]`.

[157] A. Baratin and L. Freidel, "Hidden Quantum Gravity in 4-D Feynman diagrams: Emergence of spin foams," *Class.Quant.Grav.* **24** (2007) 2027–2060, `arXiv:hep-th/0611042 [hep-th]`.

[158] B. Bahr private communication.

[159] T. Kennedy, "Introduction to Mathematical Physics – 3. RG for Ising systems,". `http://math.arizona.edu/~tgk/541/chap3.pdf`. Lecture notes, University of Arizona, 2008.

[160] B. Bahr, B. Dittrich, and J. P. Ryan, "Spin foam models with finite groups," *J.Grav.* **2013** (2013) 549824, `arXiv:1103.6264 [gr-qc]`.

[161] J. B. Kogut, "An Introduction to Lattice Gauge Theory and Spin Systems," *Rev.Mod.Phys.* **51** (1979) 659.

[162] B. Dittrich and W. Kamiński, "Topological lattice field theories from intertwiner dynamics," `arXiv:1311.1798 [gr-qc]`.

[163] M. P. Reisenberger, "On relativistic spin network vertices," *J.Math.Phys.* **40** (1999) 2046–2054, `arXiv:gr-qc/9809067 [gr-qc]`.

[164] S. Steinhaus, "Quantum group spin nets: refinement limit and relation to spin foams,". `http://relativity.phys.lsu.edu/ilqgs/steinhaus021814.pdf`. Talk given in the ILQG seminar on Feb 18th 2014, for plot see slide 36/41.

[165] B. Dittrich and J. P. Ryan, "Phase space descriptions for simplicial 4d geometries," *Class.Quant.Grav.* **28** (2011) 065006, `arXiv:0807.2806 [gr-qc]`.

[166] G. Thorleifsson, P. Bialas, and B. Petersson, "The weak coupling limit of simplicial quantum gravity," *Nucl.Phys.* **B550** (1999) 465–491, `arXiv:hep-lat/9812022 [hep-lat]`.

[167] V. Bonzom, R. Gurau, A. Riello, and V. Rivasseau, "Critical behavior of colored tensor models in the large N limit," *Nucl.Phys.* **B853** (2011) 174–195, `arXiv:1105.3122 [hep-th]`.

[168] R. Gurau and J. P. Ryan, "Melons are branched polymers," *Annales Henri Poincare* **15** no. 11, (2014) 2085–2131, `arXiv:1302.4386 [math-ph]`.

[169] C. Fleischhack, "Representations of the Weyl algebra in quantum geometry," *Commun.Math.Phys.* **285** (2009) 67–140, `arXiv:math-ph/0407006 [math-ph]`.

[170] J. Lewandowski, A. Okolow, H. Sahlmann, and T. Thiemann, "Uniqueness of diffeomorphism invariant states on holonomy-flux algebras," *Commun.Math.Phys.* **267** (2006) 703–733, `arXiv:gr-qc/0504147 [gr-qc]`.

[171] P. A. M. Dirac, *Lectures on Quantum Mechanics*. Academic Press, New York, 1965.

[172] H.-J. Matschull, "Dirac's canonical quantization program," `arXiv:quant-ph/9606031 [quant-ph]`.

[173] C. Teitelboim, "How commutators of constraints reflect the space-time structure," *Annals Phys.* **79** (1973) 542–557.

[174] J. Hartle and S. Hawking, "Wave Function of the Universe," *Phys.Rev.* **D28** (1983) 2960–2975.

[175] B. Dittrich and M. Geiller, "A new vacuum for Loop Quantum Gravity," `arXiv:1401.6441 [gr-qc]`.

[176] T. Koslowski and H. Sahlmann, "Loop quantum gravity vacuum with nondegenerate geometry," *SIGMA* **8** (2012) 026, `arXiv:1109.4688 [gr-qc]`.

[177] T. Thiemann and A. Zipfel, "Linking covariant and canonical LQG II: Spin foam projector," *Class.Quant.Grav.* **31** (2014) 125008, `arXiv:1307.5885 [gr-qc]`.

[178] R. Oeckl, "A 'General boundary' formulation for quantum mechanics and quantum gravity," *Phys.Lett.* **B575** (2003) 318–324, `arXiv:hep-th/0306025 [hep-th]`.

[179] G. Vidal, "Class of Quantum Many-Body States That Can Be Efficiently Simulated," *Phys.Rev.Lett.* **101** (2008) 110501.

[180] G. Vidal, "Entanglement Renormalization," *Phys.Rev.Lett.* **99** no. 22, (2007) 220405, `arXiv:cond-mat/0512165 [cond-mat]`.

[181] B. Swingle, "Constructing holographic spacetimes using entanglement renormalization," `arXiv:1209.3304 [hep-th]`.

[182] G. Evenbly and G. Vidal, "Tensor network states and geometry," *J. Stat. Phys.* **145** (2011) 891–918, `arXiv:1106.1082 [quant-ph]`.

[183] M. Nozaki, S. Ryu, and T. Takayanagi, "Holographic Geometry of Entanglement Renormalization in Quantum Field Theories," *JHEP* **1210** (2012) 193, `arXiv:1208.3469 [hep-th]`.

[184] K. Skenderis, "Lecture notes on holographic renormalization," *Class.Quant.Grav.* **19** (2002) 5849–5876, `arXiv:hep-th/0209067 [hep-th]`.